Cancer Cell

Volume 23
Number 3

March 18, 2013

www.cellpress.com

PHF8 Governs ATRA Response in APL

Targeting Oxidative Phosphorylation: Why, When, and How

Michael Pollak[1,2,*]
[1]Department of Oncology, McGill University, Montreal, QC H3T1E2, Canada
[2]Lady Davis Research Institute of the Jewish General Hospital, Montreal, QC H3T1E2, Canada
*Correspondence: michael.pollak@mcgill.ca
http://dx.doi.org/10.1016/j.ccr.2013.02.015

In this issue of *Cancer Cell*, Vazquez and colleagues report reduced glycolysis and increased oxidative phosphorylation in certain melanomas, revealing metabolic plasticity rather than stable Warburg pathophysiology. Furthermore, Haq and colleagues (also in this issue of *Cancer Cell*) show situations where increased oxidative phosphorylation is required for melanomas to survive inhibition of B-RAF, suggesting investigation of therapeutic combinations of B-RAF inhibitors with biguanides.

Increased glycolysis has been recognized to be a characteristic of neoplastic cells since the classic observations of Otto Warburg. It is now appreciated that the "Warburg effect" does not usually involve compensation for defects in mitochondrial ATP production as originally proposed. Rather, it is a consequence of genetic lesions that, among other sequellae, alter control systems that regulate cellular metabolism. While increased glycolytic flux may provide some benefit to cancer cells by increasing ATP production, recent studies suggest that it is advantageous mainly because it generates chemical "building blocks" required for the anabolic processes that must occur prior to cell division.

The conspicuous glycolysis of neoplastic cells has long provided a rationale for investigating inhibitors of glycolysis such as 2-deoxyglucose, but this direction of research has not yet led to clinical advances in cancer treatment. Observations reported in this issue of *Cancer Cell* by Haq et al. (2013) and Vazquez et al. (2013) provide evidence that there are circumstances in which neoplastic cells are critically dependent on oxidative phosphorylation rather than glycolysis, at least in the context of melanoma. This may represent a vulnerability that could be therapeutically exploited.

Both reports show that the lineage-specific transcription factor MITF upregulates PGC1α in a subset of melanomas, and, expectedly, this results in increased oxidative phosphorylation. Haq et al. (2013) show that mutational B-RAF activation, a common derangement in melanoma, leads to declines in MITF, PGC1α, and oxidative phosphorylation, yielding a glycolytic phenotype.

B-RAF inhibitors such as vemurafenib are used in the clinic but commonly provide only short-term benefit, followed by the rapid development of drug resistance. Interestingly, when cells with activated B-RAF are exposed to a B-RAF inhibitor, they upregulate PGC1α and demonstrate, at least for a critical period of time, increased dependency on oxidative phosphorylation. This phenomenon suggests that the efficacy of B-RAF inhibitors may be, at least in part, attributable to drug-induced reprogramming of cellular metabolism, leading to a reduction of glycolysis and an increased requirement for oxidative phosphorylation. While under this stress, cells are under selective pressure to revert to a glycolytic phenotype by activating another oncogene to substitute for the pharmacologically inhibited B-RAF (Nazarian et al., 2010). However, it is possible that before this reversion takes place, there is an opportunity for synthetic lethality by combining the kinase inhibitor with inhibition of oxidative phosphorylation.

The studies by (Haq et al. (2013) and Vazquez et al. (2013) are specific to melanoma, so it will be of interest to investigate the generality of the key findings. Many cancers with prominent glycolytic phenotypes are treated with kinase inhibitors, which reduce the oncogenic signaling that promotes glycolysis, among other consequences. Most kinase inhibitors provide a period of benefit followed by drug resistance. It is possible that one of several consequences of exposing sensitive cells to a kinase inhibitor is reduction of high glycolytic flux. Apart from the melanoma data, an example is provided by glycolytic leukemic cells driven by BCR-ABL that demonstrate upregulated oxidative phosphorylation upon exposure to imatinib (Gottschalk et al., 2004; the kinase inhibitor that targets BCR-ABL).

Consistently, Vazquez et al. (2013) show that melanomas can be classified into two groups: a conventional glycolytic group and a group characterized by high PGC1α, high rates of oxidative phosphorylation, resistance to oxidative stress, and aggressive clinical behavior. The latter group also appears to demonstrate sensitivity to the targeted inhibition of oxidative phosphorylation. Experimentally, this point is convincingly made by knocking down proteins required for oxidative phosphorylation. However, this approach is not one that is applicable to clinical testing.

Are there practical ways to target oxidative phosphorylation in the clinic? An initial impression is that this is impossible, as classic inhibitors of cellular respiration such as cyanide are well-known poisons without a suitable therapeutic index. However, there are oxidative phosphorylation inhibitors that are in common clinical use, including the antidiabetic biguanide metformin and the antimalarial agent atovaquone. Incidentally, the inhibition of cytochrome b by atovaquone is effective against *Plasmodium falciparum*, not because it inhibits mitochondrial ATP production (which is not required by the parasites), but rather because of a requirement for oxidative phosphorylation

to regenerate ubiquinone (Painter et al., 2007). (In *Plasmodium falciparum*, ubiquinone is required as the electron acceptor for dihydroorotate dehydrogenase, an essential enzyme for pyrimidine biosynthesis.) Nevertheless, the safety of atovaquone relates to the fact that it is a better inhibitor of *Plasmodium* than human cytochrome c, so it may not be a strong candidate for oncology applications.

Metformin, on the other hand, is widely used for the treatment of type II diabetes, has a favorable toxicity profile, and is already under investigation for possible oncology applications (Pollak, 2012). There are several hypotheses to explain the activity of metformin as an antineoplastic agent in experimental models. One involves systemic effects such as the reduction of insulin levels (which may be relevant for a subset of patients where the drug induces significant declines in insulin, provided their cancers are insulin responsive). A second hypothesis involves a direct action on neoplastic cells, characterized by decreased ATP levels secondary to reduced oxidative phosphorylation. This can lead to predominately cytostatic or cytotoxic effects, depending on the specific characteristics of targeted cells. In cells with intact control systems for dealing with energy stress, ATP deficit leads to the activation of AMPK, inhibition of mTOR, reduced energy consumption and growth inhibition. In cells with loss of function of these control systems (such as inactivation of LKB1), the ongoing high level of ATP consumption, despite reduced oxidative phosphorylation, leads to an energetic crisis.

Could metformin or other biguanides be practical inhibitors of oxidative phosphorylation in the context of the studies by Haq et al. (2013) and Vazquez et al. (2013)? This might not require complete inhibition of oxidative phosphorylation, but rather blocking the increase in oxidative phosphorylation following PGC1α upregulation.

If further preclinical work provides sufficient evidence that metformin can delay the development of resistance to vemurafenib or other kinase inhibitors, the safety profile of biguanides suggests that clinical trials would be feasible.

However, there are important gaps in knowledge to consider. First, with clear credentials as oxidative phosphorylation inhibitors, why are the biguanides so different from cyanide in terms of therapeutic index? Part of the reason may relate to whole organism, cellular, and subcellular pharmacokinetics. Following oral administration, biguanides accumulate in a nonhomogeneous fashion in different organs, and cellular uptake of metformin is greatly influenced by the level of anion transporter OCT1. Furthermore, mitochondrial uptake of biguanides is facilitated by the membrane potential, so as biguanide concentration rises at complex I, the membrane potential falls, reducing further import and limiting toxicity. Thus, in vivo, it is not trivial to determine the extent to which a biguanide is inhibiting oxidative phosphorylation in a particular tissue. Thus, it is unclear if the dose of metformin used in diabetes patients would be optimal for partial inhibition of oxidative phosphorylation in melanoma patients or if phenformin or other lipophilic biguanides would be more effective.

There are relevant clues and cautions in the literature. In tissue culture, biguanides clearly inhibit oxidative phosphorylation in transformed cells, often leading to compensatory increases in glycolysis (Pollak, 2012). Also, an early report provided in vitro evidence for synergy between vemurafenib and metformin (Niehr et al., 2011). On the other hand, metformin has been reported in certain contexts to upregulate VEGF expression, which is an adaptive response by the transformed cell to the inhibition of oxidative phosphorylation. This response obviously has the potential for undesired consequences, although this research revealed synergy between metformin and VEGF inhibitors (Martin et al., 2012).

Whereas many clinical trials of biguanides for cancer treatment are ongoing, most were designed with the rationale that the reduction of systemic hyperinsulinemia, if achievable, would be beneficial. The ongoing trials address neither hypotheses related to specific strategic therapeutic combinations of biguanides with kinase inhibitors nor the possibility of activity in specific tumor subsets defined by tumor characteristics such as PGC1α status. Future studies aimed at rigorously examining these possibilities will need to establish, as a first step, the extent to which clinically achievable biguanide exposure inhibits oxidative phosphorylation in neoplastic tissue in vivo.

Despite the considerable challenges, the clues concerning the sensitivity of a subset of cancers to the inhibition of oxidative phosphorylation, particularly in the context of resistance to kinase inhibitors, are tantalizing. Further work will reveal if there are practical opportunities for synthetic lethality by pharmacologically limiting the adaptive ability of transformed cells to upregulate oxidative phosphorylation when facing stresses such as oncogenic kinase inhibition.

REFERENCES

Gottschalk, S., Anderson, N., Hainz, C., Eckhardt, S.G., and Serkova, N.J. (2004). Clin. Cancer Res. *10*, 6661–6668.

Haq, R., Shoag, J., Andreu-Perez, P., Yokoyama, S., Edelman, H., Rowe, G.C., Frederick, D.T., Hurley, A.D., Nellore, A., Kung, A.L., et al. (2013). Cancer Cell *23*, this issue, 302–315.

Martin, M.J., Hayward, R., Viros, A., and Marais, R. (2012). Cancer Discov *2*, 344–355.

Nazarian, R., Shi, H., Wang, Q., Kong, X., Koya, R.C., Lee, H., Chen, Z., Lee, M.K., Attar, N., Sazegar, H., et al. (2010). Nature *468*, 973–977.

Niehr, F., von Euw, E., Attar, N., Guo, D., Matsunaga, D., Sazegar, H., Ng, C., Glaspy, J.A., Recio, J.A., Lo, R.S., et al. (2011). J. Transl. Med. *9*, 76.

Painter, H.J., Morrisey, J.M., Mather, M.W., and Vaidya, A.B. (2007). Nature *446*, 88–91.

Pollak, M.N. (2012). Cancer Discov *2*, 778–790.

Vazquez, F., Lim, J.-H., Chim, H., Bhalla, K., Girnun, G., Pierce, K., Clish, C.B., Granter, S.R., Widlund, H.R., Spiegelman, B.M., and Puigserver, P. (2013). Cancer Cell *23*, this issue, 287–301.

ROS Links Glucose Metabolism to Breast Cancer Stem Cell and EMT Phenotype

Michael S. Schieber[1] and Navdeep S. Chandel[1,2,*]
[1]Division of Pulmonary and Critical Care Medicine, Department of Medicine
[2]Department of Cell and Molecular Biology
Northwestern University Feinberg School of Medicine, Chicago, IL 60611, USA
*Correspondence: nav@northwestern.edu
http://dx.doi.org/10.1016/j.ccr.2013.02.021

Cancer stem cells display an epithelial-mesenchymal transition phenotype and are resistant to current therapies. In this issue of *Cancer Cell*, Dong and colleagues demonstrate that these phenotypes in basal-like breast cancer are promoted by a metabolic switch to glucose metabolism, resulting in decreased reactive oxygen species levels.

Cancer initiating cells, also referred to as cancer stem cells (CSCs), exhibit stem cell-like properties and have been implicated in the tumorigenesis of basal-like breast cancer (BLBC), a particularly aggressive, metastatic and chemotherapy-resistant type of breast cancer. In this issue of *Cancer Cell*, Dong et al. (2013) report a metabolic switch to glycolysis following epigenetic silencing of the gluconeogenic enzyme fructose-1,6-biphosphatase (FPB1) by the epithelial-mesenchymal transition (EMT) associated factor Snail is required for the development of BLBC.

CSCs display EMT characteristics such as loss of the adhesion protein E-cadherin (Mani et al., 2008). A number of transcription factors, including Snail, induce EMT (Kalluri and Weinberg, 2009). Previously, the same group reported that Snail interacts with G9a, a methyltransferase responsible for H3K9me2, and recruits DNA methyltransferases (DNMTs) to the E-cadherin promoter. This results in epigenetic silencing of E-cadherin expression and promotes primary tumor growth and metastasis of BLBC cells (Dong et al., 2012).

To investigate other genes regulated by the Snail-G9a-Dnmt1 complex in BLBC cells, Dong et al. (2013) performed a gene expression mircroarray analysis following G9a knockdown in a BLBC cell line and observed a substantial increase in FBP1 mRNA. Snail-G9a-Dnmt1 was then shown to directly bind and methylate the FBP1 promoter, resulting in the epigenetic silencing of FBP1. Moreover, a number of other BLBC cell lines had negligible FBP1 expression in contrast to a set of luminal breast cancer cell lines, which displayed high FBP1 levels. To test if FBP1 silencing was required for the EMT characteristics of BLBC cells, Dong et al. (2013) ectopically expressed Snail alone or together with FBP1 in ER^+-luminal breast cancer cells. Ectopic expression of Snail was sufficient to convert these cells to a BLBC phenotype, as expected. Importantly, however, Snail expression-induced EMT and basal-like phenotype was blocked when FBP1 was coexpressed under the control of a promoter that was not repressed by Snail. Moreover, ectopic expression of FBP1 in BLBC cells diminished tumor growth in mice. By contrast, loss of FBP1 in luminal breast cancer cells increased tumor growth in mice. This biological observation appears to be clinically relevant, because a retrospective analysis of patients with BLBC revealed that low FBP1 expression correlated with poor survival. The loss of FBP1 has also been previously associated with liver and gastrointestinal cancers (Chen et al., 2011). Collectively, these results suggest that epigenetic silencing of FBP1 is a critical event in tumorigenesis of BLBC.

The provocative implication of the current study is that metabolism is not simply a consequence but rather plays a causal role in dictating different phenotypic states exhibited by cancer cells. But how does an enzyme involved in glucose metabolism regulate EMT-like characteristics of BLBC? Glucose levels are maintained by two reciprocal metabolic pathways: glycolysis and gluconeogenesis. Glycolysis is an ATP- and NADH-generating reaction that results in the catabolism of glucose into two molecules of pyruvate. Under aerobic conditions, pyruvate and NADH produced by glycolysis are then imported into the mitochondria and flux through the tricarboxylic acid cycle to generate ATP through oxidative phosphorylation. Under low oxygen conditions, pyruvate can be converted to lactate, regenerating NAD^+ required for glycolysis. Conversely, gluconeogenesis produces glucose from pyruvate. Most of the enzymes in glycolysis are reversible and thus can be utilized for gluconeogenesis. However, there are three irreversible glycolytic enzymes including phosphofructose kinase 1 (PFK-1), which converts fructose 6-phosphate to fructose 1,6 bisphosphate (Figure 1). To circumvent PFK-1 during gluconeogenesis, FBP1 catalyzes the energy-consuming reaction of converting fructose 1,6-bisphosphate to fructose 6-phosphate.

Many human cancer cells display high flux through glycolysis and other metabolic pathways originating from glycolytic intermediates. These subsidiary metabolic pathways are involved in the synthesis of essential amino acids, nucleotides (via pentose phosphate shunt), and lipids. Therefore, an increase in glycolytic flux may be highly adaptive for proliferative cells with high demand for cellular macromolecules (Lunt and Vander Heiden, 2011). Indeed, Dong et al. (2013) observed that ectopic expression of FBP1 in BLBC cell lines decreased glucose uptake and diminished flux through both glycolysis and the biosynthetic subsidiary metabolic pathways. This resulted in an increase in oxygen

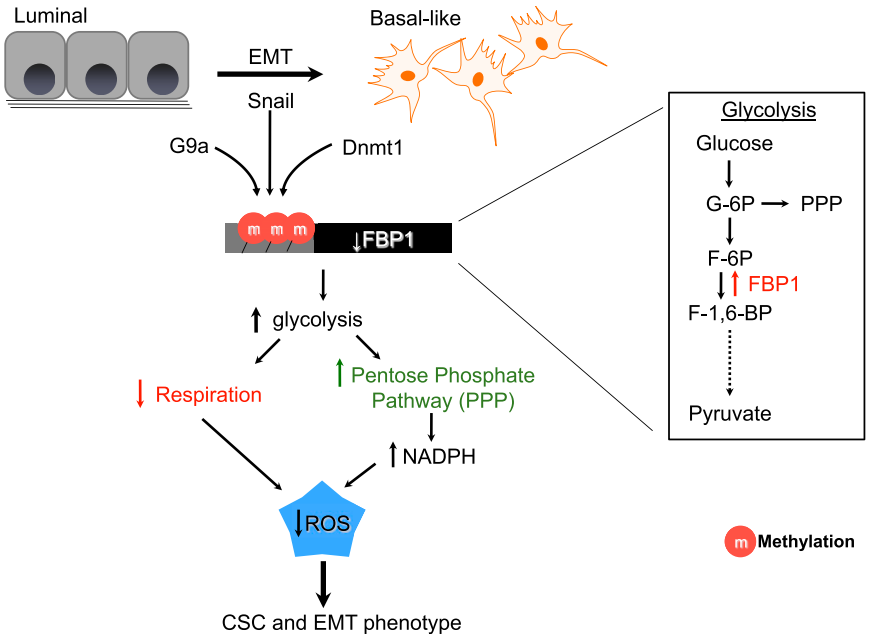

Figure 1. Epigenetic Silencing of FBP1 Decreases ROS to Promote CSC and EMT Phenotype in BLBC

FBP1 coverts F-1,6,-BP to F-6P in the rate-limiting step of gluconeogenesis (right). Epigenetic silencing of FBP1, through promoter methylation by the Snail-G9a-Dnmt1 complex, promotes glycolytic flux. An increased reliance on glucose metabolism following FBP1 silencing lowers ROS levels by two mechanisms: decreased mitochondrial respiration and increased NADPH synthesis through pentose phosphate metabolism. Lower ROS levels promote EMT and CSC phenotype in BLBC.

consumption by mitochondria. Thus, BLBC utilizes FBP1 silencing as a mechanism to maintain glucose flux through glycolysis and other associated biosynthetic metabolic pathways.

One emerging idea on how changes in glucose metabolism induce EMT-like phenotype is that mitochondrial derived reactive oxygen species (ROS) could serve as signaling molecules (Sena and Chandel, 2012). The mitochondrial electron transport chain leaks electrons from complex I, II, and III to molecular oxygen (O_2) to generate superoxide (O_2^-), which is rapidly converted to hydrogen peroxide (H_2O_2) to activate cellular signaling. However, higher levels of ROS can induce cell damage and death. Indeed, higher FBP1 expression in BLBC cell lines resulted in increased mitochondrial ROS. This increase in ROS levels due to FBP1 expression was critical for tumor suppression, which could be prevented by administration of the antioxidant N-acetylcysteine. The increased generation of H_2O_2 is likely due to enhanced mitochondrial oxygen consumption as well as the diminished flux through the pentose phosphate pathway, which generates the NADPH required for enzymes that detoxify H_2O_2 (Figure 1). Thus, the low ROS levels in BLBC due to epigenetic silencing of FBP1 allows for tumor growth of BLBC cells.

An important consequence of having low ROS levels is the maintenance of a subpopulation of CSCs within breast tumors. These CSCs are relatively insensitive to radiation and chemotherapy compared to differentiated and proliferative cancer cell populations (Diehn et al., 2009). Dong et al. (2013) show that when FPB1 is overexpressed in BLBC cell lines, the corresponding increase in ROS levels is accompanied by a significantly reduced number of $CD44^{high}/CD24^{low}/EpCAM^+$ CSC and, as a functional assay, decreased tumorsphere formation in soft agar. Because CD44 is a direct target of the β-catenin dependent transcriptional machinery, the investigators hypothesized that increased ROS, produced through FBP1 overexpression, decreased CSC by inhibiting β-catenin activation. β-catenin acts as coactivator of the transcription factor TCF4 to induce genes involved in maintaining stem-like characteristics. Indeed, FBP1 overexpression decreased β-catenin signaling by promoting its dissociation from TCF4. This interaction was restored with the antioxidant N-acetylcysteine. Taken together, these data support a mechanism where epigenetic downregulation of FBP1 increases glycolysis and decreases ROS, resulting in activation of β-catenin signaling to maintain CSCs (Figure 1).

Although Dong et al. (2013) provide a reasonable explanation for how low levels of ROS due to FBP1 silencing maintain CSCs in BLBCs, they do not mechanistically explore how modulating FBP1 protein levels can regulate E-cadherin protein expression. Presumably, the Snail-G9a-DNMT complex has access to the E-cadherin promoter in the presence or absence of FBP1. Thus, it was surprising that ectopic expression of FBP1 was sufficient to block Snail-dependent epigenetic silencing of E-cadherin. Since methylation is a balance between methyltransferase and demethylase activity, perhaps FBP1 expression triggers high levels of ROS, which affects the activity of these enzymes at the E-cadherin promoter.

A major implication of these findings is that antioxidants might not be beneficial in some cancers. A recent study indicated that non-stem cancer cells can also give rise to CSCs, indicating the bidirectionality between these two populations (Chaffer et al., 2011). If low levels of ROS maintain characteristics of CSC, which are notoriously resistant to radiation and chemotherapy, then antioxidants would possibly promote CSC. Might pharmacologically increasing ROS in BLBC promote the loss of CSCs and improve patient survival? As new therapies are developed for BLBC, it will be of interest how they affect ROS levels and glucose metabolism. Furthermore, therapies directed in diminishing glucose metabolism might be effective against BLBC.

REFERENCES

Chaffer, C.L., Brueckmann, I., Scheel, C., Kaestli, A.J., Wiggins, P.A., Rodrigues, L.O., Brooks, M., Reinhardt, F., Su, Y., Polyak, K., et al. (2011). Proc. Natl. Acad. Sci. USA *108*, 7950–7955.

Chen, M., Zhang, J., Li, N., Qian, Z., Zhu, M., Li, Q., Zheng, J., Wang, X., and Shi, G. (2011). PLoS ONE *6*, e25564.

Diehn, M., Cho, R.W., Lobo, N.A., Kalisky, T., Dorie, M.J., Kulp, A.N., Qian, D., Lam, J.S., Ailles,

L.E., Wong, M., et al. (2009). Nature *458*, 780–783.

Dong, C., Wu, Y., Yao, J., Wang, Y., Yu, Y., Rychahou, P.G., Evers, B.M., and Zhou, B.P. (2012). J. Clin. Invest. *122*, 1469–1486.

Dong, C., Yuan, T., Wu, Y., Wang, Y., Fan, T.W.M., Miriyala, S., Lin, Y., Yao, J., Shi, J., Kang, T., Lorkiewicz, P., et al. (2013). Cancer Cell *23*, this issue, 316–331.

Kalluri, R., and Weinberg, R.A. (2009). J. Clin. Invest. *119*, 1420–1428.

Lunt, S.Y., and Vander Heiden, M.G. (2011). Annu. Rev. Cell Dev. Biol. *27*, 441–464.

Mani, S.A., Guo, W., Liao, M.J., Eaton, E.N., Ayyanan, A., Zhou, A.Y., Brooks, M., Reinhard, F., Zhang, C.C., Shipitsin, M., et al. (2008). Cell *133*, 704–715.

Sena, L.A., and Chandel, N.S. (2012). Mol. Cell *48*, 158–167.

Selective Blockade of Transport via SERCA Inhibition: The Answer for Oncogenic Forms of Notch?

Ma. Xenia G. Ilagan[1,*] and Raphael Kopan[1,*]
[1]Department of Developmental Biology, Washington University School of Medicine, St. Louis, MO 63110, USA
*Correspondence: ilaganmg@wustl.edu (M.X.G.I.), kopan@wustl.edu (R.K.)
http://dx.doi.org/10.1016/j.ccr.2013.02.020

NOTCH1, **which is frequently mutated in T cell acute lymphoblastic leukemia, has been an elusive therapeutic target. In this issue of *Cancer Cell*, Roti and colleagues demonstrate that inhibiting SERCA calcium pumps preferentially impairs the maturation of the most common class of oncogenic Notch1 mutants, thus uncovering a potential therapeutic avenue.**

The four mammalian Notch receptors are large type I membrane proteins, sporting an extracellular domain with 29–36 epidermal growth factor (EGF) repeats followed by the conserved Lin12-Notch repeats (LNR) and a heterodimerization domain (HD; Figure 1A). The LNR and HD domains constitute the negative regulatory region (NRR), which maintains the "off" state of the receptor in the absence of ligand. Upon binding of Notch to ligand presented by a neighboring cell, the NRR undergoes a conformational change to expose the S2 site to ADAM metalloprotease cleavage (Figure 1B). This is followed by γ-secretase-mediated cleavage at the S3 site within the transmembrane domain (TMD), which releases the Notch intracellular domain (NICD). NICD translocates to the nucleus, associates with the DNA-binding protein RBPjκ and the transcriptional coactivator Mastermind (MAM/MAML) to activate transcription. Activation is linked to phosphorylation of the PEST domain, its recognition and ubiquitination by the E3 ubiquitin ligase FBW7, and NICD degradation (reviewed in Kopan and Ilagan, 2009).

Because the Notch signaling pathway regulates many fundamental processes during embryonic development and in self-renewing adult tissues, both gain- and loss-of-function mutations in pathway components lead to developmental disorders, cancer, and other adult onset diseases. Best known is the contribution of ligand-independent, activated forms of Notch1 to T-ALL, more than half of which gain activating mutations in the NRR, PEST, or both (Figure 1A; Weng et al., 2004). The mutations in the NRR lead to ligand hypersensitivity and ligand-independent activation, whereas the PEST domain mutations increase the stability of NICD and lead to sustained signaling activity.

The preponderance of *NOTCH1* mutations in T-ALL has fueled the search for effective anti-Notch1 therapeutics (Figure 1B; reviewed in Tzoneva and Ferrando, 2012). Because Notch activation relies on proteolysis, γ-secretase inhibitors (GSIs), which had been originally developed for Alzheimer's disease therapy, have entered clinical trials for treatment of relapsing T-ALL. However, sustained GSI inhibition is not tolerated, because pan-Notch blockade causes severe gastrointestinal toxicity and promotes progression of squamous cell carcinomas (Extance, 2010). The same problems could affect the efficacy of stapled dominant negative MAML-like peptides (SAHM) that directly target the transcription complex. More recently, receptor-specific anti-NRR1 antibodies have been developed. Despite their ability to circumvent gut toxicity, sustained treatment with these reagents will likely cause vascular neoplasms, raising additional safety concerns (Yan et al., 2010).

To identify modulators of Notch1 signaling and potential therapeutic targets for T-ALL, Roti et al. (2013; in this issue of *Cancer Cell*) conducted complementary high throughput small molecule and cDNA overexpression screens using cell-based assays reporting Notch transcriptional activity. For the compound screen, the transcriptional signature of Notch in T-ALL was assembled from previous genome-wide expression profiling studies of multiple human T-ALL cell lines treated with vehicle or GSI. They validated a group of 28 target and 4 nontarget genes to generate a robust,

L.E., Wong, M., et al. (2009). Nature *458*, 780–783.

Dong, C., Wu, Y., Yao, J., Wang, Y., Yu, Y., Rychahou, P.G., Evers, B.M., and Zhou, B.P. (2012). J. Clin. Invest. *122*, 1469–1486.

Dong, C., Yuan, T., Wu, Y., Wang, Y., Fan, T.W.M., Miriyala, S., Lin, Y., Yao, J., Shi, J., Kang, T., Lorkiewicz, P., et al. (2013). Cancer Cell *23*, this issue, 316–331.

Kalluri, R., and Weinberg, R.A. (2009). J. Clin. Invest. *119*, 1420–1428.

Lunt, S.Y., and Vander Heiden, M.G. (2011). Annu. Rev. Cell Dev. Biol. *27*, 441–464.

Mani, S.A., Guo, W., Liao, M.J., Eaton, E.N., Ayyanan, A., Zhou, A.Y., Brooks, M., Reinhard, F., Zhang, C.C., Shipitsin, M., et al. (2008). Cell *133*, 704–715.

Sena, L.A., and Chandel, N.S. (2012). Mol. Cell *48*, 158–167.

Selective Blockade of Transport via SERCA Inhibition: The Answer for Oncogenic Forms of Notch?

Ma. Xenia G. Ilagan[1,*] and Raphael Kopan[1,*]
[1]Department of Developmental Biology, Washington University School of Medicine, St. Louis, MO 63110, USA
*Correspondence: ilaganmg@wustl.edu (M.X.G.I.), kopan@wustl.edu (R.K.)
http://dx.doi.org/10.1016/j.ccr.2013.02.020

NOTCH1, **which is frequently mutated in T cell acute lymphoblastic leukemia, has been an elusive therapeutic target. In this issue of *Cancer Cell*, Roti and colleagues demonstrate that inhibiting SERCA calcium pumps preferentially impairs the maturation of the most common class of oncogenic Notch1 mutants, thus uncovering a potential therapeutic avenue.**

The four mammalian Notch receptors are large type I membrane proteins, sporting an extracellular domain with 29–36 epidermal growth factor (EGF) repeats followed by the conserved Lin12-Notch repeats (LNR) and a heterodimerization domain (HD; Figure 1A). The LNR and HD domains constitute the negative regulatory region (NRR), which maintains the "off" state of the receptor in the absence of ligand. Upon binding of Notch to ligand presented by a neighboring cell, the NRR undergoes a conformational change to expose the S2 site to ADAM metalloprotease cleavage (Figure 1B). This is followed by γ-secretase-mediated cleavage at the S3 site within the transmembrane domain (TMD), which releases the Notch intracellular domain (NICD). NICD translocates to the nucleus, associates with the DNA-binding protein RBPjκ and the transcriptional coactivator Mastermind (MAM/MAML) to activate transcription. Activation is linked to phosphorylation of the PEST domain, its recognition and ubiquitination by the E3 ubiquitin ligase FBW7, and NICD degradation (reviewed in Kopan and Ilagan, 2009).

Because the Notch signaling pathway regulates many fundamental processes during embryonic development and in self-renewing adult tissues, both gain- and loss-of-function mutations in pathway components lead to developmental disorders, cancer, and other adult onset diseases. Best known is the contribution of ligand-independent, activated forms of Notch1 to T-ALL, more than half of which gain activating mutations in the NRR, PEST, or both (Figure 1A; Weng et al., 2004). The mutations in the NRR lead to ligand hypersensitivity and ligand-independent activation, whereas the PEST domain mutations increase the stability of NICD and lead to sustained signaling activity.

The preponderance of *NOTCH1* mutations in T-ALL has fueled the search for effective anti-Notch1 therapeutics (Figure 1B; reviewed in Tzoneva and Ferrando, 2012). Because Notch activation relies on proteolysis, γ-secretase inhibitors (GSIs), which had been originally developed for Alzheimer's disease therapy, have entered clinical trials for treatment of relapsing T-ALL. However, sustained GSI inhibition is not tolerated, because pan-Notch blockade causes severe gastrointestinal toxicity and promotes progression of squamous cell carcinomas (Extance, 2010). The same problems could affect the efficacy of stapled dominant negative MAML-like peptides (SAHM) that directly target the transcription complex. More recently, receptor-specific anti-NRR1 antibodies have been developed. Despite their ability to circumvent gut toxicity, sustained treatment with these reagents will likely cause vascular neoplasms, raising additional safety concerns (Yan et al., 2010).

To identify modulators of Notch1 signaling and potential therapeutic targets for T-ALL, Roti et al. (2013; in this issue of *Cancer Cell*) conducted complementary high throughput small molecule and cDNA overexpression screens using cell-based assays reporting Notch transcriptional activity. For the compound screen, the transcriptional signature of Notch in T-ALL was assembled from previous genome-wide expression profiling studies of multiple human T-ALL cell lines treated with vehicle or GSI. They validated a group of 28 target and 4 nontarget genes to generate a robust,

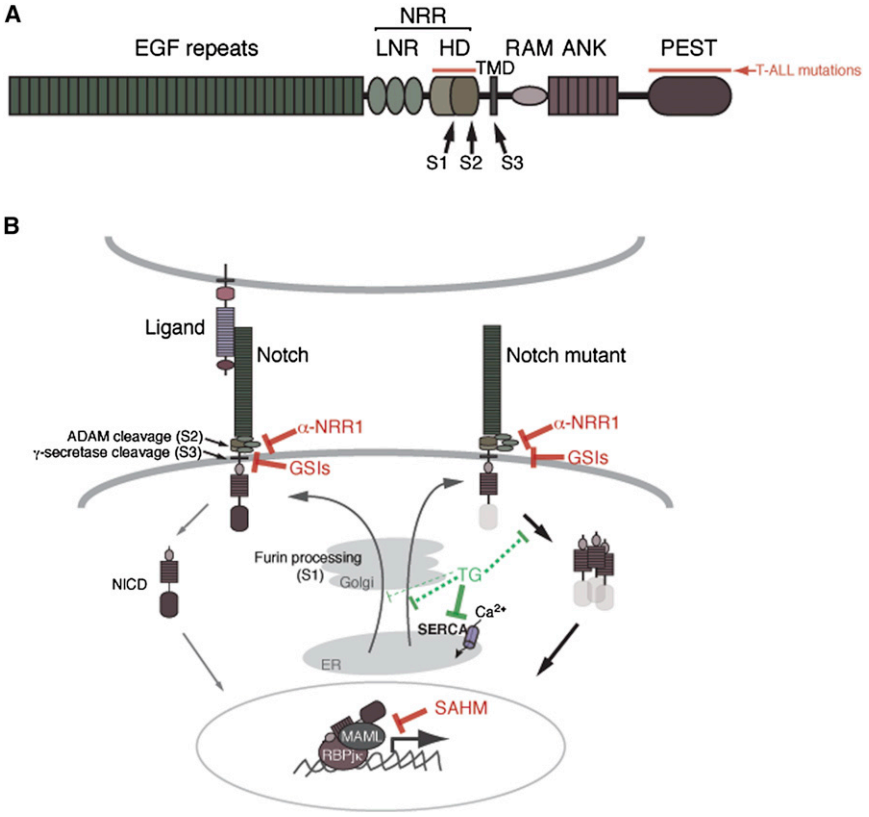

Figure 1. The Core Notch Signaling Pathway and Strategies for Therapeutic Intervention
(A) Domain organization of Notch1 (RAM, RBPjκ-association module; ANK, ankyrin repeats; PEST, proline/glutamic acid/serine/threonine degron domain). Cleavage sites for furin (S1), ADAM metalloprotease (S2), and γ-secretase (S3) are indicated. The NRR keeps the receptor "off" in the absence of ligand. Gain-of-function mutations associated with T-ALL (highlighted in red) predominantly lie within HD, which lead to ligand hypersensitivity and ligand-independent activation, or within PEST, which typically lead to deletions and truncations and therefore increased stability and prolonged signaling activity. HD and PEST activating mutations can also occur in *cis*. Notably, loss-of-function mutations throughout the entire coding region are also associated with cancer, most often in head and neck squamous cell carcinoma. (B) Core Notch signaling pathway. The Notch receptor is processed at cleavage site 1 (S1) by furin-like proteases in the Golgi and is expressed at the cell surface as an intramolecular heterodimer held together via interactions between the N- and C-terminal regions of HD. Upon ligand binding, Notch is sequentially cleaved by ADAM and by γ-secretase, thereby releasing NICD to activate transcription. Notch T-ALL mutants (HD mutant with ΔPEST shown) exhibits ligand-independent receptor activation. Various aspects of the Notch signaling mechanism can be targeted for therapeutic intervention; α-NRR1 antibodies stabilize the auto-inhibited conformation of NRR to prevent S2 cleavage; GSIs prevent cleavage and NICD release, SAHM peptides block transactivation complex function. All these modes of inhibition target wild-type and mutant receptors similarly. SERCA inhibition by thapsigargin (TG) selectively targets the maturation and activity of mutant Notch receptors carrying the most common type of HD mutations found in T-ALL (class I).

highly predictive, and Notch-dependent gene expression signature. Three thousand eight hundred one drugs and drug-like molecules were screened against a human T-ALL cell line (DND41), which carries an activating mutation in the HD of Notch1 along with a PEST domain deletion (L1594PΔPEST). In parallel, they also screened a cDNA expression library of 18,000 open reading frames to identify gene products that would enhance the activation of a transcriptional reporter downstream of another mutant Notch1 receptor identified in T-ALL patients (L1601PΔPEST) expressed in the U2OS osteosarcoma cell line. The selection of NRR mutants in both screens proved to be a fortuitous decision.

Perhaps surprisingly, calcium modulators emerged as hits in both the compound and cDNA screens. One of the top compound hits was thapsigargicin, an analog of thapsigargin, which is a potent natural product inhibitor of sarco/endoplasmic reticulum Ca^{2+}-ATPase (SERCA). Among the top cDNA hits were *ATP2A1*, *ATP2A2*, and *ATP2A3*, which encode SERCA1, SERCA2, and SERCA3, respectively. SERCAs use ATP to pump Ca^{2+} from the cytoplasm to the internal stores. Notably, previous studies in *Drosophila* identified the SERCA homolog, Ca-P60A, as a modulator of Notch transport and activity (Periz and Fortini, 1999). However, the loss of all SERCA activity in *Drosophila* demonstrated a general requirement for Ca^{2+}-ATPase for all membrane protein trafficking, which would predict a plethora of untoward effects with SERCA modulation akin to the problems experienced with GSI. This proved not to be the case at low inhibitor concentration.

Because the EGF and LNR domains of Notch all require Ca^{2+} for proper protein folding and exit from ER, Roti et al. (2013) hypothesized that SERCA inhibition was affecting the maturation process of Notch1. Indeed, thapsigargin treatment reduced the level of furin processing, a step that occurs in the trans-Golgi during transport of Notch proteins. Misfolded full-length receptors were retained in the ER/Golgi compartment, leading to diminished levels at the cell surface. Consistent with effects related to the Ca^{2+}-binding modules, constitutively active forms of Notch1 lacking the EGF and LNR domains were refractory to effects of thapsigargin. In addition, expression of NICD can rescue the negative effects of thapsigargin on the cell cycle, cell size, and cell viability of T-ALL lines in vitro and in a xenograft model.

Although the functional assays in flies (Periz and Fortini, 1999; Roti et al., 2013) clearly show that wild-type Notch function can be modulated by SERCA inhibition, the decision to screen against NRR mutants provided a critical observation; the Notch1 mutational status affected the efficacy of thapsigargin. Thapsigargin had a stronger effect on molecules containing the class I HD mutations, which encompass point substitutions and small in-frame insertions or deletions in HD and are the most common type of activating Notch1 mutants in T-ALL (Malecki et al., 2006). At thapsigargin concentrations that did not inhibit signaling from wild-type Notch1 and Notch2 receptors, signaling from the Notch1 receptor carrying the L1601PΔPEST leukemogenic mutation was impaired. Cell cycle and

cell viability were more strongly affected by thapsigargin in T-ALL lines with HD mutations in Notch1 than those carrying wild-type Notch1. Moreover, significant on-target antileukemia effects with no gastrointestinal toxicity were observed in two independent human T-ALL xenograft models carrying HD mutations. The lack of gut toxicity indicates that sufficient levels of wild-type Notch1 and Notch2 receptors reached the surface in the presence of SERCA inhibitors, whereas oncogenic Notch molecules were selectively and effectively prevented from exiting the ER.

Why would SERCA inhibition preferentially affect the maturation and activity of mutant receptors? Roti et al. (2013) speculate that the reason may reflect folding defects in many of the activating HD mutations identified in T-ALL (Malecki et al., 2006). SERCA inhibitors exploit this impaired folding and block maturation of the mutant receptor (Figure 1B). Alternatively or simultaneously, the mutant Notch1 proteins themselves trigger ER stress, making the cells more sensitive to the increase in ER stress induced by thapsigargin treatment, leading to enhanced clearance of mutant Notch proteins. Regardless of the underlying mechanism, these studies provide a therapeutic window for targeting SERCA as an antileukemia strategy for many T-ALL patients harboring mutations in the NRR.

While promising, many challenges remain before translating this strategy to the clinic. Given the fundamental role of calcium in normal physiology and the pleiotropic roles of Notch in tissue maintenance and cancer suppression (South et al., 2012), targeted delivery of SERCA inhibitors to T-ALL cells would be desirable. This was achieved with delivery of modified thapsigargin to human cancer xenografts (Denmeade et al., 2012). Even if thapsigargin can be specifically targeted, T-ALL may contain cells refractory to treatment, having lost the NRR or gained activating Myc mutations. Perhaps the most beneficial use for thapsigargin will be in combinatorial therapies aimed to combat T-ALL at its earliest manifestation before additional mutations are gained.

REFERENCES

Denmeade, S.R., Mhaka, A.M., Rosen, D.M., Brennen, W.N., Dalrymple, S., Dach, I., Olesen, C., Gurel, B., Demarzo, A.M., Wilding, G., et al. (2012). Sci. Transl. Med. *4*, 140ra186.

Extance, A. (2010). Nat. Rev. Drug Discov. *9*, 749–751.

Kopan, R., and Ilagan, M.X. (2009). Cell *137*, 216–233.

Malecki, M.J., Sanchez-Irizarry, C., Mitchell, J.L., Histen, G., Xu, M.L., Aster, J.C., and Blacklow, S.C. (2006). Mol. Cell. Biol. *26*, 4642–4651.

Periz, G., and Fortini, M.E. (1999). EMBO J. *18*, 5983–5993.

Roti, G., Carlton, A., Ross, K.N., Markstein, M., Pajcini, K., Su, A.H., Perrimon, N., Pear, W.S., Kung, A.L., Blacklow, S.C., et al. (2013). Cancer Cell *23*, this issue, 390–405.

South, A.P., Cho, R.J., and Aster, J.C. (2012). Semin. Cell Dev. Biol. *23*, 458–464.

Tzoneva, G., and Ferrando, A.A. (2012). Curr. Top. Microbiol. Immunol. *360*, 163–182.

Weng, A.P., Ferrando, A.A., Lee, W., Morris, J.P., 4th, Silverman, L.B., Sanchez-Irizarry, C., Blacklow, S.C., Look, A.T., and Aster, J.C. (2004). Science *306*, 269–271.

Yan, M., Callahan, C.A., Beyer, J.C., Allamneni, K.P., Zhang, G., Ridgway, J.B., Niessen, K., and Plowman, G.D. (2010). Nature *463*, E6–E7.

Interweaving the Strands: β-Catenin, an HIV Co-Receptor, and Schwann Cell Tumors

David Largaespada[1,2,3,4,5,6,*] and Nancy Ratner[7,*]
[1]Masonic Cancer Center
[2]Department of Genetics, Cell Biology and Development
[3]Center for Genome Engineering
[4]Brain Tumor Program
[5]Health and Natural Sciences Department
[6]Department of Pediatrics
University of Minnesota, Minneapolis, MN 55455, USA
[7]Division of Experimental Hematology and Cancer Biology, Department of Pediatrics, Cincinnati Children's Hospital Medical Center, University of Cincinnati, Cincinnati, OH 45229, USA
*Correspondence: larga002@umn.edu (D.L.), nancy.ratner@cchmc.org (N.R.)
http://dx.doi.org/10.1016/j.ccr.2013.03.001

WNT/β-catenin signaling is critical to the development of many cancer types. A paper by Mo and colleagues in a recent issue of *Cell* shows that autocrine CXCL12/CXCR4 chemokine signaling activates β-catenin signaling in a rare peripheral nerve sarcoma. Together with the availability of small molecules targeting CXCR4, this finding suggests new avenues for cancer therapy.

It is exciting to link established signaling pathways. It is especially provocative when compounds designed to target one molecule for a specific disease are shown to have potential in a novel context. In a recent issue of *Cell*, the laboratories of Luis Parada and Lu Le accomplish just this by showing that a pathway that was first identified as relevant to

cell viability were more strongly affected by thapsigargin in T-ALL lines with HD mutations in Notch1 than those carrying wild-type Notch1. Moreover, significant on-target antileukemia effects with no gastrointestinal toxicity were observed in two independent human T-ALL xenograft models carrying HD mutations. The lack of gut toxicity indicates that sufficient levels of wild-type Notch1 and Notch2 receptors reached the surface in the presence of SERCA inhibitors, whereas oncogenic Notch molecules were selectively and effectively prevented from exiting the ER.

Why would SERCA inhibition preferentially affect the maturation and activity of mutant receptors? Roti et al. (2013) speculate that the reason may reflect folding defects in many of the activating HD mutations identified in T-ALL (Malecki et al., 2006). SERCA inhibitors exploit this impaired folding and block maturation of the mutant receptor (Figure 1B). Alternatively or simultaneously, the mutant Notch1 proteins themselves trigger ER stress, making the cells more sensitive to the increase in ER stress induced by thapsigargin treatment, leading to enhanced clearance of mutant Notch proteins. Regardless of the underlying mechanism, these studies provide a therapeutic window for targeting SERCA as an antileukemia strategy for many T-ALL patients harboring mutations in the NRR.

While promising, many challenges remain before translating this strategy to the clinic. Given the fundamental role of calcium in normal physiology and the pleiotropic roles of Notch in tissue maintenance and cancer suppression (South et al., 2012), targeted delivery of SERCA inhibitors to T-ALL cells would be desirable. This was achieved with delivery of modified thapsigargin to human cancer xenografts (Denmeade et al., 2012). Even if thapsigargin can be specifically targeted, T-ALL may contain cells refractory to treatment, having lost the NRR or gained activating Myc mutations. Perhaps the most beneficial use for thapsigargin will be in combinatorial therapies aimed to combat T-ALL at its earliest manifestation before additional mutations are gained.

REFERENCES

Denmeade, S.R., Mhaka, A.M., Rosen, D.M., Brennen, W.N., Dalrymple, S., Dach, I., Olesen, C., Gurel, B., Demarzo, A.M., Wilding, G., et al. (2012). Sci. Transl. Med. *4*, 140ra186.

Extance, A. (2010). Nat. Rev. Drug Discov. *9*, 749–751.

Kopan, R., and Ilagan, M.X. (2009). Cell *137*, 216–233.

Malecki, M.J., Sanchez-Irizarry, C., Mitchell, J.L., Histen, G., Xu, M.L., Aster, J.C., and Blacklow, S.C. (2006). Mol. Cell. Biol. *26*, 4642–4651.

Periz, G., and Fortini, M.E. (1999). EMBO J. *18*, 5983–5993.

Roti, G., Carlton, A., Ross, K.N., Markstein, M., Pajcini, K., Su, A.H., Perrimon, N., Pear, W.S., Kung, A.L., Blacklow, S.C., et al. (2013). Cancer Cell *23*, this issue, 390–405.

South, A.P., Cho, R.J., and Aster, J.C. (2012). Semin. Cell Dev. Biol. *23*, 458–464.

Tzoneva, G., and Ferrando, A.A. (2012). Curr. Top. Microbiol. Immunol. *360*, 163–182.

Weng, A.P., Ferrando, A.A., Lee, W., Morris, J.P., 4th, Silverman, L.B., Sanchez-Irizarry, C., Blacklow, S.C., Look, A.T., and Aster, J.C. (2004). Science *306*, 269–271.

Yan, M., Callahan, C.A., Beyer, J.C., Allamneni, K.P., Zhang, G., Ridgway, J.B., Niessen, K., and Plowman, G.D. (2010). Nature *463*, E6–E7.

Interweaving the Strands: β-Catenin, an HIV Co-Receptor, and Schwann Cell Tumors

David Largaespada[1,2,3,4,5,6,*] and Nancy Ratner[7,*]
[1]Masonic Cancer Center
[2]Department of Genetics, Cell Biology and Development
[3]Center for Genome Engineering
[4]Brain Tumor Program
[5]Health and Natural Sciences Department
[6]Department of Pediatrics
University of Minnesota, Minneapolis, MN 55455, USA
[7]Division of Experimental Hematology and Cancer Biology, Department of Pediatrics, Cincinnati Children's Hospital Medical Center, University of Cincinnati, Cincinnati, OH 45229, USA
*Correspondence: larga002@umn.edu (D.L.), nancy.ratner@cchmc.org (N.R.)
http://dx.doi.org/10.1016/j.ccr.2013.03.001

WNT/β-catenin signaling is critical to the development of many cancer types. A paper by Mo and colleagues in a recent issue of *Cell* shows that autocrine CXCL12/CXCR4 chemokine signaling activates β-catenin signaling in a rare peripheral nerve sarcoma. Together with the availability of small molecules targeting CXCR4, this finding suggests new avenues for cancer therapy.

It is exciting to link established signaling pathways. It is especially provocative when compounds designed to target one molecule for a specific disease are shown to have potential in a novel context. In a recent issue of *Cell*, the laboratories of Luis Parada and Lu Le accomplish just this by showing that a pathway that was first identified as relevant to

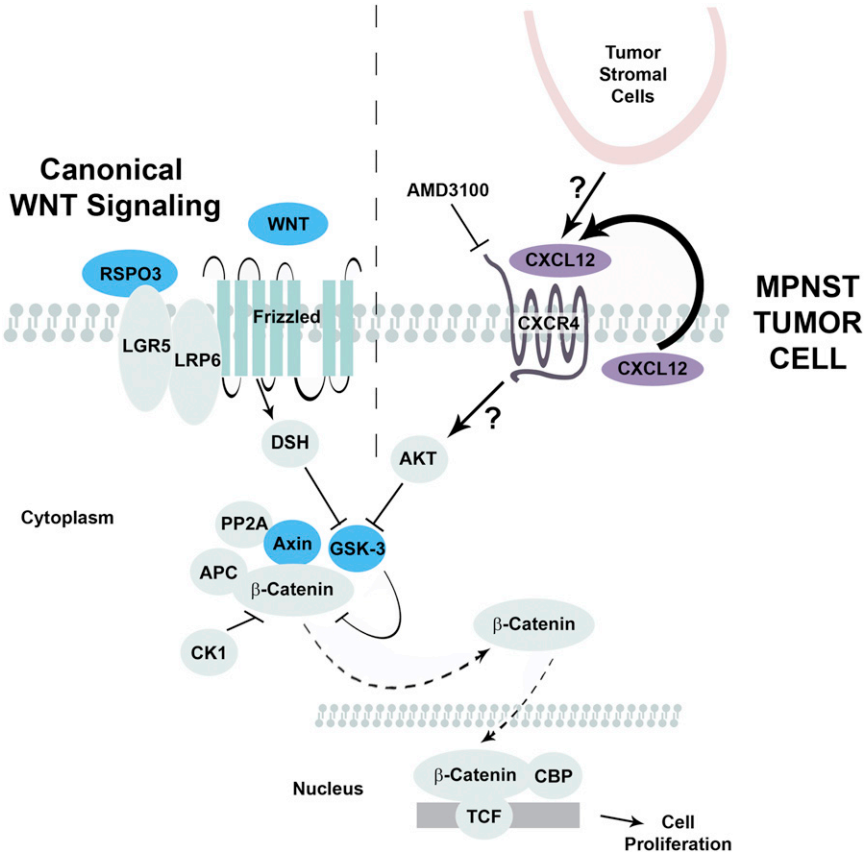

Figure 1. Canonical WNT Signaling and CXCR4 Activation of β-Catenin
In canonical WNT signaling (left of dotted line), WNT ligands activate FRIZZLED receptors; LRP and LGR are co-receptors. Receptor activation leads through inactivation of GSK3β to stabilization of β-catenin. Stabilized β-catenin moves to the nucleus and activates gene transcription. Mo et al. (2013) (right of dotted line) describe a novel mechanism in which MPNST tumor cells secrete CXCL12 ligand, activate CXCR4 receptors, and, via AKT, inactivate GSK3β and stabilizing β-catenin.

lymphocyte chemotaxis is also a driver of human Schwann cell tumor progression (Mo et al., 2013). The authors go on to find that this pathway acts via another pathway that was initially identified in organismal development and found to be corrupted in many cancers. The paper links the CXCR4 cell surface chemokine receptor, via autocrine CXCL12 ligand production, to the Wnt/β-catenin signaling pathway in malignant peripheral nerve sheath tumors (MPNSTs) (Mo et al., 2013). CXCR4 antagonists are being intensively investigated, because CXCR4 is a co-receptor for HIV on T cells, and early stage clinical studies show that blocking CXCR4 delays the onset of AIDS in HIV infected individuals (Domanska et al., 2013). The work by Mo et al. (2013) suggests that CXCR4 antagonists may be useful to treat MPNSTs, a peripheral nerve related soft tissue sarcoma with very poor prognosis, especially when they occur in the context of neurofibromatosis type 1 (NF1) disease (Widemann, 2009). In MPNST, inactivation of the *NF1* gene, which encodes a GTPase activating protein for Ras proteins, increases Ras signaling with activation of the key downstream signaling pathways MEK, AKT, and mTOR (De Raedt et al., 2011; Jessen et al., 2013). The paper by Mo et al. (2013) also shows expression of CXCR4 and Wnt/β-catenin pathway components in benign neurofibromas, which can be MPNST precursor lesions.

The WNT/β-catenin signaling pathway was identified for its roles in development and controls critical processes in worms to mammals, from the formation of teeth to the control of stem cells in the intestine (reviewed in Clevers and Nusse, 2012). Despite >7,000 papers on WNT/β-catenin signaling listed in the PubMed database, this pathway had not been directly implicated in MPNSTs. In the cells from which MPNSTs derive, which may be neural crest cells, skin-derived precursors, and/or committed Schwann cells, WNT/β-catenin signaling normally regulates cell fate decisions and transiently suppresses full differentiation (myelination) in Schwann cells, potentially explaining a role in tumor progression by differentiation block (Lewallen et al., 2011; Hari et al., 2012).

Canonical WNT/β-catenin signaling (Figure 1) plays a role in many types of cancer, including colorectal, lung, breast, ovarian, prostate, liver, and brain tumors (Clevers and Nusse, 2012; Saito-Diaz et al., 2013). β-catenin-dependent transcription can promote cell cycle progression, stem cell self-renewal, and epithelial-to-mesenchymal transition. WNT signaling in cancer can be aberrantly activated by activation of mutations in β-catenin (*CTNNB1*), overexpression of WNT ligand genes, inactivation of mutations in destruction complex genes (i.e., *AXIN1*, *GSK3B*, and *APC*), or promoter hypermethylation of negative regulators of WNT signaling (Saito-Diaz et al., 2013). Activation of the PI3K/AKT signaling pathway, either by the loss of *PTEN* or through activation of upstream tyrosine kinase receptors, also causes phosphorylation and inactivation of GSK3β, stabilizing β-catenin (Clevers and Nusse, 2012). In the study by Mo et al. (2013), WNT signaling is activated by crosstalk with the CXCL12/CXCR4 signaling, downstream of AKT (Figure 1).

CXCL12 (SDF-1) is a chemokine. CXCL12 binding to the heterotrimeric G protein-coupled receptor CXCR4 is, like β-catenin signaling, required for normal development. In many situations, stromal cells secrete CXCL12 and attract cells expressing CXCR4 receptors. In this fashion, immune cells are attracted to sites of inflammation and hematopoietic cells home to the bone marrow. This paracrine CXCL12/CXCR4 pathway has been exploited therapeutically; CXCR4 blockade facilitates the removal of cells from the bone marrow niche for use in transplantation (reviewed in Domanska et al., 2013). CXCL12/CXCR4 paracrine signaling is also relevant to tumor metastasis when tumor cells expressing CXCR4 migrate toward distant sites where ligand is produced (Domanska et al., 2013).

The paper by Mo et al. (2013) shows that autocrine, rather than paracrine, CXCL12 promotes tumor cell proliferation. The notion that tumor cells can manufacture, secrete, and respond to their own CXCL12 was discovered in prostate tumors by Sun et al. (2003). Mo et al. (2013) use antibodies against CXCL12 and CXCR4 receptor blockade, both of which decrease MPNST cell proliferation. Furthermore, whereas CXCR4 activation can recruit endothelial cells to promote neoangiogenesis, vessel density remains the same after CXCR4 blockade, providing additional evidence that the tumor cell effects are cell autonomous. CXCL12 produced in a paracrine manner by host tumor stromal cells, as in other forms of cancer, may also contribute to effects on tumor growth.

The authors show that CXCR4 activation in MPNST cells activates β-catenin by AKT-mediated phosphorylation and inactivation of GSK3β, thus stabilizing β-catenin (Figure 1). How CXCR4 activates AKT is not entirely clear. This may occur through the βγ subunits of CXCR4, known to indirectly activate AKT (Domanska et al., 2013). The authors exclude roles for activation of NF-κB, RAS/MAPK, and JAK/STAT3. Additional pathways downstream of CXCR4 might also contribute to β-catenin stabilization. CXCR4 is known to activate SRC family kinases, C-CBL, and RHO GTPases (Domanska et al., 2013), which may be relevant. β-catenin activation likely also requires additional genetic events or the activation of signaling pathways in neurofibromas and MPNSTs, particularly in MPNSTs that develop in the absence of NF1 syndrome. This is because many MPNSTs express β-catenin, but do not express CXCR4. Also, many neurofibromas express CXCR4, but not β-catenin.

The molecular mechanisms that explain CXCL12 and CXCR4 expression in MPNST cells also remain undefined. One possibility is that CXCR4/CXCL12 expression reflects the embryonic neural crest origin of MPNST cells. The authors demonstrate that CXCR4 expression frequency and intensity are especially pronounced in neurofibromas and MPNSTs associated with NF1 disease. Therefore, signaling downstream of NF1 may normally suppress expression of CXCL12/CXCR4.

Despite many efforts to identify drugs to target β-catenin signaling, no inhibitor has, to date, demonstrated the appropriate pharmacodynamic and pharmacokinetic properties to be used as a drug for the treatment of cancer patients. In this light, it is impressive that the authors have shown that the CXCR4 inhibitor AMD3100 inhibits β-catenin signaling in vitro and in vivo. With AMD3100 (Plerixafor; FDA approved for use in hematopoietic stem cell mobilization) currently in clinical testing in many settings, it should be feasible to test in human MPNST patients. Mo et al. (2013) show a clear delay in MPNST formation in human xenografts and also in a genetically engineered mouse model. Certainly, targeting the CXCR4 receptor alone is insufficient to halt MPNST growth or shrink tumors; the authors show that the main effect is proliferation arrest. Moreover, the authors note that some tumors expressed CXCR4 in a patchy manner, where the cells are not all positive. For both of these reasons, tumor ablation is likely to require co-therapy, perhaps with identified NF1/Ras pathway inhibitors (De Raedt et al., 2011; Jessen et al., 2013). Especially because *NF1* mutations have been identified in many types of cancer, it will be exciting to discover those that use the CXCL12/CXCR4 pathway to activate Wnt/β-catenin signaling and those that may benefit from CXCR4 blockade.

REFERENCES

Clevers, H., and Nusse, R. (2012). Cell *149*, 1192–1205.

De Raedt, T., Walton, Z., Yecies, J.L., Li, D., Chen, Y., Malone, C.F., Maertens, O., Jeong, S.M., Bronson, R.T., Lebleu, V., et al. (2011). Cancer Cell *20*, 400–413.

Domanska, U.M., Kruizinga, R.C., Nagengast, W.B., Timmer-Bosscha, H., Huls, G., de Vries, E.G., and Walenkamp, A.M. (2013). Eur. J. Cancer *49*, 219–230.

Hari, L., Miescher, I., Shakhova, O., Suter, U., Chin, L., Taketo, M., Richardson, W.D., Kessaris, N., and Sommer, L. (2012). Development *139*, 2107–2117.

Jessen, W.J., Miller, S.J., Jousma, E., Wu, J., Rizvi, T.A., Brundage, M.E., Eaves, D., Widemann, B., Kim, M.O., Dombi, E., et al. (2013). J. Clin. Invest. *123*, 340–347.

Lewallen, K.A., Shen, Y.A., De la Torre, A.R., Ng, B.K., Meijer, D., and Chan, J.R. (2011). J. Neurosci. *31*, 3032–3043.

Mo, W., Chen, J., Patel, A., Zhang, L., Chau, V., Li, Y., Cho, W., Lim, K., Xu, J., Lazar, A.J., et al. (2013). Cell *152*, 1077–1090.

Saito-Diaz, K., Chen, T.W., Wang, X., Thorne, C.A., Wallace, H.A., Page-McCaw, A., and Lee, E. (2013). Growth Factors *31*, 1–31.

Sun, Y.X., Wang, J., Shelburne, C.E., Lopatin, D.E., Chinnaiyan, A.M., Rubin, M.A., Pienta, K.J., and Taichman, R.S. (2003). J. Cell. Biochem. *89*, 462–473.

Widemann, B.C. (2009). Curr. Oncol. Rep. *11*, 322–328.

Cancer Cell
Previews

Tumor Dissemination: An EMT Affair

Jean Paul Thiery[1,2,5,*] and Chwee Teck Lim[3,4]
[1]Department of Biochemistry
[2]Cancer Science Institute
[3]Department of Bioengineering
[4]Mechanobiology Institute
National University of Singapore, Singapore 117599
[5]Institute of Molecular and Cell Biology, A*STAR Singapore, Singapore 138673
*Correspondence: jpthiery@imcb.a-star.edu.sg
http://dx.doi.org/10.1016/j.ccr.2013.03.004

A recent paper reports that circulating tumor cells (CTCs) from metastatic breast cancer patients exhibit heterogeneous epithelial and mesenchymal phenotypes and that CTCs display higher frequencies of partial or full-blown mesenchymal phenotype than carcinoma cells within primary tumors. Mesenchymal-like CTCs are also elevated in patients who are refractory to therapy.

Cancer cell dissemination is a hallmark of tumor progression that can potentially lead to the establishment of clinically detectable metastases (Talmadge and Fidler, 2010). Cancer cells released from primary tumors intravasate through lymph or blood vessels. Much effort has been devoted to the detection and characterization of circulating tumor cells (CTCs) in the blood, tumor cells residing in the sentinel lymph nodes, or disseminated tumor cells (DTCs) in the bone marrow (Pantel et al., 2009). Most current studies focus on CTCs because a much less invasive clinical procedure is required to obtain them, which permits frequent monitoring. In addition, different enrichment methods have been successfully developed for blood but not for bone marrow samples. These methods are currently based on antibodies (Pantel et al., 2009), cell deformability (Tan et al., 2009), or cell size (Zheng et al., 2007). CTC phenotyping and its comparison with resident primary tumor cancer cells should help to enhance our understanding of the mechanism of escape.

Experimental models show evidence for collective or individual cell migration at the periphery of primary tumors (Thiery, 2009). Collective cell migration was postulated to be involved in lymph node metastasis; such a mechanism could also account for the dissemination of tumor cell clusters and the formation of microemboli within the primary tumor bed vessels or in vessels at distant sites. Epithelial-mesenchymal (EM) transition (EMT), a well-described mechanism driving major morphogenetic events in metazoans, was also postulated to be responsible for CTC formation (Thiery, 2002). A recent study by Yu et al. (2013) reported a detailed phenotypic analysis of CTCs from patients with metastatic breast cancer, revealing that a significant number of CTCs exhibited a partial or a full-blown EMT phenotype, supportive of an EMT-driven mechanism (Figure 1).

CTCs can be enriched by loading a blood sample through a high-throughput microfluidic herringbone-chip or ^{Hb}CTC-Chip (Stott et al., 2010). This chip comprises a herringbone-patterned surface that increases the interactions of CTCs with an antibody directed against EpCAM, an epithelial marker. However, this method has been limited by the use of a single antibody directed against one relatively specific epithelial marker; this could prevent the capture of CTCs exhibiting mesenchymal characteristics. To overcome this issue, the authors coated the surface of the ^{Hb}CTC-Chip with epithelial and breast molecular subtype-specific antibodies, comprising a cocktail of EpCAM, EGFR, and HER2. The captured CTCs were phenotyped using the ^{Hb}CTC-chip via a quantitative immunofluorescence-based RNA-in situ hybridization (ISH) technology. The chip was hybridized with a mixture comprising custom-designed RNA probes directed against epithelial (E) markers (CDH1, EpCAM, KRT5, KRT7, KRT8, KRT18, and KRT19) and mesenchymal (M) markers (FN1, CDH2, and SERPINE1). The captured cells were then classified into five categories: purely E, intermediate (E > M, E = M, and M > E), or purely M. The RNA-ISH detection allowed customized probes to be used against multiple genes, enabling dual staining and the precise spectral analysis of the EM states of the CTCs. Using a threshold of five CTCs in 3 ml of blood, 17 of 41 breast cancers patients were considered positive, suggesting that this method may not detect CTCs in all metastatic patients. All 17 patients showed evidence of phenotypic changes in the CTCs. Interestingly, a large fraction of the CTCs were either double E/M- or M-positive, particularly among the HER2-positive and triple negative subtypes. Analysis of a breast cancer tissue microarray revealed that all ductal carcinoma in situ showed an E phenotype, as expected, whereas invasive carcinomas often contained cells with dual phenotype (3.3% in estrogen/progesterone [ER/PR]-positive, 2.7% in HER2-positive, and ~12.1% in triple negative [TN] tumors). These data are consistent with a tissue microarray study of 479 samples that found that TN breast cancers were particularly enriched in carcinoma cells expressing a number of mesenchymal markers, but it also showed sporadic expression of some of these mesenchymal markers in ER/PR-positive tumors (Sarrió et al., 2008). Most interestingly, the longitudinal study of ten patients showed that, after targeted therapy, CTCs from responding patients were fewer in numbers and had a more epithelial phenotype. Conversely, CTCs from refractory patients were more numerous and retained or acquired an M phenotype. CTCs with a pronounced M phenotype were also found in clusters. The question then arises as to how these cells should have formed aggregates, as it would be expected that cells with a mesenchymal

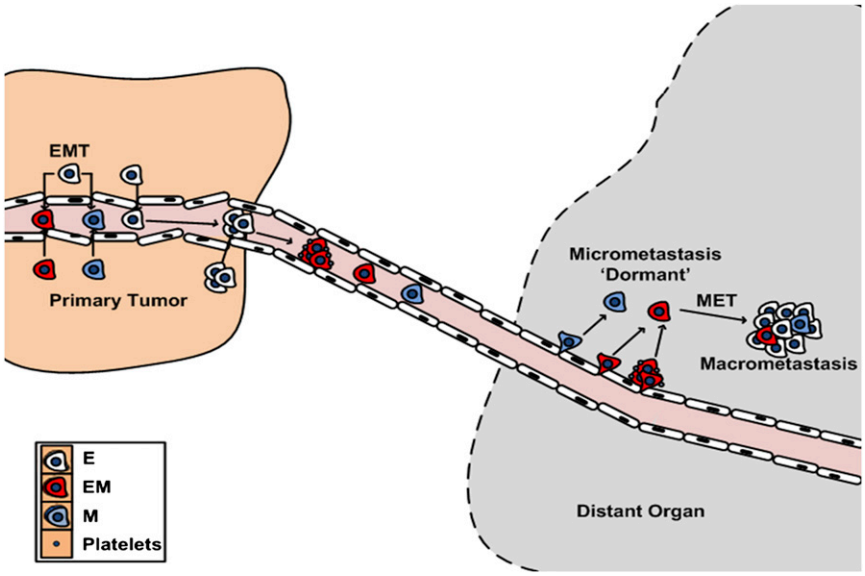

Figure 1. Hypothetical Schematic to Describe the Origin and Subsequent Fate of CTCs
Cells with different epithelial/mesenchymal (EM) phenotypes can exit the primary tumor. Epithelial (E) cells exit either through an epithelial-to-mesenchymal transition (EMT) or by other mechanisms that allow cells to be released as single cells or clusters. Microemboli can arise from EM phenotypes or from E cells. Subsequent EM phenotypes can be acquired through binding to platelets. At secondary sites, solitary cells or clusters may acquire dormancy before resuming growth through an MET (mesenchymal-to-epithelial transition) process. The metastatic tumor may express a similar proportion of EM phenotypes than the primary tumor.

phenotype should remain solitary (Figure 1). CTCs in blood can form microemboli, the presence of which indicates a worsened prognosis, but mechanisms driving microembolism formation remain unclear. Microemboli could result from the detachment of a cohesive group of cancer cells from the primary tumor, or they may be engulfed by invading neovessels. Microemboli could also form from isolated CTCs that undergo proliferation in a confined environment within the capillary bed. Several intercellular adhesion molecules, including N-cadherin, type II cadherins, or CAM-Ig family members, could be involved in cluster formation, even in E-cadherin-negative CTCs, thus promoting survival in the blood flow. Platelets also interact with CTCs and promote CTC aggregation to ensure immune escape. The present study provides evidence that CTC clusters are associated with platelets, which ensures cohesion and simultaneously induces a partial EMT phenotype through TGF-β secretion and documents the EMT phenotype by single-molecule RNA sequencing. An elegant study performed by Labelle et al. (2011) showed that platelet-secreted TGF-β and the direct interaction between platelets and cancer cells can induce an EMT phenotype through Smad and NF-κB pathways, respectively.

The study by Yu et al. (2013) prompts further investigations to better define the EMT spectrum of CTCs and ascertain their clinical relevance. Not all CTCs and DTCs have a prognostic value (Pantel et al., 2009). It will, therefore, be critical to assess their clonogenic potential in secondary sites and determine if the EMT intermediate phenotype is, in fact, most appropriate for the subsequent clonal expansion of CTCs following extravasation due to their ability to reacquire an epithelial-like phenotype (Thiery, 2002).

REFERENCES

Labelle, M., Begum, S., and Hynes, R.O. (2011). Cancer Cell *20*, 576–590.

Pantel, K., Alix-Panabières, C., and Riethdorf, S. (2009). Nat. Rev. Clin. Oncol. *6*, 339–351.

Sarrió, D., Rodriguez-Pinilla, S.M., Hardisson, D., Cano, A., Moreno-Bueno, G., and Palacios, J. (2008). Cancer Res. *68*, 989–997.

Stott, S.L., Hsu, C.H., Tsukrov, D.I., Yu, M., Miyamoto, D.T., Waltman, B.A., Rothenberg, S.M., Shah, A.M., Smas, M.E., Korir, G.K., et al. (2010). Proc. Natl. Acad. Sci. USA *107*, 18392–18397.

Talmadge, J.E., and Fidler, I.J. (2010). Cancer Res. *70*, 5649–5669.

Tan, S.J., Yobas, L., Lee, G.Y., Ong, C.N., and Lim, C.T. (2009). Biomed. Microdevices *11*, 883–892.

Thiery, J.P. (2002). Nat. Rev. Cancer *2*, 442–454.

Thiery, J.P. (2009). Curr. Biol. *19*, R1121–R1123.

Yu, M., Bardia, A., Wittner, B.S., Stott, S.L., Smas, M.E., Ting, D.T., Isakoff, S.J., Ciciliano, J.C., Wells, M.N., Shah, A.M., et al. (2013). Science *339*, 580–584.

Zheng, S., Lin, H., Liu, J.Q., Balic, M., Datar, R., Cote, R.J., and Tai, Y.C. (2007). J. Chromatogr. A *1162*, 154–161.

Cancer Cell
Previews

R-2-Hydroxyglutarate as the Key Effector of *IDH* Mutations Promoting Oncogenesis

Dan Ye,[1] Shenghong Ma,[1] Yue Xiong,[1,2] and Kun-Liang Guan[1,3,*]
[1]Key Laboratory of Molecular Medicine of Ministry of Education and Institutes of Biomedical Sciences, Shanghai Medical College, College of Life Science, Fudan University, Shanghai 200032, China
[2]Lineberger Comprehensive Cancer Center, Department of Biochemistry and Biophysics, University of North Carolina at Chapel Hill, Chapel Hill, NC 27599, USA
[3]Department of Pharmacology and Moores Cancer Center, University of California, San Diego, La Jolla, CA 92093, USA
*Correspondence: kuguan@ucsd.edu
http://dx.doi.org/10.1016/j.ccr.2013.03.005

The tumor-associated isocitrate dehydrogenase (IDH) mutants are unique in that they have lost their normal catalytic activity and gained a novel function to produce *R*-2-hydroxyglutarate (*R*-2-HG). A recent study now shows that *R*-2-HG can reversibly promote leukemogenesis in vitro, suggesting a therapeutic potential of targeting mutant IDH1 and IDH2.

Mutations in metabolic enzymes (isocitrate dehydrogenase 1 and 2 [IDH1/2], fumarate hydratase [FH], and succinate dehydrogenase [SDH]) have been found in human cancer (Oermann et al., 2012). *IDH1* and *IDH2* are the most frequently mutated metabolic genes identified in human cancers, commonly observed in secondary glioblastomas, cytogenetically normal acute myeloid leukemias (AML), cartilaginous tumors, and intrahepatic cholangiocarcinomas. The IDH enzymes normally catalyze the oxidative decarboxylation of isocitrate to produce α-ketoglutarate (α-KG) and NADPH. A remarkable feature shared by cancer-associated IDH mutations is the loss of IDH's normal catalytic activity to produce α-KG and the gain of a neomorphic function to produce the *R*-enantiomer of 2-hydroxylglutarate (*R*-2-HG) (Dang et al., 2009). IDH1/2 mutant tumor cells are thus expected to have a reduced α-KG level and an increased *R*-2-HG level, which, under normal physiological conditions, is present at extremely low concentrations, if any, but can accumulate to high levels (millimolars) in tumors. A key issue in studying IDH1/2 mutation-induced tumorigenesis is the pathophysiological function of *R*-2-HG.

2-HG is structurally similar to α-KG with the exception of the oxidation state on the carbon C-2 position, whereby a hydroxyl group in 2-HG replaces a ketone group in α-KG. This structural similarity suggests the possibility that 2-HG may act as a competitive inhibitor of α-KG by antagonizing the function of α-KG-dependent enzymes such as the α-KG-dependent dioxygenases (Loenarz and Schofield, 2008). These enzymes are involved in a wide range of cellular regulations from demethylation of DNA and histone to protein hydroxylation, including the hydroxylation and degradation of hypoxia inducible factor 1α (HIF-1α). Indeed, recent studies show that 2-HG can inhibit the activity of multiple α-KG-dependent dioxygenases (Chowdhury et al., 2011; Xu et al., 2011), among them, the JmjC domain-containing histone demethylases (KDMs) and the ten-eleven translocation (TET) family of DNA hydroxylases, which is a tumor suppressor and critically important for the demethylation of 5-methylcytosine (5mC) in DNA. 2-HG binds to the α-KG binding pocket in dioxygenases, thereby acting as a competitive inhibitor of α-KG (Xu et al., 2011). The inhibition of TET enzymes by 2-HG is particularly noteworthy because *TET2* is also frequently mutated in AML, in which *IDH1/2* mutations are common. Moreover, mutations of *IDH1/2* and *TET2* genes are mutually exclusive in AML (Figueroa et al., 2010), indicating that they may act in the same pathway. Furthermore, AML with either *IDH1/2* or *TET2* mutations display similar genomic DNA methylation and gene expression profiles, indicating that TET2 is a pathologically relevant target of 2-HG. Therefore, altered epigenetic modification is currently considered a major mechanism underlying the tumorigenesis associated with IDH1/2 mutations (Oermann et al., 2012) (Figure 1).

Despite correlative evidence for the role of 2-HG in mediating the oncogenic effects of IDH1/2 mutations, 2-HG has not been formally proven to induce oncogenic transformation. Losman et al. (2013) now provide compelling evidence that 2-HG is indeed an oncometabolite capable of stimulating proliferation and suppressing differentiation, two properties obligatory for tumorigenesis in a cell culture leukemia model. The TF-1 human erythroleukemia cell line requires the cytokine granulocyte-macrophage colony-stimulating factor (GM-CSF) for proliferation and erythropoietin (EPO) for differentiation. Using this cell line model, the authors found that expression of the cancer-associated IDH1 R132H mutant, but not wild-type IDH1, promoted TF-1 cell proliferation even in the absence of GM-CSF and inhibited differentiation in response to EPO. Moreover, expression of an IDH1 R132H mutant unable to produce *R*-2-HG did not induce transformation of TF-1 cells. These data suggest that *R*-2-HG functions as an oncometabolite by promoting cytokine-independent growth and blocking EPO-induced differentiation.

Direct evidence for an oncogenic function of *R*-2-HG was obtained by treating TF-1 cells with a cell permeable *R*-2-HG analog (Losman et al., 2013). TF-1 cells passaged in the presence of the cell permeable *R*-2-HG gained cytokine-independent growth and no longer differentiated in response to EPO, phenotypes similar to those caused by the mutant IDH1 R132H expression. These observations show that *R*-2-HG is the key factor that mediates the oncogenic function of mutant IDH1 in TF-1 cells. It took those cells several passages to acquire both

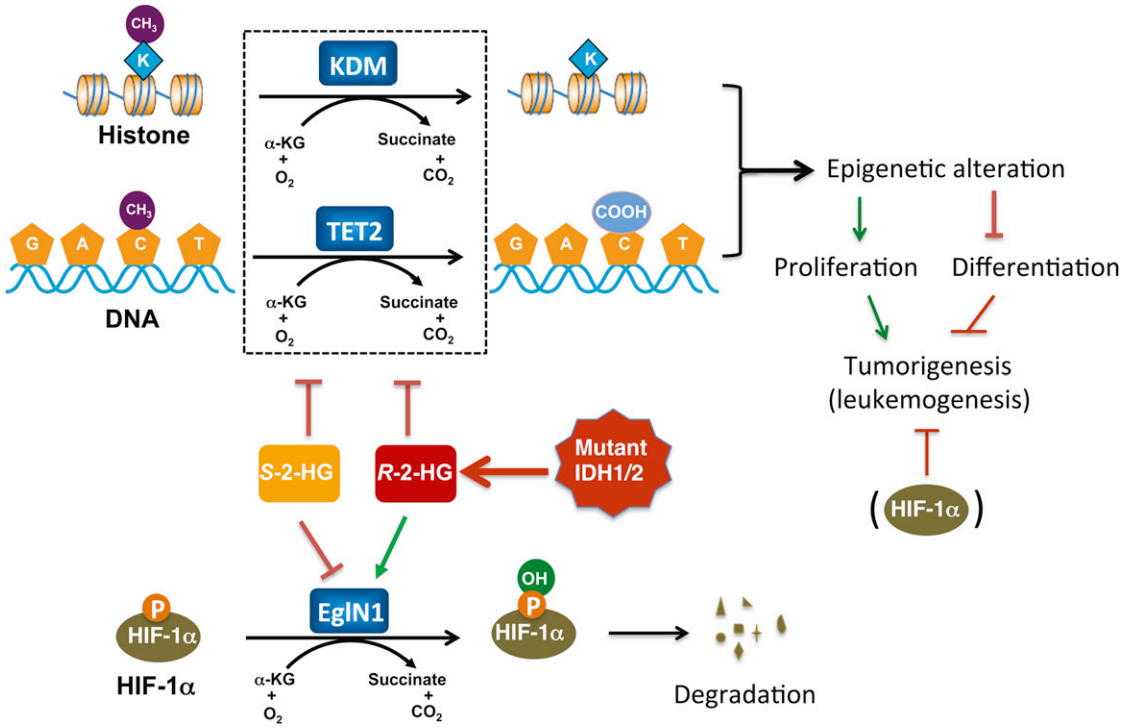

Figure 1. A Proposed Model for *R*-2-HG in Tumorigenesis

R-2-HG produced by the mutant IDH1/2 promotes tumorigenesis by inhibiting 5mC hydroxylase (TET2) and lysine demethylases (KDM), leading to the demethylation of DNA and histone, respectively. The epigenetic alterations associated with IDH1/2 mutations result in changes of gene expression and tumorigenesis. These processes can be recapitulated by *R*-2-HG, demonstrating *R*-2-HG as a true oncometabolite. *R*-2-HG does not inhibit, but rather stimulates EglN1, which promotes HIF-1α degradation by hydroxylation. HIF-1α might suppress leukemogenesis, but this may not apply to other cancer types with IDH1/2 mutations.

the cytokine independence and inability to differentiate, an observation consistent with epigenetic alterations caused by *R*-2-HG, which presumably alters both DNA and histone methylation. Interestingly, the oncogenic effects of *R*-2-HG on TF-1 cells are reversible. If *IDH1/2*-mutated tumors were similarly dependent on the continuous presence of *R*-2-HG, inhibition of mutant IDH1/2 could be an effective therapeutic treatment for these cancers.

To uncover which α-KG-dependent dioxygenase serves as the key target of *R*-2-HG in transformation, Losman et al. (2013) performed a small hairpin RNA knockdown screen of dioxygenase family members. Their data point to TET2 was likely a key α-KG-dependent dioxygenase responsible for the oncogenic function of *R*-2-HG among those tested.

There are two enantiomers of 2-HG: *R*-2-HG and *S*-2-HG. Only *R*-2-HG is produced by mutant IDH1/2. Both enantiomers inhibit many α-KG-dependent dioxygenases, with *R*-2-HG being significantly less potent than *S*-2-HG (Chowdhury et al., 2011; Xu et al., 2011; Koivunen et al., 2012). Surprisingly, Losman et al. (2013) found that *R*-2-HG, but not *S*-2-HG, promoted leukemic transformation in a dose- and passage-dependent manner. How then could *S*-2-HG, being a more potent inhibitor of TET2, be ineffective in promoting oncogenic transformation? Koivunen et al. (2012) had previously reported that *S*-2-HG inhibits EglN1, a member of the α-KG-dependent dioxygenases responsible for HIF-1α hydroxylation and degradation, whereas *R*-2-HG actually promotes EglN1 activity. The authors showed that inhibition of EglN1 by *S*-2-HG might suppress its ability to promote cytokine-independent growth and inhibit EPO-induced differentiation. This conclusion is surprising given the fact that HIF-1α is normally associated with tumor promotion rather than inhibition. The data by Losman et al. (2013) imply that inhibition of EglN1, and hence accumulation of HIF-1α, may be incompatible for leukemogeneis caused by TET2 inhibition by *R*-2-HG (Figure 1).

The function of *R*-2-HG in blocking differentiation is consistent with a previous report that supports the role of mutant IDH1 in suppressing hematopoietic differentiation (Figueroa et al., 2010). Besides altered DNA methylation, increased histone methylation has also been associated with the expression of cancer-associated mutant IDH1. Therefore, inhibition of the JmjC family of histone demethylases likely also contributes to tumorigenesis. A unified model for tumorigenesis caused by mutation in metabolic enzymes is that inhibition of α-KG-dependent dioxygenases leads to epigenetic alterations in both DNA and histone, therefore altering gene expression and oncogenic transformation (Figure 1). Consistent with this model, both KDM and TET enzymes are inhibited by succinate and fumarate, two metabolites that are structurally similar to α-KG and are accumulated in cells expressing cancer-associated mutant SDH and FH, respectively (Xiao et al., 2012). Further support for the epigenetic model comes from a mouse IDH1 R132H knockin study that reveals an increase of both DNA methylation and histone methylation (Sasaki et al., 2012). More studies are needed to demonstrate the functional significance of epigenetic

modification and expression of specific genes that are affected by cancer-associated metabolic enzyme mutations and the genetic interaction of *R*-2-HG with other oncogenes and tumor suppressor genes.

ACKNOWLEDGEMENTS

We thank members of the Fudan MCB lab for discussion and Jean Guan and Karen Tumaneng for critical reading of the manuscript. This work is supported by NIH grants (to Y.X. and K.L.G.).

REFERENCES

Chowdhury, R., Yeoh, K.K., Tian, Y.M., Hillringhaus, L., Bagg, E.A., Rose, N.R., Leung, I.K., Li, X.S., Woon, E.C., Yang, M., et al. (2011). EMBO Rep. *12*, 463–469.

Dang, L., White, D.W., Gross, S., Bennett, B.D., Bittinger, M.A., Driggers, E.M., Fantin, V.R., Jang, H.G., Jin, S., Keenan, M.C., et al. (2009). Nature *462*, 739–744.

Figueroa, M.E., Abdel-Wahab, O., Lu, C., Ward, P.S., Patel, J., Shih, A., Li, Y., Bhagwat, N., Vasanthakumar, A., Fernandez, H.F., et al. (2010). Cancer Cell *18*, 553–567.

Koivunen, P., Lee, S., Duncan, C.G., Lopez, G., Lu, G., Ramkissoon, S., Losman, J.A., Joensuu, P., Bergmann, U., Gross, S., et al. (2012). Nature *483*, 484–488.

Loenarz, C., and Schofield, C.J. (2008). Nat. Chem. Biol. *4*, 152–156.

Losman, J.A., Looper, R., Koivunen, P., Lee, S., Schneider, R.K., McMahon, C., Cowley, G., Root, D., Ebert, B.L., and Kaelin, W.G., Jr. (2013). Science. Published online February 7, 2013. http://dx.doi.org/10.1126/science.1231677.

Oermann, E.K., Wu, J., Guan, K.L., and Xiong, Y. (2012). Semin. Cell Dev. Biol. *23*, 370–380.

Sasaki, M., Knobbe, C.B., Munger, J.C., Lind, E.F., Brenner, D., Brustle, A., Harris, I.S., Holmes, R., Wakeham, A., Haight, J., et al. (2012). Nature *488*, 656–659.

Xiao, M., Yang, H., Xu, W., Ma, S., Lin, H., Zhu, H., Liu, L., Liu, Y., Yang, C., Xu, Y., et al. (2012). Genes Dev. *26*, 1326–1338.

Xu, W., Yang, H., Liu, Y., Yang, Y., Wang, P., Kim, S.H., Ito, S., Yang, C., Wang, P., Xiao, M.T., et al. (2011). Cancer Cell *19*, 17–30.

Cancer Cell
Review

Macrophage Regulation of Tumor Responses to Anticancer Therapies

Michele De Palma[1,*] and Claire E. Lewis[2,*]
[1]The Swiss Institute for Experimental Cancer Research (ISREC), School of Life Sciences, Swiss Federal Institute of Technology Lausanne (EPFL), CH-1015 Lausanne, Switzerland
[2]Department of Oncology, Sheffield Cancer Research Centre, University of Sheffield Medical School, Sheffield, S10 2RX, UK
*Correspondence: claire.lewis@sheffield.ac.uk (C.E.L.), michele.depalma@epfl.ch (M.D.P.)
http://dx.doi.org/10.1016/j.ccr.2013.02.013

Tumor-associated macrophages (TAMs) promote key processes in tumor progression, like angiogenesis, immunosuppression, invasion, and metastasis. Increasing studies have also shown that TAMs can either enhance or antagonize the antitumor efficacy of cytotoxic chemotherapy, cancer-cell targeting antibodies, and immunotherapeutic agents—depending on the type of treatment and tumor model. TAMs also drive reparative mechanisms in tumors after radiotherapy or treatment with vascular-targeting agents. Here, we discuss the biological significance and clinical implications of these findings, with an emphasis on novel approaches that effectively target TAMs to increase the efficacy of such therapies.

Introduction

Macrophages phagocytose microbes and present antigens to T cells, therefore constituting a first line of defense against invading pathogens. They also regulate tissue growth, homeostasis, repair, and remodeling via their expression of numerous cytokines, chemokines, growth factors, proteolytic enzymes, and scavenger receptors (Gordon and Martinez, 2010; Murray and Wynn, 2011). As such, macrophages play a central role in developmental processes, such as tissue morphogenesis and vascular and neuronal patterning, but also in pathophysiological responses, like inflammation and organ healing/regeneration (Mantovani et al., 2013; Nucera et al., 2011; Pollard, 2009).

In selected organs of the adult mouse, the origin of tissue macrophages can be traced back to fetal macrophages that appear before the onset of definitive hematopoiesis (Schulz et al., 2012). In inflamed and remodeling tissues, elevated macrophage turnover is sustained largely from hematopoietic progenitor cells (HPCs), which proliferate and differentiate into promonocytes in the bone marrow (BM) before they are shed into the circulation as monocytes. These then undergo final differentiation into macrophages as they extravasate in the target tissues (Shi and Pamer, 2011). During inflammation and tumor growth, BM-derived HPCs may also accumulate at extramedullary sites, such as the spleen, which can become an important site of monocyte production (Cortez-Retamozo et al., 2012).

Once resident in tissues, macrophages acquire a distinct, tissue-specific phenotype in response to signals present within individual microenvironments. The exact combination of such tissue-specific cues dictates both the differentiation and activation status of these cells. Two extreme forms of the latter are generally referred to as "classical" (or M1) and "alternative" (or M2) activation, which parallel Th1/Th2 programming of adaptive immune cells (Biswas and Mantovani, 2010; Mantovani et al., 2002). During acute inflammation, macrophages are M1-activated by toll-like receptor (TLR) agonists and Th1 cytokines (e.g., interferon [IFN]-γ). This enhances their ability to kill and phagocytose pathogens, upregulate proinflammatory cytokines (e.g., interleukin [IL]-1β, IL-12, and tumor necrosis factor-α [TNF-α]) and reactive molecular species, and present antigens via major histocompatibility complex (MHC) class II molecules (Biswas and Mantovani, 2010; Mantovani et al., 2002). Alternatively, Th2 cytokines, like IL-4 and 13, stimulate monocytes/macrophages to express an M2 activation state. This is characterized by higher production of the anti-inflammatory cytokine, IL-10; lower expression of proinflammatory cytokines; amplification of metabolic pathways that can suppress adaptive immune responses; and the upregulation of cell-surface scavenger receptors, such as mannose receptor (MRC1/CD206) and hemoglobin/aptoglobin scavenger receptor (CD163). As such, M2 macrophage activation may facilitate the resolution of inflammation and promote tissue repair (including angiogenesis) after the acute inflammatory phase (Biswas and Mantovani, 2010; Gordon and Martinez, 2010). In healthy tissues, macrophages often express a mixed M1/M2 phenotype; hence "M1" and "M2" polarization should be regarded as extreme ends of a continuum of activation states, with their exact point on the scale depending on the precise mix of local signals present in a given microenvironment (Biswas and Mantovani, 2010; Lawrence and Natoli, 2011; Sica and Mantovani, 2012).

Tumor-Associated Macrophages

Macrophages are a major cellular component of murine and human tumors, where they are commonly termed tumor-associated macrophages (TAMs). In this article, we specifically review the role of these cells and their monocyte precursors in tumor responses to anticancer therapies. Other tumor-infiltrating myeloid cells not discussed here include neutrophils, eosinophils, and activated dendritic cells (DCs) (de Visser et al., 2006). Tumors also recruit a variety of immature myeloid cells, often referred to as myeloid-derived suppressor cells (MDSCs), which comprise precursors of both the monocyte-DC (mononuclear) and neutrophil (granulocytic) lineages and are commonly identified by their expression of Gr1 (Ly6C/G) and immunosuppressive activity. Mononuclear MDSCs can further mature into TAMs (Coffelt et al., 2010; Gabrilovich et al., 2012). Finally,

there is also evidence for hematopoietic and myeloid progenitor cells homing to tumors and modulating tumor progression (Shaked and Voest, 2009).

Various mouse studies have shown that monocytes are recruited into tumors in large numbers by chemokines secreted by both malignant and stromal cells. These include chemokine (C-C motif) ligand 2 (CCL2, or MCP1), colony-stimulating factor-1 (CSF1), and chemokine (C-X-C motif) ligand 12 (CXCL12, or SDF1) (Murdoch et al., 2008). Upon monocyte differentiation into TAMs, these cells act as a source of local and systemic cues to support the proliferation, survival, and motility of the cancer cells; tumor vascularization (angiogenesis); suppression of antitumor immunity; and intravasation of cancer cells at the primary tumor site and extravasation/growth at distant metastatic sites (Bingle et al., 2006; De Palma et al., 2003; DeNardo et al., 2009; Lewis and Pollard, 2006; Lin et al., 2001; Qian et al., 2011; Qian and Pollard, 2010; Ruffell et al., 2012a; Squadrito and De Palma, 2011; Wyckoff et al., 2004). This impressive array of tumor-promoting functions is consistent with clinical studies showing high macrophage density in many human cancer types to be associated with increased tumor angiogenesis and metastasis, and/or a poor prognosis (Bingle et al., 2002; Clear et al., 2010; Heusinkveld and van der Burg, 2011; Leek et al., 1996). Furthermore, enrichment of a macrophage-related gene signature correlates with reduced survival in some types of human cancer (Engler et al., 2012; Steidl et al., 2010).

A decade ago, it was proposed that TAMs are predominantly polarized in the tumor microenvironment toward an M2-like phenotype and that this underlies their ability to promote the growth and vascularization of tumors (Mantovani et al., 2002). This is also supported by clinical studies showing the predictive value of M2-macrophage associated markers, like CD163 (Heusinkveld and van der Burg, 2011). Flow cytometry and gene expression profiling of mouse and human TAMs has shown that distinct macrophage subpopulations with a variably skewed M2-like phenotype coexist in tumors and that their relative abundance varies with the tumor type (Movahedi et al., 2010; Pucci et al., 2009; Ruffell et al., 2012b). Such complexity likely indicates diverse TAM programming in different microenvironments within individual tumors (Lewis and Pollard, 2006; Qian and Pollard, 2010; Ruffell et al., 2012a; Squadrito and De Palma, 2011). For example, M2-like TAMs reside in both perivascular and hypoxic regions of different mouse and human tumors (Mazzieri et al., 2011; Movahedi et al., 2010; Pucci et al., 2009). A population of vessel-associated TAMs—also referred to as TIE2-expressing monocytes/macrophages (TEMs)—is required for tumor angiogenesis (De Palma et al., 2005) and displays a profoundly M2-skewed phenotype characterized by enhanced expression of scavenger receptors (e.g., MRC1 and CD163) and relatively low levels of MHCII molecules and proinflammatory cytokines (Pucci et al., 2009; Squadrito et al., 2012). Interestingly, vascular endothelial cells (ECs) may induce HPCs to directly differentiate into $TIE2^{+}MRC1^{+}$ macrophages in the perivascular microenvironment, a process that appears to depend on EC-derived CSF1 (He et al., 2012). Also attesting to the complexity of TAM subtypes, recent studies have shown that both the origin and phenotype of TAMs may differ in primary versus metastatic tumors (Qian et al., 2011).

TAMs with a relatively M1-skewed phenotype may be found in incipient or regressing tumors as well as necrotic areas of progressing tumors (Prada et al., 2013; Wang et al., 2011). Gene expression profiling of M1- and M2-like TAMs, however, suggests that such TAM "subtypes" express both canonical M1 and M2 markers, albeit at significantly different levels (Movahedi et al., 2010; Pucci et al., 2009; Squadrito et al., 2012).

Macrophage Involvement in Tumor Responses to Therapy

As will be seen below, TAMs not only enhance tumor growth and progression, but also modulate the efficacy of various forms of anticancer therapy. In some circumstances, they also facilitate tumor regrowth, revascularization, and spread after the treatment.

Chemotherapy

A complex picture has emerged over the past 30 years of the role of TAMs in modulating the antitumor efficacy of chemotherapeutic agents (Figure 1). Early studies showed that the antitumor efficacy of doxorubicin (DOX; an anthracycline formerly known as adriamycin) is reduced when mice bearing immunogenic leukemia or lymphoma transplants were given macrophage toxins (Mantovani et al., 1979; Figure 1A). Furthermore, the in vivo administration of DOX enhanced the tumoricidal activity of macrophages ex vivo. Interestingly, macrophages did not enhance the efficacy of DOX against poorly immunogenic lymphomas, suggesting that tumor immunogenicity may influence the ability of macrophages to modulate the antitumor activity of DOX. In contrast, macrophage depletion failed to limit the antitumor activity of another anthracycline, daunorubicin (formerly daunomycin) (Mantovani et al., 1979), possibly because the latter is per se toxic toward macrophages in vivo (Mantovani, 1977). Together, these early reports suggested that some cytotoxic agents are able to foster the antitumor activities of TAMs, at least in leukemia and/or immunogenic (transplant) tumor models. In this regard, innate immune cells, like macrophages and DCs, are known to mediate "immunogenic cell death" (ICD), a process that encompasses chemotherapy-induced cancer cell death and release of "eat-me" signals (e.g., ATP and high-mobility group B1 [HMGB1]); activation of mononuclear phagocytes and enhancement of their antigen-presenting capacity; and promotion of T cell responses against immunogenic tumors. Of note, only a few chemotherapeutics are known to induce ICD, one of which is DOX (Kroemer et al., 2012).

TAMs can also contribute in other ways to the modulation of tumor responses to chemotherapy. Figure 1 shows that this can vary markedly between different cytotoxic agents and tumor models. For example, the antitumor activity of the taxane docetaxel involves the depletion of immunosuppressive (M2-like) TAMs and the concomitant activation or expansion of antitumoral (M1-like) monocytes/MDSCs in 4T1-Neu mammary tumor implants. Indeed, in vitro T cell assays showed that docetaxel-treated monocytes/MDSCs are able to enhance tumor-specific, cytotoxic T cell responses (Kodumudi et al., 2010). Trabectedin, a DNA-damaging agent approved for soft tissue sarcomas, inhibited the growth of mouse fibrosarcomas primarily by depleting mononuclear phagocytes, including monocytes and TAMs (Germano et al., 2013). Mechanistically, it activates caspase 8 and induces apoptosis specifically in

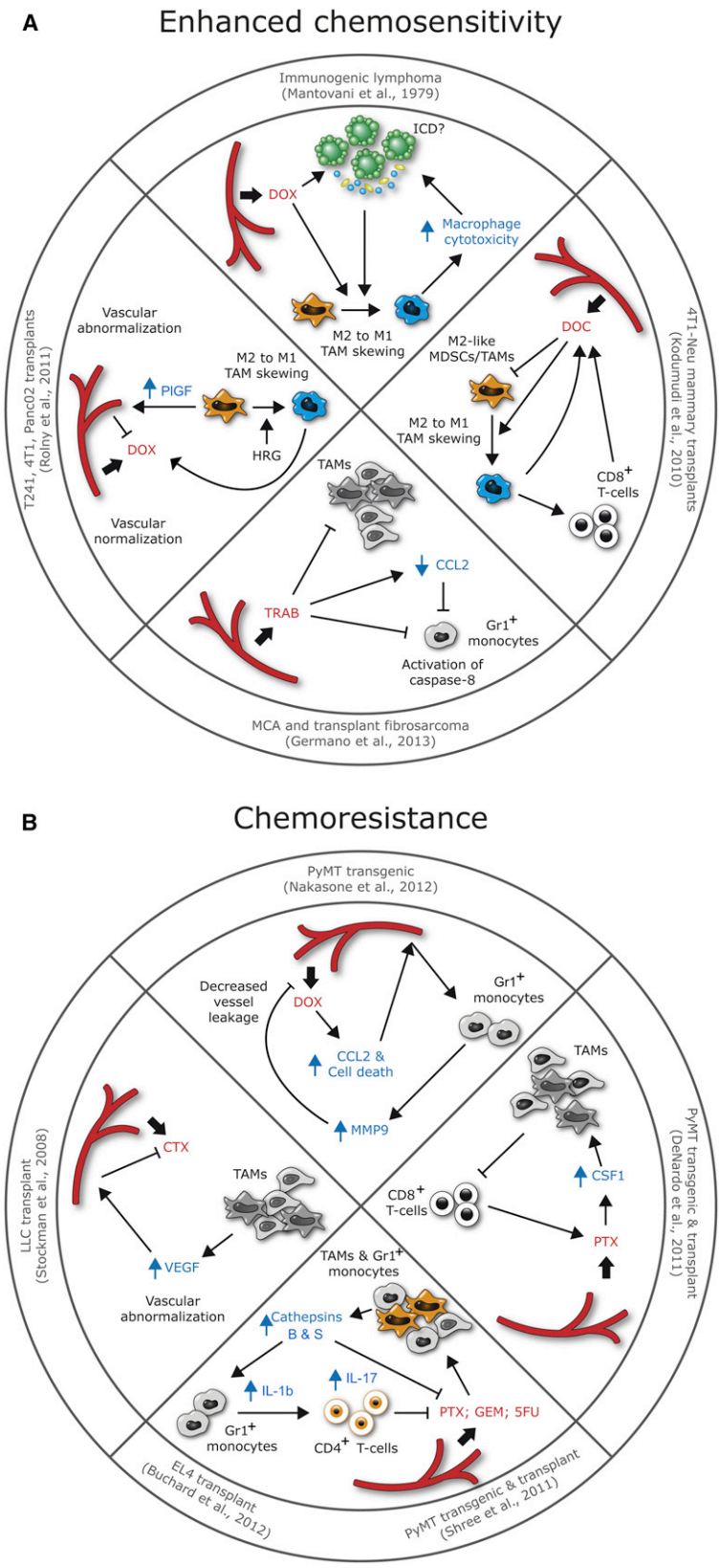

Figure 1. TAMs Enhance or Limit the Efficacy of Chemotherapy Depending on the Cytotoxic Agent Applied and/or Mouse Tumor Model Used

(A) Chemosensitivity is increased when cytotoxic agents, either directly or indirectly, increase the cytotoxicity of TAMs or deplete monocytes, TAMs, or M2-like TAMs. The latter cells can also be reprogrammed by agents like HRG, which in turn enhances chemotherapy delivery. DOX enhances the cytotoxicity of macrophages/TAMs, a process possibly involving ICD (top); DOC promotes the expansion of cytotoxic M1-like MDSCs/TAMs, which enhance antitumor T cell responses (right); TRAB depletes protumoral monocytes/TAMs via caspase-8 activation (bottom); HRG downregulates PlGF in TAMs, reprogramming them toward an M1-like phenotype, and enhances DOX delivery (left).

(B) Chemoresistance is increased when cytotoxic agents, either directly or indirectly, increase protumoral (M2-like) TAM numbers. The latter cells may also limit chemotherapy delivery by affecting vascular leakage. DOX enhances tumor infiltration by MMP9-expressing monocytes via upregulation of CCL2 (top); PTX enhances tumor infiltration by macrophages via upregulation of CSF1 (right); PTX, GEM, and 5FU enhance tumor infiltration by cathepsin-B/S-expressing monocytes/macrophages, which activate chemoprotective T cells through IL-1β and 17 (bottom); VEGF-expressing TAMs augment vascular leakiness and limit CTX delivery (left).

Abbreviations: DOC, docetaxel; TRAB, trabectedin; CTX, cyclophosphamide; GEM, gemcitabine; 5-FU, 5-fluorouracil; IL-1b, interleukin-1β; IL-17, interleukin-17.

monocytes/macrophages via TRAIL-R2, a death receptor not expressed by other leukocytes. Interestingly, trabectedin also depleted circulating monocytes and TAMs in patients with soft-tissue sarcomas. These findings support the notion that the antitumor activity of some cytotoxic agents may depend, at least in part, on their ability to reprogram or deplete protumoral mononuclear phagocytes (Kodumudi et al., 2010; Germano et al., 2013). It remains to be seen whether the mode of action of trabectedin also entails the promotion of adaptive antitumor immune responses, unleashed through the depletion of immunosuppressive TAMs (Figure 1A).

There is also compelling evidence for TAMs limiting the efficacy of chemotherapy (Figure 1B). For example, TAM depletion by anti-CSF1 antibodies enhanced the efficacy of combination chemotherapy (cyclophosphamide, methotrexate, and 5-fluorouracil) in chemoresistant, human breast cancer xenografts grown in immunodeficient mice (Paulus et al., 2006). Similarly, TAM depletion enhanced the efficacy of paclitaxel (PTX, a taxane) in immunocompetent, MMTV-PyMT mouse mammary tumors (DeNardo et al., 2011). At variance with some other cytotoxic drugs (e.g., trabectedin), PTX did not affect tumor growth by depleting TAMs. Rather, it augmented their recruitment to the tumors by upregulating tumor-derived CSF1. Consistent with the known immunosuppressive functions of TAMs, the increased TAM numbers in PTX-treated tumors limited tumor infiltration by $CD8^+$ cytotoxic T cells and possibly reduced their tumoricidal activity. These important findings suggest that TAMs may limit the therapeutic activity of PTX in breast cancer, at least in part, by suppressing specific antitumor immune responses (DeNardo et al., 2011).

TAMs may also release "chemoprotective" factors. Shree et al. (2011) reported increased TAM numbers in PTX-treated MMTV-PyMT tumors and showed that TAM secretion of the lysosomal enzymes, cathepsins B and S, protected cancer cells from PTX-induced cell death and so limited the efficacy of this agent (Shree et al., 2011). Indeed, a pan-cathepsin inhibitor improved the response of MMTV-PyMT tumors to PTX. Interestingly, coculture experiments showed that such macrophage-derived cathepsins protect cancer cells from the direct cytotoxic effects of several chemotherapeutics, including DOX and etoposide (Shree et al., 2011). In this regard, a recent study showed that two broadly used chemotherapeutics, gemcitabine and 5-fluorouracil, induce monocytes/MDSCs to release cathepsin B from lysosomes (Bruchard et al., 2013). This activates the inflammasome and enhances monocyte/MDSC secretion of IL-1β. In turn, IL-1β prompted secretion of IL-17 by $CD4^+$ T cells, which then blunted the anticancer effects of chemotherapy (Figure 1B). These data provide a molecular mechanism linking myeloid cell-derived cathepsins to chemoprotection.

While DOX may stimulate macrophage cytotoxicity toward immunogenic leukemias (Mantovani et al., 1979), its effects on TAMs appear to vary with the tumor type. In the transgenic MMTV-PyMT mammary tumor model, DOX induction of necrotic cell death led to increased tumor infiltration by CCL2 receptor $(CCR2)^+$ monocytes/TAMs, a process that relied on upregulation of CCL2 (Nakasone et al., 2012). Interestingly, the antitumor activity of DOX was enhanced in *Ccr2* knockout hosts, which lack $CCR2^+$ monocytes. While the effect of DOX on the cytotoxic activity of TAMs was not examined in this study, the authors showed that matrix-metalloproteinase (MMP)-9 produced by recruited myeloid cells decreased blood vessel leakiness and limited drug delivery to the tumors, suggesting that, at least in MMTV-PyMT tumors, increased vascular permeability is associated with a better response to DOX (Nakasone et al., 2012). It should be noted that, in other tumor models, downregulating the expression of proangiogenic factors, like vascular endothelial growth factor (VEGF) or placental growth factor (PlGF) by TAMs "normalized" the tumor-associated vasculature, decreased vessel leakiness, and enhanced chemotherapy delivery to tumors (Rolny et al., 2011; Stockmann et al., 2008; Figures 1A and 1B). It remains to be seen whether the different effects of DOX in leukemia versus the above mammary tumor model (Nakasone et al., 2012) reflect differences in tumor immunogenicity or more complex aspects of the tumor microenvironment.

Taken together, the above studies show that different chemotherapeutic agents may induce distinct responses in monocytes/macrophages, which can either enhance or antagonize the activity of the anticancer drug, possibly in a tumor-type dependent fashion. Tumor immunogenicity along with the intrinsic sensitivity of TAMs to the drug and their activation state (M1 versus M2-like) may be important determinants of such TAM-mediated responses. Furthermore, cytotoxic drugs often target multiple cell types in tumors, so tumor-type specific stromal cell signatures (Coussens et al., 2013) could influence the ability of TAMs to respond to and modulate the activity of a given chemotherapeutic. Indeed, cytotoxic drugs could have both direct and indirect effects on TAM behavior. For example, taxanes profoundly alter macrophage gene expression in vitro (Javeed et al., 2009) but also induce tumor damage and cancer cell death, which may trigger a reparative, "wound healing" response in TAMs (Mantovani et al., 2013). Further studies are now warranted to distinguish between the role of TAMs in the chemoprotection described above (DeNardo et al., 2011; Nakasone et al., 2012; Shree et al., 2011) and the reparative responses that occur in tumors after therapy.

Finally, TAMs may enhance tumor chemoresistance by providing survival signals to tumor-initiating/cancer stem cells (CSCs). For example, TAMs were found to release milk fat globule-epidermal growth factor 8 protein (MFG-E8) to help protect lung and colon CSCs from cisplatin. This relied, at least in part, on MFG-E8-induced activation of STAT3, which enhanced CSC chemoresistance (Jinushi et al., 2011). Moreover, TAM depletion has been shown to improve antitumor T cell responses and the efficacy of chemotherapy in a pancreatic cancer model, in part by decreasing the frequency, tumor-initiating capacity, and STAT3 activation of CSCs (Mitchem et al., 2013).

Tumor Irradiation

Tumor irradiation is widely used to treat many cancer types. Early studies correlated high TAM numbers in mouse tumors with poor tumor responses to irradiation (Milas et al., 1987). Recent data suggest that radiation-induced DNA damage and activation of the v-abl Abelson murine leukemia viral oncogene homolog 1 (ABL1) kinase promote *Csf1* gene transcription and upregulation of tumor CSF1, which in turn recruits CSF1R-expressing myeloid cells (including TAMs) that enhance posttherapy tumor regrowth. Indeed, a CSF1R inhibitor improved tumor response to radiotherapy in a prostate cancer model (Xu et al., 2013; Figure 2).

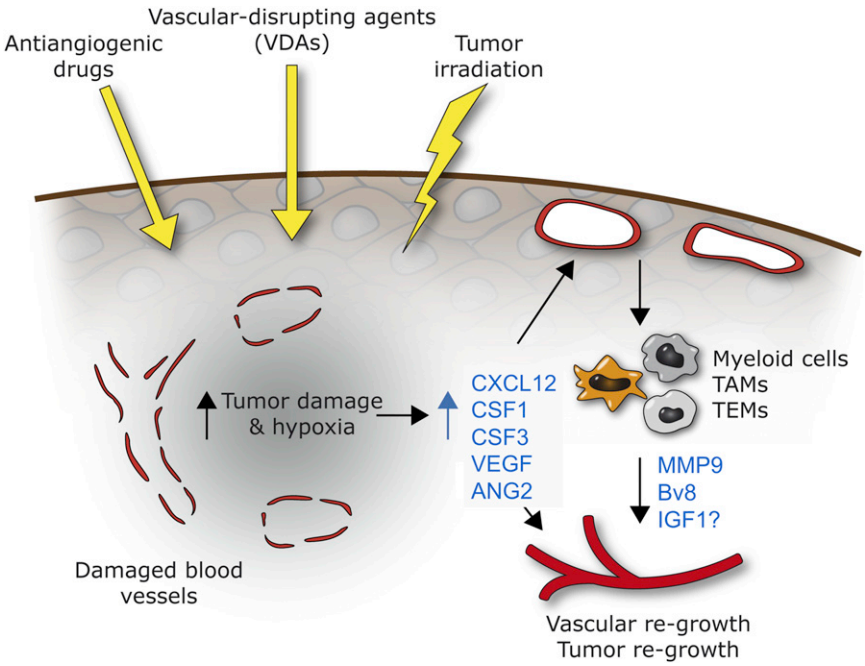

Figure 2. TAMs Promote Tumor Regrowth Following Tumor Irradiation, Antiangiogenic Drugs and VDAs

These anticancer therapies cause tumor necrosis, vascular damage, and hypoxia, which together or separately induce the upregulation of several myeloid cell/monocyte chemoattractants, including CXCL12, CSF1, CSF3, VEGF, and ANG2, in the tumor microenvironment. De novo recruitment of myeloid cells drives tumor regrowth via their effects on the tumor blood vessels (mediated, e.g., by MMP9, Bv8, and IGF1) and, possibly, the cancer cells.

Abbreviations: CSF3, granulocyte-colony stimulating factor; Bv8, prokineticin.

See also Figure 1.

Antibody-mediated depletion of $CD11b^+$ myeloid cells in human head and neck tumors grown in immunodeficient mice also reduced tumor regrowth after therapy (Ahn et al., 2010). In a model of orthotopic human glioblastoma, local irradiation dramatically enhanced tumor infiltration by $CD11b^+$ myeloid cells (Kioi et al., 2010). Interestingly, a high proportion of these cells were $F4/80^+TIE2^+$ TEMs, and their recruitment was dependent on the hypoxic induction of the chemoattractant, CXCL12, in the irradiated tumors (Figure 2). Upregulation of CXCL12 and increased TEM infiltration were also observed in lung and mammary tumors grown subcutaneously following irradiation (Kozin et al., 2010). In the latter study, TEMs congregated mainly around the remaining blood vessels in treated tumors (Kozin et al., 2010), suggesting that they may stimulate tumor recurrence by promoting EC survival and vascular regrowth through their expression of prosurvival factors like insulin growth factor 1 (IGF1) and fibroblast growth factor 2 (FGF2) (De Palma et al., 2005; Pucci et al., 2009). However, the location and, possibly, the function of M2-like TAMs in irradiated tumors may vary with tumor type. In irradiated orthotopic astrocytomas, arginase-1 $(ARG1)^+$ M2-like TAMs were found to accumulate mainly in avascular, hypoxic areas rather than at perivascular sites (Chiang et al., 2012). This suggests that the reparative mechanisms employed by M2-like TAMs in postirradiated tumors may be regulated by distinct microenvironmental signals in different tumor types. It is also conceivable that the functions of M2-like TAMs in irradiated tumors are similar to those of M2-like macrophages driving tissue repair in healing organs, such as following acute renal injury and myocardial infarction (Mantovani et al., 2013).

Vascular-Targeted Therapies

VEGF is a proangiogenic cytokine that also functions as a potent monocyte chemoattractant (Barleon et al., 1996). It is, therefore, possible that the antiangiogenic and antitumor effects of VEGF blockade could result, at least in part, from impaired monocyte/TAM recruitment. However, this seems increasingly unlikely, as it is now established that therapeutic interception of VEGF is counteracted by the compensatory induction of other proangiogenic factors, some of which are involved in monocyte/myeloid cell chemoattraction (Bergers and Hanahan, 2008; Ferrara, 2010).

Tumor hypoxia and necrosis dramatically increase after the selective destruction of tumor blood vessels by high-dose antiangiogenic drugs or vascular-disrupting agents (VDAs) (Bergers and Hanahan, 2008). When tumors are treated with VDAs, like combretastatin-A4-phosphate (CA-4-P), the selective disruption of the tumor-associated vasculature results in vessel collapse, reduced blood flow, induction of tumor hypoxia, and secondary tumor cell death. As in irradiated tumors, VDA-induced hypoxia was associated with elevated levels of CXCL12 and increased TEM infiltration in mammary tumor models (Welford et al., 2011; Figure 2). Blocking this CA-4-P-induced TEM recruitment, either using the CXCR4 antagonist, plerixafor (AMD3100), or by genetic TEM depletion, markedly increased the efficacy of CA-4-P treatment in subcutaneous N202 (Neu^+) mammary carcinomas (Welford et al., 2011).

Blocking the proangiogenic factor angiopoietin-2 (ANG2) also leads to angiogenesis inhibition and increased tumor hypoxia (Daly et al., 2013; Mazzieri et al., 2011). As seen in CA-4-P-treated tumors (Welford et al., 2011), the latter events were associated with an enhanced recruitment of $MRC1^+$ TEMs, which may have limited the efficacy of ANG2 blockade (Mazzieri et al., 2011). Sorafenib, which targets several receptor tyrosine kinases (including VEGF receptor 2 [VEGFR2] and platelet-derived growth factor receptor [PDGFR]) and Raf kinases, was also shown to increase CXCL12 levels and TAM infiltration in hepatocellular carcinoma xenografts. Depletion of TAMs by clodronate-loaded liposomes (clodrolip) augmented the inhibitory effects of sorafenib on tumor angiogenesis, growth, and metastasis in this tumor model (Zhang et al., 2010). Moreover, TAM depletion by clodrolip (Zeisberger et al., 2006) or a CSF1R inhibitor (Priceman et al., 2010) increased the antiangiogenic and antitumor effects of VEGF/VEGFR2 antibodies in subcutaneous tumor models. Together, these data support the rationale for combining antiangiogenic drugs with macrophage

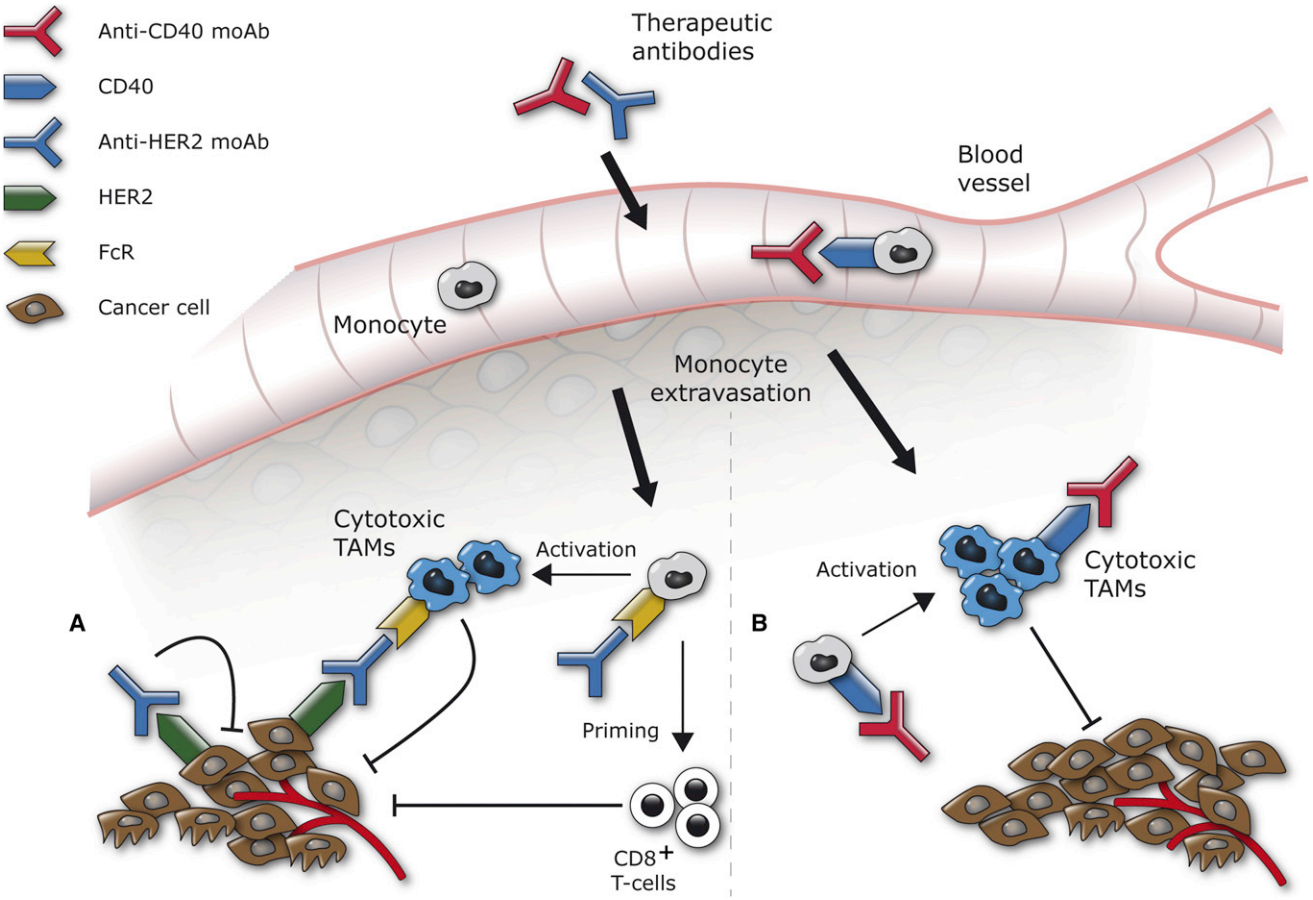

Figure 3. moAbs Activate TAMs to Express a Cytotoxic Phenotype
Binding of therapeutic antibodies to monocytes/macrophages may enhance their tumoricidal activity.
(A) Binding of therapeutic (cancer-cell targeted) moAbs (e.g., anti-HER2) to monocytes/TAMs via Fc-receptors (FcRs) induces FcR-mediated activation of macrophage cytotoxicity/phagocytosis (ADCC/ADCP) and priming of adaptive antitumor immunity (e.g., $CD8^+$ T cells).
(B) Binding of immunotherapeutic moAbs (e.g., anti-CD40) to monocytes/TAMs triggers their activation to a cytotoxic (M1-like) phenotype.

targeting strategies to increase the efficacy of the former, particularly in tumors that are refractory or develop resistance to anti-VEGF therapy.

Targeted Therapies by Monoclonal Antibodies

Although a role for TAMs in modulating the efficacy of oncogene-targeted, small molecule inhibitors has yet to be elucidated, there is now increasing evidence for TAMs contributing to the cytotoxicity of therapeutic monoclonal antibodies (moAbs). TAMs express surface receptors that bind the Fc fragment of antibodies and enable them to engage in Ab-dependent cellular cytotoxicity/phagocytosis (ADCC/ADCP). Trastuzumab, a moAb against the human epidermal growth factor receptor-2 (HER2), not only interrupts HER2 signaling in breast cancer cells, thereby slowing their proliferation rate, but also induces Fcγ receptor (FcγR)-mediated activation of macrophage cytotoxicity (Clynes et al., 2000) and priming of antigen-specific $CD8^+$ T cell responses in MMTV-Neu tumors (Park et al., 2010) (Figure 3A). In one study, TAM depletion limited the efficacy of a moAb directed against tissue factor (CD142)-expressing human breast carcinoma cells inoculated in mice (Grugan et al., 2012). Macrophages also enhance lymphoma elimination in mice in response to rituximab, a moAb against CD20, primarily through FcγR-dependent ADCP (Chao et al., 2010; Minard-Colin et al., 2008). The significance of the aforementioned studies is supported by clinical findings suggesting that certain *FCGR* polymorphisms may bear predictive value for the clinical efficacy of trastuzumab or rituximab therapy in breast cancer and lymphoma, respectively (Mellor et al., 2013). Furthermore, high TAM numbers correlate with a better prognosis in rituximab-treated patients (Taskinen et al., 2007). Engineered recombinant proteins that can enhance the interactions between FcγR-expressing immune cells and moAbs, like the recently described "grababodies" (Cai et al., 2013), may thus have the potential to increase ADCC/ADCP in tumors. It should be noted, however, that engagement of macrophage-FcγRs by serum or therapeutic antibodies (e.g., the anti-EGFR moAb cetuximab) was shown to enhance the immunosuppressive, proangiogenic, and protumoral functions of TAMs both in experimental tumor models and human cancer (Andreu et al., 2010; Pander et al., 2011).

Immunotherapies

As mentioned previously, TAMs can be potent immunosuppressors that limit the cytotoxic activity of $CD8^+$ cytotoxic T cells in progressing tumors (DeNardo et al., 2011). The analysis of human breast cancer tissues showed that a high stromal TAM

density correlates inversely with $CD8^+$ T cell numbers (DeNardo et al., 2011). In a preclinical study, clodrolip-mediated depletion of TAMs enhanced tumor infiltration by HPV16 E7-specific $CD8^+$ T cells in a HPV16 $E6^+/E7^+$ mouse model of cervical cancer (Lepique et al., 2009). TAM-mediated immunosuppression is mediated, at least in part, by induction of T cell apoptosis and nitrosylation of T cell receptors via macrophage products, like ARG1, NOS2, and peroxynitrite (Gabrilovich et al., 2012).

It should be noted that the study by DeNardo et al. (2011) analyzed the leukocyte composition of established tumors (DeNardo et al., 2011), in which immunosuppressive, M2-like TAMs likely predominate over tumoricidal (M1-like) macrophages. It is possible that incipient tumors, which are likely to be more immunogenic than established lesions, contain higher proportions of M1-like TAMs, which could initiate and/or potentiate adaptive immune responses (Prada et al., 2013; Wang et al., 2011). In this regard, macrophages were shown to acutely engulf myeloma cells inoculated subcutaneously in syngenic mice and to activate myeloma-specific $CD4^+$ Th1 cells, which then enhanced the tumoricidal activity of macrophages through IFN-γ secretion (Corthay et al., 2005). In certain immunoprivileged organs, such as the eye, macrophages promote the effector functions of $CD4^+$ T cells, and their depletion enhances rather than inhibits intraocular tumor growth (Dace et al., 2008). Thus, the type of macrophage activation—which may correlate with tumor stage (Prada et al., 2013; Wang et al., 2011)—may dictate the magnitude of antitumoral T cell responses in mouse models of cancer.

Based on the above, strategies to deplete TAMs or block cancer-induced M2-like macrophage programming (see below) may have the potential to enhance T cell-mediated antitumor responses and improve the efficacy of immunotherapies (Coussens et al., 2013; Hagemann et al., 2008; Jaiswal et al., 2010). Intriguingly, increasing data suggest that the efficacy of some forms of immunotherapy may also depend on effective reprogramming of TAMs toward an M1-like phenotype. For example, intravesical instillation of *Mycobacterium bovis* bacillus Calmette-Guérin, which is used for the treatment of superficial bladder cancer, reduces tumor recurrence by stimulating the cytotoxic activity of macrophages. Macrophage-mediated killing of bladder cancer cells relies on both direct effector-target cell contacts and the release of soluble cytotoxic factors, such as TNF-α, IFN-γ, and NO, from the macrophages (Luo and Knudson, 2010). An agonistic antibody to the TNF receptor superfamily member, CD40, was recently reported to bind to circulating monocytes, trigger their recruitment into mouse pancreatic tumors, and activate their tumoricidal functions (Figure 3B). These CD40-activated, cytotoxic (M1-skewed) TAMs were also found to enhance the efficacy of gemcitabine in a small cohort of patients with surgically incurable pancreatic cancer (Beatty et al., 2011). Finally, macrophages and DCs express programmed cell death ligand-1 (PDL1, also known as B7-H1), a major negative regulatory ligand that suppresses T cell activation through its receptor-programmed cell death protein 1. The promising therapeutic activity of anti-PDL1 moAbs in patients with advanced cancer (Brahmer et al., 2012) will no doubt prompt further studies of the possible inhibition of PDL1 expression on TAMs to improve the efficacy of chemo- or antiangiogenic therapies.

Concluding Remarks: Implications for Cancer Treatment

In light of this growing body of evidence for TAMs modulating the effects of various anticancer therapies, attempts are now being made to either target key molecules that regulate their recruitment into tumors or re-educate these cells toward a cytotoxic M1-like phenotype. The efficacy of CSF1R inhibitors in blocking the enhanced uptake of monocytes during PTX treatment in preclinical studies (DeNardo et al., 2011) has prompted clinical trials of their use in combination with either PTX or the antiproliferative agent eribulin (http://www.clinicaltrials.gov). Various preclinical studies have also highlighted ways to reprogram TAMs from an M2 to an M1-like phenotype in tumors. These include the use of histidine-rich glycoprotein (HRG), which induces macrophage downregulation of PlGF, promotes the normalization of blood vessels, and increases delivery and efficacy of chemotherapy in mouse tumor models (Rolny et al., 2011; Figure 1A). Other strategies to reprogram TAMs include blockade of nuclear factor-kB signaling (Hagemann et al., 2008) or their exposure to anti-IL-10R antibodies combined with the TLR9 ligand CpG (Guiducci et al., 2005). The latter resulted in hemorrhagic tumor necrosis, activation of DCs and cytotoxic T cells, and clearance of tumor remnants.

However, there is still much to learn about the mechanisms regulating TAM functions during chemotherapy, as well as other forms of therapy discussed in this review. Importantly, a number of key questions need to be addressed before approaches that combine macrophage targeting (or reprogramming) and conventional cancer therapies can be translated into more effective treatments. Why do preclinical studies employing distinct chemotherapeutic drugs and/or tumor models show different and, at times, contradictory roles for TAMs in modulating tumor responses to such agents? Why do TAMs apparently limit the effects of chemotherapy in some tumor types but not others? Are the distinct TAM subtypes present in individual tumors differentially responsive to chemotherapy? If yes, what are the specific features of the TAM subset(s) that either enhance or promote the antitumor activity of cytotoxic agents? And what are the signals in tumors that regulate these TAM responses? Such information might help selectively target the TAMs that limit chemotherapy while leaving antitumoral or tissue-resident macrophages unaffected. Furthermore, most preclinical studies to date have focused on primary, nonmetastatic tumors. So, are we confident that TAMs in metastatic tumors (Qian et al., 2011) behave in the same way during therapy as those in the primary tumor site?

Mouse tumor models, including genetically engineered mouse models (GEMMs), are being used extensively to study mechanisms underlying tumor (and TAM) responses to anticancer therapies. However, even sophisticated GEMMs of cancer cannot simulate the endless variations in TAM abundance, distribution, and phenotypes between and within different types and subtypes of human cancer (Coussens et al., 2013; De Palma and Hanahan, 2012). Nor do they necessarily model the ability of such tissues to recruit monocytes during therapy. Future work should therefore aim to define the identities and molecular profiles of distinct TAM subtypes in human cancer biopsies before, during, and after therapy. Specific TAM signatures could then be used to stratify patients carrying defined genetic lesions

in order to explore how such signatures correlate with the response of individual patients to chemo-, radio-, or targeted therapies, and/or the emergence of secondary resistance (DeVita and Costa, 2010). If such studies demonstrate the predictive value of specific TAM subtypes for individual tumor responses, then their further characterization in mouse tumor models could help develop more effective cancer therapies. Undeniably, such clinical approaches should consider the biological complexities on a tumor (sub)type and individual patient basis and harness them to design effective personalized therapies.

ACKNOWLEDGMENTS

We apologize to the authors whose work we could not cite or illustrate in the figures because of space constraints. The authors thank Luisa Iruela-Arispe and Livio Trusolino for critical reading of the manuscript and Bruno Liardon for help with the figures. Work in the authors' laboratories is supported by grants from the European Research Council (ERC; Tie2$^+$monocytes), National Centres of Competence in Research (Oncology program), Anna Fuller Fund (to M.D.P.), and Cancer Research UK (to C.E.L.).

REFERENCES

Ahn, G.O., Tseng, D., Liao, C.H., Dorie, M.J., Czechowicz, A., and Brown, J.M. (2010). Inhibition of Mac-1 (CD11b/CD18) enhances tumor response to radiation by reducing myeloid cell recruitment. Proc. Natl. Acad. Sci. USA *107*, 8363–8368.

Andreu, P., Johansson, M., Affara, N.I., Pucci, F., Tan, T., Junankar, S., Korets, L., Lam, J., Tawfik, D., DeNardo, D.G., et al. (2010). FcRgamma activation regulates inflammation-associated squamous carcinogenesis. Cancer Cell *17*, 121–134.

Barleon, B., Sozzani, S., Zhou, D., Weich, H.A., Mantovani, A., and Marmé, D. (1996). Migration of human monocytes in response to vascular endothelial growth factor (VEGF) is mediated via the VEGF receptor flt-1. Blood *87*, 3336–3343.

Beatty, G.L., Chiorean, E.G., Fishman, M.P., Saboury, B., Teitelbaum, U.R., Sun, W., Huhn, R.D., Song, W., Li, D., Sharp, L.L., et al. (2011). CD40 agonists alter tumor stroma and show efficacy against pancreatic carcinoma in mice and humans. Science *331*, 1612–1616.

Bergers, G., and Hanahan, D. (2008). Modes of resistance to anti-angiogenic therapy. Nat. Rev. Cancer *8*, 592–603.

Bingle, L., Brown, N.J., and Lewis, C.E. (2002). The role of tumour-associated macrophages in tumour progression: implications for new anticancer therapies. J. Pathol. *196*, 254–265.

Bingle, L., Lewis, C.E., Corke, K.P., Reed, M.W., and Brown, N.J. (2006). Macrophages promote angiogenesis in human breast tumour spheroids in vivo. Br. J. Cancer *94*, 101–107.

Biswas, S.K., and Mantovani, A. (2010). Macrophage plasticity and interaction with lymphocyte subsets: cancer as a paradigm. Nat. Immunol. *11*, 889–896.

Brahmer, J.R., Tykodi, S.S., Chow, L.Q., Hwu, W.J., Topalian, S.L., Hwu, P., Drake, C.G., Camacho, L.H., Kauh, J., Odunsi, K., et al. (2012). Safety and activity of anti-PD-L1 antibody in patients with advanced cancer. N. Engl. J. Med. *366*, 2455–2465.

Bruchard, M., Mignot, G., Derangère, V., Chalmin, F., Chevriaux, A., Végran, F., Boireau, W., Simon, B., Ryffel, B., Connat, J.L., et al. (2013). Chemotherapy-triggered cathepsin B release in myeloid-derived suppressor cells activates the Nlrp3 inflammasome and promotes tumor growth. Nat. Med. *19*, 57–64.

Cai, Z., Fu, T., Nagai, Y., Lam, L., Yee, M., Zhu, Z., and Zhang, H. (2013). scFv-based "grababody" as a general strategy to improve recruitment of immune effector cells to antibody-targeted tumors. Cancer Res.. http://dx.doi.org/10.1158/0008-5472.CAN-12-3920

Chao, M.P., Alizadeh, A.A., Tang, C., Myklebust, J.H., Varghese, B., Gill, S., Jan, M., Cha, A.C., Chan, C.K., Tan, B.T., et al. (2010). Anti-CD47 antibody synergizes with rituximab to promote phagocytosis and eradicate non-Hodgkin lymphoma. Cell *142*, 699–713.

Chiang, C.S., Fu, S.Y., Wang, S.C., Yu, C.F., Chen, F.H., Lin, C.M., and Hong, J.H. (2012). Irradiation promotes an m2 macrophage phenotype in tumor hypoxia. Front Oncol. *2*, 89.

Clear, A.J., Lee, A.M., Calaminici, M., Ramsay, A.G., Morris, K.J., Hallam, S., Kelly, G., Macdougall, F., Lister, T.A., and Gribben, J.G. (2010). Increased angiogenic sprouting in poor prognosis FL is associated with elevated numbers of CD163$^+$ macrophages within the immediate sprouting microenvironment. Blood *115*, 5053–5056.

Clynes, R.A., Towers, T.L., Presta, L.G., and Ravetch, J.V. (2000). Inhibitory Fc receptors modulate in vivo cytotoxicity against tumor targets. Nat. Med. *6*, 443–446.

Coffelt, S.B., Lewis, C.E., Naldini, L., Brown, J.M., Ferrara, N., and De Palma, M. (2010). Elusive identities and overlapping phenotypes of proangiogenic myeloid cells in tumors. Am. J. Pathol. *176*, 1564–1576.

Cortez-Retamozo, V., Etzrodt, M., Newton, A., Rauch, P.J., Chudnovskiy, A., Berger, C., Ryan, R.J., Iwamoto, Y., Marinelli, B., Gorbatov, R., et al. (2012). Origins of tumor-associated macrophages and neutrophils. Proc. Natl. Acad. Sci. USA *109*, 2491–2496.

Corthay, A., Skovseth, D.K., Lundin, K.U., Røsjø, E., Omholt, H., Hofgaard, P.O., Haraldsen, G., and Bogen, B. (2005). Primary antitumor immune response mediated by CD4$^+$ T cells. Immunity *22*, 371–383.

Coussens, L.M., Zitvogel, L., and Palucka, A.K. (2013). Neutralizing tumor-promoting chronic inflammation: a magic bullet? Science *339*, 286–291.

Dace, D.S., Chen, P.W., and Niederkorn, J.Y. (2008). CD4$^+$ T-cell-dependent tumour rejection in an immune-privileged environment requires macrophages. Immunology *123*, 367–377.

Daly, C., Eichten, A., Castanaro, C., Pasnikowski, E., Adler, A., Lalani, A.S., Papadopoulos, N., Kyle, A.H., Minchinton, A.I., Yancopoulos, G.D., and Thurston, G. (2013). Angiopoietin-2 functions as a Tie2 agonist in tumor models, where it limits the effects of VEGF inhibition. Cancer Res. *73*, 108–118.

De Palma, M., and Hanahan, D. (2012). The biology of personalized cancer medicine: facing individual complexities underlying hallmark capabilities. Mol. Oncol. *6*, 111–127.

De Palma, M., Venneri, M.A., Roca, C., and Naldini, L. (2003). Targeting exogenous genes to tumor angiogenesis by transplantation of genetically modified hematopoietic stem cells. Nat. Med. *9*, 789–795.

De Palma, M., Venneri, M.A., Galli, R., Sergi Sergi, L., Politi, L.S., Sampaolesi, M., and Naldini, L. (2005). Tie2 identifies a hematopoietic lineage of proangiogenic monocytes required for tumor vessel formation and a mesenchymal population of pericyte progenitors. Cancer Cell *8*, 211–226.

de Visser, K.E., Eichten, A., and Coussens, L.M. (2006). Paradoxical roles of the immune system during cancer development. Nat. Rev. Cancer *6*, 24–37.

DeNardo, D.G., Barreto, J.B., Andreu, P., Vasquez, L., Tawfik, D., Kolhatkar, N., and Coussens, L.M. (2009). CD4(+) T cells regulate pulmonary metastasis of mammary carcinomas by enhancing protumor properties of macrophages. Cancer Cell *16*, 91–102.

DeNardo, D.G., Brennan, D.J., Rexhepaj, E., Ruffell, B., Shiao, S.L., Madden, S.F., Gallagher, W.M., Wadhwani, N., Keil, S.D., Junaid, S.A., et al. (2011). Leukocyte complexity predicts breast cancer survival and functionally regulates response to chemotherapy. Cancer Discov. *1*, 54–67.

DeVita, V.T., Jr., and Costa, J. (2010). Toward a personalized treatment of Hodgkin's disease. N. Engl. J. Med. *362*, 942–943.

Engler, J.R., Robinson, A.E., Smirnov, I., Hodgson, J.G., Berger, M.S., Gupta, N., James, C.D., Molinaro, A., and Phillips, J.J. (2012). Increased microglia/macrophage gene expression in a subset of adult and pediatric astrocytomas. PLoS ONE *7*, e43339.

Ferrara, N. (2010). Role of myeloid cells in vascular endothelial growth factor-independent tumor angiogenesis. Curr. Opin. Hematol. *17*, 219–224.

Gabrilovich, D.I., Ostrand-Rosenberg, S., and Bronte, V. (2012). Coordinated regulation of myeloid cells by tumours. Nat. Rev. Immunol. *12*, 253–268.

Germano, G., Frapolli, R., Belgiovine, C., Anselmo, A., Pesce, S., Liguori, M., Erba, E., Uboldi, S., Zucchetti, M., Pasqualini, F., et al. (2013). Role of macrophage targeting in the antitumor activity of trabectedin. Cancer Cell *23*, 249–262.

Gordon, S., and Martinez, F.O. (2010). Alternative activation of macrophages: mechanism and functions. Immunity *32*, 593–604.

Grugan, K.D., McCabe, F.L., Kinder, M., Greenplate, A.R., Harman, B.C., Ekert, J.E., van Rooijen, N., Anderson, G.M., Nemeth, J.A., Strohl, W.R., et al. (2012). Tumor-associated macrophages promote invasion while retaining Fc-dependent anti-tumor function. J. Immunol. *189*, 5457–5466.

Guiducci, C., Vicari, A.P., Sangaletti, S., Trinchieri, G., and Colombo, M.P. (2005). Redirecting in vivo elicited tumor infiltrating macrophages and dendritic cells towards tumor rejection. Cancer Res. *65*, 3437–3446.

Hagemann, T., Lawrence, T., McNeish, I., Charles, K.A., Kulbe, H., Thompson, R.G., Robinson, S.C., and Balkwill, F.R. (2008). "Re-educating" tumor-associated macrophages by targeting NF-kappaB. J. Exp. Med. *205*, 1261–1268.

He, H., Xu, J., Warren, C.M., Duan, D., Li, X., Wu, L., and Iruela-Arispe, M.L. (2012). Endothelial cells provide an instructive niche for the differentiation and functional polarization of M2-like macrophages. Blood *120*, 3152–3162.

Heusinkveld, M., and van der Burg, S.H. (2011). Identification and manipulation of tumor associated macrophages in human cancers. J. Transl. Med. *9*, 216.

Jaiswal, S., Chao, M.P., Majeti, R., and Weissman, I.L. (2010). Macrophages as mediators of tumor immunosurveillance. Trends Immunol. *31*, 212–219.

Javeed, A., Ashraf, M., Riaz, A., Ghafoor, A., Afzal, S., and Mukhtar, M.M. (2009). Paclitaxel and immune system. Eur. J. Pharm. Sci. *38*, 283–290.

Jinushi, M., Chiba, S., Yoshiyama, H., Masutomi, K., Kinoshita, I., Dosaka-Akita, H., Yagita, H., Takaoka, A., and Tahara, H. (2011). Tumor-associated macrophages regulate tumorigenicity and anticancer drug responses of cancer stem/initiating cells. Proc. Natl. Acad. Sci. USA *108*, 12425–12430.

Kioi, M., Vogel, H., Schultz, G., Hoffman, R.M., Harsh, G.R., and Brown, J.M. (2010). Inhibition of vasculogenesis, but not angiogenesis, prevents the recurrence of glioblastoma after irradiation in mice. J. Clin. Invest. *120*, 694–705.

Kodumudi, K.N., Woan, K., Gilvary, D.L., Sahakian, E., Wei, S., and Djeu, J.Y. (2010). A novel chemoimmunomodulating property of docetaxel: suppression of myeloid-derived suppressor cells in tumor bearers. Clin. Cancer Res. *16*, 4583–4594.

Kozin, S.V., Kamoun, W.S., Huang, Y., Dawson, M.R., Jain, R.K., and Duda, D.G. (2010). Recruitment of myeloid but not endothelial precursor cells facilitates tumor regrowth after local irradiation. Cancer Res. *70*, 5679–5685.

Kroemer, G., Galluzzi, L., Kepp, O., and Zitvogel, L. (2012). Immunogenic Cell Death in Cancer Therapy. Annu. Rev. Immunol. http://dx.doi.org/10.1146/annurev-immunol-032712-100008

Lawrence, T., and Natoli, G. (2011). Transcriptional regulation of macrophage polarization: enabling diversity with identity. Nat. Rev. Immunol. *11*, 750–761.

Leek, R.D., Lewis, C.E., Whitehouse, R., Greenall, M., Clarke, J., and Harris, A.L. (1996). Association of macrophage infiltration with angiogenesis and prognosis in invasive breast carcinoma. Cancer Res. *56*, 4625–4629.

Lepique, A.P., Daghastanli, K.R., Cuccovia, I.M., and Villa, L.L. (2009). HPV16 tumor associated macrophages suppress antitumor T cell responses. Clin. Cancer Res. *15*, 4391–4400.

Lewis, C.E., and Pollard, J.W. (2006). Distinct role of macrophages in different tumor microenvironments. Cancer Res. *66*, 605–612.

Lin, E.Y., Nguyen, A.V., Russell, R.G., and Pollard, J.W. (2001). Colony-stimulating factor 1 promotes progression of mammary tumors to malignancy. J. Exp. Med. *193*, 727–740.

Luo, Y., and Knudson, M.J. (2010). Mycobacterium bovis bacillus Calmette-Guérin-induced macrophage cytotoxicity against bladder cancer cells. Clin. Dev. Immunol. *2010*, 357591.

Mantovani, A. (1977). In vitro and in vivo cytotoxicity of adriamycin and daunomycin for murine macrophages. Cancer Res. *37*, 815–820.

Mantovani, A., Polentarutti, N., Luini, W., Peri, G., and Spreafico, F. (1979). Role of host defense merchanisms in the antitumor activity of adriamycin and daunomycin in mice. J. Natl. Cancer Inst. *63*, 61–66.

Mantovani, A., Sozzani, S., Locati, M., Allavena, P., and Sica, A. (2002). Macrophage polarization: tumor-associated macrophages as a paradigm for polarized M2 mononuclear phagocytes. Trends Immunol. *23*, 549–555.

Mantovani, A., Biswas, S.K., Galdiero, M.R., Sica, A., and Locati, M. (2013). Macrophage plasticity and polarization in tissue repair and remodelling. J. Pathol. *229*, 176–185.

Mazzieri, R., Pucci, F., Moi, D., Zonari, E., Ranghetti, A., Berti, A., Politi, L.S., Gentner, B., Brown, J.L., Naldini, L., and De Palma, M. (2011). Targeting the ANG2/TIE2 axis inhibits tumor growth and metastasis by impairing angiogenesis and disabling rebounds of proangiogenic myeloid cells. Cancer Cell *19*, 512–526.

Mellor, J.D., Brown, M.P., Irving, H.R., Zalcberg, J.R., and Dobrovic, A. (2013). A critical review of the role of Fc gamma receptor polymorphisms in the response to monoclonal antibodies in cancer. J. Hematol. Oncol. *6*, 1.

Milas, L., Wike, J., Hunter, N., Volpe, J., and Basic, I. (1987). Macrophage content of murine sarcomas and carcinomas: associations with tumor growth parameters and tumor radiocurability. Cancer Res. *47*, 1069–1075.

Minard-Colin, V., Xiu, Y., Poe, J.C., Horikawa, M., Magro, C.M., Hamaguchi, Y., Haas, K.M., and Tedder, T.F. (2008). Lymphoma depletion during CD20 immunotherapy in mice is mediated by macrophage FcgammaRI, FcgammaRIII, and FcgammaRIV. Blood *112*, 1205–1213.

Mitchem, J.B., Brennan, D.J., Knolhoff, B.L., Belt, B.A., Zhu, Y., Sanford, D.E., Belaygorod, L., Carpenter, D., Collins, L., Piwnica-Worms, D., et al. (2013). Targeting tumor-infiltrating macrophages decreases tumor-initiating cells, relieves immunosuppression, and improves chemotherapeutic responses. Cancer Res. *73*, 1128–1141.

Movahedi, K., Laoui, D., Gysemans, C., Baeten, M., Stangé, G., Van den Bossche, J., Mack, M., Pipeleers, D., In't Veld, P., De Baetselier, P., and Van Ginderachter, J.A. (2010). Different tumor microenvironments contain functionally distinct subsets of macrophages derived from Ly6C(high) monocytes. Cancer Res. *70*, 5728–5739.

Murdoch, C., Muthana, M., Coffelt, S.B., and Lewis, C.E. (2008). The role of myeloid cells in the promotion of tumour angiogenesis. Nat. Rev. Cancer *8*, 618–631.

Murray, P.J., and Wynn, T.A. (2011). Protective and pathogenic functions of macrophage subsets. Nat. Rev. Immunol. *11*, 723–737.

Nakasone, E.S., Askautrud, H.A., Kees, T., Park, J.H., Plaks, V., Ewald, A.J., Fein, M., Rasch, M.G., Tan, Y.X., Qiu, J., et al. (2012). Imaging tumor-stroma interactions during chemotherapy reveals contributions of the microenvironment to resistance. Cancer Cell *21*, 488–503.

Nucera, S., Biziato, D., and De Palma, M. (2011). The interplay between macrophages and angiogenesis in development, tissue injury and regeneration. Int. J. Dev. Biol. *55*, 495–503.

Pander, J., Heusinkveld, M., van der Straaten, T., Jordanova, E.S., Baak-Pablo, R., Gelderblom, H., Morreau, H., van der Burg, S.H., Guchelaar, H.J., and van Hall, T. (2011). Activation of tumor-promoting type 2 macrophages by EGFR-targeting antibody cetuximab. Clin. Cancer Res. *17*, 5668–5673.

Park, S., Jiang, Z., Mortenson, E.D., Deng, L., Radkevich-Brown, O., Yang, X., Sattar, H., Wang, Y., Brown, N.K., Greene, M., et al. (2010). The therapeutic effect of anti-HER2/neu antibody depends on both innate and adaptive immunity. Cancer Cell *18*, 160–170.

Paulus, P., Stanley, E.R., Schäfer, R., Abraham, D., and Aharinejad, S. (2006). Colony-stimulating factor-1 antibody reverses chemoresistance in human MCF-7 breast cancer xenografts. Cancer Res. *66*, 4349–4356.

Pollard, J.W. (2009). Trophic macrophages in development and disease. Nat. Rev. Immunol. *9*, 259–270.

Prada, C.E., Jousma, E., Rizvi, T.A., Wu, J., Dunn, R.S., Mayes, D.A., Cancelas, J.A., Dombi, E., Kim, M.O., West, B.L., et al. (2013). Neurofibroma-associated macrophages play roles in tumor growth and response to pharmacological inhibition. Acta Neuropathol. *125*, 159–168.

Priceman, S.J., Sung, J.L., Shaposhnik, Z., Burton, J.B., Torres-Collado, A.X., Moughon, D.L., Johnson, M., Lusis, A.J., Cohen, D.A., Iruela-Arispe, M.L., and

Wu, L. (2010). Targeting distinct tumor-infiltrating myeloid cells by inhibiting CSF-1 receptor: combating tumor evasion of antiangiogenic therapy. Blood *115*, 1461–1471.

Pucci, F., Venneri, M.A., Biziato, D., Nonis, A., Moi, D., Sica, A., Di Serio, C., Naldini, L., and De Palma, M. (2009). A distinguishing gene signature shared by tumor-infiltrating Tie2-expressing monocytes, blood "resident" monocytes, and embryonic macrophages suggests common functions and developmental relationships. Blood *114*, 901–914.

Qian, B.Z., and Pollard, J.W. (2010). Macrophage diversity enhances tumor progression and metastasis. Cell *141*, 39–51.

Qian, B.Z., Li, J., Zhang, H., Kitamura, T., Zhang, J., Campion, L.R., Kaiser, E.A., Snyder, L.A., and Pollard, J.W. (2011). CCL2 recruits inflammatory monocytes to facilitate breast-tumour metastasis. Nature *475*, 222–225.

Rolny, C., Mazzone, M., Tugues, S., Laoui, D., Johansson, I., Coulon, C., Squadrito, M.L., Segura, I., Li, X., Knevels, E., et al. (2011). HRG inhibits tumor growth and metastasis by inducing macrophage polarization and vessel normalization through downregulation of PlGF. Cancer Cell *19*, 31–44.

Ruffell, B., Affara, N.I., and Coussens, L.M. (2012a). Differential macrophage programming in the tumor microenvironment. Trends Immunol. *33*, 119–126.

Ruffell, B., Au, A., Rugo, H.S., Esserman, L.J., Hwang, E.S., and Coussens, L.M. (2012b). Leukocyte composition of human breast cancer. Proc. Natl. Acad. Sci. USA *109*, 2796–2801.

Schulz, C., Gomez Perdiguero, E., Chorro, L., Szabo-Rogers, H., Cagnard, N., Kierdorf, K., Prinz, M., Wu, B., Jacobsen, S.E., Pollard, J.W., et al. (2012). A lineage of myeloid cells independent of Myb and hematopoietic stem cells. Science *336*, 86–90.

Shaked, Y., and Voest, E.E. (2009). Bone marrow derived cells in tumor angiogenesis and growth: are they the good, the bad or the evil? Biochim. Biophys. Acta *1796*, 1–4.

Shi, C., and Pamer, E.G. (2011). Monocyte recruitment during infection and inflammation. Nat. Rev. Immunol. *11*, 762–774.

Shree, T., Olson, O.C., Elie, B.T., Kester, J.C., Garfall, A.L., Simpson, K., Bell-McGuinn, K.M., Zabor, E.C., Brogi, E., and Joyce, J.A. (2011). Macrophages and cathepsin proteases blunt chemotherapeutic response in breast cancer. Genes Dev. *25*, 2465–2479.

Sica, A., and Mantovani, A. (2012). Macrophage plasticity and polarization: in vivo veritas. J. Clin. Invest. *122*, 787–795.

Squadrito, M.L., and De Palma, M. (2011). Macrophage regulation of tumor angiogenesis: implications for cancer therapy. Mol. Aspects Med. *32*, 123–145.

Squadrito, M.L., Pucci, F., Magri, L., Moi, D., Gilfillan, G.D., Ranghetti, A., Casazza, A., Mazzone, M., Lyle, R., Naldini, L., and De Palma, M. (2012). miR-511-3p modulates genetic programs of tumor-associated macrophages. Cell Rep. *1*, 141–154.

Steidl, C., Lee, T., Shah, S.P., Farinha, P., Han, G., Nayar, T., Delaney, A., Jones, S.J., Iqbal, J., Weisenburger, D.D., et al. (2010). Tumor-associated macrophages and survival in classic Hodgkin's lymphoma. N. Engl. J. Med. *362*, 875–885.

Stockmann, C., Doedens, A., Weidemann, A., Zhang, N., Takeda, N., Greenberg, J.I., Cheresh, D.A., and Johnson, R.S. (2008). Deletion of vascular endothelial growth factor in myeloid cells accelerates tumorigenesis. Nature *456*, 814–818.

Taskinen, M., Karjalainen-Lindsberg, M.L., Nyman, H., Eerola, L.M., and Leppä, S. (2007). A high tumor-associated macrophage content predicts favorable outcome in follicular lymphoma patients treated with rituximab and cyclophosphamide-doxorubicin-vincristine-prednisone. Clin. Cancer Res. *13*, 5784–5789.

Wang, B., Li, Q., Qin, L., Zhao, S., Wang, J., and Chen, X. (2011). Transition of tumor-associated macrophages from MHC class II(hi) to MHC class II(low) mediates tumor progression in mice. BMC Immunol. *12*, 43.

Welford, A.F., Biziato, D., Coffelt, S.B., Nucera, S., Fisher, M., Pucci, F., Di Serio, C., Naldini, L., De Palma, M., Tozer, G.M., and Lewis, C.E. (2011). TIE2-expressing macrophages limit the therapeutic efficacy of the vascular-disrupting agent combretastatin A4 phosphate in mice. J. Clin. Invest. *121*, 1969–1973.

Wyckoff, J., Wang, W., Lin, E.Y., Wang, Y., Pixley, F., Stanley, E.R., Graf, T., Pollard, J.W., Segall, J., and Condeelis, J. (2004). A paracrine loop between tumor cells and macrophages is required for tumor cell migration in mammary tumors. Cancer Res. *64*, 7022–7029.

Xu, J., Escamilla, J., Mok, S., David, J., Priceman, S.J., West, B.L., Bollag, G., McBride, W.H., and Wu, L. (2013). Abrogating the protumorigenic influences of tumor-infiltrating myeloid cells by CSF1R signaling blockade improves the efficacy of radiotherapy in prostate cancer. Cancer Res. Published online February 19, 2013. http://dx.doi.org/10.1158/0008-5472.CAN-12-3981.

Zeisberger, S.M., Odermatt, B., Marty, C., Zehnder-Fjällman, A.H., Ballmer-Hofer, K., and Schwendener, R.A. (2006). Clodronate-liposome-mediated depletion of tumour-associated macrophages: a new and highly effective antiangiogenic therapy approach. Br. J. Cancer *95*, 272–281.

Zhang, W., Zhu, X.D., Sun, H.C., Xiong, Y.Q., Zhuang, P.Y., Xu, H.X., Kong, L.Q., Wang, L., Wu, W.Z., and Tang, Z.Y. (2010). Depletion of tumor-associated macrophages enhances the effect of sorafenib in metastatic liver cancer models by antimetastatic and antiangiogenic effects. Clin. Cancer Res. *16*, 3420–3430.

Cancer Cell
Article

PGC1α Expression Defines a Subset of Human Melanoma Tumors with Increased Mitochondrial Capacity and Resistance to Oxidative Stress

Francisca Vazquez,[1,6] Ji-Hong Lim,[1,6] Helen Chim,[1] Kavita Bhalla,[2] Geoff Girnun,[2] Kerry Pierce,[3] Clary B. Clish,[3] Scott R. Granter,[4] Hans R. Widlund,[5] Bruce M. Spiegelman,[1] and Pere Puigserver[1,*]
[1]Department of Cancer Biology, Dana-Farber Cancer Institute and Department of Cell Biology, Harvard Medical School, Boston, MA 02115, USA
[2]Stewart Greenebaum Cancer Center, Department of Pathology, University of Maryland School of Medicine, Baltimore, MD 21201, USA
[3]Metabolite Profiling Initiative, Broad Institute of MIT and Harvard, 7 Cambridge Center, Cambridge, MA 02142, USA
[4]Department of Pathology
[5]Department of Dermatology
Harvard Skin Disease Research Center, Brigham and Women's Hospital, Boston, MA 02115, USA
[6]These authors contributed equally to this work
*Correspondence: pere_puigserver@dfci.harvard.edu
http://dx.doi.org/10.1016/j.ccr.2012.11.020

SUMMARY

Cancer cells reprogram their metabolism using different strategies to meet energy and anabolic demands to maintain growth and survival. Understanding the molecular and genetic determinants of these metabolic programs is critical to successfully exploit them for therapy. Here, we report that the oncogenic melanocyte lineage-specification transcription factor MITF drives *PGC1α* (*PPARGC1A*) overexpression in a subset of human melanomas and derived cell lines. Functionally, PGC1α positive melanoma cells exhibit increased mitochondrial energy metabolism and reactive oxygen species (ROS) detoxification capacities that enable survival under oxidative stress conditions. Conversely, PGC1α negative melanoma cells are more glycolytic and sensitive to ROS-inducing drugs. These results demonstrate that differences in PGC1α levels in melanoma tumors have a profound impact in their metabolism, biology, and drug sensitivity.

INTRODUCTION

Tumors reprogram their metabolism to meet increased energetic and anabolic demands. A frequent metabolic adaptation that cancer cells acquire is an increase in glucose uptake and aerobic glycolysis together with decrease in oxidative metabolism. It is clear, however, that there is not one single tumor-specific metabolic state, and tumors can utilize a variety of different metabolic strategies that have only now begun to be elucidated. For example, tumor cells are able to generate ATP through mitochondrial oxidation of fatty acids and amino acids, such as glutamine when glucose becomes limiting (Zaugg et al., 2011; Choo et al., 2010; Gao et al., 2009; Wise et al., 2008).

An increase in reactive oxygen species (ROS), due to an enhanced and unbalanced metabolic activity (Hanahan and Weinberg, 2011) is a common stressor to which tumors must adapt. This increased generation of ROS can play a dual role in the cancer phenotype. On one hand, it can play a tumorigenic role by stimulating cell proliferation and promoting genomic instability (Weinberg and Chandel, 2009). On the other hand, above a certain threshold, ROS can be toxic and induce cellular damage, leading to cell death (Trachootham et al., 2009; Diehn et al., 2009). Cancer cells develop adaptive responses against oxidative stress, often by upregulating their antioxidant-scavenging capacity. One clear example is the constitutive activation of the Keap1-Nrf2 pathway in squamous cell carcinomas, either

Significance

Tumor cells reprogram a variety of central metabolic and bioenergetic pathways to maintain exacerbated growth and survival rates. The identification of the genetic factors responsible for specific metabolic programs is key to exploit this reprogramming for cancer therapy. Here, we show that, in melanomas, overexpression of the transcriptional coactivator PGC1α, a key regulator of mitochondrial respiration, metabolically defines melanoma tumors with high bioenergetic and ROS detoxification capacities. These metabolic capacities allow PGC1α-positive melanomas higher rates of survival under oxidative stress compared to PGC1α-negative melanomas. Our results underscore how different metabolic vulnerabilities defined by PGC1α expression could be therapeutically exploited to treat melanoma tumors.

by activating mutations in *Nrf2* or through inactivating mutations in *KEAP1* (an Nrf2 cytoplasmic repressor) (Padmanabhan et al., 2006; Singh et al., 2006; Shibata et al., 2008; Ohta et al., 2008). Whereas some of these components of the oxidative stress response have been identified in cancer cells, it is likely that key regulators in this response that contribute to tumorigenesis are still missing.

PPARGC1A, named hereafter PGC1α, is part of a small family of transcriptional coactivators, including PGC1β and PRC, that promote mitochondrial biogenesis and respiration (Puigserver and Spiegelman, 2003; Scarpulla, 2011). PGC1α is the best studied, particularly in brown fat, skeletal and cardiac muscle, liver, and fat tissues, where it is a key regulator of mitochondrial mass, thermogenic programs, and adaptation to fasting conditions (Kelly and Scarpulla, 2004). PGC1α can also potently reduce generation of mitochondrial-driven ROS (St-Pierre et al., 2006). PGC1α is typically expressed at low levels under normal conditions and is strongly induced and activated in response to increased metabolic and energetic demands in highly metabolic tissues. For example, exercise increases PGC1α levels in skeletal muscle, where it induces mitochondrial biogenesis and oxidative capacity (Handschin et al., 2007). Cold exposure rapidly increases PGC1α levels in brown/beige adipose tissue to program a thermogenic response based on mitochondrial function (Puigserver et al., 1998). In liver, fasting increases PGC1α to induce fatty acid oxidation, hepatic glucose production, and ketogenesis (Rhee et al., 2003). In many of these cell types, the cyclic AMP (cAMP) pathway plays a central role through the activation of a cAMP response element binding protein (CREB) response element at the *PGC1α* promoter (Herzig et al., 2001). Other signals contribute to increases in *PGC1α* gene expression, such as calcium signaling and MEF2 transcriptional activity in skeletal muscle (Lin et al., 2002). It is unknown, however, whether and how oncogenic signals impact PGC1α expression and what are the metabolic and growth consequences this might cause to the tumor phenotype.

RESULTS

A Subset of Human Melanoma Tumors Expresses High Levels of PGC1α and Mitochondrial Genes of Oxidative Metabolism

Given the central role of PGC1α in oxidative metabolism and ROS detoxification in a variety of tissues (Puigserver and Spiegelman, 2003; Kelly and Scarpulla, 2004; Fernandez-Marcos and Auwerx, 2011; St-Pierre et al., 2006), we hypothesized that PGC1α could be aberrantly activated in some tumors, thereby conferring them an adaptive advantage. Since *PGC1α* is strongly regulated at the messenger RNA (mRNA) level, publicly available gene expression databases were surveyed. In several data sets, a subset of melanoma tumors and melanoma-derived cell lines expressed very high relative levels of *PGC1α* mRNA. Figures 1A and S1A (available online) show the relative *PGC1α* mRNA levels from 56 melanoma tumors (GSE7553) (Riker et al., 2008) and 82 short-term melanoma cultures (Lin et al., 2008). Levels of 10.7% for Riker melanoma data set and 8.4% for short-term melanoma cultures showed *PGC1α* expression levels that are at least one standard deviation above the average. To assess if the high *PGC1α* levels in these melanoma tumors were associated with its known metabolic gene expression program, we used Gene Set Enrichment Analysis (GSEA) to find gene expression signatures that correlated with *PGC1α* expression. Consistent with previous and established PGC1α targets in skeletal muscle cells (Mootha et al., 2003), gene expression sets of mitochondrial genes, energy metabolism, and estrogen-related receptor alpha target genes were all significantly correlated with *PGC1α* expression in both melanoma tumors and short-term melanoma cultures (Table 1; Table S1). Using an additional data set of metastatic melanoma tumors with clinical outcome data (Bogunovic et al., 2009), we found that tumors expressing high *PGC1α* levels were associated with lower survival (long-rank p value 0.0230) compared to low *PGC1α*-expressing tumors (Figure 1B). The high and low expressing tumors were defined by selecting the top and bottom 25% *PGC1α* expressing tumors. Other clinical parameters were not affected (Figure S1B). The overexpression results were validated using patient-derived long-term melanoma cell lines. Remarkably, all melanoma cell lines tested fell into two categories with very high levels (PGC1α positive) or undetectable or very low levels (PGC1α negative) of PGC1α mRNA (Figure 1C) and protein (Figure 1D). PGC1α-positive cell lines had elevated levels of mitochondrial respiratory chain proteins from all different complexes tested (Figure 1D). These results suggest that PGC1α induces a mitochondrial metabolism gene expression program in these tumors and tumor-derived cell lines.

To confirm that PGC1α was driving the mitochondrial metabolism gene expression signature, we used lentiviral small hairpin RNA (shRNA) to reduce its expression in a PGC1α-positive melanoma cell line (A375P) and performed gene-expression microarray followed by GSEA analysis. Similar gene expression sets of mitochondrial energy metabolism as the ones found in melanoma tumors and short-term melanoma cultures were enriched in control versus PGC1α knockdown cell lines (Figure 1E; Table S2). Some of the targets were confirmed using quantitative PCR (qPCR) in A375P and two other PGC1α-positive melanoma cell lines (MeWo and G361) (Figure 1F). As expected, downregulation of mitochondrial genes in PGC1α-depleted A375P cells translated into decreases of protein levels. Several components of the oxidative phosphorylation complex were substantially decreased in PGC1α knockdown cells, particularly proteins that are part of Complex I and Complex IV (Figure 1G). PGC1α expression was also sufficient to induce this mitochondrial program. Modest ectopic expression of PGC1α in a PGC1α-negative cell line (A375, a metastatic clone derived from A375P) increased mitochondrial gene targets and protein levels (Figures S1C and S1D). We then compared the levels of PGC1α between nontransformed melanocytes and melanoma cells. The relative levels of *PGC1α* mRNA expression were measured in cultured immortal primary melanocytes and in a PGC1α-positive and negative melanoma cell lines. *PGC1α* mRNA expression levels in primary melanocytes were higher than PGC1α-negative melanoma cells but dramatically lower than PGC1α-positive melanoma cells (Figure S1E). Together, these results indicate that PGC1α is overexpressed in a subset of melanoma tumors and drives a mitochondrial gene expression program.

Interestingly, the overexpression of PGC1α and correlation with oxidative metabolism is not only present in melanomas.

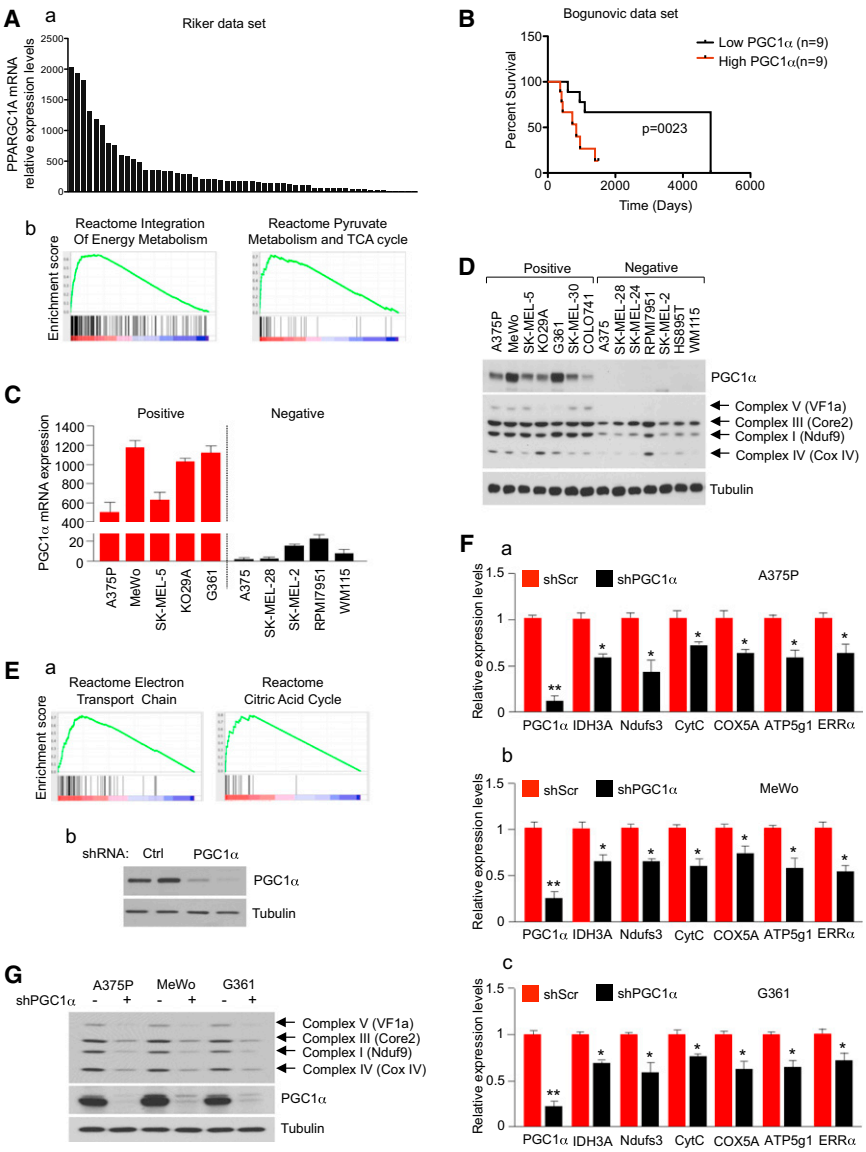

Figure 1. PGC1α Drives the Expression of a Mitochondrial Respiration Program in a Subset of Human Melanoma Tumors and Derived Cell Lines

(A) (a) Relative expression levels of *PGC1α* in 56 melanoma tumors included in the data set GSEA7553 (Riker et al., 2008). (b) Plots for two of the top gene sets from GSEA analysis of genes positively correlated with *PGC1α* expression.

(B) Kaplan-Meier survival curves for metastatic melanoma tumors with high and low *PGC1α* expression from data set GSE19232 (Bogunovic et al., 2009). Survival curves for the 18 metastatic melanoma patients with tumors expressing the 25% highest and lowest *PGC1α* levels were calculated using Kaplan-Meier analysis with test of statistical significance using the Mantel–Cox log-rank test. The long-rank p value was 0.0230.

(C) *PGC1α* mRNA expression levels in ten human melanoma cell lines. mRNA levels were quantified using qRT-PCR. Values represent mean ± SD of two independent experiments performed in triplicate.

(D) Protein levels of PGC1α and mitochondrial respiration-associated proteins in human melanoma cell lines.

(E) (a) Plots for two of the top gene sets of the GSEA analysis in control versus PGC1α knocked down A375P cells. (b) PGC1α protein levels in the control and PGC1α knocked down cells.

(F) mRNA levels of PGC1α mitochondrial target genes measured using qRT-PCR analysis after PGC1α knockdown in PGC1α-positive cell lines: (a) A375P; (b) MeWo; and (c) G361. Values represent mean ± SD of three independent experiments performed in triplicate. *p < 0.05 and **p < 0.01.

(G) Protein expression levels of mitochondrial respiration-associated proteins and PGC1α in A375P stably expressing a control or *PGC1α* shRNA.

See also Figure S1 and Tables S1–S3.

We found that levels of *PGC1α* expression in lung adenocarcinoma cell lines also correlate with an oxidative metabolism signature (Figure S1; Table S3).

MITF Expression in Human Melanoma Cells Drives High Levels of PGC1α Gene Expression

In order to identify the key factors responsible for the high levels of *PGC1α* expression in melanoma, we used publicly available data on gene expression, copy number, and mutations from the Cancer Cell Line Encyclopedia (CCLE) database (http://www.broadinstitute.org/ccle) (Barretina et al., 2012). We found no correlation between *PGC1α* copy number levels and gene expression. Only one melanoma cell line (SK-MEL1)—out of 60 melanoma cell lines with copy number data available at the time (Figure S2A, data from the CCLE database)—was found to have *PGC1α* amplification, suggesting that amplification is not a common mechanism to increase *PGC1α* expression levels. Since p53 has been shown to negatively regulate *PGC1α* levels (Sahin et al., 2011; Sen et al., 2011), we searched if there was an association between p53 mutation status and *PGC1α* expression, but no correlation was found in 60 cell lines with expression and mutation status data. Similarly, there was no correlation with BRAF mutations status (Figure S2B). The Riker melanoma data set was classified by their *PGC1α* expression levels to identify genes that were upregulated in high *PGC1α* versus low *PGC1α*-expressing tumors (Figure 2A). Intriguingly, among the top classifying genes identified was microphthalmia-associated transcription factor (*MITF*), a melanocyte-lineage transcription factor and bona fide melanoma oncogene (Garraway et al., 2005; Yokoyama et al., 2011; Bertolotto et al., 2011). Similar results were obtained comparing high- versus low-expressing *PGC1α* melanoma cell lines. Furthermore, the levels of several MITF downstream target genes, such as *SLC45A2*, *CDK2*, *PMEL*, *TYR*, *TYRP1*, *MLANA*, and *DCT*, were also differentially expressed (Figure 2B, data from the CCLE database). Hence, within both melanoma specimens and melanoma cell lines, the

Table 1. GSEA of Genes Ranked by Positive Correlation with PGC1α Expression in Melanoma Tumors

Name	NES	FDR q-value
Reactome_integration_of_energy_metabolism	2.15	0.02
Reactome_glucose_regulation_of_insulin_secretion	2.08	0.03
Reactome_regulation_of_insulin_secretion	2.09	0.04
Reactome_pyruvate_metabolism_and_TCA_cycle	1.94	0.1
Reactome_citric_acid_cycle	1.88	0.13
Reactome_peroxisomal_lipid_metabolism	1.88	0.16
Reactome_electron_transport_chain	1.86	0.13

Gene expression of 56 melanoma tumors extracted from the GSEA7553 data set (Riker et al., 2008) was ranked for positive correlation with *PGC1α* expression and analyzed with the GSEA algorithm using the reactome gene sets; the significant ($q < 0.25$) gene sets ranked by normalized enrichment score are shown. NES, normalized enrichment score.

expression levels of *PGC1α* correlated with *MITF* levels, indicating that they may be affecting each other in an epistatic manner. To forward this notion, we analyzed mRNA and protein levels of MITF in five PGC1α-positive and five PGC1α-negative cell lines. We found that both the mRNA and protein levels were higher in PGC1α-positive cell lines (Figure 2C). Interestingly, one of the outlier cell lines (SK-MEL-28) that expresses high levels of *MITF* but is *PGC1α*-negative expresses high levels of *PGC1β*.

Based on these data, we investigated if MITF was a causal driver for the high levels of *PGC1α* gene expression. Hence, we used lentiviral shRNA to reduce endogenous MITF levels in three PGC1α-positive melanoma cell lines (A375P, G361, and SK-MEL5) and found that it strongly downregulated PGC1α both at the mRNA and protein levels (Figures 2D and 2E). Notably, *PGC1α* expression levels were suppressed even further than the known MITF target *TYR*. Moreover, PGC1α protein levels were almost undetectable after MITF knockdown. As expected, MITF knockdown-induced PGC1α downregulation resulted in decrease of PGC1α targets, including mitochondrial genes (Figure S2C). These results indicate that MITF is necessary to maintain high levels of PGC1α expression in PGC1α-positive melanoma cell lines.

Next we investigated whether MITF was sufficient to induce *PGC1α* expression in melanoma cell lines. Hence, ectopic expression of MITF using retroviral transduction in A375, a PGC1α-negative cell line, caused induction of PGC1α mRNA levels, including PGC1α targets, comparable to the known MITF target genes, *TYR* and *DCT* (Figure 2F). Because MITF is a transcription factor, it could directly bind the upstream regulatory promoter of *PGC1α*, as this region contains several E-boxes sequences (Figure S2D). Transfection of HEK293T cells with MITF induced a 2Kb *PGC1α* promoter-driving luciferase that was dependent on both E-boxes (Figure 2Ga). Conversely, MITF knockdown experiments in A375P cells reduced the activity of this promoter (Figure 2Gb). In addition, chromatin immunoprecipitation (ChiP) assays showed that endogenous MITF is bound to the PGC1α promoter (Figure 2H), consistent with previously reported ChiP sequencing data set (Strub et al., 2011; Figure S2E).

Gene expression profiling analysis of melanoma tumors has previously identified two expression signatures associated with proliferative or invasive phenotype. *MITF* expression was higher in melanoma samples with the proliferative signature and lower in samples with an invasive signature (Hoek et al., 2008). Consistently, we found that melanoma tumors with high *PGC1α* levels also correlated with the proliferative signature (Figure S2F).

Collectively, these results indicate that MITF is necessary and contributes to the high levels of PGC1α expression found in a subset of human melanoma cells.

PGC1α Defines the Metabolic State of Melanoma Cells

To test whether PGC1α expression levels drive the metabolic program of melanoma cells, we compared key cellular metabolic and bioenergetic parameters between PGC1α-positive and negative melanoma cells. PGC1α-positive cells exhibited substantial increased basal and maximal oxygen consumption rates (Figure 3A). Additionally, the respiration reserve capacity, calculated by subtracting the basal to the maximal respiration capacity, was significantly higher in PGC1α-expressing melanoma cells. Glucose uptake was slightly decreased in PGC1α-positive cells that paralleled diminished levels of secreted lactate compared to PGC1α-negative cells (Figure 3B). Consistent with glycolytic metabolism generating lower ATP levels compared to oxidative metabolism, intracellular ATP levels of PGC1α-negative melanoma cell lines were reduced (Figure 3B). These differences in metabolic parameters were caused by PGC1α expression. Depletion of PGC1α levels in A375P largely recapitulated the metabolic and bioenergetic patterns of PGC1α-negative cells, e.g., decreased in basal, maximal, and reserved oxygen consumption rate (OCR) and intracellular ATP levels, decreased glucose uptake, and increased lactate production (Figures 3C and 3D). Metabolomic analysis showed that shRNA *PGC1α* cells had increased glycolytic but decreased tricarboxylic acid (TCA) intermediates (Figure S3). In addition, a modest increase in PGC1α levels through forced expression (Figure S1C) in a PGC1α-negative cell line resulted in a reversal of these metabolic parameters (Figure 3E). In summary, these results indicate that cells with undetectable levels of PGC1α have lower rates of mitochondrial oxidative metabolism but elevated rates of glycolysis and lactate production consistent with a more pronounced glycolytic "Warburg" state. In contrast, PGC1α-positive cells have the reversed metabolic phenotype, leading to an elevated cellular energetic state.

PGC1α-Positive Melanoma Cells Are Dependent on PGC1α for Survival and Tumor Progression

Given the central role of PGC1α in the metabolic and energetic state of a subset of melanoma cells with high expression levels, we investigated whether these cells may have become dependent on PGC1α for survival. Thus, we suppressed the expression of PGC1α in five positive cell lines and measured its effect on cell viability. Figure 4A shows that knockdown of PGC1α significantly decreased cell number. As expected, knockdown of PGC1α had no significant effect on PGC1α-negative cells. As an additional control, we tested the effect of RPS6 knockdown in a PGC1α-positive and negative cell line and observed a similar effect of decreased cell number in both PGC1α-positive and negative cell lines (Figure S4A). Overexpression of PGC1α, similar to

MITF, was not sufficient to induce proliferation in PGC1α-negative melanoma cells (Figures S4B–S4D) underscoring the context dependency of the effects.

We next investigated the mechanism responsible for the reduced cell number after PGC1α knockdown. PGC1α knockdown resulted in a more than 3-fold induction in the percentage of apoptotic cells in two PGC1α-positive cell lines (A375P and MeWo) but not in a negative cell line (A375) (Figure 4B). This apoptosis was mediated through the intrinsic pathway, as caspases 9 and 3 but not 8 were activated in PGC1α-depleted cells. Other apoptotic markers, including cleavage of poly (ADP-ribose) polymerase (PARP), was also induced in PGC1α knockdown cells (Figure 4C). The apoptotic effect was largely reversed by overexpression of PGC1α, indicating that it is a result of PGC1α depletion (Figure 4D). To further support the involvement of caspases, the inhibitor Q-VD-OPH significantly reduced the number of cells entering apoptosis (Figure 4E). These results indicate that suppression of PGC1α activates the intrinsic mitochondrial apoptotic pathway and strongly suggest that PGC1α-positive melanoma cells have become dependent on PGC1α for survival.

PGC1α Suppression Results in a Reduction of ROS Detoxification Genes and Increase in ROS Levels Leading to Apoptosis

The fact that the intrinsic apoptotic pathway was activated in PGC1α-depleted cells suggested that the mitochondria was involved in the induction of apoptosis. One of the mechanisms by which mitochondrial failure causes apoptosis is through the loss of membrane potential and generation of ROS (Tait and Green, 2010). Consistent with induction of this process, knockdown of PGC1α in A375P cells showed a strong decrease in mitochondrial membrane potential as measured using J-aggregation fluorescent assay (Figure 5A). Intracellular concentrations of ROS were significantly increased in PGC1α-depleted cells (Figure 5B), and this was associated with a decrease in glutathione (GSH), cystathionine, and 5-adenosylhomocysteine levels (Figure 5C). Importantly, elevated ROS levels were necessary to mediate apoptosis in PGC1α knockdown cells, because two different antioxidants, N-acetyl-L-cysteine (NAC) and Trolox, largely suppressed caspase and PARP cleavages and the number of apoptotic cells (Figure 5D).

To determine whether ROS detoxification genes decrease in PGC1α-depleted cells and might contribute to apoptosis, we analyze the microarray data described in Figure 1. Consistent with previous data in non-transformed cells (St-Pierre et al., 2006), a set of genes involved in the ROS detoxification, including different glutathione synthase enzymes, thioredoxins, glutaredoxin, peroxiredoxins, and *SOD2*, were decreased in PGC1α knockdown cells. These results were confirmed using qPCR of several of these genes (Figure 5E). SOD2 protein levels were substantially decreased in PGC1α-depleted melanoma cells (Figure 5F). Moreover, ectopic expression of PGC1α in A375 increased ROS detoxification genes (Figure 5G). These data supports a key role for PGC1α in activating the ROS detoxification gene program to maintain melanoma cell survival.

As we have showed that *PGC1α* is a target of MITF, we next investigated the role of PGC1α downstream of MITF in promoting survival and proliferation. Overexpression of PGC1α could partially overcome the effects of knockdown MITF on DNA damage and increase of p27 levels (Figure S5A). In addition, treatment of MITF-depleted cells with the antioxidant NAC partially blocked the apoptotic effects (Figure S5B). Together, these results suggest that downregulation of PGC1α contributes to the phenotypic effects of MITF knockdown in PGC1α-expressing cells.

Depletion of Several PGC1α Respiratory Chain Targets Mimic the Metabolic and ROS-Dependent Apoptotic Effects of PGC1α Suppression

The reduction in ROS detoxification genes and GSH levels could be one of the mechanisms by which depletion of PGC1α in melanoma cells induces intracellular ROS levels. However, defects in mitochondrial bioenergetic function are also known to generate toxic ROS levels. Thus, to understand how PGC1α deficiency caused ROS-mediated apoptosis, we tested whether knockdown of different proteins of the mitochondrial respiratory complexes, which are PGC1α targets, produced similar metabolic and apoptotic defects as PGC1α depletion. Therefore, Ndufs3, Cox5a, and ATP5b were efficiently knocked down in A375P melanoma cells (Figure 6A). Individual depletion of these three mitochondrial proteins caused a similar metabolic phenotype as PGC1α knockdown cells, leading to decreases in oxygen consumption and increases in glucose uptake and lactate secretion (Figures 6B and 6C). Consistent with an increase in intracellular ROS levels in these cells, GSH levels were also decreased (Figure 6D). Moreover, increased ROS concentrations caused by depletion of these mitochondrial proteins lead to increased cleavage of proapoptotic proteins (Figures 6E and 6F). To support the role of ROS mediating cell death, treatment with antioxidants NAC and Trolox largely prevented PARP cleavage (Figure 6G). Together, these results suggest that PGC1α-positive melanoma cells are highly sensitive to the induction of ROS due, at least in part, to the disruption of the mitochondria respiratory complex.

PGC1α Protects against ROS-Induced Apoptosis in Human Melanoma Cells and Tumors

The increased ROS levels in cancer cells makes them more dependent in their antioxidant capacity for cell survival, a principle that is exploited by anticancer drugs, such as piperlongumine or phenethyl isothiocyanate (PEITC). In fact, transformed cells have been shown to be exquisitely more sensitive to ROS-inducing drugs than nontransformed cells (Trachootham et al., 2006; Raj et al., 2011). Based on the results presented above that PGC1α controls the antioxidant capacity affecting cell survival, we investigated if PGC1α, by reducing ROS levels and enhancing the antioxidant capacity, could influence the sensitivity to ROS-inducing drugs in melanoma cells. Depletion of PGC1α in A375P cells enhanced their sensitivity to apoptosis induced by H_2O_2, PEITC, or piperlongumine, all of which are known to increase intracellular ROS concentrations (Trachootham et al., 2006; Raj et al., 2011). These effects were not generalized to all drugs, as the B-Raf inhibitor PLX4032 had similar effects in PGC1α control or knockdown A375P cells (Figures 7A and S6A). Furthermore, similar effects on the sensitivity to these compounds were observed after knockdown of several mitochondrial proteins (Ndufs3, Cox5a, and ATP5b)

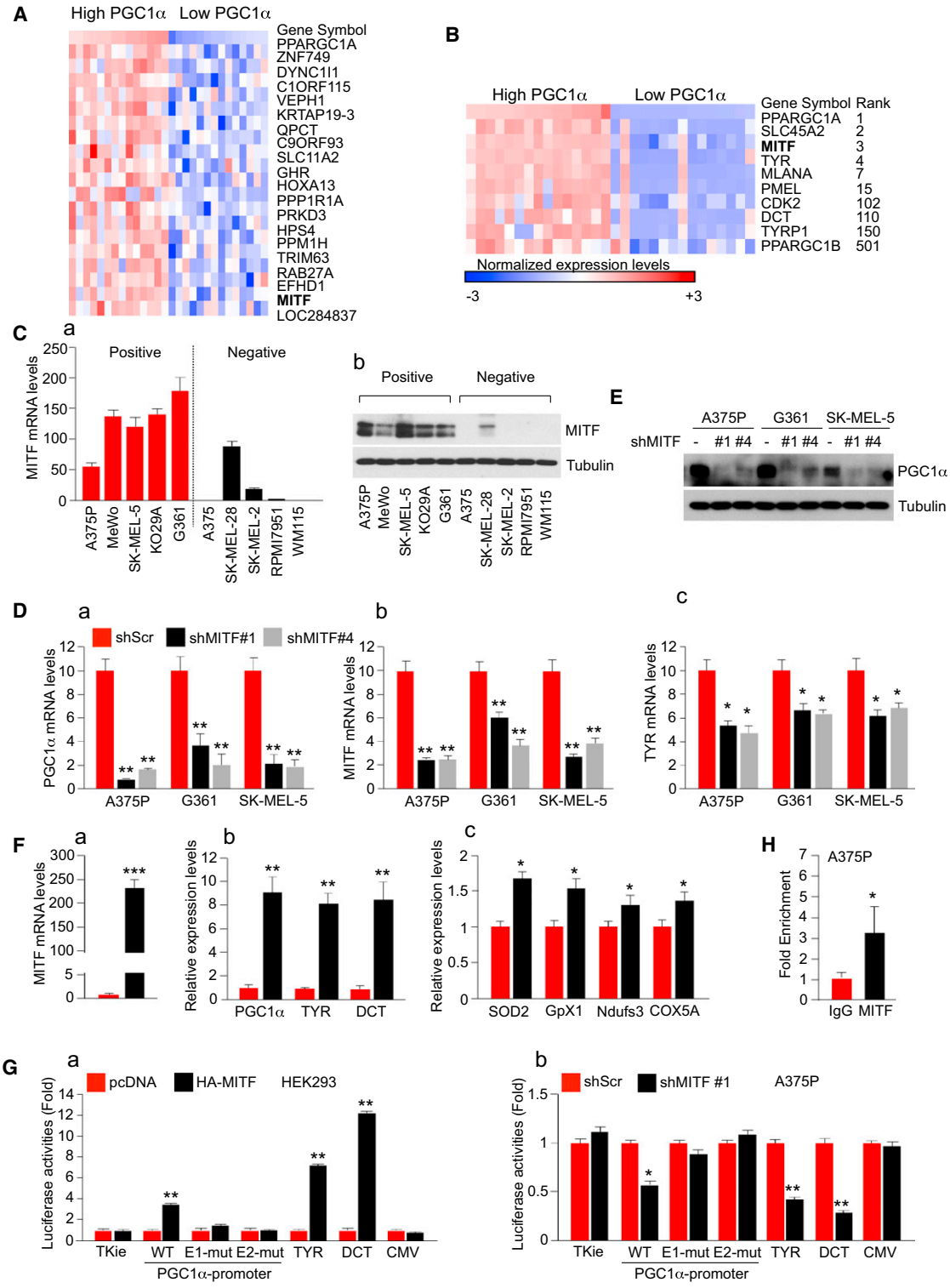

Figure 2. MITF Is Necessary to Maintain High Levels of PGC1α Gene Expression in Melanoma Cells

(A) Heat map of the top 20 genes differentially expressed between the top and the bottom 25% of melanoma samples ranked by *PGC1α* expression levels. Expression data were extracted from the GSE7553 data set. The gene list shown is ranked by signal to noise.

(B) Heat map of selected differentially expressed genes between the top and the bottom 25% of melanoma samples ranked by *PGC1α* expression levels. Expression data were extracted from the CCLE database. The rank of the genes by signal to noise is shown.

(C) (a) *MITF* mRNA and (b) protein expression levels in five PGC1α-positive and five PGC1α-negative melanoma cell lines. Values represent mean ± SD of three independent experiments performed in triplicate.

(legend continued on next page)

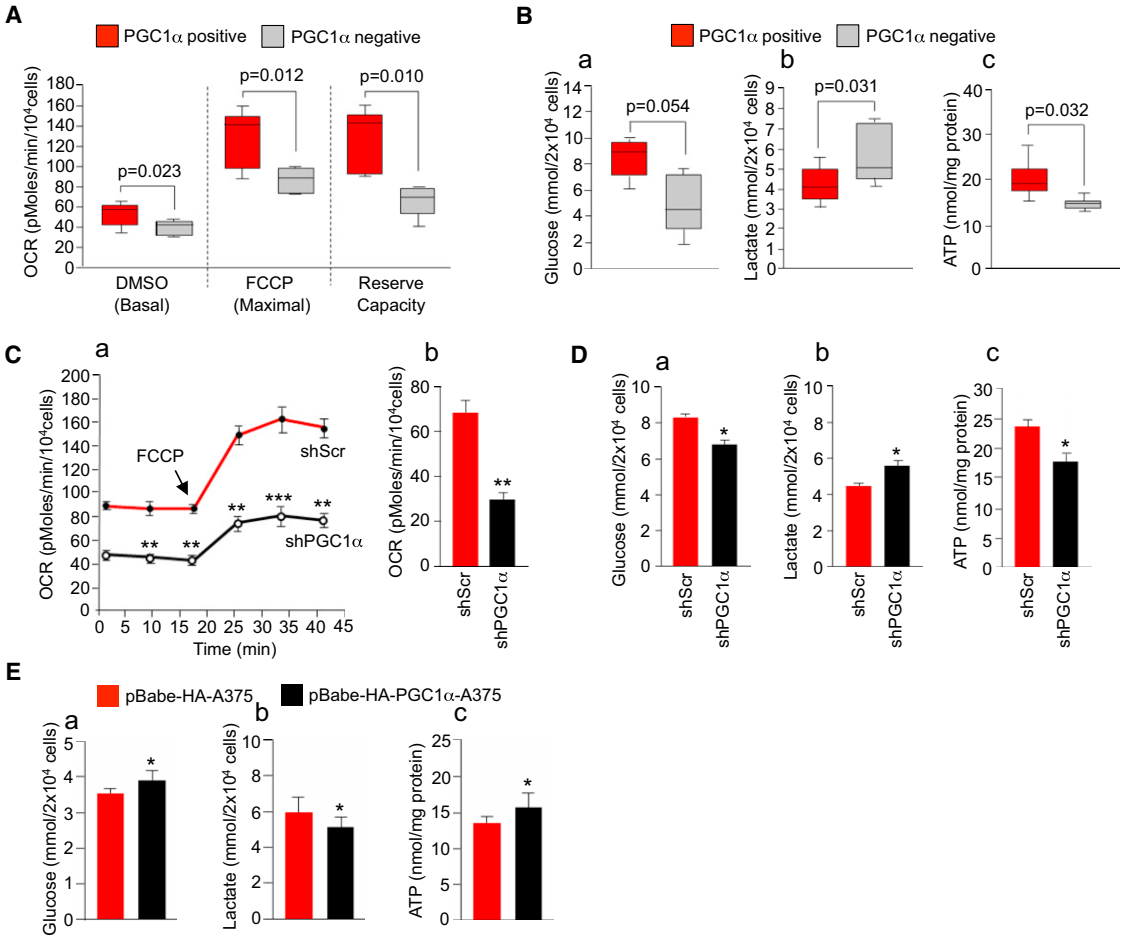

Figure 3. PGC1α Defines the Metabolic and Energetic Program of Human Melanoma Cells

(A) Basal and maximal oxygen consumption rates (OCR) in PGC1α-positive and negative cells measured in DMSO control or FCCP-treated cells. The reserve capacity was calculated by subtracting the basal from the maximum OCR. Values of two independent experiments performed in quadruplicate were averaged. The whiskers in the box plots represent the maximum and the minimum value.

(B) (a) Glucose (in the culture media), (b) lactate (in the culture media), and (c) intracellular ATP levels of PGC1α-positive compared to PGC1α-negative cells. Values of three independent experiments performed in duplicate were averaged. The whiskers in the box plots represent the maximum and the minimum value.

(C) (a) Real-time measurement of basal and maximal (after addition of FCCP) OCR and (b) basal OCR in control and PGC1α knockdown cells. Values represent mean ± SD of two independent experiments performed in quadruplicate. **p < 0.01 and ***p < 0.001.

(D) (a) Glucose (in the culture media), (b) lactate (in the culture media), and (c) intracellular ATP levels in control and PGC1α knockdown cells. Values represent mean ± SD of three independent experiments performed in duplicate. *p < 0.05.

(E) (a) Glucose (in the culture media), (b) lactate (in the culture media), and (c) intracellular ATP levels in cells overexpressing PGC1α. A375 cells stably expressing HA-PGC1α were used. Values represent mean ± SD of three independent experiments performed in duplicate. *p < 0.05.

See also Figure S3.

(Figure 7A). Consistent with these results, piperlongumine had a more potent effect, inducing apoptosis in PGC1α-negative cells (Figures 7B and 7C). Furthermore, ROS levels after piperlongumine treatment were higher in four out of the five PGC1α-negative compared to five PGC1α-positive cell lines tested (Figures 7D and S6B). To further support the role of

(D) qPCR analysis of (a) *PGC1α*, (b) MITF targets, and (c) *TYR* in shRNA *MITF* melanoma cell lines. Values represent mean ± SD of three independent experiments performed in triplicate. *p < 0.05 and **p < 0.01.

(E) Western blot analysis of PGC1α protein expression levels in control and MITF knockdown melanoma cell lines.

(F) qPCR analysis of (a) *MITF*, (b) MITF targets, and (c) PGC1α target mRNAs in A375 melanoma cells ectopically expressing MITF. Values represent mean ± SD of two independent experiments performed in triplicate. *p < 0.05, **p < 0.01, and ***p < 0.001.

(G) *PGC1α* promoter luciferase analysis using transient transfection with the indicated plasmids performed in (a) 293 and (b) A375P cells. Values represent mean ± SD of two independent experiments performed in triplicate. *p < 0.05 and **p < 0.01. A representation of the construct is shown in Figure S2D.

(H) ChiP analysis at the *PGC1α* promoter in A375P cells using an antibody against MITF and immunoglobulin G (IgG) as a control. Values represent mean ± SD of two independent experiments performed in triplicate. *p < 0.05.

See also Figure S2.

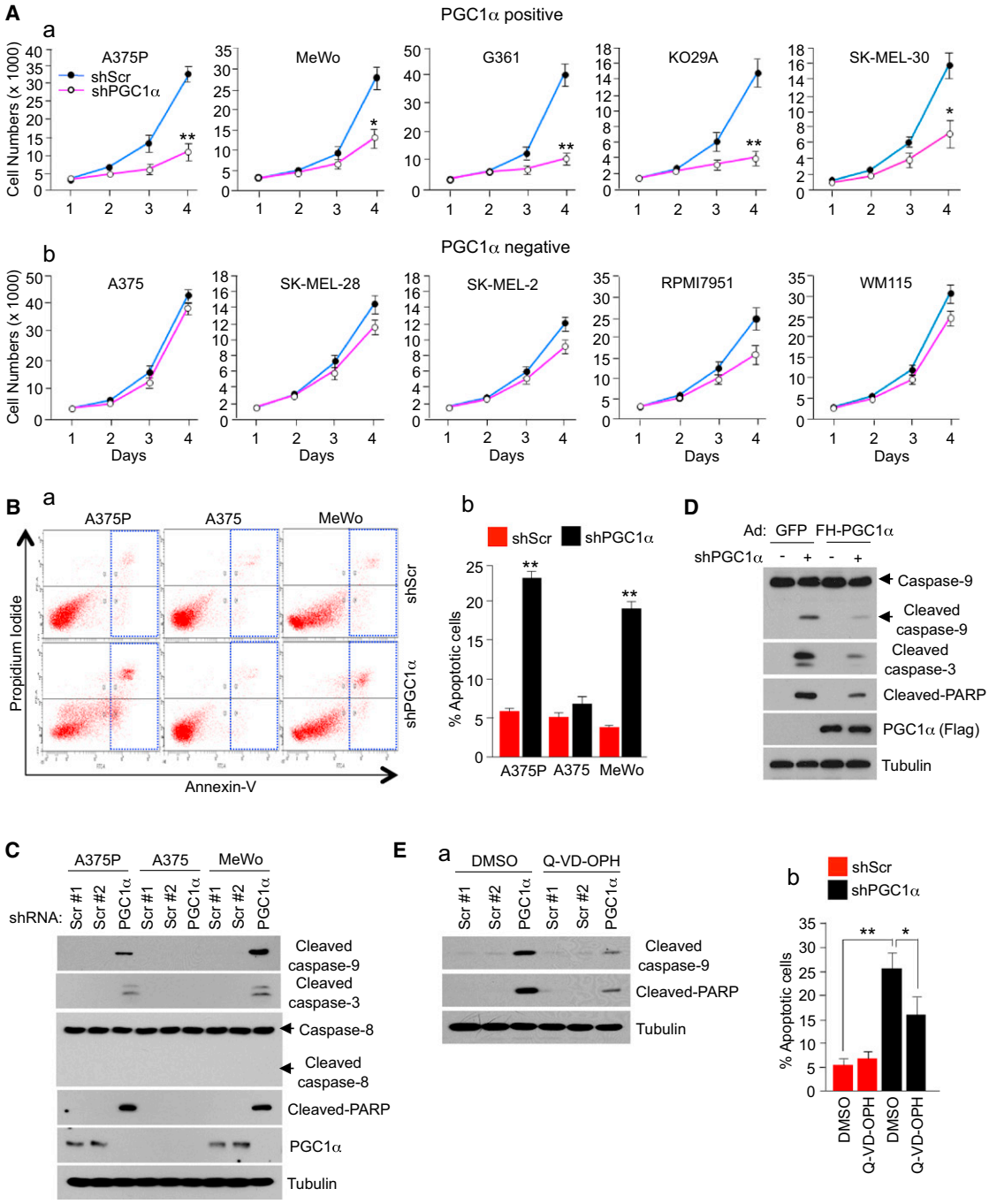

Figure 4. PGC1α Is Essential for Survival in Human Melanoma Cells

(A) Cell number analysis after PGC1α knockdown in (a) PGC1α-positive and (b) PGC1α-negative melanoma cells measured for 4 days after puromycin selection. Values on the graph represent mean ± SD of three independent experiments performed in quadruplicate. *$p < 0.05$ and **$p < 0.01$.

(B) (a) Annexin V analysis of apoptosis after PGC1α knockdown in PGC1α-positive melanoma cells. (b) Quantitation of the percentage of apoptotic cells. Data represent mean ± SD of three independent experiments performed in triplicate. **$p < 0.01$.

(C) Western blot analysis of cleaved apoptotic proteins in PGC1α knocked down and control melanoma cells.

(D) Western blot analysis of cleaved apoptotic proteins in cells expressing ectopic PGC1α in control and PGC1α knockdown A375P melanoma cells.

(E) Apoptosis measured by (a) western blot analysis of caspases and PARP cleavages or (b) Annexin V assays in PGC1α knocked down and control A375P cells treated with 20 μM Q-VD-OPH (a pan-caspase inhibitor) for 2 days. Values on the graph represent mean ± SD of three independent experiments performed in triplicate. *$p < 0.05$ and **$p < 0.01$.

See also Figure S4.

PGC1α-mediating resistance to ROS-induced apoptosis, ectopic expression of PGC1α in PGC1α-negative cell lines prevented piperlongumine-induced cleavage of caspase 9 and PARP (Figure 7E).

Finally, to evaluate the impact of PGC1α depletion on tumor growth, subcutaneous injections of control and PGC1α-depleted A375P cells were performed in nude mice and the size of the resulting tumors was measured. As shown in Figure 8A, there was a significant reduction in tumor size in PGC1α-depleted cells, suggesting that PGC1α is important for tumor progression. Importantly, piperlongumine treatment for 7 days had a greater reduction of tumor volume of xenografts derived from PGC1α knockdown cells compared to control xenografts. The magnitude of these effects correlated with induction of apoptotic markers in these tumors (Figure 8B). The growth of these tumors did not affect body weight (Figure 8C). Collectively, these data suggest that PGC1α expression confers resistance to drugs that induce intracellular ROS levels in melanoma cells and tumors.

DISCUSSION

Cancer cells reprogram their metabolism to meet anabolic and energetic demands necessary for growth and survival. It is becoming clear, however, that tumor cells do not employ a single strategy to accomplish this, as cancers can choose from a variety of metabolic programs to meet their demands. Here, we provide a clear example of this metabolic reprogramming heterogeneity by showing that cells derived from the one tumor type can have profound differences in their metabolic state. In melanomas, expression levels of PGC1α metabolically define two types of tumors with different bioenergetic and ROS detoxification capacities, thereby affecting the ability to survive under oxidative stress. It is conceivable that, in certain low nutrient conditions, elevated mitochondrial capacity might be more efficient to generate ATP necessary for survival without compromising anaplerotic reactions to support cell growth.

Our findings show that a subset of melanoma cells acquire high levels of PGC1α that depend on an increased activity of the melanoma oncogene MITF. This would confer a selective advantage to melanocytic tumor cells by providing a strong protection against oxidative damage. A large subset of melanoma tumors has very low or undetectable levels of *PGC1α* that, to a large extent, overlaps with low levels of *MITF*. These less differentiated tumors use a different metabolic strategy of increased glycolysis for growth and survival. It is also possible that melanoma tumors transit through different states during tumor progression with high or low expression levels of PGC1α. In fact, we provide here an example of this possibility: the PGC1α-negative melanoma cell line A375 was derived from a metastatic tumor produced by the PGC1α-positive parental cell line A375P (Clark et al., 2000). It is likely that A375 cells lost their melanocytic differentiation state, since they express very low levels of MITF and differentiation markers. Concomitant to this loss of differentiation, they became MITF and PGC1α independent for tumor progression. Thus, similar to MITF, PGC1α effects on melanomagenesis may be context dependent. PGC1α controls *MITF* gene expression. contributing to the maintenance of survival in melanomas. Interestingly, peroxisome proliferator-activated receptor γ, a transcription factor known to bind PGC1α (Puigserver et al., 1998), regulates *MITF* (Grabacka et al., 2008), suggesting that it might be involved in this process.

These results provide the basis for some potential anticancer therapeutic strategies targeting cellular metabolism. PGC1α-positive cells depend on PGC1α for survival, suggesting that PGC1α itself or one of its target genes could be a therapeutic target. In this regard, although small molecules targeting PGC1α do not currently exist, inhibitors of estrogen-related receptors (ERRs), key PGC1 transcription factor partners (Mootha et al., 2004; Chang et al., 2011; Schreiber et al., 2004; Eichner and Giguère, 2011; Wende et al., 2005), could potentially be used to inhibit PGC1α function. Because several transcription factors, including nuclear respiratory factors, ERRs, and YY1 (Scarpulla, 2011; Knutti and Kralli, 2001; Cunningham et al., 2007), control PGC1α function, future studies will focus to assess which transcription factor(s) partners with PGC1α to control mitochondrial function and ROS detoxification genes in melanomas. Our data also show that PGC1α-positive cells are more sensitive to disruption of mitochondrial respiration, suggesting that specific inhibition of respiratory chain complexes could be another vulnerability that could be exploited in this tumor subtype. Importantly, melanoma cells can adapt their metabolism and become PGC1α independent, underscoring metabolic flexibility as a potential hurdle on developing drugs against metabolic targets. Conversely, PGC1α-negative melanoma cells have reduced bioenergetic capacity together with lower levels of antioxidant enzymes. As a result, these tumor cells are more sensitive and vulnerable to toxic oxidative stress. This metabolic vulnerability provides a therapeutic strategy to treat this subtype of melanoma tumors (Figure 7). In fact, here we find that ROS-inducing drugs, such as piperlongumine or PEITC, that have been shown to preferentially kill transformed over normal cells (Raj et al., 2011; Trachootham et al., 2006) showed increased potency in PGC1α-negative melanoma cells.

In summary, our work has revealed that melanoma tumors present heterogeneous metabolic and energetic states defined by levels of PGC1α expression. These studies illustrate how reprogramming metabolism and energy in tumor cells is genetic dependent and how this information might be used to develop cancer therapy targeting regulatory metabolic networks.

EXPERIMENTAL PROCEDURES

Cell Culture and Virus Infection

Melanoma cell lines were cultured in high glucose Dulbecco's modified Eagle's medium supplemented with 10% fetal bovine serum. Immortalized primary melanocytes transduced with pBABE-hygro-*hTERT*, pLNCX2-*CDK4*(R24C), and pBABE-puro-*p53*DD were generated as described (Garraway et al., 2005). Lentiviruses were produced by transfecting HEK293T cells with pLKO and packaging vectors, as previously described (Moffat et al., 2006) using PolyFect (QIAGEN). Retroviral particles were produced by transfecting HEK293T cells with the pBabe or pWZL vectors and packaging vector (pCL-Ampho) using PolyFect (QIAGEN). GFP control and Flag-HA-PGC1α adenovirus have been previously described (Lerin et al., 2006).

Animal Studies

All animal studies were performed with an approved protocol from the Beth Israel Deaconess Medical Center Institutional Animal Care and Use Committee

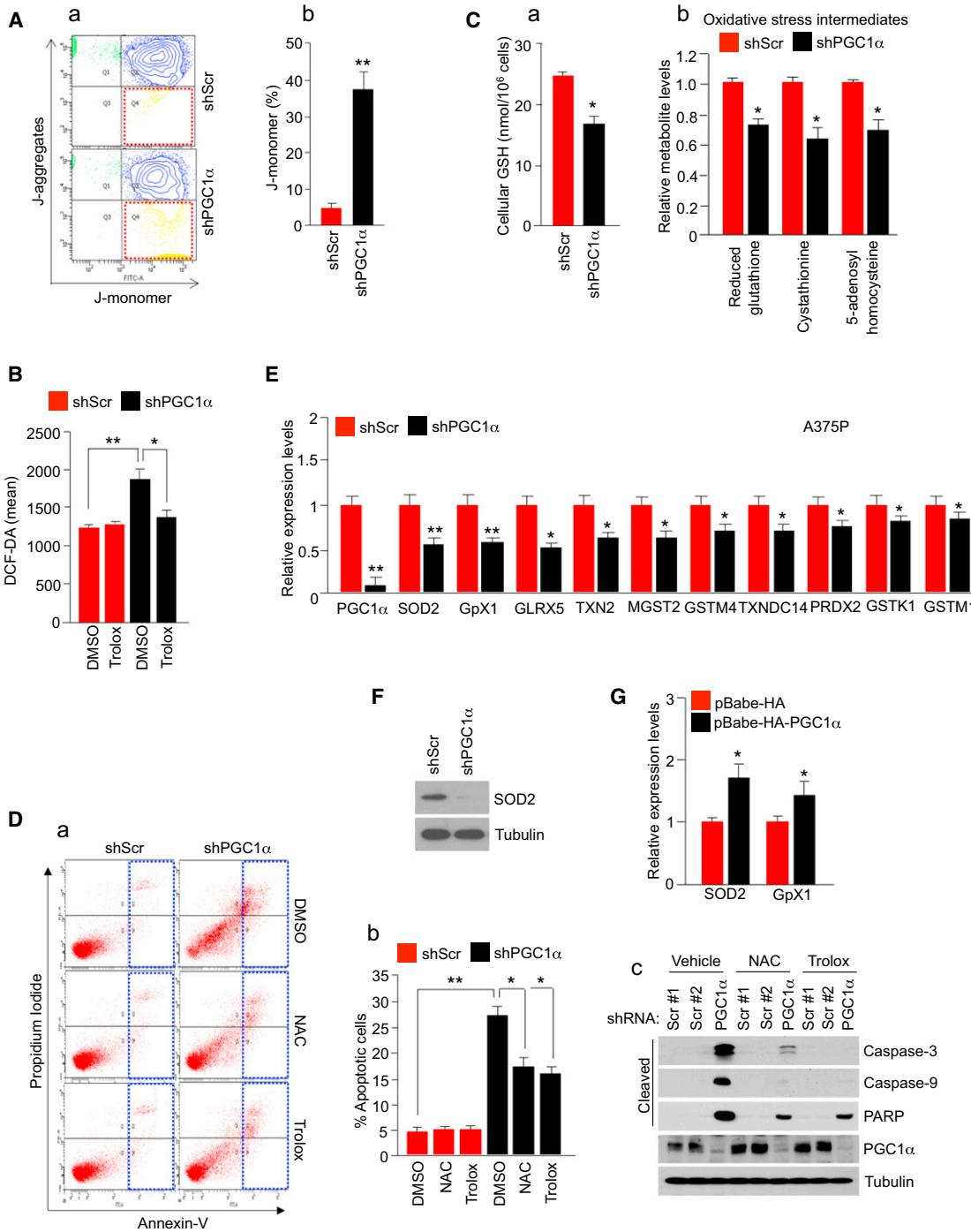

Figure 5. Depletion of PGC1α Triggers an Increase in ROS Levels, Causing Apoptosis

(A) (a) Mitochondrial membrane potential measured by the JC-1 dye in PGC1α knocked down and control A375P cells. (b) Quantitation of the percentage of J-monomer. Values on the graph represent mean ± SD of three independent experiments performed in duplicate. **$p < 0.01$.

(B) ROS levels in control and PGC1α knockdown A375P cells measured using the DCF-DA dye. Values represent mean ± SD of three independent experiments performed in triplicate. *$p < 0.05$ and **$p < 0.01$.

(C) (a) Total GSH levels and (b) oxidative stress intermediates in PGC1α knocked down and control A375P cells. Values represent mean ± SD of three independent experiments performed in triplicate. *$p < 0.05$.

(D) Analysis of apoptosis in A375P cells (control and PGC1α knocked down) treated with 2 mM NAC or 100 μM Trolox for 2 days. (a) Annexin V diagram, (b) quantitation of the percentage of apoptotic cells using the Annexin V assay, and (c) western blot analysis of caspases and PARP cleavages. Values on the graph represent mean ± SD three independent experiments performed in triplicate. *$p < 0.05$ and **$p < 0.01$.

(E) mRNA expression levels of ROS detoxification genes in PGC1α knockdown A375P melanoma cells. Values represent mean ± SD of three independent experiments performed in triplicate. *$p < 0.05$ and **$p < 0.01$.

(legend continued on next page)

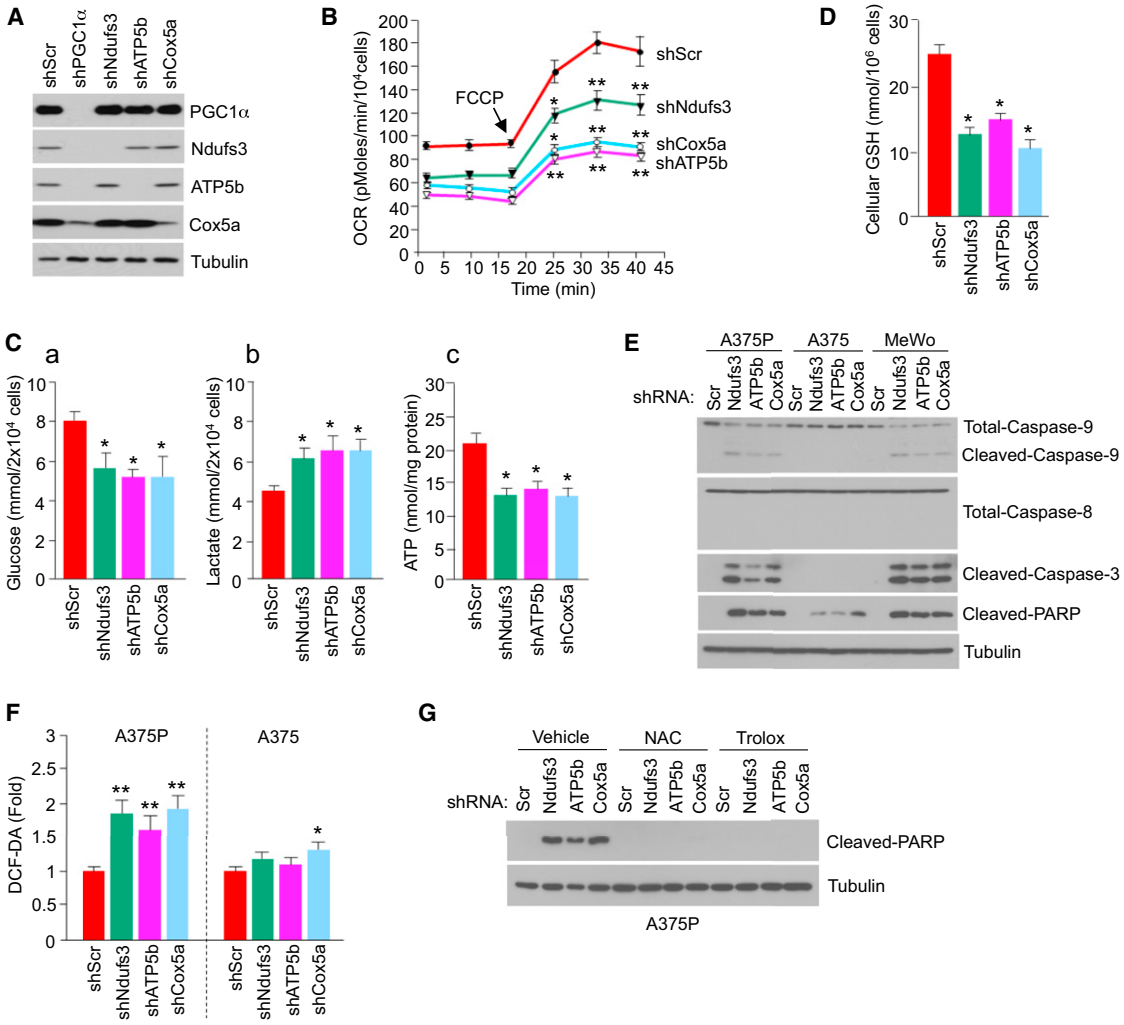

Figure 6. Induction of ROS-Mediated Apoptosis by Depletion of Mitochondrial Respiration PGC1α Target Genes

(A) Depletion of PGC1α and mitochondrial proteins in A375P melanoma cells.

(B) Real-time measurement of basal and maximal (after addition of FCCP) OCR after knockdown of the indicated genes encoding mitochondrial proteins in A375P. Values represent mean ± SD of two independent experiments performed in triplicate. *$p < 0.05$ and **$p < 0.01$.

(C) (a) Glucose (in the culture media), (b) lactate (in the culture media), and (c) intracellular ATP levels in A375P after knockdown of the indicated mitochondrial genes. Values represent mean ± SD of three independent experiments in duplicate. *$p < 0.05$.

(D) Cellular GSH levels in A375P after knockdown of the indicated mitochondrial genes. Values represent mean ± SD of three independent experiments in duplicate. *$p < 0.05$.

(E) Western blot analysis of apoptotic markers after knockdown of the indicated genes in PGC1α-positive melanoma cells.

(F) ROS levels, measured by DCF-DA fluorescent dye, after depletion of mitochondrial proteins in A375P or A375 melanoma cells. Values represent mean ± SD of three independent experiments in duplicate. *$p < 0.05$ and **$p < 0.01$.

(G) Protein expression levels of cleaved PARP after depletion of mitochondrial proteins in A375P melanoma cells treated with the indicated antioxidants.

(Protocol number 105-2011). For xenograft studies, 1×10^6 A375P cells stably expressing scrambled shRNA control or *PGC1α* shRNA were injected subcutaneously into the flank of nude mice (Taconic) in 100 μl of media. After cell injection, mice were incubated for 15 days to allow tumor growth, and then mice were treated with DMSO or piperlongumine (1.5 mg/kg, intraperitoneally [i.p.]) once a day for 6 days. Tumor volumes were measured with a caliper and calculated using the equation volume = $ab^2/2$, where "a" is the maximal width and "b" is maximal orthogonal width.

Arrays and Gene Set Enrichment Analysis

To generate gene-expression arrays, A375P cells were infected with a control shRNA (small hairpin *GFP* or scrambled short hairpin RNA) or a *PGC1α* shRNA

(F) Western blot analysis of SOD2 protein levels in A375P cells.

(G) *SOD2* and *GpX1* mRNA levels after ectopic expression of PGC1α in A375 cells. Values represent mean ± SD of two independent experiments performed in triplicate. *$p < 0.05$.

See also Figure S5.

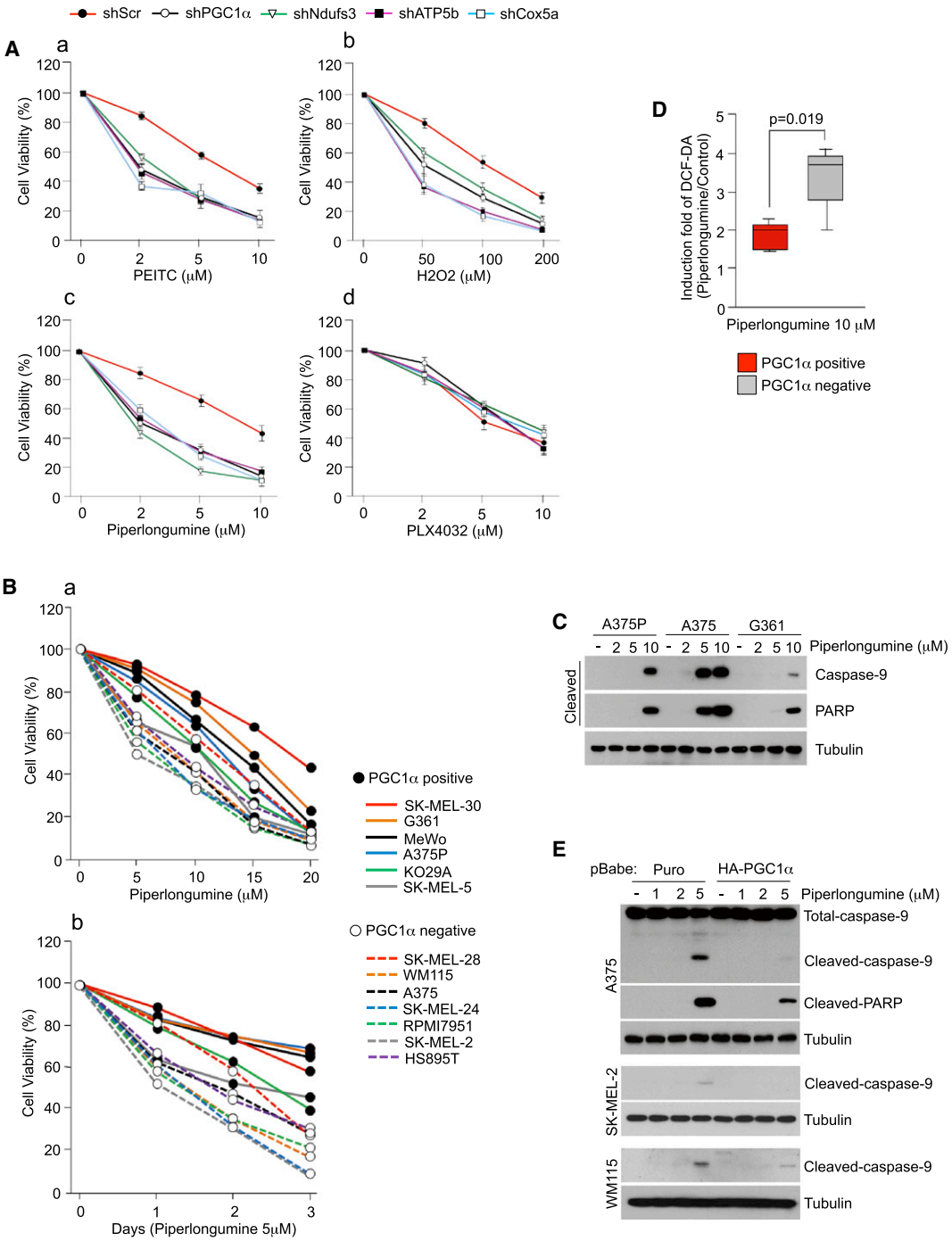

Figure 7. PGC1α Expression Decreases Apoptotic Sensitivity to ROS-Inducing Drugs in Human Melanoma Cells

(A) Cell viability, measured using cell titer glo, after treatment with (a) PEITC, (b) H2O2, (c) piperlongumine, and (d) PLX4032 in A375P cells stably expressing the indicated shRNAs. Values represent mean ± SD of three independent experiments in triplicate.

(B) Cell viability of PGC1α-positive and negative melanoma cell lines treated with piperlongumine at (a) different concentrations and (b) times. Values represent mean of three independent experiments in triplicate.

(C) Analysis of cleaved caspase-9 and PARP in two PGC1α-positive (A375P and G361) and one PGC1α-negative (A375) cell lines treated with piperlongumine.

(D) ROS levels in PGC1α-positive and -negative melanoma cell lines treated with piperlongumine. Values of three independent experiments performed in duplicate were averaged. The whiskers in the box plots represent the maximum and the minimum value.

(E) Analysis of apoptosis using cleavage of apoptotic markers in PGC1α-negative melanoma cell lines ectopically expressing PGC1α and treated with piperlongumine.

See also Figure S6.

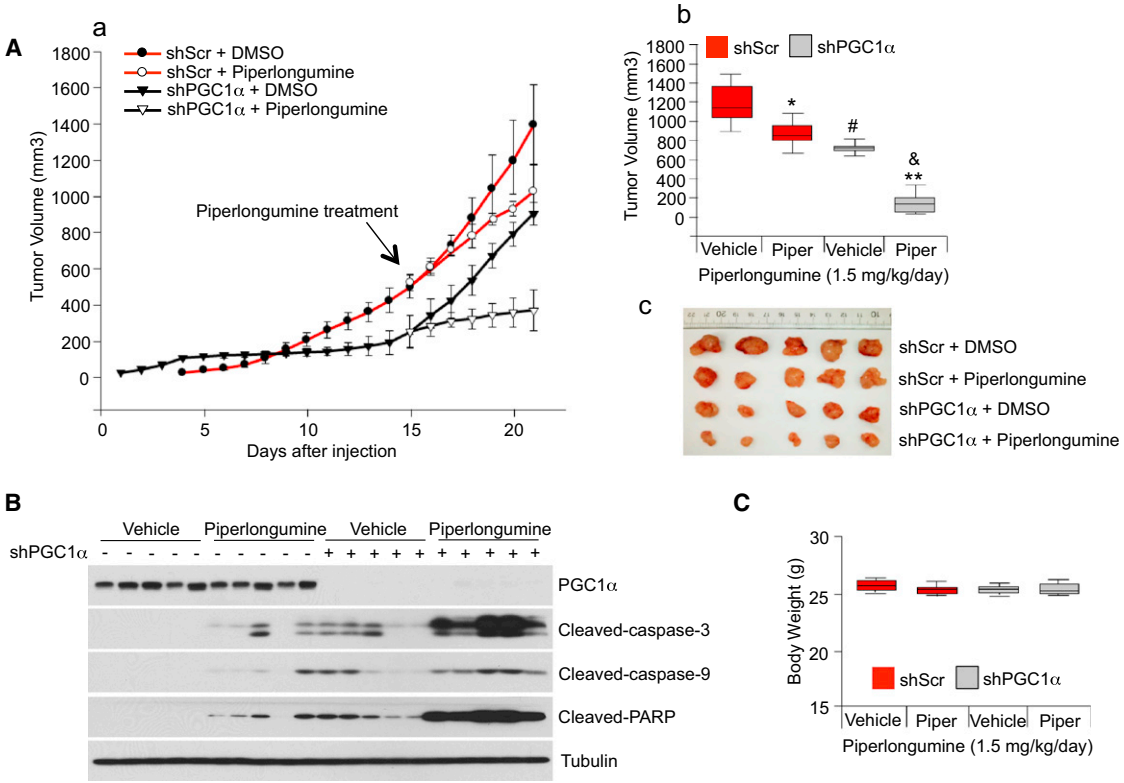

Figure 8. PGC1α Expression Decreases Sensitivity to ROS-Inducing Drugs in Human Melanomas

(A) (a) Tumor volume analysis of xenografts of A375P cells expressing shRNAs against *PGC1α* or control shRNAs. Fifteen days after cell injection, mice were injected daily with piperlongumine (1.5 mg/kg) or DMSO. The tumor growth curves are plotted as mean ± SEM (n = 10, each group). Statistical significance of tumor volumes were calculated by one-way ANOVA with a Tukey posttest; *p < 0.05; **p < 0.01, DMSO versus piperlongumine; #p < 0.05, DMSO/control shRNA versus DMSO/*PGC1α* shRNA; &p < 0.01, piperlongumine/control shRNA versus piperlongumine/*PGC1α* shRNA. (b) In the box plots, final tumor volumes are represented (n = 10). The whiskers in the box plots represent the maximum and the minimum value. (c) Representative images of tumors are shown.
(B) Western blot analysis of apoptotic, cleaved caspases and PARP in PGC1α knocked down tumors treated with piperlongumine.
(C) Body weight measured at the end of experiment. The whiskers in the box plots represent the maximum and the minimum value.

(described in Supplemental Experimental Procedures) in duplicate and selected with puromycin for 48 hr. Four days after selection, RNA was extracted and gene expression arrays were performed using Human Genome U133A 2.0 arrays. To create a gene expression file, CEL files were used as input for the GenePattern (http://www.genepattern.broadinstitute.org) module Expression File Creator using robust multiarray average (RMA) and quantile normalization. The gct file created was used as input for the GSEA analysis.

For the melanoma tumors gene expression analysis, the normalized data set GSE7553 was imported from GEO using the software Gene-e (http://www.broadinstitute.org/software/gene-e). The melanoma samples from the data set were selected to create a gct file. This gct file was used as input for the GSEA algorithm.

To find differentially expressed genes, the probes' values were collapsed using maximum average probe and log2 transformed. The signal to noise marker selection tool from Gene-e was used to find genes differentially expressed between the top and the bottom 25% *PGC1α*-expressing melanoma tumors with 10,000 permutations. The cutoff to select the gene list was fold change >2, false discovery rate (FDR) q < 0.25. For the melanoma cell lines gene expression analysis, the gene-centric RMA-normalized CCLE expression data set was used (http://www.broadinstitute.org/ccle).

The GSEA software v2.0 (http://www.broadinstitute.org/gsea; Subramanian et al., 2005) was used to perform the GSEA analysis. In all the analysis, the Reactome gene sets were used and the number of permutations was changed to 5,000. For the GSEA7553 slice data set, the values of the 219195_at probe (corresponding to *PPARGC1A*) were used as phenotype and the default parameters were used with the exception that Pearson correlation was computed to rank the genes. For the analysis of the A375P data set, the default parameters were used but the permutation type was changed to gene set.

Oxygen Consumption

The oxygen consumption rate was measured using an optical fluorescent oxygen sensor in a Seahorse Bioscience XF24 Extracellular Flux Analyzer. Briefly, cells were seeded in quadruplicate at equal densities (25,000 cells per well) into XF24 tissue culture plates. Cell media was changed 12 hr after cell seeding into unbuffered Dulbecco's modified Eagle's medium (DMEM) (8.3 g/l DMEM [Sigma], 200 mM GlutaMax-1 [Invitrogen], 25 mM D-glucose [Sigma], 63.3 mM NaCl [Sigma], and phenol red [Sigma], adjusted pH to 7.4 with NaOH), according to the manufacturer's protocol. Oxygen consumption was measured under basal conditions and mitochondrial uncoupler trifluoromethoxy carbonyl cyanide phenyl hydrazone (FCCP) (2 μM). Oxygen consumption values were normalized to cell number.

Intracellular ROS and Cellular GSH Levels

To measure intracellular ROS levels, 2 μM dichlorofluorescein diacetate (DCF-DA) (Invitrogen) was used as a fluorescent dye. An equal number of cells were seeded in six well plates, after 72 hr cells were trypsinized, washed once with PBS, and stained with DCF-DA in Hank's balanced salt solution for 30 min at 37°C. Samples were then immediately analyzed by flow cytometry.

A glutathione colorimetric detection kit (BioVision Research Products) was used to measure total cellular glutathione according to the manufacturer's instructions.

ACCESSION NUMBERS

The Gene Expression Omnibus accession number for the gene expression data reported is GSE36879.

SUPPLEMENTAL INFORMATION

Supplemental Information includes six figures, three tables, and Supplemental Experimental Procedures and can be found with this article online at http://dx.doi.org/10.1016/j.ccr.2012.11.020.

ACKNOWLEDGMENTS

We thank the Dana-Farber Cancer Institute Microarray Core Facility for performing the gene-expression arrays and the Dana-Farber RNAi facility for the shRNA constructs. These studies were funded by the Claudia Adams Barr Program in Cancer Research and Dana-Farber Cancer Institute funds. H.R.W. acknowledges support from P50CA093683.

Received: March 30, 2012
Revised: August 3, 2012
Accepted: November 30, 2012
Published: February 14, 2013

REFERENCES

Barretina, J., Caponigro, G., Stransky, N., Venkatesan, K., Margolin, A.A., Kim, S., Wilson, C.J., Lehár, J., Kryukov, G.V., Sonkin, D., et al. (2012). The Cancer Cell Line Encyclopedia enables predictive modelling of anticancer drug sensitivity. Nature *483*, 603–607.

Bertolotto, C., Lesueur, F., Giuliano, S., Strub, T., de Lichy, M., Bille, K., Dessen, P., d'Hayer, B., Mohamdi, H., Remenieras, A., et al.; French Familial Melanoma Study Group (2011). A SUMOylation-defective MITF germline mutation predisposes to melanoma and renal carcinoma. Nature *480*, 94–98.

Bogunovic, D., O'Neill, D.W., Belitskaya-Levy, I., Vacic, V., Yu, Y.L., Adams, S., Darvishian, F., Berman, R., Shapiro, R., Pavlick, A.C., et al. (2009). Immune profile and mitotic index of metastatic melanoma lesions enhance clinical staging in predicting patient survival. Proc. Natl. Acad. Sci. USA *106*, 20429–20434.

Chang, C.Y., Kazmin, D., Jasper, J.S., Kunder, R., Zuercher, W.J., and McDonnell, D.P. (2011). The metabolic regulator ERRα, a downstream target of HER2/IGF-1R, as a therapeutic target in breast cancer. Cancer Cell *20*, 500–510.

Choo, A.Y., Kim, S.G., Vander Heiden, M.G., Mahoney, S.J., Vu, H., Yoon, S.O., Cantley, L.C., and Blenis, J. (2010). Glucose addiction of TSC null cells is caused by failed mTORC1-dependent balancing of metabolic demand with supply. Mol. Cell *38*, 487–499.

Clark, E.A., Golub, T.R., Lander, E.S., and Hynes, R.O. (2000). Genomic analysis of metastasis reveals an essential role for RhoC. Nature *406*, 532–535.

Cunningham, J.T., Rodgers, J.T., Arlow, D.H., Vazquez, F., Mootha, V.K., and Puigserver, P. (2007). mTOR controls mitochondrial oxidative function through a YY1-PGC-1alpha transcriptional complex. Nature *450*, 736–740.

Diehn, M., Cho, R.W., Lobo, N.A., Kalisky, T., Dorie, M.J., Kulp, A.N., Qian, D., Lam, J.S., Ailles, L.E., Wong, M., et al. (2009). Association of reactive oxygen species levels and radioresistance in cancer stem cells. Nature *458*, 780–783.

Eichner, L.J., and Giguère, V. (2011). Estrogen related receptors (ERRs): a new dawn in transcriptional control of mitochondrial gene networks. Mitochondrion *11*, 544–552.

Fernandez-Marcos, P.J., and Auwerx, J. (2011). Regulation of PGC-1α, a nodal regulator of mitochondrial biogenesis. Am. J. Clin. Nutr. *93*, 884S–890S.

Gao, P., Tchernyshyov, I., Chang, T.C., Lee, Y.S., Kita, K., Ochi, T., Zeller, K.I., De Marzo, A.M., Van Eyk, J.E., Mendell, J.T., and Dang, C.V. (2009). c-Myc suppression of miR-23a/b enhances mitochondrial glutaminase expression and glutamine metabolism. Nature *458*, 762–765.

Garraway, L.A., Widlund, H.R., Rubin, M.A., Getz, G., Berger, A.J., Ramaswamy, S., Beroukhim, R., Milner, D.A., Granter, S.R., Du, J., et al. (2005). Integrative genomic analyses identify MITF as a lineage survival oncogene amplified in malignant melanoma. Nature *436*, 117–122.

Grabacka, M., Placha, W., Urbanska, K., Laidler, P., Plonka, P.M., and Reiss, K. (2008). PPAR gamma regulates MITF and beta-catenin expression and promotes a differentiated phenotype in mouse melanoma S91. Pigment Cell Melanoma Res. *21*, 388–396.

Hanahan, D., and Weinberg, R.A. (2011). Hallmarks of cancer: the next generation. Cell *144*, 646–674.

Handschin, C., Chin, S., Li, P., Liu, F., Maratos-Flier, E., Lebrasseur, N.K., Yan, Z., and Spiegelman, B.M. (2007). Skeletal muscle fiber-type switching, exercise intolerance, and myopathy in PGC-1alpha muscle-specific knock-out animals. J. Biol. Chem. *282*, 30014–30021.

Herzig, S., Long, F., Jhala, U.S., Hedrick, S., Quinn, R., Bauer, A., Rudolph, D., Schutz, G., Yoon, C., Puigserver, P., et al. (2001). CREB regulates hepatic gluconeogenesis through the coactivator PGC-1. Nature *413*, 179–183.

Hoek, K.S., Eichhoff, O.M., Schlegel, N.C., Döbbeling, U., Kobert, N., Schaerer, L., Hemmi, S., and Dummer, R. (2008). In vivo switching of human melanoma cells between proliferative and invasive states. Cancer Res. *68*, 650–656.

Kelly, D.P., and Scarpulla, R.C. (2004). Transcriptional regulatory circuits controlling mitochondrial biogenesis and function. Genes Dev. *18*, 357–368.

Knutti, D., and Kralli, A. (2001). PGC-1, a versatile coactivator. Trends Endocrinol. Metab. *12*, 360–365.

Lerin, C., Rodgers, J.T., Kalume, D.E., Kim, S.H., Pandey, A., and Puigserver, P. (2006). GCN5 acetyltransferase complex controls glucose metabolism through transcriptional repression of PGC-1alpha. Cell Metab. *3*, 429–438.

Lin, J., Wu, H., Tarr, P.T., Zhang, C.Y., Wu, Z., Boss, O., Michael, L.F., Puigserver, P., Isotani, E., Olson, E.N., et al. (2002). Transcriptional co-activator PGC-1 alpha drives the formation of slow-twitch muscle fibres. Nature *418*, 797–801.

Lin, W.M., Baker, A.C., Beroukhim, R., Winckler, W., Feng, W., Marmion, J.M., Laine, E., Greulich, H., Tseng, H., Gates, C., et al. (2008). Modeling genomic diversity and tumor dependency in malignant melanoma. Cancer Res. *68*, 664–673.

Moffat, J., Grueneberg, D.A., Yang, X., Kim, S.Y., Kloepfer, A.M., Hinkle, G., Piqani, B., Eisenhaure, T.M., Luo, B., Grenier, J.K., et al. (2006). A lentiviral RNAi library for human and mouse genes applied to an arrayed viral high-content screen. Cell *124*, 1283–1298.

Mootha, V.K., Lindgren, C.M., Eriksson, K.F., Subramanian, A., Sihag, S., Lehar, J., Puigserver, P., Carlsson, E., Ridderstråle, M., Laurila, E., et al. (2003). PGC-1alpha-responsive genes involved in oxidative phosphorylation are coordinately downregulated in human diabetes. Nat. Genet. *34*, 267–273.

Mootha, V.K., Handschin, C., Arlow, D., Xie, X., St Pierre, J., Sihag, S., Yang, W., Altshuler, D., Puigserver, P., Patterson, N., et al. (2004). Erralpha and Gabpa/b specify PGC-1alpha-dependent oxidative phosphorylation gene expression that is altered in diabetic muscle. Proc. Natl. Acad. Sci. USA *101*, 6570–6575.

Ohta, T., Iijima, K., Miyamoto, M., Nakahara, I., Tanaka, H., Ohtsuji, M., Suzuki, T., Kobayashi, A., Yokota, J., Sakiyama, T., et al. (2008). Loss of Keap1 function activates Nrf2 and provides advantages for lung cancer cell growth. Cancer Res. *68*, 1303–1309.

Padmanabhan, B., Tong, K.I., Ohta, T., Nakamura, Y., Scharlock, M., Ohtsuji, M., Kang, M.I., Kobayashi, A., Yokoyama, S., and Yamamoto, M. (2006). Structural basis for defects of Keap1 activity provoked by its point mutations in lung cancer. Mol. Cell *21*, 689–700.

Puigserver, P., and Spiegelman, B.M. (2003). Peroxisome proliferator-activated receptor-gamma coactivator 1 alpha (PGC-1 alpha): transcriptional coactivator and metabolic regulator. Endocr. Rev. *24*, 78–90.

Puigserver, P., Wu, Z., Park, C.W., Graves, R., Wright, M., and Spiegelman, B.M. (1998). A cold-inducible coactivator of nuclear receptors linked to adaptive thermogenesis. Cell *92*, 829–839.

Raj, L., Ide, T., Gurkar, A.U., Foley, M., Schenone, M., Li, X., Tolliday, N.J., Golub, T.R., Carr, S.A., Shamji, A.F., et al. (2011). Selective killing of cancer cells by a small molecule targeting the stress response to ROS. Nature *475*, 231–234.

Rhee, J., Inoue, Y., Yoon, J.C., Puigserver, P., Fan, M., Gonzalez, F.J., and Spiegelman, B.M. (2003). Regulation of hepatic fasting response by PPARgamma coactivator-1alpha (PGC-1): requirement for hepatocyte nuclear factor 4alpha in gluconeogenesis. Proc. Natl. Acad. Sci. USA *100*, 4012–4017.

Riker, A.I., Enkemann, S.A., Fodstad, O., Liu, S., Ren, S., Morris, C., Xi, Y., Howell, P., Metge, B., Samant, R.S., et al. (2008). The gene expression profiles of primary and metastatic melanoma yields a transition point of tumor progression and metastasis. BMC Med. Genomics *1*, 13.

Sahin, E., Colla, S., Liesa, M., Moslehi, J., Müller, F.L., Guo, M., Cooper, M., Kotton, D., Fabian, A.J., Walkey, C., et al. (2011). Telomere dysfunction induces metabolic and mitochondrial compromise. Nature *470*, 359–365.

Scarpulla, R.C. (2011). Metabolic control of mitochondrial biogenesis through the PGC-1 family regulatory network. Biochim. Biophys. Acta *1813*, 1269–1278.

Schreiber, S.N., Emter, R., Hock, M.B., Knutti, D., Cardenas, J., Podvinec, M., Oakeley, E.J., and Kralli, A. (2004). The estrogen-related receptor alpha (ERRalpha) functions in PPARgamma coactivator 1alpha (PGC-1alpha)-induced mitochondrial biogenesis. Proc. Natl. Acad. Sci. USA *101*, 6472–6477.

Sen, N., Satija, Y.K., and Das, S. (2011). PGC-1α, a key modulator of p53, promotes cell survival upon metabolic stress. Mol. Cell *44*, 621–634.

Shibata, T., Ohta, T., Tong, K.I., Kokubu, A., Odogawa, R., Tsuta, K., Asamura, H., Yamamoto, M., and Hirohashi, S. (2008). Cancer related mutations in NRF2 impair its recognition by Keap1-Cul3 E3 ligase and promote malignancy. Proc. Natl. Acad. Sci. USA *105*, 13568–13573.

Singh, A., Misra, V., Thimmulappa, R.K., Lee, H., Ames, S., Hoque, M.O., Herman, J.G., Baylin, S.B., Sidransky, D., Gabrielson, E., et al. (2006). Dysfunctional KEAP1-NRF2 interaction in non-small-cell lung cancer. PLoS Med. *3*, e420.

St-Pierre, J., Drori, S., Uldry, M., Silvaggi, J.M., Rhee, J., Jäger, S., Handschin, C., Zheng, K., Lin, J., Yang, W., et al. (2006). Suppression of reactive oxygen species and neurodegeneration by the PGC-1 transcriptional coactivators. Cell *127*, 397–408.

Strub, T., Giuliano, S., Ye, T., Bonet, C., Keime, C., Kobi, D., Le Gras, S., Cormont, M., Ballotti, R., Bertolotto, C., and Davidson, I. (2011). Essential role of microphthalmia transcription factor for DNA replication, mitosis and genomic stability in melanoma. Oncogene *30*, 2319–2332.

Subramanian, A., Tamayo, P., Mootha, V.K., Mukherjee, S., Ebert, B.L., Gillette, M.A., Paulovich, A., Pomeroy, S.L., Golub, T.R., Lander, E.S., and Mesirov, J.P. (2005). Gene set enrichment analysis: a knowledge-based approach for interpreting genome-wide expression profiles. Proc. Natl. Acad. Sci. USA *102*, 15545–15550.

Tait, S.W., and Green, D.R. (2010). Mitochondria and cell death: outer membrane permeabilization and beyond. Nature Rev. Mol. Cell Biol. *11*, 621–632.

Trachootham, D., Zhou, Y., Zhang, H., Demizu, Y., Chen, Z., Pelicano, H., Chiao, P.J., Achanta, G., Arlinghaus, R.B., Liu, J., and Huang, P. (2006). Selective killing of oncogenically transformed cells through a ROS-mediated mechanism by beta-phenylethyl isothiocyanate. Cancer Cell *10*, 241–252.

Trachootham, D., Alexandre, J., and Huang, P. (2009). Targeting cancer cells by ROS-mediated mechanisms: a radical therapeutic approach? Nat. Rev. Drug Discov. *8*, 579–591.

Weinberg, F., and Chandel, N.S. (2009). Mitochondrial metabolism and cancer. Ann. N Y Acad. Sci. *1177*, 66–73.

Wende, A.R., Huss, J.M., Schaeffer, P.J., Giguère, V., and Kelly, D.P. (2005). PGC-1alpha coactivates PDK4 gene expression via the orphan nuclear receptor ERRalpha: a mechanism for transcriptional control of muscle glucose metabolism. Mol. Cell. Biol. *25*, 10684–10694.

Wise, D.R., DeBerardinis, R.J., Mancuso, A., Sayed, N., Zhang, X.Y., Pfeiffer, H.K., Nissim, I., Daikhin, E., Yudkoff, M., McMahon, S.B., and Thompson, C.B. (2008). Myc regulates a transcriptional program that stimulates mitochondrial glutaminolysis and leads to glutamine addiction. Proc. Natl. Acad. Sci. USA *105*, 18782–18787.

Yokoyama, S., Woods, S.L., Boyle, G.M., Aoude, L.G., MacGregor, S., Zismann, V., Gartside, M., Cust, A.E., Haq, R., Harland, M., et al. (2011). A novel recurrent mutation in MITF predisposes to familial and sporadic melanoma. Nature *480*, 99–103.

Zaugg, K., Yao, Y., Reilly, P.T., Kannan, K., Kiarash, R., Mason, J., Huang, P., Sawyer, S.K., Fuerth, B., Faubert, B., et al. (2011). Carnitine palmitoyltransferase 1C promotes cell survival and tumor growth under conditions of metabolic stress. Genes Dev. *25*, 1041–1051.

Cancer Cell
Article

Oncogenic BRAF Regulates Oxidative Metabolism via PGC1α and MITF

Rizwan Haq,[1,2] Jonathan Shoag,[4] Pedro Andreu-Perez,[2] Satoru Yokoyama,[2,5] Hannah Edelman,[2] Glenn C. Rowe,[4] Dennie T. Frederick,[3] Aeron D. Hurley,[6] Abhinav Nellore,[7] Andrew L. Kung,[8] Jennifer A. Wargo,[3] Jun S. Song,[7] David E. Fisher,[1,2,9,*] Zolt Arany,[4,9,*] and Hans R. Widlund[6,9,*]

[1]Massachusetts General Hospital Cancer Center
[2]Department of Dermatology, Cutaneous Biology Research Center
[3]Department of Surgery
Massachusetts General Hospital, 55 Fruit Street, Boston, MA 02114, USA
[4]Cardiovascular Institute, Beth Israel Deaconess Medical Center, Boston, MA 02116, USA
[5]Division of Pathogenic Biochemistry, Institute of Natural Medicine, University of Toyama, 2630 Sugitani, Toyama 930-0194, Japan
[6]Department of Dermatology, Brigham and Women's Hospital, Boston, MA 02115, USA
[7]Department of Epidemiology and Biostatistics, Institute for Human Genetics, University of California, San Francisco, San Francisco, CA 94143-0794, USA
[8]Department of Pediatrics, Columbia University Medical Center, New York, NY 10032, USA
[9]These authors contributed equally to this work
*Correspondence: dfisher3@partners.org (D.E.F.), zarany@bidmc.harvard.edu (Z.A.), hwidlund@bics.bwh.harvard.edu (H.R.W.)
http://dx.doi.org/10.1016/j.ccr.2013.02.003

SUMMARY

Activating mutations in *BRAF* are the most common genetic alterations in melanoma. Inhibition of BRAF by small molecules leads to cell-cycle arrest and apoptosis. We show here that BRAF inhibition also induces an oxidative phosphorylation gene program, mitochondrial biogenesis, and the increased expression of the mitochondrial master regulator, PGC1α. We further show that a target of BRAF, the melanocyte lineage factor MITF, directly regulates the expression of PGC1α. Melanomas with activation of the BRAF/MAPK pathway have suppressed levels of *MITF* and *PGC1α* and decreased oxidative metabolism. Conversely, treatment of BRAF-mutated melanomas with BRAF inhibitors renders them addicted to oxidative phosphorylation. Our data thus identify an adaptive metabolic program that limits the efficacy of BRAF inhibitors.

INTRODUCTION

Activating mutations in the BRAF protein kinase are the most common genetic alterations in melanoma, found in ~50% of tumors (Davies et al., 2002; Curtin et al., 2005). The most frequent BRAF mutation is the substitution of valine at position 600 by glutamic acid (BRAF V600E) that results in the constitutive activation of its serine/threonine kinase activity and sustained activation of the mitogen-activated protein kinase (MAPK) signal transduction pathway (Davies et al., 2002; Wan et al., 2004). BRAF directly phosphorylates the dual-specificity kinases MEK1 and MEK2, which in turn phosphorylate and activate the MAPKs, ERK1 and ERK2. BRAF has been shown by overexpression and knockdown experiments to be a critical mediator of melanomagenesis. In mice, activation of BRAF in combination with deletion of the tumor suppressor genes *PTEN* or *INK4A* leads to melanoma with complete penetrance (Dankort et al., 2009; Dhomen et al., 2009). Conversely, treatment of BRAF mutant melanomas in vitro with chemical inhibitors of BRAF or MEK1/MEK2 promotes cell-cycle arrest and apoptosis (Hingorani et al., 2003; Karasarides et al., 2004; Hoeflich et al., 2006; Wellbrock et al., 2008). Moreover, the BRAF inhibitor vemurafenib (PLX4032) leads to tumor regression and improved overall survival in patients whose melanomas have

Significance

BRAF mutations are the most common genetic aberrations in melanoma, but the mechanisms by which they promote oncogenesis are poorly understood. Here, we show that activated BRAF promotes metabolic reprogramming by suppression of oxidative phosphorylation through the actions of the melanocyte lineage factor *MITF* and the mitochondrial master regulator PGC1α. BRAF inhibitors, which transiently suppress melanoma growth in vitro and in patients, induce PGC1α and oxidative phosphorylation. This addiction to oxidative phosphorylation in melanomas treated with BRAF-targeted therapy therefore suggests that mitochondrial inhibitors should be evaluated in combination with BRAF pathway inhibitors in vivo.

the BRAF(V600E) mutation, leading to its approval as a treatment for patients with metastatic melanoma (Flaherty et al., 2010; Chapman et al., 2011; Sosman et al., 2012). Despite the promise and dramatic initial effects of BRAF inhibitors in the clinic, patients eventually relapse within a few months, suggesting that combination therapies may be needed to overcome intrinsic or acquired resistance (Gray-Schopfer et al., 2007; Poulikakos and Rosen, 2011).

Although melanomas with BRAF mutations have constitutively active growth signals, how they sustain their growth in the setting of nutrient scarcity is not well understood. In 1930, Otto Warburg proposed that cancer cells have a high rate of glycolysis as compared to oxidative metabolism even under conditions of high oxygen, a phenomenon known as the Warburg effect (Warburg, 1956; Vander Heiden et al., 2009). Oxidative phosphorylation depends on the ability of functionally intact mitochondria to metabolize oxygen, whereas glycolysis can occur independently of mitochondria. Warburg theorized that this metabolic switch facilitated the uptake and incorporation of nutrients that were required for cellular proliferation. Although poorly understood in melanoma, the molecular mechanisms of metabolic reprogramming in cancer have been described in other tumor types. *TP53*-deficient tumor cells have diminished levels of the genes *TIGAR* and *SCO2*, which regulate glycolysis and assembly of the mitochondrial cytochrome *c* oxidase complex, respectively (Bensaad et al., 2006; Matoba et al., 2006). Similarly, the dysregulation of the proto-oncogene *MYC* leads to profound effects on tumor metabolism through multiple mechanisms (reviewed in Dang, 2012).

These observations have raised the possibility of targeting key metabolic pathways to inhibit cancer growth. Yun et al. demonstrated that several colorectal cancers with KRAS or BRAF mutations have increased glucose uptake and glycolysis and survived better in low-glucose conditions compared to nonmutated cell lines (Yun et al., 2009). Suppression of glycolysis with 3-bromopyruvate (a nonactive intermediary in the glycolysis pathway) reactivates mitochondrial metabolism in tumor cells, induces their selective killing, and suppresses cancer growth. Similarly, suppression of glycolysis by inhibiting conversion of pyruvate to lactate enhances oxidative phosphorylation and suppressed the growth of breast cancer cell lines (Fantin et al., 2006; Bonnet et al., 2007). Thus, whereas metabolic reprogramming is commonly found in cancer, the mechanism and details of metabolic alterations in melanoma are unknown.

Mitochondrial biogenesis and oxidative phosphorylation are well known to be controlled by the members of the peroxisome proliferator-activated receptor γ coactivator 1 (PGC-1) family of transcriptional coactivators (PGC1α, PGC1β, PPRC1) (Lin et al., 2005a; Finck and Kelly, 2006; Handschin, 2009; Leone and Kelly, 2011). The best-studied PGC-1 family member, PGC1α, potently activates coordinated gene expression programs by interacting with transcription factors, the basal transcriptional machinery, histone-modifying enzymes, and the RNA-splicing machinery. PGC1α drives mitochondrial biogenesis in multiple contexts, including brown and white adipocytes (Wu et al., 1999; Uldry et al., 2006), skeletal muscle (Lin et al., 2002), and the heart (Lehman et al., 2000). PGC1α mRNA expression is sensitive to numerous signaling inputs that have been implicated in cancer biology (Herzig et al., 2001; Yoon et al., 2001; Chinsomboon et al., 2009; Arany et al., 2008). PGC1β shares significant sequence homology and functional overlap with PGC1α, including the activation of mitochondrial biogenesis and oxidative phosphorylation, but also has several distinct functions in different tissues (Lin et al., 2005b; Uldry et al., 2006; Wolfrum and Stoffel, 2006). The regulation of PGC1β has been less extensively studied. Although little is known about the role of the PGC-1s in melanoma, they have recently been implicated in metabolic shifts in breast cancer cells and colon cancers (Eichner et al., 2010; Bhalla et al., 2011; Sahin et al., 2011; Wang and Moraes, 2011; Girnun, 2012; Klimcakova et al., 2012). Here, we comprehensively evaluate the effect of BRAF pathway activation on metabolic gene expression and function in melanoma.

RESULTS

BRAF Regulates Metabolic Reprogramming of Melanomas

The mechanisms by which oncogenic BRAF promotes oncogenesis are incompletely understood. Gene set enrichment analysis (GSEA) provides a bioinformatics approach to identify gene signatures among microarray data sets that are induced or suppressed as small coordinated changes in individual genes (Mootha et al., 2003). In order to identify gene expression programs altered by oncogenic BRAF, we evaluated previously published gene expression profiles of BRAF mutant melanomas treated with the BRAF inhibitor vemurafenib (Joseph et al., 2010). As shown in Figure 1A, treatment of BRAF mutant melanomas with vemurafenib resulted in significant increases in the expression of the citric acid cycle gene set (Figure 1A) as well as multiple oxidative phosphorylation and ATP synthesis gene sets (Table S1 available online). Similarly, melanoma cells treated with PD0325901, a preclinical inhibitor of the MEK1/MEK2 protein kinases (Pratilas et al., 2009; Joseph et al., 2010), also exhibited a trend toward induction of the citric acid cycle and oxidative phosphorylation gene sets (Table S2). In contrast, we did not find enrichment of oxidative phosphorylation, or citric acid cycle gene sets in BRAF mutant nonmelanomas treated with PD0325901 (Table S3). We validated the effects of vemurafenib on OXPHOS gene expression in three melanoma cell lines by quantitative PCR (qPCR) (Figures S1A–S1C).

To directly evaluate the effect of BRAF inhibition on oxidative phosphorylation and mitochondrial number and function, we treated melanoma cell lines with PLX4720, a preclinical analog of vemurafenib (Tsai et al., 2008). PLX4720 increased the mitochondrial density of two BRAF mutant melanomas as detected by MitoTracker Green, which localizes to mitochondria independent of membrane potential. PLX4720 did not affect the mitochondrial density of MeWo cells that are BRAF wild-type (Figure 1B). PLX4720 also induced MitoTracker Red fluorescence, a measure of mitochondrial activity and mass (Figure 1C), and increased the production of mitochondrial oxidative stress measured by the MitoSOX fluorescence assay (Figure 1D). To confirm these findings, we also evaluated mitochondrial number by electron microscopy after treatment of the BRAF mutant melanoma cell line UACC62 with PLX4720. As seen in Figures 1E and S1D, inhibition of BRAF led to a significant increase in the number of mitochondria per cell.

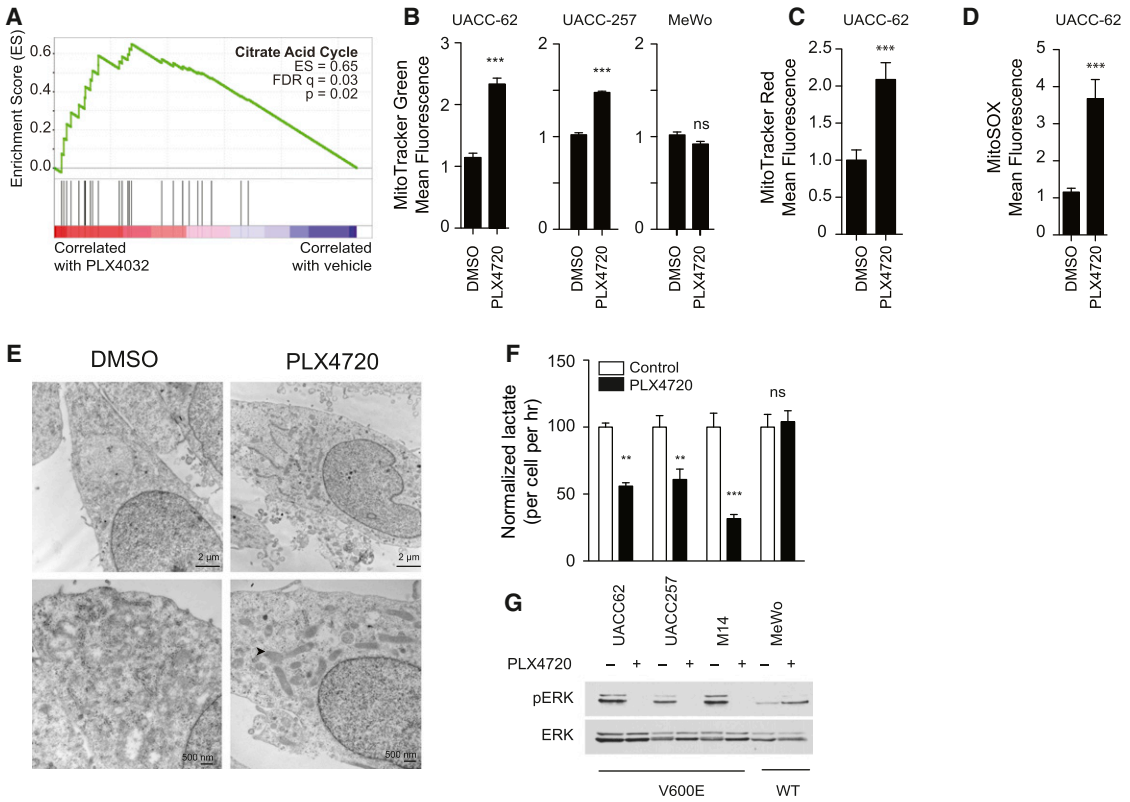

Figure 1. BRAF Inhibitors Induce Mitochondrial Biogenesis and Oxidative Metabolism

(A) GSEA plot of melanoma cells treated with vemurafenib showing the most significantly changed gene set. FDR, false-discovery rate; ES, enrichment score.

(B) MitoTracker Green fluorescence of BRAF mutant (UACC-62 and UACC-257) or BRAF wild-type (MeWo) melanoma cell lines treated with PLX4720 (1 μM, 72 hr) and subjected to analysis by flow cytometry.

(C and D) MitoTracker Red fluorescence (C) or MitoSOX fluorescence (D) of UACC-62 cells treated with PLX4720.

(E) Electron micrographs of UACC-62 cells treated with PLX4720 or vehicle control. Representative photographs of cells at 22,000× (upper panel) or 44,000× (lower panel) are shown. Arrowhead indicates a representative mitochondrion.

(F) Lactate levels in media conditioned from the indicated cell lines treated with PLX4720 or vehicle control for 16 hr.

(G) Cells in (F) were concomitantly evaluated for ERK activity by western blotting using phospho-ERK antibodies.

Error bars represent SEM of at least three independent replicates. ***$p < 0.001$; **$p < 0.01$. ns, not significant.

See also Tables S1–S3 and Figure S1.

The conversion of glucose to lactate, as noted by Warburg, can be due to the shunting of pyruvate away from oxidative phosphorylation (Vander Heiden et al., 2009). In line with our findings above, PLX4720 reduced lactate levels in all BRAF mutant melanomas evaluated (Figure 1F). Lactate levels did not change upon treatment of a melanoma cell line that does not contain the BRAF mutation, consistent with the inability of PLX4720 to suppress ERK signaling in these cells (Figure 1G). Collectively, our data suggest that BRAF suppresses oxidative phosphorylation gene expression and mitochondrial density in melanoma.

BRAF and MAPK Activation Suppresses PGC1α

Because oxidative phosphorylation depends on mitochondrial number and activity, their alteration may contribute to altered tumor metabolism. Candidate pathways, which physiologically regulate mitochondrial content and function, include the mitochondrial transcription factors A (TFAM) and B (TFB1M, *TFB2M*), nuclear respiratory factor 1 (NRF1), GA binding proteins (*GABPA*, *GABPB2*), peroxisome proliferator-activated receptors (PPARα, *PPARβ*), *PPAR-γ* coactivators (PGC1α, PGC1β), and PGC1-related coactivator 1 (PPRC1) (reviewed in Kelly and Scarpulla, 2004).

We observed that BRAF(V600E) expression suppressed *PGC1α*, a well-known regulator of mitochondrial metabolism in the microarray data sets above. To validate these observations, we treated a series of BRAF mutant melanomas and nonmelanoma cell lines with PLX4720 and evaluated the effect on *PGC1α* mRNA (Figure 2A). In all melanomas with BRAF mutations, PLX4720 induced 3- to 14-fold increases in *PGC1α* mRNA. We did not observe any changes in the expression of *PGC1α* in a BRAF wild-type MeWo cell line treated with PLX4720. Surprisingly, we did not observe any effects of PLX4720 on *PGC1α* expression in two BRAF mutant colon cancer cell lines, despite suppression of ERK phosphorylation similar to that seen in melanomas (Figure 2B). We did not observe any change in *PGC1β* mRNA upon treatment with PLX4720 or any effects in a BRAF wild-type melanoma over 24 hr (Figures S2A and S2B). These data suggested that there

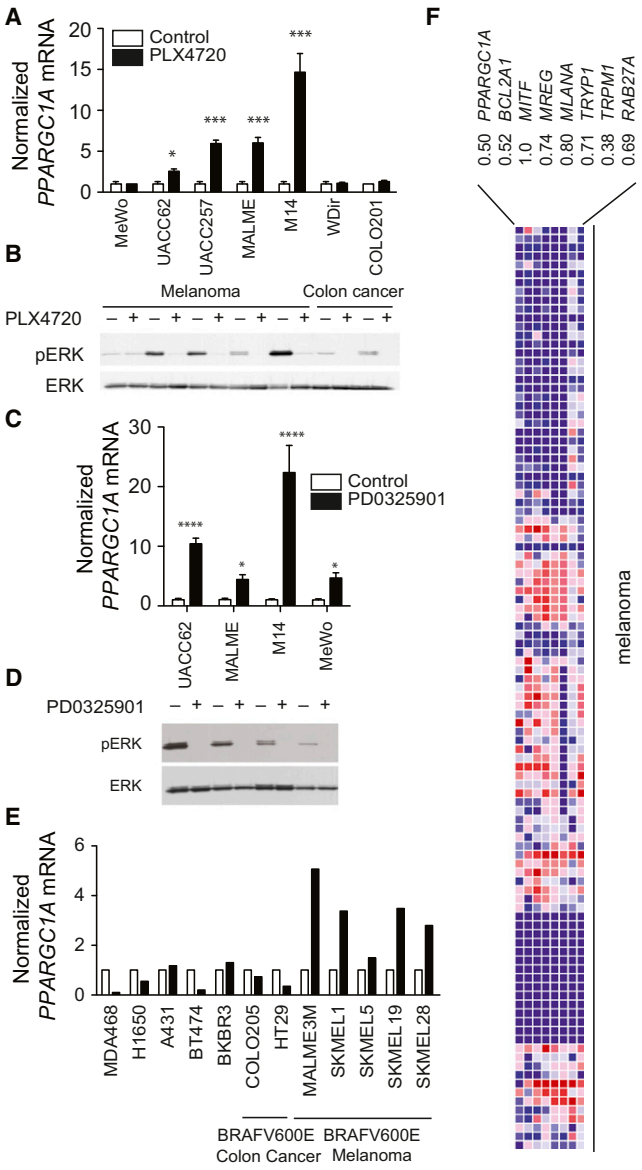

Figure 2. BRAF Inhibitors Induce PGC1α Expression

(A and B) PGC1α mRNA (A) and phospho-ERK levels (B) in melanoma or colon cancer cells treated with PLX4720 (1 μM) for 24 hr.

(C and D) PGC1α mRNA (C) and ERK activity (D) in melanoma cells treated with the MEK inhibitor PD0325901 (10 nM) for 24 hr.

(E) Microarray analysis (GSE10086) of PGC1α mRNA in cell lines treated with 10 nM PD0325901 for 24 hr.

(F) Comparison of *PGC1α* mRNA with MITF, melanocytic markers, and MITF targets in 105 melanoma cell cultures (Hoek et al., 2006). Pearson correlation coefficient is shown below each gene.

Error bars represent SEM of at least three independent replicates. ****p < 0.0001; ***p < 0.001; *p < 0.01.

See also Figure S2.

might be lineage-specific differences in the regulation of PGC1α by BRAF. To validate our findings using a structurally unrelated small molecule, we treated several melanoma cell lines with the MEK inhibitor PD0325901. Induction of *PGC1α* mRNA (Figure 2C) and suppression of ERK phosphorylation (Figure 2D) were seen in all cell lines tested including the BRAF wild-type melanoma MeWo, suggesting that the BRAF/MEK/ERK pathway regulates *PGC1α* expression in melanoma cells. These results were also confirmed with additional NRAS mutant melanoma cell lines treated with a MEK1/MEK2 inhibitor (Figures S2C and S2D). Finally, we evaluated the expression of PGC1α in an independent data set of A375 melanoma cells selected for resistance to BRAF inhibitors (Greger et al., 2012). We observed that *PGC1α* expression was 10-fold lower in cells that had acquired resistance to BRAF inhibitors (Figure S2E), likely reflecting their higher demonstrated basal MAPK activity.

We also interrogated a publicly available microarray of 12 breast, lung, colon, and melanoma cell lines treated with PD0325901 (Joseph et al., 2010). Suppression of MEK only affected PGC1α mRNA in melanoma cell lines (Figure 2E; $p < 0.0001$), suggesting that the regulation of PGC1α mRNA by the BRAF/MEK/ERK pathway is unique to the melanocytic lineage. Consistent with our results, we found that PGC1α expression was significantly correlated with melanocyte-specific antigen expression in a data set comprising of 105 melanoma cell cultures (Hoek et al., 2006) (Figure 2F).

PGC1α mRNA Is Directly Regulated by the MITF Transcription Factor

To elucidate how BRAF may regulate *PGC1α*, we compared the expression pattern of all human transcription factors to PGC1α in a large microarray data set of short-term melanoma cultures (Lin et al., 2008). Among the transcription factors whose expression most closely paralleled PGC1α, we observed that both transcription factor EB (*TFEB*) and the microphthalmia-associated transcription factor *(MITF*) were significantly associated with *PGC1α* expression ($q < 0.001$) (Figure 3A). Both TFEB and MITF are members of a four-member family of distinctly encoded transcription factors (TFEB, TFEC, TFE3, and MITF) that share a common structure, binding recognition sequence, and function (Haq and Fisher, 2011). Whereas TFEB, TFEC, and TFE3 are ubiquitously expressed, MITF is largely restricted to the melanocytic lineage. The correlation of *PGC1α* to *MITF* was therefore interesting in light of our data suggesting BRAF regulation of *PGC1α* in melanoma, but not in other lineages (see Figures 2A and 2E). *MITF* expression correlated with *PGC1α* as shown above (see Figure 2F).

We therefore evaluated the requirement of TFE3, TFEB, and MITF for the expression of *PGC1α* by siRNA. In both M14 melanoma cells and primary human melanocytes, suppression of MITF but not TFEB or TFE3 (Figures 3B and S3A) led to a significant suppression of *PGC1α* (Figures 3C and S3B) despite similar knockdown efficiency. We were unable to reliably detect *TFEC* expression in the cell lines tested (data not shown). MITF suppression in two other melanoma lines also significantly reduced *PGC1α* expression (Figure S3C), which was validated using two independent shRNAs (Figure S3D).

In silico analysis of the *PGC1α* promoter identified three putative MITF recognition sequences ("E boxes"), which were conserved among mammalian species. One E box was located approximately 420 bp upstream of the transcriptional start site, whereas a proximal E box was located within 20 bp of the start site (Figure 3D). Another E box was located approximately 10 kb upstream of these sequences, in the promoter sequences of an

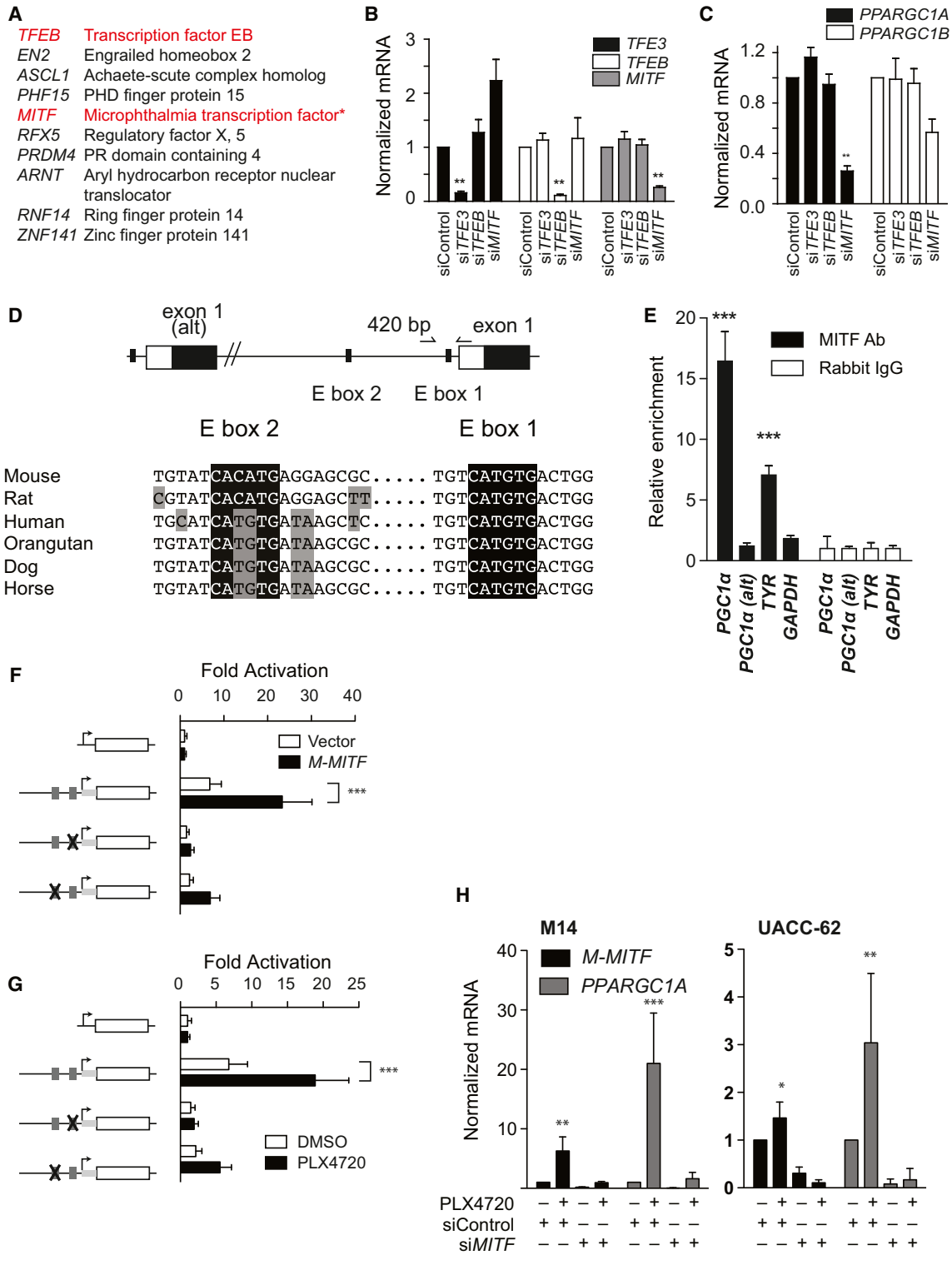

Figure 3. PGC1α Is Regulated by MITF in the Melanocytic Lineage

(A) Top ten transcription factors correlated to PGC1α mRNA in Lin et al. (2008). *q < 0.05.

(B and C) Requirement of MiT family members for PGC1α expression in M14 melanoma cells. Knockdown of each family member is shown in (B).

(D) Structure of PGC1α promoter in mammalian species showing the location of alternative (alt) exon 1 and exon 1. Also depicted are the locations of E box 1 and E box 2 and primers used for ChIP.

(E) ChIP of indicated genomic region with anti-MITF, or rabbit IgG in primary melanocytes. Precipitated DNA was amplified using primers depicted in (D). ***p < 0.001 compared to rabbit IgG control.

(legend continued on next page)

alternative exon 1 (PGC1α-alt) (Miura et al., 2008; Chinsomboon et al., 2009). To evaluate if MITF could directly bind to the *PGC1α* promoter, we performed chromatin immunoprecipitation (ChIP) using primers located either near alternative exon 1 or exon 1 (see Figure 3D). As shown in Figure 3E, MITF was found to bind to the proximal *PGC1α* promoter but not to the *PGC1α*-alt promoter in primary melanocytes. Due to limits in the resolution of this assay, we were unable to distinguish if MITF binds to E box 1, E box 2, or both. We therefore utilized a *PGC1α* promoter cloned upstream of the luciferase reporter gene (Handschin et al., 2003) and mutated each E box by site-directed mutagenesis (Figure 3F). MITF overexpression (Figure 3F) or treatment with PLX4720 (Figure 3G) led to the induction of the wild-type promoter, whereas mutation of either of the two E boxes significantly inhibited this response. Collectively, these data indicate that MITF binds and directly regulates the *PGC1α* gene in the melanocyte lineage. To evaluate if BRAF regulates PGC1α via MITF, we suppressed MITF using siRNA, then used PLX4720 to inhibit BRAF(V600E) activity. As shown in Figure 3H, treatment with PLX4720 strongly induced *PGC1α* mRNA in M14 cells and ~3-fold in UACC62 cells, and this induction was absent in cells in which MITF was knocked down by siRNA. These data indicate that BRAF regulates *PGC1α* via MITF.

BRAF Negatively Regulates MITF Activity

The relationship between BRAF and MITF is poorly understood because oncogenic BRAF and the ERK pathway promote MITF activation but also lead to its degradation (Hemesath et al., 1998; Wu et al., 2000; Wellbrock and Marais, 2005; Wellbrock et al., 2008; Boni et al., 2010). We therefore examined the consequences of ectopic BRAF(V600E) expression in immortalized melanocytes. Introduction of oncogenic BRAF was associated with decreased levels of *M-MITF* protein (the melanocyte-specific isoform), but not other isoforms (Figure 4A). Conversely, the MEK inhibitor PD0325901 induced the expression of *TRPM1* and other direct targets of MITF in published microarrays (Figure 4B) and by qPCR (Figure 4C). As shown in Figure 4D, knockdown of MITF blocked induction of TRPM1, suggesting these effects were dependent on MITF. In line with these findings, we observed that treatment of UACC-257 cells with PLX4720 for 72 hr led to increased pigmentation, reflecting MITF's essential role in melanin synthesis and pigmentation (Figure 4E).

We were unable to detect a correlation between BRAF mutation status and *PGC1α* or *MITF* expression in short-term cultures. Given the prevalence of MAPK pathway mutations other than BRAF(V600E) in melanoma, we evaluated the expression of *PGC1α* and *MITF* in melanomas with either high or low expression of a MAPK activation gene signature. Both *MITF* (t test, $p = 1.4 \times 10^{-14}$) and *PGC1α* (t test, $p = 1.34 \times 10^{-5}$) expression inversely correlated with MAPK activity (Figure 4F). Collectively, these data suggest that BRAF/MAPK inhibition leads to activation of MITF mRNA and protein and that this induction leads to induction of MITF targets including *PGC1α*.

To evaluate if BRAF suppression alters the BRAF/MITF/PGC1α pathway described here in vivo, we obtained serial biopsies from 11 patients prior to treatment with BRAF/MEK inhibitors and 10–14 days after beginning treatment (patient characteristics described in Straussman et al., 2012). Of eight samples that had detectable phosphorylated ERK at baseline (Figure 5A), all had induction of PGC1α upon treatment (Figure 5B). Comparison to separately analyzed levels of *M-MITF* induction following BRAF-targeted therapy revealed a significant correlation to PGC1α induction within these patient-derived specimens (J.A.W., unpublished data). Together, these data indicate that the OXPHOS adaptive response described here exists in vivo.

MITF Promotes Expression of Oxidative Phosphorylation Genes

Up to 30% of melanomas harbor genomic amplifications of *MITF* (Garraway et al., 2005), and MITF is required for the survival of at least a subset of melanomas. Activating point mutations have also been identified in melanoma (Bertolotto et al., 2011; Yokoyama et al., 2011). These data have led to the designation of MITF as a lineage-specific melanoma oncogene (Garraway et al., 2005). Comprehensive expression profiling approaches have identified roles for MITF in promoting cell growth and survival, organelle biogenesis, the oxidative stress response, and miRNA regulation (Vachtenheim and Borovanský, 2010; Haq and Fisher, 2011). However, a role for MITF in regulating metabolism has not been previously described. We therefore tested if *MITF* expression correlated with oxidative phosphorylation by classifying melanomas into two groups based on a previously defined oxidative phosphorylation signature. As seen in Figure 6A, melanomas with high *MITF* expression had significantly higher oxidative phosphorylation gene expression ($p = 5.51 \times 10^{-5}$). Similarly, *MITF* expression correlated with PGC1α-regulated gene expression ($p = 1.42 \times 10^{-15}$).

To evaluate if MITF was sufficient to drive oxidative phosphorylation in melanoma, we evaluated two matched human cell lines derived from primary melanocytes. These two cell lines (termed pmel*+BRAF(V600E) and pmel*+BRAF(V600E)+MITF) are derived from primary normal human melanocytes by immortalization using telomerase, with a constitutively active allele of cyclin-dependent kinase 4 and dominant-negative p53 (Garraway et al., 2005). These cells are therefore isogenic with the exception of the expression of *MITF*. Consistent with published reports by Garraway et al. (2005) and our results above, expression of M-MITF protein was undetectable in pmel*+BRAF(V600E) cells but strongly expressed in the derived MITF-expressing cells, which correlated with PGC1α expression (Figure 6B). BRAF(V600E) cells expressing MITF were able to form tumors in immunocompromised mice, whereas control cells were not

(F and G) Activity of *PGC1α* promoters upstream of the luciferase gene mutated as depicted in response to transfection of MITF (F) or treatment with PLX4720 (G). Gray boxes indicate the location of E boxes.
(H) Expression of PGC1α following knockdown of MITF (48 hr) and treatment with PLX4720 (1 μM, 24 hr) in M14 cells (left) or UACC-62 cells (right).
Error bars represent SEM of at least three independent replicates. **$p < 0.0$; ***$p < 0.001$.
See also Figure S3.

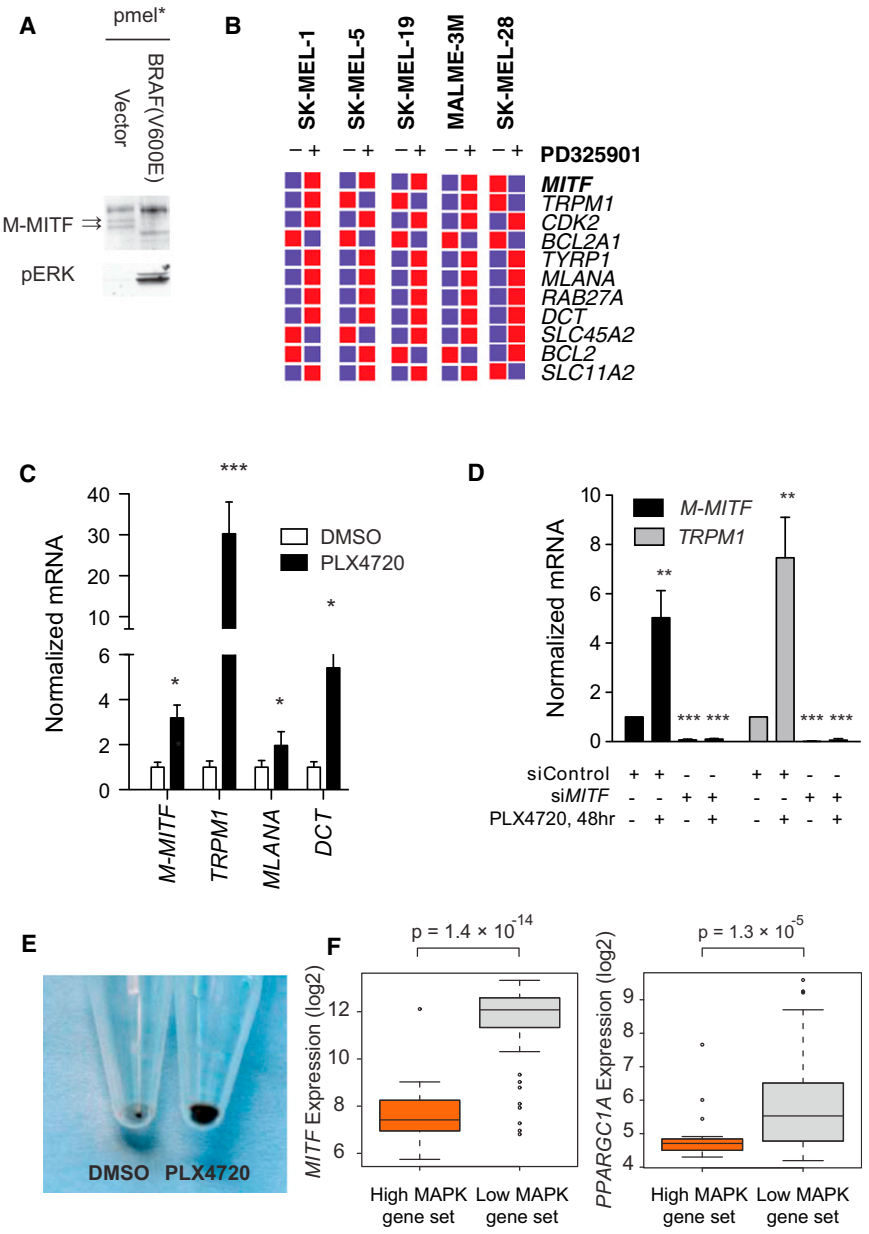

Figure 4. BRAF Suppresses MITF Expression and Activity

(A) Levels of M-MITF (arrows) and phosphorylated ERK in pmel* and pmel* BRAF(V600E).

(B) Effects of MEK inhibitor PD0325901 on *MITF* mRNA and MITF targets by published microarray (Pratilas et al., 2009).

(C) Response of MITF and MITF targets to PLX4720 in UACC-257 cells by qPCR. *$p < 0.01$; ***$p < 0.001$ relative to DMSO control.

(D) Effect of MITF suppression on induction of MITF-target *TRPM1* by PLX4720. **$p < 0.01$; ***$p < 0.001$ relative to siControl. Error bars represent SEM of at least three independent replicates.

(E) Consequence of PLX4720 (72 hr) on UACC-257 pigmentation. Equal number of cells were pelleted by centrifugation.

(F) Box plots showing expression of *MITF* (left) and *PGC1α* in melanoma cells with high or low MAPK activation from 88 short-term melanoma cultures (Lin et al., 2008).

(Figure 6C), paralleling previous data from soft agar growth (Garraway et al., 2005). Similar to our findings with BRAF inhibition, GSEA of microarray data identified a highly significant induction of the oxidative phosphorylation gene set in MITF-expressing cells compared to control cells ($q = 0.0$, $p < 5 \times 10^{-4}$; see Figure 6C). We found that a large majority of the oxidative phosphorylation gene set was induced by MITF overexpression (Figure S4A), consistent with the ability of PGC1α to strongly upregulate many oxidative phosphorylation genes (Mootha et al., 2003). We validated the expression of differentially expressed genes (chosen to represent different mitochondrial processes) by qPCR (Figure S4B) and found significant increases in several oxidative phosphorylation genes. Similarly, expression of the oxidative phosphorylation genes was suppressed by oncogenic BRAF (Figure S4C).

To evaluate the metabolic consequence of MITF overexpression directly, we evaluated glycolysis and oxidative phosphorylation in the isogenic cells. Overexpression of MITF did not increase glucose uptake (Figure 6D) but, strikingly decreased lactate production (Figure 6E) and increased oxygen consumption (Figure 6F), consistent with enhanced mitochondrial metabolism. Conversely, BRAF(V600E) cells had elevated sensitivity to knockdown of pyruvate kinase (muscle isoform), the final step in the glycolysis pathway, compared to isogenic cells expressing MITF (Figure S4D), despite similar degrees of knockdown efficiency in the two cell lines (Figure S4E).

To further validate these findings in patient-derived melanomas, we suppressed MITF by shRNA and performed gene expression profiling. We identified several genes involved in oxidative phosphorylation that were dependent on MITF (Figure S4F), consistent with the aforementioned gene expression data. With the exception of PGC1α, whose promoter was found to be directly bound by MITF, oxidative phosphorylation genes were not bound by MITF but have been identified as PGC1α targets in other cell lineages (Mootha et al., 2003). We conclude that MITF overexpression is sufficient and necessary to drive oxidative metabolism and metabolic reprogramming in the melanocyte lineage.

BRAF Inhibition Leads to Bioenergetic Adaptation by Induction of MITF and PGC1α

Collectively, the data above support the notion that BRAF inhibition endangers ATP production, which is rescued by concomitant induction of MITF, PGC1α, and oxidative metabolism. To

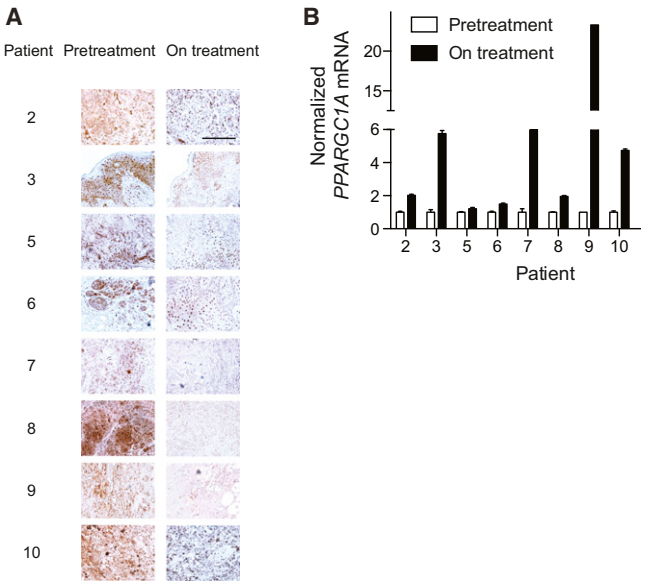

Figure 5. Validation of Induction of PGC1α Pathway In Vivo following BRAF Inhibition

(A) Expression of phospho-ERK in eight matched patient biopsies prior or during (10–14 days) treatment with BRAF/MEK inhibitors. Scale bar represents 100 μm.

(B) Expression of PGC1α mRNA prior and during treatment with BRAF/MEK inhibitors. Error bars represent SEM of at least three technical replicates.

experimentally test this hypothesis, we evaluated the response of the isogenic cell lines expressing BRAF(V600E) with or without M-MITF overexpression to PLX4032. Inhibition of BRAF resulted in a 42% drop in ATP in BRAF(V600E) parental cells, whereas the magnitude of this drop was reduced in MITF-overexpressing cells (Figure 6G), despite similar basal ATP concentrations. Consistent with MITF effects on oxidative metabolism, BRAF(V600E)+MITF cells were significantly more sensitive to the mitochondrial uncoupler 2,4-dinitrophenol (DNP; Figure 7A).

We also evaluated the magnitude of bioenergetic compensation in eight patient-derived melanoma cell lines. As shown in Figure 7B, in all cases, there was induction of PGC1α following vemurafenib treatment, which varied in magnitude by cell line. We also measured ATP levels before and after treatment with vemurafenib, and we observed a significant correlation between induction of PGC1α and ATP levels in BRAF mutant cells ($R = 0.72$, $p = 0.03$; Figure 7C). Strikingly, the two lines with highest ATP levels following BRAF inhibition are the ones with the strongest induction of PGC1α. These data suggest that the metabolic switch to "normal" varies in magnitude among different melanoma cell lines and suggest that the inhibition of BRAF leads to a bioenergetic crisis that can be variably rescued by induction of the MITF/PGC1α pathway.

We next asked whether oxidative metabolism could be exploited to inhibit the growth of melanoma cells. We compared the sensitivity of melanoma cells to primary melanocytes (Figure S5). All melanoma cells were more sensitive to DNP than primary melanocytes, except A375P. Treatment of UACC257 cells, but not A375P cells, with DNP led to a decrease in ATP and increases in lactate, consistent with inhibition of OXPHOS (Figures 7D and 7E). To validate the effects of mitochondrial inhibitors on tumor growth in vivo, we treated animals bearing tumor xenografts of A375P and UACC257 melanoma cells with DNP. Consistent with the in vitro data, we found that longitudinal treatment of UACC257 xenografts profoundly inhibited tumor growth, similar to the effects of PLX4032 (Figure 7F), whereas A375P cells were insensitive to 2,4-DNP (Figure 7G).

Melanomas Treated with BRAF Inhibitors Are Addicted to Oxidative Metabolism

Our observations that BRAF and MITF regulate *PGC1α* expression prompted us to evaluate if oxidative metabolism affected response to BRAF inhibitors. We observed that high levels of PGC1α were associated with poorer prognosis in patients with stage III melanoma (Figure S6A) (Bogunovic et al., 2009). To this end, forced expression of PGC1α protected cells from PLX4720, as demonstrated using three cell lines that expressed low levels of PGC1α (Figures 8A–8C). Because our data suggest that BRAF regulates PGC1α and oxidative phosphorylation, we evaluated the effects of inhibitors of oxidative phosphorylation in combination with BRAF inhibitors. In addition, the cells were found to be relatively insensitive to the mitochondrial uncoupler CCCP, but addition of PLX4720 enhanced the cytotoxicity of this drug (Figure 8D). Melanoma cells treated with 2,4-DNP, or oligomycin A, which inhibits oxidative phosphorylation through different mechanisms, additively enhanced the efficacy of PLX4720 in vitro (Figure 8E). We also found similar data using rotenone and the complex II inhibitor, TTFA (Figures S6B and S6C). Together, the data indicate that induction of oxidative phosphorylation in response to BRAF inhibition limits the therapeutic efficacy of BRAF inhibitors.

DISCUSSION

Previous studies have suggested a role for BRAF signaling in the regulation of tumor metabolism. Clinically, patients with BRAF mutant melanomas have higher levels of serum lactate consistent with diminished oxidative phosphorylation (Board et al., 2009). In addition, BRAF mutant melanomas have an order of magnitude increased uptake of glucose compared to normal tissues in vivo as assessed by functional imaging (Bollag et al., 2010). However, the mechanism by which BRAF regulates metabolism in melanoma is poorly understood. This study identifies a pathway by which the oncogenic BRAF pathway regulates energy metabolism in melanoma. Our findings show that BRAF activation is associated with diminished oxidative enzymes, diminished mitochondrial number and function, and increased production of lactate. This metabolic reprogramming triggered by BRAF(V600E) is accompanied by a suppression of MITF and PGC1α, a major regulator of mitochondrial biogenesis and function.

We identify the melanocyte master regulator *MITF* as a direct and essential mediator of BRAF-regulated PGC1α transcription. Consistent with the restricted expression of *MITF* to the melanocyte lineage, the ERK pathway does not appear to regulate PGC1α transcription in BRAF mutant cancers that lack *MITF* expression. The MITF-PGC1 connection thus explains the lineage-specific effects of BRAF activation and inhibition.

Although BRAF inhibitors can suppress glycolysis and induce oxidative phosphorylation, we found that MITF only regulates mitochondrial respiration. Consistent with this, MITF and PGC1α expression correlate with oxidative phosphorylation genes in

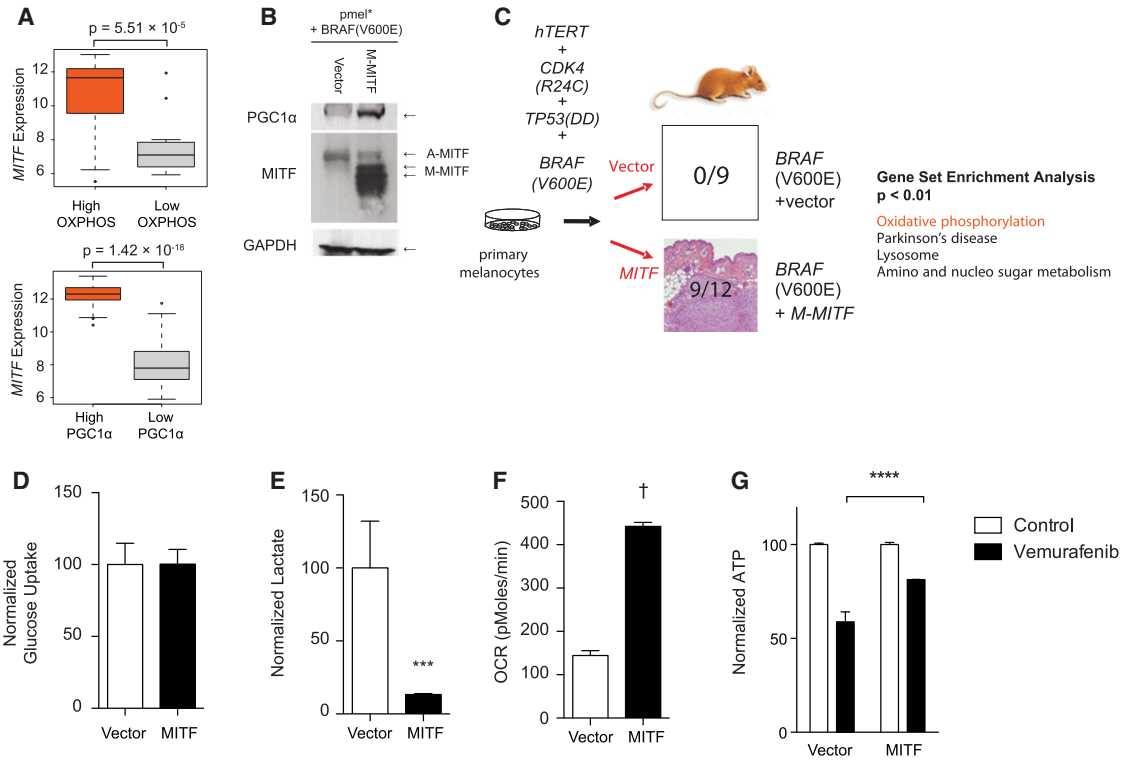

Figure 6. MITF Regulates Oxidative Phosphorylation

(A) Box plots depicting *MITF* expression in melanomas with high expression of a PGC1α-target gene set (bottom) or oxidative phosphorylation gene set (top).

(B) Western blotting showing expression of MITF and PGC1α in pmel* BRAF(V600E) with and without MITF overexpression.

(C) Schema showing isogenic system evaluating the effect of MITF overexpression in BRAF(V600E) melanoma cells. The tumorigenicity of the paired cell lines was assessed in FoxN^{nu} mice, and the number of formed tumors per injection of each cell line is shown. GSEA of the paired cell lines with the most highly induced gene sets is shown (right).

(D–F) Glucose uptake (D), lactate levels (E), and oxygen consumption (F) were measured as relative amounts in each cell line, normalized to cell number. †$p < 0.0001$.

(G) ATP levels, normalized to cell number in BRAF(V600E)+vector and BRAF(V600E)+MITF treated with PLX4032 (1 μM) for 24 hr.

***$p < 0.001$ compared to control cells. Error bars represent SEM of at least three independent replicates.

See also Figure S4.

a large series of melanoma short-term cultures, but we have not observed an inverse correlation with glycolytic gene expression. We also found that MITF expression did not affect glucose uptake but decreased lactate production and increased oxygen consumption, consistent with a shift to oxidative metabolism. Thus, consistent with Warburg's initial hypothesis, the activation of glycolysis and the suppression of oxidative metabolism, as shown here to be initiated by oncogenic BRAF, are likely separate processes.

Overall, our data suggest that MITF is a major regulator of mitochondrial respiration in the melanocyte lineage by acting via PGC1α. Tumors likely generate ATP via both glycolysis and oxidative phosphorylation (Colombi et al., 2011; Weinberg et al., 2010), and tumor cells may require mitochondria for functions other than ATP generation, such as fatty acid synthesis and glutaminolysis in some cases (Wise and Thompson, 2010; Dang, 2012). However, we show here that MITF-expressing melanomas have a higher level of oxidative gene expression. These data therefore suggest that MITF expression may serve as a biomarker for greater dependence on mitochondrial function. Because MITF has been difficult to drug directly (Haq and Fisher, 2011), the dependence of MITF-dependent melanoma on oxidative phosphorylation thus presents a theoretical therapeutic approach. However, MITF paradoxically can promote tumorigenesis (e.g., Garraway et al., 2005; Yokoyama et al., 2011), whereas activation of MITF expression in normal melanocytes typically induces differentiation, which likely antagonizes tumorigenesis (D'Orazio et al., 2006; Carreira et al., 2006; Haq and Fisher, 2011). A rheostat model has been proposed to explain the apparent paradox of MITF (Goding, 2011), but definitive evidence of this model remains an area of active investigation. We show that BRAF inhibitors induce some, but not all, MITF target genes, implying that the context in which MITF is regulated may also contribute to its physiologic effects. Finally, it is also highly likely that MITF has protumorigenic effects outside of its induction of OXPHOS, so that any antitumorigenic effect of inducing OXPHOS may well be countered by other protumorigenic effects. In the future, it will be of great interest to examine how MITF can coordinate its numerous downstream effects.

Eight patients treated with vemurafenib had induction of PGC1α,but a larger sample size will therefore be needed to evaluate the diagnostic and predictive role of PGC1α induction in response to BRAF inhibitors. Interestingly, mutations in PGC1α have been detected in recent melanoma whole-genome

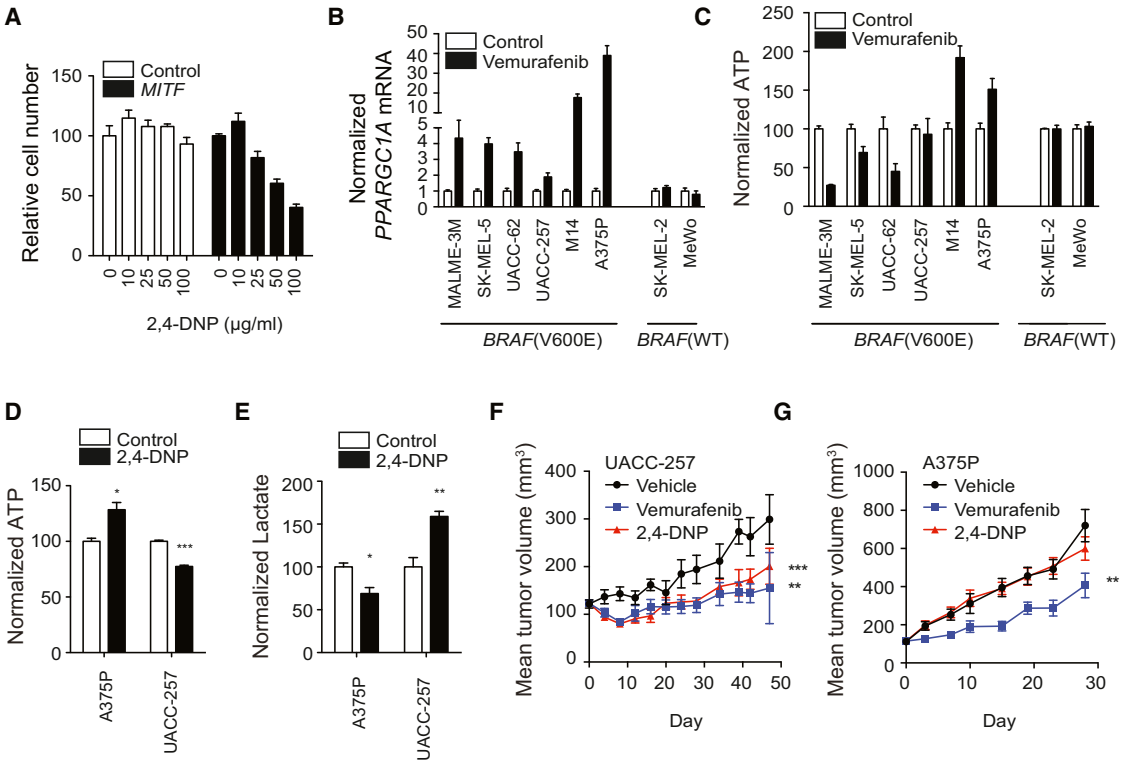

Figure 7. Effects of 2,4-DNP on Growth Melanoma Cells In Vitro and In Vivo

(A) Number of BRAF(V600E)+vector and BRAF(V600E)+MITF melanoma cells following treatment with 2,4-DNP with indicated dose for 72 hr.

(B and C) Levels of PGC1α mRNA (B) and ATP (C) in melanoma cell lines treated with vemurafenib (1 μM) for 24 hr.

(D and E) Effects of 2,4-DNP (50 μg/ml, 24 hr) on ATP (D) and lactate levels (E) in indicated cell lines in vitro. *$p < 0.05$.

(F and G) Effect of 2,4-DNP (20 mg/kg/day) or vemurafenib (75 mg/kg/day) on murine xenografts of indicated cell line (n = 7–8 per group). **$p < 0.01$ and ***$p < 0.001$ compared to vehicle group. Error bars represent SEM of at least three independent replicates.

See also Figure S5.

sequencing efforts (Prickett et al., 2009; Stark et al., 2012). Our data nonetheless suggest that dysregulation of PGC1α may have profound effects on metabolism of melanoma cells and may contribute to oncogenesis in certain cases.

We found that BRAF mutant melanomas treated with PLX4720 are dependent on ATP generation by mitochondria. Our data suggest that inhibition of mitochondrial metabolism may be most effective as initial therapy because most patients that have relapsed following BRAF inhibitors have reactivation of the MAPK pathway, which we have shown correlates with a decreased level of MITF and PGC1α. Although mitochondrial function would likely be difficult to target therapeutically in many cancer types, agents that exploit bioenergetic and metabolic alterations in mitochondria have been proposed by Fantin and Leder (2006). We find that mitochondrial uncouplers enhanced the efficacy of PLX4720 in BRAF mutant melanomas, but demonstration of the in vivo efficacy of this combination remains to be firmly established, which possibly will involve derivation of improved mitochondrial pharmacologic agents. Although available drugs have generally unfavorable pharmacologic properties, 2,4-DNP had been used extensively in diet pills (Cutting and Tainter, 1933), and over 100,000 people had been treated worldwide with the drug at the time of its discontinuation (Tainter et al., 1934). Cases of dangerous side effects such as fatal hyperthermia led to its official discontinuation by 1938. Given the toxicities of the drugs, further development of alternative oxidative phosphorylation inhibitors should be considered. Despite the recent successes of BRAF inhibition in the clinical arena, recurrence rates remain high, and survival is only extended several months. Although further in vivo studies will be crucial, uncouplers such as DNP, or other inhibitors of oxidative phosphorylation may be an alternative approach to enhance the effect of BRAF inhibitors in patients with melanoma.

EXPERIMENTAL PROCEDURES

Gene Expression and Bioinformatics

Immortal melanocytes (pmel*) and their transformed counterparts, pmel* BRAF(V600E)-vector and pmel*BRAF(V600E)+MITF, were maintained as described by Garraway et al. (2005). Global gene expression analysis was carried out using HG-U133A microarrays (Affymetrix).

RNA Isolation, ChIP, and Quantitative Real-Time PCR

ChIP was performed in primary human melanocytes using previously described methods by Cui et al. (2007). Chromatin was immunoprecipitated using rabbit polyclonal anti-MITF, or normal rabbit IgG as a control. Results are normalized to input DNA.

Clinical Samples

All patients gave informed consent for tissue acquisition as per an IRB-approved protocol (Office for Human Research Studies, Dana-Farber/Harvard Cancer Center). Tumors were biopsied before treatment (day 0), at 10–14 days during treatment.

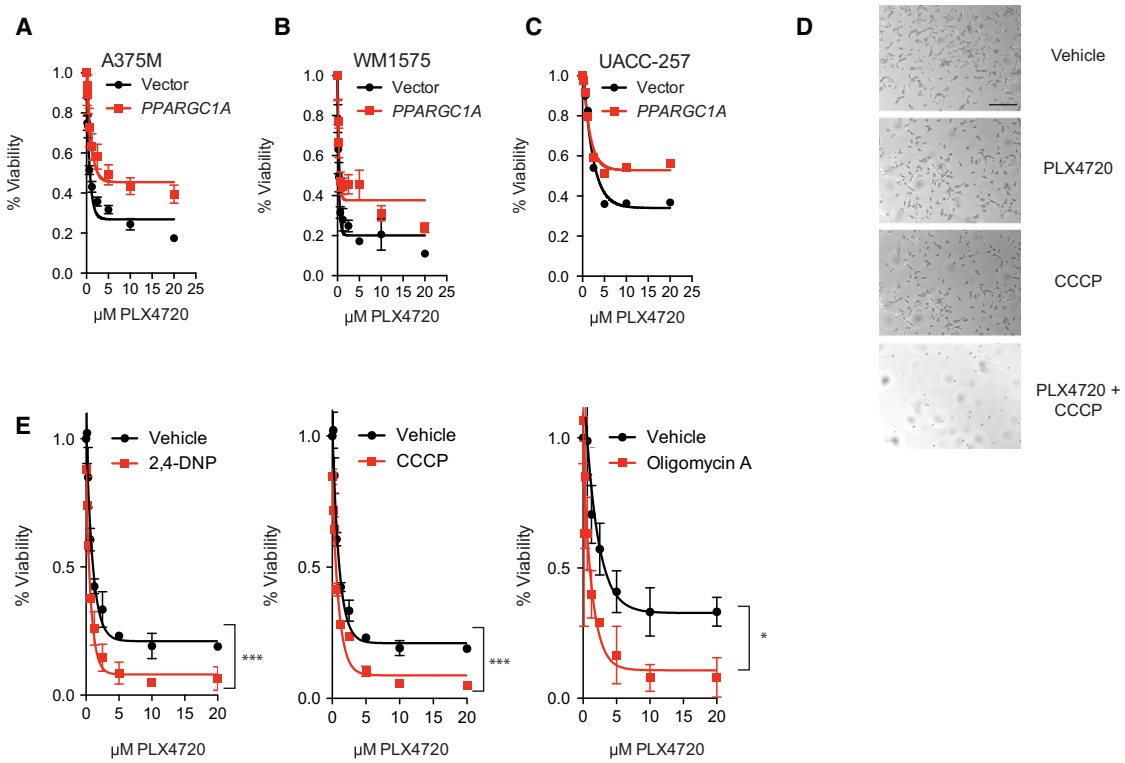

Figure 8. BRAF Inhibitors Enhance Dependence on Mitochondrial Metabolism

(A–C) Sensitivity of A375M (A), WM1575 (B), and UACC-257 (C) melanoma cells overexpressing PGC1α to treatment with PLX4720 for 72 hr.

(D) Photograph of M14 cells treated with PLX4720 (5 μM), CCCP (20 μM), or the combination for 72 hr. Scale bar represents 100 μm.

(E) Cell number following treatment with mitochondrial uncouplers oligomycin A (1μM), CCCP (5 μM), or 2,4-DNP (200 μg/ml). Cell number was estimated after 72 hr of treatment.

*$p < 0.05$ and ***$p < 0.001$ compared to control. Error bars represent SEM of at least three independent replicates.

See also Figure S6.

siRNA Delivery and Analysis

siRNAs SMARTpools (Dharmacon) were delivered using the lipidoid delivery agent C12-133-B as described by Li et al. (2012).

Promoter Assays and Luciferase Experiments

The murine *PGC1α* promoter was obtained from Addgene. Mutagenesis was performed using the QuikChange Site-Directed Mutagenesis Kit (Stratagene). Mutant promoters were verified by sequencing. UACC-62 cells were transfected with each promoter construct, pRL-CMV *Renilla* control, and a *M*-MITF overexpression vector. PLX4720 treatment was for 48 hr. Results reported are averages of at least three independent experiments, normalized for transfection efficiency using *Renilla* luciferase.

Xenograft Tumor Studies

All mouse experiments were done in accordance with Institutional Animal Care and Use Committee-approved animal protocols at Dana-Farber Cancer Institute as described in the Supplemental Experimental Procedures.

Electron Microscopy

Electron microscopy of UACC-62 melanoma cells treated with vehicle or PLX4720 (3 μM, 72 hr) was performed at the PMB Microscopy Core as described in Supplemental Experimental Procedures.

ACCESSION NUMBERS

Expression array data are deposited under GEO accession GSE38007.

SUPPLEMENTAL INFORMATION

Supplemental Information includes three tables, six figures, and Supplemental Experimental Procedures and can be found with this article online at http://dx.doi.org/10.1016/j.ccr.2013.02.003.

ACKNOWLEDGMENTS

We thank A. Winant for assistance with manuscript writing, M. McKee for electron microscopy, and A. Saur at the Luria Family Imaging Center (Dana-Farber Cancer Institute) for assistance with mouse xenograft experiments. This work was supported by the American Skin Association (to R.H.), NIAMS/NIH (R01 AR043369-16), Melanoma Research Alliance, Dr. Miriam and Sheldon G. Adelson Medical Research Foundation (to D.E.F.), and The National Cancer Institute (R01CA163336 to J.S.S. and P50CA093683 to H.R.W.).

Received: May 21, 2012
Revised: November 27, 2012
Accepted: February 5, 2013
Published: March 7, 2013

REFERENCES

Arany, Z., Foo, S.Y., Ma, Y., Ruas, J.L., Bommi-Reddy, A., Girnun, G., Cooper, M., Laznik, D., Chinsomboon, J., Rangwala, S.M., et al. (2008). HIF-independent regulation of VEGF and angiogenesis by the transcriptional coactivator PGC-1alpha. Nature *451*, 1008–1012.

Bensaad, K., Tsuruta, A., Selak, M.A., Vidal, M.N.C., Nakano, K., Bartrons, R., Gottlieb, E., and Vousden, K.H. (2006). TIGAR, a p53-inducible regulator of glycolysis and apoptosis. Cell *126*, 107–120.

Bertolotto, C., Lesueur, F., Giuliano, S., Strub, T., de Lichy, M., Bille, K., Dessen, P., d'Hayer, B., Mohamdi, H., Remenieras, A., et al.; French Familial Melanoma Study Group. (2011). A SUMOylation-defective MITF germline mutation predisposes to melanoma and renal carcinoma. Nature *480*, 94–98.

Bhalla, K., Hwang, B.J., Dewi, R.E., Ou, L., Twaddel, W., Fang, H.B., Vafai, S.B., Vazquez, F., Puigserver, P., Boros, L., and Girnun, G.D. (2011). PGC1α promotes tumor growth by inducing gene expression programs supporting lipogenesis. Cancer Res. *71*, 6888–6898.

Board, R.E., Ellison, G., Orr, M.C.M., Kemsley, K.R., McWalter, G., Blockley, L.Y., Dearden, S.P., Morris, C., Ranson, M., Cantarini, M.V., et al. (2009). Detection of BRAF mutations in the tumour and serum of patients enrolled in the AZD6244 (ARRY-142886) advanced melanoma phase II study. Br. J. Cancer *101*, 1724–1730.

Bogunovic, D., O'Neill, D.W., Belitskaya-Levy, I., Vacic, V., Yu, Y.-L., Adams, S., Darvishian, F., Berman, R., Shapiro, R., Pavlick, A.C., et al. (2009). Immune profile and mitotic index of metastatic melanoma lesions enhance clinical staging in predicting patient survival. Proc. Natl. Acad. Sci. USA *106*, 20429–20434.

Bollag, G., Hirth, P., Tsai, J., Zhang, J., Ibrahim, P.N., Cho, H., Spevak, W., Zhang, C., Zhang, Y., Habets, G., et al. (2010). Clinical efficacy of a RAF inhibitor needs broad target blockade in BRAF-mutant melanoma. Nature *467*, 596–599.

Boni, A., Cogdill, A.P., Dang, P., Udayakumar, D., Njauw, C.N.J., Sloss, C.M., Ferrone, C.R., Flaherty, K.T., Lawrence, D.P., Fisher, D.E., et al. (2010). Selective BRAFV600E inhibition enhances T-cell recognition of melanoma without affecting lymphocyte function. Cancer Res. *70*, 5213–5219.

Bonnet, S., Archer, S.L., Allalunis-Turner, J., Haromy, A., Beaulieu, C., Thompson, R., Lee, C.T., Lopaschuk, G.D., Puttagunta, L., Bonnet, S., et al. (2007). A mitochondria-K+ channel axis is suppressed in cancer and its normalization promotes apoptosis and inhibits cancer growth. Cancer Cell *11*, 37–51.

Carreira, S., Goodall, J., Denat, L., Rodriguez, M., Nuciforo, P., Hoek, K.S., Testori, A., Larue, L., and Goding, C.R. (2006). Mitf regulation of Dia1 controls melanoma proliferation and invasiveness. Genes Dev. *20*, 3426–3439.

Chapman, P.B., Hauschild, A., Robert, C., Haanen, J.B., Ascierto, P., Larkin, J., Dummer, R., Garbe, C., Testori, A., Maio, M., et al.; BRIM-3 Study Group. (2011). Improved survival with vemurafenib in melanoma with BRAF V600E mutation. N. Engl. J. Med. *364*, 2507–2516.

Chinsomboon, J., Ruas, J., Gupta, R.K., Thom, R., Shoag, J., Rowe, G.C., Sawada, N., Raghuram, S., and Arany, Z. (2009). The transcriptional coactivator PGC-1alpha mediates exercise-induced angiogenesis in skeletal muscle. Proc. Natl. Acad. Sci. USA *106*, 21401–21406.

Colombi, M., Molle, K.D., Benjamin, D., Rattenbacher-Kiser, K., Schaefer, C., Betz, C., Thiemeyer, A., Regenass, U., Hall, M.N., and Moroni, C. (2011). Genome-wide shRNA screen reveals increased mitochondrial dependence upon mTORC2 addiction. Oncogene *30*, 1551–1565.

Cui, R., Widlund, H.R., Feige, E., Lin, J.Y., Wilensky, D.L., Igras, V.E., D'Orazio, J., Fung, C.Y., Schanbacher, C.F., Granter, S.R., and Fisher, D.E. (2007). Central role of p53 in the suntan response and pathologic hyperpigmentation. Cell *128*, 853–864.

Curtin, J.A., Fridlyand, J., Kageshita, T., Patel, H.N., Busam, K.J., Kutzner, H., Cho, K.-H., Aiba, S., Bröcker, E.B., LeBoit, P.E., et al. (2005). Distinct sets of genetic alterations in melanoma. N. Engl. J. Med. *353*, 2135–2147.

Cutting, W.C., and Tainter, M.L. (1933). Metabolic actions of dinitrophenol with the use of balanced and unbalanced diets. J. Am. Med. Assoc. *101*, 2099–2012.

Dang, C.V. (2012). Links between metabolism and cancer. Genes Dev. *26*, 877–890.

Dankort, D., Curley, D.P., Cartlidge, R.A., Nelson, B., Karnezis, A.N., Damsky, W.E., Jr., You, M.J., DePinho, R.A., McMahon, M., and Bosenberg, M. (2009). Braf(V600E) cooperates with Pten loss to induce metastatic melanoma. Nat. Genet. *41*, 544–552.

Davies, H., Bignell, G.R., Cox, C., Stephens, P., Edkins, S., Clegg, S., Teague, J., Woffendin, H., Garnett, M.J., Bottomley, W., et al. (2002). Mutations of the BRAF gene in human cancer. Nature *417*, 949–954.

Dhomen, N., Reis-Filho, J.S., da Rocha Dias, S., Hayward, R., Savage, K., Delmas, V., Larue, L., Pritchard, C., and Marais, R. (2009). Oncogenic Braf induces melanocyte senescence and melanoma in mice. Cancer Cell *15*, 294–303.

D'Orazio, J.A., Nobuhisa, T., Cui, R., Arya, M., Spry, M., Wakamatsu, K., Igras, V., Kunisada, T., Granter, S.R., Nishimura, E.K., et al. (2006). Topical drug rescue strategy and skin protection based on the role of Mc1r in UV-induced tanning. Nature *443*, 340–344.

Eichner, L.J., Perry, M.-C., Dufour, C.R., Bertos, N., Park, M., St-Pierre, J., and Giguère, V. (2010). miR-378(*) mediates metabolic shift in breast cancer cells via the PGC-1β/ERRγ transcriptional pathway. Cell Metab. *12*, 352–361.

Fantin, V.R., and Leder, P. (2006). Mitochondriotoxic compounds for cancer therapy. Oncogene *25*, 4787–4797.

Fantin, V.R., St-Pierre, J., and Leder, P. (2006). Attenuation of LDH-A expression uncovers a link between glycolysis, mitochondrial physiology, and tumor maintenance. Cancer Cell *9*, 425–434.

Finck, B.N., and Kelly, D.P. (2006). PGC-1 coactivators: inducible regulators of energy metabolism in health and disease. J. Clin. Invest. *116*, 615–622.

Flaherty, K.T., Puzanov, I., Kim, K.B., Ribas, A., McArthur, G.A., Sosman, J.A., O'Dwyer, P.J., Lee, R.J., Grippo, J.F., Nolop, K., and Chapman, P.B. (2010). Inhibition of mutated, activated BRAF in metastatic melanoma. N. Engl. J. Med. *363*, 809–819.

Garraway, L.A., Widlund, H.R., Rubin, M.A., Getz, G., Berger, A.J., Ramaswamy, S., Beroukhim, R., Milner, D.A., Granter, S.R., Du, J., et al. (2005). Integrative genomic analyses identify MITF as a lineage survival oncogene amplified in malignant melanoma. Nature *436*, 117–122.

Girnun, G.D. (2012). The diverse role of the PPARγ coactivator 1 family of transcriptional coactivators in cancer. Semin. Cell Dev. Biol. *23*, 381–388.

Goding, C.R. (2011). Commentary. A picture of Mitf in melanoma immortality. Oncogene *30*, 2304–2306.

Gray-Schopfer, V., Wellbrock, C., and Marais, R. (2007). Melanoma biology and new targeted therapy. Nature *445*, 851–857.

Greger, J.G., Eastman, S.D., Zhang, V., Bleam, M.R., Hughes, A.M., Smitheman, K.N., Dickerson, S.H., Laquerre, S.G., Liu, L., and Gilmer, T.M. (2012). Combinations of BRAF, MEK, and PI3K/mTOR inhibitors overcome acquired resistance to the BRAF inhibitor GSK2118436 dabrafenib, mediated by NRAS or MEK mutations. Mol. Cancer Ther. *11*, 909–920.

Handschin, C. (2009). The biology of PGC-1α and its therapeutic potential. Trends Pharmacol. Sci. *30*, 322–329.

Handschin, C., Rhee, J., Lin, J., Tarr, P.T., and Spiegelman, B.M. (2003). An autoregulatory loop controls peroxisome proliferator-activated receptor gamma coactivator 1alpha expression in muscle. Proc. Natl. Acad. Sci. USA *100*, 7111–7116.

Haq, R., and Fisher, D.E. (2011). Biology and clinical relevance of the micropthalmia family of transcription factors in human cancer. J. Clin. Oncol. *29*, 3474–3482.

Hemesath, T.J., Price, E.R., Takemoto, C., Badalian, T., and Fisher, D.E. (1998). MAP kinase links the transcription factor Microphthalmia to c-Kit signalling in melanocytes. Nature *391*, 298–301.

Herzig, S., Long, F., Jhala, U.S., Hedrick, S., Quinn, R., Bauer, A., Rudolph, D., Schutz, G., Yoon, C., Puigserver, P., et al. (2001). CREB regulates hepatic gluconeogenesis through the coactivator PGC-1. Nature *413*, 179–183.

Hingorani, S.R., Jacobetz, M.A., Robertson, G.P., Herlyn, M., and Tuveson, D.A. (2003). Suppression of BRAF(V599E) in human melanoma abrogates transformation. Cancer Res. *63*, 5198–5202.

Hoeflich, K.P., Gray, D.C., Eby, M.T., Tien, J.Y., Wong, L., Bower, J., Gogineni, A., Zha, J., Cole, M.J., Stern, H.M., et al. (2006). Oncogenic BRAF is required for tumor growth and maintenance in melanoma models. Cancer Res. *66*, 999–1006.

Hoek, K.S., Schlegel, N.C., Brafford, P., Sucker, A., Ugurel, S., Kumar, R., Weber, B.L., Nathanson, K.L., Phillips, D.J., Herlyn, M., et al. (2006). Metastatic potential of melanomas defined by specific gene expression profiles with no BRAF signature. Pigment Cell Res. *19*, 290–302.

Joseph, E.W., Pratilas, C.A., Poulikakos, P.I., Tadi, M., Wang, W., Taylor, B.S., Halilovic, E., Persaud, Y., Xing, F., Viale, A., et al. (2010). The RAF inhibitor PLX4032 inhibits ERK signaling and tumor cell proliferation in a V600E BRAF-selective manner. Proc. Natl. Acad. Sci. USA *107*, 14903–14908.

Karasarides, M., Chiloeches, A., Hayward, R., Niculescu-Duvaz, D., Scanlon, I., Friedlos, F., Ogilvie, L., Hedley, D., Martin, J., Marshall, C.J., et al. (2004). B-RAF is a therapeutic target in melanoma. Oncogene *23*, 6292–6298.

Kelly, D.P., and Scarpulla, R.C. (2004). Transcriptional regulatory circuits controlling mitochondrial biogenesis and function. Genes Dev. *18*, 357–368.

Klimcakova, E., Chénard, V., McGuirk, S., Germain, D., Avizonis, D., Muller, W.J., and St-Pierre, J. (2012). PGC-1α promotes the growth of ErbB2/Neu-induced mammary tumors by regulating nutrient supply. Cancer Res. *72*, 1538–1546.

Lehman, J.J., Barger, P.M., Kovacs, A., Saffitz, J.E., Medeiros, D.M., and Kelly, D.P. (2000). Peroxisome proliferator-activated receptor gamma coactivator-1 promotes cardiac mitochondrial biogenesis. J. Clin. Invest. *106*, 847–856.

Leone, T.C., and Kelly, D.P. (2011). Transcriptional control of cardiac fuel metabolism and mitochondrial function. Cold Spring Harb. Symp. Quant. Biol. *76*, 175–182.

Li, J., Song, J.S., Bell, R.J.A., Tran, T.-N.T., Haq, R., Liu, H., Love, K.T., Langer, R., Anderson, D.G., Larue, L., and Fisher, D.E. (2012). YY1 regulates melanocyte development and function by cooperating with MITF. PLoS Genet. *8*, e1002688.

Lin, J., Wu, H., Tarr, P.T., Zhang, C.-Y., Wu, Z., Boss, O., Michael, L.F., Puigserver, P., Isotani, E., Olson, E.N., et al. (2002). Transcriptional co-activator PGC-1 alpha drives the formation of slow-twitch muscle fibres. Nature *418*, 797–801.

Lin, J., Handschin, C., and Spiegelman, B.M. (2005a). Metabolic control through the PGC-1 family of transcription coactivators. Cell Metab. *1*, 361–370.

Lin, J., Yang, R., Tarr, P.T., Wu, P.-H., Handschin, C., Li, S., Yang, W., Pei, L., Uldry, M., Tontonoz, P., et al. (2005b). Hyperlipidemic effects of dietary saturated fats mediated through PGC-1β coactivation of SREBP. Cell *120*, 261–273.

Lin, W.M., Baker, A.C., Beroukhim, R., Winckler, W., Feng, W., Marmion, J.M., Laine, E., Greulich, H., Tseng, H., Gates, C., et al. (2008). Modeling genomic diversity and tumor dependency in malignant melanoma. Cancer Res. *68*, 664–673.

Matoba, S., Kang, J.G., Patino, W.D., Wragg, A., Boehm, M., Gavrilova, O., Hurley, P.J., Bunz, F., and Hwang, P.M. (2006). p53 regulates mitochondrial respiration. Science *312*, 1650–1653.

Miura, S., Kai, Y., Kamei, Y., and Ezaki, O. (2008). Isoform-specific increases in murine skeletal muscle peroxisome proliferator-activated receptor-gamma coactivator-1alpha (PGC-1alpha) mRNA in response to beta2-adrenergic receptor activation and exercise. Endocrinology *149*, 4527–4533.

Mootha, V.K., Lindgren, C.M., Eriksson, K.F., Subramanian, A., Sihag, S., Lehár, J., Puigserver, P., Carlsson, E., Ridderstråle, M., Laurila, E., et al. (2003). PGC-1alpha-responsive genes involved in oxidative phosphorylation are coordinately downregulated in human diabetes. Nat. Genet. *34*, 267–273.

Poulikakos, P.I., and Rosen, N. (2011). Mutant BRAF melanomas—dependence and resistance. Cancer Cell *19*, 11–15.

Pratilas, C.A., Taylor, B.S., Ye, Q., Viale, A., Sander, C., Solit, D.B., and Rosen, N. (2009). (V600E)BRAF is associated with disabled feedback inhibition of RAF-MEK signaling and elevated transcriptional output of the pathway. Proc. Natl. Acad. Sci. USA *106*, 4519–4524.

Prickett, T.D., Agrawal, N.S., Wei, X., Yates, K.E., Lin, J.C., Wunderlich, J.R., Cronin, J.C., Cruz, P., Rosenberg, S.A., and Samuels, Y. (2009). Analysis of the tyrosine kinome in melanoma reveals recurrent mutations in ERBB4. Nat. Genet. *41*, 1127–1132.

Sahin, E., Colla, S., Liesa, M., Moslehi, J., Müller, F.L., Guo, M., Cooper, M., Kotton, D., Fabian, A.J., Walkey, C., et al. (2011). Telomere dysfunction induces metabolic and mitochondrial compromise. Nature *470*, 359–365.

Sosman, J.A., Kim, K.B., Schuchter, L., Gonzalez, R., Pavlick, A.C., Weber, J.S., McArthur, G.A., Hutson, T.E., Moschos, S.J., Flaherty, K.T., et al. (2012). Survival in BRAF V600-mutant advanced melanoma treated with vemurafenib. N. Engl. J. Med. *366*, 707–714.

Stark, M.S., Woods, S.L., Gartside, M.G., Bonazzi, V.F., Dutton-Regester, K., Aoude, L.G., Chow, D., Sereduk, C., Niemi, N.M., Tang, N., et al. (2012). Frequent somatic mutations in MAP3K5 and MAP3K9 in metastatic melanoma identified by exome sequencing. Nat. Genet. *44*, 165–169.

Straussman, R., Morikawa, T., Shee, K., Barzily-Rokni, M., Qian, Z.R., Du, J., Davis, A., Mongare, M.M., Gould, J., Frederick, D.T., et al. (2012). Tumour micro-environment elicits innate resistance to RAF inhibitors through HGF secretion. Nature *487*, 500–504.

Tainter, M.L., Cutting, W.C., and Stockton, A.B. (1934). Use of dinitrophenol in nutritional disorders : a critical survey of clinical results. Am. J. Public Health Nations Health *24*, 1045–1053.

Tsai, J., Lee, J.T., Wang, W., Zhang, J., Cho, H., Mamo, S., Bremer, R., Gillette, S., Kong, J., Haass, N.K., et al. (2008). Discovery of a selective inhibitor of oncogenic B-Raf kinase with potent antimelanoma activity. Proc. Natl. Acad. Sci. USA *105*, 3041–3046.

Uldry, M., Yang, W., St-Pierre, J., Lin, J., Seale, P., and Spiegelman, B.M. (2006). Complementary action of the PGC-1 coactivators in mitochondrial biogenesis and brown fat differentiation. Cell Metab. *3*, 333–341.

Vachtenheim, J., and Borovanský, J. (2010). "Transcription physiology" of pigment formation in melanocytes: central role of MITF. Exp. Dermatol. *19*, 617–627.

Vander Heiden, M.G., Cantley, L.C., and Thompson, C.B. (2009). Understanding the Warburg effect: the metabolic requirements of cell proliferation. Science *324*, 1029–1033.

Wan, P.T.C., Garnett, M.J., Roe, S.M., Lee, S., Niculescu-Duvaz, D., Good, V.M., Jones, C.M., Marshall, C.J., Springer, C.J., Barford, D., and Marais, R.; Cancer Genome Project. (2004). Mechanism of activation of the RAF-ERK signaling pathway by oncogenic mutations of B-RAF. Cell *116*, 855–867.

Wang, X., and Moraes, C.T. (2011). Increases in mitochondrial biogenesis impair carcinogenesis at multiple levels. Mol. Oncol. *5*, 399–409.

Warburg, O. (1956). On the origin of cancer cells. Science *123*, 309–314.

Weinberg, F., Hamanaka, R., Wheaton, W.W., Weinberg, S., Joseph, J., Lopez, M., Kalyanaraman, B., Mutlu, G.M., Budinger, G.R.S., and Chandel, N.S. (2010). Mitochondrial metabolism and ROS generation are essential for Kras-mediated tumorigenicity. Proc. Natl. Acad. Sci. USA *107*, 8788–8793.

Wellbrock, C., and Marais, R. (2005). Elevated expression of MITF counteracts B-RAF-stimulated melanocyte and melanoma cell proliferation. J. Cell Biol. *170*, 703–708.

Wellbrock, C., Rana, S., Paterson, H., Pickersgill, H., Brummelkamp, T., and Marais, R. (2008). Oncogenic BRAF regulates melanoma proliferation through the lineage specific factor MITF. PLoS One *3*, e2734.

Wise, D.R., and Thompson, C.B. (2010). Glutamine addiction: a new therapeutic target in cancer. Trends Biochem. Sci. *35*, 427–433.

Wolfrum, C., and Stoffel, M. (2006). Coactivation of Foxa2 through Pgc-1beta promotes liver fatty acid oxidation and triglyceride/VLDL secretion. Cell Metab. *3*, 99–110.

Wu, Z., Puigserver, P., Andersson, U., Zhang, C., Adelmant, G., Mootha, V., Troy, A., Cinti, S., Lowell, B., Scarpulla, R.C., and Spiegelman, B.M. (1999). Mechanisms controlling mitochondrial biogenesis and respiration through the thermogenic coactivator PGC-1. Cell *98*, 115–124.

Wu, M., Hemesath, T.J., Takemoto, C.M., Horstmann, M.A., Wells, A.G., Price, E.R., Fisher, D.Z., and Fisher, D.E. (2000). c-Kit triggers dual phosphorylations, which couple activation and degradation of the essential melanocyte factor Mi. Genes Dev. *14*, 301–312.

Yokoyama, S., Woods, S.L., Boyle, G.M., Aoude, L.G., MacGregor, S., Zismann, V., Gartside, M., Cust, A.E., Haq, R., Harland, M., et al. (2011). A novel recurrent mutation in MITF predisposes to familial and sporadic melanoma. Nature *480*, 99–103.

Yoon, J.C., Puigserver, P., Chen, G., Donovan, J., Wu, Z., Rhee, J., Adelmant, G., Stafford, J., Kahn, C.R., Granner, D.K., et al. (2001). Control of hepatic gluconeogenesis through the transcriptional coactivator PGC-1. Nature *413*, 131–138.

Yun, J., Rago, C., Cheong, I., Pagliarini, R., Angenendt, P., Rajagopalan, H., Schmidt, K., Willson, J.K., Markowitz, S., Zhou, S., et al. (2009). Glucose deprivation contributes to the development of KRAS pathway mutations in tumor cells. Science *325*, 1555–1559.

Cancer Cell
Article

Loss of FBP1 by Snail-Mediated Repression Provides Metabolic Advantages in Basal-like Breast Cancer

Chenfang Dong,[1,5] Tingting Yuan,[1,5,11] Yadi Wu,[2,5,11] Yifan Wang,[1,5,11] Teresa W.M. Fan,[6] Sumitra Miriyala,[4,5] Yiwei Lin,[1,5] Jun Yao,[7] Jian Shi,[1,5] Tiebang Kang,[9] Pawel Lorkiewicz,[6] Daret St Clair,[4,5] Mien-Chie Hung,[8,10] B. Mark Evers,[1,3,5] and Binhua P. Zhou[1,5,*]

[1]Department of Molecular and Cellular Biochemistry
[2]Department of Molecular and Biomedical Pharmacology
[3]Department of Surgery
[4]Graduate Center for Toxicology
[5]Markey Cancer Center
The University of Kentucky, College of Medicine, Lexington, KY 40506, USA
[6]Center for Regulatory and Environmental Analytical Metabolomics, Department of Chemistry and J.G. Brown Cancer Center, University of Louisville, Louisville, KY 40202, USA
[7]Department of Neuro-Oncology
[8]Department of Molecular and Cellular Oncology
The University of Texas M. D. Anderson Cancer Center, Houston, TX 77030, USA
[9]State Key Laboratory of Oncology in South China, Guangzhou 510060, China
[10]Center for Molecular Medicine and Graduate Institute of Cancer Biology, China Medical University, Taichung, Taiwan
[11]These authors contributed equally to this study
*Correspondence: peter.zhou@uky.edu
http://dx.doi.org/10.1016/j.ccr.2013.01.022

SUMMARY

The epithelial-mesenchymal transition (EMT) enhances cancer invasiveness and confers tumor cells with cancer stem cell (CSC)-like characteristics. We show that the Snail-G9a-Dnmt1 complex, which is critical for E-cadherin promoter silencing, is also required for the promoter methylation of fructose-1,6-biphosphatase (FBP1) in basal-like breast cancer (BLBC). Loss of FBP1 induces glycolysis and results in increased glucose uptake, macromolecule biosynthesis, formation of tetrameric PKM2, and maintenance of ATP production under hypoxia. Loss of FBP1 also inhibits oxygen consumption and reactive oxygen species production by suppressing mitochondrial complex I activity; this metabolic reprogramming results in an increased CSC-like property and tumorigenicity by enhancing the interaction of β-catenin with T-cell factor. Our study indicates that the loss of FBP1 is a critical oncogenic event in EMT and BLBC.

INTRODUCTION

The increased motility and invasiveness of metastatic tumor cells are reminiscent of the events that occur at the epithelial-mesenchymal transition (EMT), a characteristic of embryonic development, tissue remodeling, and wound healing (Polyak and Weinberg, 2009; Thiery et al., 2009). EMT also bestows tumor cells with cancer stem cell (CSC)-like characteristics, providing them with therapeutic resistance and conferred tumor recurrence. Although metabolism plays a fundamental role in essentially every function of a cell, little is known about how the cell's metabolism contributes to the morphological and molecular changes in EMT. Understanding the causes and consequences of altered metabolism, particularly glucose, in EMT may permit the identification of drug targets for treating metastatic breast cancer.

Glucose homeostasis is reciprocally controlled by the catabolic glycolysis/oxidative phosphorylation (OXPHOS) and the

Significance

BLBC is associated with an aggressive clinical history, development of recurrence, distant metastasis, and shorter patient survival. BLBC contains abundant EMT markers and possesses many CSC-like characteristics, but the metabolic program associates with these changes remain unknown. We showed that the Snail-G9a-Dnmt1 complex repressed FBP1 expression in BLBC; this results in increased CSC-like characteristics and tumorigenicity by enhancing aerobic glycolysis and by suppressing ROS production. This metabolic reprogramming is intertwined with the development of BLBC, because loss of FBP1 is required for EMT induction, the conversion from luminal to basal-like phenotype, and is associated with poor patient survival. Our study suggests that targeting the Snail complex may be an effective approach for treating BLBC.

anabolic gluconeogenesis pathway. In the catabolic reaction, glucose is converted to pyruvate in the absence of oxygen, which can be further metabolized to lactate in the cytoplasm (glycolysis). In the presence of oxygen, pyruvate is channeled to the tricarboxylic acid (TCA) cycle to fuel OXPHOS for the maximal ATP production in the mitochondria. Otto Warburg noticed that some tumor cells preferentially metabolized glucose to lactate in the presence of ample oxygen, a process called aerobic glycolysis (Koppenol et al., 2011). Activation of several oncogenes contributes to the Warburg effect in tumor cells. For example, AKT1 stimulates glucose uptake by enhancing Glu-4 expression and by activating hexokinase (Elstrom et al., 2004; Robey and Hay, 2009). Activation of Myc also induces glycolysis by inducing LDH-A and PDK1 expression, which inhibits the conversion of pyruvate to acetyl-CoA and facilitates the production of lactate (Dang et al., 2008). Tumor cells can increase an embryonic form of pyruvate kinase M2 (PKM2) to trigger glycolysis in lung cancer (Christofk et al., 2008).

Much attention has focused on regulation of the catabolic pathway of glucose. Gluconeogenesis is less investigated and may play an equally important role in the switch to aerobic glycolysis in tumor cells. Fructose-1,6-bisphosphatase (FBP1), which catalyzes the splitting of fructose-1,6-bisphosphate (F-1,6-BP) into fructose 6-phosphate and inorganic phosphate, is a rate-limiting enzyme in gluconeogenesis. An autosomal recessive inherited disorder of FBP1 deficiency is characterized by hypoglycemia and lactic acidosis, which often causes sudden infant death (Emery et al., 1988). This suggests that loss of FBP1 increases glucose uptake and glycolysis, leading to hypoglycemia and lactic acidosis in patients. Consistent with these observations, inhibition of FBP1 significantly increases glucose sensitivity and utilization in type 2 diabetic mouse models (van Poelje et al., 2006). Interestingly, loss of FBP1 expression due to promoter DNA methylation has been observed in liver, colon, and gastric cancers (Chen et al., 2011; Liu et al., 2010), suggesting that epigenetic regulation of FBP1 plays a critical role in modulating glucose metabolism in cancer.

Breast cancer can be divided into four subtypes based on gene expression profiling: luminal A, luminal B, HER2, and basal-like (BLBC). BLBC is defined by expression of markers characteristic of basal/myoepithelial cells and is identified as a subgroup of breast cancers that may originate from undifferentiated stem cells (Polyak, 2011). Consistent with this notion, BLBC contains many EMT markers and CSC-like characteristics. We recently showed that Snail interacted with H3K9 methyltransferase G9a and DNA methyltransferase Dnmt1 to silence E-cadherin expression in BLBC cells (Dong et al., 2012). We carried out this study to identify other targets regulated by the Snail-G9a-Dnmt1 complex and investigate their contributions to BLBC.

RESULTS

FBP1 Expression Is Inversely Correlated with Snail in Breast Cancer

To identify potential targets regulated by the Snail-G9a-Dnmt1 complex, we performed microarray analysis in MDA-MB231 cells with knockdown of G9a (GSE34925). Similar to E-cadherin, FBP1 mRNA was greatly elevated after knockdown of G9a. FBP1 has been identified as a marker to distinguish estrogen receptor (ER)-positive breast cancer from ER-negative subtype (van 't Veer et al., 2002). To reveal the potential function of FBP1 in breast cancer, we analyzed FBP1 expression in five gene expression data sets and noticed that FBP1 expression positively correlated with ERα expression (Figure S1A available online). In two data sets (NKI295 and GSE1456) with information on breast cancer subtypes, we found FBP1 expression was high in luminal subtype and significantly lower in BLBC (Figure 1A). Using immunohistochemistry staining, we also found that FBP1 expression positively correlated with ERα expression (Figures 1B and S1B). This correlation was further confirmed using immunoblotting. We found that FBP1 and ERα were highly expressed in luminal subtype but lowly expressed in triple-negative breast cancer, which are mostly also BLBC (Figure S1C; six samples from both cases are shown in Figure 1C). Consistent with the notion that BLBC express EMT molecules, Snail protein level was high in triple-negative breast cancer, and its level inversely correlated with expression of FBP1, ERα, and E-cadherin (Figures 1C and S1C). Furthermore, we examined the expression of FBP1, ERα, and Snail in breast cancer cell lines. BLBC cells lose expression of luminal epithelial molecules (ERα and E-cadherin) and contain high levels of mesenchymal markers (vimentin, N-cadherin, and Snail). Similar to E-cadherin and ERα, FBP1 was high in luminal cell lines and absent in BLBC cell lines (Figure 1D).

FBP1 Is a Direct Target of Snail

To investigate the causal relationship between Snail and FBP1, we expressed Snail in two luminal breast cancer cell lines. Expression of Snail downregulated E-cadherin expression, induced EMT, and converted luminal cells into basal-like phenotype (Dhasarathy et al., 2011) (Figures 2A–2D). This phenotypic conversion is associated with the loss of luminal markers and gain of basal markers (Figures 2D and S2). Similar to E-cadherin, Snail almost completely suppressed FBP1 expression in these cells (Figures 2B–2D). To examine whether FBP1 repression is required for Snail-mediated EMT and basal-like phenotype conversion, Snail was co-expressed with exogenous FBP1 (under the control of CMV promoter and thus not repressed by Snail) in luminal cells (Figure 2A). Ectopic FBP1 expression blocked the downregulation of E-cadherin, inhibited morphological changes indicative of EMT, and suppressed the basal-like phenotype conversion in these cells (Figures 2B, 2D, and S2), indicating that FBP1 repression is required for this event.

We noticed that the FBP1 promoter contained nine consensus Snail-binding E-boxes (CAGGTG) (Figure 2E). We cloned FBP1 promoter (FL1 = −1669 to +331 bp) and generated several deletion mutants of promoter-luciferase constructs based on the location of these E-boxes. By expressing a full-length FBP1 promoter reporter (FL1) in HEK293, HeLa, and MCF7 cells, we found Snail significantly repressed FBP1 promoter activity (Figure 2F). When the E-box at −1273 bp was deleted (FL1 versus FL2), we did not notice any changes in Snail-mediated FBP1 promoter-luciferase repression (Figure 2G), suggesting that the E-box at −1273 is not critical for Snail-mediated FBP1 repression. However, two E-boxes upstream of transcriptional starting site (TSS) (−657 and −358 bp) as well as six consecutive

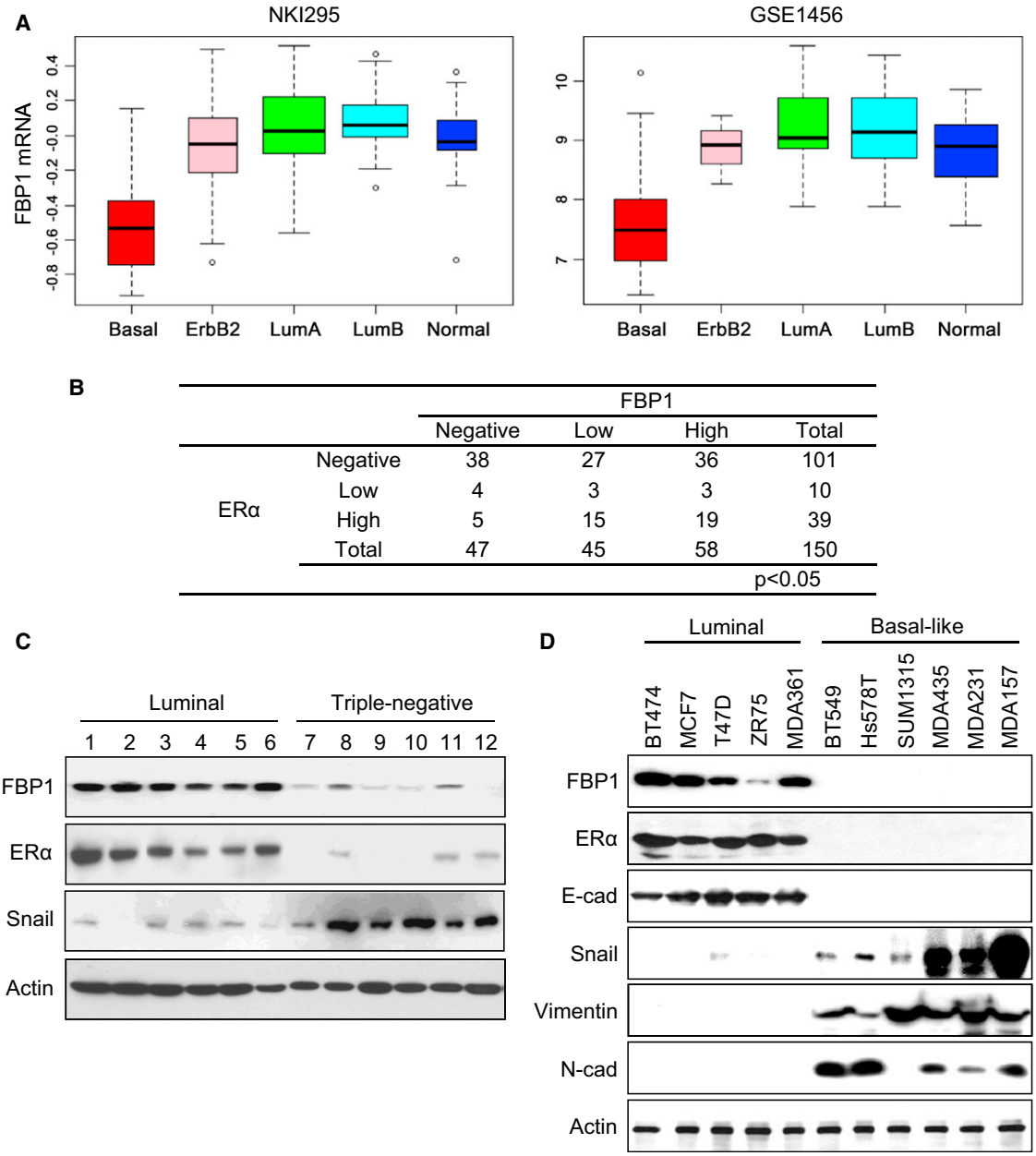

Figure 1. FBP1 Expression Inversely Correlates with Snail in Breast Cancer

(A) Box-plots indicate FBP1 expression in different subtypes of breast cancer.

(B) Statistical analysis of 150 cases of breast tumor samples immunostained using antibodies against FBP1, ER-α, and a control serum.

(C) Expression of FBP1, ER-α, and Snail were analyzed on fresh frozen tumor samples from six cases of luminal and six cases of triple-negative breast cancer.

(D) Expression of FBP1, ER-α, E-cadherin, Snail, and other EMT markers was determined by western blotting on five luminal and six BLBC cell lines (MDA-MB231, MDA-MB435, MDA-MB157, and MDA-MB361 are abbreviated to MDA231, MDA435, MDA157, and MDA361 in all figures).

See also Figure S1.

E-boxes between TSS and ATG sites were important for Snail-mediated FBP1 repression, as deletion constructs (FL3 and FL4) that removed these two regions separately became less sensitive to Snail-mediated repression (Figure 2H). Mutations on these E-boxes almost completely abolished Snail-mediated repression on FBP1 promoter luciferase (Figure 2H).

To examine whether Snail binds to FBP1 promoter, we performed chromatin immunoprecipitation (ChIP) by using three sets of primers (Figure 3A). Primer set 2, which covers nucleotides from −369 to −161, worked effectively and thus was used for the subsequent ChIP experiments. In cells that had undergone Snail-mediated EMT (Figure 2B), we found that Snail was associated with the FBP1 promoter (Figure 3B). In addition, we found endogenous Snail bound to FBP1 promoter in BLBC cells but not luminal cell lines (Figure 3C). These results indicate that FBP1 is a direct target of Snail.

Loss of FBP1 Expression Is Associated with Elevated H3K9me2 and DNA Methylation at the FBP1 Promoter

We hypothesized that the Snail-G9a-Dnmts complex also binds to the FBP1 promoter and is responsible for FBP1 repression in BLBC. In three luminal cell lines that had undergone Snail-mediated EMT, we found that downregulation of FBP1 was associated with an increased G9a and H3K9me2 and decreased H3K9ac at the FBP1 promoter (Figure 3B). We also found FBP1 promoter was completely unmethylated in vector control cell lines; however, de novo DNA methylation occurred at the FBP1 promoter in cells that had undergone Snail-mediated EMT (Figure 3B). The increased G9a association, H3K9me2, and DNA methylation on FBP1 promoter correlated well with the downregulation of FBP1 in these luminal cell lines (Figure 3B).

We also detected a dramatic increase of H3K9me2 and decrease of H3K9ac on the FBP1 promoter in six BLBC cell lines compared to those in five luminal cell lines (Figure 3C). The increase of H3K9me2 at the FBP1 promoter was likely due to the association of the Snail-G9a-Dnmts complex because the occupancy of Snail and G9a at the FBP1 promoter was also significantly higher in BLBC cell lines than in luminal cell lines (Figure 3C). Consistently, all BLBC cell lines showed a significant increase of DNA methylation on the FBP1 promoter, whereas no detectable FBP1 promoter DNA methylation in luminal cell lines was observed (Figure 3C). When analyzing 25 cases of luminal and 16 cases of triple-negative breast tumor tissues (Figure S1C), we found that the association of G9a and the level of H3K9me2 and DNA methylation on the FBP1 promoter were significantly increased in triple-negative breast cancer compared with the luminal subtype (Figure 3D). Knockdown of G9a in MDA-MB231 cells increased the mRNA and protein levels of FBP1 in a way similar to that of E-cadherin (Figure 3E). Knockdown of Snail also increased the expression of FBP1 and E-cadherin in MDA-MB231 cells (Figure S3). Together, these results indicate that the association of Snail and G9a and the corresponding increased H3K9me2 and DNA methylation on FBP1 promoter are critical for the silencing of FBP1 expression in BLBC.

FBP1 Inhibits Glucose Uptake and Sensitivity in BLBC Cells

To examine the function of FBP1 in breast cancer, we established stable clones with FBP1 expression or knockdown in six BLBC and two luminal breast cancer cell lines, respectively (Figure 4A). We first measured glucose uptake and found that FBP1 expression significantly decreased glucose uptake in BLBC cell lines, whereas knockdown of FBP1 enhanced glucose uptake in luminal cell lines (Figure 4B). Intracellular glucose is sensed by MondoA and ChREBP (Li et al., 2006). Following an increase in intracellular glucose-derived metabolites, MondoA and ChREBP shuttle to the nucleus, where they interact with Mlx and activate transcription of target genes. TXNIP is a major direct target of MondoA-Mlx complex and is commonly used as an intracellular glucose sensor (Peterson et al., 2010). We thus examined TXNIP induction by depleting glucose for 12 hr, followed by glucose stimulation for additional 3 hr. TXNIP was robustly induced in BLBC cell lines; however, FBP1 suppressed TXNIP induction. In contrast, knockdown of FBP1 stimulated TXNIP induction in luminal cells (Figure 4C). Because the cells had been glucose-deprived for 12 hr, the TXNIP levels were re-set to baseline (lane 2 versus lane 1, Figure S4A); the induction of TXNIP after glucose stimulation reflects glucose uptake and resultant steady-state level of intracellular glucose. Indeed, following glucose stimulation for different time intervals, TXNIP induction was greatly delayed in FBP1-expressing MDA-MB231 cells. In contrast, TXNIP induction was robustly increased in FBP1-knockdown MCF7 cells (Figure S4A). Because insulin is the major hormone regulating glucose uptake, we measured insulin sensitivity by examining tyrosine phosphorylation of the insulin receptor (IR) after insulin stimulation. We found that FBP1 expression suppressed the intensity and duration of IR phosphorylation in BLBC cell lines. Conversely, knockdown of FBP1 increased the intensity and duration of IR phosphorylation in luminal cell lines (Figure S4B). These results indicate that FBP1 is critical in inhibiting glucose uptake exemplified by downregulating glucose and insulin sensitivities.

FBP1 Reduces Lactate Generation and Increases Oxygen Consumption in BLBC Cells

To examine whether FBP1 changes glucose metabolism from aerobic glycolysis to OXPHOS, we measured lactate production and found that FBP1-expressing BLBC cells produced less lactate than their vector control cells, whereas FBP1-knockdown luminal cells had more lactate production (Figure 4D). We then investigated FBP1's role on cell growth under different oxygen conditions. At normoxic condition (21% oxygen), FBP1 expression induced a minor inhibition in cell growth in BLBC cell lines. Similarly, knockdown of FBP1 did not cause an apparent effect on the growth of luminal cells (Figure S4C). However, under hypoxic condition (0.1% oxygen), FBP1 expression induced a drastic growth inhibition in BLBC cell lines, whereas knockdown of FBP1 significantly reduced hypoxia-mediated growth inhibition in luminal cell lines (Figure 4E), suggesting that the effect of FBP1 on cell growth depends on oxygen. We thus examined oxygen consumption rate (OCR). We found that the basal OCR significantly increased in FBP1-expressing BLBC cells, whereas FBP1-knockdown luminal cells displayed a decrease in basal OCR (Figure 4F). Similar results were obtained in the analysis of ATP-linked and maximal OCR (Figure 4F).

FBP1 Inhibits Glycolysis and Increases OXPHOS

For every glucose molecule a cell consumes, aerobic glycolysis produces 2 ATP, whereas OXPHOS produces 36 ATP. We found that FBP1 expression or knockdown did not alter the steady-state level of ATP in BLBC or luminal cells under normoxic condition (Figure S5A). However, under hypoxia, the steady-state level of ATP was significantly decreased in FBP1-expressing BLBC cells, whereas knockdown of FBP1 greatly reduced hypoxia-mediated ATP reduction in luminal cells (Figure S5A). Consistent with these observations, oligomycin treatment resulted in a significant growth inhibition in FBP1-expressing BLBC cells. Conversely, knockdown of FBP1 provided luminal cells with resistance to this compound (Figure S5B). Although BLBC cell lines are less sensitive to growth inhibition mediated by hypoxia or oligomycin compared with their FBP1-expressing clones, they were extremely sensitive to glucose deprivation, as indicated by massive cell death and

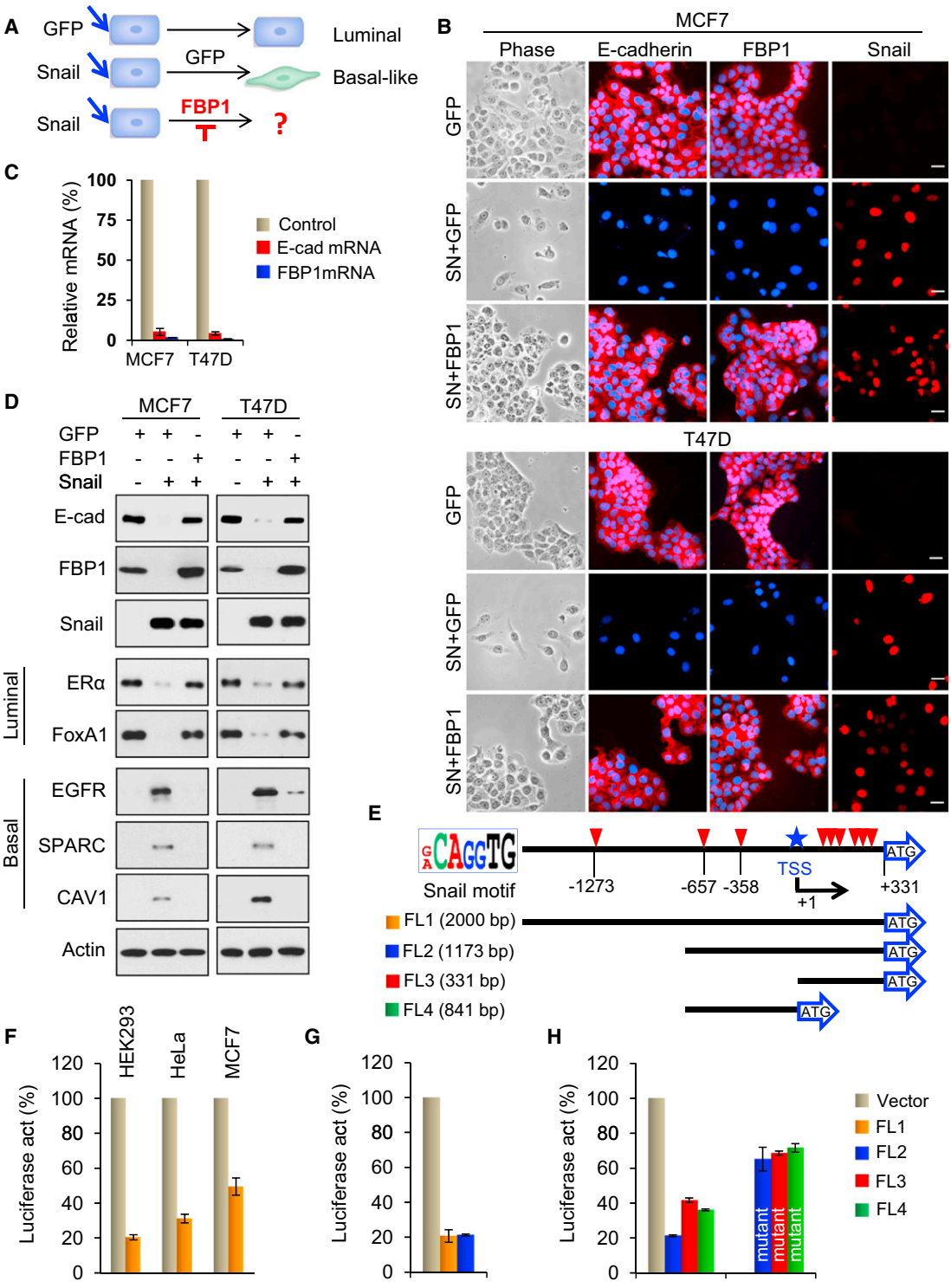

Figure 2. Snail Represses FBP1 Expression

(A) Schematic diagram showing that Snail was coexpressed with vector (GFP) or FBP1 (CMV promoter) in luminal subtype breast tumor cells.

(B) Snail was coexpressed with vector (GFP) or FBP1 in MCF7 and T47D cells for 4 days. Morphologic changes indicative of EMT are shown in the phase contrast images; expression of FBP1 and E-cadherin were analyzed by immunofluorescent staining. Nuclei were visualized with DAPI (blue). Scale bar = 20 μm.

(C) The mRNA levels of E-cadherin and FBP1 were quantitated by real-time PCR (mean ± SD in three separate experiments).

(D) Expression of E-cadherin, FBP1, Snail, luminal markers (ER-α and FoxA1), and basal markers (EGFR, SPARC, and Caveolin-1) for cells in (B) was analyzed by western blotting.

(E) Schematic diagram showing positions of nine potential Snail-binding E-boxes on the FBP1 promoter and FBP1 promoter luciferase construct used.

(legend continued on next page)

detachment from the cell substratum after 48 hr of glucose depletion (Figure S5C).

We further investigated the metabolic fate of [U-^{13}C]-glucose in vector- and FBP1-expressing MDA-MB231 cells by using stable isotope-resolved metabolomics (SIRM) (Fan et al., 2009; Fan et al., 2011; Le et al., 2012). Nuclear magnetic resonance (NMR) analysis of the culture media demonstrated a reduced $^{13}C_6$-glucose uptake and $^{13}C_3$-lactate excretion, leading to an overall decrease of $^{13}C_6$-glucose to $^{13}C_3$-lactate conversion in FBP1-expressing cells (Figures 5A and S5D). NMR analysis of ^{13}C-labeled metabolites in cell extracts also indicated a reduced $^{13}C_3$-lactate in FBP1-expressing cells (Figure 5B), consisting of reduced $^{13}C_3$-lactate excretion into the media. Interestingly, FBP1 expression also reduced ^{13}C abundance in the ribosyl unit of ribonucleotides and derivatives (i.e., AXP, UXP, NAD^+, and UDPG) (Figure 5B), suggesting that the pentose phosphate pathway (PPP), which is responsible for generating ribose-5-phosphate for the synthesis of ribonucleotides and NADPH production, is inhibited. In line with this finding, the ratio of $NADP^+$/NADPH was increased in FBP1-expressing MDA-MB231 cells, whereas this ratio was decreased in FBP1-knockdown MCF7 cells (Figure S5E). The decreased level of ^{13}C-UDPG in FBP1-expressing cells suggests that the glycosylation process is reduced. The same cell extracts were further analyzed by GC-MS to quantify ^{13}C-metabolites involved in glycolysis and the TCA cycle (Figure 5C). We found that the production of the m3 or $^{13}C_3$-isotopologues of glycerol-3-phosphate (G3P) and serine were significantly reduced in FBP1-expresing cells, which is again consistent with attenuated glycolytic activity. In line with the observations that FBP1 increased OXPHOS, the production of $^{13}C_2$ or m2-succinate, fumarate, and malate (markers of the first turn of the TCA cycle) as well as the $^{13}C_4$- or m4-citrate (markers of the second turn of the TCA cycle) (Fan et al., 2010) were increased in FBP1-expressing cells (Figure 5C). Together, these results indicate that FBP1 inhibits glycolytic flux, reduces biosynthesis (nucleotides via PPP, G3P for triacylglycerol synthesis, and serine for protein), and enhances OXPHOS.

FBP1 Suppresses PKM2 Activation and Increases Mitochondrial Complex I Activity and Reactive Oxygen Species Generation

To explore the underlying mechanisms of increased OXPHOS by FBP1, we first assessed the level of F-1,6-BP. FBP1 expression caused a dramatic decrease of F-1,6-BP level in BLBC cells, whereas knockdown of FBP1 led to a marked increase of F-1,6-BP in luminal cell lines (Figure 6A). We also measured pyruvate kinase (PK) activity and found that FBP1 significantly decreased PK activity in two BLBC cell lines; whereas knockdown of FBP1 increased PK activity in two luminal cells (Figure S6A). The PK activity contained both PKM1 and PKM2 activities and thus we could not distinguish the activation of PKM2 by F-1,6-BP. We next examined the tetrameric form of PKM2 using cross-linking agent. Surprisingly, PKM2 existed mainly in tetrameric form in two BLBC cell lines, whereas it appeared in monomer state in two luminal cell lines (Figure 6B). FBP1 expression significantly decreased the tetrameric PKM2, whereas knockdown of FBP1 increased the formation of tetrameric PKM2. These data indicate that loss of FBP1 activates PKM2, which facilitates lactate production and triggers the switch to aerobic glycolysis.

Because FBP1 expression enhanced oxygen consumption, we reasoned that FBP1 expression stimulates activity in the mitochondrial electron transport complexes (I, II, III, and IV of ETC) (Figure 6C). Complexes I and II use electrons donated from NADH and FADH2, respectively, to reduce coenzyme Q, which shuttles these electrons to complex III, where they are transferred to cytochrome c. Complex IV uses electrons from cytochrome c to reduce molecular oxygen to water. These actions produce a proton electrochemical potential gradient, and the free energy released is converted to ATP by ATP synthase (Chatterjee et al., 2011). We first compared the activity of the mitochondrial complexes I and II in terms of their contribution to the overall oxygen consumption. Complex I and II activity could be blocked by rotenone and TTFA, respectively, thus the oxygen consumption relies on the electron transport activity of the remaining active complex. As shown in Figure 6C, although OCR was higher in FBP1-expressing BLBC cell lines, addition of TTFA slightly and proportionally decreased OCR in both vector- and FBP1-expressing BLBC cells. A consistent trend was observed in vector- and FBP1-knockdown luminal cell lines (Figure 6C). However, treatment with rotenone dramatically reduced OCR in FBP1-expressing BLBC cells to levels found in vector control cells (Figure 6C). Consistently, treatment with rotenone also decreased OCR in luminal cells to levels similar to those found in the FBP1-knockdown luminal cells. We also measured complex I activity using purified mitochondria from these cells. FBP1-expressing BLBC cell lines had significant higher complex I activity, whereas FBP1-knockdown luminal cell lines had decreased complex I activity (Figure 6D). To identify the underlying mechanism, we performed microarray analysis (GSE41158) and determined that mitochondrial transcription factor B1M (TFB1M) was significantly higher in FBP1-expressing BLBC cells (Figure S6B). TFB1M is a nuclear gene encoding mitochondrial transcription factor that is essential for the mitochondrial biogenesis (Metodiev et al., 2009). Loss of TFB1M causes defects of protein translation in mitochondrial complex I components, resulting in impaired OXPHOS (Koeck et al., 2011). We found that TFB1M expression was increased in FBP1-expressing MDA-MB231 cells, whereas its expression was decreased in FBP1-knockdown MCF7 cells (Figures S6B and S6C). In addition, two targets of TFB1M from mitochondrial complex I, ND1 and ND5, but not components from complex

(F) FBP1 promoter luciferase construct (FL1) was coexpressed with Snail or vector in HEK293, HeLa, and MCF7 cells, respectively. After 48 hr, luciferase activities were determined and normalized (mean ± SD in three separate experiments).
(G) FBP1 promoter luciferase constructs (FL1 and FL2) were coexpressed with Snail or vector in HEK293 cells. Luciferase activities were determined as in (F).
(H) FBP1 promoter luciferase constructs (FL2, FL3, and FL4 as well as their E-box mutants) were coexpressed with Snail or vector in HEK293 cells. Luciferase activities were determined as in (F).
See also Figure S2.

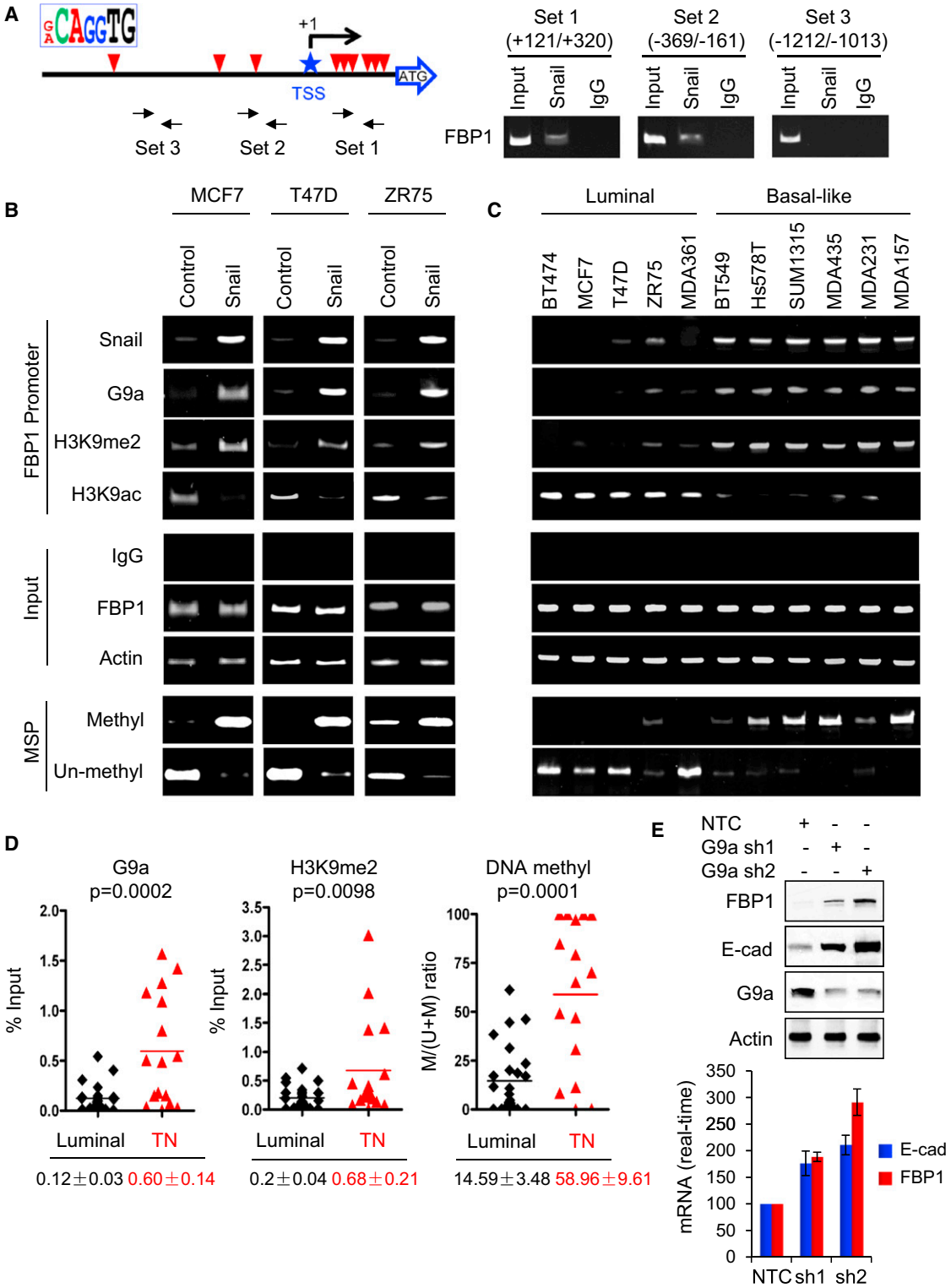

Figure 3. Snail and G9a Are Required for H3K9me2 and DNA Methylation at the FBP1 Promoter

(A) Three sets of primers used for FBP1 promoter ChIP are shown.

(B and C) The association of Snail and G9a, and the level of H3K9me2 and H3K9ac at the FBP1 promoter in cells that have undergone Snail-mediated EMT (B) and cell lines from Figure 1D (C) were analyzed by ChIP. DNA methylation at the FBP1 promoter was analyzed by MSP.

(D) The association of G9a, and the level of H3K9me2 and DNA methylation at the FBP1 promoter in luminal (25 cases) and triple-negative (16 cases) breast cancer tissues were analyzed by ChIP and MSP, respectively. Horizontal lines represent mean values. Statistical analyses (mean ± SD in three separate experiments) are shown below.

(legend continued on next page)

II-IV were also elevated in FBP1-expressing cells. Together, these data indicate that the rise of complex I activity is the main factor underlying the increase of mitochondrial oxygen consumption in FBP1-expressing cells.

In ETC, a small percentage of electrons are prematurely leaked to oxygen, mainly from complex I and/or complex III, forming the majority of reactive oxygen species (ROS; Chatterjee et al., 2011). To test whether an increase in mitochondrial OCR and complex I activity by FBP1 would accompany an increase of ROS, we examined intracellular ROS levels using CellROX deep red. FBP1-expressing BLBC cells showed a substantial increase in ROS levels, whereas FBP1-knockdown luminal cell lines induced a significant decrease of ROS (Figures 6E and 6F). A similar finding was observed for superoxide production using Mito-Sox Red and DHE staining (Figure S6D). These data indicate that FBP1 expression contributes to the increase of cellular ROS.

FBP1 Suppresses CSCs and Inhibits Tumorigenicity of Breast Cancer

To examine whether FBP1 expression alters CSC characteristics of BLBC, we examined tumorsphere formation of these cells under normoxic and hypoxic conditions. FBP1 expression greatly suppressed tumorsphere formation in BLBC cell lines (Figure 7A), and this inhibitory effect was enhanced by hypoxia (Figure S7A). Conversely, knockdown of FBP1 in luminal cell lines enhanced tumorsphere formation in normoxic condition, and this effect was also substantiated under hypoxia.

Breast CSCs are enriched in cells with a $CD44^{high}/CD24^{low}/EpCAM^{+}$ phenotype (Blick et al., 2010). We found that FBP1 expression significantly reduced the percentage of $CD44^{high}/CD24^{low}/EpCAM^{+}$ population in BLBC cell lines (Figures 7B and 7C). Conversely, knockdown of FBP1 induced a significant increase of $CD44^{high}/CD24^{low}/EpCAM^{+}$ population in luminal cell lines. Because CD44 is a known target of β-catenin, and because activation of β-catenin is often found in BLBC (DiMeo et al., 2009; Zeilstra et al., 2008), we reasoned that the elevated ROS caused by FBP1 expression compromises β-catenin activity. In the cellular aging process, ROS antagonizes β-catenin activity by shifting the interaction of β-catenin with TCF4 toward FOXO3a (Figure 7D) (Bowerman, 2005; Essers et al., 2005; Manolagas and Almeida, 2007). We found that β-catenin interacted with TCF4 in BLBC cells. However, the interaction of β-catenin with TCF4 was significantly decreased and substituted with an increased interaction of β-catenin with FOXO3a in FBP1-expressing cells (Figure 7E). Similarly, knockdown of FBP1 in luminal cells increased the interaction of β-catenin with TCF4. The differential interactions of β-catenin with TCF4 were consistent with the luciferase reporter assays showing that FBP1-expressing cells had lower TOP-Flash and higher FOXO3a luciferase activities than vector control cells (Figure S7B). In addition, expression of several target genes of β-catenin (Axin2, CD44, and ID2) and FOXO3a (CDKN2A and SOD2) were in line with these binding and promoter luciferase assays (Figure S7C). Consistently, NAC treatment restored the interaction of β-catenin with TCF4 as well as their luciferase activities and target gene expression (Figures 7E, S7B, and S7C). In addition, treatment with NAC and EUK134 restored tumorsphere formation in FBP1-expressing BLBC cells (Figure S7D).

We also measured the in vitro tumorigenicity of these cells using soft-agar assay. Although BT549 and SUM1315 cells could not form colonies, the other FBP1-expressing BLBC cell lines had significantly fewer colonies than their corresponding vector controls; whereas knockdown of FBP1 increased colony formation in luminal cell lines (Figure 8A). NAC treatment restored colony growth in FBP1-expressing BLBC cells, indicating that the elevated ROS impairs their tumorigenicity in vitro (Figure S8A). To examine the tumorigenicity in vivo, we injected mammary fat pads of SCID mice with the following three pairs of cell lines: (1) vector- and FBP1-expressing MDA-MB231 cells, (2) vector- and FBP1-expressing MDA-MB435 cells, and (3) vector- and FBP1-knockdown MCF7 cells. As shown in Figure 8B, FBP1-expressing MDA-MB231 cells failed to form tumors in all six mice. Similarly, tumors derived from FBP1-expressing MDA-MB435 cells had a significantly reduced tumor size compared with vector control cells. In line with these findings, FBP1-knockdown MCF7 cells showed significantly enhanced tumor growth compared with vector control cells (Figure 8B). Strikingly, NAC treatment greatly increased tumor formation in FBP1-expressing MDA-MB231 and MDA-MB435 cells (Figures S8B and S8C). Together, these data indicate that FBP1 expression increases ROS production, which compromises CSC properties by shifting the interaction of β-catenin from TCF4 to FOXO3a, and thus inhibits tumorigenicity in vitro and tumor formation in vivo.

We then examined the correlation of FBP1 expression with patient survival in NKI295 that consists of 295 patients with node-negative breast cancer (van de Vijver et al., 2002). Expression of FBP1 can separate patients into two prognostic groups, with high FBP1 expression having a better survival rate (Figure 8C). This clinical validation supports the finding that FBP1 repression is critical in EMT and BLBC.

DISCUSSION

Our study provides several insights into EMT and breast cancer. First, loss of FBP1 is essential to trigger glycolytic reprogramming and results in several metabolic benefits in BLBC: (1) increase glucose uptake and sensitivity as evidenced by elevated TXNIP and IR phosphorylation after stimulation, (2) increased glycolytic intermediates for biosynthesis (such as PPP, glycerol-3-phosphate, and serine), (3) maintenance of ATP production under hypoxia, and (4) reduced oxygen dependence and ROS production (Figure 8D). These observations are consistent with the notion that FBP1 deficiency causes hypoglycemia and acidosis in patients and that inhibition of FBP1 restores glucose uptake in the type 2 diabetic model.

(E) Expression of FBP1 and E-cadherin was examined in MDA-MB231 cells with knockdown of G9a expression (top panel). Their mRNA levels were also quantified by real-time PCR (bottom panel). Data are presented as a percentage of non-target control (NTC) values (mean ± SD in three separate experiments in duplicates).
See also Figure S3.

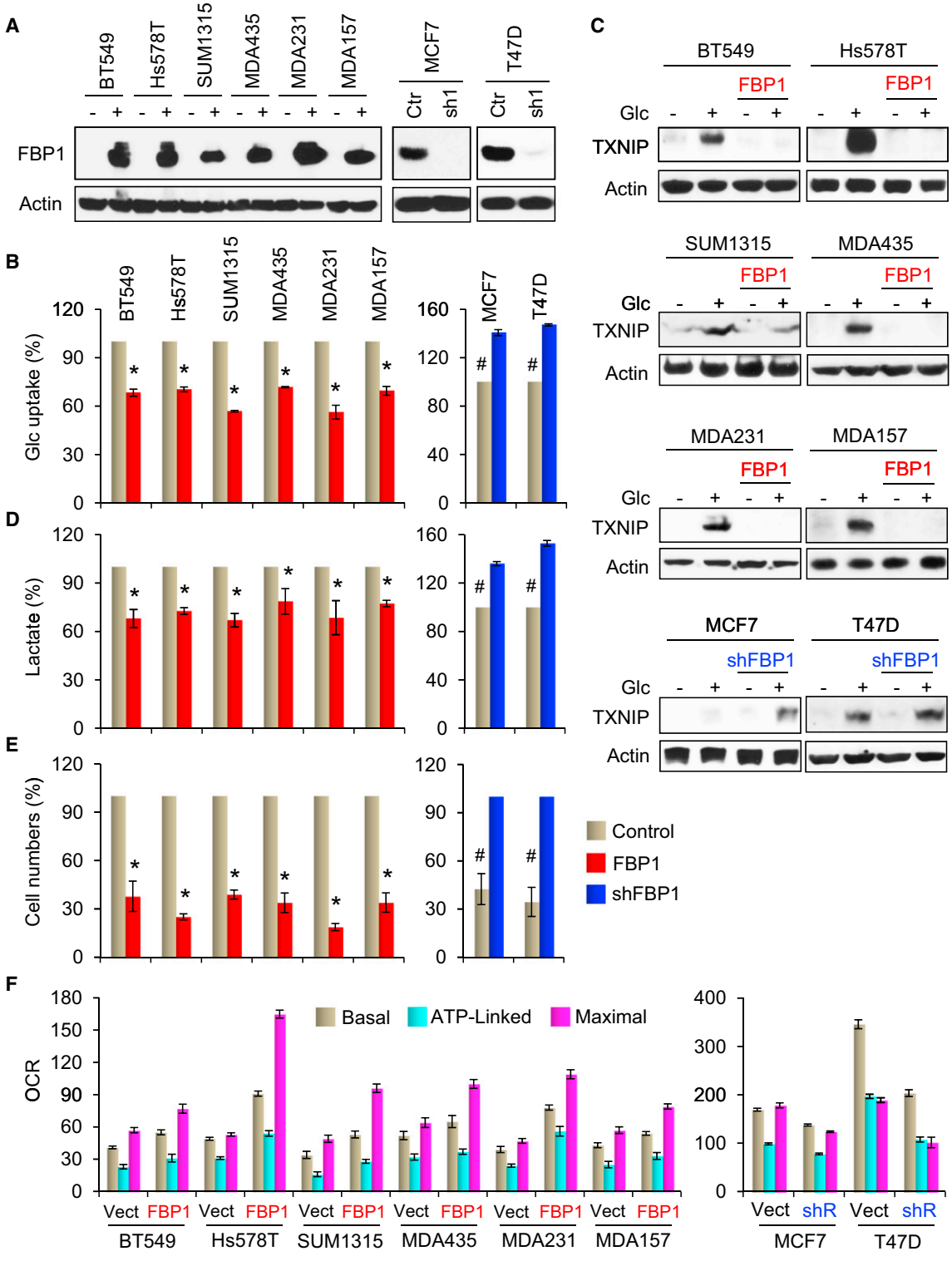

Figure 4. FBP1 Inhibits Glucose Uptake and Sensitivity and Suppresses Cell Growth under Hypoxia

(A) Stable clones with FBP1 expression or knockdown were established in six BLBC and two luminal cell lines, respectively.

(B) Glucose uptake was measured.

(C) Cells were deprived for glucose for 12 hr followed by glucose stimulation for additional 3 hr. TXNIP expression was examined by western blotting.

(D) Lactate excretion was measured.

(E) Cell growth under hypoxic condition was measured by cell-count assay for 2 days. Data are presented as a percentage of vector control values for BLBC cells, whereas data are presented as a percentage of FBP1-knockdown groups for luminal cells (mean ± SD in three separate experiments in triplicates).

(legend continued on next page)

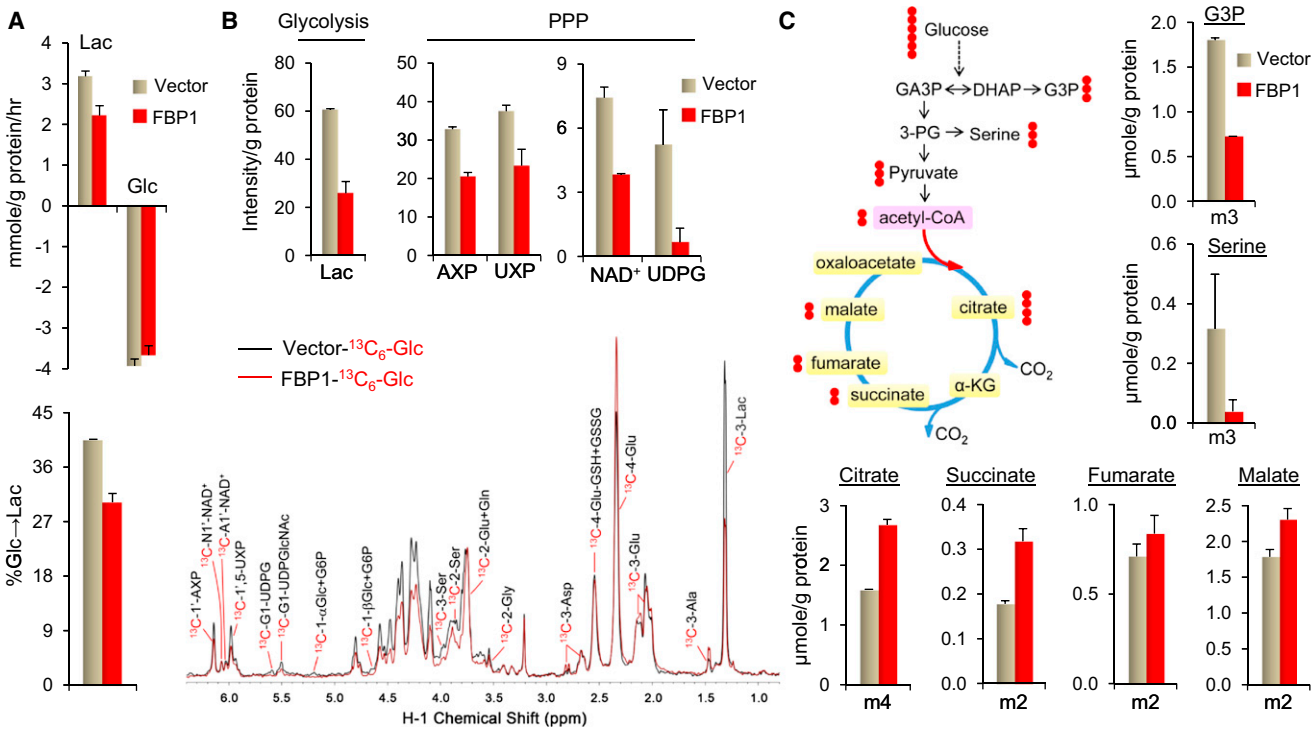

Figure 5. FBP1 Inhibits Glycolysis and Increases OXPHOS

(A) $^{13}C_6$-Glucose uptake, $^{13}C_3$-lactate production, and the conversion of $^{13}C_6$-Glucose to $^{13}C_3$-lactate were measured by 1D ^{1}H NMR analysis of the media of vector- and FBP1-expressing MDA-MB231 cells grown in $^{13}C_6$-Glucose (mean ± SEM in duplicate). ^{1}H NMR spectra from the media are shown in Figure S5D.

(B) A pair of representative 1D ^{1}H{^{13}C} HSQC NMR spectra show the changes in ^{13}C abundance (represented by the intensity of ^{13}C-attached ^{1}H peaks) of various assigned metabolites elicited by FBP1 expression in MDA-MB231 cells (black, control vector; red, FBP1, bottom panel). The relative ^{13}C abundance of indicated metabolites from cell extracts was quantified from their HSQC peak intensity (Fan and Lane, 2008) (mean ± SEM in duplicate). Lac, lactate; AXP, adenine nucleotides; UXP, uracil nucleotides; UDPG, UDP-glucose.

(C) Top left panel shows the expected ^{13}C (●) labeling patterns of glycolytic and TCA cycle metabolites with $^{13}C_6$-Glc as tracer. The doubly ^{13}C labeled TCA cycle metabolites are derived from the first turn of the TCA cycle while the quadruply ^{13}C labeled citrate is produced from the second turn of the cycle. The levels of several indicated ^{13}C isotopologues of glycolytic and TCA cycle metabolites were obtained from the GC-MS analysis of the same cell extracts as in (B) (mean ± SEM in duplicate).

See also Figure S5.

The activity of PKM2 oscillates between the activated tetrameric form and inactivated monomeric state, which constitutes the metabolic budget system in tumor metabolism (Mazurek et al., 2005). F-1,6-BP increases the formation of tetrameric PKM2. Glucose is then fueled to lactate along with ATP production until F-1,6-BP levels drop below a minimum signal level, which causes the disassembly of the tetrameric PKM2 into a monomeric state. We found that PKM2 mainly existed in tetrameric form in BLBC cells and existed predominantly in a monomeric state in luminal cells. This observation corresponds with the findings that BLBC cells contain a high level of F-1,6-BP, an increased PK activity, and increased lactate production. FBP1 expression significantly decreased the formation of tetrameric PKM2 in BLBC cells by reducing F-1,6-BP. Because the major function of glycolysis is to provide high levels of glycolytic intermediates for biomass synthesis, we speculate that two modes of PKM2 are used in glycolysis. The first mode is the inhibition of PKM2 (economic mode), which blocks glycolytic flux for accumulation of intermediates required for biosynthesis. The second mode is the overall increase of glycolytic flux with activation of PKM2 (luxury mode). The rise of intermediates results not from a block of PKM2, but from an increased load of glycolysis through glucose (Figure 8D). As pointed out by Vander Heiden and colleagues, although this seems wasteful, it ensures that the glycolytic intermediates will not be depleted and maintain precursor concentrations at constant and ample levels for allowing maximum biosynthesis during rapid cell growth (Lunt and Vander Heiden, 2011). Our study indicates that BLBC cells employ the luxury mode of glycolysis by suppressing FBP1 for increasing glucose assimilation and rapid channeling of glycolytic intermediates in biosynthesis at the cost of host.

PKM2 is the main enzyme for ATP production in glycolysis. This inefficient but faster mode of ATP production may be

(F) Oxygen consumption was measured (mean ± SD in three separate experiments in triplicate).

For B and D, data are presented as a percentage of vector control values (mean ± SD in three separate experiments in triplicates). For B, D, and E, *$p < 0.01$ and #$p < 0.01$ for vector control cells compared with their FBP1-expressing or FBP1-knockdown clones, respectively.

See also Figure S4.

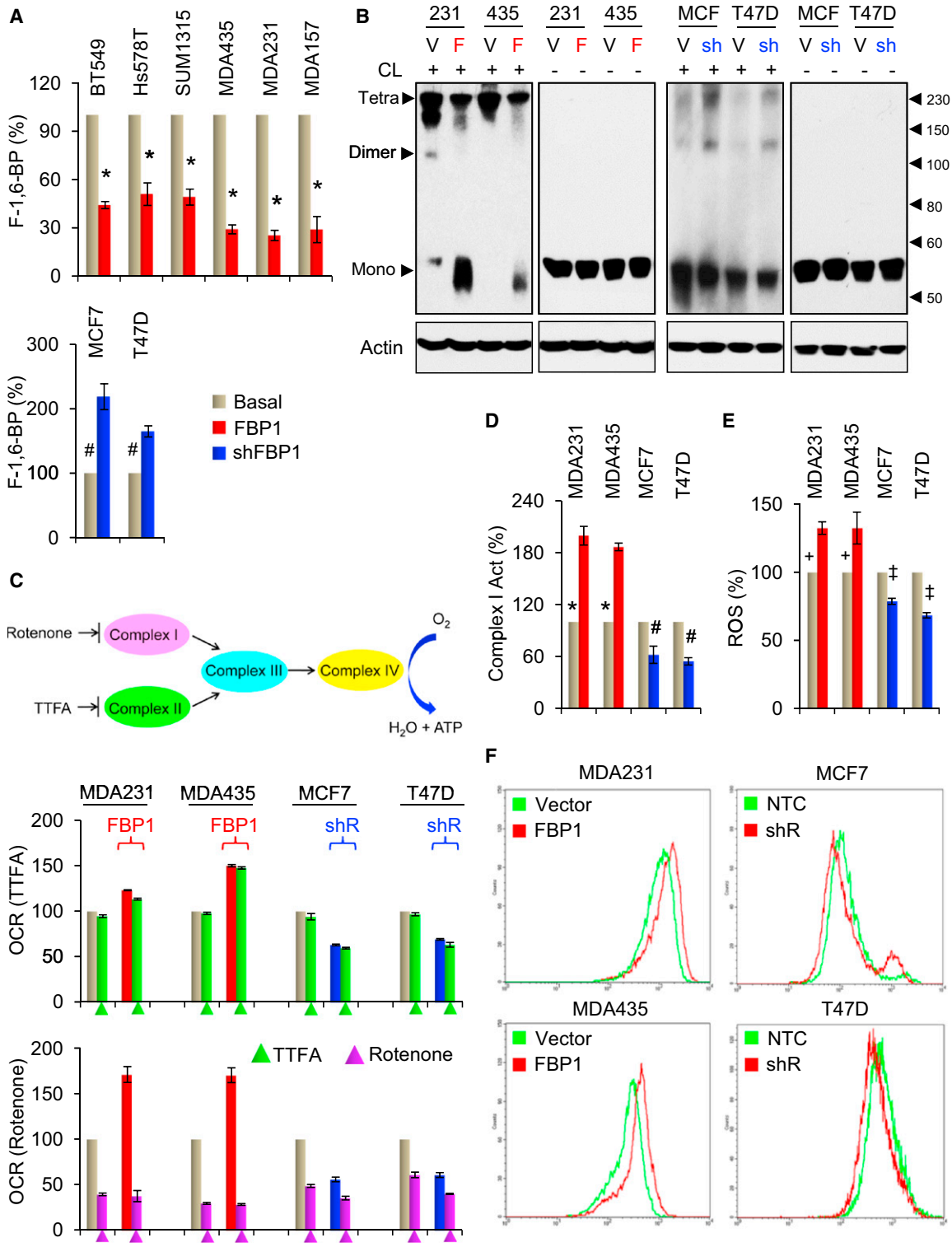

Figure 6. FBP1 Suppresses PKM2 Activation and Increases Complex I Activity and ROS Production

(A) F-1,6-BP was measured in FBP1-expressing and FBP1-knockdown clones.

(B) Cells were either treated with (+) or without (−) 1% formaldehyde (crosslinker; CL) for 20 min immediately after cell lysis. The states of monomer, dimer, and tetramer of PKM2 were analyzed by western blotting.

(C) Schematic diagram showing the electron transfer from mitochondrial complex I to IV. Cells were treated with Rotenone and TTFA, respectively. Oxygen consumption was measured (mean ± SD in three separate experiments in triplicate).

(D) Complex I activity was measured from mitochondria isolated from cells in (C).

(legend continued on next page)

preferred to meet the cellular demands of BLBC, particularly under hypoxic condition. Under hypoxia, the steady-state level of ATP in BLBC cells declined slightly; however, FBP1 expression resulted in a dramatic plunge in ATP level. This is in line with the observation that BLBC cells are less sensitive to growth inhibition under hypoxia or by oligomycin. Given that BLBC cells are highly invasive, this metabolic switch empowers them to absorb glucose and maintain ATP level in a nutrient-poor and hypoxic condition. In addition, the acidic microenvironment created by excreted lactate facilitates the degradation of extracellular matrix and protects BLBC cells from inhibition by an immune response at the metastatic site (Figure 8D).

The phenomenon during which increased glucose uptake and exacerbated glycolytic activity often accompany OXPHOS inhibition is known as a Crabtree effect and had been identified in tumors and other mitotically active tissues (Crabtree, 1929). We found that the inhibition of complex I activity is mainly responsible for the Crabtree effect in BLBC cells. Expression of FBP1 significantly increased mitochondrial complex I activity by inducing the expression of TFB1M, which is required for the translation of ND1 and ND5 of mitochondrial complex I (Koeck et al., 2011). These data provide mechanistic insights and support our finding that loss of FBP1 suppresses OXPHOS in BLBC cells.

Second, our results indicate that the glycolytic switch enhances CSC characteristics in BLBC by reducing ROS. It has been noted that somatic cells primarily utilize OXPHOS for their energy production, whereas pluripotent cells rely on glycolysis (Facucho-Oliveira and St John, 2009). Using an iPSC as a model in stem cell reprogramming, mitochondria were found to change from a mature cristae-rich morphology in somatic cells to more immature spherical and cristae-poor structures in iPSCs. Intriguingly, the glycolytic change occurs in cells prior to their acquisition of pluripotent markers, suggesting that the glycolytic switch plays a causative role in the iPSC reprogramming rather than simply being a consequence of acquiring pluripotency. The induction of pluripotency with a glycolytic switch is consistent with the observation that a hypoxic environment maintains the stem cell state and hypoxia facilitates the reprogramming process (Mohyeldin et al., 2010). In the stem cell niche, protection from ROS is critical for the maintenance of self-renewal of hematopoietic stem cells and human and mouse breast CSCs (Diehn et al., 2009). These observations indicate that the self-renewal potential of CSCs is exquisitely sensitive to the level of ROS. We found that FBP1-expressing BLBC cells increased OXPHOS and ROS production. The increased ROS was associated with the suppression of tumorsphere and decreased CSC markers ($CD44^{high}/CD24^{low}/EpCAM^{+}$). In addition, FBP1 expression in BLBC cells inhibited tumorigenicity in vitro and suppressed tumor formation in vivo. Mechanistically, elevated ROS shifts the interaction of β-catenin from TCF4 to FOXO3a and thus compromises β-catenin activity, which is essential for the maintenance of pluripotency. NAC treatment returns the interaction of β-catenin with TCF4 and restores tumorigenicity in vitro and in vivo. Together, these data indicate that the loss of FBP1 greatly increases CSC traits by repressing ROS production and maintaining the interaction of β-catenin with TCF4 in BLBC.

Third, our study indicates that FBP1 is a major downstream target of Snail in controlling glycolysis. We identified that the Snail-G9a-Dnmt1 complex, which is required for E-cadherin silencing, is responsible for FBP1 repression in BLBC. FBP1 silencing is required for Snail-mediated EMT and the conversion from luminal to basal-like phenotype in breast cancer. In addition, knockdown of Snail or G9a restores the expression of E-cadherin and FBP1. Our results indicate that this metabolic reprogramming (resulting from the loss of FBP1) synergizes with the loss of E-cadherin to sustain CSC-like properties during dissemination and metastasis. Our study strengthens the notion that metabolic reprogramming is inextricably intertwined with tumorigenesis and fortifies Warburg's historical claim that metabolism is an actionable event instead of an accompanied biomarker in oncogenesis (Ward and Thompson, 2012). Our study also reveals that the Snail-mediated epigenetic regulation may represent the Achilles' heel of BLBC. Thus, targeting this chromatin modification complex will generate an entirely effective approach for treating metastatic breast cancer.

EXPERIMENTAL PROCEDURES

Plasmids, siRNA, and Antibodies

FBP1 shRNA was purchased from MISSION shRNA at Sigma-Aldrich (St Louis, MO). Human FBP1 was amplified from a HeLa cDNA library and subcloned into pLenti6.3. Antibody information is provided in the Supplemental Experimental Procedures.

Cell Culture

Breast cancer cell lines were cultured as described previously (Dong et al., 2012). For establishing stable transfectants with expression or knockdown of FBP1, BLBC cells and luminal cells were transfected with pLenti6.3/FBP1 and FBP1 shRNA, respectively; stable clones were selected with puromycin (300 ng/ml) for 4 weeks.

Immunostaining, Immunoprecipitation, Immunoblotting, Immunohistochemical Staining

All protocols are described in detail in the Supplemental Experimental Procedures.

Human Breast Tumors

The frozen fresh tumor samples were collected from resected breast tumors from patients at the University of Texas MD Anderson Cancer Center with informed consent and institutional IRB approval. These frozen samples were snap-frozen in liquid nitrogen and stored at −80°C. Data regarding the stage, grade, and expression of ER-α, PR, and HER2 are described previously (Dong et al., 2012).

Metabolic Assays

Glucose uptake, lactate production, ATP levels, and PK activity were measured by assay kits from BioVision (San Francisco, CA). Oxygen consumption was determined using the Seahorse Extracellular Flux (XF-96)

(E and F) ROS generation was analyzed by flow cytometry (mean ± SD in three separate experiments in duplicates). Representative images are shown (F). $^{+}p < 0.05$ and $^{‡}p < 0.05$ for vector control cells compared with their FBP1-expressing or FBP1-knockdown clones, respectively.
For A and D, data are presented as a percentage of vector control values (mean ± SD in three separate experiments in triplicates). $^{*}p < 0.01$ and $\#p < 0.01$ for vector control cells compared with their FBP1-expressing or FBP1-knockdown clones, respectively.
See also Figure S6.

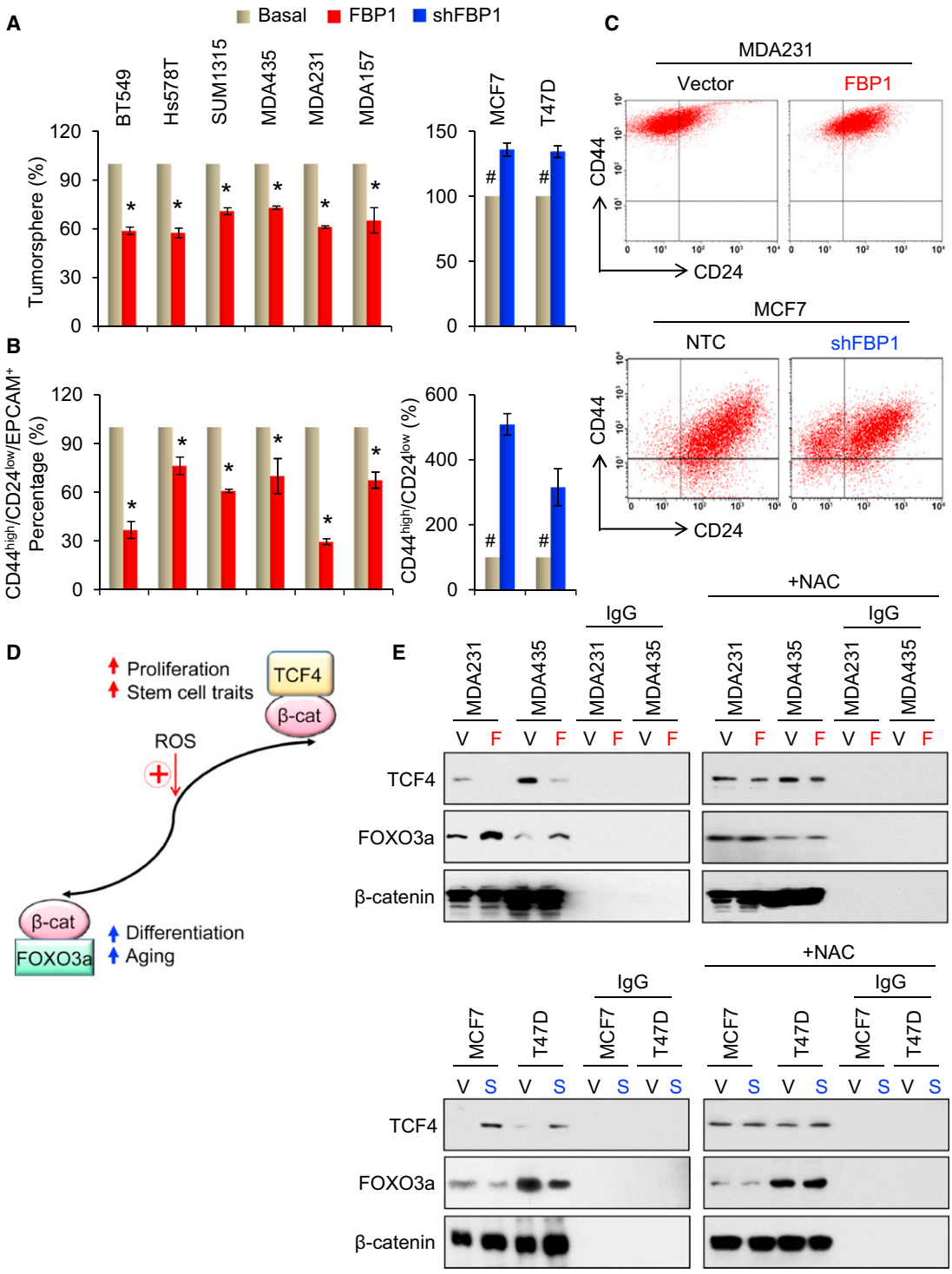

Figure 7. FBP1 Inhibits Tumorsphere Formation and Reduces CSC Population

(A) Tumorsphere formation was assessed under normoxic conditions.

(B and C) The CSC population ($CD44^{high}/CD24^{low}/EpCAM^{+}$) was analyzed by flow cytometry. Representative images for MDA-MB231 and MCF7 cells are shown in (C).

(D) Schematic diagram of the interaction of β-catenin with TCF4 and FOXO3a.

(E) FBP1-expressing BLBC cells (F) as well as in FBP1-knockdown luminal cells (S) were treated with or without NAC overnight; the interactions of β-catenin with TCF4 and FOXO3a were examined by immunoprecipitating β-catenin following immunoblot of TCF4 and FOXO3a.

For A and B, data are presented as a percentage of vector control values (mean ± SD in three separate experiments in duplicates). *$p < 0.01$ and #$p < 0.01$ for vector control cells compared with their FBP1-expressing or FBP1-knockdown clones, respectively.

See also Figure S7.

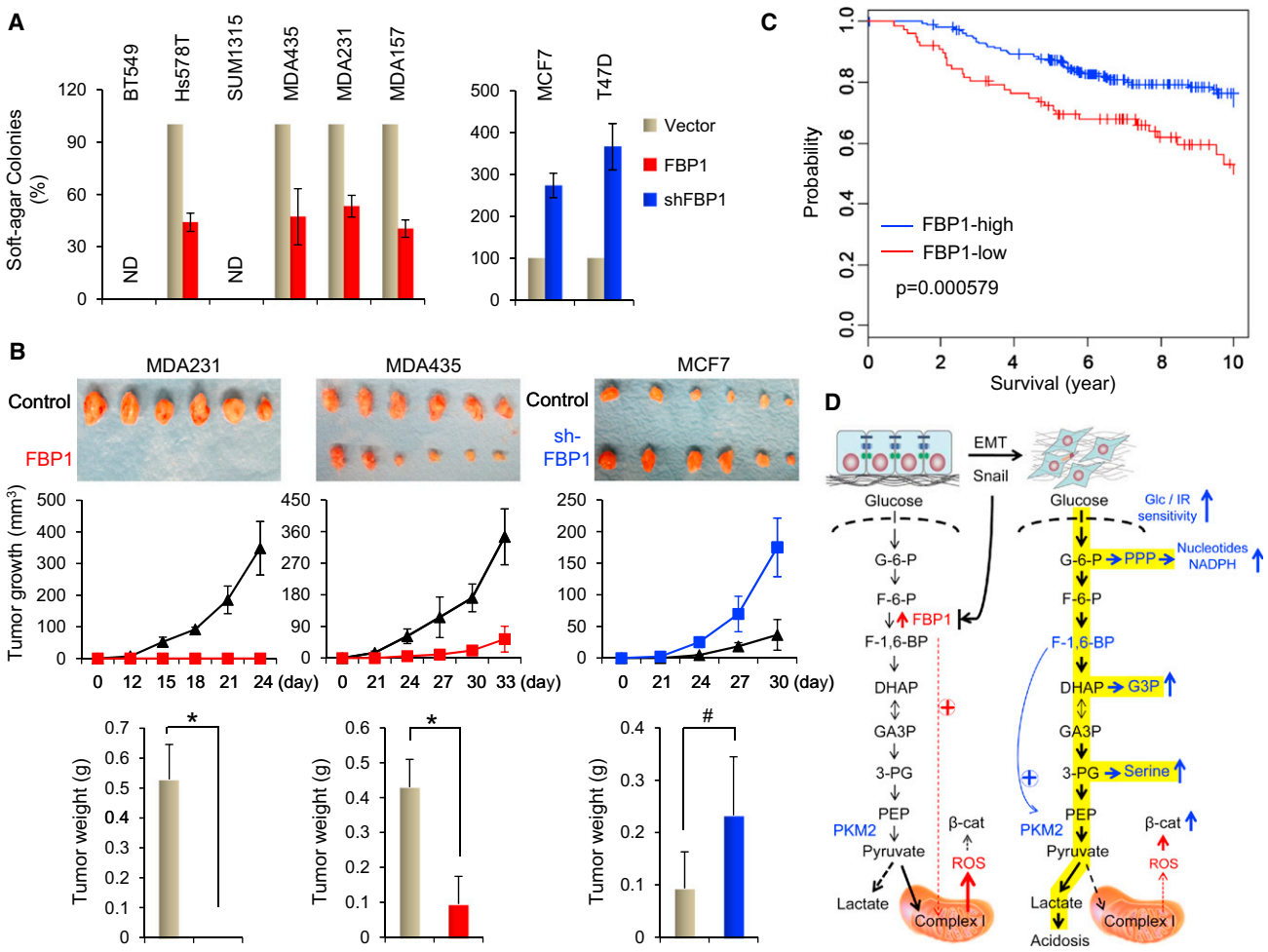

Figure 8. FBP1 Suppresses Tumorigenicity In Vitro and In Vivo

(A) Data of soft-agar assay are presented as a percentage of vector control cell lines (mean ± SD in three separate experiments with duplicates). ND, no colonies detected.

(B) Tumor growth was monitored every 3 days; tumor size and weight were recorded. Data are represented as mean ± SEM from six mice. *$p < 0.01$ and #$p < 0.01$ for vector control cells compared with their FBP1-expressing or FBP1-knockdown clones, respectively.

(C) Kaplan-Meier overall survival curve separates the tumors into two groups based on FBP1 expression.

(D) A proposed model to illustrate the transcription repression of FBP1 by Snail in EMT and BLBC, which results in the switch to aerobic glycolysis and increased β-catenin activity.

See also Figure S8.

analyzer (Seahorse Bioscience, Chicopee, MA). To allow comparison between experiments, data are presented as OCR in pMol/min/104 cells. Basal OCR were measured four times and plotted as a function of cells with and without treatment under the basal condition followed by the sequential addition of oligomycin (1 μg/ml) and FCCP (1 μM) as indicated. The progress curve is annotated to show the relative contribution of basal, ATP-linked and maximal oxygen consumption after the addition of FCCP, and the reserve capacity of the cells. The intracellular concentration of F-1,6-BP was examined by treating cells with 1.25 ml of perchloric acid; cells were then pelleted by centrifugation at 2500× g for 10 min. The cell pellet was resuspended in 0.2 ml of perchloric acid (6%) and 0.2 ml of water. After centrifugation, the pH of the combined supernatant was adjusted to 3.5 with 1% potassium carbonate. F-1,6-BP in the supernatant was determined spectrophotometrically by measuring the decrease of NADH to NAD^+ at 340 nm. Complex I specific activity was assayed as described by Sinthupibulyakit (Sinthupibulyakit et al., 2010) by following the decrease in absorbance due to the oxidation of NADH at 340 nm. The activity was calculated by the differences with and without the complex I inhibitor, rotenone.

For the [U-$^{13}C_6$]-glucose tracer experiment, Vector- and FBP1-expressing MDA-MB231 cells were cultured in the DMEM medium with glucose replaced by 0.1% $^{13}C_6$-glucose for 24 hr. Polar metabolites were extracted from cells and media using the acetonitrile/water/chloroform partitioning and 10% trichloracetic acid methods, respectively. The extracts were subjected to 1D ^1H and $^1H\{^{13}C\}$ HSQC NMR and GC-MS analysis, as previously described (Fan et al., 2011; Le et al., 2012).

DNA Methylation Analysis, ChIP, Quantitative Real-Time PCR, and Luciferase Reporter Assay

The methods used are described in the Supplemental Experimental Procedures.

Metabolic Assays, Colony Formation Assay, Mammosphere Assay, and Flow Cytometry Analysis

All methods are described in detail in the Supplemental Experimental Procedures.

Xenograft Studies

Female ICR-SCID mice (6–8 weeks old) were purchased from Taconic (Germantown, NY) and maintained and treated under specific pathogen-free conditions. All procedures were approved by the Institutional Animal Care and Use Committee at the University of Kentucky College of Medicine and conformed to the legal mandates and federal guidelines for the care and maintenance of laboratory animals. The mice were injected with 1×10^6 FBP1-expressing or knockdown cells on the right MFP and control cells on the left MFP. The mice were then randomly divided into two groups: standard water supply and water supplemented with 40 mM NAC. Tumor formation was examined every 2 to 3 days for the whole duration of the experiment. Tumors were harvested and weighed at the experimental endpoint, and the tumor mass derived from cells with FBP1 expression or knockdown and vector control in both flanks of each mouse were compared.

Statistical Analysis

Experiments were repeated at least twice. Results are expressed as mean ± SD or SEM as indicated. An independent Student's t test was performed to analyze the assay results; a two-tailed Student's t test was used to compare the intergroup differences. A p value < 0.05 was considered statistically significant.

ACCESSION NUMBERS

Microarray data of FBP1 expression in MDA-MB231 and Hs578T cells were deposited at the Gene Expression Omnibus with the accession number GSE41158.

SUPPLEMENTAL INFORMATION

Supplemental Information includes eight figures and Supplemental Experimental Procedures and can be found with this article online at http://dx.doi.org/10.1016/j.ccr.2013.01.022.

ACKNOWLEDGMENTS

We thank Ms. Ramya Balasubramaniam for technical assistance in metabolomics experiments, Dr. Sam Arumugam at J.G. Brown Cancer Center NMR facility for NMR data acquisition, and Dr. Cathy Anthony for critical reading and editing of this manuscript. This work was supported by grants from NIH (CA125454 to B.P.Z.; CA049797 and CA073599 to D.St.C.; P20CA1530343 to B.M.E.; CA118434-01A2 and 1R01ES022191-01 to T.W.M.F.), Susan G Komen Foundation (KG081310), Mary Kay Ash Foundation (to B.P.Z.), National Science Foundation (EPS-0447479 to T.W.M.F.), Edward P. Evans Foundation (to D.St.C.), and pre-doctoral fellowship (BC101068) from DoD Breast Cancer Research Program (to Y.L.).

Received: April 1, 2012
Revised: September 25, 2012
Accepted: January 29, 2013
Published: February 28, 2013

REFERENCES

Blick, T., Hugo, H., Widodo, E., Waltham, M., Pinto, C., Mani, S.A., Weinberg, R.A., Neve, R.M., Lenburg, M.E., and Thompson, E.W. (2010). Epithelial mesenchymal transition traits in human breast cancer cell lines parallel the CD44(hi/)CD24 (lo/-) stem cell phenotype in human breast cancer. J. Mammary Gland Biol. Neoplasia *15*, 235–252.

Bowerman, B. (2005). Cell biology. Oxidative stress and cancer: a beta-catenin convergence. Science *308*, 1119–1120.

Chatterjee, A., Dasgupta, S., and Sidransky, D. (2011). Mitochondrial subversion in cancer. Cancer Prev. Res. (Phila.) *4*, 638–654.

Chen, M., Zhang, J., Li, N., Qian, Z., Zhu, M., Li, Q., Zheng, J., Wang, X., and Shi, G. (2011). Promoter hypermethylation mediated downregulation of FBP1 in human hepatocellular carcinoma and colon cancer. PLoS ONE *6*, e25564.

Christofk, H.R., Vander Heiden, M.G., Harris, M.H., Ramanathan, A., Gerszten, R.E., Wei, R., Fleming, M.D., Schreiber, S.L., and Cantley, L.C. (2008). The M2 splice isoform of pyruvate kinase is important for cancer metabolism and tumour growth. Nature *452*, 230–233.

Crabtree, H.G. (1929). Observations on the carbohydrate metabolism of tumours. Biochem. J. *23*, 536–545.

Dang, C.V., Kim, J.W., Gao, P., and Yustein, J. (2008). The interplay between MYC and HIF in cancer. Nat. Rev. Cancer *8*, 51–56.

Dhasarathy, A., Phadke, D., Mav, D., Shah, R.R., and Wade, P.A. (2011). The transcription factors Snail and Slug activate the transforming growth factor-beta signaling pathway in breast cancer. PLoS ONE *6*, e26514.

Diehn, M., Cho, R.W., Lobo, N.A., Kalisky, T., Dorie, M.J., Kulp, A.N., Qian, D., Lam, J.S., Ailles, L.E., Wong, M., et al. (2009). Association of reactive oxygen species levels and radioresistance in cancer stem cells. Nature *458*, 780–783.

DiMeo, T.A., Anderson, K., Phadke, P., Fan, C., Perou, C.M., Naber, S., and Kuperwasser, C. (2009). A novel lung metastasis signature links Wnt signaling with cancer cell self-renewal and epithelial-mesenchymal transition in basal-like breast cancer. Cancer Res. *69*, 5364–5373.

Dong, C., Wu, Y., Yao, J., Wang, Y., Yu, Y., Rychahou, P.G., Evers, B.M., and Zhou, B.P. (2012). G9a interacts with Snail and is critical for Snail-mediated E-cadherin repression in human breast cancer. J. Clin. Invest. *122*, 1469–1486.

Elstrom, R.L., Bauer, D.E., Buzzai, M., Karnauskas, R., Harris, M.H., Plas, D.R., Zhuang, H., Cinalli, R.M., Alavi, A., Rudin, C.M., and Thompson, C.B. (2004). Akt stimulates aerobic glycolysis in cancer cells. Cancer Res. *64*, 3892–3899.

Emery, J.L., Howat, A.J., Variend, S., and Vawter, G.F. (1988). Investigation of inborn errors of metabolism in unexpected infant deaths. Lancet *2*, 29–31.

Essers, M.A., de Vries-Smits, L.M., Barker, N., Polderman, P.E., Burgering, B.M., and Korswagen, H.C. (2005). Functional interaction between beta-catenin and FOXO in oxidative stress signaling. Science *308*, 1181–1184.

Facucho-Oliveira, J.M., and St John, J.C. (2009). The relationship between pluripotency and mitochondrial DNA proliferation during early embryo development and embryonic stem cell differentiation. Stem Cell Rev. *5*, 140–158.

Fan, T.W., Lane, A.N., Higashi, R.M., Farag, M.A., Gao, H., Bousamra, M., and Miller, D.M. (2009). Altered regulation of metabolic pathways in human lung cancer discerned by (13)C stable isotope-resolved metabolomics (SIRM). Mol. Cancer *8*, 41.

Fan, T.W., Yuan, P., Lane, A.N., Higashi, R.M., Wang, Y., Hamidi, A.B., Zhou, R., Guitart, X., Chen, G., Manji, H.K., and Kaddurah-Daouk, R. (2010). Stable isotope-resolved metabolomic analysis of lithium effects on glial-neuronal metabolism and interactions. Metabolomics *6*, 165–179.

Fan, T.W., Lane, A.N., Higashi, R.M., and Yan, J. (2011). Stable isotope resolved metabolomics of lung cancer in a SCID mouse model. Metabolomics *7*, 257–269.

Fan, T.W.M., and Lane, A.N. (2008). Structure-based profiling of metabolites and isotopomers by NMR. Prog. Nucl. Magn. Reson. Spectrosc. *52*, 69–117.

Koeck, T., Olsson, A.H., Nitert, M.D., Sharoyko, V.V., Ladenvall, C., Kotova, O., Reiling, E., Ronn, T., Parikh, H., Taneera, J., et al. (2011). A common variant in TFB1M is associated with reduced insulin secretion and increased future risk of type 2 diabetes. Cell Metab. *13*, 80–91.

Koppenol, W.H., Bounds, P.L., and Dang, C.V. (2011). Otto Warburg's contributions to current concepts of cancer metabolism. Nat. Rev. Cancer *11*, 325–337.

Le, A., Lane, A.N., Hamaker, M., Bose, S., Gouw, A., Barbi, J., Tsukamoto, T., Rojas, C.J., Slusher, B.S., Zhang, H., et al. (2012). Glucose-independent glutamine metabolism via TCA cycling for proliferation and survival in B cells. Cell Metab. *15*, 110–121.

Li, M.V., Chang, B., Imamura, M., Poungvarin, N., and Chan, L. (2006). Glucose-dependent transcriptional regulation by an evolutionarily conserved glucose-sensing module. Diabetes *55*, 1179–1189.

Liu, X., Wang, X., Zhang, J., Lam, E.K., Shin, V.Y., Cheng, A.S., Yu, J., Chan, F.K., Sung, J.J., and Jin, H.C. (2010). Warburg effect revisited: an epigenetic link between glycolysis and gastric carcinogenesis. Oncogene *29*, 442–450.

Lunt, S.Y., and Vander Heiden, M.G. (2011). Aerobic glycolysis: meeting the metabolic requirements of cell proliferation. Annu. Rev. Cell Dev. Biol. *27*, 441–464.

Manolagas, S.C., and Almeida, M. (2007). Gone with the Wnts: beta-catenin, T-cell factor, forkhead box O, and oxidative stress in age-dependent diseases of bone, lipid, and glucose metabolism. Mol. Endocrinol. *21*, 2605–2614.

Mazurek, S., Boschek, C.B., Hugo, F., and Eigenbrodt, E. (2005). Pyruvate kinase type M2 and its role in tumor growth and spreading. Semin. Cancer Biol. *15*, 300–308.

Metodiev, M.D., Lesko, N., Park, C.B., Camara, Y., Shi, Y., Wibom, R., Hultenby, K., Gustafsson, C.M., and Larsson, N.G. (2009). Methylation of 12S rRNA is necessary for in vivo stability of the small subunit of the mammalian mitochondrial ribosome. Cell Metab. *9*, 386–397.

Mohyeldin, A., Garzon-Muvdi, T., and Quinones-Hinojosa, A. (2010). Oxygen in stem cell biology: a critical component of the stem cell niche. Cell Stem Cell *7*, 150–161.

Peterson, C.W., Stoltzman, C.A., Sighinolfi, M.P., Han, K.S., and Ayer, D.E. (2010). Glucose controls nuclear accumulation, promoter binding, and transcriptional activity of the MondoA-Mlx heterodimer. Mol. Cell. Biol. *30*, 2887–2895.

Polyak, K. (2011). Heterogeneity in breast cancer. J. Clin. Invest. *121*, 3786–3788.

Polyak, K., and Weinberg, R.A. (2009). Transitions between epithelial and mesenchymal states: acquisition of malignant and stem cell traits. Nat. Rev. Cancer *9*, 265–273.

Robey, R.B., and Hay, N. (2009). Is Akt the "Warburg kinase"?-Akt-energy metabolism interactions and oncogenesis. Semin. Cancer Biol. *19*, 25–31.

Sinthupibulyakit, C., Ittarat, W., St Clair, W.H., and St Clair, D.K. (2010). p53 Protects lung cancer cells against metabolic stress. Int. J. Oncol. *37*, 1575–1581.

Thiery, J.P., Acloque, H., Huang, R.Y., and Nieto, M.A. (2009). Epithelial-mesenchymal transitions in development and disease. Cell *139*, 871–890.

van de Vijver, M.J., He, Y.D., van't Veer, L.J., Dai, H., Hart, A.A., Voskuil, D.W., Schreiber, G.J., Peterse, J.L., Roberts, C., Marton, M.J., et al. (2002). A gene-expression signature as a predictor of survival in breast cancer. N. Engl. J. Med. *347*, 1999–2009.

van Poelje, P.D., Potter, S.C., Chandramouli, V.C., Landau, B.R., Dang, Q., and Erion, M.D. (2006). Inhibition of fructose 1,6-bisphosphatase reduces excessive endogenous glucose production and attenuates hyperglycemia in Zucker diabetic fatty rats. Diabetes *55*, 1747–1754.

van 't Veer, L.J., Dai, H., van de Vijver, M.J., He, Y.D., Hart, A.A., Mao, M., Peterse, H.L., van der Kooy, K., Marton, M.J., Witteveen, A.T., et al. (2002). Gene expression profiling predicts clinical outcome of breast cancer. Nature *415*, 530–536.

Ward, P.S., and Thompson, C.B. (2012). Metabolic reprogramming: a cancer hallmark even warburg did not anticipate. Cancer Cell *21*, 297–308.

Zeilstra, J., Joosten, S.P., Dokter, M., Verwiel, E., Spaargaren, M., and Pals, S.T. (2008). Deletion of the WNT target and cancer stem cell marker CD44 in Apc(Min/+) mice attenuates intestinal tumorigenesis. Cancer Res. *68*, 3655–3661.

Cancer Cell
Article

The E3 Ubiquitin Ligase Siah2 Contributes to Castration-Resistant Prostate Cancer by Regulation of Androgen Receptor Transcriptional Activity

Jianfei Qi,[1,*] Manisha Tripathi,[2] Rajeev Mishra,[2] Natasha Sahgal,[3] Ladan Fazil,[4] Susan Ettinger,[4] William J. Placzek,[1] Giuseppina Claps,[1] Leland W.K. Chung,[2] David Bowtell,[5] Martin Gleave,[4] Neil Bhowmick,[2] and Ze'ev A. Ronai[1,*]
[1]Signal Transduction Program, Cancer Center, Sanford-Burnham Medical Research Institute, La Jolla 92037, CA, USA
[2]Uro-Oncology Research Program, Department of Medicine, Cedars-Sinai Medical Center, Los Angeles 90048, CA, USA
[3]Bioinformatics and Statistical Genetics, Wellcome Trust Center for Human Genetics, University of Oxford, Oxford OX3 7BN, UK
[4]Vancouver Prostate Centre, University of British Columbia, Vancouver, BC V6T 1Z4, Canada
[5]Research Division, Peter McCallum Cancer Centre, Melbourne, VIC 3002, Australia
*Correspondence: jfqi@sbmri.org (J.Q.), ronai@sbmri.org (Z.A.R.)
http://dx.doi.org/10.1016/j.ccr.2013.02.016

SUMMARY

Understanding the mechanism underlying the regulation of the androgen receptor (AR), a central player in the development of castration-resistant prostate cancer (CRPC), holds promise for overcoming the challenge of treating CRPC. We demonstrate that the ubiquitin ligase Siah2 targets a select pool of NCOR1-bound, transcriptionally-inactive AR for ubiquitin-dependent degradation, thereby promoting expression of select AR target genes implicated in lipid metabolism, cell motility, and proliferation. Siah2 is required for prostate cancer cell growth under androgen-deprivation conditions in vitro and in vivo, and Siah2 inhibition promotes prostate cancer regression upon castration. Notably, Siah2 expression is markedly increased in human CRPCs. Collectively, we find that selective regulation of AR transcriptional activity by the ubiquitin ligase Siah2 is important for CRPC development.

INTRODUCTION

In American men, prostate cancer (PCa) is the most commonly diagnosed malignancy and the second leading cause of cancer death. Signaling through the androgen receptor (AR), a member of the nuclear receptor superfamily activated by steroids, plays an essential role in the initiation and progression of PCa (Shen and Abate-Shen, 2010). AR consists of an N-terminal domain, a central DNA-binding domain (DBD), a hinge region, and a C-terminal ligand-binding domain (LBD). AR transcriptional activity is mediated via AF1 and AF2, two transactivation domains located within the N-terminal and the LBD domains, respectively. Upon ligand binding, AR translocates to the nucleus and regulates gene expression through binding to androgen-responsive elements (AREs) on the AR target genes.

Given the central role AR plays in the development of PCa, androgen-deprivation therapy (ADT) is used as a first-line treatment for metastatic PCa. Although such therapy achieves significant clinical response, patients with advanced prostate cancer invariably relapse with a more aggressive form of PCa known as castration-resistant PCa (CRPC). Studies on the pathogenesis of CRPC have revealed that resumption of AR-dependent transcriptional activity is a critical event in nearly all cases (Waltering et al., 2012). Several mechanisms have been suggested to mediate AR reactivation during CRPC progression, including AR gene amplification or overexpression, AR mutations conferring ligand promiscuity, expression of AR splice variants allowing androgen-independent activity, and intratumoral androgen production.

Similar to other transcription factors, AR is subject to regulation by the ubiquitin-proteasome pathway, and the E3 ubiquitin ligases Mdm2 and CHIP have been implicated in the control of AR stability and activity (Chymkowitch et al., 2011; Lin et al., 2002). In humans, Siah1 and Siah2 comprise a two-member

Significance

Increased androgen receptor (AR) activity is central to the development of castration-resistant prostate cancer (CRPC), which is a major obstacle to the treatment of advanced/metastatic prostate cancer with hormone therapy. We find that the ubiquitin ligase Siah2 enhances the transcriptional activity of AR by degrading a transcriptionally-inactive pool of AR on select gene promoters/enhancers. Consequently, Siah2 promotes the expression of select AR target genes, leading to the growth of CRPC cells under androgen-deprivation conditions. Our findings point to the importance of targeting a select subpopulation of AR target genes for the treatment of CRPC and the possible consideration of Siah2 for such an approach.

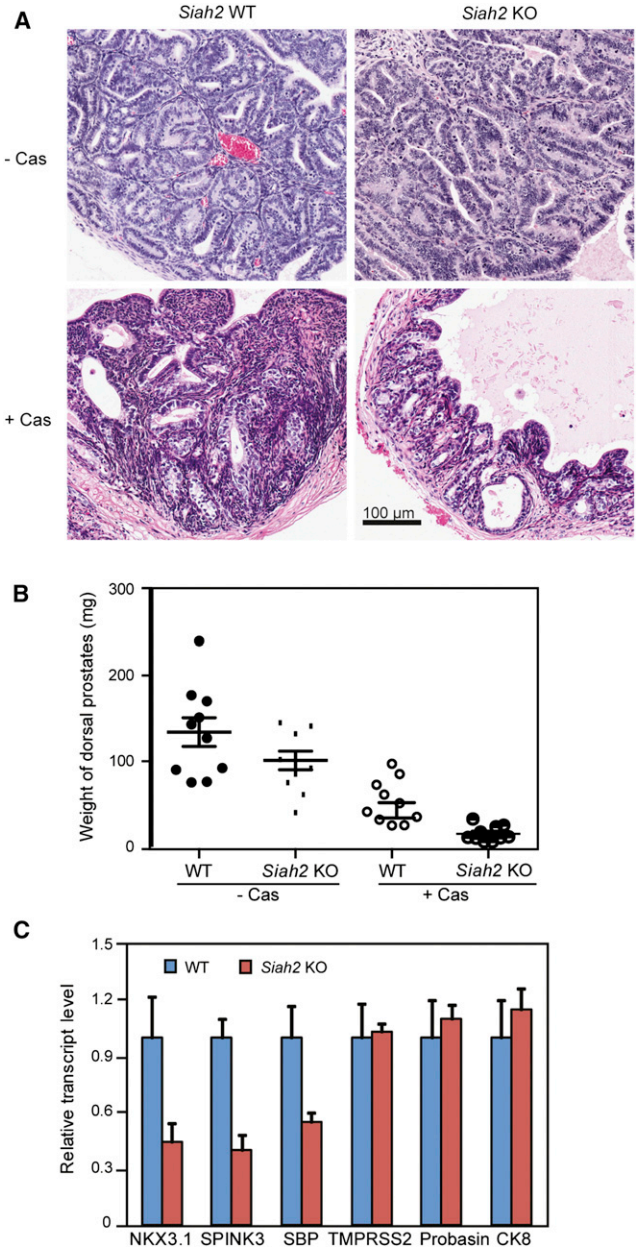

Figure 1. Siah2 Is Required for the Castration Sensitivity and Expression of Select AR Targets in the TRAMP Atypical Hyperplasia Model

(A) H&E staining of AH in the dorsal prostates of *Siah2*$^{+/+}$*;TRAMP* or *Siah2*$^{-/-}$*;TRAMP* mice before and after castration.

(B) The scatter plot showing the average weight of dorsal prostates microdissected from 5-month-old mice with or without 3-week castration (n = 10 for each group). p = 0.17 for WT versus Siah KO, − castration; p < 0.005 for WT versus Siah KO, + castration.

(C) Transcript levels of selected AR target genes in the prostates of *Siah2*$^{-/-}$*;TRAMP* mice after castration. RNA for qRT-PCR was isolated from the dorsal prostates of 5-month-old mice with 3 week castration. p < 0.01 for NKX3.1, p < 0.005 for SPINK3, p < 0.05 for SBP, p > 0.1 for TMPRSS2, probasin, or CK8. Data are mean ± SD.

See also Figure S1.

family of evolutionarily conserved RING finger E3 ubiquitin ligases. The Siah proteins regulate ubiquitination-dependent degradation of multiple substrates, including nuclear corepressor (NCOR1), β-catenin, TRAF2, α-ketoglutarate dehydrogenase, and Sprouty 2, and thus influence an array of regulatory functions such as the MAPK signaling, cell survival, and mitochondrial biogenesis (Kim et al., 2011; Nakayama et al., 2009). Siah1 and Siah2 also enhance the availability and activity of hypoxia-inducible factor (HIF-α) by mediating the ubiquitination and degradation of HIF-α-negative regulators, including PHD1/3, HIPK2, and FIH (Calzado et al., 2009; Fukuba et al., 2008; Nakayama et al., 2004). Here, we identify Siah2 as an E3 ligase that targets a select pool of chromatin-bound ARs, through which Siah2 controls the growth, survival, and tumorigenic capacity of PCa cells, especially under conditions of androgen deprivation.

RESULTS

Siah2 Deletion Increases the Castration Sensitivity of TRAMP Mice

We previously reported that crossing *Siah2*$^{-/-}$mice with *TRAMP* (transgenic adenocarcinoma of the mouse prostate) mice abolished the spontaneous formation of prostate NE tumors (Qi et al., 2010). In the TRAMP model, prostate-specific expression of SV40 T-antigen results in two types of lesions: NE carcinoma, found in the ventral lobe, and atypical hyperplasia (AH; often termed adenocarcinoma), which occurs in all lobes (Chiaverotti et al., 2008). To further investigate the possible role of Siah2 in the development of prostate tumors, we subjected *Siah2*$^{-/-}$*;TRAMP* mice to castration. As expected, castration caused shrinkage of AH in the dorsal prostate lobes of both genotypes (Figure 1A). However, the weight of dorsal prostate lobes was reduced approximately 10-fold in *Siah2*$^{-/-}$*;TRAMP* mice compared with 2.5-fold in the *Siah2*$^{+/+}$*;TRAMP* mice (Figure 1B). These results indicate that in *TRAMP* mice Siah2 deletion increased the sensitivity of AH to castration, implying that Siah2 may be required for AR signaling when androgen levels are low. Indeed, comparing expression of AR target genes in the dorsal prostate from *Siah2*$^{-/-}$*;TRAMP* mice with *Siah2*$^{+/+}$*;TRAMP* mice identified a greater reduction in transcript and protein levels of some AR target genes (i.e., *NKX3.1* and *SPINK3*, but not probasin and *TMPRSS2*; Figure 1C and Figure S1A available online), pointing to the possibility that Siah2 regulates the expression of a specific subset of AR target genes. The reduction in lesions observed in *Siah2*-deficient mice is not likely to be due to *probasin*-driven SV40 T-antigen expression, as the level of probasin transcripts and SV40 T-antigen protein were similar in *Siah2*$^{+/+}$ and *Siah2*$^{-/-}$*;TRAMP* tissues (Figures 1C and S1B). In agreement, the dorsal prostates from both genotypes expressed similar transcript levels of the luminal marker CK8 (Figure 1C), suggesting that the reduced expression of AR target genes was not due to a change in cellular differentiation.

Siah2 Is Required for Expression of a Subset of AR Target Genes

To determine if Siah2 regulates AR activity in human PCa cells, we used shRNA to inhibit Siah2 expression in androgen-dependent LNCaP cells. Four of the 10 different Siah2 shRNAs

examined elicited 70%–90% knockdown (Figure S2A). To determine if Siah2 regulated transcription of PSA, a well-established AR target gene, LNCaP cells were cultured in medium supplemented with 5% charcoal stripped (CS)-fetal bovine serum (FBS) for 2 days and then stimulated with the synthetic androgen R1881 for 16 hr. Siah2 knockdown reduced PSA transcripts by 80%–90% in the absence of R1881 (Figure 2A) and by 50% in the presence of a physiologic level of R1881 (0.5 nM), consistent with changes reported upon knockdown of AR in LNCaP cells (Bao et al., 2008). In the presence of high levels of R1881 (10 nM), the degree of reduced PSA transcript was limited to 20% (Figure 2A). These results indicate that Siah2 is required for PSA transcription under conditions of both low and physiologic concentrations of androgen.

We next knocked down Siah2 in the androgen-independent PCa cell line, CWR22Rv1 (Rv1), which expresses constitutively active AR. Under androgen-deprivation conditions, Siah2 knockdown led to an 80% reduction in PSA transcript levels in Rv1 cells in the presence or absence of androgen (R1881; Figure 2B), confirming the importance of Siah2 for transcription of AR target genes.

Because Siah2 plays an important role in regulating the cellular response to hypoxia (Nakayama et al., 2004) and hypoxia has been reported to activate AR activity, we examined transcription of AR target genes under 1% O_2. Surprisingly, the relative change in PSA transcript levels upon Siah2 knockdown was similar under normoxia and hypoxia (Figures 2B and 2C). Notably, Siah2 knockdown reduced the transcript level of CA9, a HIF target gene, only under hypoxia (Figures 2B and 2C). These findings suggest that the effect of Siah2 on AR target gene expression is independent of its established role in the hypoxia response.

We next used qRT-PCR to compare the expression of representative androgen-responsive genes (ARGs) in LNCaP or Rv1 cells subjected to inhibition of AR or Siah2 expression. Siah2 knockdown in LNCaP or Rv1 cells reduced the expression of a subset of ARGs; transcripts of PSA, NKX3.1, PMEPA1, and SLC45A3 were reduced by Siah2 knockdown while TMPRSS2 and FKBP5 transcripts were unaffected (Figures 2D and 2E). In contrast, AR knockdown reduced the transcript levels of all these representative ARGs (Figures 2D, S2B, and S2C). These analyses confirmed that Siah2 modulates the expression of a specific pool of AR target genes in both LNCaP and Rv1 cells. To determine whether the effect of Siah2 on PSA transcripts is AR dependent, we knocked down Siah2 in LNCaP or Rv1 cells stably expressing AR shRNA. Although Siah2 knockdown reduced the PSA transcript level in control cells, it failed to do so in AR-knockdown cells (Figure 2F), suggesting that the Siah2 effect on PSA is AR dependent.

To evaluate the global effect of Siah2 on transcription of ARGs, we performed array-based gene expression analyses on Rv1 cells stably expressing Siah2 shRNA. Siah2 knockdown resulted in downregulation of 981 genes (>1.5-fold; Table S1). Gene network analysis, using the IPA software, was performed to identify possible enrichment of regulatory networks among the 981 genes. Notably, the AR-related genes were ranked among the top three transcriptional networks that were responsive to Siah2 inhibition (Figure 3A), with the other two being hypoxia- and HNF4A-related. Changes in hypoxia-response genes are consistent with the established role of Siah2 in control of HIF-1α expression, stability, and activity (Calzado et al., 2009; Fukuba et al., 2008; Nakayama et al., 2004). Further restricting the analysis to genes that are primarily associated with prostate cancer, we ranked the AR gene network as the primary one to be altered upon Siah2 knockdown (Figure 3B). These analyses point to AR as the major signaling pathway underlying Siah2-dependent gene expression in the Rv1 cells. About 10% (98/981) of Siah2-dependent genes were identified within the androgen-induced gene cluster in an ARG data set (Figure 3C; Table S1). Correspondingly, about 13% (98/759) of androgen-induced genes in the ARG data set were enriched within the Siah2-dependent expression cluster (Figure 3C). IPA analysis for molecular and cellular functions revealed that the 98 Siah2-dependent ARGs were associated with lipid metabolism, cell movement, and cell proliferation (Figures 3D and 3E), whereas the remaining 883 Siah2-dependent genes were associated with DNA replication/repair, and cell morphology and proliferation (Figure 3F). Independent analysis using the GO pathway software package confirmed lipid metabolism, steroid metabolism, and cholesterol metabolism as the primary pathways enriched in the 98 Siah2-dependent ARGs (Figure 3G; Table S2), whereas the remaining 883 Siah2-dependent genes were associated with oxidation, protein polymerization, and organic acid metabolism (Figure 3H; Table S2). Together, these gene expression analyses substantiate the role of Siah2 in the regulation of a subset of ARGs, while identifying distinct functional networks that are associated with the Siah2-dependent ARGs.

To determine whether the Siah2-regulated ARGs are important for the proliferation of PCa cells under the low androgen condition, we performed a siRNA screen in which we have targeted each of 98 Siah2-dependent ARGs. We identified 48 out of 98 siRNAs capable of inhibiting the proliferation of Rv1 cells grown in the CS-FBS medium by 10%–40% (Table S3). Notably, the most pronounced inhibition was observed by Siah2 siRNA. The siRNA screen also revealed that 8/16 Siah2-dependent ARGs involved in the metabolisms of lipids, cholesterol, and steroids (Figure 3E) were required for the proliferation and survival of Rv1 cells (Table S3). Since SREBF1, a master transcriptional regulator for lipid and cholesterol metabolism, was found among the Siah2-dependent ARGs, we further assessed the importance of SREBF1 for Siah2-dependent effects on Rv1 cells maintained in the CS-FBS medium. Significantly, inhibition of Rv1 cell proliferation upon Siah2 knockdown could be partially rescued upon re-expression of SREBF1 (Figures S3A and S3B). These findings substantiate the importance of the Siah2-AR regulatory axis in control of lipid metabolism for androgen-independent growth of Rv1 cells.

Comparison of the Siah2-dependent genes identified in our study with the published profiling arrays on prostate cancers revealed that 53 genes that were downregulated upon Siah2 knockdown in Rv1 cells were found to exhibit increased expression in the CRPC xenograft tumor model (Table S4) (Ettinger et al., 2004), and 44 of those genes were upregulated in high-grade prostate cancers (Table S5) (Taylor et al., 2010). Furthermore, analyses of profiling array data obtained from 35 CRPC and 58 primary PCa samples (Grasso et al., 2012) confirmed that 25% of Siah2-dependent ARGs identified in our current study were upregulated in CRPCs and enriched for genes

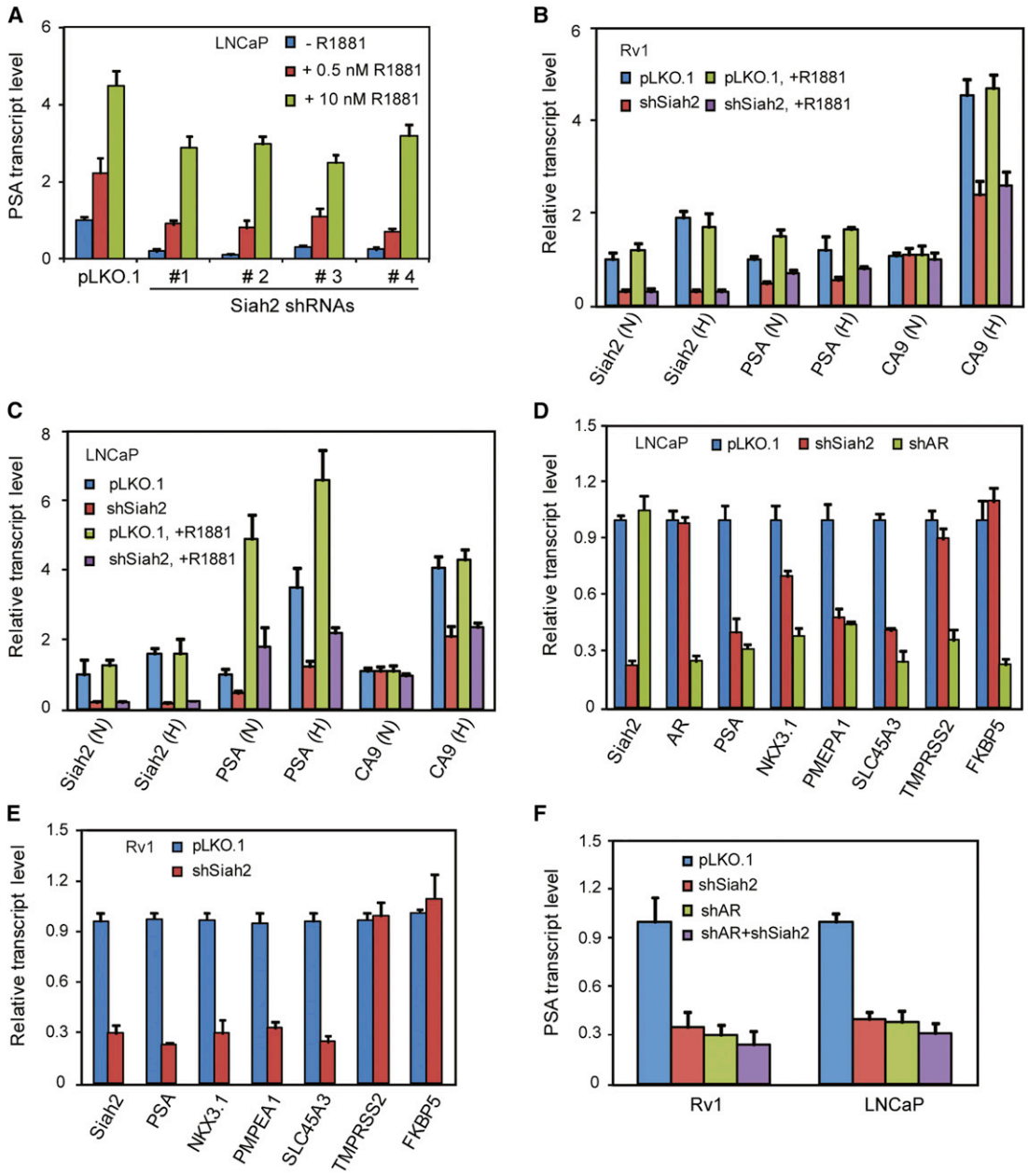

Figure 2. Siah2 Is Required for the Expression of Select AR Targets in Human Prostate Cancer Cells

(A) Effect of Siah2 knockdown in LNCaP cells on the PSA transcript levels. Siah2 was knocked down in LNCaP cells using four different Siah2 shRNAs. LNCaP transfectants were grown in medium containing 5% CS-FBS for 48 hr before treatment with 0.5 nM or 10 nM of synthetic androgen R1881 for 16 hr. The differences in PSA transcript levels between Siah2-knockdown and pLKO.1-transfected control cells were statistically significant ($p < 0.005$) in the presence and absence of androgen.

(B) Effect of Siah2 knockdown in Rv1 cells on the PSA transcript levels under normoxia or hypoxia. Rv1 cells transfected with Siah2 shRNA were grown in medium containing 5% CS-FBS for 48 hr and then treated for 16 hr with or without hypoxia or 10 nM R1881. Hypoxia did not increase the PSA transcript level in either pLKO.1 control or Siah2-knockdown cells ($p > 0.1$). N, normoxia; H, hypoxia.

(C) Effect of Siah2 knockdown in LNCaP cells on the PSA transcript levels under normoxia or hypoxia. The analysis was performed as for (B).

(D) qRT-PCR analysis of the indicated AR target genes in LNCaP cells transfected with shSiah2 or shAR vectors. Reduction in transcripts of PSA, NKX3.1, PMEPA1, and SLC45A3 by shSiah2 or shAR was statistically significant. Transcripts of TMPRSS2 or FKBP5 were reduced by shAR ($p < 0.01$) but not by shSiah2 ($p > 0.1$).

(E) qRT-PCR analysis of the indicated AR target genes in Rv1 cells transfected with shSiah2 vector. Reduction in transcripts of PSA, NKX3.1, PMEPA1, and SLC45A3 by shSiah2 was statistically significant ($p < 0.01$).

(F) qRT-PCR analysis of PSA transcripts in the indicated transfectants of LNCaP or Rv1 cells. The reduction of PSA transcript in the indicated knockdown cells was statistically significant ($p < 0.0005$). Data are mean ± SD.

See also Figure S2.

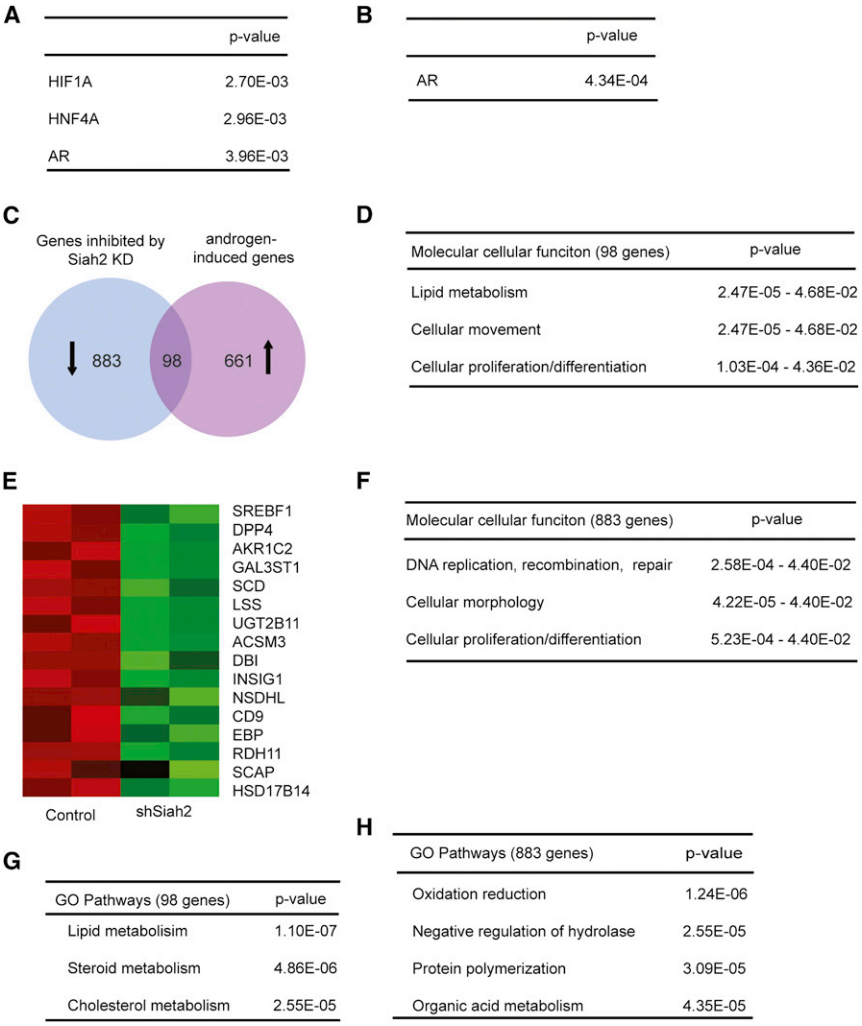

Figure 3. Bioinformatic Analyses of Siah2-Dependent Genes in Rv1 Cells

(A) Top three transcription factors predicted to underlie Siah2-dependent transcription by IPA. A total of 981 genes downregulated upon Siah2 knockdown were subjected to IPA analysis against canonical gene pathways.

(B) IPA analysis of transcription factors enriched within the 981 genes, as described in (A), against human prostate cancer cell data set.

(C) Venn diagram depicting overlap between genes downregulated by Siah2 knockdown and those induced by androgen signaling. The androgen-induced ARGs in prostate cancer cells were extracted from an ARG data set.

(D) The molecular and cellular functions of the 98 Siah2-dependent ARGs revealed by IPA analyses.

(E) Heatmap of the Siah2-dependet ARGs that regulate biosynthesis and metabolism of lipid, cholesterol, and steroids. Upregulated genes, red; downregulated genes, green.

(F) The molecular and cellular functions of the 883 genes (Siah2-dependent but AR-independent) revealed by IPA analyses.

(G) DAVID GOBP analyses of pathways enriched in the 98 Siah2-dependent ARGs.

(H) DAVID GOBP analyses of pathways enriched in the 833 genes (Siah2-dependent, but AR-independent).

See also Figure S3 and Tables S1, S2, S3, S4, S5, and S6.

involved in the biosynthesis of lipids, cholesterol, and steroids (Table S6). This observation substantiates the finding of metabolism and biosynthesis of lipids, cholesterol, and steroids as the primary ARGs regulated by Siah2 (Figures 3D and 3E). Importantly, Siah2 expression was found to be upregulated in the CRPC samples (Table S6), supporting a key role of Siah2 in CRPC. These results further confirm Siah2-dependent expression of a select subset of genes that are implicated in the progression and development of CRPC.

Siah2 Functions as an E3 Ubiquitin Ligase for AR

We next set to determine the mechanism underlying Siah2 effect on AR. First, we determined whether Siah2 and AR interacted by co-expressing AR with a wild-type (Siah2WT) or catalytically inactive RING mutant form of Siah2 (Siah2RM), which forms stable complexes with Siah2 substrates (Nakayama et al., 2004). Analysis of AR immunoprecipitates showed that Siah2RM or Siah2WT bound to AR protein (Figures 4A and S4A). Expression of Siah2WT, but not Siah2RM, reduced the levels of AR overexpressed in 293T cells (Figure 4B) or PC3 cells (Figure S4B). Overexpression of Siah2 in PCa cells also reduced the endogenous levels of AR (Figure S4C). Similarly, reduction of AR levels was observed following expression of WT but not the RING mutant form of Siah1a (S1aRM; Figure S4D). The effect of Siah2 on AR levels was partially blocked by treatment of 293T or PC3 cells with the proteasome inhibitor MG132 (Figures S4E and S4F), suggesting that Siah2 induces AR degradation via the ubiquitin-proteasome pathway. To determine if AR was polyubiquitinated by Siah2, we co-expressed Siah2, AR, and ubiquitin in 293T cells and found that Siah2WT, but not Siah2RM, induced AR polyubiquitination in the presence or absence of R1881 (Figure 4C). Similarly, purified GST-Siah2 induced polyubiquitination of AR in vitro (Figure S4G). Because polyubiquitination of AR can occur on lysine residues other than lysine 48 (K48) (Xu et al., 2009), we examined the topology of the AR ubiquitin chains by co-expressing AR, Siah2, and expression vectors for K48 or K63 mutant ubiquitin (Figure 4D). Siah2 expression was found to enhance polyubiquitination of AR in the presence of K63, but not K48, mutant ubiquitin, suggesting that Siah2 promotes K48-linked ubiquitination of AR. To determine whether Siah2 alters the half-life of AR, we performed cycloheximide chase assays in 293T cells ectopically expressing AR, with or without Siah2. Expression of Siah2 reduced the half-life of AR from 6 hr to less than 2 hr (Figure S4H). These findings suggest that Siah2 regulates AR stability by targeting it for ubiquitination-dependent degradation by the proteasomes.

We next mapped the AR domains required for Siah2 interaction by making domain-deletion mutants of AR and

co-expressing them with Siah2 in 293T cells. Western blot analyses indicated that AR mutants containing the AF2 domain were degraded by Siah2, whereas AF2-deficient mutants were resistant to Siah2-induced degradation (Figures S4I and S4J), suggesting that Siah2 interacts with the AF2 domain of AR. Indeed, GST-Siah2 was able to pull down the AF2, but not the AF1, domain of AR (Figure 4E). Siah2 consists of an N-terminal domain, a central RING domain/zinc finger domain, and a C-terminal substrate-binding domain (SBD) (Figure S4K). To map the Siah2 domain required for AR interaction, we generated truncation mutants of Siah2 and co-expressed them with AR in 293T cells. Immunoblotting revealed that both the Siah2 SBD and central RING domain/zinc finger domains interacted with AR (Figure 4F).

Because Siah2 interacts with the AR LBD, we tested whether the presence of androgen affects the AR–Siah2 interaction and whether Siah2 affects androgen–AR binding. The interaction between ectopic AR and Siah2 was unaffected by R1881 (Figure S4L), suggesting that ligand binding does not affect the AR–Siah2 interaction. Further, knockdown of Siah2 in Rv1 cells did not influence the affinity of [^{3}H]-labeled R1881 for the endogenous AR or its dissociation rate (Figure S4M). These observations indicate that ligand binding does not affect the AR–Siah2 interaction, nor does Siah2 affect the androgen–AR interaction.

AR Contains Two Major Siah2-Binding Sites

To identify the regions of the AR LBD that interacted with Siah2, we mutated AR with a series of single amino acid mutations that had been previously characterized in human PCa samples. The mutated ARs were individually co-expressed with Siah2RM in 293T cells, and the binding between AR mutants and Siah2RM was assessed by co-immunoprecipitation experiments.

AR constructs with the mutations R726L, Q798E, and F754L, all containing solvent-accessible side chains, showed the greatest reduction in Siah2 binding. R726L is clustered in the AF2 site with three other mutations (V715M, H874Y, and V730M) that cause moderate inhibition of Siah2 binding (Figures 4G–4I). Two additional mutations (L701H and T877A) in the AR ligand-binding pocket proximal to the AF2 site had moderate effects on Siah2 binding to AR.

The two remaining mutations that strongly reduced Siah2–AR binding (Q798E and F754L) are located in proximity in a hydrophobic cleft on the opposite side of the AR hinge region (Figure 4I). Interestingly, a mutation at V757, which lies just under this cleft, does not significantly decrease the Siah2–AR association, which points to its specific recognition of this cleft. In summary, the mutational analysis identified two solvent-accessible surfaces on AR LBD that are required for the interaction with Siah2.

To determine whether the Siah2–AR interaction is essential for AR transcriptional activity, we monitored the PSA promoter-driven luciferase activity in AR null PC3 cells transfected with AR mutants. Although knockdown of Siah2 reduced luciferase activity induced by WT AR or an AR mutant (G683A) capable of associating with Siah2 under both low and normal androgen conditions, it had limited effect on luciferase activity induced by AR mutants (R726L or Q798E) with markedly (70%) reduced Siah2-binding abilities (Figure 4J). Consistently, AR mutants R726L or Q798E showed impaired Siah2-dependent ubiquitination, compared with WT AR or G683A mutant AR (Figure S4N). These observations indicate that AR mutations that prevent Siah2-binding also prevent Siah2-mediated ubiquitination of AR and regulation of AR transcriptional activity, and further support the importance of the Siah2-AR association in the control of selected AR target genes, illustrated here by the PSA promoter.

Siah2 Is Required for Degradation of NCOR1-Bound AR on AREs of Selective AR Target Genes

To further understand Siah2 regulation of AR activity, we assessed whether knockdown of Siah2 affected levels of total, nuclear, or chromatin-bound AR in PCa cells. Significantly, Siah2 had no effect on any of these AR pools (Figures S5A–S5F). Overexpression of Siah2 in 293T cells did not affect the AR intermolecular N-terminal and C-terminal interaction (Figure S5G), which is known to regulate AR transcriptional activity. Because Siah2 knockdown reduced transcripts of specific AR target genes (Figure 2), we determined if Siah2 modulates AR binding to target gene promoters/enhancers. For this, we used *PSA*, *NKX3.1*, and *PMEPA1* as representative Siah2-regulated AR target genes and *TMPRSS2* as a Siah2-independent AR target gene. The results of ChIP assays confirmed androgen-dependent association of Siah2 with the AREs of *PSA*, *NKX3.1*, and *PMEPA1* in LNCaP cells, but not with ARE of *TMPRSS2* (Figure 5A). Binding of Siah2 to the AREs of *PSA*, *NKX3.1*, and *PMEPA1* was reduced by knockdown of AR or Siah2 (Figure 5A), suggesting that Siah2 was recruited to these chromatin regions by AR. Similar results were observed for the Siah2 ChIP assays performed in Rv1 cells (Figure 5B). Because NCOR1 is a known AR corepressor and a Siah2 substrate (Frasor et al., 2005; Zhang et al., 1998), we performed ChIP assays to determine whether Siah2 knockdown affected the binding of AR and NCOR1 to the AR target genes. Siah2 knockdown in LNCaP and Rv1 cells increased the level of AR and NCOR1 on the AREs of *PSA*, *NKX3.1*, and *PMEPA1* (Figures 5C, 5D, S5H, and S5I). As expected, binding of AR and NCOR1 to the ARE of *TMPRSS2* was unaffected by Siah2 knockdown (Figures 5D and S5J). Knockdown of Siah2 had no effect on the global level of AR (Figure S5A) or NCOR1 (Figure S5K). These results suggest that Siah2 is required for the degradation of AR and NCOR1, at selective AR target genes. To further evaluate this hypothesis, we performed additional ChIP assays with 29 randomly selected AR targets (16 Siah2-dependent and 13 Siah2-independent, based on our global gene expression analysis; Figure 3). ChIP was performed on Rv1 cells (pLKO.1 control versus Siah2 knockdown cells) using antibodies to Siah2, NCOR1, and AR, and the precipitated chromatins were subjected to qRT-PCR analyses for AREs of the 29 AR targets. Some of the AREs have been reported in the literature; for the remainder, we consulted published ChIP-seq or ChIP-on-chip studies and then validated AR binding to the AREs by ChIP-PCR analyses. These experiments revealed that Siah2 knockdown increased the levels of AR and NCOR1 bound to 11 of the 16 Siah2-dependent AR targets (68.75%) (Figures S5L and S5M), whereas none of the 13 Siah2-independent AR targets showed such change (data not shown). This analysis satisfied statistical power analyses, which indicated

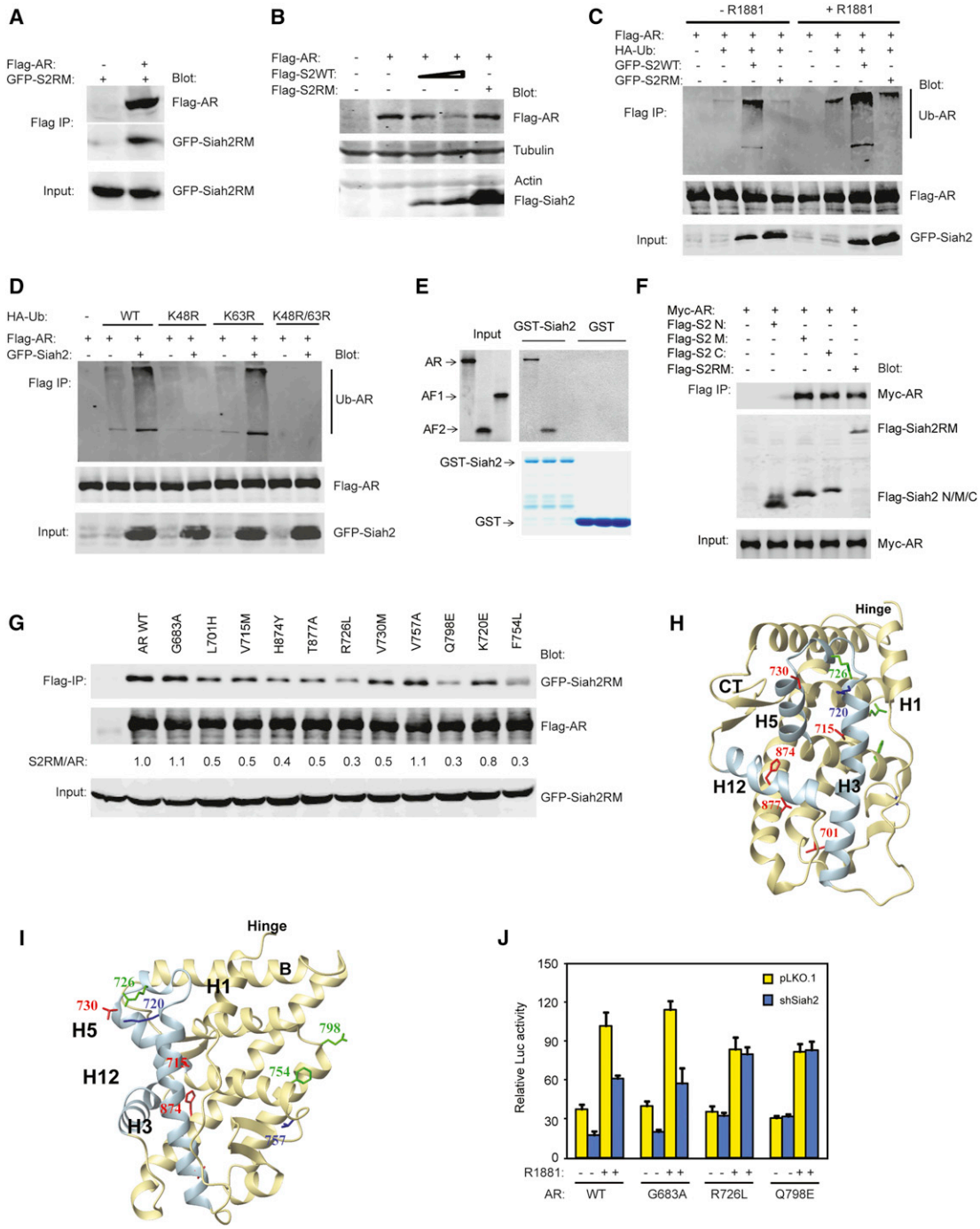

Figure 4. Siah2 Interacts with and Ubiquitinates AR for Proteasome-Dependent Degradation

(A) 293T cells were transfected with Flag-AR and GFP-Siah2RM for 24 hr before immunoprecipitation with anti-Flag M2 beads. Bound proteins were eluted and analyzed by western blotting with Flag or GFP antibodies.

(B) 293T cells were transfected with Flag-tagged AR and Siah2 (WT or RM) for 24 hr. Whole cell lysates were analyzed by western blotting with the antibodies of Flag, tubulin, and actin.

(C) 293T cells were transfected with Flag-AR, HA-Ub, and GFP-Siah2 (WT or RM) for 24 hr in the presence or absence of 10 nM R1881. Cells were treated with 20 μM MG132 for 5 hr and then Flag-AR was immunoprecipitated with M2 beads under denaturing conditions. The immunoprecipitates were analyzed by western blotting with HA or Flag antibody. The input of GFP-Siah2 was immunoblotted with GFP antibody.

(D) 293T cells were transfected with Flag-AR, HA-Ub (WT, K48 mutant, K63 mutant, and K48/K63 double mutant), and GFP-Siah2. The analysis was performed as described for (C).

(E) Flag-AF2 or-AF1 was in vitro translated (^{35}S labeling), purified, and incubated with GST-Siah2. Proteins bound to GST-Siah2 were analyzed by SDS-PAGE and phosphoimaging.

(legend continued on next page)

a requirement for 12 genes per group to reach 95% confidence. Notably, Siah2 binding was demonstrated for nine of the 11 Siah2-dependent AR targets that exhibited increased AR/NCOR1 binding, compared with only one of the five Siah2-dependent AR targets that did not show increased AR/NCOR1 binding (Figure S5N). The association between Siah2 binding to AREs in control cells and the increased NCOR1/AR binding to these AREs upon Siah2 knockdown was statistically significant ($p < 0.05$, Fisher's exact test). Importantly, none of the Siah2-independent AR targets exhibited Siah2 binding (data not shown).

Collectively, the above data substantiate our conclusion that Siah2 targets the degradation of NCOR1-bound AR on a select group of AR target genes. Consistent with this, ChIP assays revealed that Siah2 knockdown reduced the level of ubiquitinated proteins on AREs of *PSA*, *NKX3.1*, and *PMEPA1*, but not *TMPRSS2* (Figure 5E). Notably, knockdown of NCOR1 attenuated the recruitment of Siah2 (Figures 5B and S5O) and the accumulation of AR on AREs of *PSA*, *NKX3.1*, and *PMEPA1* was further reduced upon Siah2 knockdown (Figures 5C, S5H, and S5I). Moreover, coprecipitation experiments showed a markedly higher association of Siah2 with the AR/NCOR1 complex than with AR alone (Figure 5F). These results suggest that the NCOR1-bound AR recruits Siah2 more efficiently. Indeed, knockdown of NCOR1 in Rv1 cells increased the transcripts of PSA, NKX3.1, and PMEPA1 in both control and Siah2-knockdown cells, but the effect was more pronounced in Siah2-knockdown cells (Figure 5G). Together, these results suggest that Siah2 may promote the AR transcriptional output via degradation of the transcriptionally-inactive AR (marked by NCOR1 binding) on the AREs of selective AR targets.

To investigate whether Siah2-mediated degradation of NCOR1-bound AR could affect binding of a co-activator to AR, we performed ChIP-reChIP assays that enable detection of multiple protein-protein interactions on specific chromatin regions. ChIP of Siah2 followed by reChIP of AR, NCOR1, and co-activator p300 revealed that Siah2 interacted with AR and NCOR1 but not with p300 on the PSA promoter (Figure 5H). Consistent with this, ChIP-reChIP assays revealed that NCOR1 and co-activator p300 are present in distinct AR complexes on the promoter of PSA gene (Figure 5I), and knockdown of NCOR1 increased the amount of p300 and acetylated histone H3 on the PSA promoter (Figures 5J and 5K), suggesting that competitive binding between p300 and NCOR1 to the AR modulates PSA promoter activity, consistent with findings from a previous report (Yoon and Wong, 2006). Interestingly, knockdown of Siah2 decreased the amount of p300 and acetylated histone H3 on the PSA promoter (Figures 5J and 5K), opposite to what was seen upon NCOR1 knockdown. Given that Siah2 knockdown increased the amount of NCOR1-bound AR on the PSA promoter (Figure 5C), these results suggest that Siah2-mediated degradation of NCOR1-bound AR (transcriptionally inactive) on PSA promoter allows the subsequent recruitment of p300-bound AR (transcriptionally active), leading to an increase in the transcription of PSA gene.

Knockdown of the E3 ubiquitin ligase Mdm2 in MEFs expressing ectopic AR has also been reported to disrupt AR turnover at the PSA promoter (Chymkowitch et al., 2011). To compare the effects of Siah2 and Mdm2 on AR transcriptional activity, we knocked down Mdm2 in Rv1 cells and examined transcripts of representative ARGs. The expression of some ARGs was regulated by both Siah2 and Mdm2 (e.g., *PSA*, *SLC45A3*), while others were regulated only by Siah2 (e.g., *NKX3.1*, *PMEPA1*) or Mdm2 (e.g., *TMPRSS2*), and some were unaffected by either protein (e.g., *FKBP5*) (Figures 2E and S5P). Knockdown of Mdm2 had little effect on the total level of AR (Figure S5Q), as had been observed with Siah2 knockdown. Additional regulatory layers (i.e., posttranslational modifications) are expected to exist in the control of AR by distinct ubiquitin ligases.

Modulation of AR Transcriptional Activity by Siah2 Is Required for Growth and Motility of Prostate Cancer Cells

We next evaluated the physiologic significance of Siah2 regulation of AR activity. Knockdown of Siah2 or AR significantly reduced proliferation of Rv1 and LNCaP cells (Figures 6A and 6B). However, knockdown of Siah2 in AR-knockdown cells did not further reduce cell proliferation (Figure 6B), suggesting that the Siah2 effect on cell proliferation may be AR dependent. Similarly, knockdown of Siah2 or AR in Rv1 or C4-2 cells (a castration-resistant subline of LNCaP) abolished anchorage-independent growth, as demonstrated by an inability to form colonies in soft agar (Figures 6C and 6D). In contrast, knockdown of Siah2 in AR-negative PC3 or DU145 cells (Figure S6A) had no apparent effect on cell growth (Figure 6A) or anchorage-independent growth (Figure S6B). Knockdown of Siah2 or AR in Rv1 cells reduced sphere formation in three-dimensional Matrigel to the levels seen with control Rv1 cells cultured under androgen-deprivation conditions (Figures 6E and S6C). Further, Siah2 or AR knockdown inhibited Rv1 and LNCaP cell motility in transwell

(F) Identification of the AR-interacting domains of Siah2. Myc-AR was cotransfected with Flag-tagged Siah2 fragments (N, N-terminal part; C, C-terminal part; M, middle part) in 293T cells. Siah2 fragments were immunoprecipitated with M2 beads and coprecipitated Myc-AR was analyzed by western blotting using Flag or AR antibody.

(G) 293T cells were cotransfected with GFP-Siah2RM and Flag-AR mutants as indicated. After 24 hr, immunoprecipitation was performed using M2 beads and samples were analyzed by western blotting using GFP or Flag antibody. The intensity ratios between GFP-S2RM and Flag-ARs are shown. The input of GFP-Siah2RM is shown at the bottom panel.

(H and I) Structural location of AR LBD mutants in WT AR. Ribbon presentation of the LBD with the AF2 site helices highlighted in blue and labeled in addition to the key helix H1 (H). The side chains of residues that were mutated are drawn as sticks, labeled, and colored green (strong), red (moderate), or blue (no effect) depending on their effect on Siah2 interaction. A 90° rotation of the model is shown to highlight the location of V757, F754, and Q798 (I).

(J) PC3 cells (pLKO.1 or shSiah2) were cotransfected with a PSA promoter *Gaussia* luciferase construct, a control *Cypridina* luciferase construct, and the mutant ARs indicated. Cells were grown in medium containing 5% CS-FBS for 48 hr and treated with 1 nM of R1881 for 16 hr. *Gaussia* luciferase activity was normalized to the *Cypridina* luciferase activity (n = 3). Data are mean ± SD. Siah2 knockdown reduced PSA promoter activity in cells expressing WT AR or G683 mutant AR in the absence or presence of R1881 ($p < 0.05$).

See also Figure S4.

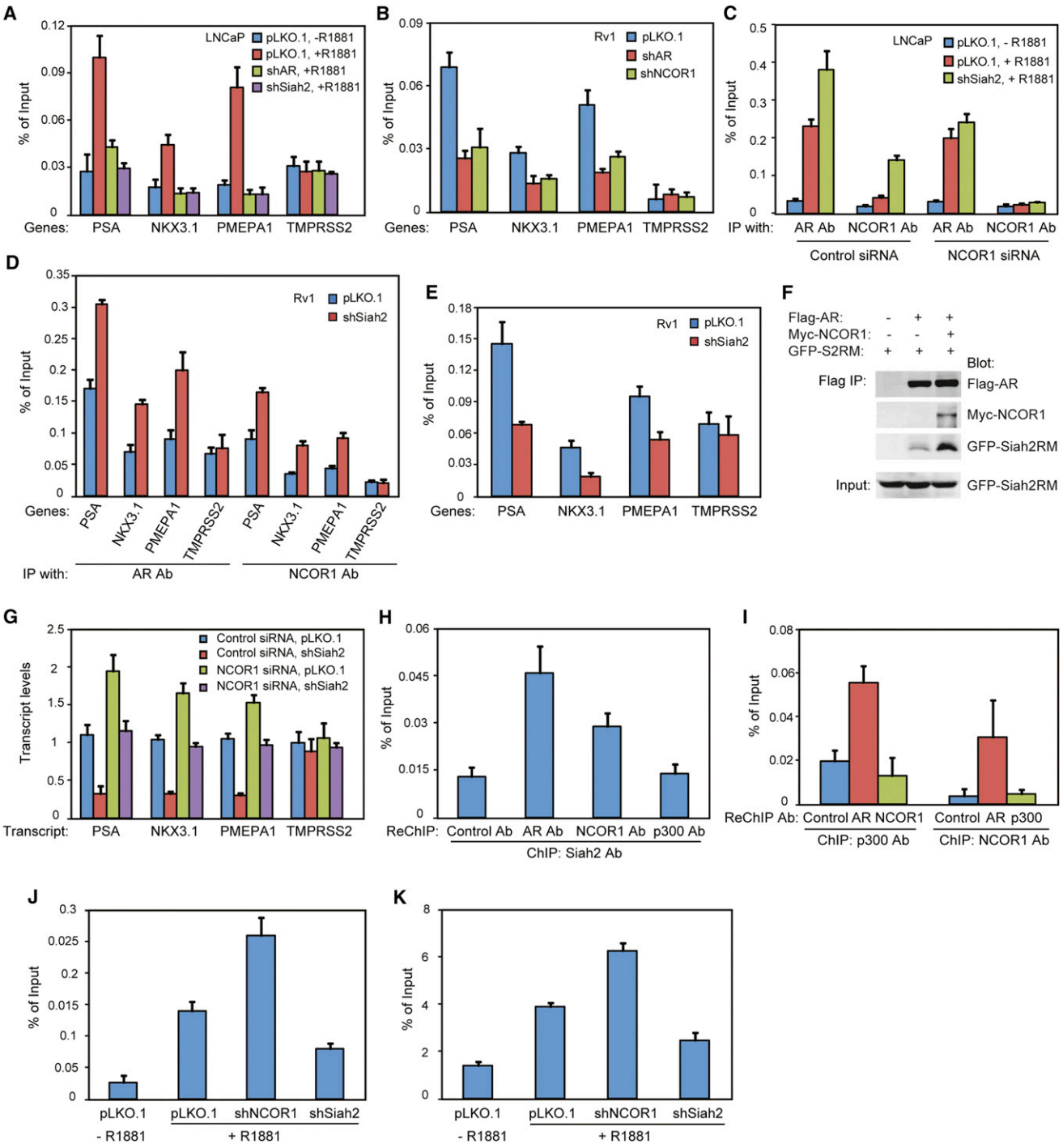

Figure 5. Siah2 Promotes the AR Transcriptional Activity by Targeting the NCOR1-Bound AR

(A) LNCaP cells stably transfected with control, AR shRNA, or Siah2 shRNA were grown in the absence or presence of 1 nM of R1881 for 12 hr, treated with 20 μM MG132 for 5 hr, and collected for ChIP assays using an anti-Siah2 antibody. Purified chromatin was analyzed by qPCR for the ARE regions of PSA, NKX3.1, PMEPA1, and TMPRSS2. Siah2 was enriched on AREs of PSA, NKX3.1, and PMEPA1 in the presence of R1881 ($p < 0.05$), but not on the ARE of TMPRSS2 gene ($p = 0.62$).

(B) Rv1 cells stably transfected with control, AR shRNA, or NCOR1 shRNA were grown in the normal growth medium, treated with 20 μM MG132 for 5 hr, and collected for the ChIP assays using anti-Siah2 antibody as described in (A). AR or NCOR1 knockdown affected Siah2 presence on the AREs of PSA, NKX3.1, and PMEPA1 ($p < 0.05$) and TMPRSS2 ($p > 0.1$).

(C) Effect of Siah2 knockdown in LNCaP cells on the association of AR and NCOR1 with the PSA promoter. ChIP assays were performed on LNCaP cells (pLKO.1 or shSiah2) using anti-AR or anti-NCOR1 antibodies and purified chromatins were analyzed by qPCR for the ARE region of PSA gene. Relative change in AR ($p < 0.05$) or NCOR1 ($p < 0.0005$) in the presence of R1881 or upon knockdown of Siah2, or NCOR1 ($p > 0.1$) is shown.

(legend continued on next page)

assays, and this effect was amplified under androgen-deprivation conditions (Figures 6F, 6G, and S6D). In contrast, knockdown of Siah2 in AR-negative PC3 cells showed no effect on cell motility (Figure S6E). Collectively, these data strongly support a key role for Siah2 in the growth and motility of PCa cells, which is mediated at least partially through regulation of AR activity.

Siah2 Is Important for Growth of Castration-Resistant Prostate Tumors

Having established that Siah2 influences the growth and motility of AR-positive PCa cells in vitro, we next addressed its role in vivo. To establish CRPC, we used an orthotopic prostate tumor model in which the androgen-independent C4-2 cell line was injected into the dorsal prostate lobes of nude mice. We established C4-2 cells with stable knockdown of Siah2 and verified that they were similar to LNCaP Siah2-knockdown cells in both transcript levels of ARGs and in vitro growth characteristics (Figures S7A–S7C). Tumors derived from the Siah2-knockdown C4-2 cells were about half the size of those derived from control C4-2 cells (Figure 7A). Castration had no effect on tumor size of control cells, consistent with the fact that growth of C4-2 cells is androgen independent. Interestingly, the size of Siah2-knockdown tumors was reduced in response to castration (Figure 7A), suggesting that Siah2 contributed to the castration resistance of human PCa cells. qRT-PCR analyses revealed lower transcript levels of selective ARGs in the Siah2-knockdown C4-2 tumors, which were further lowered after castration (Figure 7B). In agreement, knockdown of AR reduced the C4-2 xenograft tumor size and PSA level in the castrated mice (Snoek et al., 2009). These findings suggest that Siah2-dependent regulation of AR activity may contribute to the castration resistance of C4-2 tumors.

Prostatic stromal cells from transgenic mice with a conditional knockout of the *tumor growth factor-β* (*TGF-β*) *receptor type II* in fibroblasts (*Tgfbr2*^{fspKO} and *Tgfbr2*^{ColTKO}) conferred resistance to castration in the prostate cancer models (Bhowmick et al., 2004). To further test the role of Siah2 in castration resistance, we knocked down Siah2 expression in a mouse prostate cancer cell line MPC3, knocked out for *Pten* and *Trp53*. Knockdown of Siah2 in MPC3 cells also reduced the transcription of selective AR targets (Figure S7D), characteristic of the Pten prostate cancer model (Mulholland et al., 2011). Tissue-recombination experiments combining WT or *Tgfbr2*-KO prostate stromal cells with MPC3 cells (control or Siah2 knockdown) were orthotopically grafted. The tumors grew diffusely in the mouse prostate and did not form a distinctive mass. The growth of MPC3 cells in vivo was evaluated by phosphorylated-histone H3, Ki67, and TUNEL staining. Knockdown of Siah2 in MPC3 cells recombined with WT prostate stromal cells led to reduced phospho-histone H3, Ki67, and TUNEL staining in castrated mice (Figures 7C, 7D, S7E, and S7F), indicative of Siah2′s role in the castration-resistant growth of MPC3 cells. Notably, co-culture of the Siah2-knockdown MPC3 cells with *Tgfbr2*-KO prostate stromal cells diminished the requirement of Siah2 for the proliferation of MPC3 cells in the castrated mice (Figures 7D and S7F). *Tgfbr2*-KO prostate stromal cells are known to promote the castration resistance of prostate epithelia via paracrine secretion of growth factors such as Wnt3a, interleukin-6 (IL-6), IL-1β, and human growth factor (HGF) (Bhowmick et al., 2004; Kiskowski et al., 2011), which can bypass the requirement for androgen signaling and thus Siah2 for the progression of MPC3 cells in the castrated mice. Together, these observations substantiate the role of Siah2 in the progression of CRPC.

Siah2 Expression Is Upregulated in Castration-Resistant Human Prostate Cancer

To verify the relevance of our findings to human PCa, we measured Siah2 expression in human castration-resistant prostate tumor samples. Siah2 was detected immunohistochemically in a PCa tissue microarray (TMA) containing representative samples of different Gleason stage tumors and castration-resistant tumors (Figures 7E–7G; Table S7). Siah2 showed a nuclear expression pattern in both the benign and the cancer cells. However, in the benign tissues, Siah2 was mostly present in basal cells, not luminal cells (Figure 7E). Compared to benign tissues, Siah2 expression was upregulated in PCa tissues, and

(D) Effect of Siah2 knockdown in Rv1 cells on the association of AR and NCOR1 with the AREs of PSA, NKX3.1 and PMEPA1. ChIP assays were performed on Rv1 cells (pLKO.1 control or shSiah2) using anti-AR or anti-NCOR1 antibodies and purified chromatins were analyzed by qPCR for ARE regions of PSA, NKX3.1, PMEPA1 and TMPRSS2. Level of AR ($p < 0.05$) and NCOR1 ($p < 0.05$) on the AREs of PSA, NKX3.1, and PMEPA1 upon Siah2 KD, compared with the ARE of TMPRSS2 ($p > 0.1$).
(E) Effect of Siah2 knockdown in Rv1 cells on the association of ubiquitinated proteins with the AREs of PSA, NKX3.1, and PMEPA1. ChIP assays were performed on Rv1 cells (pLKO.1 control or shSiah2) using anti-ubiquitin antibody and analyzed as described in (D). Level of ubiquitinated proteins upon Siah2 KD on the ARE regions of PSA, NKX3.1, and PMEPA1 ($p < 0.05$), compared with the ARE on TMPRSS2 gene ($p = 0.55$).
(F) 293T cells were transfected with Flag-AR or Flag-AR/myc-NCOR1, which were isolated by purification on M2 beads and then incubated with 293T lysates expressing GFP-Siah2RM. After three washes, the proteins were eluted and analyzed by western blotting using the antibodies of Flag, Myc or GFP.
(G) qRT-PCR of the indicated genes was performed on Rv1 cells (pLKO.1 or shSiah2) transfected with NCOR1 siRNA. Shown is the change in transcripts of PSA, NKX3.1, and PMEPA1 in pLKO.1 or Siah2 KD cells by the NCOR1 siRNA ($p < 0.05$).
(H) LNCaP cells were treated with 1 nM of R1881 for 12 hr, 20 μM MG132 for 5 hr, and collected for the first round of IP (ChIP) using Siah2 antibody. The eluates of the first IP were used for the second round of IP (reChIP) using antibodies indicated. The purified chromatins by the reChIP were analyzed by qPCR for the ARE region of PSA promoter. Relative enrichment by AR or NCOR1 antibody ($p < 0.05$), or p300 antibody ($p = 0.76$) is shown.
(I) LNCaP cells were treated with 1 nM of R1881 for 12 hr, and collected for the first round of IP (ChIP) using p300 (left columns) or NCOR1 (right columns) antibody followed by the second round of IP (reChIP) using the antibodies indicated, and analyzed by qPCR for the ARE region of PSA gene. Enrichment of reChIP by AR antibody is shown ($p < 0.05$).
(J) LNCaP cells subjected to NCOR1 or Siah2 KD were treated with 1 nM of R1881 for 12 hr, collected for the ChIP assays using p300 antibody, and analyzed by qPCR of the ARE region of PSA promoter. p300 enrichment upon NCOR1 or Siah2 KD ($p < 0.05$) is shown.
(K) ChIP assays using acetylated histone H3 antibody were performed on LNCaP cells as described in J. Shown is the relative enrichment of acetylated histone H3 antibody on PSA promoter upon NCOR1 or Siah2 knockdown ($p < 0.05$). Data are mean ± SD.
See also Figure S5.

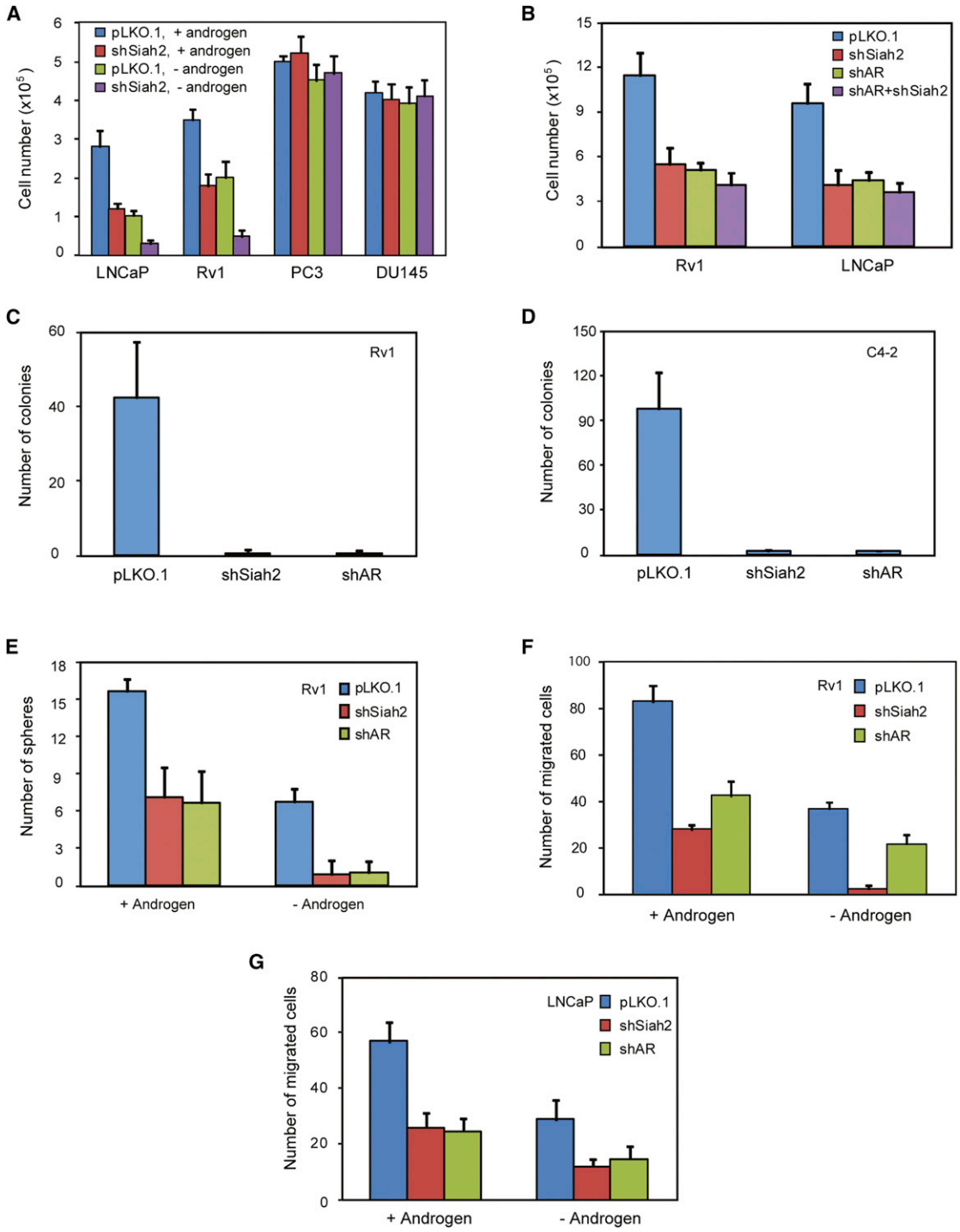

Figure 6. The Siah2 Effect on AR for the Proliferation and Motility of PCa Cells

(A) Effect of Siah2 knockdown on the growth of human PCa cells. LNCaP, Rv1, PC3, or DU145 cells were stably transfected with Siah2 shRNA or control pLKO.1 vector. Equal numbers of cells (1×10^4) were seeded in 12-well plates in medium containing 5% FBS (+androgen) or 5% CS-FBS (−androgen) and cells were counted after 5 days (n = 3). Change in cell growth upon Siah2 KD in LNCaP or Rv1 cells was maintained in the presence or absence of androgen ($p < 0.05$).

(B) Siah2 or AR was stably knocked down individually or in combination in LNCaP or Rv1 cells. Equal numbers of cells (5×10^4) were grown in six-well plates and cells were counted after 5 days (n = 3). Change in growth of Rv1 ($p < 0.01$) or LNCaP ($p < 0.005$) is shown.

(C) Knockdown of Siah2 or AR in Rv1 cells on the colony formation in soft agar assays. Cells (pKLO.1 control, shSiah2, or shAR) were maintained in soft agar for 3 weeks before staining with p-iodonitrotetrazolium violet. The number of colonies per field was quantified ($p < 0.0001$).

(D) Siah2 or AR KD effect on colony formation of C4-2 cells ($p < 0.00005$), was carried out as detailed in (C).

(legend continued on next page)

interestingly, Siah2 upregulation was seen across Gleason stages within this cohort (Figure 7F). Significantly, levels of Siah2 expression were closely associated with ADT and development of CRPC, reflected in reduction of Siah2 levels after ADT and elevation of Siah2 levels in CRPC (Figure 7G). Interestingly the level of Siah2 protein in human CRPC resembles the changes seen in Siah2 transcripts in the human CRPC xenograft model; while the level of Siah2 transcripts was reduced upon castration, it increased during development of CRPC (Figure S7G). Notably, whereas Siah2 level is associated with clinical recurrence upon ADT, it is not associated with recurrence after prostatectomy (Figure 7H). Consistent with the upregulation of Siah2 in CRPCs, the endogenous Siah2 level is higher in the two androgen-independent PCa cell lines C4-2 and Rv1 than in the androgen-dependent LNCaP cells or the AR null PC3 cells (Figure S7H). Immunohistochemical staining of CLGN and ACPP (Siah2-dependent AR targets) in the human PCa tumor microarray revealed their elevated expression (~30% increase, $p < 0.05$) in CRPCs compared with the naive PCa samples (Figure S7I, data not shown). The latter substantiate the significance of Siah2-dependent AR targets in CRPCs.

DISCUSSION

Understanding the mechanisms underlying AR activity is important for the development of effective therapeutic modalities to treat CRPC. Here, we identified an undisclosed facet of AR regulation and demonstrated its consequences for the growth of castration-resistant prostate tumors. Our studies reveal that the E3 ubiquitin ligase Siah2 regulates a subset of AR, bound to the corepressor NCOR1, resulting in removal of the transcriptionally-inactive AR from chromatin. The specificity of Siah2 for the NCOR1-bound AR is achieved through Siah2 interaction with two accessible surfaces on AR, concomitant with its interaction with the AR/NCOR1 complex. Siah2-dependent removal of NCOR1-bound AR allows the binding of p300-bound AR to the AREs of PSA gene. Collectively, our findings suggest a model whereby Siah2 recognition and degradation of a specific inactive AR pool enables recycling of AR, whereby inactive AR-NCOR1 is replaced with active AR-p300, thereby sustaining constitutive AR-dependent transcription from selected promoters/enhancers.

The finding that Siah2 ubiquitin ligase controls a subset of AR is consistent with the concept that some transcription factors are removed from target promoters via the ubiquitin-proteasome pathway to allow binding of new factors and continued transcription (Muratani and Tansey, 2003). A similar mechanism has been proposed for regulation of PSA by Mdm2 (Chymkowitch et al., 2011), and interestingly, both Mdm2 and Siah2 reportedly regulate HIPK2 stability (Calzado et al., 2009; Rinaldo et al., 2007). Thus, the interplay between these two ligases may dictate the duration, level, and/or specificity of transcriptional output. It is equally plausible that Siah2 and Mdm2 play distinct roles in AR turnover for different pools of AR target genes, or under varying physiologic conditions. We favor the latter possibility, which is supported by the observation that Siah2 and Mdm2 regulate different AR targets (Figures 2E and S5P). Although we provide evidence that Siah2 contributes to AR turnover on the AREs of selective AR targets, we cannot exclude the possibility that it regulates AR activity through additional mechanisms, such as promoting recruitment of co-activators or degrading/displacing corepressors.

How do the Siah2-regulated ARGs contribute to CRPC? Our gene expression profiling studies point to Siah2-dependent regulation of AR target genes associated with sterol and lipid metabolism. These findings were confirmed by qPCR analyses in PCa cells and identification of this gene cluster in independent data sets reported for PCa and CRPC. Of those, a master regulator of lipid metabolism, SREBF1, a Siah2-dependent ARG, plays an important role in the proliferation of Rv1 cells under low androgen condition (Figure S3B) and is upregulated in CRPC (Table S6). SREBF1 induces the expression of enzymes involved in fatty acid and cholesterol synthesis, thereby providing CRPC cells with fatty acids for energy and membrane synthesis, and cholesterol for intratumoral de novo synthesis of androgens (Ettinger et al., 2004; Locke et al., 2008). Among the enzymes underlying the intratumoral androgen metabolism are AKR1C2, AKR1C3, and UGT2B15, which are upregulated in CRPC (Cai et al., 2011; Stanbrough et al., 2006), consistent with their downregulation in the Siah2-knockdown Rv1 cells.

We previously reported that Siah2-dependent regulation of HIF was important to the neuroendocrine differentiation (NED) of PCa cells under chronic hypoxic conditions (Qi et al., 2010). Here, we show that Siah2-dependent regulation of AR activity is equivalent under normoxia and hypoxia. Notably, NED foci of prostate cancer express little or no AR protein (Huang et al., 2006), suggesting that the effect of Siah2 on AR activity is not applicable for NED foci, where the Siah2 contribution is mediated through its concerted regulation of HIF-1α and FoxA2 (Qi et al., 2010). Siah2 thus elicit distinct effects in different PCa cell populations: it enhances HIF activity in NED foci and promotes AR activity in PCa cells surrounding these foci. Importantly, through independent mechanisms in each of these cell populations, Siah2 contributes to the castration resistance of PCa. Thus, the role played by Siah2 in controlling AR signaling, castration resistance, and NED of PCa makes it a promising target for PCa therapy, either alone or in combination with other therapeutic approaches.

EXPERIMENTAL PROCEDURES

Prostate Tumor Samples

A total of 194 prostate cancer specimens were obtained from the Vancouver Prostate Tissue Bank under approval by Clinical Research Ethics Board

(E and F) Rv1 cells (pLKO.1, shSiah2, and shAR) were grown in the three-dimensional Matrigel in the presence (5% FBS) or absence (5% CS-FBS) of androgen for 1 week (E). The number of spheres (>25 μm in diameter) grown in the presence ($p < 0.05$) or absence ($p < 0.005$) of androgen is shown (F). Rv1 cells (pLKO.1, shSiah2, and shAR) were subjected to transwell assays in the presence (5% FBS; $p < 0.0005$) or absence (5% CS-FBS; $p < 0.05$) of androgen for 24 hr.
(G) Migration of LNCaP cells upon KD of Siah2 or AR in the presence ($p < 0.0005$) or absence ($p < 0.001$) of androgen, monitored using the transwell assays as described in (F). Data are mean ± SD.
See also Figure S6.

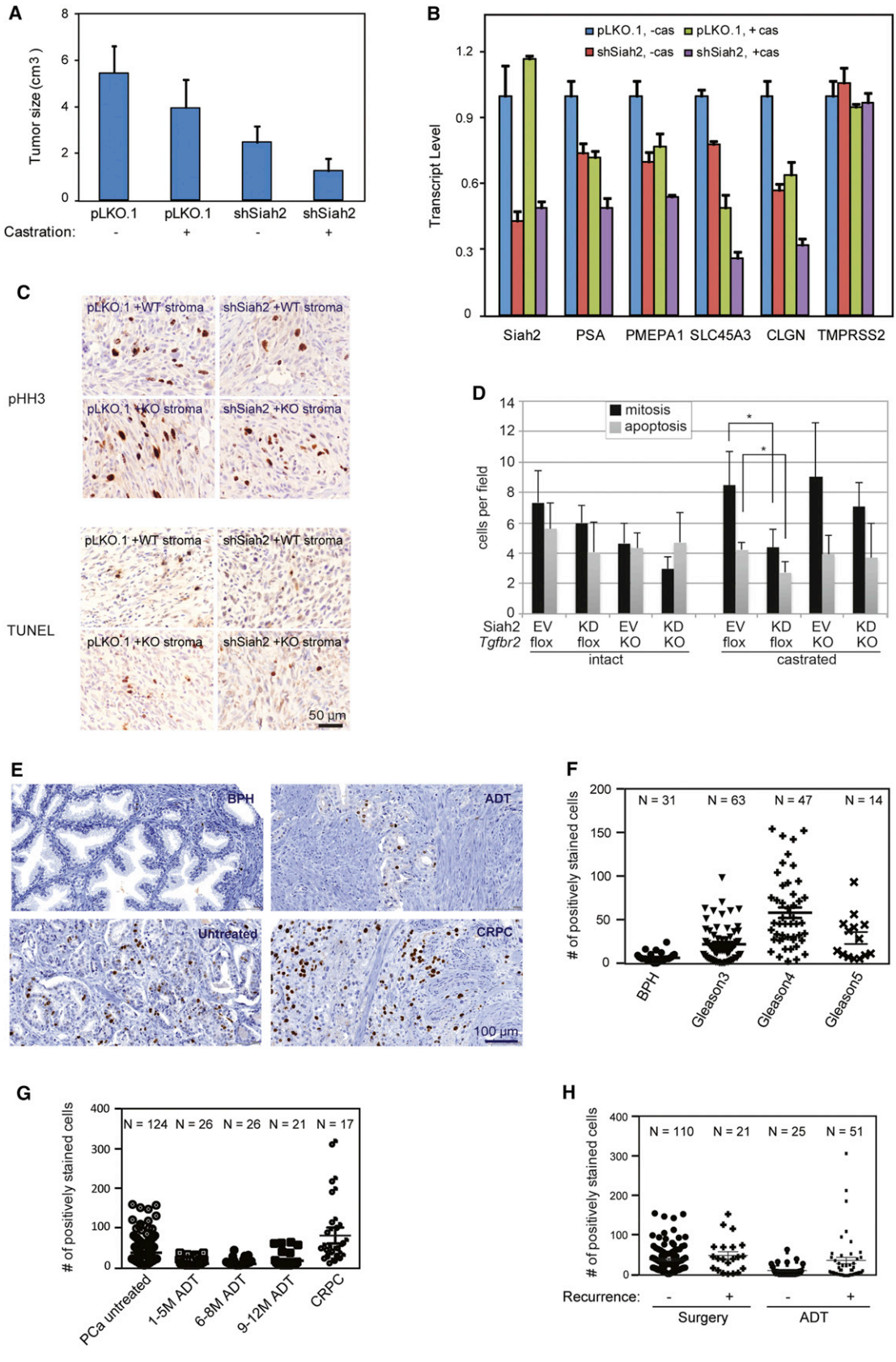

(legend on next page)

(# H09-01628; informed consent was obtained from all subjects). All the specimens were from radical prostatectomy except the 12 CRPC samples, which were obtained from transurethral resections of prostate. The hematoxylin and eosin (H&E) slides were reviewed and the desired areas were marked. Three TMAs were manually constructed (Beecher Instruments, MD, USA) by punching duplicate cores of 1 mm from each sample.

Animal Studies

Animals were housed in the Sanford-Burnham Medical Research Institute (SBMRI) animal facility, or Cedars-Sinai Medical Center (CSMC). All experiments were approved by the Institutional Animal Care and Use Committee (IACUC # 55545 and 56155 at SBMRI and IACUC # 3679 at CSMC) and were conducted following the Institute's animal policy in accordance with National Institutes of Health (NIH) guidelines.

Cell Lines

LNCaP, C4-2, PC3, DU145, and CWR22 Rv1 cells were maintained in RPMI 1640 medium supplemented with 10% FBS and antibiotics.

Generation of Siah2$^{-/-}$;TRAMP Mice

Siah2$^{+/-}$ mice (129/SvJ background) were crossed with *TRAMP* transgenic mice (C57BL/6 background) to obtain *Siah2*$^{+/-}$*;TRAMP* mice. Female *Siah2*$^{+/-}$*;TRAMP* mice were crossed with male *Siah2*$^{+/-}$ mice to generate mice of the genotypes *Siah2*$^{+/+}$*;TRAMP*, *Siah2*$^{+/-}$*;TRAMP*, and *Siah2*$^{-/-}$*;TRAMP* (Qi et al., 2010).

Antibodies and Reagents

Antibodies to AR, p300, ubiquitin, GFP, myc, Mdm2, tubulin, actin (Santa Cruz), NCOR1, Histone H3, GFP, NKX3.1, Ki67, SV40 T-antigen (Abcam), acetylated histone H3 (anti-AcH3-K9, Upstate Biotechnology), Siah2 (Novus Biologicals), ACPP (Pierce), CLGN (Abgent), phospho-histone H3, SPINK3 (cell signaling), and Flag (Sigma) were used according to the manufacturers' recommendations.

Statistical Analysis

The data were analyzed by Student's t test, one-way ANOVA, or Fisher's exact test. A p value < 0.05 was considered statistically significant.

ACCESSION NUMBER

The GEO accession number for the microarray data reported in this paper is GSE38851.

SUPPLEMENTAL INFORMATION

Supplemental Information includes seven figures, seven tables, and Supplemental Experimental Procedures and can be found with this article online at http://dx.doi.org/10.1016/j.ccr.2013.02.016.

ACKNOWLEDGMENTS

We thank members of the Ronai Lab for helpful discussions. We thank Dr. Yun Qiu for the human AR expression plasmid and AR luciferase reporters, Dr. McDonnell Donald for the pcDNA-myc-NCOR1 plasmid, Dr. Wen-Chin Huang for SREBF1 construct, and Dr. Estelle Li for the preparation, staining, and analysis of the prostate tumor TMA. Support by NCI grants CA111515 (to Z.R.) and CA154888 (to J.Q.) is gratefully acknowledged. J.Q. was initially supported by a CIHR fellowship. N.S. is supported by the Wellcome Trust Core Award (090532/Z/09/Z).

Received: June 8, 2012
Revised: October 22, 2012
Accepted: February 13, 2013
Published: March 18, 2013

REFERENCES

Bao, B.Y., Chuang, B.F., Wang, Q., Sartor, O., Balk, S.P., Brown, M., Kantoff, P.W., and Lee, G.S. (2008). Androgen receptor mediates the expression of UDP-glucuronosyltransferase 2 B15 and B17 genes. Prostate *68*, 839–848.

Bhowmick, N.A., Chytil, A., Plieth, D., Gorska, A.E., Dumont, N., Shappell, S., Washington, M.K., Neilson, E.G., and Moses, H.L. (2004). TGF-beta signaling in fibroblasts modulates the oncogenic potential of adjacent epithelia. Science *303*, 848–851.

Cai, C., Chen, S., Ng, P., Bubley, G.J., Nelson, P.S., Mostaghel, E.A., Marck, B., Matsumoto, A.M., Simon, N.I., Wang, H., et al. (2011). Intratumoral de novo steroid synthesis activates androgen receptor in castration-resistant prostate cancer and is upregulated by treatment with CYP17A1 inhibitors. Cancer Res. *71*, 6503–6513.

Calzado, M.A., de la Vega, L., Möller, A., Bowtell, D.D., and Schmitz, M.L. (2009). An inducible autoregulatory loop between HIPK2 and Siah2 at the apex of the hypoxic response. Nat. Cell Biol. *11*, 85–91.

Chiaverotti, T., Couto, S.S., Donjacour, A., Mao, J.H., Nagase, H., Cardiff, R.D., Cunha, G.R., and Balmain, A. (2008). Dissociation of epithelial and neuroendocrine carcinoma lineages in the transgenic adenocarcinoma of mouse prostate model of prostate cancer. Am. J. Pathol. *172*, 236–246.

Figure 7. Siah2 Promotes the Growth of CRPC Orthotopic Tumors, and Its Expression Is Elevated in Human CRPC Samples

(A) Orthotopic tumor size of C4-2 cells expressing Siah2 shRNA with or without castration. C4-2 cells (pLKO.1 or shSiah2) were injected into the dorsal prostates of nude mice and 3 weeks later one group of mice was castrated for 4 weeks. The size of tumors formed was quantified (n = 6 for each group). $p < 0.005$ for pLKO.1, − castration versus shSiah2, − castration; $p < 0.01$ for shSiah2, − castration versus shSiah2, + castration; $p = 0.16$ for pLKO.1, − castration versus pLKO.1, + castration.

(B) qRT-PCR analysis of the indicated genes on RNA samples extracted from the orthotopic tumors. Change in transcripts level for PSA, PMEPA1, SLC45A3, and CLGN upon Siah2 KD with or without castration ($p < 0.05$).

(C) The phospho-histone and TUNEL staining on the MPC3 tumor tissues collected from the indicated mice after castration. MPC3 pLKO.1 cells or Siah2-KD cells were recombined with WT or *Tgfr2* KO prostate stromal cells for an orthotopic injection. One month after injection, mice were castrated, and 4 days later tissues were collected and subjected to IHC analyses.

(D) Quantification of phospho-histone and TUNEL staining shown in (C).

(E) Representative images of Siah2 IHC staining on the PCa TMA. BPH, benign prostate hyperplasia.

(F) Quantification of Siah2 IHC staining on the BPH and PCa samples of different Gleason scores. ANOVA with Tukey's multiple comparison indicates $p < 0.0001$, except Gleason3 versus Gleason5 (lower number of cases in Gleason5 group).

(G) Quantification of Siah2 IHC staining on the PCa samples without or with ADT or the CRPC samples. ANOVA with posthoc results indicates $p < 0.0001$ for CRPC compared with all other groups and for untreated PCa compared with all other groups.

(H) Quantification of Siah2 staining on the PCa samples after prostatectomy or ADT (with or without clinical recurrence). ANOVA analyses of Siah2 staining between recurrent and nonrecurrent cases in samples after ADT ($p < 0.0001$), and between recurrent and nonrecurrent cases in samples obtained after prostatectomy ($p < 0.1$). Data are mean ± SD.

See also Figure S7 and Table S7.

Chymkowitch, P., Le May, N., Charneau, P., Compe, E., and Egly, J.M. (2011). The phosphorylation of the androgen receptor by TFIIH directs the ubiquitin/proteasome process. EMBO J. *30*, 468–479.

Ettinger, S.L., Sobel, R., Whitmore, T.G., Akbari, M., Bradley, D.R., Gleave, M.E., and Nelson, C.C. (2004). Dysregulation of sterol response element-binding proteins and downstream effectors in prostate cancer during progression to androgen independence. Cancer Res. *64*, 2212–2221.

Frasor, J., Danes, J.M., Funk, C.C., and Katzenellenbogen, B.S. (2005). Estrogen down-regulation of the corepressor N-CoR: mechanism and implications for estrogen derepression of N-CoR-regulated genes. Proc. Natl. Acad. Sci. USA *102*, 13153–13157.

Fukuba, H., Takahashi, T., Jin, H.G., Kohriyama, T., and Matsumoto, M. (2008). Abundance of aspargynyl-hydroxylase FIH is regulated by Siah-1 under normoxic conditions. Neurosci. Lett. *433*, 209–214.

Grasso, C.S., Wu, Y.M., Robinson, D.R., Cao, X., Dhanasekaran, S.M., Khan, A.P., Quist, M.J., Jing, X., Lonigro, R.J., Brenner, J.C., et al. (2012). The mutational landscape of lethal castration-resistant prostate cancer. Nature *487*, 239–243.

Huang, J., Yao, J.L., di Sant'Agnese, P.A., Yang, Q., Bourne, P.A., and Na, Y. (2006). Immunohistochemical characterization of neuroendocrine cells in prostate cancer. Prostate *66*, 1399–1406.

Kim, H., Scimia, M.C., Wilkinson, D., Trelles, R.D., Wood, M.R., Bowtell, D., Dillin, A., Mercola, M., and Ronai, Z.A. (2011). Fine-tuning of Drp1/Fis1 availability by AKAP121/Siah2 regulates mitochondrial adaptation to hypoxia. Mol. Cell *44*, 532–544.

Kiskowski, M.A., Jackson, R.S., 2nd, Banerjee, J., Li, X., Kang, M., Iturregui, J.M., Franco, O.E., Hayward, S.W., and Bhowmick, N.A. (2011). Role for stromal heterogeneity in prostate tumorigenesis. Cancer Res. *71*, 3459–3470.

Lin, H.K., Wang, L., Hu, Y.C., Altuwaijri, S., and Chang, C. (2002). Phosphorylation-dependent ubiquitylation and degradation of androgen receptor by Akt require Mdm2 E3 ligase. EMBO J. *21*, 4037–4048.

Locke, J.A., Guns, E.S., Lubik, A.A., Adomat, H.H., Hendy, S.C., Wood, C.A., Ettinger, S.L., Gleave, M.E., and Nelson, C.C. (2008). Androgen levels increase by intratumoral de novo steroidogenesis during progression of castration-resistant prostate cancer. Cancer Res. *68*, 6407–6415.

Mulholland, D.J., Tran, L.M., Li, Y., Cai, H., Morim, A., Wang, S., Plaisier, S., Garraway, I.P., Huang, J., Graeber, T.G., and Wu, H. (2011). Cell autonomous role of PTEN in regulating castration-resistant prostate cancer growth. Cancer Cell *19*, 792–804.

Muratani, M., and Tansey, W.P. (2003). How the ubiquitin-proteasome system controls transcription. Nat. Rev. Mol. Cell Biol. *4*, 192–201.

Nakayama, K., Qi, J., and Ronai, Z. (2009). The ubiquitin ligase Siah2 and the hypoxia response. Mol. Cancer Res. *7*, 443–451.

Nakayama, K., Frew, I.J., Hagensen, M., Skals, M., Habelhah, H., Bhoumik, A., Kadoya, T., Erdjument-Bromage, H., Tempst, P., Frappell, P.B., et al. (2004). Siah2 regulates stability of prolyl-hydroxylases, controls HIF1alpha abundance, and modulates physiological responses to hypoxia. Cell *117*, 941–952.

Qi, J., Nakayama, K., Cardiff, R.D., Borowsky, A.D., Kaul, K., Williams, R., Krajewski, S., Mercola, D., Carpenter, P.M., Bowtell, D., and Ronai, Z.A. (2010). Siah2-dependent concerted activity of HIF and FoxA2 regulates formation of neuroendocrine phenotype and neuroendocrine prostate tumors. Cancer Cell *18*, 23–38.

Rinaldo, C., Prodosmo, A., Mancini, F., Iacovelli, S., Sacchi, A., Moretti, F., and Soddu, S. (2007). MDM2-regulated degradation of HIPK2 prevents p53Ser46 phosphorylation and DNA damage-induced apoptosis. Mol. Cell *25*, 739–750.

Shen, M.M., and Abate-Shen, C. (2010). Molecular genetics of prostate cancer: new prospects for old challenges. Genes Dev. *24*, 1967–2000.

Snoek, R., Cheng, H., Margiotti, K., Wafa, L.A., Wong, C.A., Wong, E.C., Fazli, L., Nelson, C.C., Gleave, M.E., and Rennie, P.S. (2009). In vivo knockdown of the androgen receptor results in growth inhibition and regression of well-established, castration-resistant prostate tumors. Clin. Cancer Res. *15*, 39–47.

Stanbrough, M., Bubley, G.J., Ross, K., Golub, T.R., Rubin, M.A., Penning, T.M., Febbo, P.G., and Balk, S.P. (2006). Increased expression of genes converting adrenal androgens to testosterone in androgen-independent prostate cancer. Cancer Res. *66*, 2815–2825.

Taylor, B.S., Schultz, N., Hieronymus, H., Gopalan, A., Xiao, Y., Carver, B.S., Arora, V.K., Kaushik, P., Cerami, E., Reva, B., et al. (2010). Integrative genomic profiling of human prostate cancer. Cancer Cell *18*, 11–22.

Waltering, K.K., Urbanucci, A., and Visakorpi, T. (2012). Androgen receptor (AR) aberrations in castration-resistant prostate cancer. Mol. Cell. Endocrinol. *360*, 38–43.

Xu, K., Shimelis, H., Linn, D.E., Jiang, R., Yang, X., Sun, F., Guo, Z., Chen, H., Li, W., Chen, H., et al. (2009). Regulation of androgen receptor transcriptional activity and specificity by RNF6-induced ubiquitination. Cancer Cell *15*, 270–282.

Yoon, H.G., and Wong, J. (2006). The corepressors silencing mediator of retinoid and thyroid hormone receptor and nuclear receptor corepressor are involved in agonist- and antagonist-regulated transcription by androgen receptor. Mol. Endocrinol. *20*, 1048–1060.

Zhang, J., Guenther, M.G., Carthew, R.W., and Lazar, M.A. (1998). Proteasomal regulation of nuclear receptor corepressor-mediated repression. Genes Dev. *12*, 1775–1780.

Cancer Cell
Article

Ablation of Fbxw7 Eliminates Leukemia-Initiating Cells by Preventing Quiescence

Shoichiro Takeishi,[1,2] Akinobu Matsumoto,[1,2] Ichiro Onoyama,[1,2] Kazuhito Naka,[3] Atsushi Hirao,[2,3] and Keiichi I. Nakayama[1,2,*]

[1]Department of Molecular and Cellular Biology, Medical Institute of Bioregulation, Kyushu University, 3-1-1 Maidashi, Higashi-ku, Fukuoka, Fukuoka 812-8582, Japan

[2]CREST (Core Research for Evolutional Science and Technology), Japan Science and Technology Agency, Kawaguchi, Saitama 332-0012, Japan

[3]Division of Molecular Genetics, Center for Cancer and Stem Cell Research, Cancer Research Institute, Kanazawa University, Kakuma-machi, Kanazawa, Ishikawa 920-1192, Japan

*Correspondence: nakayak1@bioreg.kyushu-u.ac.jp

http://dx.doi.org/10.1016/j.ccr.2013.01.026

SUMMARY

Imatinib eradicates dividing progenitor cells of chronic myeloid leukemia (CML) but does not effectively target nondividing leukemia-initiating cells (LICs); thus, the disease often relapse after its discontinuation. We now show that Fbxw7 plays a pivotal role in maintenance of quiescence in LICs of CML by reducing the level of c-Myc. Abrogation of quiescence in LICs by Fbxw7 ablation increased their sensitivity to imatinib, and the combination of Fbxw7 ablation with imatinib treatment resulted in a greater depletion of LICs than of normal hematopoietic stem cells in mice. Purging of LICs by targeting Fbxw7 to interrupt their quiescence and subsequent treatment with imatinib may thus provide the basis for a promising therapeutic approach to CML.

INTRODUCTION

Cancer-initiating cells (CICs) are thought to constitute a minor subpopulation of cancer cells that is required for the initiation and maintenance of cancer (Clevers, 2011; Huntly and Gilliland, 2005). This notion is based largely on the characterization of leukemia-initiating cells (LICs), a rare subpopulation of cells that propagates leukemia (Lapidot et al., 1994). LICs were recently shown to share many properties, including self-renewal, pluripotency, and quiescence, with normal hematopoietic stem cells (HSCs) (Clevers, 2011; Huntly and Gilliland, 2005). A fundamental problem in treating leukemia is that the quiescent LIC subpopulation is particularly resistant to conventional chemotherapy and radiation, both of which target cells undergoing DNA replication and are therefore not effective against quiescent (noncycling) cells (Clevers, 2011; Huntly and Gilliland, 2005). Failure to eradicate quiescent LICs may result in reinitiation of malignancy after a period of latency. The development of therapeutic approaches that target quiescent CICs might therefore be expected to have a profound impact on cancer eradication.

Chronic myeloid leukemia (CML) in humans is characterized by the presence of the Philadelphia chromosome, which is generated by a chromosomal translocation that joins the *BCR* gene on chromosome 22 to the *ABL* gene on chromosome 9 (de Klein et al., 1982; Rowley, 1973). CML is a biphasic myeloproliferative disorder, which initially assumes a chronic phase before progressing to an accelerated phase and finally to blast crisis. Given that individuals with CML in blast crisis have a poor prognosis associated with a short survival time, it is critical to treat CML patients during the chronic phase. Several lines

Significance

Most cancer-initiating cells (CICs) are quiescent and therefore resistant to anticancer drugs that preferentially target dividing cells. CICs that survive therapy are a potential cause of relapse. Elucidation of the mechanism by which CICs maintain quiescence is thus critical for the elimination of cancer. Here, we show that Fbxw7 plays a pivotal role in maintenance of quiescence in leukemia-initiating cells (LICs) of chronic myeloid leukemia. Our findings reveal that ablation of Fbxw7 in LICs results in deregulated activation of c-Myc and impaired maintenance of quiescence followed by p53-dependent apoptosis and consequent cell exhaustion. Moreover, they provide a rationale for Fbxw7-targeted therapy to sensitize LICs to currently available drugs by interrupting their quiescence, potentially resulting in a substantial survival benefit.

of evidence indicate that LICs of CML emerge as a result of expression of BCR-ABL in normal HSCs (Pear et al., 1998), supporting the notion that CML is a "stem cell disease."

The BCR-ABL fusion protein possesses constitutive tyrosine kinase activity and triggers molecular events that result in the expansion of malignant hematopoiesis (Deininger et al., 2000). The recent development of the tyrosine kinase inhibitor (TKI) imatinib represented a breakthrough in treatment of the chronic phase of CML, resulting in a marked improvement in the prognosis of CML patients (Druker et al., 2001; Kantarjian et al., 2002). The French CML Intergroup Stop Imatinib study recently found that ~40% of CML patients in complete molecular remission for >2 years while on treatment with imatinib did not relapse within 12 months after discontinuation of imatinib treatment (Mahon et al., 2010). However, this observation suggests that LICs of CML persist in more than half of patients treated with imatinib alone, resulting in relapse after discontinuation of imatinib treatment. Several mechanisms of resistance of CML LICs to imatinib therapy have been suggested, including the maintenance of quiescence (Holtz et al., 2007) and the lack of addiction to BCR-ABL in these cells (Corbin et al., 2011). Although more potent TKIs such as nilotinib and dasatinib have been developed, these drugs also do not target quiescent LICs of CML (Copland et al., 2006; Jørgensen et al., 2007). Therapy with these TKIs thus serves to suppress, not to eliminate, the disease. Moreover, quiescence in CML LICs is thought not only to contribute to TKI resistance but also to be essential for their long-term maintenance. Elucidation of the molecular mechanism by which LICs maintain quiescence is therefore expected to provide a basis for the development of approaches to sensitize CML LICs to TKI therapy, thereby allowing efficient eradication of leukemia cells, prevention of relapse, and increased patient survival. Although several key molecules and signaling pathways have been implicated in LIC maintenance (Ito et al., 2008; Naka et al., 2010; Zhao et al., 2007), the mechanism by which LICs maintain quiescence has been poorly understood.

c-Myc is one of the best characterized proteins found to determine the state of cell proliferation or quiescence (Laurenti et al., 2009). Regulation of the abundance of c-Myc is achieved at several levels, one of which is control of protein stability mediated by posttranslational modification. We and others have shown that the F-box protein Fbxw7 (also known as Fbw7, Sel-10, hCdc4, or hAgo), the substrate-recognition subunit of an SCF-type ubiquitin ligase complex, interacts with and mediates the ubiquitylation of c-Myc (Nakayama and Nakayama, 2006). The ubiquitin-dependent degradation of c-Myc mediated by Fbxw7 has been found to be essential for maintenance of the quiescence and reconstitution capacity of normal HSCs (Matsuoka et al., 2008; Reavie et al., 2010; Thompson et al., 2008). Given that LICs share many properties with normal HSCs, we hypothesized that Fbxw7 might also be required for the maintenance of LICs and that the Fbxw7–c-Myc axis might be a promising target for leukemia therapy.

RESULTS

Fbxw7 Is Required for Maintenance of Quiescence in LICs

To examine whether Fbxw7 expression is modulated during leukemogenesis, we first measured the amount of Fbxw7 mRNA at various stages of the differentiation of leukemic cells in a mouse model of CML caused by the human BCR-ABL fusion protein (Pear et al., 1998). For generation of the model, a c-Kit$^+$Sca-1$^+$Lin$^-$ (KSL) fraction of bone marrow cells, which represents immature hematopoietic cells, was infected with a retrovirus encoding both p210$^{BCR-ABL}$ and green fluorescent protein (GFP) and was subsequently transplanted into syngeneic recipients (Figure 1A). Recipient mice developed signs of CML, including decreased activity, weight loss, an increased number of myeloid cells in peripheral blood, and splenomegaly, and all mice died within 4 weeks after transplantation. Bone marrow cells were collected from the recipient mice after they began to show such signs of CML. Reverse transcription (RT) and real-time PCR analysis revealed that Fbxw7 mRNA was highly abundant in the LIC compartment (GFP$^+$KSL population), whereas it was present in much smaller amounts in the leukemic progenitor compartment (GFP$^+$c-Kit$^+$Sca-1$^-$Lin$^-$ population) and its abundance decreased further as cell differentiation progressed (Figure 1B). Similar results were obtained by quantification of the copy number of Fbxw7 mRNA per cell in these various compartments (Figure S1A available online). These data thus suggested that Fbxw7 expression during leukemogenesis is regulated at least in part at the transcriptional level.

We next examined the role of Fbxw7 in the maintenance of LIC quiescence by conditional disruption of the Fbxw7 gene in this CML mouse model. KSL cells from Mx1-Cre;*Fbxw7*$^{+/+}$ (control) and Mx1-Cre;*Fbxw7*$^{F/F}$ mice were infected with the retrovirus encoding BCR-ABL and GFP and were then transplanted into syngeneic wild-type mice. The donor mice harbored wild-type (+) or floxed (F) alleles of *Fbxw7*, as well as a transgene for Cre recombinase under the control of the Mx1 gene promoter. The number of white blood cells in peripheral blood of the recipient mice was determined every 5 days; when it had increased to >20,000/μl, GFP$^+$KSL cells (2×10^4) were collected from the recipients and transplanted into additional recipient mice (first bone marrow transplantation [BMT]). These recipients were then injected with polyinosinic:polycytidylic acid (pIpC) beginning the day after the first BMT to activate the Mx1-Cre transgene and thereby to delete the floxed *Fbxw7* allele in Mx1-Cre;*Fbxw7*$^{F/F}$ leukemia cells (to yield the *Fbxw7*$^{\Delta/\Delta}$ genotype) (Figure 1C). One week after the final injection of pIpC, we confirmed that almost all floxed alleles of *Fbxw7* were inactivated in each fraction of the targeted leukemia cells (Figure S1B). Analysis of the cell cycle status of leukemic cells from the recipients of the first BMT by flow cytometry revealed that the frequency of Hoechst^{low}pyronin Y^{low} cells, which represent cells in G_0 phase (quiescence), was significantly smaller in the GFP$^+$KSL compartment of *Fbxw7*$^{\Delta/\Delta}$ leukemia cells than in the corresponding compartment of pIpC-treated Mx1-Cre;*Fbxw7*$^{+/+}$ (control) leukemia cells (Figure 1D). Given that gene ablation induced by pIpC is mediated by interferon, which has been shown to act directly on HSCs to induce cell cycle progression (Essers et al., 2009), recipients of control bone marrow cells as well as those of Mx1-Cre;*Fbxw7*$^{F/F}$ cells were injected with pIpC to eliminate any bias attributable to interferon action. In contrast to LICs, most cells in the GFP$^+$c-Kit$^+$Sca-1$^-$Lin$^-$ compartment were actively cycling, and the proportion of quiescent cells in this compartment did not differ between the two genotypes (Figure 1D), consistent with our observation that

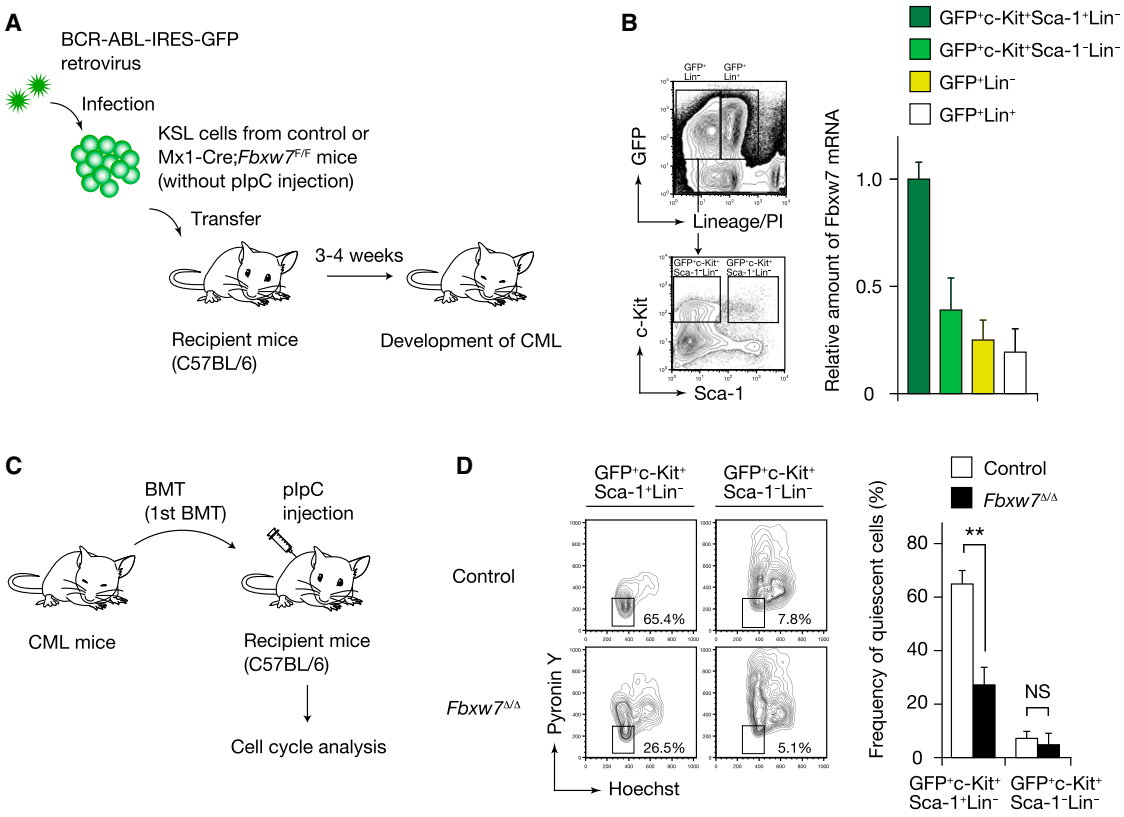

Figure 1. Loss of Fbxw7 in LICs Promotes Cell Cycle Progression

(A) Experimental strategy for generation of a mouse model of CML.

(B) GFP$^+$ cells of control CML bone marrow were fractionated by FACS as indicated (left panels; PI, propidium iodide) and then assayed for Fbxw7 mRNA by RT and real-time PCR analysis (right panel; n = 3).

(C) Experimental strategy for deletion of the floxed *Fbxw7* allele in leukemic cells.

(D) CML bone marrow cells from recipients of the first BMT were subjected to flow cytometry (left panels) for determination of the percentage of quiescent cells in the indicated fractions (right panel; n = 3).

Data are means ± SD. **p < 0.01; NS, not significant. See also Figure S1.

these cells express *Fbxw7* at a low level (Figure 1B). Together, these results suggested that Fbxw7 is expressed predominantly in the LIC fraction of leukemia cells and is required for maintenance of quiescence in LICs.

Fbxw7 Is Required for Leukemic Stemness

The critical role of Fbxw7 in the maintenance of quiescence in LICs and the fact that quiescence is thought to be essential for maintenance of normal HSCs prompted us to examine whether Fbxw7 is essential for LIC maintenance. To test this possibility, we first performed long-term culture-initiating cell assays. Control and *Fbxw7*$^{\Delta/\Delta}$ GFP$^+$KSL cells were isolated from recipients of the first BMT, cultured on OP-9 stromal cells for 2 or 6 weeks, and then subjected to colony-formation assays (Figure 2A). In these assays, the number of colony-forming cells arising after short-term culture (2 weeks) on OP-9 cells mainly reflects progenitor function, whereas that arising after long-term culture (6 weeks) reflects stem cell function (Matsumoto et al., 2011b). We confirmed that the floxed alleles of *Fbxw7* were indeed inactivated efficiently in the *Fbxw7*$^{\Delta/\Delta}$ leukemic cells cultured on OP-9 cells (Figure S2A). The number of cells derived from *Fbxw7*$^{\Delta/\Delta}$ GFP$^+$KSL cells during culture on OP-9 cells was smaller than that derived from the corresponding control cells (Figure S2B). Furthermore, whereas the number of colonies derived from the cells cultured for the short term (2 weeks) did not differ between the two genotypes (Figure 2B), the number of colonies formed by *Fbxw7*$^{\Delta/\Delta}$ GFP$^+$KSL cells was significantly smaller than that formed by the control cells after long-term culture (6 weeks), suggesting that increased cycling of *Fbxw7*$^{\Delta/\Delta}$ LICs eventually results in their exhaustion. We also performed serial replating assays and confirmed that almost all floxed alleles of *Fbxw7* were inactivated in the targeted leukemic cells after serial replating (Figure S2C). Whereas the number of colonies formed did not differ between control and Fbxw7-deficient LICs in the first plating, the number of colonies derived from Fbxw7-deficient LICs was significantly smaller than that derived from control LICs in the second plating (Figure S2D).

To assess the repopulating ability of *Fbxw7*$^{\Delta/\Delta}$ LICs in vivo, we performed serial BMT experiments in which we collected control and *Fbxw7*$^{\Delta/\Delta}$ GFP$^+$KSL cells (2×10^4) from the recipients of the first BMT and transplanted these cells into new recipients (second BMT) (Figure 2C). Almost all floxed alleles of *Fbxw7* were inactivated in the targeted leukemic cells isolated from the recipients of the second BMT (Figure S2E). Whereas the

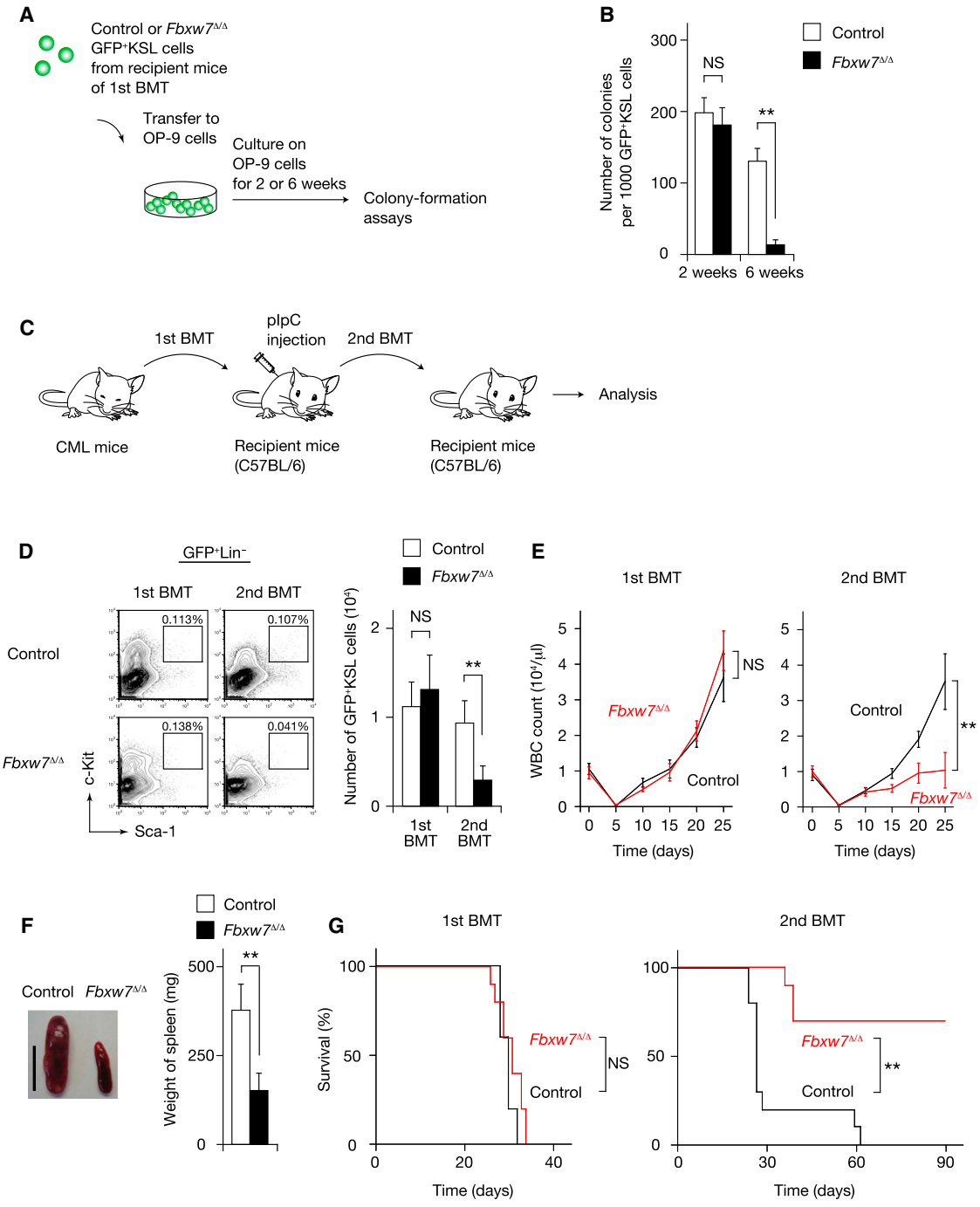

Figure 2. Loss of Fbxw7 in LICs Results in Cell Exhaustion

(A) Experimental strategy for colony formation assays.

(B) Colony formation by BCR-ABL-transduced KSL cells of the indicated genotypes after 2 or 6 weeks of culture on OP-9 cells (n = 3).

(C) Experimental strategy for serial BMT experiments.

(D) Flow-cytometric determination of the absolute number of GFP$^+$KSL cells in bone marrow of recipients (n = 5) after the first and second BMTs.

(E) Numbers of white blood cells (WBC) in peripheral blood of recipient mice (n = 10) after the first and second BMTs.

(F) Representative appearance (scale bar, 10 mm) and weight (n = 5) of the spleen in recipients of the second BMT.

(G) Survival of recipient mice (n = 10) after the first and second BMTs.

Data are means ± SD. **p < 0.01; NS, not significant. See also Figure S2.

number of GFP$^+$KSL cells isolated from recipients of the first BMT did not differ between the two genotypes, that of GFP$^+$KSL cells isolated from recipients of the second BMT was greatly reduced in the case of *Fbxw7*$^{\Delta/\Delta}$ donor cells compared with that for control donor cells (Figure 2D). These results thus suggested that the loss of Fbxw7 results in disruption of quiescence, followed by eventual exhaustion of LICs. We also observed that both the proportion and absolute number of Fbxw7-deficient leukemic progenitors were significantly smaller than those of control leukemic progenitors in recipients of the second BMT (Figures S2F and S2G). Given that Fbxw7 deficiency did not affect the cell cycle status of the progenitors (Figure 1D), these latter results were likely attributable to a functional defect in Fbxw7-deficient LICs. Consistent with these observations, the timing of CML development did not differ between the two types of recipients of the first BMT (Figure 2E). In contrast, after the second BMT, Fbxw7 deficiency prevented the propagation of leukemic cells in peripheral blood (Figure 2E) and the spleen (Figure 2F). Furthermore, whereas most recipients of control LICs died of CML at ~30 days after the second BMT, ~70% of mice receiving *Fbxw7*$^{\Delta/\Delta}$ LICs survived for >120 days (Figure 2G; data not shown). In a similar mouse model of CML, LICs were also shown to give rise to acute lymphocytic leukemia (ALL) with a long latency (Pear et al., 1998). Notably, we did not observe development of ALL or CML in recipients of *Fbxw7*$^{\Delta/\Delta}$ LICs later than 40 days after the second BMT. Flow cytometric analysis and histological examination revealed the almost complete absence of leukemic cells in peripheral blood and no infiltration of leukemic cells in the spleen, liver, or lungs of the recipients of Fbxw7-deficient LICs that survived for >90 days after the second BMT (Figure S2H), suggesting that Fbxw7-deficient LICs lose their potential to generate malignancies. Fbxw7 thus appears to be essential for the long-term maintenance of leukemia-initiating potential.

Accumulation of c-Myc Is Responsible for Loss of Leukemic Stemness

We next investigated the mechanism underlying LIC exhaustion associated with Fbxw7 deficiency. Fbxw7 targets many proteins related to HSC maintenance, including c-Myc, Notch1 intracellular domain (NICD1), and mammalian target of rapamycin (mTOR) (Nakayama and Nakayama, 2006). To determine whether these substrates accumulate in Fbxw7-deficient LICs, we examined their abundance in LICs isolated from recipients of the first BMT and found that the abundance of c-Myc was increased in *Fbxw7*$^{\Delta/\Delta}$ GFP$^+$KSL cells compared with control GFP$^+$KSL cells (Figure 3A). In contrast, the expression levels of NICD1 and mTOR did not differ between control and Fbxw7-deficient GFP$^+$KSL cells (Figures S3A and S3B).

To determine whether c-Myc accumulation is responsible for the phenotype of *Fbxw7*$^{\Delta/\Delta}$ LICs, we first cultured control and *Fbxw7*$^{\Delta/\Delta}$ GFP$^+$KSL cells isolated from recipients of the first BMT with the c-Myc inhibitor 10058-F4 (Follis et al., 2009). A colony-formation assay performed after culture of GFP$^+$KSL cells for 2 or 6 weeks in the presence of 10058-F4 revealed that the number of colonies did not differ between the two genotypes (Figure 3B). To confirm that 10058-F4 indeed inhibited c-Myc function in these cells, we measured the abundance of mRNAs for cyclin D2 and ornithine decarboxylase 1 (ODC1), the genes for which are direct targets of c-Myc. The abundance of these mRNAs was increased in Fbxw7-deficient LICs compared with that in control cells, and each increase was attenuated by 10058-F4, suggesting that 10058-F4 indeed inhibits c-Myc activity in these cells (Figure 3C). To demonstrate further that c-Myc accumulation contributes to the phenotype of Fbxw7-deficient LICs, we next generated Mx1-Cre;*Fbxw7*$^{F/F}$;*c-Myc*$^{+/F}$ mice in order to analyze the cell cycle status and colony-forming ability of *Fbxw7*$^{\Delta/\Delta}$;*c-Myc*$^{+/\Delta}$ LICs. The loss of quiescence and impaired colony-forming ability apparent for *Fbxw7*-deficient LICs were normalized by the additional deletion of one allele of the c-Myc gene (Figures 3D and 3E). In contrast, neither a γ-secretase inhibitor, *N*-[*N*-(3,5-difluorophenacetyl)-L-alanyl]-*S*-phenylglycine *t*-butyl ester (DAPT), which antagonizes Notch signaling, nor rapamycin, which antagonizes mTOR, mimicked the effects of 10058-F4 or c-Myc depletion (Figures S3C and S3D), suggesting that neither Notch nor mTOR contributes to the phenotype of Fbxw7-deficient LICs. Collectively, these results thus indeed suggested that the phenotype of *Fbxw7*$^{\Delta/\Delta}$ LICs is attributable to increased activity of c-Myc.

We next compared the amount of BCR-ABL between control and Fbxw7-deficient LICs. Immunoblot analysis revealed no substantial difference in the level of BCR-ABL between these cells (Figure S3E). We further examined whether Fbxw7 deficiency affects signaling downstream of BCR-ABL in LICs by analyzing the phosphorylation of Stat5 (on Tyr^{694}), Crkl (on Tyr^{207}), and Akt (on Ser^{473}). Intracellular flow cytometric analysis revealed that the proportions of cells expressing the phosphorylated forms of Stat5 or Crkl were similar for control and Fbxw7-deficient LICs (Figures S3F and S3G). In contrast, the frequency of cells positive for phosphorylated Akt was greater for Fbxw7-deficient LICs than for control LICs (Figure S3H). We previously showed that Akt phosphorylation is inhibited by transforming growth factor–β (TGF-β) signaling in CML LICs (Naka et al., 2010), and a recent study indicated that TGF-β is activated by a niche for HSCs (Yamazaki et al., 2011). These observations suggest that Fbxw7-deficient LICs might enter the cell cycle and cease to interact with a LIC niche, resulting in a decrease in TGF-β signaling and an increase in Akt phosphorylation. Consistent with this notion, we found that the frequency of cells positive for phosphorylated Smad2/3 was smaller for *Fbxw7*$^{\Delta/\Delta}$ GFP$^+$KSL cells than for control cells (Figure S3I). Moreover, TGF-β1 treatment reversed the increase in the proportion of Fbxw7-deficient LICs positive for phosphorylated Akt (Figure S3J), suggesting that downregulation of TGF-β signaling indeed contributes to this increase. Collectively, our results exclude the possibility that the phenotype of Fbxw7-deficient LICs is attributable to downregulation of BCR-ABL itself or of signaling downstream of BCR-ABL.

To further exclude the possibility that Fbxw7 deficiency in LICs impairs their homing ability, we collected the same number of control and *Fbxw7*$^{\Delta/\Delta}$ GFP$^+$KSL cells from recipients of the first BMT, transplanted the cells into new recipient mice, and determined the proportion of GFP$^+$ cells among bone marrow cells by flow cytometry at 12 hr after transplantation. We found that the frequency of GFP$^+$ cells did not differ significantly between the two genotypes (Figure S3K), suggesting that the phenotype of mice receiving Fbxw7-deficient LICs was not likely a consequence of impaired homing.

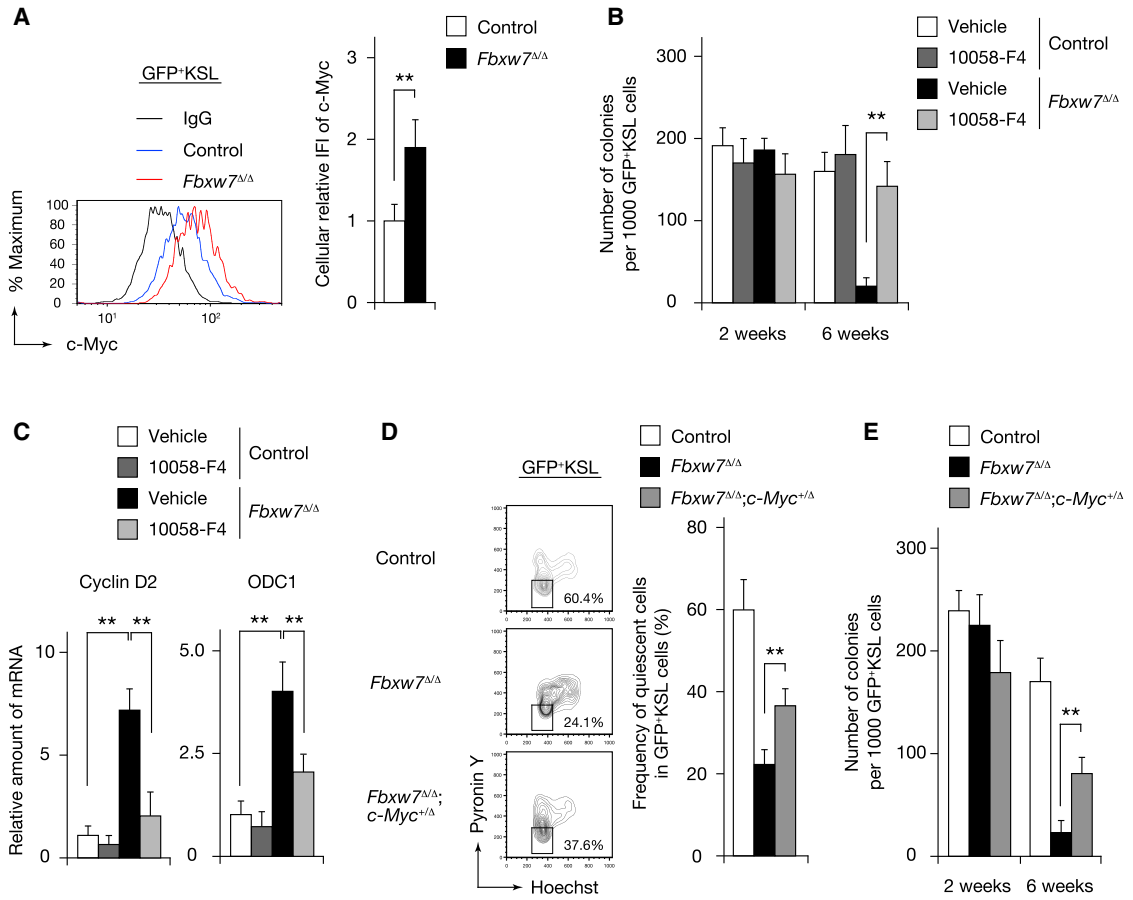

Figure 3. Inhibition of c-Myc Rescues the Phenotype of Fbxw7-Deficient LICs

(A) The abundance of c-Myc in *Fbxw7*$^{\Delta/\Delta}$ or control GFP$^+$KSL cells from mouse recipients of the first BMT was measured by flow cytometry (left panel). Relative c-Myc immunofluorescence intensity (IFI) was determined (n = 5) (right panel). IgG, immunoglobulin G.

(B) Colony formation by *Fbxw7*$^{\Delta/\Delta}$ and control LICs after culture for 2 or 6 weeks with or without 10058-F4 (n = 5).

(C) Control and *Fbxw7*$^{\Delta/\Delta}$ LICs were assayed for cyclin D2 and ODC1 mRNAs by RT and real-time PCR analysis after culture on OP-9 cells for 2 weeks with or without 10058-F4 (n = 5).

(D) The percentage of quiescent cells among GFP$^+$KSL cells was determined for control, *Fbxw7*$^{\Delta/\Delta}$, or *Fbxw7*$^{\Delta/\Delta}$;*c-Myc*$^{+/\Delta}$ bone marrow cells from recipients (n = 5) of the first BMT.

(E) Colony formation by BCR-ABL-transduced KSL cells of the indicated genotypes after 2 or 6 weeks of culture on OP-9 cells (n = 3).

Data are means ± SD. **p < 0.01. See also Figure S3.

Loss of Fbxw7 in LICs Induces Apoptosis in a p53-Dependent Manner

Given that deregulation of c-Myc activation often triggers apoptosis in a p53-dependent manner (Matsuoka et al., 2008; Onoyama et al., 2007), we postulated that p53-dependent apoptosis might be induced by accumulation of c-Myc in Fbxw7-deficient LICs and contribute to LIC exhaustion. The proportion of apoptotic cells did not differ significantly between control and Fbxw7-deficient LICs isolated from recipients of the first BMT. However, the frequency of annexin V$^+$ apoptotic cells was markedly greater among *Fbxw7*$^{\Delta/\Delta}$ GFP$^+$KSL cells than among control GFP$^+$KSL cells from recipients of the second BMT, whereas such a difference was not apparent for leukemic progenitors (Figure 4A). To determine whether this apoptosis in Fbxw7-deficient LICs is induced in a p53-dependent manner, we next cultured control or *Fbxw7*$^{\Delta/\Delta}$ GFP$^+$KSL cells isolated from recipients of the first BMT with the p53 inhibitor pifithrin-α (PFTα) (Komarov et al., 1999). Analysis of colony formation revealed that the exhaustion apparent in *Fbxw7*$^{\Delta/\Delta}$ GFP$^+$KSL cells after 6 weeks of culture was efficiently inhibited by treatment of the cells with PFTα (Figure 4B). To confirm that PFTα indeed inhibits p53 function in these cells, we measured the abundance of mRNAs for p21 and Noxa, the genes for which are direct targets of p53. The amounts of these mRNAs were increased in Fbxw7-deficient LICs compared with those in control cells, and each increase was attenuated by treatment with PFTα (Figure 4C), suggesting that PFTα indeed inhibits p53 activity in these cells. To further show that Fbxw7 deficiency in LICs induces apoptosis in a p53-dependent manner, we generated Mx1-Cre;*Fbxw7*$^{F/F}$;*p53*$^{-/-}$ mice in order to determine the proportion of apoptotic cells and colony-forming ability for *Fbxw7*$^{\Delta/\Delta}$;*p53*$^{-/-}$ LICs. The increase in the frequency of apoptosis apparent for Fbxw7-deficient LICs from recipients of the second BMT was not observed with *Fbxw7*$^{\Delta/\Delta}$;*p53*$^{-/-}$ LICs

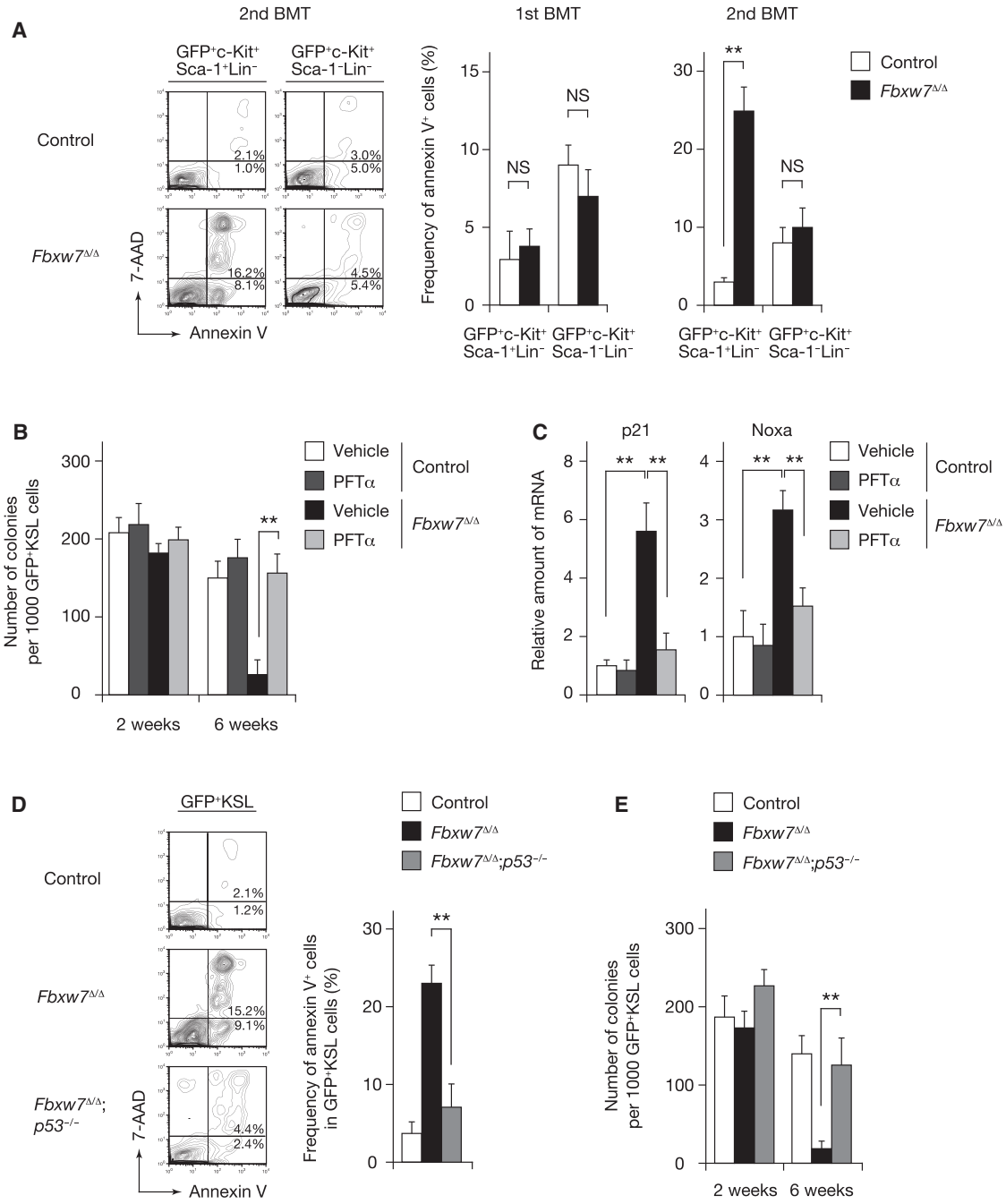

Figure 4. Apoptosis Is Induced in Fbxw7-Deficient LICs in a p53-Dependent Manner

(A) The frequency of annexin V$^+$ cells among *Fbxw7*$^{\Delta/\Delta}$ and control cells of the indicated fractions from mouse recipients (n = 3) of the first or second BMT was determined by flow cytometry. 7-AAD, 7-aminoactinomycin D.

(B) Colony formation by *Fbxw7*$^{\Delta/\Delta}$ and control LICs after culture for 2 or 6 weeks with or without PFTα (n = 5).

(C) Control and *Fbxw7*$^{\Delta/\Delta}$ LICs were assayed for p21 and Noxa mRNAs by RT and real-time PCR analysis after culture on OP-9 cells for 2 weeks with or without PFTα (n = 5).

(D) The proportion of annexin V$^+$ cells among GFP$^+$KSL cells was determined by flow cytometry for control, *Fbxw7*$^{\Delta/\Delta}$, or *Fbxw7*$^{\Delta/\Delta}$;*p53*$^{-/-}$ bone marrow cells from recipients (n = 3) of the second BMT.

(E) Colony formation by cells of the indicated genotypes after culture for 2 or 6 weeks on OP-9 cells (n = 3).

Data are means ± SD. **p < 0.01; NS, not significant.

(Figure 4D). Consistent with this finding, the decrease in the number of colonies derived from Fbxw7-deficient LICs after 6 weeks of culture on OP-9 cells was reversed by deletion of the p53 gene (Figure 4E). Collectively, these results indicated that Fbxw7 deficiency in LICs results in deregulated c-Myc activation, impaired maintenance of quiescence, subsequent apoptosis as a result of p53 induction, and consequent cell exhaustion.

The Combination of Fbxw7 Ablation and Anticancer Drug Treatment Is Effective for LIC Eradication

Although our results implicated Fbxw7 as a potential target for leukemia therapy, the timing of CML development and the survival rate did not differ between the recipients of the first BMT harboring control or Fbxw7-deficient LICs (Figures 2E and 2G), suggesting that inhibition of Fbxw7 alone would not suffice as an effective therapy for CML. To address this problem, we examined the effects of combining Fbxw7 ablation with imatinib. Recipients of the first BMT were injected with pIpC on 7 alternate days beginning the day after transplantation and were then administered imatinib twice a day at 100 mg/kg for 2 weeks beginning 20 days after transplantation (Figure 5A). Determination of the proportion of annexin V^+ cells among GFP^+KSL cells revealed that the frequency of apoptosis among imatinib-treated *Fbxw7*$^{\Delta/\Delta}$ LICs was significantly greater than that among imatinib-treated control LICs (Figure 5B), indicating that Fbxw7-deficient LICs are sensitive to imatinib. In contrast, imatinib was able to efficiently induce apoptosis in both control and Fbxw7-deficient leukemic progenitors and bulk leukemic cells. The number of colonies formed by imatinib-treated *Fbxw7*$^{\Delta/\Delta}$ GFP^+KSL cells was smaller than that formed by vehicle-treated *Fbxw7*$^{\Delta/\Delta}$ GFP^+KSL cells or by imatinib-treated control GFP^+KSL cells (Figure 5C).

Analysis of the effects of this combination therapy on CML development in vivo revealed that it markedly reduced the number of Fbxw7-deficient LICs (Figure 5D). Consistent with these findings, most mice treated with imatinib alone showed a moderate delay in the onset of disease but developed CML after discontinuation of imatinib (Figure 5E), dying within 60 days after BMT (Figure 5F). In contrast, combination therapy with Fbxw7 ablation and imatinib resulted in a marked attenuation of CML development that remained apparent even after discontinuation of imatinib treatment (Figures 5E and 5F). Furthermore, when LICs isolated from recipients of the first BMT were transplanted into new recipients, we found that, whereas LICs treated with imatinib alone still had the potential to confer disease, an apparently complete cure was achieved in all recipients of LICs treated with the combination therapy of Fbxw7 ablation and imatinib (Figure 5F). These results indicated that the effectiveness of the combination therapy is attributable to disrupted maintenance of LICs. We also combined *Fbxw7* deletion and treatment with the conventional anticancer drug cytosine arabinoside (Ara-C) and obtained similar results (Figures S4A–S4D). Analysis of signaling downstream of BCR-ABL in GFP^+KSL cells isolated from recipients of the first BMT at 36 days after transplantation revealed no differences in the proportions of cells expressing phosphorylated forms of Stat5, Crkl, or Akt between imatinib-treated control and *Fbxw7*$^{\Delta/\Delta}$ LICs (Figures S4E–S4G). Collectively, these data thus suggested that LICs whose quiescence is interrupted by Fbxw7 loss are actively cycling and thus sensitive to imatinib or Ara-C treatment and that these combination therapies of Fbxw7 ablation and anticancer drug administration are able to eradicate LICs and provide a survival advantage compared with currently available treatments.

Fbxw7 Deficiency Affects LICs More than It Does Normal HSCs

Given that Fbxw7 is essential for maintenance of both HSCs and LICs, the targeting of LICs by Fbxw7 ablation combined with anticancer drugs might also be expected to damage HSCs. We thus compared the sensitivity of HSCs and LICs to Fbxw7 ablation. To this end, we infected KSL cells from control or Mx1-Cre;*Fbxw7*$^{F/F}$ mice with the retrovirus encoding the $p210^{BCR\text{-}ABL}$ oncoprotein and GFP (to yield LICs) or with a virus encoding GFP alone (to yield HSCs) and then transplanted the cells into recipient mice. GFP^+KSL cells from these mice were subsequently transferred to new recipients, which were then injected with pIpC (Figure 6A). Analysis of GFP^+KSL cells from these latter recipients revealed that exit from quiescence induced by Fbxw7 ablation was more pronounced for LICs than for HSCs (Figure 6B). Accordingly, whereas the proportion of apoptotic cells among LICs did not differ from that among HSCs isolated from recipients of the first BMT, it was greater for Fbxw7-deficient LICs than for Fbxw7-deficient HSCs isolated from recipients of a second BMT (Figure 6C). Consistent with these results, whereas Fbxw7 deficiency did not affect the number of HSCs or LICs in recipients of the first BMT, it reduced the number of LICs to a greater extent than it did that of HSCs in recipients of the second BMT (Figure 6D).

To examine the mechanism underlying this difference in sensitivity to Fbxw7 deficiency between HSCs and LICs, we first compared the amount of Fbxw7 mRNA in these cells. RT and real-time PCR analysis revealed that the abundance of Fbxw7 mRNA in LICs was more than twice that in HSCs (Figure S5A). Given that such an increase in the amount of Fbxw7 mRNA was not observed in KSL cells expressing a kinase-dead (K1176R) mutant of BCR-ABL (Zhang and Ren, 1998), the upregulation of Fbxw7 mRNA in LICs is likely attributable to BCR-ABL kinase activity. The level of c-Myc mRNA was also markedly increased in LICs compared with that in HSCs or in KSL cells expressing the kinase-dead mutant of BCR-ABL (Figure S5B), and intracellular flow cytometric analysis revealed that the abundance of c-Myc in LICs was about five times that in HSCs or in KSL cells expressing the BCR-ABL mutant (Figure S5C). We also confirmed that these effects of BCR-ABL on KSL cells were reversed by imatinib treatment (Figures S5A–S5C). We further examined whether the difference in sensitivity to Fbxw7 deficiency between HSCs and LICs might be attributable to the difference in the abundance of c-Myc in these cells. Both exit from quiescence and apoptosis induced by *Fbxw7* deletion were more pronounced in HSCs overexpressing c-Myc and were less pronounced in *c-Myc*$^{+/\Delta}$ HSCs, than in control HSCs (Figures S5D and S5E). Accordingly, the decrease in the number of stem cells induced by Fbxw7 ablation in recipients of the second BMT was greater for HSCs overexpressing c-Myc, and smaller for *c-Myc*$^{+/\Delta}$ HSCs, than for control HSCs (Figure S5F). We next compared sensitivity to combination therapy with

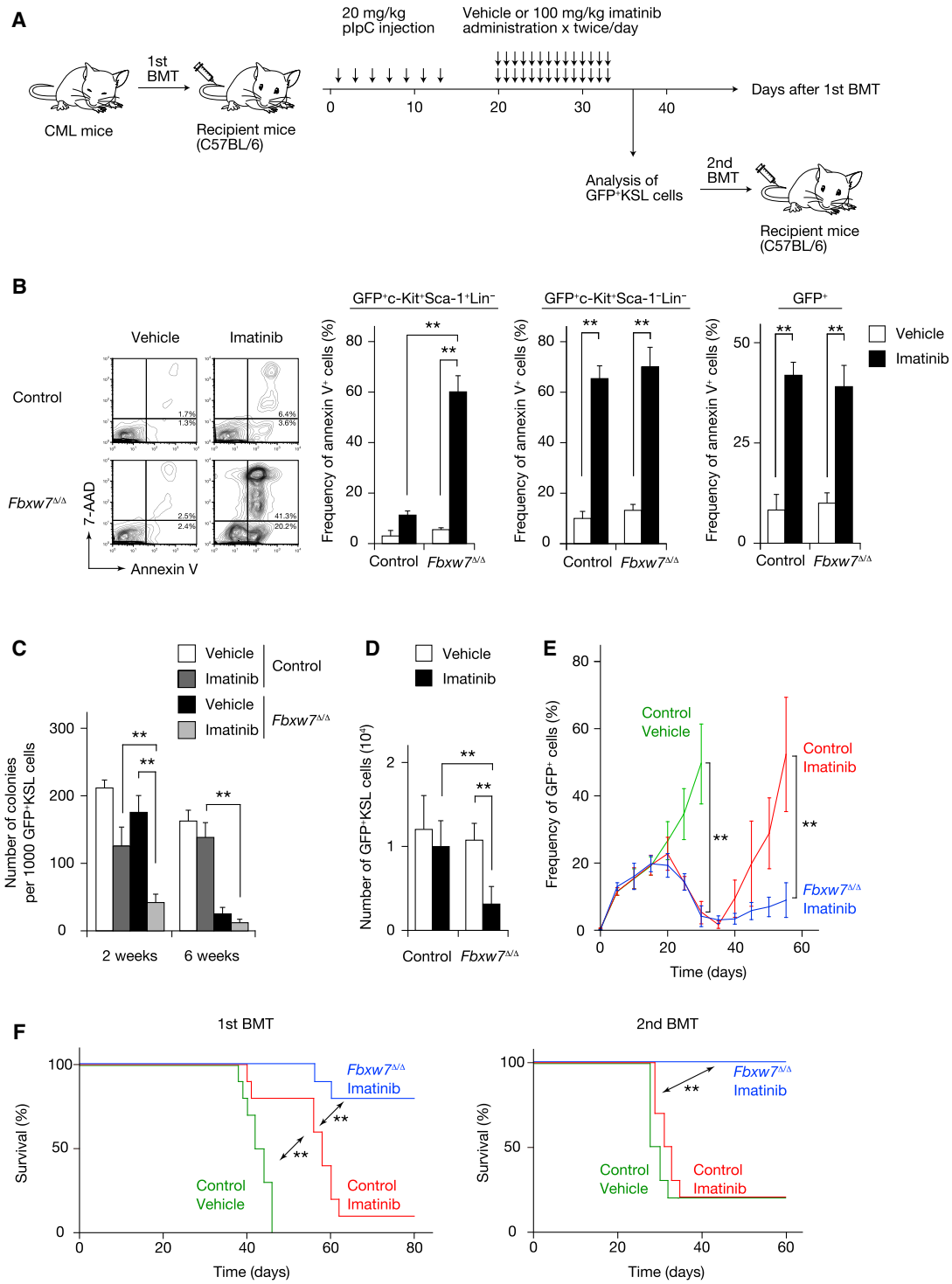

Figure 5. Combination Therapy with Fbxw7 Ablation and Imatinib Eliminates LICs

(A) Experimental strategy for combination therapy with Fbxw7 ablation and imatinib administration.

(B) Frequency of annexin V positivity among *Fbxw7*$^{\Delta/\Delta}$ or control cells of the indicated fractions isolated from recipients (n = 3) of the first BMT after treatment with imatinib or vehicle.

(C) Colony formation by *Fbxw7*$^{\Delta/\Delta}$ and control LICs cultured on OP-9 cells with imatinib or vehicle for 2 or 6 weeks (n = 3).

(D) Absolute number of GFP$^+$KSL cells in bone marrow from mice (n = 5) treated as in (A).

(E) Frequency of GFP$^+$ cells in peripheral blood from mice (n = 10) treated as in (A).

(F) Survival of recipients (n = 10) of the first and second BMT treated as in (A).

Data are means ± SD. **p < 0.01. See also Figure S4.

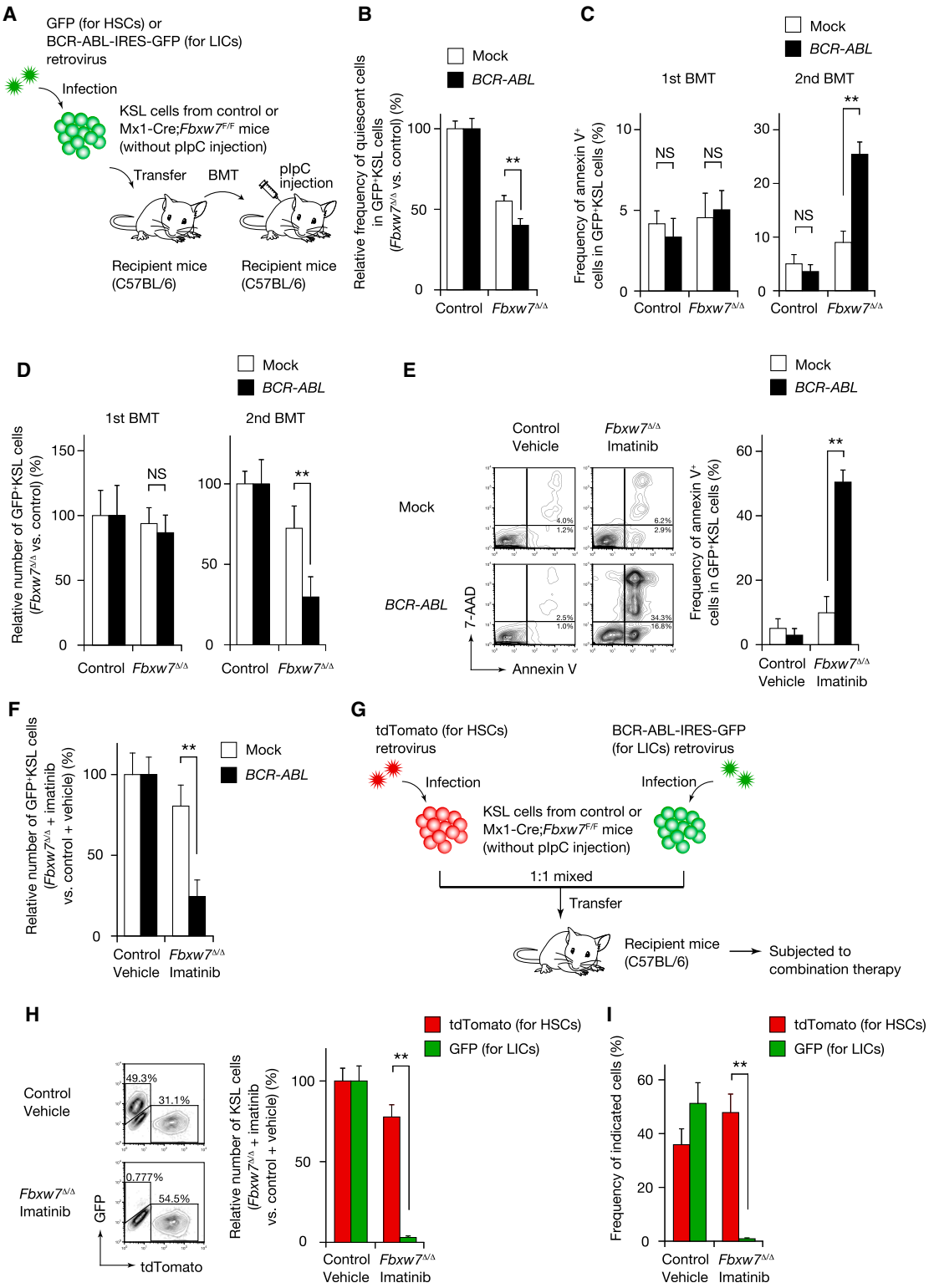

Figure 6. Fbxw7 Deficiency Affects LICs to a Greater Extent than It Does Normal HSCs

(A) Experimental strategy to compare the sensitivity of LICs to Fbxw7 deficiency with that of normal HSCs.

(B) The relative percentage of quiescent cells among GFP$^+$KSL cells for *Fbxw7*$^{\Delta/\Delta}$ cells compared with that for control cells infected with the corresponding vector was determined for recipients of the first BMT (n = 5).

(C) The frequency of annexin V$^+$ cells among GFP$^+$KSL cells for *Fbxw7*$^{\Delta/\Delta}$ cells compared with that for control cells infected with the corresponding vector was determined for recipients of the first and second BMTs (n = 3).

(legend continued on next page)

Fbxw7 ablation and imatinib administration between HSCs and LICs. The frequency of apoptosis among cells from recipient mice treated with this combination therapy was markedly greater for LICs than for HSCs (Figure 6E). Consistent with these results, the decrease in the number of stem cells was more prominent for LICs than for HSCs after combination therapy (Figure 6F).

Finally, to determine directly whether this combination therapy is able to eradicate LICs while preserving normal HSC function, we transplanted an equal number (1×10^4) of KSL cells infected with a retrovirus encoding the fluorescent marker tdTomato (to yield HSCs) and of KSL cells infected with the virus for BCR-ABL and GFP (to yield LICs) into the same recipient mice and then subjected the animals to combination therapy (Figure 6G). Flow cytometric analysis revealed that this regimen reduced the number of GFP^+KSL cells (LICs) to a greater extent than it did that of $tdTomato^+$KSL cells (HSCs) (Figure S5G). We then collected the same number (1×10^4) of $tdTomato^+$KSL cells and GFP^+KSL cells from these recipients and again transplanted them together into new recipients. Whereas Fbxw7-deficient $tdTomato^+$KSL cells (HSCs) persisted in these new recipients, almost all Fbxw7-deficient GFP^+KSL cells (LICs) were eradicated (Figure 6H). Furthermore, whereas $tdTomato^+$ cells (normal progeny of HSCs) were detected in the peripheral blood, virtually no GFP^+ cells (leukemic progeny of LICs) were detected (Figure 6I). Collectively, these observations thus reveal a difference in sensitivity to the combination therapy between HSCs and LICs, referred to as a ''therapeutic window,'' and they thus provide a rationale for further development of this potential approach to the treatment of human leukemia.

Downregulation of Fbxw7 Is Effective for Eradication of Human LICs

To examine whether Fbxw7 ablation is indeed effective for eradication of human LICs in CML, we first measured the amount of Fbxw7 mRNA at various stages of the differentiation of bone marrow cells from patients in the chronic phase of CML. Similar to our findings with the mouse model of CML (Figure 1B), Fbxw7 mRNA was abundant in the LIC compartment ($CD34^+CD38^-Lin^-$ fraction), and its amount decreased markedly as the cells differentiated (Figure 7A). We next transfected bone marrow cells from such patients with small interfering RNAs (siRNAs) specific for Fbxw7 by electroporation, and we confirmed that almost all LICs were successfully transfected without induction of a substantial level of apoptosis by the procedure (Figure S6A) and that Fbxw7 mRNA was depleted efficiently (Figure 7B). Transfection with either of two independent such siRNAs resulted in a decrease in the proportion of quiescent cells in the LIC compartment (Figure 7C). Depletion of Fbxw7 in human LICs resulted in marked enhancement of the induction of apoptosis (Figure 7D) and the inhibition of colony formation (Figure 7E) by imatinib. Similar results were obtained with human LICs subjected to combination therapy with Fbxw7 depletion and Ara-C (Figures S6B and S6C).

Finally, we compared the sensitivity to Fbxw7 deficiency and combination therapy between human HSCs and LICs. We first measured the amount of Fbxw7 mRNA at various stages of the differentiation of bone marrow cells from healthy volunteers and found that Fbxw7 mRNA was abundant in HSCs and was downregulated during cell differentiation (Figure S6D). Depletion of Fbxw7 induced entry of human HSCs into the cell cycle (Figure S6E), and, as with mouse HSCs and LICs, this effect was greater in LICs than in HSCs (Figure 7F). In addition, induction of apoptosis and inhibition of colony formation by the combination of Fbxw7 depletion and imatinib treatment were more pronounced in LICs than in HSCs (Figures 7G and 7H; Figure S6F). Together, these results suggested that the sensitivity to combination therapy differs markedly between human HSCs and LICs, as was the case with mouse HSCs and LICs and that such therapy is a promising approach to the treatment of human CML.

DISCUSSION

With the use of a mouse model of CML, we have found that Fbxw7 has an indispensable role in maintenance of the quiescence as well as the stemness of LICs. Fbxw7-deficient LICs became exhausted with time and incapable of generating CML in transplanted animals. In contrast to LICs, leukemic progenitors proliferated rapidly, and their cell cycle status was not affected by Fbxw7 deficiency. The abundance of Fbxw7 mRNA was high in LICs and relatively low in leukemic progenitors, suggesting that Fbxw7 expression is regulated at the transcriptional level during leukemogenesis. The difference in cell cycle status between LICs and leukemic progenitors is therefore likely attributable, at least in part, to the difference in the abundance of Fbxw7 in these cells. Although the mechanisms responsible for regulation of Fbxw7 expression remain unknown, given that the HSC niche is thought to maintain HSCs in a quiescent state, it is possible that signals from the LIC niche may control Fbxw7 expression in LICs.

Our data also provide mechanistic insight into the maintenance of LIC quiescence by Fbxw7. We found that c-Myc accumulated in Fbxw7-deficient LICs, and either treatment with a c-Myc inhibitor or deletion of one allele of the c-Myc gene

(D) The relative number of GFP^+KSL cells among $Fbxw7^{\Delta/\Delta}$ cells compared with that for control cells infected with the corresponding vector was determined for recipients of the first and second BMTs (n = 5).
(E) The proportion of apoptotic cells among GFP^+KSL cells isolated from recipient mice harboring retrovirus-infected Mx1-Cre;$Fbxw7^{F/F}$ or control cells and injected with pIpC and then treated with imatinib or vehicle for 14 days was determined (n = 3).
(F) The number of GFP^+KSL cells in recipient mice processed as in (E) was determined relative to that in corresponding vehicle-treated recipients (n = 5).
(G) Experimental strategy to examine directly the difference in sensitivity to combination therapy between LICs and normal HSCs.
(H) An equal number (1×10^4) of $tdTomato^+$KSL cells and GFP^+KSL cells was collected from the recipients treated as in (G) and transplanted into new recipient mice together with 2×10^5 bone marrow cells from wild-type mice (second BMT). The relative numbers of $tdTomato^+$KSL cells and GFP^+KSL cells in the recipients (n = 5) of the second BMT were determined.
(I) The frequencies of $tdTomato^+$ cells and GFP^+ cells in peripheral blood from the recipients (n = 10) of the second BMT obtained as in (H) were determined.
Data are means ± SD. $^{**}p < 0.01$; NS, not significant. See also Figure S5.

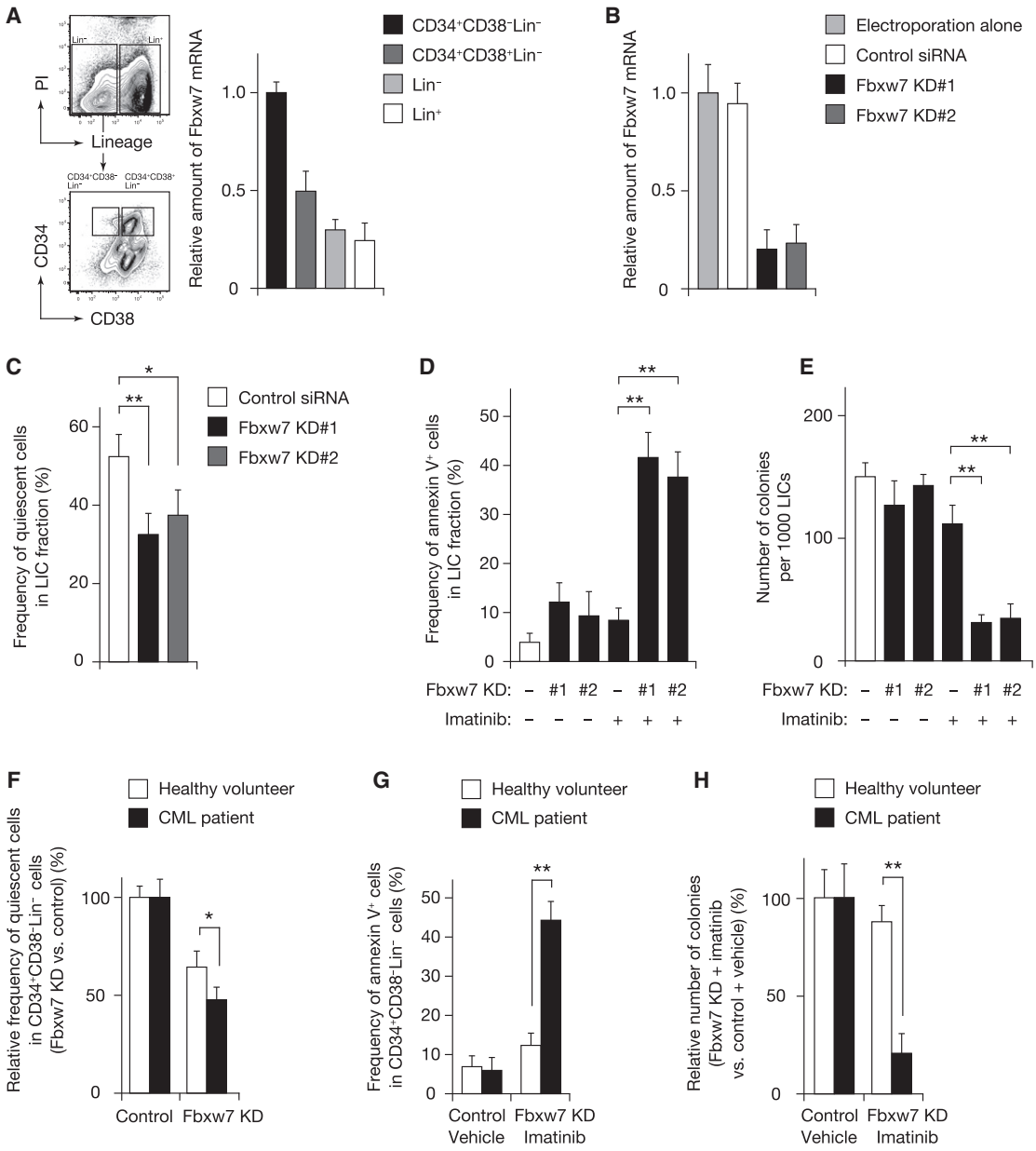

Figure 7. Combination Therapy with Fbxw7 Downregulation and Imatinib Is Effective for Eradication of Human LICs

(A) Bone marrow cells at various stages of differentiation from CML patients were fractionated by FACS and assayed for Fbxw7 mRNA by RT and real-time PCR analysis (n = 3).

(B) Bone marrow cells from patients with CML were transfected with a control siRNA or one of two independent Fbxw7 siRNAs (KD#1 or KD#2), after which the $CD34^+CD38^-Lin^-$ fraction was cultured on OP-9 cells for 3 days and then assayed for Fbxw7 mRNA (n = 3).

(C) Bone marrow cells from CML patients were transfected with Fbxw7 siRNAs, after which the $CD34^+CD38^-Lin^-$ fraction was sorted and cultured on OP-9 cells as in (B). The frequency of quiescent cells was then measured by flow cytometry (n = 3).

(D) Cells from CML patients were transfected, sorted, and cultured on OP-9 cells for 7 days. The cells were exposed (or not) to imatinib for the last 4 days of the culture, after which the proportion of apoptotic cells was determined by staining with annexin V (n = 3).

(E) Colony formation by human CML LICs transfected with Fbxw7 siRNAs and treated with imatinib as in (D) (n = 3).

(F) The relative frequencies of quiescent cells among human HSCs and LICs transfected with Fbxw7 or control siRNAs were determined as in (C) (n = 3).

(G) The frequency of annexin V^+ cells in human HSCs and LICs treated as in (D) (n = 3).

(H) The relative numbers of colonies formed by human HSCs and LICs transfected with Fbxw7 or control siRNAs and treated with vehicle or imatinib as in (D) were determined (n = 3).

Data are means ± SD. *$p < 0.05$; **$p < 0.01$. NS, not significant. See also Figure S6.

normalized the phenotype of these cells, including their cell cycle status and colony formation capacity. These results support the notion that c-Myc activation is responsible for cell cycle progression and the resulting exhaustion of Fbxw7-deficient LICs. Previous studies have indicated that an increase in metabolic growth signaling alone, including activation of the mTOR signaling pathway, is sufficient to drive quiescent HSCs into the proliferative state (Yilmaz et al., 2006). Given that mTOR is a candidate substrate of Fbxw7 (Mao et al., 2008), it was possible that increased mTOR activity might be responsible for the phenotype of Fbxw7-deficient LICs. However, we found that mTOR did not accumulate in Fbxw7-deficient LICs, and the mTOR signaling inhibitor rapamycin did not rescue the phenotype of these cells. We therefore conclude that mTOR activity is not related to the phenotype of Fbxw7-deficient LICs.

We also provide evidence that Fbxw7-deficient LICs are sensitive to anticancer drugs and that combination therapy with Fbxw7 ablation and such drugs is effective for LIC eradication, resulting in a survival advantage over treatment with anticancer drugs alone. Although the development of imatinib has substantially improved the prognosis of CML patients (Druker et al., 2001; Kantarjian et al., 2002), CML LICs are resistant to imatinib and residual LICs give rise to relapse after discontinuation of imatinib treatment (Mahon et al., 2010). Several mechanisms underlying resistance to imatinib have been proposed, including quiescence, BCR-ABL mutations such as T315I, and the lack of addiction to BCR-ABL in LICs (Corbin et al., 2011; Gorre et al., 2001; Holtz et al., 2007). Although more potent TKIs such as nilotinib and dasatinib have been developed, these drugs are also not able to overcome these mechanisms of TKI resistance in LICs (Copland et al., 2006; Jørgensen et al., 2007). We now show that combination therapy with Fbxw7 ablation and imatinib markedly reduced the rate of relapse after discontinuation of imatinib. We also obtained results suggesting that such combination therapy is effective for eradication of LICs in human CML.

Although our study suggests that inhibition of Fbxw7 might represent a promising therapeutic approach for CML patients, the application of Fbxw7 inhibition to the treatment of cancer warrants careful consideration. Given that Fbxw7 has been regarded as an oncosuppressor protein because it targets many proto-oncoproteins, growth promoters, and antiapoptotic molecules including cyclin E, c-Myc, Notch, c-Jun (Nakayama and Nakayama, 2006), mTOR (Mao et al., 2008), and Mcl-1 (Inuzuka et al., 2011; Wertz et al., 2011), suppression of Fbxw7 might induce carcinogenesis or promote cancer growth. Nevertheless, our experimental evidence indicates that the combination therapy with Fbxw7 ablation and anticancer drugs is effective for treatment of CML in a mouse model at the animal level as well as for eradication of human LICs.

Another concern about Fbxw7-targeted therapy is whether normal stem cells might be damaged. Fbxw7 also plays a pivotal role in HSC maintenance (Matsuoka et al., 2008; Thompson et al., 2008), and recent studies have shown that Fbxw7 is a key regulator of the viability of neural stem and progenitor cells (Hoeck et al., 2010; Matsumoto et al., 2011a). Although we found that LICs are more sensitive to Fbxw7 deficiency than are HSCs, suggesting that there is a therapeutic window in targeting Fbxw7 for therapy, it remains to be determined to what extent Fbxw7 inhibition might damage stem cells in other tissues. To minimize damage to normal stem cells, we propose that Fbxw7 inhibitors should be used for only a limited period. Our present study suggests that the difference in sensitivity to Fbxw7 inhibition between LICs and HSCs is attributable at least in part to the difference in the abundance of Fbxw7 or c-Myc in these cells and that such therapy may be expandable to other types of human cancer. Fbxw7 is therefore a promising target for the discovery of anticancer drugs with a broad spectrum of activity against many human cancers.

EXPERIMENTAL PROCEDURES

Mice

Generation of *Fbxw7*$^{F/F}$ mice was described previously (Onoyama et al., 2007). They were crossed with Mx1-Cre transgenic mice (kindly provided by K. Rajewsky) to generate Mx1-Cre;*Fbxw7*$^{F/F}$ mice, and Mx1-Cre;*Fbxw7*$^{+/+}$ mice were used as controls. *Fbxw7*$^{F/F}$ mice were also crossed with *c-Myc*$^{F/F}$ mice (kindly provided by I.M. de Alboran) or *p53*$^{-/-}$ mice (Taconic). All these mice were backcrossed with C57BL/6 mice for more than five generations. Expression of Cre recombinase in transplant recipients was induced by intraperitoneal injection of pIpC (Merck) at a dose of 20 mg per kilogram of body mass on 7 alternate days. C57BL/6 mice were obtained from The Jackson Laboratory and were used as recipients. All mouse experiments were approved by the Animal Ethics Committee of Kyushu University. For some experiments, mice were injected intraperitoneally with Ara-C (Sigma) at a dose of 150 mg/kg. Imatinib (Novartis) was administered by oral gavage twice a day at a dose of 100 mg/kg.

Generation of CML Model

Immature c-Kit$^+$Sca-1$^+$Lin$^-$ hematopoietic cells (KSL cells) were isolated by fluorescence-activated cell sorting (FACS) from bone marrow of Mx1-Cre;*Fbxw7*$^{F/F}$ and Mx1-Cre;*Fbxw7*$^{+/+}$ mice and were cultured in serum-free S-Clone SF-O3 medium (Sanko Junyaku) supplemented with mouse stem cell factor (Wako) at 100 ng/ml as well as human thrombopoietin (PeproTech) at 100 ng/ml. For generation of the CML mouse model, the KSL cells were infected for 2 days with a retrovirus harboring the MSCV-BCR-ABL-IRES-GFP construct (see Supplemental Experimental Procedures) with the use of CombiMag (OZ Biosciences). GFP$^+$ cells (2×10^4) were then isolated by FACS and were injected intravenously into lethally irradiated (9.5 Gy) C57BL/6 mice together with 2×10^5 bone marrow cells from C57BL/6 mice. The efficiency of gene transduction as evaluated on the basis of GFP expression was 30 to 40% in all experiments. When the number of white blood cells had increased to >20,000 /μl, we collected 2×10^4 GFP$^+$KSL cells from the recipient mice and transferred them to new recipients together with 2×10^5 bone marrow cells from C57BL/6 mice (first BMT). These new recipients were injected with pIpC beginning the day after BMT as described earlier. For serial transplantation, 1×10^4 or 2×10^4 GFP$^+$KSL cells were collected from recipient mice 3 weeks after the first BMT and were transplanted into other recipient mice together with 2×10^5 bone marrow cells from C57BL/6 mice (second BMT).

Colony Formation Assays

Colony formation by mouse cells was examined with the use of Methocult medium (MethoCult GF M3434, StemCell Technologies). Control and *Fbxw7*$^{\Delta/\Delta}$ GFP$^+$KSL cells (1×10^3) were collected from recipients of the first BMT and then cultured under hypoxic (5% O_2) conditions with OP-9 stromal cells (Kodama et al., 1994) (RIKEN Cell Bank) for 2 or 6 weeks in six-well dishes containing α–minimum essential medium (Sigma) supplemented with 12.5% fetal bovine serum (Invitrogen), 12.5% horse serum (Invitrogen), and 1 nM dexamethasone (Wako). The cells (2×10^4) were then collected and transferred to Methocult medium. Colonies were scored 1 week after plating for determination of the number of colonies per 1000 GFP$^+$KSL cells. For some experiments, 100 μM 10058-F4 (Merck), 10 μM DAPT (Merck), 25 nM rapamycin (Cell Signaling Technology), 10 μM PFTα (Merck), 100 nM Ara-C, or 5 μM imatinib was added to the culture medium.

Analysis of Primary Human CML Samples

Viable bone marrow mononuclear cells from treatment-naive patients in the chronic phase of CML and from healthy volunteers who had given informed consent were obtained from AllCells. The use of these purchased samples was considered exempt by the Ethics Committee of Kyushu University. To examine the role of Fbxw7 in the maintenance of LICs for human CML and normal HSCs, we transfected bone marrow mononuclear cells with 300 nM Fbxw7 siRNAs (Stealth Select RNAi siRNA, Invitrogen) by electroporation with the use of an Amaxa Nucleofector II device (Lonza) according to the recommended protocol. The transfected cells were then stained with antibodies to human CD34 (8G12), CD38 (HIT2), CD3 (SK7), CD16 (3G8), CD19 (SJ25C1), CD20 (L27), CD14 (MϕP9), and CD56 (NCAM16.2) (BD Biosciences). CD3, CD16, CD19, CD20, CD14, and CD56 were used as lineage markers. $CD34^{+}CD38^{-}Lin^{-}$ cells (1×10^{3}) were purified by FACS and cocultured with OP-9 cells for 7 days. For some experiments, 100 nM Ara-C or 5 μM imatinib was added to the cultures for Days 3 to 7. The human cells were then assayed for apoptosis (see Supplemental Experimental Procedures) or for colony formation; for the latter assay, the cells were transferred to Methocult medium (MethoCult GF H4435, StemCell Technologies), and the number of colonies was counted 1 week after plating.

Statistical Analysis

Quantitative data are presented as means ± SD and were analyzed by Student's t test, with the exception that survival curves were analyzed by the log-rank nonparametric test. A p value of < 0.05 was considered statistically significant.

Other Experimental Procedures

Flow cytometry, preparation of recombinant retroviruses, cell cycle analysis, detection of apoptosis, RT and real-time PCR analysis, and immunoblot analysis are described in Supplemental Experimental Procedures.

SUPPLEMENTAL INFORMATION

Supplemental Information includes six figures and Supplemental Experimental Procedures and can be found in this article online at http://dx.doi.org/10.1016/j.ccr.2013.01.026.

ACKNOWLEDGMENTS

We thank K. Rajewsky for Mx1-Cre transgenic mice, I.M. de Alboran for *c-Myc*$^{F/F}$ mice, H. Honda for BCR-ABL cDNA, and T. Kitamura for Plat-E retroviral packaging cells.

Received: June 29, 2011
Revised: April 25, 2012
Accepted: January 22, 2013
Published: March 18, 2013

REFERENCES

Clevers, H. (2011). The cancer stem cell: premises, promises and challenges. Nat. Med. *17*, 313–319.

Copland, M., Hamilton, A., Elrick, L.J., Baird, J.W., Allan, E.K., Jordanides, N., Barow, M., Mountford, J.C., and Holyoake, T.L. (2006). Dasatinib (BMS-354825) targets an earlier progenitor population than imatinib in primary CML but does not eliminate the quiescent fraction. Blood *107*, 4532–4539.

Corbin, A.S., Agarwal, A., Loriaux, M., Cortes, J., Deininger, M.W., and Druker, B.J. (2011). Human chronic myeloid leukemia stem cells are insensitive to imatinib despite inhibition of BCR-ABL activity. J. Clin. Invest. *121*, 396–409.

de Klein, A., van Kessel, A.G., Grosveld, G., Bartram, C.R., Hagemeijer, A., Bootsma, D., Spurr, N.K., Heisterkamp, N., Groffen, J., and Stephenson, J.R. (1982). A cellular oncogene is translocated to the Philadelphia chromosome in chronic myelocytic leukaemia. Nature *300*, 765–767.

Deininger, M.W., Goldman, J.M., and Melo, J.V. (2000). The molecular biology of chronic myeloid leukemia. Blood *96*, 3343–3356.

Druker, B.J., Talpaz, M., Resta, D.J., Peng, B., Buchdunger, E., Ford, J.M., Lydon, N.B., Kantarjian, H., Capdeville, R., Ohno-Jones, S., and Sawyers, C.L. (2001). Efficacy and safety of a specific inhibitor of the BCR-ABL tyrosine kinase in chronic myeloid leukemia. N. Engl. J. Med. *344*, 1031–1037.

Essers, M.A., Offner, S., Blanco-Bose, W.E., Waibler, Z., Kalinke, U., Duchosal, M.A., and Trumpp, A. (2009). IFNalpha activates dormant haematopoietic stem cells in vivo. Nature *458*, 904–908.

Follis, A.V., Hammoudeh, D.I., Daab, A.T., and Metallo, S.J. (2009). Small-molecule perturbation of competing interactions between c-Myc and Max. Bioorg. Med. Chem. Lett. *19*, 807–810.

Gorre, M.E., Mohammed, M., Ellwood, K., Hsu, N., Paquette, R., Rao, P.N., and Sawyers, C.L. (2001). Clinical resistance to STI-571 cancer therapy caused by BCR-ABL gene mutation or amplification. Science *293*, 876–880.

Hoeck, J.D., Jandke, A., Blake, S.M., Nye, E., Spencer-Dene, B., Brandner, S., and Behrens, A. (2010). Fbw7 controls neural stem cell differentiation and progenitor apoptosis via Notch and c-Jun. Nat. Neurosci. *13*, 1365–1372.

Holtz, M., Forman, S.J., and Bhatia, R. (2007). Growth factor stimulation reduces residual quiescent chronic myelogenous leukemia progenitors remaining after imatinib treatment. Cancer Res. *67*, 1113–1120.

Huntly, B.J., and Gilliland, D.G. (2005). Leukaemia stem cells and the evolution of cancer-stem-cell research. Nat. Rev. Cancer *5*, 311–321.

Inuzuka, H., Shaik, S., Onoyama, I., Gao, D., Tseng, A., Maser, R.S., Zhai, B., Wan, L., Gutierrez, A., Lau, A.W., et al. (2011). $SCF^{(FBW7)}$ regulates cellular apoptosis by targeting MCL1 for ubiquitylation and destruction. Nature *471*, 104–109.

Ito, K., Bernardi, R., Morotti, A., Matsuoka, S., Saglio, G., Ikeda, Y., Rosenblatt, J., Avigan, D.E., Teruya-Feldstein, J., and Pandolfi, P.P. (2008). PML targeting eradicates quiescent leukaemia-initiating cells. Nature *453*, 1072–1078.

Jørgensen, H.G., Allan, E.K., Jordanides, N.E., Mountford, J.C., and Holyoake, T.L. (2007). Nilotinib exerts equipotent antiproliferative effects to imatinib and does not induce apoptosis in $CD34^{+}$ CML cells. Blood *109*, 4016–4019.

Kantarjian, H., Sawyers, C., Hochhaus, A., Guilhot, F., Schiffer, C., Gambacorti-Passerini, C., Niederwieser, D., Resta, D., Capdeville, R., Zoellner, U., et al.; International STI571 CML Study Group. (2002). Hematologic and cytogenetic responses to imatinib mesylate in chronic myelogenous leukemia. N. Engl. J. Med. *346*, 645–652.

Kodama, H., Nose, M., Niida, S., Nishikawa, S., and Nishikawa, S. (1994). Involvement of the c-kit receptor in the adhesion of hematopoietic stem cells to stromal cells. Exp. Hematol. *22*, 979–984.

Komarov, P.G., Komarova, E.A., Kondratov, R.V., Christov-Tselkov, K., Coon, J.S., Chernov, M.V., and Gudkov, A.V. (1999). A chemical inhibitor of p53 that protects mice from the side effects of cancer therapy. Science *285*, 1733–1737.

Lapidot, T., Sirard, C., Vormoor, J., Murdoch, B., Hoang, T., Caceres-Cortes, J., Minden, M., Paterson, B., Caligiuri, M.A., and Dick, J.E. (1994). A cell initiating human acute myeloid leukaemia after transplantation into SCID mice. Nature *367*, 645–648.

Laurenti, E., Wilson, A., and Trumpp, A. (2009). Myc's other life: stem cells and beyond. Curr. Opin. Cell Biol. *21*, 844–854.

Mahon, F.X., Réa, D., Guilhot, J., Guilhot, F., Huguet, F., Nicolini, F., Legros, L., Charbonnier, A., Guerci, A., Varet, B., et al.; Intergroupe Français des Leucémies Myéloïdes Chroniques. (2010). Discontinuation of imatinib in patients with chronic myeloid leukaemia who have maintained complete molecular remission for at least 2 years: the prospective, multicentre Stop Imatinib (STIM) trial. Lancet Oncol. *11*, 1029–1035.

Mao, J.H., Kim, I.J., Wu, D., Climent, J., Kang, H.C., DelRosario, R., and Balmain, A. (2008). FBXW7 targets mTOR for degradation and cooperates with PTEN in tumor suppression. Science *321*, 1499–1502.

Matsumoto, A., Onoyama, I., Sunabori, T., Kageyama, R., Okano, H., and Nakayama, K.I. (2011a). Fbxw7-dependent degradation of Notch is required for control of "stemness" and neuronal-glial differentiation in neural stem cells. J. Biol. Chem. *286*, 13754–13764.

Matsumoto, A., Takeishi, S., Kanie, T., Susaki, E., Onoyama, I., Tateishi, Y., Nakayama, K., and Nakayama, K.I. (2011b). p57 is required for quiescence and maintenance of adult hematopoietic stem cells. Cell Stem Cell *9*, 262–271.

Matsuoka, S., Oike, Y., Onoyama, I., Iwama, A., Arai, F., Takubo, K., Mashimo, Y., Oguro, H., Nitta, E., Ito, K., et al. (2008). Fbxw7 acts as a critical fail-safe against premature loss of hematopoietic stem cells and development of T-ALL. Genes Dev. *22*, 986–991.

Naka, K., Hoshii, T., Muraguchi, T., Tadokoro, Y., Ooshio, T., Kondo, Y., Nakao, S., Motoyama, N., and Hirao, A. (2010). TGF-β-FOXO signalling maintains leukaemia-initiating cells in chronic myeloid leukaemia. Nature *463*, 676–680.

Nakayama, K.I., and Nakayama, K. (2006). Ubiquitin ligases: cell-cycle control and cancer. Nat. Rev. Cancer *6*, 369–381.

Onoyama, I., Tsunematsu, R., Matsumoto, A., Kimura, T., de Alborán, I.M., Nakayama, K., and Nakayama, K.I. (2007). Conditional inactivation of Fbxw7 impairs cell-cycle exit during T cell differentiation and results in lymphomatogenesis. J. Exp. Med. *204*, 2875–2888.

Pear, W.S., Miller, J.P., Xu, L., Pui, J.C., Soffer, B., Quackenbush, R.C., Pendergast, A.M., Bronson, R., Aster, J.C., Scott, M.L., and Baltimore, D. (1998). Efficient and rapid induction of a chronic myelogenous leukemia-like myeloproliferative disease in mice receiving P210 bcr/abl-transduced bone marrow. Blood *92*, 3780–3792.

Reavie, L., Della Gatta, G., Crusio, K., Aranda-Orgilles, B., Buckley, S.M., Thompson, B., Lee, E., Gao, J., Bredemeyer, A.L., Helmink, B.A., et al. (2010). Regulation of hematopoietic stem cell differentiation by a single ubiquitin ligase-substrate complex. Nat. Immunol. *11*, 207–215.

Rowley, J.D. (1973). Letter: A new consistent chromosomal abnormality in chronic myelogenous leukaemia identified by quinacrine fluorescence and Giemsa staining. Nature *243*, 290–293.

Thompson, B.J., Jankovic, V., Gao, J., Buonamici, S., Vest, A., Lee, J.M., Zavadil, J., Nimer, S.D., and Aifantis, I. (2008). Control of hematopoietic stem cell quiescence by the E3 ubiquitin ligase Fbw7. J. Exp. Med. *205*, 1395–1408.

Wertz, I.E., Kusam, S., Lam, C., Okamoto, T., Sandoval, W., Anderson, D.J., Helgason, E., Ernst, J.A., Eby, M., Liu, J., et al. (2011). Sensitivity to antitubulin chemotherapeutics is regulated by MCL1 and FBW7. Nature *471*, 110–114.

Yamazaki, S., Ema, H., Karlsson, G., Yamaguchi, T., Miyoshi, H., Shioda, S., Taketo, M.M., Karlsson, S., Iwama, A., and Nakauchi, H. (2011). Nonmyelinating Schwann cells maintain hematopoietic stem cell hibernation in the bone marrow niche. Cell *147*, 1146–1158.

Yilmaz, O.H., Valdez, R., Theisen, B.K., Guo, W., Ferguson, D.O., Wu, H., and Morrison, S.J. (2006). Pten dependence distinguishes haematopoietic stem cells from leukaemia-initiating cells. Nature *441*, 475–482.

Zhang, X., and Ren, R. (1998). Bcr-Abl efficiently induces a myeloproliferative disease and production of excess interleukin-3 and granulocyte-macrophage colony-stimulating factor in mice: a novel model for chronic myelogenous leukemia. Blood *92*, 3829–3840.

Zhao, C., Blum, J., Chen, A., Kwon, H.Y., Jung, S.H., Cook, J.M., Lagoo, A., and Reya, T. (2007). Loss of β-catenin impairs the renewal of normal and CML stem cells in vivo. Cancer Cell *12*, 528–541.

Cancer Cell
Article

Regulation of c-Myc Ubiquitination Controls Chronic Myelogenous Leukemia Initiation and Progression

Linsey Reavie,[1,2,6] Shannon M. Buckley,[1,2,6] Evangelia Loizou,[1,2] Shoichiro Takeishi,[3] Beatriz Aranda-Orgilles,[1,2] Delphine Ndiaye-Lobry,[1,2] Omar Abdel-Wahab,[4,5] Sherif Ibrahim,[2] Keiichi I. Nakayama,[3] and Iannis Aifantis[1,2,*]
[1]Howard Hughes Medical Institute and Department of Pathology
[2]Cancer Institute
New York University School of Medicine, New York, NY 10016, USA
[3]Department of Molecular and Cellular Biology, Medical Institute of Bioregulation, Kyushu University, 3-1-1 Maidashi, Higashi-ku, Fukuoka, Fukuoka 812-8582, Japan
[4]Human Oncology and Pathogenesis Program
[5]Leukemia Service
Department of Medicine, Memorial Sloan-Kettering Cancer, New York, NY 10016, USA
[6]These authors contributed equally to this work
*Correspondence: iannis.aifantis@nyumc.org
http://dx.doi.org/10.1016/j.ccr.2013.01.025

SUMMARY

The molecular mechanisms regulating leukemia-initiating cell (LIC) function are of important clinical significance. We use chronic myelogenous leukemia (CML) as a model of LIC-dependent malignancy and identify the interaction between the ubiquitin ligase Fbw7 and its substrate c-Myc as a regulator of LIC homeostasis. Deletion of Fbw7 leads to c-Myc overexpression, p53-dependent LIC-specific apoptosis, and the eventual inhibition of tumor progression. A decrease of either c-Myc protein levels or attenuation of the p53 response rescues LIC activity and disease progression. Further experiments showed that Fbw7 expression is required for survival and maintenance of human CML LIC. These studies identify a ubiquitin ligase:substrate pair regulating LIC activity, suggesting that targeting of the Fbw7:c-Myc axis is an attractive therapy target in refractory CML.

INTRODUCTION

Chronic myeloid leukemia (CML) was the first type of cancer for which a specific chromosomal abnormality was identified—the Philadelphia chromosome (Nowell and Hungerford, 1960). Subsequent studies identified that the translocation event occurred between t(9;22)(q34;q11), which fused the breakpoint cluster region gene (*BCR*) with the Abelson kinase gene (*ABL1*) to produce the *BCR-ABL* oncogene (Bartram et al., 1983; Rowley, 1973). This Bcr-Abl fusion protein possesses constitutive tyrosine kinase activity resulting in development of myeloid leukemia through aberrant differentiation of hematopoietic stem cells (HSC) toward the myeloid lineage. CML is dependent on Bcr-Abl-induced c-Myc expression (Sawyers et al., 1992). Clinically, CML progresses through at least three different phases: a chronic phase (CP), a late chronic/accelerated phase (AP), and a blast crisis (BC).

Patients diagnosed with CML in the early CP have been successfully treated with tyrosine kinase inhibitors (TKIs), such as imatinib, that inhibit the tyrosine kinase activity of Bcr-Abl and have a 5-year progression-free survival rate of 89% (Druker et al., 2006). However, only a fraction of TKI-treated patients achieve long-term remission, suggesting that the compound is unable to target CML-initiating cells (de Lavallade et al., 2008;

Significance

CML is initiated by the *BCR-ABL* translocation and maintained by LIC. Although current therapies can suppress disease, they are insufficient to target LIC. Utilizing a Bcr-Abl model of CML and human CML samples, we demonstrate that the E3 ligase Fbw7 is required for the initiation and progression of CML as well as maintenance of the LIC. We demonstrate that interaction between Fbw7 and its protein substrate c-Myc is required for CML progression, and Fbw7 deletion leads to p53-mediated apoptosis of LIC. In agreement with these findings, silencing of FBW7 leads to loss of human CML LIC self-renewal. These studies identify Fbw7 ligase as an essential regulator of CML LIC maintenance and open the way for targeting Fbw7 activity in CML.

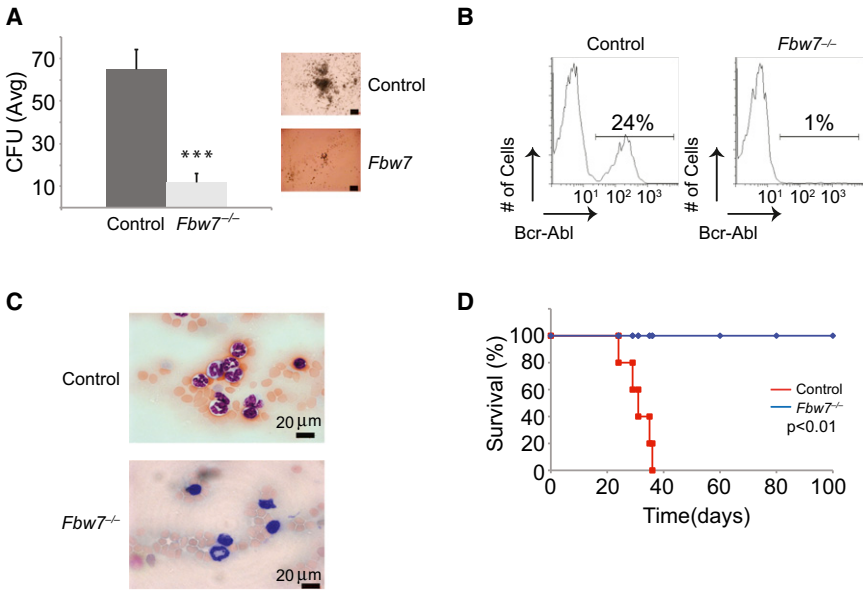

Figure 1. *Fbw7* Deletion Suppresses Initiation of Bcr-Abl-Induced CML

(A) Average CFU from *VavCre*$^{+}$;*Fbw7*$^{+/+}$ and *VavCre*$^{+}$;*Fbw7*$^{-/-}$ cells infected with Bcr-Abl-expressing retrovirus at the first plating. Images on right are representative colonies from control or *Fbw7*$^{-/-}$ Bcr-Abl^{+} LSKs. Scale bar, 100 μm.

(B and C) FACS analysis (B) and blood smears (C) of PB taken from host mice transplanted with *VavCre*$^{+}$;*Fbw7*$^{+/+}$ (Control) or *VavCre*$^{+}$;*Fbw7*$^{-/-}$ Bcr-Abl^{+} LSK cells.

(D) Kaplan Meier survival curves of irradiated animals that were transplanted with *VavCre*$^{+}$;*Fbw7*$^{+/+}$ or *VavCre*$^{+}$;*Fbw7*$^{-/-}$ Bcr-Abl^{+} LSKs. (n = 5 for each genotype). Error bars indicate ± SD. ***p < 0.0001.

See also Figure S1.

Hochhaus et al., 2009). Indeed, the majority of the patients experience relapse upon cessation of treatment (Michor et al., 2005). Moreover, resistance to imatinib treatment can develop in some patients, particularly those who present with advanced disease (O'Hare et al., 2006). The mechanisms thought to drive resistance and disease relapse include the acquisition of mutations in the kinase domain of Bcr-Abl, amplification of *BCR-ABL*, and clonal evolution (Gorre et al., 2001; le Coutre et al., 2000; Shah et al., 2002).

An increasing body of work has suggested that disease relapse upon cessation of TKI therapy could be due to a rare population of leukemia-initiating cells (LICs) that are resistant or refractory to treatment (Bhatia et al., 2003; Corbin et al., 2011; Jankowska et al., 2009). LICs are thought to possess properties similar to normal HSC such as self-renewal, quiescence, and resistance to traditional chemotherapy (Bonnet and Dick, 1997; Huntly and Gilliland, 2005). Thus, the LIC subset might act as a reservoir contributing to relapse by passing *BCR-ABL* on to its progeny. In different types of leukemia, evidence in support of the LIC determined that only a small fraction of acute myeloid leukemia cells from patients were able to recapitulate the disease when transplanted into immunocompromised animals (Bonnet and Dick, 1997; Lapidot et al., 1994). Using similar assays, putative LIC populations were also identified in patients diagnosed with CP and BC CML (Jamieson et al., 2004; Sirard et al., 1996; Wang et al., 1998).

The development of disease animal models, which proved that expression of Bcr-Abl is indeed leukemogenic, provided an important tool to investigate the mechanisms involved in LIC maintenance (Daley et al., 1990; Heisterkamp et al., 1990; Pear et al., 1998). Over the years, Bcr-Abl has been shown to contribute to tumorigenesis through deregulation of molecular pathways that control HSC self-renewal and differentiation (Heidel et al., 2012; Zhao et al., 2007, 2009). Moreover, transplantation studies in mouse models of Bcr-Abl-induced CP CML suggested that LIC activity is confined to Bcr-Abl-expressing Lineage (Lin)$^{-}$Sca1^{+}c-Kit^{+} (LSK) cells, which contain the HSC population (Neering et al., 2007).

Fbw7 is an E3 ubiquitin ligase and is a substrate recognition component of the Cullin-1/SCF complex that targets specific substrate proteins for poly-ubiquitination and degradation by the 26S proteasome. Fbw7 has been shown to regulate a number of oncoproteins such as c-Myc, Notch, and cyclinE (Gupta-Rossi et al., 2001; Koepp et al., 2001; Welcker et al., 2004; Yada et al., 2004). Moreover, we and others have shown that Fbw7 is essential for the maintenance of adult HSC quiescence (Matsuoka et al., 2008; Thompson et al., 2008). Indeed, deletion of Fbw7 in HSC leads to c-Myc accumulation, aberrant cell cycle entry, and eventual HSC exhaustion (Reavie et al., 2010). Here, we explore the role of the Fbw7:c-Myc axis and relative abundance of c-Myc protein in the maintenance of CML LIC.

RESULTS

Fbw7 Deletion Suppresses Initiation of Bcr-Abl-Induced CML

To address the role of Fbw7 in the self-renewal and differentiation of LIC, we used a well-established animal model of Bcr-Abl-induced CP CML (Pear et al., 1998). In this model, Bcr-Abl-expressing retroviruses are used to infect highly-purified hematopoietic stem and progenitor cells, LSK. Transduced LSKs are then transplanted into lethally irradiated recipients, which develop a CML-like disease that is characterized by the accumulation of Bcr-Abl^{+}CD11b^{+}Gr1^{+} cells in the peripheral blood (PB), splenomegaly, and tissue infiltration. The pathology of the disease replicates the CP of CML due to less than 2% of the mononuclear population in the PB has blast morphology, a hallmark of disease progression, whereas the majority displays morphology consistent with mature myeloid cells. Mice succumb to disease starting at ~25–30 days posttransplantation (Figure 1 and data not shown). To initially test the role of Fbw7 function in CML in vitro, we used a conditional *Fbw7* allele (*Vav1cre*$^{+}$;*Fbw7*$^{f/f}$) that specifically targets deletion in hematopoietic cells, starting from the HSC subset during development, and purified LSK cells from 2- to 4-week-old mice (before any significant alterations of the LSK compartment are evident)

(Matsuoka et al., 2008; Stadtfeld and Graf, 2005; Thompson et al., 2007, 2008). *Fbw7*$^{-/-}$ and *Fbw7*$^{+/+}$ LSK cells were infected with Bcr-Abl retroviruses, sorted by flow cytometry for Bcr-Abl^{+}, and plated on colony-forming unit (CFU) assays. Control (Bcr-Abl^{+};*Fbw7*$^{+/+}$) LSK cells generated colonies at the first plating and were able to serially replate demonstrating extensive proliferation potential (Figure 1A and data not shown). Interestingly, Bcr-Abl^{+};*Fbw7*$^{-/-}$ LSK cells generated only a few small colonies at the first plating and were unable to replate, suggesting direct effects of *Fbw7* deletion on survival of the cells. This was an unexpected finding, as WT (Bcr-Abl^{-}) *Fbw7*$^{-/-}$ LSK cells are able to efficiently generate colonies at the first plating, and their colony-forming ability is only progressively lost (Figure S1 available online), suggesting distinct responses to *Fbw7* deletion between physiologic and leukemic LSK cells (Thompson et al., 2008). To address Fbw7 function in CML in vivo, LSKs were infected with Bcr-Abl-expressing retroviruses and transplanted into lethally irradiated recipient mice. Control Bcr-Abl-expressing cells were able to initiate disease and progress to lethal CML (Figures 1B–1D). On the other hand, Bcr-Abl-expressing *Fbw7*$^{-/-}$ LSK cells were unable to initiate disease and recipient animals did not develop CML (Figures 1B–1D). These effects on the initiation of CML were not a consequence of *Fbw7* deletion on HSC homing and engraftment, suggesting a direct role on the maintenance of Bcr-Abl^{+} cells (Figure S1; data not shown). These data suggest that *Fbw7* deletion inhibits Bcr-Abl induction of CML due to direct effects on Bcr-Abl^{+} LSK cell maintenance.

Fbw7 Deletion Suppress Bcr-Abl-Induced Disease Progression

The above experiments address the effects of Fbw7 on transformation but do not study its role during progression of CML in vivo. To experimentally address this question we took advantage of an inducible *Fbw7* allele and crossed these mice to the Mx1cre strain, of which Cre-recombinase is expressed as early as the HSC stage upon administration of poly(I:C) (*Mx1cre*$^{+}$;*Fbw7*$^{f/f}$) and allows for gene deletion after the onset of the disease. In these experiments, CML was established by Bcr-Abl-expressing *Mx1cre*$^{+}$;*Fbw7*$^{f/f}$ and littermate control LSK cells. Disease onset was verified by flow cytometry 7 days posttransplantation (Figure 2A). *Fbw7* deletion was achieved by three poly(I:C) injections and confirmed by quantitative reverse transcriptase PCR (qRT-PCR) analysis (Figure 2B). Notably, tumor LSKs expressed the highest levels of *Fbw7* when compared to more differentiated subsets (Figure 2B). Control recipients developed CML as characterized by the accumulation of Bcr-Abl^{+}CD11b^{+}Gr1^{+} cells in the bone marrow (BM) (Figure 2C), PB (Figures 2A and 2D), and peripheral organs such as the spleen, liver, and lung (Figure 2E and data not shown). In contrast, poly(I:C)-mediated deletion of *Fbw7* led to a rapid reversal of CML progression (as judged by both Bcr-Abl^{+} and CD11b^{+} absolute cell numbers, Figures 2A and 2C), resulting in almost no infiltration of secondary tissues by leukemic cells (Figure 2E). More importantly, while all control mice succumbed to the disease by day 50 posttransplantation, the majority of recipient animals transplanted with Bcr-Abl^{+};*Mx1cre*$^{+}$;*Fbw7*$^{f/f}$ cells and injected with poly(I:C) survived (Figure 2F). These studies demonstrated that *Fbw7* deletion suppresses further development of CML and leads to disease remission, suggesting effects on putative leukemia-initiating cells.

Fbw7-Deficient Bcr-Abl Cells Have No Leukemia-Initiating Activity In Vivo

To directly test the self-renewal capacity of the LIC fraction, we performed secondary transplantation experiments using whole spleen cells isolated ~10 days after poly(I:C)-treatment from *Mx1cre*$^{+}$;*Fbw7*$^{-/-}$ and littermate controls. To ensure that identical numbers of Bcr-Abl^{+} LSKs were transplanted in both cohorts, we normalized the total number of spleen cells based on the frequency of Bcr-Abl^{+} LSK cells. In agreement with our previous findings, recipients of *Fbw7*$^{-/-}$ tumor cells did not develop CML (Figure S2). In contrast, control Bcr-Abl^{+} cells harbored LIC activity when transplanted into secondary recipients and transferred disease exhibiting the same hallmarks as the primary CML (Figure S2). These results strongly suggested that *Fbw7* deletion specifically inhibits CML LIC activity.

Fbw7 Deletion Affects Survival of CML-Initiating Cell Populations

It was previously shown that the LIC activity in Bcr-Abl-induced CML is confined to the Lin^{-}c-Kit^{+} and specifically the LSK subset of the Bcr-Abl-expressing tumor (Neering et al., 2007). To directly study putative effects of *Fbw7* deletion in these subsets, we studied both their relative representation and their absolute numbers in response to *Fbw7* deletion (using the inducible *Mx1cre*$^{+}$;*Fbw7*$^{f/f}$ *in vivo* model). *Fbw7* deletion in established CML led to the rapid and significant loss of Bcr-Abl^{+} Lin-c-Kit^{+} and more specifically the Bcr-Abl^{+} LSK population (Figure 3A). Interestingly, at the same time points, we were able to detect more differentiated Bcr-Abl-expressing tumor cells, suggesting that deletion of Fbw7 specifically targets immature LIC subsets (Figure 2C). The acute loss of Bcr-Abl^{+} LSK cells following *Fbw7* deletion was significantly more rapid than what has been reported for WT LSK cells, which takes 3–4 months (Matsuoka et al., 2008; Thompson et al., 2008). QRT-PCR studies showed that CML LSK cells express slightly higher levels of *Fbw7* mRNA than WT LSK but the difference is not statistically significant (Figure S1D). To identify a putative mechanism to explain the impact of *Fbw7* deletion on the Bcr-Abl^{+} LSK population, we evaluated apoptosis and cell death using Annexin-V and 7AAD. As shown in Figure 3B, *Fbw7* deletion led to a rapid and significant increase (5- to 8-fold) in the fraction of the Bcr-Abl^{+} LSK cells undergoing apoptosis, suggesting direct induction of cell death in this stem and progenitor subset. We further evaluated p53 pathway target genes associated with cell survival by qRT-PCR and found *Puma, Bax, p21*, and *Noxa* upregulated in *Fbw7*$^{-/-}$ tumor LSKs (Figure 3C and data not shown), suggesting that p53 pathway activation mediates the induced death of *Fbw7*-deficient Bcr-Abl^{+} LSK cells. These studies provide the biologic mechanism explaining the loss of Bcr-Abl^{+} LICs and the suppression of disease progression in response to *Fbw7* deletion.

c-Myc Is the Key Substrate Targeted by Fbw7 in CML-Initiating Cell Populations

As we have previously shown that c-Myc is an Fbw7 substrate during early hematopoiesis (Reavie et al., 2010) and CML is

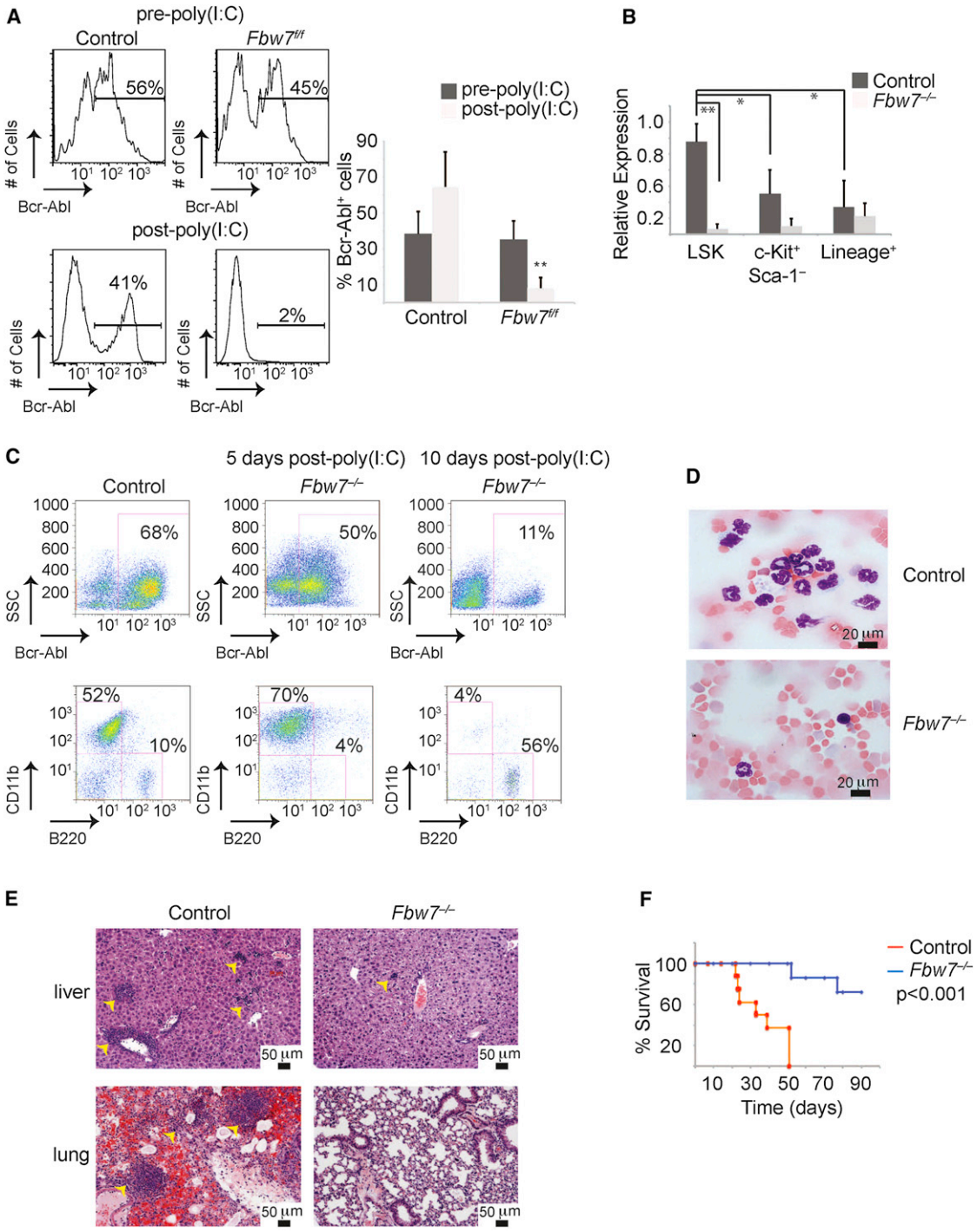

Figure 2. Fbw7 Is Essential for Progression of Established CML In Vivo

(A) PB from mice transplanted with *MxCre*$^{+}$;*Fbw7*$^{+/+}$ and *MxCre*$^{+}$;*Fbw7*$^{-/-}$ Bcr-Abl infected LSK cells. The bar graph on right is a quantification of Bcr-Abl^{+} cells in the PB.

(B) qRT-PCR analysis of *Fbw7* expression in sorted populations from WT and *Fbw7*$^{-/-}$ CML 5 days after the post-poly(I:C) injection.

(C) FACS analysis of the BM of animals transplanted with Bcr-Abl^{+} LSK cells.

(D) Blood smears ~10 days post-poly(I:C) injections.

(E) Hematoxylin and eosin (H&E) staining of liver and lung.

(F) Kaplan Meier survival curves of irradiated animals that were transplanted with *Fbw7*$^{+/+}$ or *Fbw7*$^{-/-}$ Bcr-Abl^{+} LSKs. (n = 9 for each genotype). Error bars indicate ±SD. *p < 0.01, **p < 0.001.

See also Figure S2.

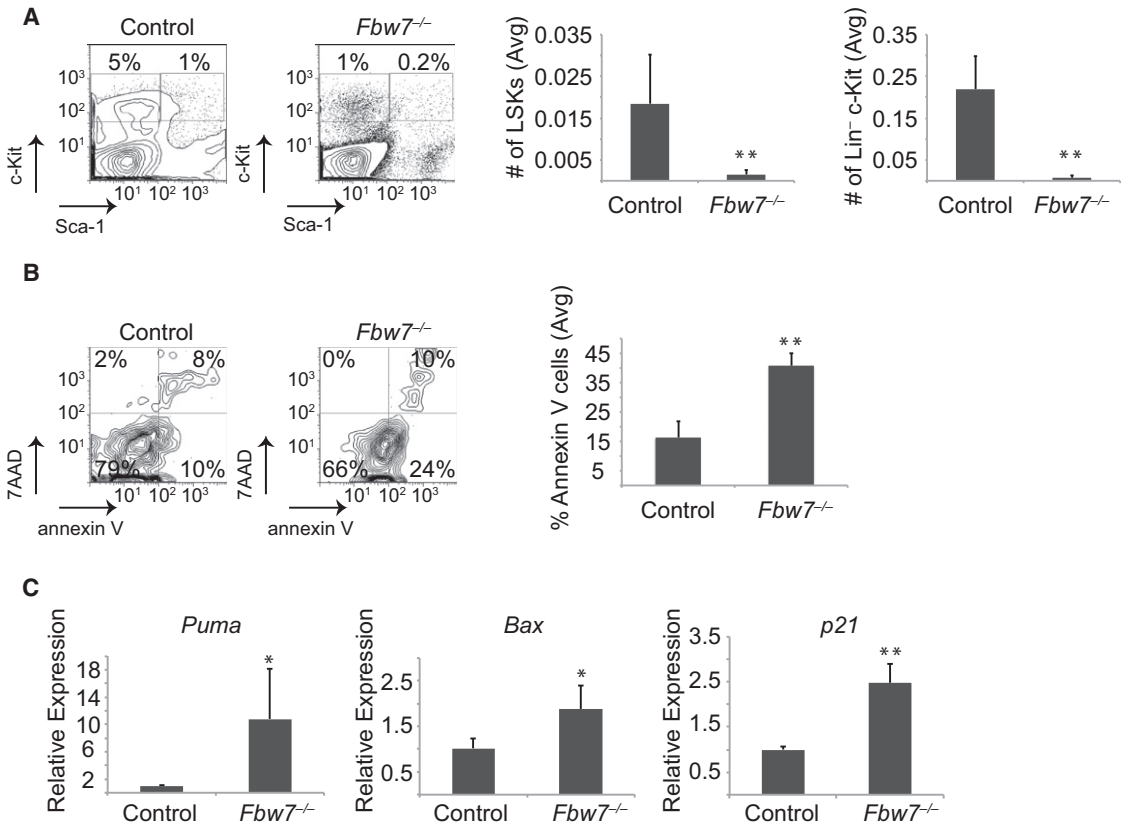

Figure 3. Fbw7 Deletion Affects CML-Initiating Cell Survival through the Activation of the p53 Pathway

(A) FACS plots depicting the relative percentage of Bcr-Abl expressing stem and progenitor (LSK), and progenitors ($Lin^-c\text{-}Kit^+Sca^-$) cells in the BM of *MxCre*$^+$;*Fbw7*$^{+/+}$ or *MxCre*$^+$;*Fbw7*$^{-/-}$ mice. Bar graphs depict the number of tumor stem and progenitor cells based on the frequency of LSK in total number of BM cells.

(B) FACS plots showing relative annexin V and 7-AA-positive cells in the Bcr-Abl$^+$ LSK subset in the BM. Graph on right represents percent of annexin V$^+$ cells in the Bcr-Abl$^+$ LSK.

(C) qRT-PCR analysis showing expression of the p53 target genes, *Puma*, *Bax*, and *p21*, in sorted control or *Fbw7*$^{-/-}$ LSKs from the tumor. Error bars indicate ± SD (n = 4 for each genotype). *p < 0.05, **p < 0.01.

dependent on c-Myc induced by Bcr-Abl (Sawyers et al., 1992), we investigated the possibility that unphysiologically high levels of the oncogenic c-Myc protein could cause the cell death observed upon loss of Fbw7 expression in CML. We further hypothesized that this was most likely through activation of the p53 pathway since p53 target genes were upregulated in *Fbw7*$^{-/-}$ Bcr-Abl$^+$ LSKs (Figure 3C). Because we have shown differential effects of *Fbw7* deletion on WT and Bcr-Abl$^+$ LSK function in vitro (Figures 1 and S1), we directly compared levels of c-Myc protein in these two subsets using a targeted c-Myc allele that expresses a c-Myc-eGFP fusion protein (c-Myc^{eGFP}), which has been shown to be a functional protein fusion and a faithful indicator of endogenous c-Myc protein levels (Huang et al., 2008). Despite the fact that *c-Myc* mRNA levels were unchanged between control and *Fbw7*-deficient Bcr-Abl$^+$ LSKs (Figure 4A), using this allele (*Mx1cre*$^+$;*Fbw7*$^{f/f}$;*c-Myc*$^{eGFP/+}$), we showed that Bcr-Abl$^+$ LSK cells expressed significantly higher c-Myc protein levels than WT LSK cells (Figure 4B). These data were further corroborated by western blot (Figure 4C). Notably, c-Myc protein levels were higher in leukemic LSKs when compared to both WT LSK and *Fbw7*$^{-/-}$ LSKs, explaining the different physiologic responses observed between nonleukemic and leukemic LSKs in response to *Fbw7* deletion (Figure 4C). In Bcr-Abl$^+$ LSK cells, loss of *Fbw7* expression further induced the levels of c-Myc protein beyond that observed in WT leukemic LSK cells (Figure 4D). These observations suggested that slight changes in c-Myc protein abundance could result in distinct phenotypic responses.

Additional Fbw7 substrates, particularly Notch, have been previously implicated in CML progression (Ito et al., 2010) and could influence the observed LIC defects upon *Fbw7* deletion in Bcr-Abl$^+$ LSKs. To address this question, we initially evaluated the expression level of cleaved Notch1 in WT and *Fbw7*$^{-/-}$ Bcr-Abl$^+$ c-Kit$^+$ cells. Expression of Notch1 was not detected in either population (Figure S3A). Of note, Notch1 and Notch2 do not appear to be important Fbw7 substrates in WT HSCs because generation of triple knockout mice (*MxCre*$^+$;*Fbw7*$^{f/f}$;*Notch1*$^{f/f}$;*Notch2*$^{f/f}$) could not rescue the HSC defects observed in *Fbw7*$^{-/-}$LSKs (nonleukemic) (Figures S3B–S3E). More specifically, the frequency (total cell number) of CD150$^+$ CD48$^-$ LSKs and aberrant cell cycle status were unaffected by reducing Notch levels in *Fbw7*-deficient mice (Figures S3B–S3D;

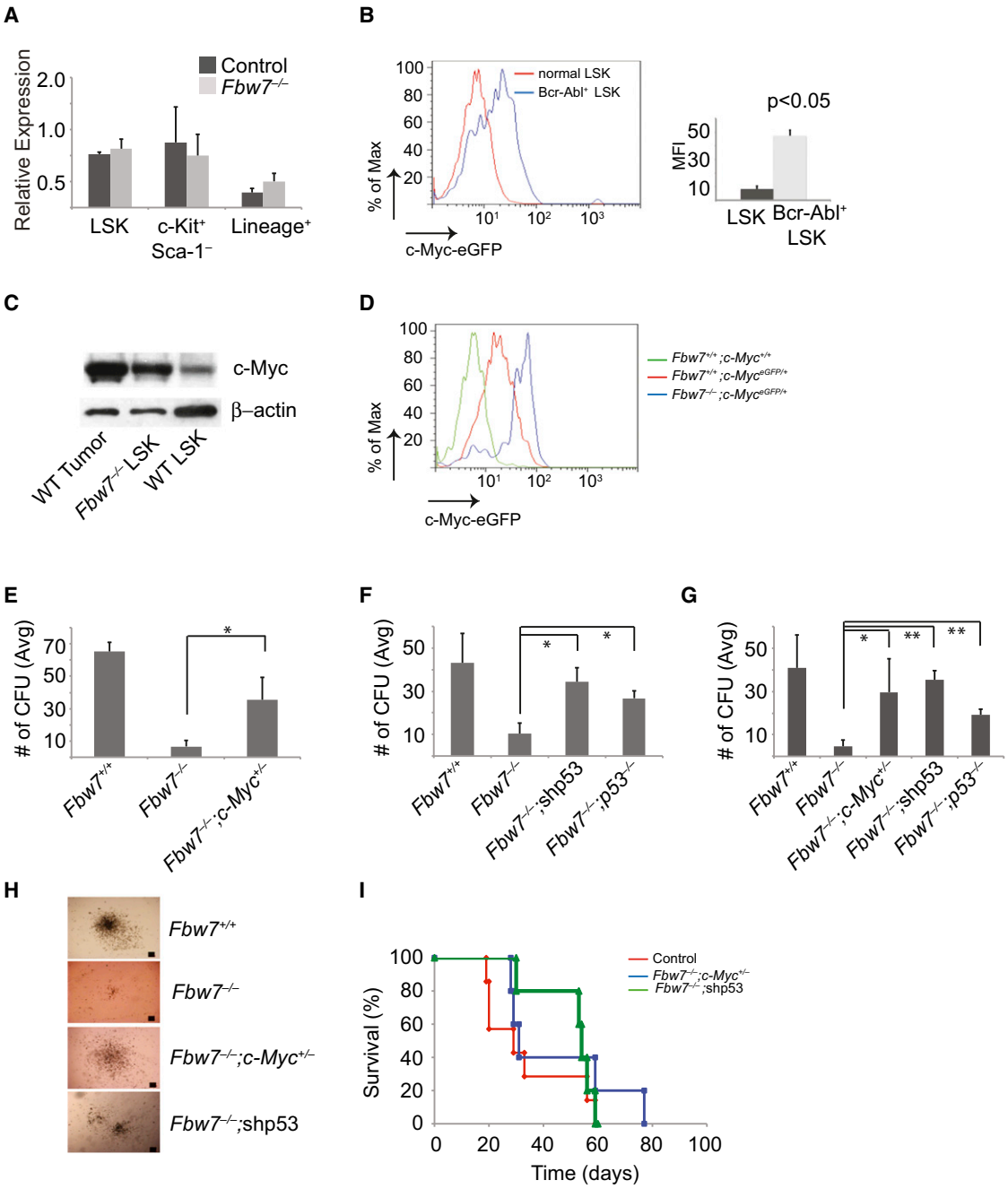

Figure 4. Decrease of c-Myc Protein Levels and Inhibition of p53 Activation Rescue CML-Initiating Activity

(A) qRT-PCR analysis of *c-Myc* expression in sorted tumor subsets (LSK, c-Kit$^+$, and Lin$^+$).

(B) c-Myc protein expression in normal and Bcr-Abl$^+$ LSK cells in the BM. Graph on right shows mean fluorescence intensity (MFI) for eGFP (c-Myc protein).

(C) Western blot analysis of c-Myc protein expression in LSKs sorted from WT tumor, *Fbw7*$^{-/-}$ and WT mice.

(D) c-Myc protein expression in *MxCre*$^+$;*Fbw7*$^{+/+}$ or *MxCre*$^+$;*Fbw7*$^{-/-}$ Bcr-Abl$^+$ LSK.

(E) Average CFU from sorted Bcr-Abl$^+$ LSK cells from *MxCre*$^+$;*Fbw7*$^{+/+}$, *MxCre*$^+$;*Fbw7*$^{-/-}$, or *MxCre*$^+$;*Fbw7*$^{-/-}$;*Myc*$^{+/-}$ mice.

(F and G) Average CFU from sorted Bcr-Abl$^+$ LSK cells from *MxCre*$^+$;*Fbw7*$^{+/+}$, *MxCre*$^+$;*Fbw7*$^{-/-}$, *MxCre*$^+$;*Fbw7*$^{-/-}$;shp53, or *MxCre*$^+$;*Fbw7*$^{-/-}$;*p53*$^{-/-}$ mice on the first (F) and secondary (G) platings.

(H) Images of Bcr-Abl$^+$ colonies generated from the indicated genotypes (n = 3 for each genotype). Scale bar 100 μm.

(I) Kaplan Meier survival curves of animals transplanted with control (red), *Fbw7*$^{-/-}$;*Myc*$^{+/-}$ (blue) LSKs transduced with a retrovirus expressing Bcr-Abl, or *Fbw7*$^{-/-}$ LSKs transduced with a retrovirus expressing Bcr-Abl and a shRNA targeting p53 (green). Error bars indicate ± SD. *p < 0.01, **p < 0.001.

See also Figure S3.

Thompson et al., 2008 and unpublished). These in vivo studies have defined the effects of *Fbw7* on leukemia-initiating cell populations. They have also demonstrated that c-Myc (and not Notch1/2) is the major Fbw7 substrate in CML. However, we cannot exclude that other Fbw7 substrates may play a part in the regulation of CML LIC.

Decrease of c-Myc Protein Levels and p53 Silencing Rescues *Fbw7*$^{-/-}$ LIC Function

To directly address the mechanisms of action of Fbw7 in CML-initiating cells, we attempted to genetically rescue *Fbw7* deletion effects on the survival of the Bcr-Abl$^+$ LSK population. We generated *Mx1cre*$^+$;*Fbw7*$^{f/f}$;*c-Myc*$^{f/+}$ mice and silenced p53 expression in *Mx1cre*$^+$;*Fbw7*$^{f/f}$ cells by using a p53-specific shRNA or by deleting *p53*, *Mx1cre*$^+$;*Fbw7*$^{f/f}$;*p53*$^{-/-}$ mice (Bric et al., 2009). We hypothesized that a decrease in c-Myc protein levels or the inhibition of p53 response could rescue the ability of *Fbw7*$^{-/-}$ Bcr-Abl$^+$LSK cells to maintain CML disease progression in vivo and serially replate in vitro. As shown in Figures 4E–4I, both genetic modifications led to a significant rescue of the ability of the Fbw7-deficient LSK cells to generate colonies in vitro and to induce disease in vivo. The *Fbw7*$^{-/-}$;*c-Myc*$^{-/+}$, *Fbw7*$^{-/-}$;shp53 and *Fbw7*$^{-/-}$;*p53*$^{-/-}$ colonies were almost indistinguishable in numbers from colonies generated by WT cells and no lineage differences were noted (Figures 4E–4H). *Fbw7*$^{-/-}$;*c-Myc*$^{-/+}$ and *Fbw7*$^{-/-}$;*p53*$^{-/-}$ colonies were able to serially replate in a fashion identical to WT counterparts (Figure 4G). To directly assess the self-renewal ability of LICs, we transplanted transduced LSKs from *Fbw7*$^{-/-}$;*c-Myc*$^{-/+}$ or *Fbw7*$^{-/-}$;shp53 into lethally irradiated recipients. Importantly, mice receiving Bcr-Abl$^+$ LSKs from *Fbw7*$^{-/-}$;*c-Myc*$^{-/+}$ developed a CML-like disease with similar kinetics to Bcr-Abl$^+$ control cells restoring *Fbw7*$^{-/-}$LIC self-renewal capacity (Figure 4I). However, as previously shown by Lowe and colleagues, loss of p53 in CML leads to disease progression, and Bcr-Abl$^+$ shp53$^+$ LSKs from *Fbw7*$^{-/-}$ progressed to an AP based on pathology and ~5% blasts in the periphery (data not shown) (Wendel et al., 2006). These experiments demonstrate that c-Myc overexpression and p53-mediated cell death are responsible for the apoptotic phenotype of the Fbw7-deficient LIC.

In Vivo Visualization of c-Myc Protein Expression in CML

These studies suggested that CML-initiating cells express c-Myc protein and depend on its activity. Although it was previously shown that Bcr-Abl induces the transcription of c-Myc (Nakamura et al., 2012; Xie et al., 2002), it is unclear whether c-Myc function is essential for the initiation and/or the progression of the disease in vivo. To address this question, we utilized the *c-Myc*^{eGFP} genetic model and visualized c-Myc expression in established CML. As shown in Figure 5A, only a minority of CML (Bcr-Abl$^+$) cells express detectable levels of c-Myc protein. All c-Myc protein expression is confined within the Lin$^-$ fraction and comprises approximately 10%–20% of the bulk of the tumor. Myc protein expression was detected in both Bcr-Abl$^+$ Lin$^-$ c-Kit$^+$ and Bcr-Abl$^+$ LSK populations. In contrast, Bcr-Abl$^+$ CD11b$^+$Gr1$^+$ cells are negative for GFP expression (Figure 5A). To test whether there is a correlation between leukemia-initiating activity and c-Myc protein expression, identical numbers of purified different tumor subsets were transplanted into secondary recipients. Neither the Lin$^+$ c-Myc/eGFP$^-$ nor the Lin$^-$ c-Myc/eGFP$^-$ fractions were able to transfer disease (Figure S4 and data not shown). On the other hand, all leukemia-initiating activity was confined to the c-Myc^{eGFP} leukemic cell fraction (Figures S4B and S4C). However, flow-cytometry-based separation of Bcr-Abl$^+$Lin$^-$c-Kit$^+$Sca1$^-$ and Bcr-Abl$^+$ Lin$^-$c-Kit$^+$Sca1$^+$ fractions, coupled to subsequent transplantation experiments, demonstrated that only the LSK fraction could transfer disease in secondary hosts (Figures S4B and S4C). This finding contrasts with c-Myc protein expression and function in normal LSK cells, where two distinct populations exist. The c-Myc$^-$ population contains HSC activity and a c-Myc$^+$ population contains multipotential progenitors (Reavie et al., 2010). These studies demonstrate in vivo c-Myc visualization in leukemia and suggest that although LIC activity lies within the c-Myc-expressing fraction, c-Myc protein expression is not sufficient to guarantee leukemia initiation.

Bcr-Abl-Induced CML Is Addicted to c-Myc Expression and Function

To test the importance of c-Myc protein expression in CML initiation and progression, we used a conditional *c-Myc* allele (*Mx1cre*$^+$;*c-Myc*$^{f/f}$). All genotypes prior to deletion were able to initiate disease as verified by PB analysis (Figure 5B). Once disease onset was verified, *c-Myc* was deleted using poly(I:C) administration. Deletion of *c-Myc* led to an almost complete absence of Bcr-Abl$^+$ cells from PB and infiltration in secondary tissues such as liver and lung within 3 weeks (Figures 5B and 5C). Mice carrying *c-Myc*$^{-/-}$ Bcr-Abl$^+$ cells were followed up to 6–8 months posttransplantation and never developed any signs of a CML-like disease. On the other hand, control mice carrying *Mx1cre*$^+$;*c-Myc*$^{+/+}$ Bcr-Abl$^+$ cells succumbed to a lethal CML-like disease within 5 weeks posttransplantation (Figure 5D).

To further quantify c-Myc protein levels, we utilized mice carrying only one allele of c-Myc (*Mx1cre*$^+$;*c-Myc*$^{f/w}$). We had previously shown that these LSK cells express lower levels of c-Myc protein (Reavie et al., 2010). Bcr-Abl$^+$c-Myc$^{+/-}$ LSK cells were able to generate colonies in vitro, at similiar efficiency to their Bcr-Abl$^+$c-Myc$^{+/+}$ counterparts in both primary and secondary platings (Figure S4D). We then initiated disease by transplanting Bcr-Abl-expressing LSK (Bcr-Abl$^+$c-Myc$^{+/-}$) cells and upon verification of CML initiation, deleted one *c-Myc* allele by poly(I:C) administration. Interestingly, a single allele of *c-Myc* was sufficient to maintain disease progression (Figures S4E–S4G). These studies suggest that there are well-defined thresholds of c-Myc protein expression, which is controlled by Fbw7-mediated ubiquitination, essential for CML induction and progression. Indeed, both are lacking and nonphysiologically increased levels of c-Myc severely affect CML progression.

Fbw7 Deletion Inhibits Progression of Established, Bcr-Abl-Induced B-Cell Acute Lymphoblastic Leukemia

The *BCR-ABL* translocation is also found in B cell acute lymphoblastic leukemia (B-ALL). We thus determined whether Fbw7 plays a role in progression of B-ALL. To establish B-ALL, we transduced *MxCre*$^+$;*Fbw7*$^{+/+}$ or *MxCre*$^+$;*Fbw7*$^{f/f}$ whole BM with retrovirus expressing Bcr-Abl-GFP followed by transplantation into lethally irradiated recipient mice. PB was analyzed 12 days posttransplantation to determine initiation of disease

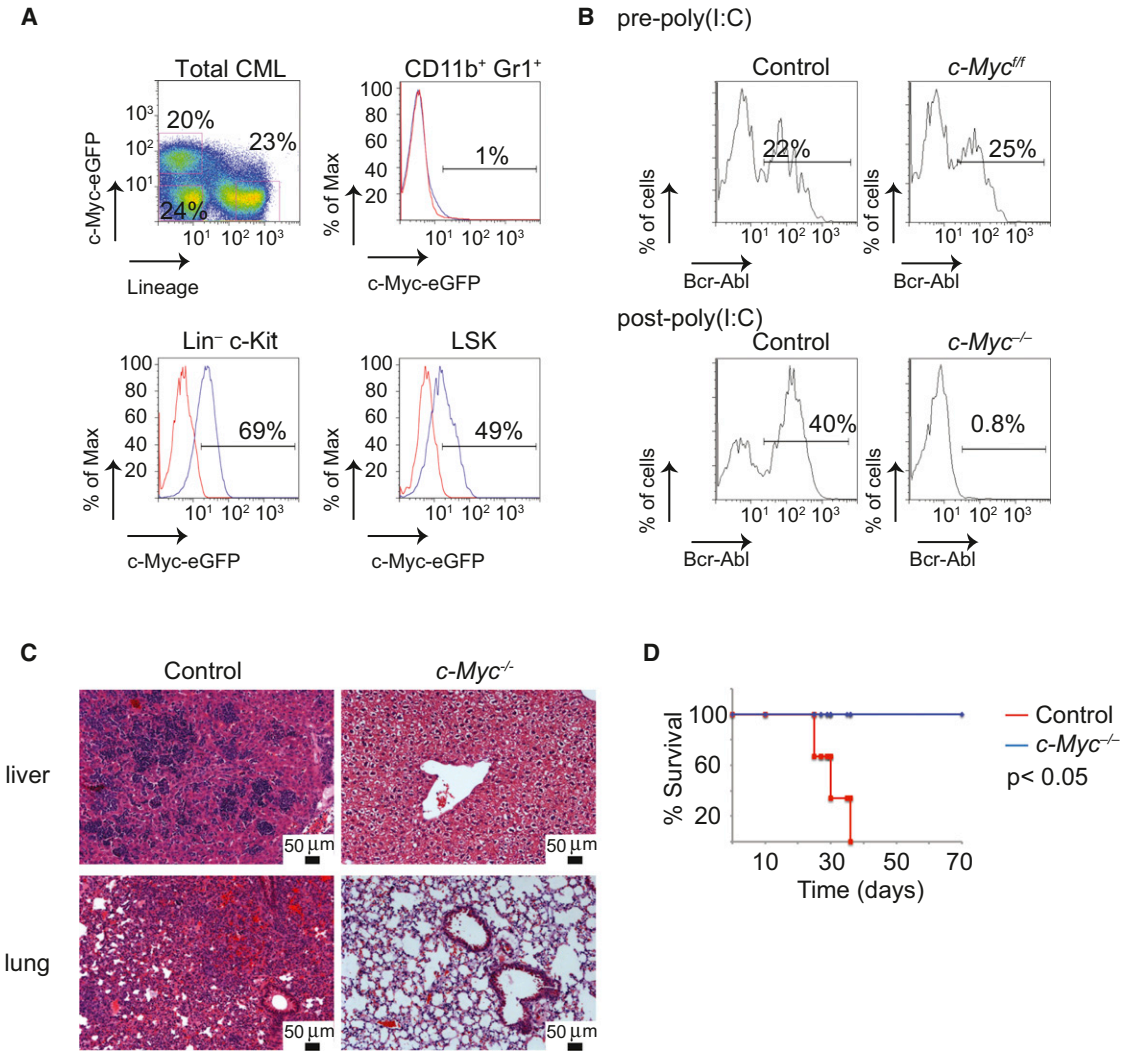

Figure 5. CML-Initiating Cell Activity and Disease Progression Depends on c-Myc Expression and Activity

(A) c-Myc protein expression in Bcr-Abl$^+$ CML tumor subsets.

(B–D) Mice transplanted with LSKs expressing Bcr-Abl from *MxCre*$^+$;*c-Myc*$^{+/+}$ and *MxCre*$^+$;*c-Myc*$^{f/f}$ mice and treated with poly(I:C) following disease initiation. PB analysis of mice (B), H&E staining of liver and lung (C), and Kaplan Meier survival curves of animals transplanted with *MxCre*$^+$;*Myc*$^{+/+}$ (red), *MxCre*$^+$;*Myc*$^{-/-}$ (blue) (n = 5 for each genotype) (D).

See also Figure S4.

by Bcr-Abl$^+$B220$^+$. Both cohorts of mice showed approximately 40% Bcr-Abl$^+$B220$^+$ cells. At that point, deletion of *Fbw7* was initiated by administration of poly(I:C) (Figure 6A) and disease progression was monitored. As expected, mice transplanted with Bcr-Abl$^+$*MxCre*$^+$;*Fbw7*$^{+/+}$ BM had an increase in the percentage of Bcr-Abl$^+$B220$^+$ cells in the PB. However, mice transplanted with Bcr-Abl$^+$ *MxCre*$^+$;*Fbw7*$^{f/f}$ BM showed a significant reduction in Bcr-Abl$^+$B220$^+$ cells (Figure 6A) and these cells were virtually undetectable 3 weeks after the initiation of *Fbw7* deletion (Figure 6B). *MxCre*$^+$;*Fbw7*$^{+/+}$ mice showed signs of B-ALL including infiltration of secondary tissues and splenomegaly, whereas mice transplanted with *MxCre*$^+$;*Fbw7*$^{f/f}$ showed no sign of disease following treatment with poly(I:C) (Figures 6C–6E). Once more, utilizing the *c-Myc*^{eGFP} mouse model, we evaluated c-Myc protein expression in the tumor to determine whether loss of B-ALL was due to stabilization of c-Myc as seen in the CML model. Unlike the CML model, approximately 100% of Bcr-Abl$^+$ cells were B220$^+$ and Bcr-Abl$^+$ LSKs were not observed. Although a significantly greater percentage of the tumor in *Fbw7*$^{-/-}$ expressed *c-Myc*^{eGFP}, no overall increase in expression was observed suggesting that Fbw7 could have additional substrates in B-ALL (Figures 6F and 6G). Analysis of Annexin V and 7-AAD in the Bcr-Abl$^+$ B220$^+$ BM cells showed a significant increase in cell apoptosis and cell death along with induction of apoptosis-associated p53 targets in *MxCre*$^+$;*Fbw7*$^{-/-}$ BM (Figures 6H and 6I). This is an exciting finding because it suggests that Fbw7 could be an attractive therapeutic target in Bcr-Abl$^+$ B-ALL. In agreement with this notion, sequencing of *FBW7* in the cDNA of patients with B-ALL failed to identify any inactivating mutations (0/50

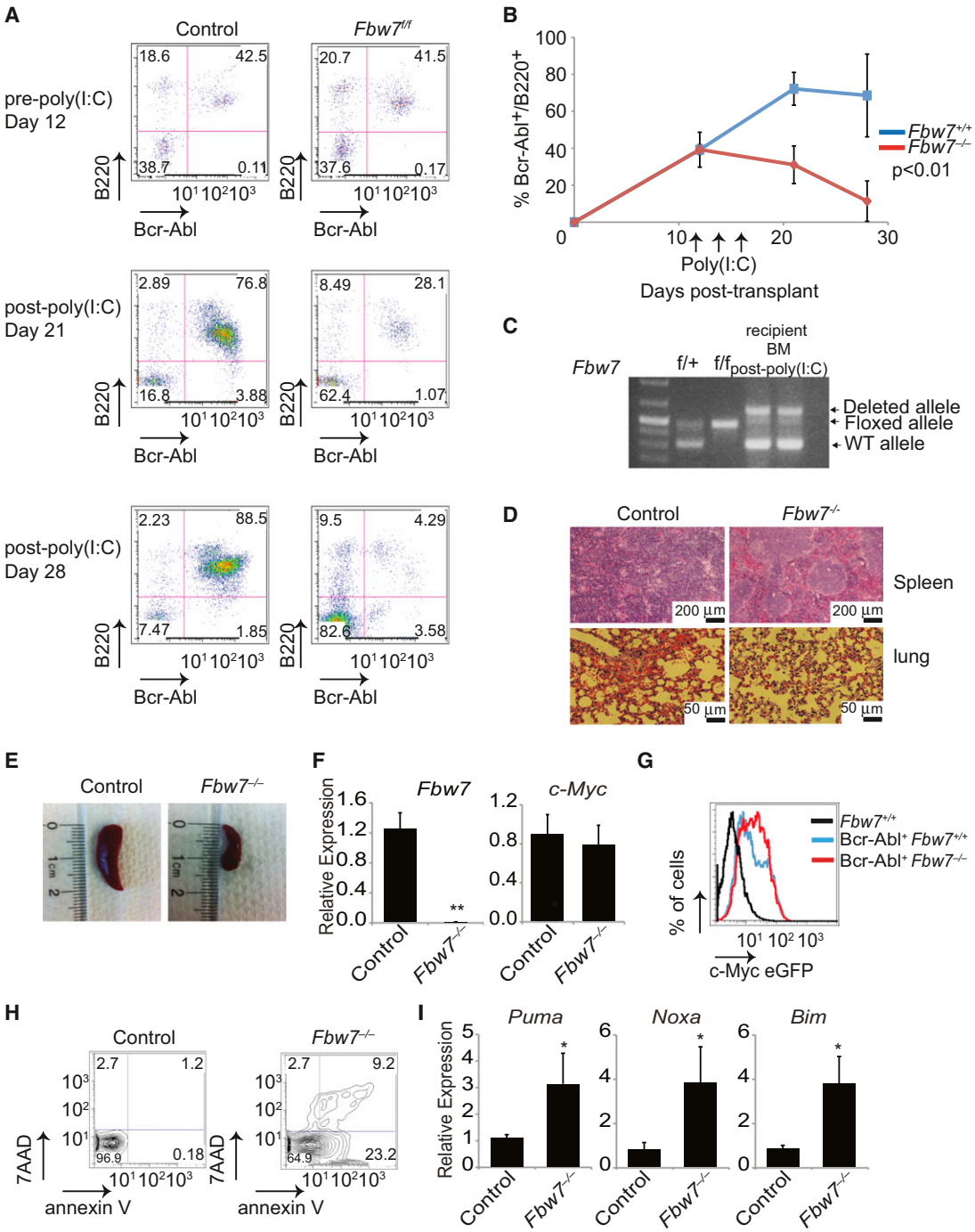

Figure 6. Depletion of Fbw7 Inhibits Progression of B-ALL

(A) FACS analysis of PB from mice transplanted with *MxCre*$^{+}$;*Fbw7*$^{+/+}$ and *MxCre*$^{+}$;*Fbw7*$^{-/-}$ total BM cells expressing Bcr-Abl. Upper panel: 12 days post-transplant but prior to poly(I:C) treatment. Middle and lower panels: d21 and 28 days post-poly(I:C) treatment, respectively.

(B) Graph depicting the percent of Bcr-Abl^{+} B220^{+} cells in the PB of both cohorts.

(C) Genotyping PCR from recipient BM.

(D) H&E staining of spleen and lung.

(E) Representative spleen at day 28.

(F) qRT-PCR analysis of *Fbw7* and *c-Myc* expression in sorted tumor.

(G) c-Myc protein expression in spleen of recipient animals gated on Bcr-Abl^{+} B220^{+}.

(H) FACS plots showing annexin V^{+} and 7-AAD^{+} cells in the Bcr-Abl^{+} B220^{+} cells in the BM.

(I) qRT-PCR analysis showing the expression of p53 target genes, *Puma, Bim,* and *Noxa*, in sorted control or *Fbw7*$^{-/-}$ tumors. Error bars indicate ± SD. *$p < 0.01$, **$p < 0.001$.

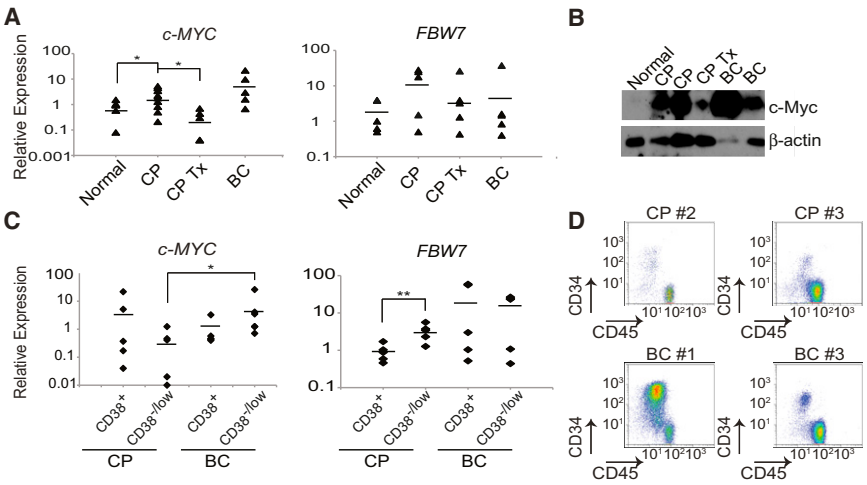

Figure 7. *FBW7* and *c-MYC* Expression Patterns in Human CML

(A and B) *FBW7* and *c-MYC* mRNA levels (A, determined by qRT-PCR, bar indicates average) and c-Myc protein levels (B, determined by western blot) from total PBMNCs in healthy individuals (normal), CML patients in CP without treatment (CP) or being treated with Imatinib (CP Tx), or in BC (BC).

(C) qRT-PCR for *c-MYC* and *FBW7* mRNA levels from $CD34^+CD38^+$ and $CD34^+CD38^{low}$ populations from BM of patients in CP, and BC normalized to normal UCB derived $CD34^+CD38^{low}$. Bar indicates average.

(D) FACS plots showing CD45 and CD34 expression in human CML patients used to sort $CD34^+CD38^+$ and $CD34^+CD38^{low}$ cell populations. *$p < 0.01$, **$p < 0.001$.

samples), suggesting that FBW7 function is required for B-ALL disease progression (data not shown).

Human CML Leukemia-Initiating Cells Require FBW7 Function

Depletion of *Fbw7* in the mouse model eradicates the CML LIC; we next asked whether these findings are relevant to the human disease. Consistent with the findings that Bcr-Abl induces *c-MYC* expression (Xie et al., 2002), we observed that *c-MYC* expression level in PB mononuclear cells (PBMNCs) of patients is higher in patients with newly diagnosed or untreated CP CML than in normal PBMNC. Patients with TKI-treated CML CP displayed almost physiologic levels of *c-MYC* (Figure 7A). c-Myc protein levels followed similar patterns of expression (Figure 7B). On the other hand, no significant differences in the levels of *FBW7* expression were noted (Figure 7A), consistent with the idea that *FBW7* is also controlled at the activity level and not merely transcriptionally.

We further determined the levels of *c-MYC* and *FBW7* expression in stem and progenitor populations in patients with CML by sorting $CD34^+CD38^+$ and $CD34^+CD38^{low}$ populations, respectively, from CP, and patient BC BM samples (Figures 7C and 7D). *c-MYC* mRNA expression was detected in all subsets; however, its highest level was in BC $CD34^+CD38^{low}$ cells. Interestingly, although *FBW7* was also expressed in all samples, CP $CD34^+CD38^{low}$ cells expressed significantly higher levels than $CD34^+CD38^+$ cells from the same samples, in agreement with our animal modeling data that detected the highest Fbw7 expression in the LSK LIC population.

To address whether Fbw7 possesses a similar functional role in human CML, we transduced the Bcr-Abl^+ human CML cell line KU812with lentiviruses expressing shRNAs against Fbw7. Efficient knockdown was confirmed by qRT-PCR (Figure S5A). Loss of Fbw7 induced apoptosis and lead to the accumulation of c-Myc (Figures S5B and S5C). Degradation of c-Myc requires a priming phosphorylation event on T58 by GSK3β (Gregory et al., 2003), and in agreement with this, Fbw7 silencing lead to the specific enrichment of phosphorylated c-Myc (Figure S5C). To further study potential Fbw7 functions in human cells, we first silenced Fbw7 using lentiviruses expressing shRNAs against Fbw7 in normal umbilical cord blood (UCB)-derived $CD34^+$ with or without co-infection with Bcr-Abl retrovirus and subsequently plated the cells in colony-forming assays. Fbw7 silencing showed no alterations in the colony-forming ability of normal $CD34^+$ cells, but significantly decreased plating capacity of Bcr-Abl^+ $CD34^+$ cells (Figures 8A and 8B). Fbw7 silencing led to accumulation of both c-Myc and phospo-c-Myc protein in total progeny derived from Bcr-Abl^+-infected $CD34^+$ cells (Figure 8C). Overexpression of c-Myc protein was further verified in the Bcr-Abl^+ $CD34^+$ population compared to normal $CD34^+$ population by intracellular FACS for c-Myc expression. Consistent with the finding in the mouse model, Bcr-Abl expression results in increased c-Myc expression, which is further increased by silencing of Fbw7 (Figure 8D). Finally, FBW7 silencing in purified primary human CP (from either newly diagnosed or untreated patients) CML CD34+ cells led to a significant loss of plating ability in CFU assays (Figures 8E, S5D, and S5E), most likely due to the elevated levels of c-Myc, and significant induction of cell death (Figures 8F, 8G, and S5F). These combined human data are in agreement with our animal experiments.

DISCUSSION

We demonstrate here the essential function of the Fbw7 E3 ligase for the initiation and the progression of CML. *Fbw7* deletion leads to LIC apoptosis due to aberrantly high levels of c-Myc protein expression and activation of the p53 pathway. Interestingly, p53 mutations can accompany disease progression in human CML and p53 loss in some cases impedes the antileukemic response to Bcr-Abl inhibition (Kelman et al., 1989; Wendel et al., 2006), suggesting that loss of p53 in some tumors could constitute an adaptive response to the increase in the levels of c-Myc during CML progression. Overall, our experiments suggest that Fbw7 expression is absolutely essential for the maintenance of nontoxic levels of c-Myc protein within CML LIC cells. Interestingly, although Fbw7 is a ubiquitin ligase capable of targeting a large number of substrates, our results suggest that c-Myc is its key substrate in CML, in contrast with human T-ALL, where Notch1 appears to be a main targets (O'Neil et al., 2007; Thompson et al., 2008). However, we cannot

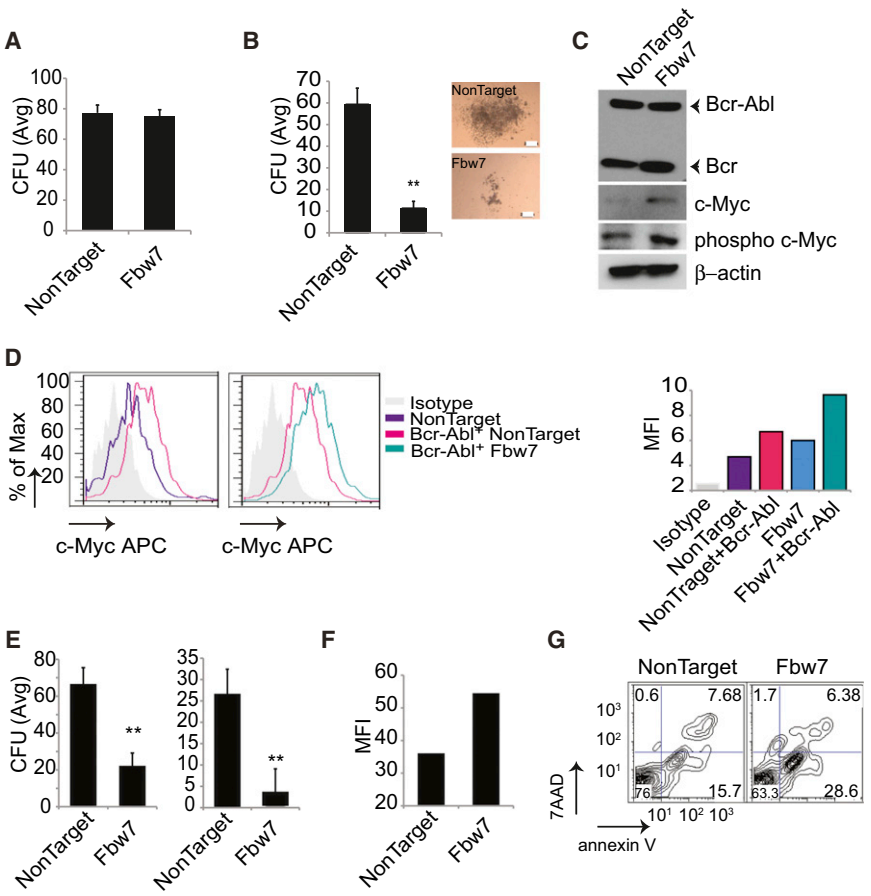

Figure 8. Fbw7 Silencing in Human CML-Initiating Cells Leads to Induction of Apoptosis and Loss of Differentiation Potential

(A) Average CFU from normal UCB derived CD34$^+$ cells expressing shRNA against either NonTarget or Fbw7.

(B–D) Normal UCB-derived CD34$^+$-expressing Bcr-Abl together with shRNAs against either NonTarget or Fbw7. Progeny of cells were plated in CFU assay (B; scale bar, 200 μm) and western blot for c-Myc, Phospho-c-Myc, and Bcr-Abl in total progeny of CD34$^+$ cells (C). c-Myc expression determined by intracellular FACS gated on CD34$^+$ population (D). Graph on right shows MFI for c-Myc protein.

(E–G) CP patient BM derived CD34$^+$ cells were transduced with lentivirus expressing either control or shRNAs against Fbw7, puromycin selected for 48 hr. Average CFU assay from CD34+ progeny in two different patients (E). MFI for c-Myc protein for representative CML patient derived CD34$^+$ cells following Fbw7 silencing (F). Representative annexin V staining of patient derived CD34$^+$ cells following lentiviral transduction (G). Error bars indicate ± SD. *p < 0.01, **p < 0.001.

See also Figure S5.

exclude that additional Fbw7 substrates, except for Notch1, play roles in its function. Further studies are required to address the identity and function of such substrates.

We were able to visualize, using flow cytometry, c-Myc protein abundance in vivo, and show that c-Myc expression is restricted within the LIC population, with the bulk of the tumor being c-Myc$^-$. These results prove that Fbw7 function is specifically required by cells with leukemia-initiating activity but is dispensable for the maintenance of the more differentiated CML subset. Moreover, genetic deletion of c-Myc during disease progression showed that Bcr-Abl-driven CML is addicted to physiologic c-Myc function, suggesting that the disease requires well-defined and Fbw7-regulated thresholds of c-Myc abundance and activity. This is an intriguing idea with potential important clinical ramifications in the field of cancer biology, as it would suggest that both depletion and overabundance of c-Myc protein levels in tumors could lead to similar clinical outcomes, albeit with distinct mechanisms of action. Recent development of small molecules targeting c-Myc co-activator bromodomain inhibitors (Delmore et al., 2011) opens the way for therapeutic protocols that include c-Myc activity inhibition in established CML.

Classic experiments have shown that introduction of v-abl in a myeloid cell line can specifically induce c-Myc expression in a tyrosine kinase-dependent manner (Cleveland et al., 1989). Subsequent seminal studies by Sawyers and colleagues demonstrated that Bcr-Abl-induced transformation could be suppressed by dominant negative Myc mutants in vitro (Sawyers et al., 1992). In agreement with these studies, we visualized c-Myc protein levels in vivo in progressing CML and identify the populations that retain c-Myc protein expression. Interestingly, only a minority of the established leukemia cells express c-Myc^{eGFP}. These cells are characterized by the expression of c-Kit and include the CML LSK population, previously suggested to possess all LIC activity (Neering et al., 2007; Reynaud et al., 2011). When we subdivided the c-Myc-expressing population using the c-Myc^{eGFP} reporter, we were able to transplant disease only using the c-Myc^{eGFP} LSK fraction suggesting that although LIC activity lies within the c-Myc-expressing fraction, c-Myc protein expression is not sufficient to guarantee leukemia-initiating properties. This is an intriguing distinction between normal and leukemic hematopoiesis as we showed that normal c-Myc^{eGFP} LSK cells are multipotential progenitors but not bona fide HSC (Reavie et al., 2010).

We have shown that Fbw7 is required for normal hematopoiesis, because its deletion leads to progressive adult stem cell exhaustion. This would suggest that inhibition of Fbw7 activity is not an ideal therapeutic target in leukemia. However, the response of normal and malignant stem and progenitor cells to the deletion of *Fbw7* is vastly distinct. Putative LIC respond acutely, as *Fbw7* deletion leads to rapid (<2 weeks) loss of cell numbers and activity, whereas the response of normal HSC is delayed and there are no significant changes in the number of HSC cells until 10–12 weeks post *Fbw7* deletion (Matsuoka et al., 2008; Thompson et al., 2008) (data not shown). We believe that this differential response to *Fbw7* deletion can be explained

by the significantly higher levels of c-Myc protein in the Bcr-Abl-expressing LIC. These data suggest that it should be possible to define a therapeutic window altering either the concentration of the inhibitor or the length of the treatment. Drug combination could be another therapeutic avenue, especially as TKI fail to target CML LIC. Indeed, Nakayama and colleagues have demonstrated that Fbw7 inhibition can be used in combination with other established CML treatments, including imatinib, to achieve efficient targeting of CML-initiating cells (Takeishi et al., 2013), both in animal models and primary human disease. At this point, no Fbw7 inhibitors have been identified. However, recent studies suggested that a small molecule targeting Fbw7 is a feasible approach. Tyers and collegues have recently identified a biplanar dicarboxylic acid compound as an inhibitor of substrate recognition by the yeast Fbw7 ortholog (Cdc4) (Aghajan et al., 2010; Orlicky et al., 2010). Moreover, as Fbw7-mediated c-Myc recognition is induced by the priming phosphorylation of c-Myc^{Thr58} by GSK3, GSK3 inhibitors could also be used to target Fbw7 function and c-Myc stability. Such inhibitors have been developed and their efficacy in vivo was tested using MLL-induced models of AML (Wang et al., 2008). These GSK3 inhibitors are currently in Phase II clinical trials for the treatment of Alzheimer disease (Martinez et al., 2011), opening the way for their future use for the treatment of CML in combination with TKIs. Finally, because c-Myc activity is a driver of distinct tumor types, it is conceivable that Fbw7 inhibitors could be promising therapeutic tools in a wide range of blood and solid tumors.

EXPERIMENTAL PROCEDURES

Animals

Fbw7^{flox} mice were previously published (Thompson et al., 2008). *Myc^{flox}* mice were a kind gift from F. Alt (de Alboran et al., 2001), and *Myc^{eGFP}* mice were a kind gift from Dr. Barry Sleckman (Huang et al., 2008). Interferon-α-inducible *Mx1cre*, *p53* germline knockout, and C57Bl6 recipient mice were purchased from Jackson Laboratories. All mice were housed in a pathogen-free animal facility at the NYU School of Medicine. All animal procedures were approved by Institutional Animal Care and Use Committee of the NYU School of Medicine and carried out in compliance with NIH guidelines.

Generation and Analysis of CML Animals

LSK were isolated from 4- to 6-week-old mice using the mouse hematopoietic progenitor enrichment kit (Stem Cell Technologies) per manufacturer's protocol and stained with a lineage cocktail, c-Kit, and Sca-1 antibodies followed by FACS purification. LSK were cells were infected with Bcr-Abl-NGFR or Bcr-Abl-GFP retrovirus (Wertheim et al., 2002) and spun at 2500 rpm for 90 min at 30°C. Forty-eight to 72 hr posttransfection, ~20,000–40,000 Lin$^-$ Bcr-Abl$^+$ LSKs were transplanted intravenously into lethally irradiated recipient mice with 2–5 × 10^5 support BM cells. For donor cells deleted posttransplantation, deletion was initiated on day 7 posttransplantation with three injections of poly(I:C) (Amersham) at a concentration of 5 μg/g of body weight, and disease was monitored by flow cytometry. Further details of culture and analysis are provided in the Supplemental Experimental Procedures.

Analysis and Culture of Human CML Samples

Primary patient samples were obtained with informed consent from all donors in accordance with the Declaration of Helsinki and studies were approved by the Institutional Review Boards at NYU Medical Center, and Memorial Sloan-Kettering Cancer Center. UCB or patient BM CD34$^+$ cells were isolated using CD34$^+$ selection kit following manufacturer's instructions (Stem Cell Technologies). Cells were cultured in Stemspan (Stem Cell Technologies), supplemented with 50 ng/ml SCF, 50 ng/ml Flt3L, and 100 ng/ml Tpo for 24 hr followed by lentiviral transduction. Further details of culture and analysis are provided in the Supplemental Experimental Procedures.

FACS Analysis

All antibodies used for FACS analysis were procured from e-Bioscience. Specifically, the antibodies we used were as follows: c-Kit (2B8), Sca-1 (D7), Mac-1 (M1/70), Gr-1 (RB6-8C5), NK1.1 (PK136), TER-119, CD3 (145-2C11), CD19 (1D3), IL7R (RAM34), CD4 (RM4-5), CD8 (53-6.7), CD271 (NGFR), and (ME20.4). BM lineage antibody cocktail includes the following: Mac-1, Gr-1, NK1.1, TER-119, CD4, CD8, IL7R, and CD19. Apoptosis was detected using an Annexiv-V PE-conjugated detection kit (BD PharMingen) along with 7-AAD following manufacturer's protocol. For intracellular c-Myc staining, cells were stained with anti-CD34 (BD PharMingen), washed, fixed, and permeabilized using BD cytofix/cytoperm kit following manufacturer's protocol. Stainings were performed with rabbit anti-c-Myc (Cell Signaling) followed by goat anti-rabbit Alexa Fluor 647 (Invitrogen).

Quantitative Real-Time PCR

Total RNA was harvested from cells using the QIAGEN RNeasy Kit (QIAGEN, Germany). RNA was quantified by absorbance at A260 nm and 2 μg of total RNA used for cDNA synthesis using Superscript III first strand synthesis kit (Invitrogen). qRT-PCR was carried out using SYBR green universal mix PCR reaction buffer (Roche) using an Roche lightcycler 480 II (Roche). All signals are normalized to levels of *Gapdh*.

Statistical Analysis

All statistical analyses were performed using an unpaired two-tailed Student's t test, unless otherwise specified.

SUPPLEMENTAL INFORMATION

Supplemental Information includes five figures and Supplemental Experimental Procedures and can be found with this article online at http://dx.doi.org/10.1016/j.ccr.2013.01.025.

ACKNOWLEDGMENTS

We would like to thank Dr. B. Sleckman for providing the c-Myc^{eGFP} knockin mice, J. Silva for the anti-p53 shRNA vector, and W. Pear for the Bcr-Abl vectors. We would also like to thank the members of the Aifantis lab for valuable advice and discussions and the NYU Flow Cytometry facility for expert cell sorting. I.A. is supported by the National Institutes of Health (RO1CA133379, RO1CA105129, 1RO1CA173636, RO1CA149655, and RO1GM088847), the Leukemia and Lymphoma Society (TRP program grants), the Chemotherapy Foundation, the William Lawrence Blanche Hughes Foundation, and the V Foundation for Cancer Research. L.R. is supported by an NIH Ruth L. Kirchstein Award. S.M.B. is supported by the NYU Hematology/Oncology NIH training grant (5T32HL007151-33) and the NIH institutional training grant (1T32CA160002-01). B.A-O. is supported by the Alexander von Humboldt Foundation. I.A. is a Howard Hughes Medical Institute Early Career Scientist. We would like to dedicate this paper to our mice lost in the fury of hurricane Sandy.

Received: August 12, 2011
Revised: April 25, 2012
Accepted: January 29, 2013
Published: March 18, 2013

REFERENCES

Aghajan, M., Jonai, N., Flick, K., Fu, F., Luo, M., Cai, X., Ouni, I., Pierce, N., Tang, X., Lomenick, B., et al. (2010). Chemical genetics screen for enhancers of rapamycin identifies a specific inhibitor of an SCF family E3 ubiquitin ligase. Nat. Biotechnol. *28*, 738–742.

Bartram, C.R., de Klein, A., Hagemeijer, A., van Agthoven, T., Geurts van Kessel, A., Bootsma, D., Grosveld, G., Ferguson-Smith, M.A., Davies, T., Stone, M., et al. (1983). Translocation of c-ab1 oncogene correlates with the

presence of a Philadelphia chromosome in chronic myelocytic leukaemia. Nature *306*, 277–280.

Bhatia, R., Holtz, M., Niu, N., Gray, R., Snyder, D.S., Sawyers, C.L., Arber, D.A., Slovak, M.L., and Forman, S.J. (2003). Persistence of malignant hematopoietic progenitors in chronic myelogenous leukemia patients in complete cytogenetic remission following imatinib mesylate treatment. Blood *101*, 4701–4707.

Bonnet, D., and Dick, J.E. (1997). Human acute myeloid leukemia is organized as a hierarchy that originates from a primitive hematopoietic cell. Nat. Med. *3*, 730–737.

Bric, A., Miething, C., Bialucha, C.U., Scuoppo, C., Zender, L., Krasnitz, A., Xuan, Z., Zuber, J., Wigler, M., Hicks, J., et al. (2009). Functional identification of tumor-suppressor genes through an in vivo RNA interference screen in a mouse lymphoma model. Cancer Cell *16*, 324–335.

Cleveland, J.L., Dean, M., Rosenberg, N., Wang, J.Y., and Rapp, U.R. (1989). Tyrosine kinase oncogenes abrogate interleukin-3 dependence of murine myeloid cells through signaling pathways involving c-myc: conditional regulation of c-myc transcription by temperature-sensitive v-abl. Mol. Cell. Biol. *9*, 5685–5695.

Corbin, A.S., Agarwal, A., Loriaux, M., Cortes, J., Deininger, M.W., and Druker, B.J. (2011). Human chronic myeloid leukemia stem cells are insensitive to imatinib despite inhibition of BCR-ABL activity. J. Clin. Invest. *121*, 396–409.

Daley, G.Q., Van Etten, R.A., and Baltimore, D. (1990). Induction of chronic myelogenous leukemia in mice by the P210bcr/abl gene of the Philadelphia chromosome. Science *247*, 824–830.

de Alboran, I.M., O'Hagan, R.C., Gärtner, F., Malynn, B., Davidson, L., Rickert, R., Rajewsky, K., DePinho, R.A., and Alt, F.W. (2001). Analysis of C-MYC function in normal cells via conditional gene-targeted mutation. Immunity *14*, 45–55.

de Lavallade, H., Apperley, J.F., Khorashad, J.S., Milojkovic, D., Reid, A.G., Bua, M., Szydlo, R., Olavarria, E., Kaeda, J., Goldman, J.M., and Marin, D. (2008). Imatinib for newly diagnosed patients with chronic myeloid leukemia: incidence of sustained responses in an intention-to-treat analysis. J. Clin. Oncol. *26*, 3358–3363.

Delmore, J.E., Issa, G.C., Lemieux, M.E., Rahl, P.B., Shi, J., Jacobs, H.M., Kastritis, E., Gilpatrick, T., Paranal, R.M., Qi, J., et al. (2011). BET bromodomain inhibition as a therapeutic strategy to target c-Myc. Cell *146*, 904–917.

Druker, B.J., Guilhot, F., O'Brien, S.G., Gathmann, I., Kantarjian, H., Gattermann, N., Deininger, M.W., Silver, R.T., Goldman, J.M., Stone, R.M., et al.; IRIS Investigators. (2006). Five-year follow-up of patients receiving imatinib for chronic myeloid leukemia. N. Engl. J. Med. *355*, 2408–2417.

Gorre, M.E., Mohammed, M., Ellwood, K., Hsu, N., Paquette, R., Rao, P.N., and Sawyers, C.L. (2001). Clinical resistance to STI-571 cancer therapy caused by BCR-ABL gene mutation or amplification. Science *293*, 876–880.

Gregory, M.A., Qi, Y., and Hann, S.R. (2003). Phosphorylation by glycogen synthase kinase-3 controls c-myc proteolysis and subnuclear localization. J. Biol. Chem. *278*, 51606–51612.

Gupta-Rossi, N., Le Bail, O., Gonen, H., Brou, C., Logeat, F., Six, E., Ciechanover, A., and Israël, A. (2001). Functional interaction between SEL-10, an F-box protein, and the nuclear form of activated Notch1 receptor. J. Biol. Chem. *276*, 34371–34378.

Heidel, F.H., Bullinger, L., Feng, Z., Wang, Z., Neff, T.A., Stein, L., Kalaitzidis, D., Lane, S.W., and Armstrong, S.A. (2012). Genetic and pharmacologic inhibition of β-catenin targets imatinib-resistant leukemia stem cells in CML. Cell Stem Cell *10*, 412–424.

Heisterkamp, N., Jenster, G., ten Hoeve, J., Zovich, D., Pattengale, P.K., and Groffen, J. (1990). Acute leukaemia in bcr/abl transgenic mice. Nature *344*, 251–253.

Hochhaus, A., O'Brien, S.G., Guilhot, F., Druker, B.J., Branford, S., Foroni, L., Goldman, J.M., Müller, M.C., Radich, J.P., Rudoltz, M., et al.; IRIS Investigators. (2009). Six-year follow-up of patients receiving imatinib for the first-line treatment of chronic myeloid leukemia. Leukemia *23*, 1054–1061.

Huang, C.Y., Bredemeyer, A.L., Walker, L.M., Bassing, C.H., and Sleckman, B.P. (2008). Dynamic regulation of c-Myc proto-oncogene expression during lymphocyte development revealed by a GFP-c-Myc knock-in mouse. Eur. J. Immunol. *38*, 342–349.

Huntly, B.J., and Gilliland, D.G. (2005). Leukaemia stem cells and the evolution of cancer-stem-cell research. Nat. Rev. Cancer *5*, 311–321.

Ito, T., Kwon, H.Y., Zimdahl, B., Congdon, K.L., Blum, J., Lento, W.E., Zhao, C., Lagoo, A., Gerrard, G., Foroni, L., et al. (2010). Regulation of myeloid leukaemia by the cell-fate determinant Musashi. Nature *466*, 765–768.

Jamieson, C.H., Ailles, L.E., Dylla, S.J., Muijtjens, M., Jones, C., Zehnder, J.L., Gotlib, J., Li, K., Manz, M.G., Keating, A., et al. (2004). Granulocyte-macrophage progenitors as candidate leukemic stem cells in blast-crisis CML. N. Engl. J. Med. *351*, 657–667.

Jankowska, A.M., Szpurka, H., Tiu, R.V., Makishima, H., Afable, M., Huh, J., O'Keefe, C.L., Ganetzky, R., McDevitt, M.A., and Maciejewski, J.P. (2009). Loss of heterozygosity 4q24 and TET2 mutations associated with myelodysplastic/myeloproliferative neoplasms. Blood *113*, 6403–6410.

Kelman, Z., Prokocimer, M., Peller, S., Kahn, Y., Rechavi, G., Manor, Y., Cohen, A., and Rotter, V. (1989). Rearrangements in the p53 gene in Philadelphia chromosome positive chronic myelogenous leukemia. Blood *74*, 2318–2324.

Koepp, D.M., Schaefer, L.K., Ye, X., Keyomarsi, K., Chu, C., Harper, J.W., and Elledge, S.J. (2001). Phosphorylation-dependent ubiquitination of cyclin E by the SCFFbw7 ubiquitin ligase. Science *294*, 173–177.

Lapidot, T., Sirard, C., Vormoor, J., Murdoch, B., Hoang, T., Caceres-Cortes, J., Minden, M., Paterson, B., Caligiuri, M.A., and Dick, J.E. (1994). A cell initiating human acute myeloid leukaemia after transplantation into SCID mice. Nature *367*, 645–648.

le Coutre, P., Tassi, E., Varella-Garcia, M., Barni, R., Mologni, L., Cabrita, G., Marchesi, E., Supino, R., and Gambacorti-Passerini, C. (2000). Induction of resistance to the Abelson inhibitor STI571 in human leukemic cells through gene amplification. Blood *95*, 1758–1766.

Martinez, A., Gil, C., and Perez, D.I. (2011). Glycogen synthase kinase 3 inhibitors in the next horizon for Alzheimer's disease treatment. Int. J. Alzheimers Dis. *2011*, 280502.

Matsuoka, S., Oike, Y., Onoyama, I., Iwama, A., Arai, F., Takubo, K., Mashimo, Y., Oguro, H., Nitta, E., Ito, K., et al. (2008). Fbxw7 acts as a critical fail-safe against premature loss of hematopoietic stem cells and development of T-ALL. Genes Dev. *22*, 986–991.

Michor, F., Hughes, T.P., Iwasa, Y., Branford, S., Shah, N.P., Sawyers, C.L., and Nowak, M.A. (2005). Dynamics of chronic myeloid leukaemia. Nature *435*, 1267–1270.

Nakamura, S., Yokota, D., Tan, L., Nagata, Y., Takemura, T., Hirano, I., Shigeno, K., Shibata, K., Fujisawa, S., and Ohnishi, K. (2012). Down-regulation of Thanatos-associated protein 11 by BCR-ABL promotes CML cell proliferation through c-Myc expression. Int. J. Cancer. *130*, 1046–1059.

Neering, S.J., Bushnell, T., Sozer, S., Ashton, J., Rossi, R.M., Wang, P.Y., Bell, D.R., Heinrich, D., Bottaro, A., and Jordan, C.T. (2007). Leukemia stem cells in a genetically defined murine model of blast-crisis CML. Blood *110*, 2578–2585.

Nowell, P.C., and Hungerford, D.A. (1960). Chromosome studies on normal and leukemic human leukocytes. J. Natl. Cancer Inst. *25*, 85–109.

O'Hare, T., Corbin, A.S., and Druker, B.J. (2006). Targeted CML therapy: controlling drug resistance, seeking cure. Curr. Opin. Genet. Dev. *16*, 92–99.

O'Neil, J., Grim, J., Strack, P., Rao, S., Tibbitts, D., Winter, C., Hardwick, J., Welcker, M., Meijerink, J.P., Pieters, R., et al. (2007). FBW7 mutations in leukemic cells mediate NOTCH pathway activation and resistance to gamma-secretase inhibitors. J. Exp. Med. *204*, 1813–1824.

Orlicky, S., Tang, X., Neduva, V., Elowe, N., Brown, E.D., Sicheri, F., and Tyers, M. (2010). An allosteric inhibitor of substrate recognition by the SCF(Cdc4) ubiquitin ligase. Nat. Biotechnol. *28*, 733–737.

Pear, W.S., Miller, J.P., Xu, L., Pui, J.C., Soffer, B., Quackenbush, R.C., Pendergast, A.M., Bronson, R., Aster, J.C., Scott, M.L., and Baltimore, D. (1998). Efficient and rapid induction of a chronic myelogenous leukemia-like myeloproliferative disease in mice receiving P210 bcr/abl-transduced bone marrow. Blood *92*, 3780–3792.

Reavie, L., Della Gatta, G., Crusio, K., Aranda-Orgilles, B., Buckley, S.M., Thompson, B., Lee, E., Gao, J., Bredemeyer, A.L., Helmink, B.A., et al. (2010). Regulation of hematopoietic stem cell differentiation by a single ubiquitin ligase-substrate complex. Nat. Immunol. *11*, 207–215.

Reynaud, D., Pietras, E., Barry-Holson, K., Mir, A., Binnewies, M., Jeanne, M., Sala-Torra, O., Radich, J.P., and Passegué, E. (2011). IL-6 controls leukemic multipotent progenitor cell fate and contributes to chronic myelogenous leukemia development. Cancer Cell *20*, 661–673.

Rowley, J.D. (1973). Letter: A new consistent chromosomal abnormality in chronic myelogenous leukaemia identified by quinacrine fluorescence and Giemsa staining. Nature *243*, 290–293.

Sawyers, C.L., Callahan, W., and Witte, O.N. (1992). Dominant negative MYC blocks transformation by ABL oncogenes. Cell *70*, 901–910.

Shah, N.P., Nicoll, J.M., Nagar, B., Gorre, M.E., Paquette, R.L., Kuriyan, J., and Sawyers, C.L. (2002). Multiple BCR-ABL kinase domain mutations confer polyclonal resistance to the tyrosine kinase inhibitor imatinib (STI571) in chronic phase and blast crisis chronic myeloid leukemia. Cancer Cell *2*, 117–125.

Sirard, C., Lapidot, T., Vormoor, J., Cashman, J.D., Doedens, M., Murdoch, B., Jamal, N., Messner, H., Addey, L., Minden, M., et al. (1996). Normal and leukemic SCID-repopulating cells (SRC) coexist in the bone marrow and peripheral blood from CML patients in chronic phase, whereas leukemic SRC are detected in blast crisis. Blood *87*, 1539–1548.

Stadtfeld, M., and Graf, T. (2005). Assessing the role of hematopoietic plasticity for endothelial and hepatocyte development by non-invasive lineage tracing. Development *132*, 203–213.

Takeishi, S., Matsumoto, A., Onoyama, I., Naka, K., Hirao, A., and Nakayama, K.I. (2013). Ablation of Fbw7 eliminates leukemia-intiating cells by preventing quiescence. Cancer Cell *23*, this issue, 347–361.

Thompson, B.J., Buonamici, S., Sulis, M.L., Palomero, T., Vilimas, T., Basso, G., Ferrando, A., and Aifantis, I. (2007). The SCFFBW7 ubiquitin ligase complex as a tumor suppressor in T cell leukemia. J. Exp. Med. *204*, 1825–1835.

Thompson, B.J., Jankovic, V., Gao, J., Buonamici, S., Vest, A., Lee, J.M., Zavadil, J., Nimer, S.D., and Aifantis, I. (2008). Control of hematopoietic stem cell quiescence by the E3 ubiquitin ligase Fbw7. J. Exp. Med. *205*, 1395–1408.

Wang, J.C., Lapidot, T., Cashman, J.D., Doedens, M., Addy, L., Sutherland, D.R., Nayar, R., Laraya, P., Minden, M., Keating, A., et al. (1998). High level engraftment of NOD/SCID mice by primitive normal and leukemic hematopoietic cells from patients with chronic myeloid leukemia in chronic phase. Blood *91*, 2406–2414.

Wang, Z., Smith, K.S., Murphy, M., Piloto, O., Somervaille, T.C., and Cleary, M.L. (2008). Glycogen synthase kinase 3 in MLL leukaemia maintenance and targeted therapy. Nature *455*, 1205–1209.

Welcker, M., Orian, A., Jin, J., Grim, J.E., Harper, J.W., Eisenman, R.N., and Clurman, B.E. (2004). The Fbw7 tumor suppressor regulates glycogen synthase kinase 3 phosphorylation-dependent c-Myc protein degradation. Proc. Natl. Acad. Sci. USA *101*, 9085–9090.

Wendel, H.G., de Stanchina, E., Cepero, E., Ray, S., Emig, M., Fridman, J.S., Veach, D.R., Bornmann, W.G., Clarkson, B., McCombie, W.R., et al. (2006). Loss of p53 impedes the antileukemic response to BCR-ABL inhibition. Proc. Natl. Acad. Sci. USA *103*, 7444–7449.

Wertheim, J.A., Forsythe, K., Druker, B.J., Hammer, D., Boettiger, D., and Pear, W.S. (2002). BCR-ABL-induced adhesion defects are tyrosine kinase-independent. Blood *99*, 4122–4130.

Xie, S., Lin, H., Sun, T., and Arlinghaus, R.B. (2002). Jak2 is involved in c-Myc induction by Bcr-Abl. Oncogene *21*, 7137–7146.

Yada, M., Hatakeyama, S., Kamura, T., Nishiyama, M., Tsunematsu, R., Imaki, H., Ishida, N., Okumura, F., Nakayama, K., and Nakayama, K.I. (2004). Phosphorylation-dependent degradation of c-Myc is mediated by the F-box protein Fbw7. EMBO J. *23*, 2116–2125.

Zhao, C., Blum, J., Chen, A., Kwon, H.Y., Jung, S.H., Cook, J.M., Lagoo, A., and Reya, T. (2007). Loss of beta-catenin impairs the renewal of normal and CML stem cells in vivo. Cancer Cell *12*, 528–541.

Zhao, C., Chen, A., Jamieson, C.H., Fereshteh, M., Abrahamsson, A., Blum, J., Kwon, H.Y., Kim, J., Chute, J.P., Rizzieri, D., et al. (2009). Hedgehog signalling is essential for maintenance of cancer stem cells in myeloid leukaemia. Nature *458*, 776–779.

Cancer Cell
Article

The Histone Demethylase PHF8 Governs Retinoic Acid Response in Acute Promyelocytic Leukemia

Maria Francisca Arteaga,[1] Jan-Henrik Mikesch,[1] Jihui Qiu,[2] Jesper Christensen,[3,4] Kristian Helin,[3,4,5] Scott C. Kogan,[6] Shuo Dong,[2] and Chi Wai Eric So[1,*]
[1]Leukaemia and Stem Cell Biology Group, Department of Haematological Medicine, King's College London, Denmark Hill, London SE5 9NU, UK
[2]Department of Medicine, Baylor College of Medicine, Houston, TX 77030, USA
[3]Biotech Research and Innovation Centre (BRIC)
[4]Centre for Epigenetics
[5]The Danish Stem Cell Center (Danstem)
University of Copenhagen, 2200 Copenhagen, Denmark
[6]Helen Diller Family Comprehensive Cancer Center and Department of Laboratory Medicine, University of California, San Francisco, San Francisco, CA 94143, USA
*Correspondence: eric.so@kcl.ac.uk
http://dx.doi.org/10.1016/j.ccr.2013.02.014

SUMMARY

While all-*trans* retinoic acid (ATRA) treatment in acute promyelocytic leukemia (APL) has been the paradigm of targeted therapy for oncogenic transcription factors, the underlying mechanisms remain largely unknown, and a significant number of patients still relapse and become ATRA resistant. We identified the histone demethylase PHF8 as a coactivator that is specifically recruited by RARα fusions to activate expression of their downstream targets upon ATRA treatment. Forced expression of PHF8 resensitizes ATRA-resistant APL cells, whereas its downregulation confers resistance. ATRA sensitivity depends on the enzymatic activity and phosphorylation status of PHF8, which can be pharmacologically manipulated to resurrect ATRA sensitivity to resistant cells. These findings provide important molecular insights into ATRA response and a promising avenue for overcoming ATRA resistance.

INTRODUCTION

Transcriptional deregulation plays a key role in a large array of human malignancies, in particular, in acute leukemia, which is mostly initiated by chimeric transcription factors (CTFs) that induce oncogenic transcriptional programs resulting in cellular transformation (Cheung and So, 2011). The successful application of all-*trans* retinoic acid (ATRA) treatment to acute promyelocytic leukemia (APL) induced by RARα fusion proteins represents a major breakthrough and is the paradigm for targeted therapy of oncogenic transcription factors (Wang and Chen, 2008). In spite of its success in achieving a complete remission (CR), APL patients receiving ATRA treatment alone do not achieve definite cure of the disease. Although refined APL treatment regimens in combination with anthracycline-based chemotherapy or arsenic trioxide (ATO) result in 90% of initial CR, a significant proportion of patients still relapse and are resistant to the treatment with 3 years overall survival in second remission of only around 50% (Sanz and Lo-Coco, 2011). Also, while the success of ATRA treatment in APL sets the stage for targeted therapy of oncogenic transcription factors, retinoic acid (RA) treatment is ineffective to other malignant diseases. Therefore, understanding the molecular mechanisms of APL pathogenesis and ATRA response are of major interest, because

Significance

Identification of the molecular functions of oncogenic transcription factors and their associated epigenetic-modifying enzymes in drug response has been an important goal for development of targeted therapy. In this study, we discover the histone demethylase PHF8 as a critical molecular sensor for mediating retinoic acid (RA) treatment response in RARα-fusion-induced leukemia. RA sensitivity is governed by both the enzymatic activity and phosphorylation status of PHF8, which mediate transactivation of downstream targets. Molecular or pharmacological manipulation of PHF8 activity can enhance or even resurrect RA response to resistant leukemic cells. These results reveal a critical function of histone demethylase in mediating drug response and open up an attractive avenue for modulation of RA sensitivity for cancer therapeutics.

it may help to design better therapeutic strategies to overcome ATRA resistance and potentially extend its application to other malignancies.

Over the years, we and others have shown that RARα fusions form high-order homo-oligomers (Kwok et al., 2006; Lin and Evans, 2000; Minucci et al., 2000; Sternsdorf et al., 2006) that aberrantly recruit DNA binding cofactor RXRα (Zeisig et al., 2007; Zhu et al., 2007) and epigenetic modifying enzymes such as histone deacetylases (HDACs) (Grignani et al., 1998; Lin et al., 1998) and polycomb-repressive complexes (PRCs) (Boukarabila et al., 2009; Smith et al., 2011; Villa et al., 2007) for transcriptional suppression of their downstream targets (e.g., *RARB*) and oncogenic transformation. A pharmacological level of ATRA induces conformational changes of RARα fusions, which result in dissociation of corepressor complexes and recruitment of coactivators, leading to activation of downstream targets and subsequent degradation of the fusion proteins (de Thé and Chen, 2010; Wang and Chen, 2008). In spite of its critical functions in mediating ATRA response, the identity of the coactivator complex responsible for gene activation upon ATRA treatment remains unknown, and this becomes a major hurdle that significantly hinders the progress in understanding underlying mechanisms of ATRA response and designing more effective therapeutic strategies for overcoming resistance (Martens et al., 2010; Mikesch et al., 2010).

Emerging evidence indicates that dynamic histone modifications by lysine methyltransferases (KMTs) and demethylases (KDMs) play a key role in regulation of gene expression (Cheung and So, 2011; Kouzarides, 2007). Members of Jumonji-C domain (JmjC) KDMs involved in diverse biological processes including embryonic development, stem cell self-renewal, and differentiation are known to work closely together with specific KMTs by removing opposite epigenetic marks to govern gene expression (Cheung and So, 2011; Kooistra and Helin, 2012). PHF8 (also called KDM7B) is a member of the plant homeodomain finger (PHF) family KDM harboring an N-terminal plant homeodomain (PHD) that mediates binding to nucleosomes at active gene promoters as well as an active JmjC domain that is able to catalyze the demethylation of mono- or dimethyl-lysines (Feng et al., 2010; Fortschegger et al., 2010; Kleine-Kohlbrecher et al., 2010; Liu et al., 2010; Loenarz et al., 2010; Qi et al., 2010). PHF8 preferentially acts on H3K9me2 and H3K9me1 (however, some results also suggest that it can demethylate H4K20me1) and associates with transcriptional activation and retinoic acid signaling pathway in neuronal differentiation (Qiu et al., 2010). Mutations in the *PHF8* gene are found in patients with X-linked mental retardation (XLMR), and knockdown of PHF8 homolog leads to brain defects in zebrafish (Abidi et al., 2007; Koivisto et al., 2007; Laumonnier et al., 2005), revealing its potential involvement in human disease.

RESULTS

PHF8 Interacts with PML-RARα and Functions as a Transcriptional Coactivator in Response to ATRA Treatment

Given the critical functions of JmjC-KDMs in transcriptional regulation, we performed a systematic biochemical screening by immunoprecipitation assay in human 293T cells for interactions between PML-RARα and seven different JmjC-KDMs from each of the subfamily (KDM2-7) with known enzymatic activity upon ATRA treatment. As a result, we identified PHF8 as the only KDM that exhibited a highly specific interaction with PML-RARα, and this interaction increased significantly in the presence of ATRA (Figure 1A; data not shown). To validate this finding in APL, we showed that endogenous PHF8 binds to PML-RARα in human NB4 cells (Figure S1A available online), which express the PML-RARα fusion.

To further characterize this interaction, a series of PML-RARα and PHF8 mutants were constructed for structure/function analyses to define the respective interaction domains. In contrast to the regions D (hinge region), E (ligand binding domain, LDB), and F (unknown function) of the PML-RARα that were dispensable for PHF8 interaction, the region C that partly overlaps with the DNA binding domain in the PML-RARα fusion was absolutely required for the recruitment of PHF8 (Figure 1B). On the other hand, the JmjC domain but not the catalytic activity of PHF8 was essential for the interaction with PML-RARα (Figure 1C). In contrast, the PHD domain and the C-terminal domain of PHF8 were not part of the PML-RARα-interacting motif (Figure 1C). Consistent with the recent findings of its involvement in retinoic acid signaling (Qiu et al., 2010), mapping of the PML-RARα interaction domain to the region C suggests a potential interaction between PHF8 and wild-type RARα. To gain further insights into this issue, we revealed that PML-RARα had a much higher ability than wild-type RARα to form complex with PHF8 in the presence of ATRA (Figure 1D). Moreover, the interaction between wild-type RARα and PHF8 rapidly dissociated under the stringent washing condition, while the one between PML-RARα and PHF8 remained stable (Figure 1E). Consistently, only the PML-RARα/PHF8 interaction could be detected upon ATRA treatment even when wild-type RARα was coexpressed at the almost identical level as PML-RARα in the same cells with endogenous or ectopic expression of PHF8 (Figure 1F). Together these results indicate that PML-RARα is by far the dominant PHF8 binding partner compared to wild-type RARα in response to the ATRA treatment.

To assess the effect of PHF8 expression on histone modification, we ectopically expressed PHF8 in NB4 and 293T cells. As shown in Figures 1G, 1H, and S1B, PHF8 expression resulted in a significant reduction of H3K9me2 levels in NB4 and 293T cells, consistent with its role in promoting transcriptional activation (Feng et al., 2010; Fortschegger et al., 2010; Kleine-Kohlbrecher et al., 2010; Liu et al., 2010; Loenarz et al., 2010; Qi et al., 2010). To further demonstrate that PHF8 is indeed recruited by PML-RARα to activate expression of downstream targets upon ATRA treatment in APL cells, chromatin immunoprecipitation (ChIP) assays revealed specific binding of PHF8 to the promoter region of *RARB*, a RARα fusion target, but not to *GAPDH* control, upon ATRA treatment in NB4 cells (Figure 1I). Recruitment of PHF8 was also associated with a reduction of the H3K9me2 repressive mark, increase in H3K4me3 and H3K9Ac activation marks (Figure 1J), and an increased in *RARB* mRNA level (Figure S1C). These results demonstrate that PHF8 binds to and modifies the promoter regions of PML-RARα targets for active gene expression in APL cells upon ATRA treatment.

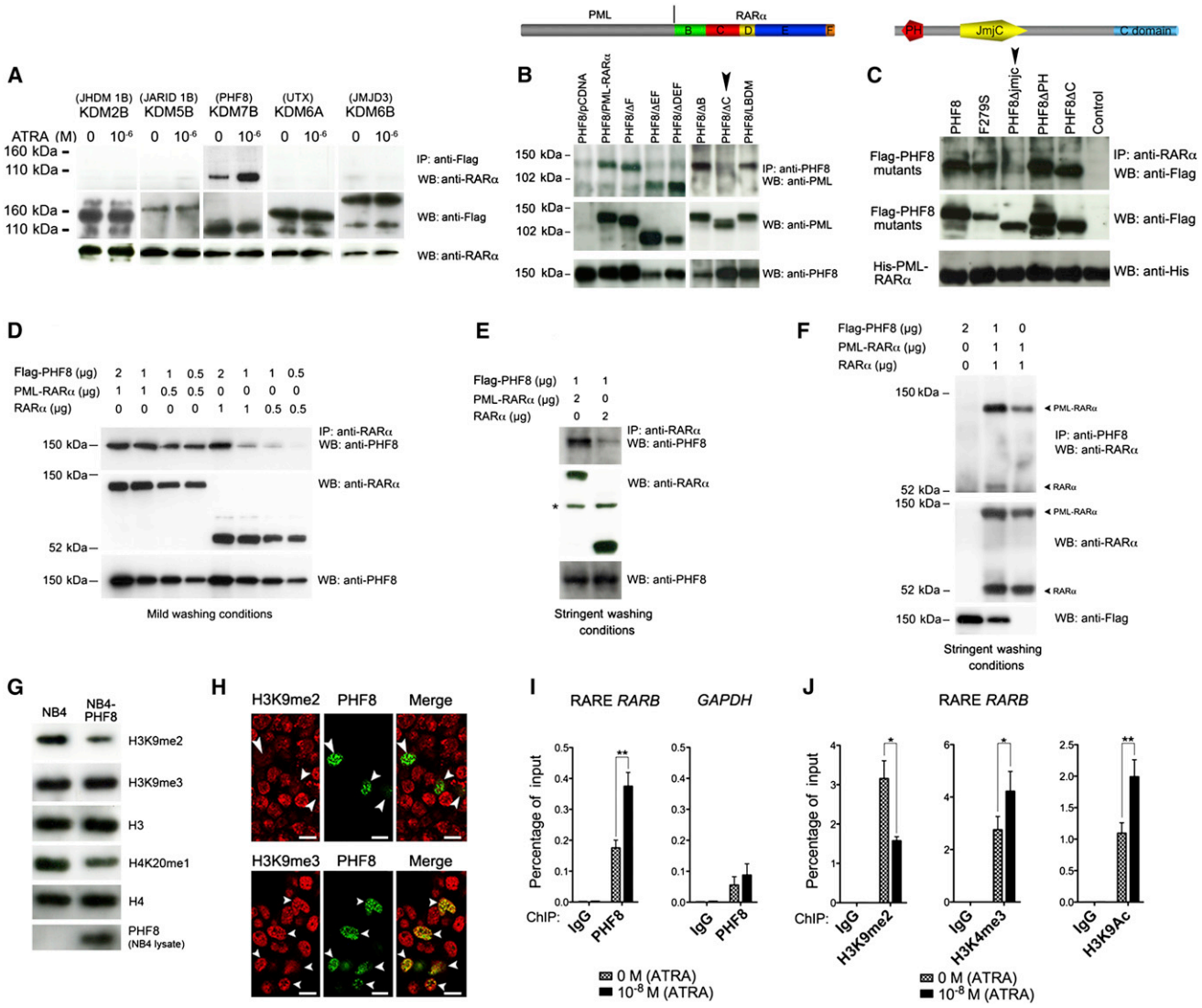

Figure 1. Specific Interaction of PHF8 with PML-RARα Results in Alternation of Histone Marks of Transcriptional Targets in Response to ATRA Treatment

(A–F) Representative coimmunoprecipitation (coIP) analysis in 293T cells coexpressing PML-RARα and Flag-tagged Jumonji family members cultured in the presence or absence of ATRA (A). Deleted or point mutants of PML-RARα were coexpressed with PHF8 (B), or deleted or point mutants of PHF8 were coexpressed with His-PML-RARα (C); and all samples were processed in presence of ATRA. Black arrowheads indicate mutants that cannot interact. PML-RARα or/and wild-type RARα were expressed with Flag-tagged PHF8 using the indicated amounts of expression vectors, and cells were treated with ATRA as indicated; samples were processed under mild washing conditions (D) or stringent washing conditions (E and F). Asterisk indicates unspecific band.

(G) Immunoblotting of purified histone extracts from NB4 and NB4-PHF8 cells.

(H) Histone demethylase activity of YFP-tagged PHF8 protein in 293T cells was assessed by immunostaining using confocal microscopy. White arrowheads indicate cells transfected with YFP-PHF8. Scale bar, 10 μm. Anti-H3K9me2 and anti-H3K9me3 antibodies were used.

(I and J) ChIP analysis of the binding of the endogenous PHF8 (I) and histone H3 modifications (J) on typical RARE *RARB* promoter region in human NB4 cells after 24 hr with or without 10^{-8} M ATRA.

Data representative of at least three independent experiments are shown (±SD, *$p < 0.05$, **$p < 0.01$). See also Figure S1.

PHF8 Sensitizes APL Cells to Physiological Levels of ATRA

To investigate the functional significance of PML-RARα/PHF8 interaction in mediating cellular response to ATRA treatment, we performed both gain-of-function and loss-of-function studies using human NB4 cells and mouse primary hematopoietic cells transformed by APL fusion proteins (Kwok et al., 2006; Zeisig et al., 2007). NB4 cells are highly sensitive to pharmacological concentrations (10^{-6} M) but only have a mild response to physiological level (10^{-8} M) of ATRA as assessed by activation of a RARα fusion target, *RARB,* and inhibition of transformation (Figures S2A and S2B). Strikingly, forced expression of PHF8 in NB4 cells (Figures 2A, 2B, S2C, and S2D) or primary hematopoietic cells transformed by different RARα fusions, including

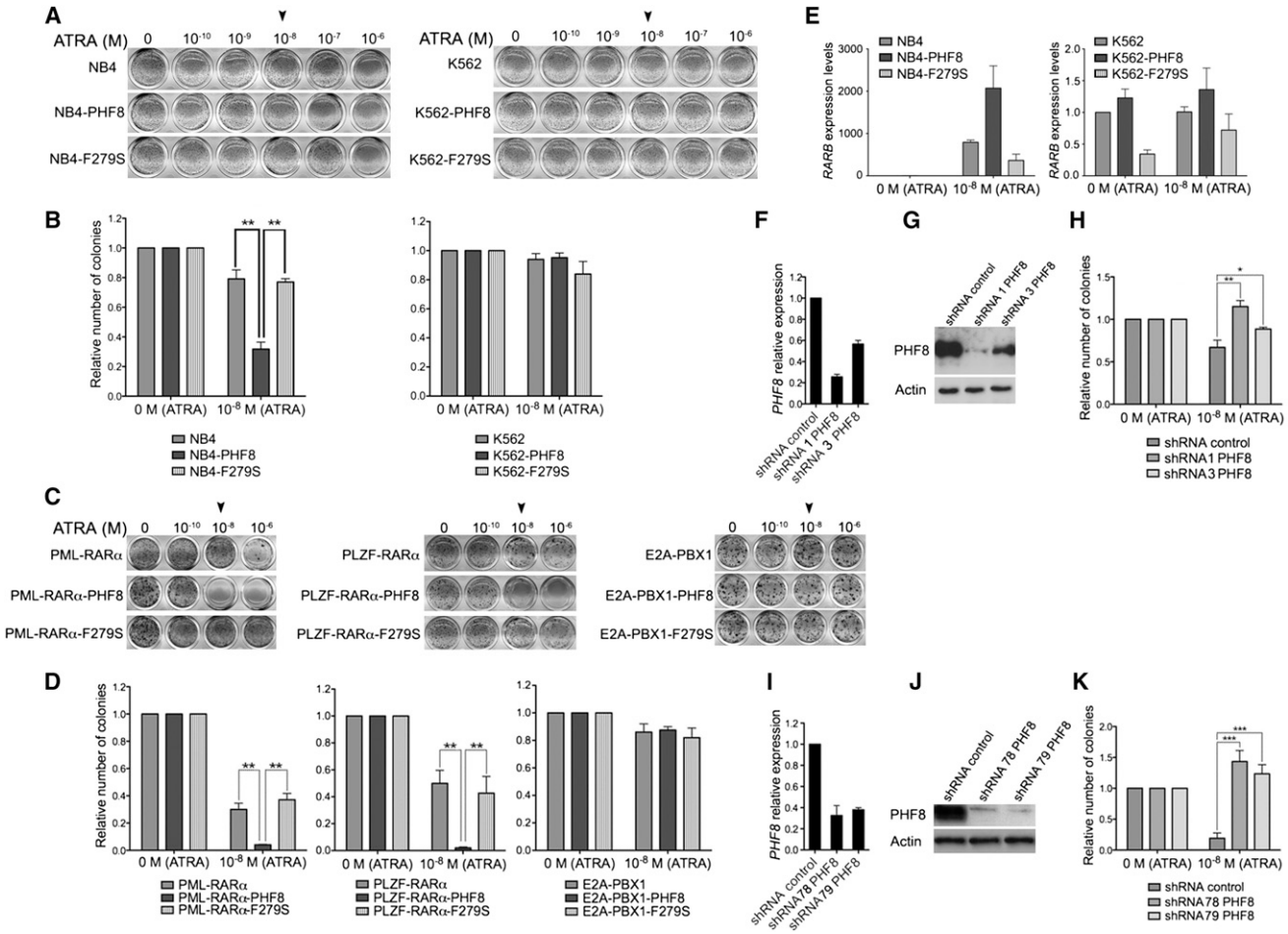

Figure 2. PHF8 Governs ATRA Sensitivity of APL Cells

(A–D) Typical p-iodonitrotetrazolium-violet (INT)-stained colony pictures and bar charts representing normalized colony number of human NB4 and K562 cells (A and B) or murine primary bone marrow cells transformed by the indicated RARα fusion constructs (C and D) treated with and without indicated concentration of ATRA. Black arrowheads indicate the lowest optimal ATRA concentration employed in most of the subsequent studies. Representative data of three experiments are shown (±SEM, $^{**}p < 0.01$).

(E) Quantitative RT-PCR (qRT-PCR) analysis for *RARB* expression in the indicated cells.

(F–J) qRT-PCR (F and I) and western blot analysis (G and J) for *PHF8* expression in cell transduced with specific human (F and G) or mouse (I and J) *PHF8* shRNA. Error bars indicate SD of at least three independent experiments. (H) Human NB4 cells or (K) murine primary bone marrow cells transformed by PLZF-RARα were transduced with either shRNAs for specific PHF8 knockdown (KD) or scramble control before they were plated into methylcellulose medium in the absence or presence of ATRA for colony formation assay.

Data representative of three experiments are shown (±SEM, $^{*}p < 0.05$, $^{**}p < 0.01$, $^{***}p < 0.001$). See also Figure S2.

PLZF-RARα-transformed cells that are usually more resistant to ATRA treatment in the presence of the reciprocal RARα-PLZF fusion (Guidez et al., 2007), significantly sensitized their response to ATRA (Figures 2C, 2D, S2E, and S2F). This function of PHF8 highly depended on the following: (1) its enzymatic activity as a single-point mutation F279S on the catalytic domain identified in X-linked mental retardation patients (Kleine-Kohlbrecher et al., 2010; Koivisto et al., 2007) completely abolished the enhanced ATRA sensitivity including colony suppression (Figures 2A–2D and S2D), enhanced *RARB* expression (Figures 2E and S2G), and differentiation of APL cells (Figure S2H); and (2) the presence of RARα fusions as expression of PHF8 had no effect on the ATRA response in the control human K562 leukemic cells or E2A-PBX1-transformed primary cells (Figures 2A–2E, S2G, and S2I), which expressed the same or even higher levels of RARα protein compared with those in NB4 cells and PML-RARα-transformed primary cells, respectively (Figure S2J). Consistently, the levels of PML-RARα were much higher than those of wild-type RARα in both NB4 and PML-RARα-transformed cells (Figure S2J). Together with the competitive/dilution assays in Figures 1D–1F, these results strongly suggest that PML-RARα is the major and dominant mediator for the PHF8/ATRA response.

To demonstrate a critical function of endogenous PHF8 in governing ATRA response, we further confirmed the expression of endogenous PHF8 in NB4, which was indeed much higher than that in the ATRA-resistant variant, NB4-MR2 cells (Figure S2K), suggesting an association of ATRA resistance with

a reduced level of PHF8. To further validate this hypothesis, endogenous PHF8 expression was downmodulated by small hairpin RNAs (shRNAs) in human NB4 cells (Figures 2F–2H) or RARα-fusion-transformed primary cells (Figures 2I–2K). As a result, suppression of PHF8 conferred ATRA resistance in both NB4 cells (Figure 2H) and RARα-fusion-transformed primary cells (Figure 2K), although the effect was more pronounced in the latter with a more defined genetic background. Together, these results indicate that PHF8 may act as a sensor to mediate ATRA response in APL and its level may govern ATRA sensitivity.

PHF8 Resensitizes ATRA-Resistant APL Cells In Vitro and In Vivo

To investigate if PHF8 can indeed sensitize ATRA-resistant cells to the treatment, we induced expression of wild-type PHF8 and the catalytically dead mutant PHF8-F279S in the ATRA-resistant NB4-MR2 cells (Figures S3A and S3B). NB4-MR2 cells have an increased level of topoisomerase 2β (TOP2β) that could decrease ATRA-mediated gene expression and granulocytic differentiation by enhancing the association of repressor complexes with PML-RARα downstream target genes including *RARB* (McNamara et al., 2008). NB4-MR2-PHF8 cells showed a significant reduction in colony number, induction of the *RARB* expression, and increased differentiation of the APL cells after ATRA treatment (Figures 3A–3C and S3C–S3E). On the contrary, expression of PHF8-F279S failed to sensitize NB4-MR2 cells to the treatment, indicating an important enzymatic-activity-dependent function of PHF8, in governing ATRA response even in resistant cells (Figures 3A–3C and S3A–S3E). To further assess if PHF8 is also able to sensitize ATRA-resistant cells to treatment in vivo, we transplanted NB4-MR2, NB4-MR2-PHF8, and NB4-MR2-F279S cells into sublethally irradiated NOD-SCID-Gamma (NSG) mice for in vivo leukemogenic assay (Figures 3D and 3E). As expected, mice transplanted with NB4-MR2 cells succumbed to leukemia regardless of ATRA treatment. Strikingly, mice transplanted with NB4-MR2-PHF8 cells responded very well to the ATRA treatment, and most of them remained healthy (Figure 3D). This was in stark contrast to the untreated NB4-MR2-PHF8 control group that rapidly succumbed to leukemia. Consistent with the in vitro results (Figures 3A–3C), mice transplanted with NB4-MR2-F279S failed to respond to the ATRA treatment in vivo and developed leukemia with a similar latency as the untreated controls, confirming the importance of its enzymatic activity in ATRA response (Figure 3E). These results strongly indicate that PHF8 plays a critical role in mediating ATRA response, and its activation by an overexpression approach reverses ATRA resistance in APL cells.

Another major mechanism for ATRA resistance in human APL is the mutation of ligand binding domain (LBD) of PML-RARα (Côté et al., 2000). To further extend the role of PHF8 in ATRA-resistant APL, we employed two different APL models, namely, human NB4-LR2 cells (Roussel and Lanotte, 2001) and primary leukemic cells from a PML-RARαm4 transgenic mouse (designated "M4" herein) (Kogan et al., 2000), each carrying a different PML-RARα LBD mutation identified in human APL patients. As expected, NB4-LR2 cells were resistant to ATRA (Figures 3F, 3G, and S3F–S3H). Conversely, expression of PHF8 resensitized their response to ATRA 10^{-8} M (Figures 3F, 3G, and S3F–S3H). However, this effect disappeared when the mutation abolishing the catalytic activity was introduced to PHF8, consistently indicating the critical function of PHF8 enzymatic activity in mediating the ATRA response even in the PML-RARα LBD mutant (Figures 3F and 3G, S3A, and S3F–S3H). Finally, transplantation of NB4-LR2 cells into NGS mice induced ATRA-resistant leukemia, which could, however, be sensitized to ATRA treatment again when PHF8 was expressed (Figure 3H). To further validate these results in a well-defined genetic background, we performed similar in vivo experiments using the well-characterized ATRA-resistant M4 primary cell model (Kogan et al., 2000). M4 cells induced leukemia in mice regardless ATRA treatment. M4 cells expressing PHF8 also induced leukemia in mice. However, expression of active PHF8 in combination with ATRA treatment significantly extended the survival of mice and induced differentiation of M4 cells (Figures 3I and 3J). Together, these results strongly indicate that activation of PHF8 can resurrect ATRA sensitivity in a wide range of clinically relevant ATRA-resistant APL cells.

PHF8 Switches Promoter Occupancy after ATRA Treatment

It has been shown that the binding of PHF8 to its targets is regulated by its phosphorylation status (Liu et al., 2010). PHF8 binds to promoter regions of genes involved in cell cycle progression such as *RBL1* to remove H4K20me1 mark and dissociates from these promoters upon phosphorylation of S33/S84 residues by CDK1 (Liu et al., 2010). To gain further insights into the molecular regulation of PHF8 upon ATRA treatment in APL, we investigated the dynamics of PHF8 promoter occupancy by ChIP analysis in NB4-MR2 cells. Upon ATRA treatment, the binding of PHF8 to the promoter regions of multiple RARα fusion targets, including *RARB*, *PRAM1*, *TGM2*, and *ID1* (Martens et al., 2010; Wang et al., 2010), was increased (Figure 4A), while its binding to naive PHF8 targets such as *RBL1* and *CCNE1* promoters that are occupied by PHF8 in the absence of ATRA was reduced (Figure 4B). ATRA treatment had no effect on the binding of PHF8 at the control *GAPDH* promoter (Figure 4C). This switch in promoter occupancy was also accompanied by changes in corresponding histone marks. A significant reduction in PHF8-specific repression marks (H3K9me2) and an increase in activation marks (H3K4me3 and H3K9Ac) were detected in the same promoter regions of *RARB* (Figure 4D), *PRAM1* (Figure 4E), *TGM2* (Figure 4F), and *ID1* (Figure 4G), whereas H4K20me1 histone mark was significantly increased at the *RBL1* (Figure 4I) and *CCNE1* (Figure 4J) promoters. None of these changes could be detected in the noncoding control region (NC1) of NB4-MR2 cells (Figures 4H and 4K) or the same *RARB* regions in K562 cells that do not carry RARα fusions (Figures S4A and S4B). Thus, these findings suggest that PHF8 may switch promoter occupancy for driving the expression of PML-RARα targets in human APL cells upon ATRA treatment.

PHF8-Mediated ATRA Response Is Regulated by Serine Phosphorylation

Interestingly, ATRA is known to relocate cyclin A to the nuclear compartment in leukemic cells, resulting in activation of CDK1 in AML cells (Ekberg et al., 2004). Thus, we speculated that the promoter occupancy of PHF8 might be regulated by ATRA

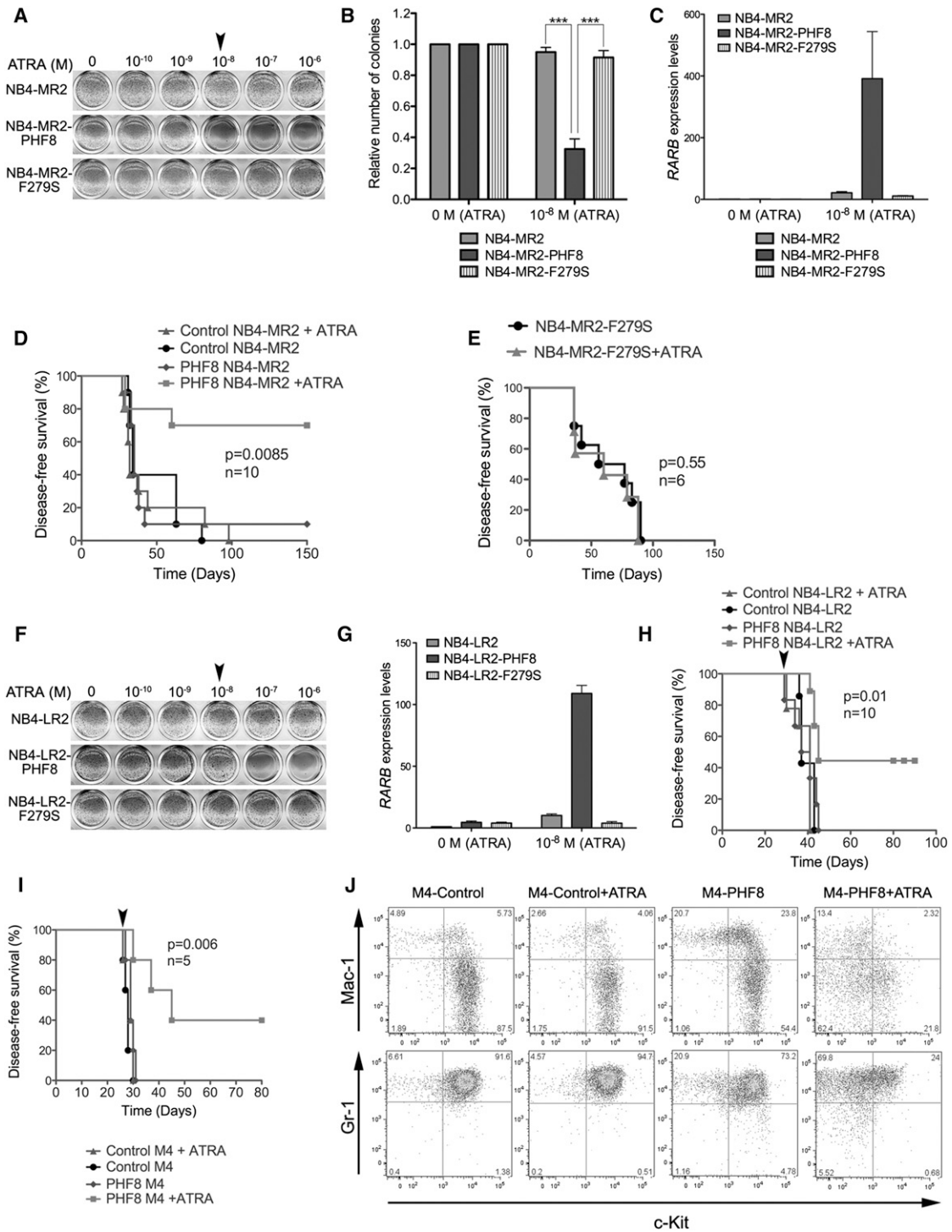

Figure 3. PHF8 Sensitizes ATRA-Resistant APL Cells to Physiological Concentrations of ATRA

(A–H) Human APL cells transduced with vector control or PHF8 wild-type or its catalytically inactive mutant F279S were treated with and without ATRA at the indicated concentrations. Typical INT-stained colony pictures of NB4-MR2 (A) and NB4-LR2 (F) cell lines. The bar charts represent NB4-MR2 normalized numbers of colonies (B). Error bars are representative of four independent experiments. (±SEM, ***$p < 0.001$). qRT-PCR analysis for human *RARB* expression in NB4-MR2 (C) or NB4-LR2 (G) cell lines. Error bars indicate SD of three independent experiments. Disease-free survival of NSG mice injected with NB4-MR2, NB4-MR2-PHF8 cells (D), NB4-MR2-F279S cells (E), or NB4-LR2, NB4-LR2-PHF8 cells (H), with and without ATRA treatment.

(I and J) M4 cells from PML-RARα LBD transgenic mouse model transduced with vector control (control M4) or PHF8 wild-type (PHF8 M4). Disease-free survival of FVB mice injected with control M4 or PHF8 M4 cells with and without ATRA treatment. Black arrowheads indicate the end of ATRA treatment (I). FACS analysis of bone marrow cells stained with Gr-1, Mac-1, and c-Kit markers for differentiation status of murine myeloid cells (J).

See also Figure S3.

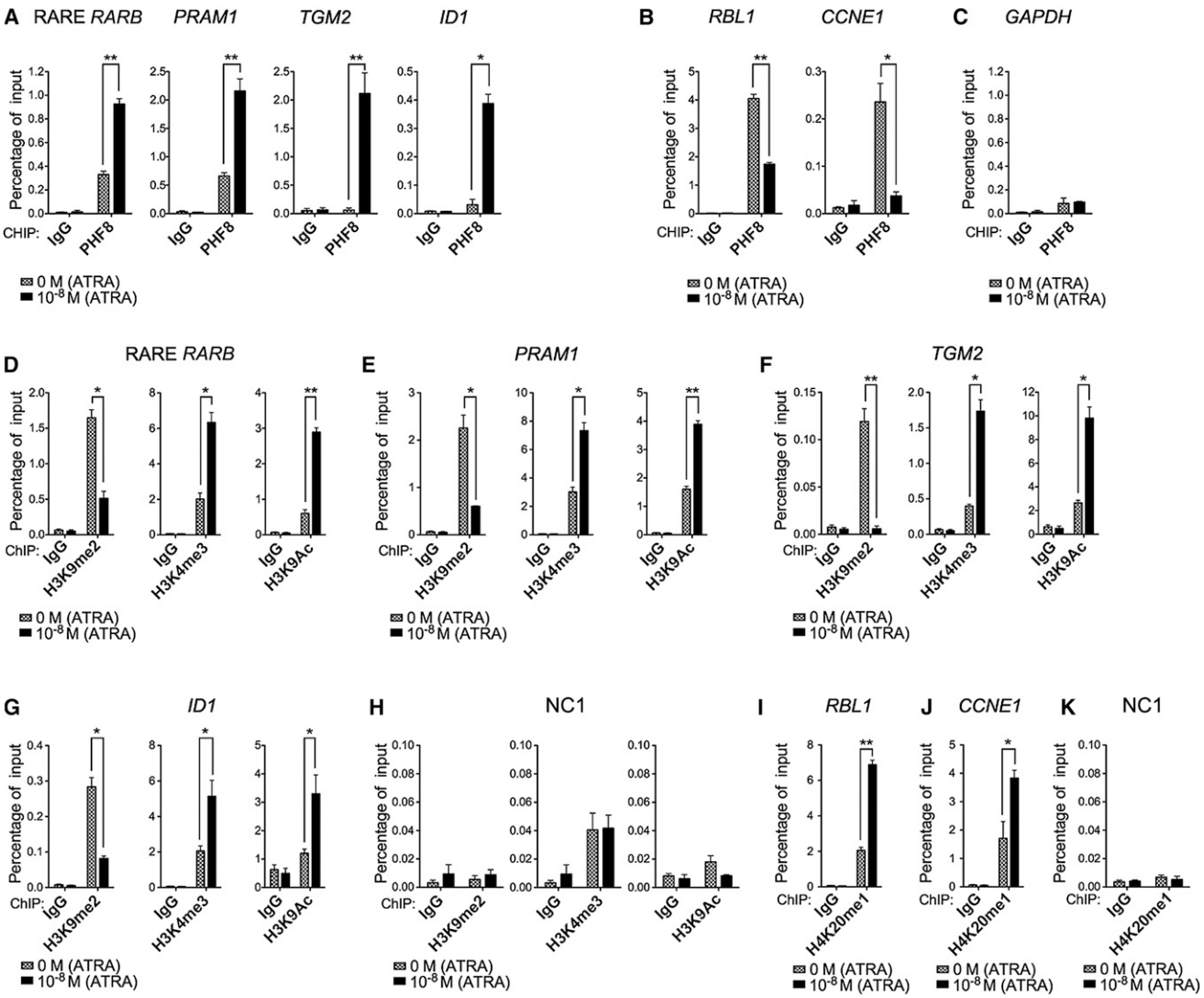

Figure 4. Changes of PHF8 Promoter Occupancy and Associated Histone Modifications after ATRA Induction

ChIP analysis of PHF8 (A–C) or various histone marks including H3K9me2, H3K4me3, H3K9Ac, H4K20me1 (D–K) on both RARα-fusion-targeted promoters (e.g., *RARB*, *PRAM1*, *TGM2*, and *ID1*) and naive PHF8-targeted promoters (e.g., *RBL1*, *CCNE1*) before and after 24 hr of ATRA treatment at 0 M or 10^{-8} M in NB4-MR2-PHF8 cells. ChIP signals are presented as percentage of input. Error bars indicate SD of three independent experiments (±SD, *$p < 0.05$, **$p < 0.01$). *GAPDH* was used as negative control for PHF8 occupancy, and NC1 was used as negative control for histone marks. See also Figure S4.

in part by CDK1-mediated phosphorylation. Indeed, we detected an increase in PHF8 phosphorylation with increasing levels of ATRA in NB4-MR2-PHF8 cells (Figure 5A). Next, we investigated if CDK1-mediated PHF8 phosphorylation would be able to mimic ATRA response in PHF8-transduced NB4 or NB4-MR2 cells (Figures 5B–5D, S5A, and S5B). In the absence of ATRA treatment, cells transduced with PHF8 (NB4-MR2-PHF8) or CDK1 (NB4-MR2-CDK1) exhibited a mild increase of *RARB* gene expression as compared with vector-control (NB4-MR2)-transduced cells (Figure 5B). In contrast, cells cotransduced with CDK1 and PHF8 (NB4-MR2-CDK1-PHF8) significantly activated *RARB* expression even in the absence of ATRA (Figure 5B). These transcriptional activities also directly correlated with the biological readouts, in which coexpression of PHF8 with CDK1 significantly suppressed transformation and enhanced differentiation of NB4-MR2 cells even in the absence of ATRA treatment (Figures 5C and 5D). Similar results could also be obtained for NB4 cells (Figure S5B). These results suggest a critical function of CDK1 in mediating PHF8 functions, although it is known that CDK1 can have many different targets and functions, and likewise other kinases may also be able to modulate PHF8 activity. To confirm the critical role of PHF8 phosphorylation in mediating ATRA response, we generated two additional PHF8 variants at those two serine phosphorylation sites by replacing S33 and S84 with either alanines to generate a phosphorylation defective mutant (PHF8AA) or aspartic acids to mimic a constitutively phosphorylated form (PHF8DD) (Liu et al., 2010). To further demonstrate their specific activity in mediating ATRA response, these three PHF8 variants were fused to the ligand binding domain of the

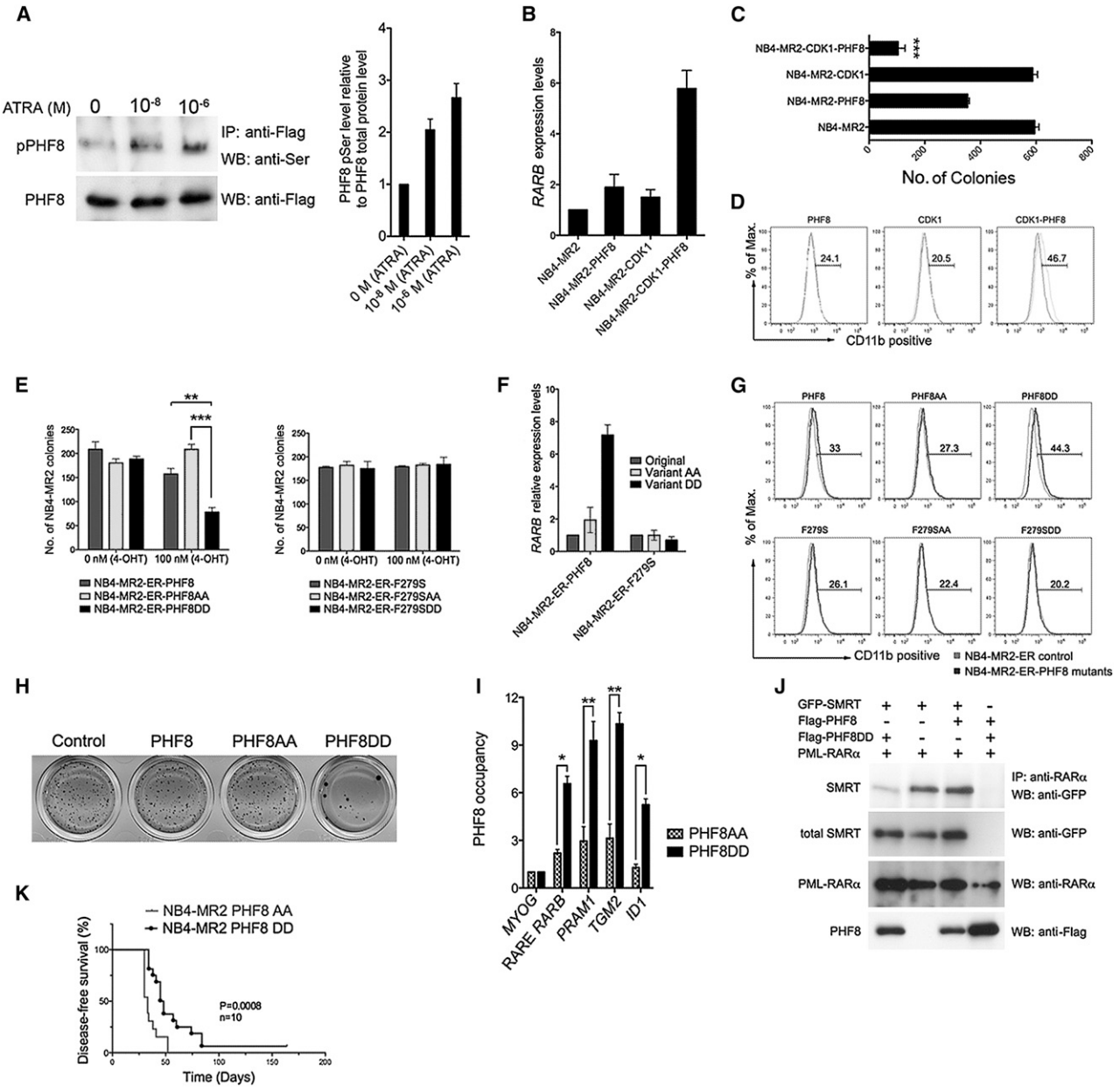

Figure 5. PHF8-Mediated ATRA Response Is Regulated by Serine Phosphorylation

(A) PHF8 was immunoprecipitated from total cell lysate of NB4-MR2-PHF8 cells treated with the indicated concentrations of ATRA and immunoblotted for phospho-Ser (upper panel); the membrane was stripped and then immunoblotted for total PHF8 protein (lower panel). The bar chart at the right represents quantification of serine-phosphorylated PHF8 relative to the total PHF8 protein. Error bars represent SD of three independent experiments.

(B–D) NB4-MR2 cells were transduced with empty vector control, wild-type PHF8, wild-type CDK1, or PHF8 and CDK1 together. The *RARB* mRNA level (B, measured by qRT-PCR, error bars indicate SD of three independent experiments), the number of colony formed (C, error bars represent SEM of three independent experiments, ***$p < 0.001$), and expression of the differentiation marker for myeloid cells CD11b (D, FACS analysis) of these cells were determined.

(E) The number of colonies of NB4-MR2 cells transduced with ER-fused enzymatic active (left) or dead (right) PHF8, PHF8AA, or PHF8DD in the absence or presence of 100 nM 4-OHT. Error bars represent three independent experiments (±SEM, **$p < 0.01$, ***$p < 0.001$).

(F) *RARB* mRNA level in cells transduced with indicated PHF8 constructs after induction with 100 nM 4-OHT shown in (E). Error bars indicate SD of three independent experiments.

(G) FACS analysis for CD11b expression of NB4-MR2-ER cells expressing PHF8 or different PHF8 mutants.

(H) Typical INT-stained colony pictures of NB4-MR2 cells transduced with empty vector control, PHF8, PHF8AA, or PHF8DD.

(I) ChIP analysis comparing the PHF8 occupancy at the indicated promoter regions of NB4-MR2 cells transduced with PHF8AA and PHF8DD variants. ChIP signals are presented as fold enrichment over *MYOG* (±SD, *$p < 0.05$, **$p < 0.01$).

(J) Representative coimmunoprecipitation (coIP) analysis in 293T cells. PML-RARα was coexpressed in the presence of GFP-SMRT, Flag-PHF8, or Flag-PHF8DD.

(K) Disease-free survival curves of NSG mice injected with NB4-MR2 cells expressing PHF8AA or PHF8DD.

See also Figure S5.

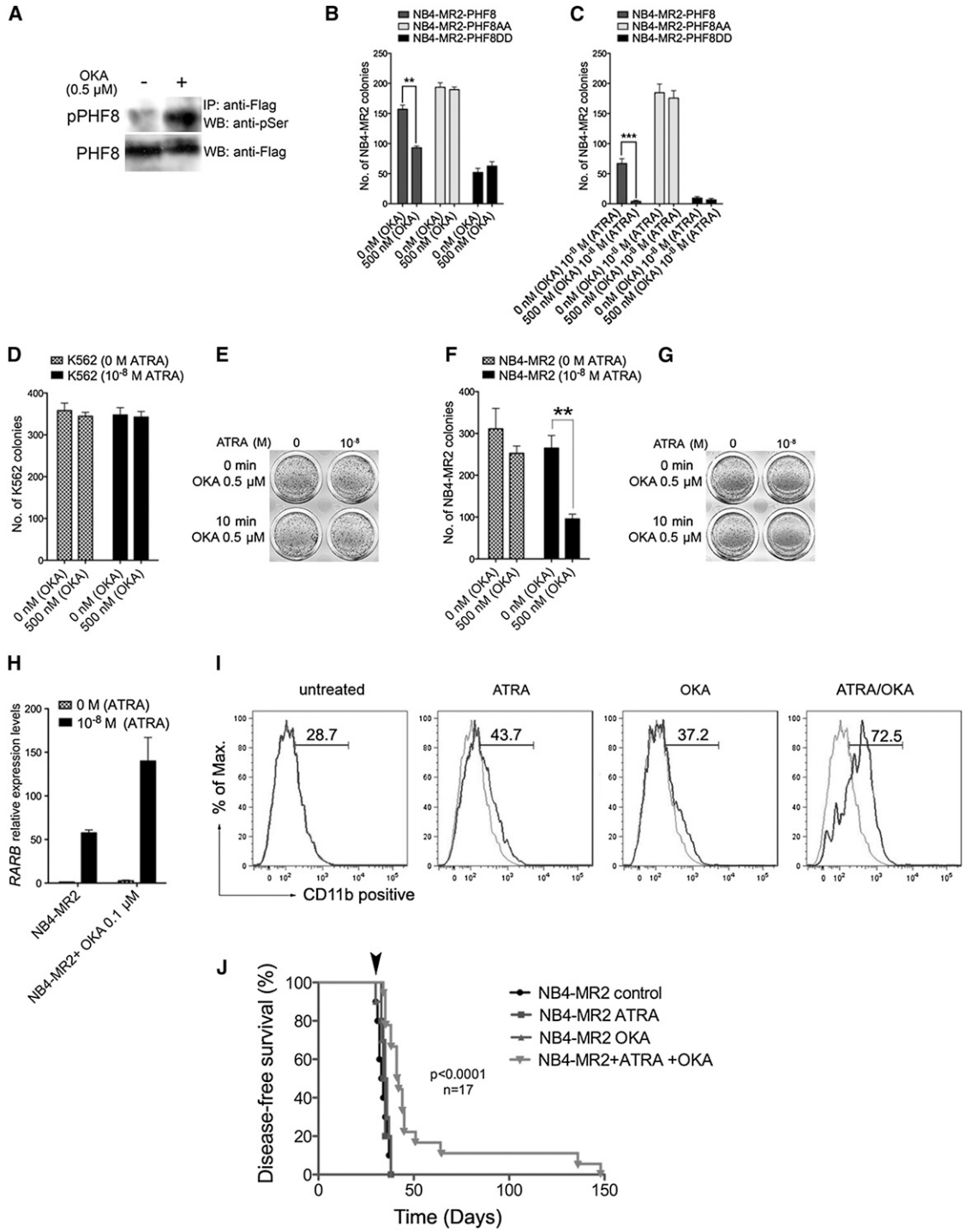

Figure 6. Okadaic Acid Specifically Inhibits PHF8 Dephosphorylation and Sensitizes NB4-MR2 Cells to ATRA Treatment

(A) Western blot analysis of PHF8 phosphorylation in NB4-MR2-PHF8 cells upon 10 min treatment with 0.5 μM OKA. Flag-tagged PHF8 was immunoprecipitated from the total lysate using anti-Flag antibody and blotted for phospho-Ser detection (upper panel) or for total PHF8 protein on the stripped membrane (lower panel).

(B and C) The effect of OKA treatment on NB4-MR2 cells transduced with PHF8, PHF8AA, or PHF8DD. Cells were plated in methylcellulose after 10 min of OKA pretreatment at the indicated concentrations without (B) or with (C) ATRA treatment. Data are representative of three independent experiments (±SEM, $^{**}p < 0.01$, $^{***}p < 0.001$).

(D–G) K562 and NB4-MR2 cells were pretreated with OKA as described above and plated in methylcellulose with or without 10^{-8} M ATRA. The bar charts show the number of colonies after indicated treatment for K562 (D) and NB4-MR2 (F), while INT-stained represent typical results for K562 (E) and NB4-MR2 (G) colony formation assay. Data are representative of three independent experiments (±SEM, $^{**}p < 0.01$).

(legend continued on next page)

estrogen receptor (ER) to allow an inducible activation of the proteins by 4-hydroxy-tamoxifen (4-OHT) treatment. As expected, activation of PHF8 in the absence of ATRA had little impact on NB4-MR2 cells, and similar results were obtained for PHF8AA mutant (Figures 5E–5G, S5C, and S5D). However, expression of PHF8DD mutant significantly suppressed colony formation (Figure 5E) as well as enhanced expression of *RARB* (Figure 5F) and differentiation (Figure 5G) of APL cells without a significant impact on apoptosis (Figure S5D) even in the absence of ATRA. These results from ER-inducible mutants could also be directly reproduced using corresponding constitutive mutants (Figure 5H), in which the PHF8AA mutant as expected failed to collaborate with CDK1 for suppression of NB4-MR2 colony formation in the absence of ATRA (Figure S5E). Moreover, PHF8DD as compared with PHF8AA exhibited a much stronger binding to target promoters of PML-RARα (e.g., *RARB*, *PRAM1*, *TGM2*, and *ID1*) but not the *MYOG* control, consistent with a critical function of phosphorylation status in determining the promoter occupancy (Figure 5I). To further investigate if the inhibitory effects by PHF8DD mutant also require enzymatic activity of PHF8, the F279S mutation was introduced to these three PHF8 variants. The F279S mutation completely abolished both the transformation suppressive function and the transactivation activity of PHF8DD (Figures 5E–5G), strongly suggesting that ATRA response mediated by PHF8 is regulated by both serine phosphorylation and enzymatic activity of PHF8. Consistently, expression of PHF8DD mutant but not wild-type PHF8 could displace the transcriptional corepressor SMRT from PML-RARα in the absence of ATRA (Figure 5J). To further demonstrate that phosphorylation of PHF8 plays a key role in mediating ATRA response in APL in vivo, NB4-MR2 cells expressing either PHF8AA or PHF8DD mutant were transplanted into NSG mice for in vivo leukemogenic assay. PHF8DD significantly extended the disease latency even in the absence of ATRA treatment, confirming a key role of PHF8 phosphorylation status for APL leukemogenesis (Figure 5K).

Inhibition of PHF8 Dephosphorylation by Okadaic Acid Sensitizes ATRA-Resistant Human APL Cells to the Treatment

Considering the critical function of PHF8 in mediating ATRA response, we asked if pharmacological inhibition of PHF8 dephosphorylation could sensitize resistant APL cells to the ATRA treatment. To this end, we tested the effect of two common phosphatase inhibitors, calyculin A and okadaic acid (OKA), on NB4-MR2-PHF8 cells for their ability to suppress dephosphorylation of PHF8. OKA showed good efficacy in inhibiting PHF8 dephosphorylation as revealed by a significant increase of PHF8 serine phosphorylation in NB4-MR2-PHF8 cells upon OKA treatment (Figure 6A; data not shown). Consistent with this result, colony formation assays revealed that OKA alone could suppress colony formation by NB4-MR2-PHF8 cells, while it had no effect on NB4-MR2 cells expressing phosphorylation mutants NB4-MR2-PHF8AA and NB4-MR2-PHF8DD (Figure 6B). In addition, combined OKA/ATRA treatment had further enhanced tumor suppression effect on NB4-MR2-PHF8 cells but not on NB4-MR2 cells expressing PHF8AA or PHF8DD mutants (Figure 6C), indicating a critical function of these two PHF8 phosphorylation sites in mediating OKA response. To further assess if OKA can be used to sensitize ATRA-resistant APL to the treatment without genetic manipulation of PHF8, NB4-MR2 cells and K562 control cells were treated with OKA, ATRA, or their combination and subjected to colony formation assay (Figures 6D–6I). As expected, K562 cells did not respond to any of the treatments with ATRA, OKA, or their combination (Figures 6D and 6E). NB4-MR2 cells were also refractory to ATRA treatment and exhibited a very mild response to OKA treatment alone (Figures 6F and 6G). However, the combined treatment of ATRA and OKA could significantly reduce the colony formation ability of NB4-MR2 cells (Figures 6F and 6G), which was also accompanied by increased expression of *RARB* (Figure 6H) and expression of differentiation marker CD11b (Figure 6I). Consistently, very similar effects were also obtained using NB4 cells and NB4-LR2 cells carrying wild-type and LBD mutant of PML-RARα (Figures S6A and S6B), indicating a more general effect of OKA on different ATRA-resistant APL cells. Finally, in order to assess the in vivo efficacy of OKA/ATRA treatment on ATRA-resistant APL, NB4-MR2 cells were transplanted into NSG mice and subjected to the treatments. Mice receiving ATRA or OKA treatment alone died at almost the identical time points as the untreated control (Figure 6J). In contrast, combined OKA/ATRA treatment significantly prolonged the survival of mice even after ceasing treatment (Figure 6J). Together, these results reveal PHF8 as a critical sensor in mediating ATRA response, and pharmacological manipulation of its activity represents a potential avenue to sensitize resistant APL cells to the ATRA treatment.

DISCUSSION

Transcriptional deregulation plays a key role in a large array of human cancer, in particular, in acute leukemia, which is mostly initiated by mutations affecting master transcription factors (Cheung and So, 2011). While development of small molecule inhibitors targeting transcriptional machinery has been proved extremely difficult, the discovery of epigenetic modifying enzymes such as EZH2 and DNMT3 with rigid catalytic domains that are mutated or aberrantly recruited by oncogenic transcription factors for their functions have fueled the enthusiasm for targeting these classically intractable factors (Zeisig et al., 2012). This has also led to a recent burst of international efforts in developing specific inhibitors toward these enzymes (Arrowsmith et al., 2012). In addition to their emerging role in disease development, here we reveal a critical function of KDM in regulation of treatment response, in which PHF8 governs the ATRA sensitivity in APL.

(H and I) NB4-MR2 cells were treated with OKA and ATRA as indicated and then analyzed for the expression of *RARB* by qRT-PCR (H, error bars indicate SD of three independent experiments) or CD11b by FACS (I).
(J) Disease-free survival curves of NSG mice transplanted with NB4-MR2 cells and then treated as indicated. Arrow indicates the end point of the treatment. See also Figure S6.

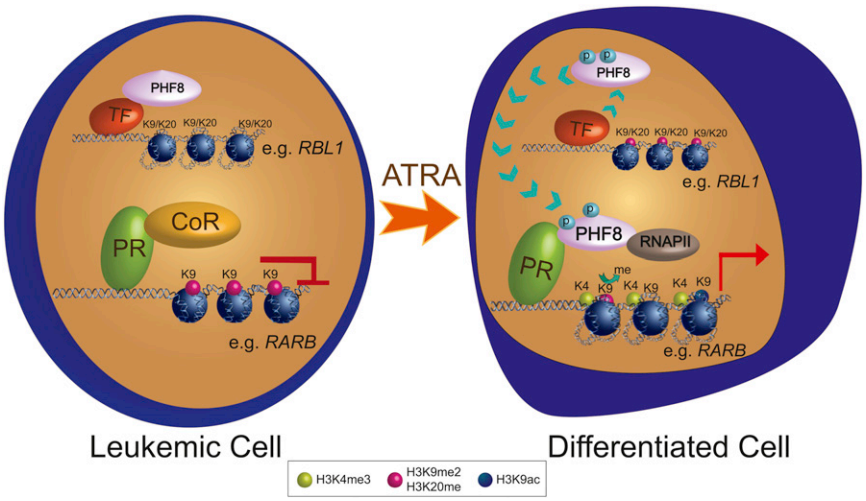

Figure 7. Schematic Diagram Illustrates the Molecular Regulation of PHF8 in Mediating ATRA Response in APL

In leukemia, PML-RARα (PR) recruits corepressor complexes (CoR) to suppress expression of downstream targets. Upon ATRA treatment, PHF8 is phosphorylated and detaches from the original binding sites (naive PHF8 targets, e.g., *RBL1* promoter) to bind to PR. PHF8 removes H3K9me2 marks and recruits additional histone modification enzymes and RNA polymerase II (RNAPII) to drive the expression of PR downstream targets (e.g., *RARB*) for differentiation.

Although significant progress has been made in recent years in characterizing the corepressor complexes and the resultant epigenetic landscapes in APL cells (Martens et al., 2010; Wang et al., 2010), the molecular basis and regulation of the resultant transcriptional reactivation upon ATRA treatment are still largely unknown (Mikesch et al., 2010). In this study, we provide several lines of evidence that PHF8 functions as a critical coactivator and molecular sensor in regulating transcriptional and cellular responses to ATRA treatment in APL. In contrast to HDAC or PRC2, PHF8 is differentially recruited by the RARα fusions to remove repressive histone marks and favors active gene transcription in response to ATRA treatment, which is in agreement with PHF8 as a class of transcriptional coactivators recruited by RARα fusions to create a more permissive chromatin environment at promoters in response to ATRA treatment (Figure 7). Activation of PHF8 activity by increasing its level of either expression or phosphorylation at S33/S84 residues can sensitize ATRA-responsive or ATRA-resistant APL. Under these conditions, the respective demethylated lysine residues can be targets for acetylation and additional interactions with RNA polymerases and other proteins, which may further stimulate transcription (Fortschegger et al., 2010). Consistently, inhibition of LSD1 resulting in an increase of H3K4me2 has recently been shown to be able to reactivate ATRA differentiation pathway in AML (Schenk et al., 2012), whereas histone acetylation has been one of the highly regulated histone marks in RARE binding sites with a strong correlation with RNA polymerase II occupancy near PML-RARα binding sites upon ATRA treatment (Martens et al., 2010; Mikesch et al., 2010). Interestingly, inhibition of TOP2β that overcame ATRA resistance in NB4-MR2 also caused hyperaceylation of H3K9 (McNamara et al., 2008), which is consistent with the observed transcriptional function of PHF8. Thus, identification of PHF8 as a coactivator for RARα fusions may provide a molecular explanation for epigenetic changes associated with ATRA response and opens up promising avenues to sensitize cancer cells to ATRA treatment.

RA signaling and subsequent activation of target genes for induction of differentiation, cell cycle arrest, and apoptosis have been a focus for development of differentiation-based cancer therapy (Gronemeyer et al., 2004). ATRA and 13-*cis* RA have been used in the clinic to treat cutaneous T cell lymphoma (CTCL) and neuroblastoma (NB) by targeting endogenous RAR to induce cell proliferation arrest and morphological differentiation in these tumors. While RA treatment after completion of chemoradiotherapy significantly improves event-free survival in high-risk NB patients (Matthay et al., 2009), more than 40% of the patients will relapse, and virtually all become resistant to the treatment. Interestingly, PHF8 can also interact with endogenous RAR in the absence of RARα fusions, and its knockdown suppresses RA-induced neuronal differentiation from mouse embryonic P19 cells (Qiu et al., 2010), suggesting its potential function in regulating RA response in the neuronal lineage. This property is reminiscent of ZNF423, which is activated by tumor suppressor NF1 (Hölzel et al., 2010) and is critically required for RA-induced differentiation of NB cells (Huang et al., 2009). However, ZNF423 constitutively associates with RAR regardless of ATRA treatment; thus, additional RA modulators (RAMs) that are differentially recruited to RAR/RXR complexes are likely required to mediate the RA response in NB. While PRAME has been reported to differentially bind to RAR upon RA treatment, it acts as a transcriptional repressor to prevent ligand-induced activation (Epping et al., 2005), and the equivalent positive RAM is still missing. In analogy to PRAME, PHF8 is differentially recruited to RAR in response to ATRA. Instead of complexing with EZH2 for making transcriptional repressive marks (Epping et al., 2005), PHF8 possesses enzymatic activity that can actively remove repressive marks and recruits other epigenetic modifying enzymes and basal transcriptional machinery for active gene expression. Discovery of the critical functions of PHF8 in ATRA-mediated transcriptional and in vivo cellular responses in APL may also suggest PHF8 as the missing positive RAM. While the activity of RAM is likely tissue specific and requires other cofactors to mediate its full response, it will be of interest to determine if PHF8 may fulfill the role of positive RAM in mediating RA response in other cell types as well. As a proof-of-principle study, we were able to show that combined treatment of ATRA and OKA, a phosphatase inhibitor suppressing PHF8 dephosphorylation, could be used successfully to treat ATRA-resistant human APL cells in vivo. Together, these results describe an important molecular regulation of PHF8 in mediating ATRA response and raise hope to develop effective therapeutic strategies combining ATRA treatment with drugs inducing

specific epigenetic modifications to target RA-resistant cancer cells.

EXPERIMENTAL PROCEDURES

Plasmids and antibodies are described in Supplemental Experimental Procedures.

Immunoprecipitation and Western Blot Analysis

For generic immunoprecipitation, transfected cells were lysed in 0.5% NP-40 lysis buffer (50 mM Tris-HCl [pH 8], 150 mM NaCl, 5 mM EDTA, 0.2 μM DTT, 10% glycerol, protease inhibitor, 0.5% NP-40 detergent) for mild conditions or RIPA lysis buffer (50 mM Tris-HCL [pH 8], 150 mM NaCl, 1% NP-40, 0.5% sodium deoxycholate, 0.1% SDS, protease inhibitors) for stringent condition during 1 hr at 4°C. They were then incubated with the respective antibody overnight, precipitated with protein A/G Dynal beads (Invitrogen) at 4°C for 1 hr, and then washed with mild 0.5% NP-40 lysis buffer or stringent RIPA buffer. The indicated amount of ATRA was present throughout the processes. Eluted proteins were resolved by SDS-PAGE. Membranes were probed with described antibodies.

Histone Purification

Nuclei were extracted in acidic conditions to selectively remove histones, which were used subsequently for immunoblotting analysis. Details are in Supplemental Experimental Procedures.

Immunofluorescence Staining

Cytospins of a total of 5×10^4 cells were performed onto glass microscope slides and then fixed with 4% formaldehyde in phosphate-buffered saline (PBS) (pH 7.4) for 30 min on ice. Cells were washed in PBS, permeabilized, and blocked using 10% fetal calf serum (FCS)/1% BSA/0.2% TX-100/PBS for 15 min. Anti-H3K4 was used at 1:50 dilution in 10% FCS/1% BSA/PBS and incubated overnight at 4°C. Slides were washed three times with PBS and subsequently incubated with 1:100 donkey anti-mouse fluorescein isothiocyanate for 30 min at room temperature. Slides were washed five times with PBS and mounted with Vectashield (Vector Laboratories, Peterborough, UK).

Chromatin Immunoprecipitation

NB4, NB4-MR2, and K562 cells were cultured in R10 medium at 37°C and, when indicated, treated for 24 hr with 10^{-8} M ATRA and crosslinked with 1% formaldehyde (Sigma). Details are described in Supplemental Experimental Procedures.

Retroviral/Lentiviral Transduction and Transformation Assays

Retroviral/lentiviral transduction and transformation assays (RTTAs) were performed on primary murine or human hematopoietic cells as previously described (Zeisig and So, 2009). In brief, c-kit$^+$ cells were isolated from murine bone marrow and cultured overnight in R10 medium (RPMI 1640, 10% FCS, 2 mM L-glutamine) supplemented with 20 ng/ml SCF, 10 ng/ml IL-3, and IL-6. Spinoculation was carried out by centrifugation at 800 × *g* in the presence of 5 μg/ml polybrene (Sigma-Aldrich, UK) at 32°C for 2 hr. Cells were plated in M3231 methylcellulose medium (Stem Cell Technologies, Canada) supplemented with recombinant murine 20 ng/ml SCF, 10 ng/ml IL-3, IL-6, and GM-CSF (PeproTech EC, UK), and antibiotic on the following day. Colonies were scored and replated every 7 days.

For human cell studies, cells were transduced as described before and kept in R10 with appropriate antibiotics until cells were plated into methylcellulose medium. Colonies were scored after 8 days of culture.

Flow Cytometric Analysis

Immunophenotypic analysis was performed by flow cytometric analysis using fluorochrome-conjugated monoclonal antibody to human CD11b (PE/Cy5 anti-human CD11b Clone ICRF44 Biolegend). Protocols and reagents used for murine cell analysis were as previously described (Yeung and So, 2009) and detailed in Supplemental Experimental Procedures.

In Vitro Drug Studies

Drug studies were carried out by pretreating cells at 3×10^3 cells/ml in R10 with different concentrations of Okadaic Acid (Sigma-Aldrich), 0, 100, 250, and 500 nM at different time points 0, 5, 10, or 20 min. After washing, cells were plated in 1 ml of methylcellulose in the absence or presence of 10^{-8} M ATRA (Sigma-Aldrich). Colony formation was examined after 8 days of incubation at 37°C in 5% CO_2.

Animals and Drug Treatment Studies

All experimental procedures were approved by King's College London and conform to the UK Home Office regulations. NOD.Cg-*Prkdc*^{scid} *Il2rg*^{tm1Wjl}/SzJ (also termed NSG) (Shultz et al., 2005) or FVB mice were used for transplantation experiments. Mice were given 2.5 Gy total body gamma-irradiation and injected intravenously with up to 1×10^5 test cells. For drug studies, all treatments commenced on the next day after injection of cells. Mice were given intraperitoneal injection of daily 1 μg ATRA/g of body weight (He et al., 1998) or/and 50 ng OKA/g of body weight every other day.

Statistical Analysis

Two-tailed Student's test was used to determine statistical significance for all bar charts. The log-rank test and Gehan-Breslow-Wilcoxon test were used to compare survival curves as previously described (Yeung et al., 2010). The p values less than 0.05 were considered statistically significant.

SUPPLEMENTAL INFORMATION

Supplemental Information includes six figures and Supplemental Experimental Procedures and can be found with this article online at http://dx.doi.org/10.1016/j.ccr.2013.02.014.

ACKNOWLEDGMENTS

We would like to thank Drs. Bernd Zeisig for technical advice and inputs, Hinrich Gronemeyer for RARα antibody and insightful discussion, Hugues de Thé for PML-RARα mutant constructs, David Grimwade and Marc Timmers for critical comments on the manuscript, Miles Houslay, David Adams, and Grazia Saturno for helpful advice on the enzymology and structural basis of PHF8/PML-RARα/ATRA interaction, members of So's lab for constructive discussion, and Pui Yi Tse for professional graphic assistance. The Leukaemia and Lymphoma Research (LLR) in the United Kingdom supported the majority of the work. The work carried out in the Helin lab was supported by the Danish Cancer Society, the Novo Nordisk Foundation, the Danish National Research Foundation, and the Excellence Program of the University of Copenhagen. M.F.A. performed all the experiments with assistance from J.-H.M. and J.Q. J.C. and K.H. supplied the PHF8 antibody. S.C.K. provided the M4 transgenic cells. C.W.E.S., M.F.A., J.-H.M., and S.D. analyzed the data. C.W.E.S. and M.F.A. wrote the manuscript with inputs from J.-H.M., S.D., and K.H. C.W.E.S. designed the overall experimental direction.

Received: May 14, 2012
Revised: November 26, 2012
Accepted: February 15, 2013
Published: March 18, 2013

REFERENCES

Abidi, F.E., Miano, M.G., Murray, J.C., and Schwartz, C.E. (2007). A novel mutation in the PHF8 gene is associated with X-linked mental retardation with cleft lip/cleft palate. Clin. Genet. *72*, 19–22.

Arrowsmith, C.H., Bountra, C., Fish, P.V., Lee, K., and Schapira, M. (2012). Epigenetic protein families: a new frontier for drug discovery. Nat. Rev. Drug Discov. *11*, 384–400.

Boukarabila, H., Saurin, A.J., Batsché, E., Mossadegh, N., van Lohuizen, M., Otte, A.P., Pradel, J., Muchardt, C., Sieweke, M., and Duprez, E. (2009). The PRC1 Polycomb group complex interacts with PLZF/RARA to mediate leukemic transformation. Genes Dev. *23*, 1195–1206.

Cheung, N., and So, C.W. (2011). Transcriptional and epigenetic networks in haematological malignancy. FEBS Lett. *585*, 2100–2111.

Côté, S., Zhou, D., Bianchini, A., Nervi, C., Gallagher, R.E., and Miller, W.H., Jr. (2000). Altered ligand binding and transcriptional regulation by mutations in the PML/RARalpha ligand-binding domain arising in retinoic acid-resistant patients with acute promyelocytic leukemia. Blood *96*, 3200–3208.

de Thé, H., and Chen, Z. (2010). Acute promyelocytic leukaemia: novel insights into the mechanisms of cure. Nat. Rev. Cancer *10*, 775–783.

Ekberg, J., Landberg, G., Holm, C., Richter, J., Wolgemuth, D.J., and Persson, J.L. (2004). Regulation of the cyclin A1 protein is associated with its differential subcellular localization in hematopoietic and leukemic cells. Oncogene *23*, 9082–9089.

Epping, M.T., Wang, L., Edel, M.J., Carlée, L., Hernandez, M., and Bernards, R. (2005). The human tumor antigen PRAME is a dominant repressor of retinoic acid receptor signaling. Cell *122*, 835–847.

Feng, W., Yonezawa, M., Ye, J., Jenuwein, T., and Grummt, I. (2010). PHF8 activates transcription of rRNA genes through H3K4me3 binding and H3K9me1/2 demethylation. Nat. Struct. Mol. Biol. *17*, 445–450.

Fortschegger, K., de Graaf, P., Outchkourov, N.S., van Schaik, F.M., Timmers, H.T., and Shiekhattar, R. (2010). PHF8 targets histone methylation and RNA polymerase II to activate transcription. Mol. Cell. Biol. *30*, 3286–3298.

Grignani, F., De Matteis, S., Nervi, C., Tomassoni, L., Gelmetti, V., Cioce, M., Fanelli, M., Ruthardt, M., Ferrara, F.F., Zamir, I., et al. (1998). Fusion proteins of the retinoic acid receptor-alpha recruit histone deacetylase in promyelocytic leukaemia. Nature *391*, 815–818.

Gronemeyer, H., Gustafsson, J.A., and Laudet, V. (2004). Principles for modulation of the nuclear receptor superfamily. Nat. Rev. Drug Discov. *3*, 950–964.

Guidez, F., Parks, S., Wong, H., Jovanovic, J.V., Mays, A., Gilkes, A.F., Mills, K.I., Guillemin, M.C., Hobbs, R.M., Pandolfi, P.P., et al. (2007). RARalpha-PLZF overcomes PLZF-mediated repression of CRABPI, contributing to retinoid resistance in t(11;17) acute promyelocytic leukemia. Proc. Natl. Acad. Sci. USA *104*, 18694–18699.

He, L.Z., Guidez, F., Tribioli, C., Peruzzi, D., Ruthardt, M., Zelent, A., and Pandolfi, P.P. (1998). Distinct interactions of PML-RARalpha and PLZF-RARalpha with co-repressors determine differential responses to RA in APL. Nat. Genet. *18*, 126–135.

Hölzel, M., Huang, S., Koster, J., Ora, I., Lakeman, A., Caron, H., Nijkamp, W., Xie, J., Callens, T., Asgharzadeh, S., et al. (2010). NF1 is a tumor suppressor in neuroblastoma that determines retinoic acid response and disease outcome. Cell *142*, 218–229.

Huang, S., Laoukili, J., Epping, M.T., Koster, J., Hölzel, M., Westerman, B.A., Nijkamp, W., Hata, A., Asgharzadeh, S., Seeger, R.C., et al. (2009). ZNF423 is critically required for retinoic acid-induced differentiation and is a marker of neuroblastoma outcome. Cancer Cell *15*, 328–340.

Kleine-Kohlbrecher, D., Christensen, J., Vandamme, J., Abarrategui, I., Bak, M., Tommerup, N., Shi, X., Gozani, O., Rappsilber, J., Salcini, A.E., and Helin, K. (2010). A functional link between the histone demethylase PHF8 and the transcription factor ZNF711 in X-linked mental retardation. Mol. Cell *38*, 165–178.

Kogan, S.C., Hong, S.H., Shultz, D.B., Privalsky, M.L., and Bishop, J.M. (2000). Leukemia initiated by PMLRARalpha: the PML domain plays a critical role while retinoic acid-mediated transactivation is dispensable. Blood *95*, 1541–1550.

Koivisto, A.M., Ala-Mello, S., Lemmelä, S., Komu, H.A., Rautio, J., and Järvelä, I. (2007). Screening of mutations in the PHF8 gene and identification of a novel mutation in a Finnish family with XLMR and cleft lip/cleft palate. Clin. Genet. *72*, 145–149.

Kooistra, S.M., and Helin, K. (2012). Molecular mechanisms and potential functions of histone demethylases. Nat. Rev. Mol. Cell Biol. *13*, 297–311.

Kouzarides, T. (2007). Chromatin modifications and their function. Cell *128*, 693–705.

Kwok, C., Zeisig, B.B., Dong, S., and So, C.W. (2006). Forced homo-oligomerization of RARalpha leads to transformation of primary hematopoietic cells. Cancer Cell *9*, 95–108.

Laumonnier, F., Holbert, S., Ronce, N., Faravelli, F., Lenzner, S., Schwartz, C.E., Lespinasse, J., Van Esch, H., Lacombe, D., Goizet, C., et al. (2005). Mutations in PHF8 are associated with X linked mental retardation and cleft lip/cleft palate. J. Med. Genet. *42*, 780–786.

Lin, R.J., and Evans, R.M. (2000). Acquisition of oncogenic potential by RAR chimeras in acute promyelocytic leukemia through formation of homodimers. Mol. Cell *5*, 821–830.

Lin, R.J., Nagy, L., Inoue, S., Shao, W., Miller, W.H., Jr., and Evans, R.M. (1998). Role of the histone deacetylase complex in acute promyelocytic leukaemia. Nature *391*, 811–814.

Liu, W., Tanasa, B., Tyurina, O.V., Zhou, T.Y., Gassmann, R., Liu, W.T., Ohgi, K.A., Benner, C., Garcia-Bassets, I., Aggarwal, A.K., et al. (2010). PHF8 mediates histone H4 lysine 20 demethylation events involved in cell cycle progression. Nature *466*, 508–512.

Loenarz, C., Ge, W., Coleman, M.L., Rose, N.R., Cooper, C.D., Klose, R.J., Ratcliffe, P.J., and Schofield, C.J. (2010). PHF8, a gene associated with cleft lip/palate and mental retardation, encodes for an Nepsilon-dimethyl lysine demethylase. Hum. Mol. Genet. *19*, 217–222.

Martens, J.H., Brinkman, A.B., Simmer, F., Francoijs, K.J., Nebbioso, A., Ferrara, F., Altucci, L., and Stunnenberg, H.G. (2010). PML-RARalpha/RXR Alters the Epigenetic Landscape in Acute Promyelocytic Leukemia. Cancer Cell *17*, 173–185.

Matthay, K.K., Reynolds, C.P., Seeger, R.C., Shimada, H., Adkins, E.S., Haas-Kogan, D., Gerbing, R.B., London, W.B., and Villablanca, J.G. (2009). Long-term results for children with high-risk neuroblastoma treated on a randomized trial of myeloablative therapy followed by 13-cis-retinoic acid: a children's oncology group study. J. Clin. Oncol. *27*, 1007–1013.

McNamara, S., Wang, H., Hanna, N., and Miller, W.H., Jr. (2008). Topoisomerase IIbeta negatively modulates retinoic acid receptor alpha function: a novel mechanism of retinoic acid resistance. Mol. Cell. Biol. *28*, 2066–2077.

Mikesch, J.H., Gronemeyer, H., and So, C.W. (2010). Discovery of novel transcriptional and epigenetic targets in APL by global ChIP analyses: Emerging opportunity and challenge. Cancer Cell *17*, 112–114.

Minucci, S., Maccarana, M., Cioce, M., De Luca, P., Gelmetti, V., Segalla, S., Di Croce, L., Giavara, S., Matteucci, C., Gobbi, A., et al. (2000). Oligomerization of RAR and AML1 transcription factors as a novel mechanism of oncogenic activation. Mol. Cell *5*, 811–820.

Qi, H.H., Sarkissian, M., Hu, G.Q., Wang, Z., Bhattacharjee, A., Gordon, D.B., Gonzales, M., Lan, F., Ongusaha, P.P., Huarte, M., et al. (2010). Histone H4K20/H3K9 demethylase PHF8 regulates zebrafish brain and craniofacial development. Nature *466*, 503–507.

Qiu, J., Shi, G., Jia, Y., Li, J., Wu, M., Li, J., Dong, S., and Wong, J. (2010). The X-linked mental retardation gene PHF8 is a histone demethylase involved in neuronal differentiation. Cell Res. *20*, 908–918.

Roussel, M.J., and Lanotte, M. (2001). Maturation sensitive and resistant t(15;17) NB4 cell lines as tools for APL physiopathology: nomenclature of cells and repertory of their known genetic alterations and phenotypes. Oncogene *20*, 7287–7291.

Sanz, M.A., and Lo-Coco, F. (2011). Modern approaches to treating acute promyelocytic leukemia. J. Clin. Oncol. *29*, 495–503.

Schenk, T., Chen, W.C., Göllner, S., Howell, L., Jin, L., Hebestreit, K., Klein, H.U., Popescu, A.C., Burnett, A., Mills, K., et al. (2012). Inhibition of the LSD1 (KDM1A) demethylase reactivates the all-trans-retinoic acid differentiation pathway in acute myeloid leukemia. Nat. Med. *18*, 605–611.

Shultz, L.D., Lyons, B.L., Burzenski, L.M., Gott, B., Chen, X., Chaleff, S., Kotb, M., Gillies, S.D., King, M., Mangada, J., et al. (2005). Human lymphoid and myeloid cell development in NOD/LtSz-scid IL2R gamma null mice engrafted with mobilized human hemopoietic stem cells. J. Immunol. *174*, 6477–6489.

Smith, L.L., Yeung, J., Zeisig, B.B., Popov, N., Huijbers, I., Barnes, J., Wilson, A.J., Taskesen, E., Delwel, R., Gil, J., et al. (2011). Functional crosstalk between Bmi1 and MLL/Hoxa9 axis in establishment of normal hematopoietic and leukemic stem cells. Cell Stem Cell *8*, 649–662.

Sternsdorf, T., Phan, V.T., Maunakea, M.L., Ocampo, C.B., Sohal, J., Silletto, A., Galimi, F., Le Beau, M.M., Evans, R.M., and Kogan, S.C. (2006). Forced retinoic acid receptor alpha homodimers prime mice for APL-like leukemia. Cancer Cell *9*, 81–94.

Villa, R., Pasini, D., Gutierrez, A., Morey, L., Occhionorelli, M., Viré, E., Nomdedeu, J.F., Jenuwein, T., Pelicci, P.G., Minucci, S., et al. (2007). Role of the polycomb repressive complex 2 in acute promyelocytic leukemia. Cancer Cell *11*, 513–525.

Wang, Z.Y., and Chen, Z. (2008). Acute promyelocytic leukemia: from highly fatal to highly curable. Blood *111*, 2505–2515.

Wang, K., Wang, P., Shi, J., Zhu, X., He, M., Jia, X., Yang, X., Qiu, F., Jin, W., Qian, M., et al. (2010). PML/RARalpha targets promoter regions containing PU.1 consensus and RARE half sites in acute promyelocytic leukemia. Cancer Cell *17*, 186–197.

Yeung, J., and So, C.W. (2009). Identification and characterization of hematopoietic stem and progenitor cell populations in mouse bone marrow by flow cytometry. Methods Mol. Biol. *538*, 301–315.

Yeung, J., Esposito, M.T., Gandillet, A., Zeisig, B.B., Griessinger, E., Bonnet, D., and So, C.W. (2010). β-Catenin mediates the establishment and drug resistance of MLL leukemic stem cells. Cancer Cell *18*, 606–618.

Zeisig, B.B., and So, C.W. (2009). Retroviral/Lentiviral transduction and transformation assay. Methods Mol. Biol. *538*, 207–229.

Zeisig, B.B., Kwok, C., Zelent, A., Shankaranarayanan, P., Gronemeyer, H., Dong, S., and So, C.W. (2007). Recruitment of RXR by homotetrameric RARalpha fusion proteins is essential for transformation. Cancer Cell *12*, 36–51.

Zeisig, B.B., Kulasekararaj, A.G., Mufti, G.J., and So, C.W. (2012). Acute Myeloid Leukemia: Snapshot. Cancer Cell *22*, 698.

Zhu, J., Nasr, R., Pérès, L., Riaucoux-Lormière, F., Honoré, N., Berthier, C., Kamashev, D., Zhou, J., Vitoux, D., Lavau, C., and de Thé, H. (2007). RXR is an essential component of the oncogenic PML/RARA complex in vivo. Cancer Cell *12*, 23–35.

Cancer Cell
Article

Complementary Genomic Screens Identify SERCA as a Therapeutic Target in *NOTCH1* Mutated Cancer

Giovanni Roti,[1,3] Anne Carlton,[1,3] Kenneth N. Ross,[4] Michele Markstein,[5] Kostandin Pajcini,[6,7] Angela H. Su,[1,3] Norbert Perrimon,[8,11] Warren S. Pear,[6,7] Andrew L. Kung,[12] Stephen C. Blacklow,[2,9] Jon C. Aster,[10] and Kimberly Stegmaier[1,3,4,*]

[1]Department of Pediatric Oncology
[2]Cancer Biology Program
Dana-Farber Cancer Institute, Boston, MA 02215, USA
[3]Division of Hematology/Oncology, Boston Children's Hospital, Boston, MA 02115, USA
[4]Broad Institute of Harvard and Massachusetts Institute of Technology, Cambridge, MA 02142, USA
[5]Department of Biology, University of Massachusetts Amherst, Amherst, MA 01003, USA
[6]Abramson Family Cancer Research Institute
[7]Department of Pathology and Laboratory Medicine
University of Pennsylvania, Philadelphia, PA 19104, USA
[8]Department of Genetics
[9]Department of Biological Chemistry and Molecular Pharmacology
[10]Department of Pathology, Brigham & Women's Hospital
[11]Howard Hughes Medical Institute
Harvard Medical School, Boston, MA 02115, USA
[12]Department of Pediatrics, Columbia University Medical Center, New York, NY 10032, USA
*Correspondence: kimberly_stegmaier@dfci.harvard.edu
http://dx.doi.org/10.1016/j.ccr.2013.01.015

SUMMARY

Notch1 is a rational therapeutic target in several human cancers, but as a transcriptional regulator, it poses a drug discovery challenge. To identify Notch1 modulators, we performed two cell-based, high-throughput screens for small-molecule inhibitors and cDNA enhancers of a *NOTCH1* allele bearing a leukemia-associated mutation. Sarco/endoplasmic reticulum calcium ATPase (SERCA) channels emerged at the intersection of these complementary screens. SERCA inhibition preferentially impairs the maturation and activity of mutated Notch1 receptors and induces a G_0/G_1 arrest in *NOTCH1*-mutated human leukemia cells. A small-molecule SERCA inhibitor has on-target activity in two mouse models of human leukemia and interferes with Notch signaling in *Drosophila*. These studies "credential" SERCA as a therapeutic target in cancers associated with *NOTCH1* mutations.

INTRODUCTION

Selective expression of transcription factors directs the hierarchical specification of the hematopoietic lineage, and acquired mutations that perturb the function of these factors have a central role in leukemia pathogenesis. A prime example involves Notch1, a surface receptor that is essential for T-cell progenitor specification and maturation. Acquired mutations that activate Notch1 are found in 40% to 70% of childhood and adult T-cell acute lymphoblastic leukemia (T-ALL) (Lee et al., 2005; Mansour et al., 2006; Weng et al., 2004). Moreover, recent reports identified *NOTCH1* activating mutations in 10%–15% of chronic lymphocytic leukemia (CLL) (Di Ianni et al., 2009; Puente et al., 2011) and mantle cell lymphoma (Kridel et al., 2012).

Notch receptors regulate many aspects of normal development and tissue homeostasis (reviewed in Kopan and Ilagan,

Significance

Notch1 is aberrant in many malignancies, with both gain and loss-of-function mutations reported, highlighting the need for therapies selectively targeting mutant Notch1 receptors. T cell acute lymphoblastic leukemia (T-ALL), a high-risk leukemia in need of better treatment approaches, is one disease notable for frequent, activating mutations in *NOTCH1*. In this study, we identify SERCA inhibition as an approach to selectively impair the maturation of mutant Notch1 receptors in T-ALL and demonstrate the antileukemia activity of this strategy both in vitro and in vivo. With increasing evidence of SERCA mutations in hereditary diseases and cancer, our study also suggests that aberrant SERCA activity might contribute to diseases linked to altered Notch signaling.

2009). Mammalian Notch receptors are processed during maturation by a furin-like protease, leading to the formation of two, noncovalently associated subunits. Signaling is normally initiated by binding of the Notch ectodomain to a ligand of the DSL family expressed on a neighboring cell. This interaction triggers two additional, successive proteolytic cleavages in the Notch transmembrane subunit. The first, mediated by ADAM-10 or ADAM-17 (Brou et al., 2000), occurs within a juxtamembrane negative regulatory region (NRR) at a site that is protected in the Notch *off* state (Gordon et al., 2009; Gordon et al., 2007). This cleavage within the Notch transmembrane domain creates a short-lived intermediate that is primed for secondary cleavage by the γ-secretase complex, an event that liberates the intracellular domain of Notch1 (ICN). ICN translocates to the nucleus, associates with the DNA-binding factor RBPJ, and recruits coactivators of the Mastermind-like (MAML) family to activate expression of target genes.

Each of the proteolytic steps involved in the activation of Notch receptors is a potential therapeutic target. Indeed, γ-secretase inhibitors (GSIs) have anti-T-ALL activity in vitro (Weng et al., 2004) and in vivo (Cullion et al., 2009; Real et al., 2009). The GSI MK-0752 was tested in a phase I clinical trial in patients with relapsed acute leukemia (DeAngelo et al., 2006). This trial was halted, however, due to gastrointestinal toxicity thought to be related to chronic pan-Notch receptor inhibition in gut progenitor cells (Wong et al., 2004). Thus, other approaches to Notch1 inhibition are desirable.

Historically, it has been difficult to develop high-throughput assays for small molecules that disrupt protein-DNA or protein-protein interactions (Darnell, 2002). Recently, there has been renewed interest in cell-based screening to address the problem of ''undruggable'' targets using various approaches (Carpenter, 2007; Inglese et al., 2007; Stegmaier et al., 2004). Gene expression-based high-throughput screening (GE-HTS) is a chemical genomic approach in which gene expression signatures serve as surrogates for cellular states (Hahn et al., 2008; Stegmaier et al., 2004). One application of GE-HTS is for the identification of small molecules that modulate transcriptional signatures produced by aberrantly activated transcription factors (Corsello et al., 2009). A limitation of cell-based assays is that identifying the biologically relevant target of the small molecule can be a daunting task. One way to overcome this challenge is to design multiple, integrated cell-based screens and then to focus on common emerging hits. With the availability of genome-scale cDNA collections, overexpression screens have also proven to be powerful tools to probe biological pathways and to identify the protein targets of small molecules. Here, we used complementary GE-HTS and cDNA overexpression screens to search for small-molecule modulators of Notch1 signaling in T-ALL.

RESULTS

Development of a GE-HTS Assay for Notch1 Inhibitors

Figure 1A outlines our approach. We first defined a robust Notch1 transcriptional signature for the GE-HTS assay. We selected a set of genes that defined the Notch1 activation state from genomewide expression profiling of seven *NOTCH1*-mutated T-ALL cell lines treated with the GSI compound E (Cpd E) (Palomero et al., 2006b). From a set of approximately 500 genes with differences of $p < 0.01$ by two-sided Student's t test, 28 genes with mean fold changes > 1.5 between the Notch1 *on* versus *off* states (Figure 1B) and four invariant control genes were selected and validated (Figure S1A available online). To confirm that the signature reports on Notch1 inhibition and not GSI treatment per se, we transduced DND41 cells with Notch1-specific shRNA and demonstrated induction of the Notch1 *off* signature (Figures S1B–S1D). This is consistent with prior work in which we showed that GE-HTS identified a Notch1 *off* signature in T-ALL cells treated with a Notch1-specific inhibitory antibody (Aste-Amézaga et al., 2010). To ensure that the signature does not identify generic growth inhibitors or cellular toxins, we treated DND41 cells with drugs known to be active against T-ALL cells. These drugs inhibited growth but did not induce the Notch1 *off* signature (Figures S1E–S1F).

Identification of Small Molecules that Modulate Notch1

We screened 3,801 drugs or drug-like compounds in the human T-ALL cell line DND41. GE-HTS data were collected after 72 hr of treatment as previously described (Peck et al., 2006). Because true-positives are more likely to score by multiple scoring metrics, we applied a consensus classification system requiring hits to score in multiple algorithms: summed score, weighted summed score, K-nearest neighbor, naive Bayes classification, and support vector machine (Figure 1C; Figure S1G) (Banerji et al., 2012). A total of 16 compounds (Table S1) selected for validation based on these criteria were retested in a 2-fold dose-response series in DND41, MOLT4, and PF382 cell lines. Notably, multiple compounds reported to modulate calcium ion flux scored as dose-dependent Notch pathway inhibitors in all of the cell lines tested (Figures S1H–S1J).

A cDNA Library Screen Identifies SERCA as a Notch Signaling Enhancer

A complementary cDNA library screen for factors that enhance the signaling activity of the Notch1 mutant L1601PΔP was simultaneously conducted in the osteosarcoma cell line U2OS. L1601PΔP contains the same heterodimerization mutation that is present in the MOLT4 and KOPTK1 cell lines in *cis* with a PEST domain deletion (Chiang et al., 2008), a combination that is found in approximately 10%–15% of human T-ALL (Weng et al., 2004). U2OS cells were selected for the screen because they are readily transfected and have very low basal Notch signaling tone, a feature that produces favorable signal-to-noise ratios. A total of 18,000 open reading frames were scored for their ability to enhance L1601PΔP-dependent activation of a Notch luciferase reporter. Among the top hits were *ATP2A1*, *ATP2A2*, and *ATP2A3* (Figure 1D), which encode SERCA1, SERCA2, and SERCA3, respectively. Sarco/endoplasmic reticulum calcium ATPases (SERCAs) are closely related, inwardly directed, ATP-dependent calcium pumps that localize to the endoplasmic reticulum (ER). Retesting confirmed that *ATP2A2* and *ATP2A3* potentiate L1601PΔP-dependent signaling (Figure 1E). Of note, loss-of-function mutations in a *Drosophila* SERCA homolog, Ca-P60A, have been reported to produce Notch loss-of-function phenotypes in this model organism by altering Notch trafficking (Periz and Fortini, 1999).

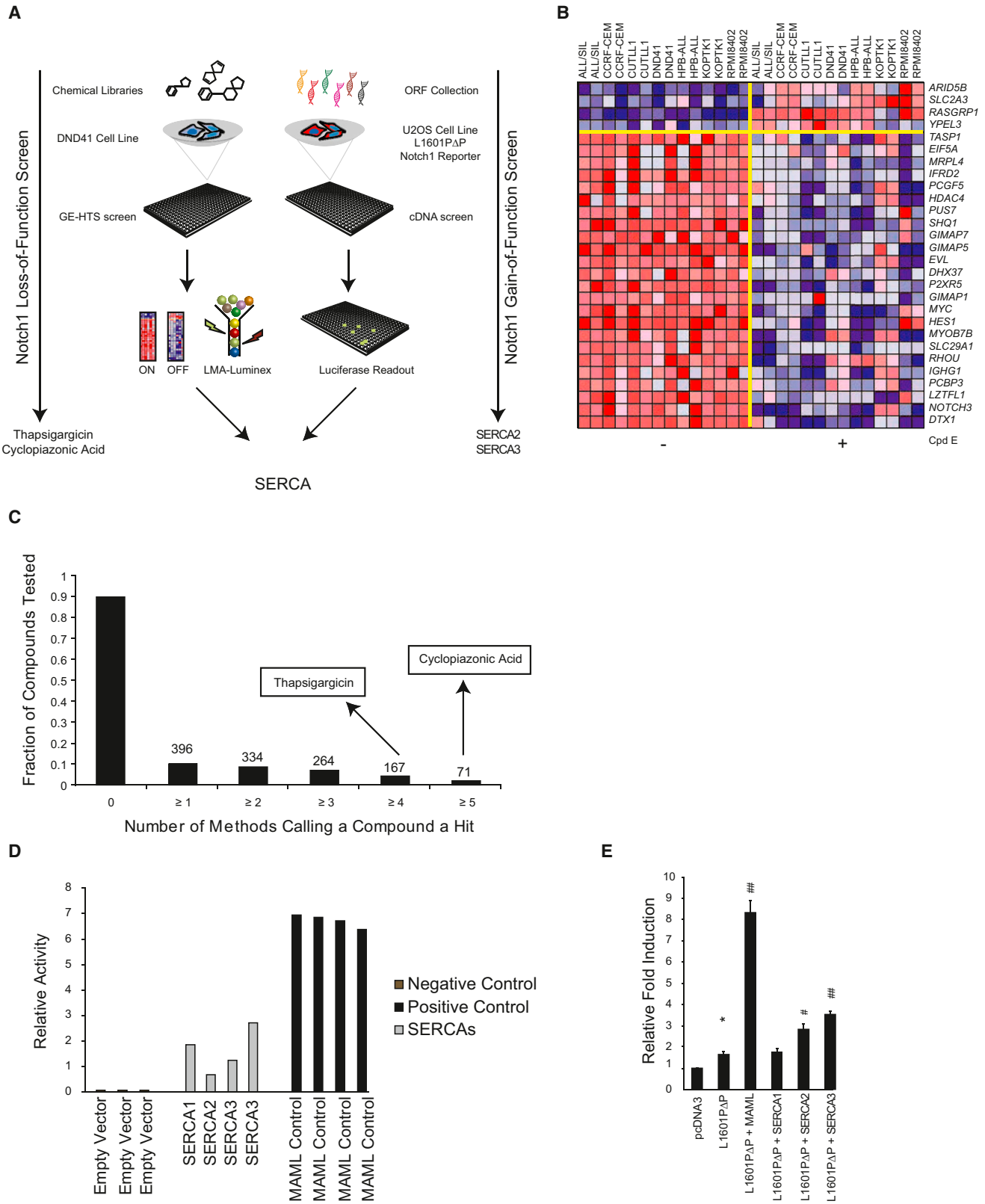

Figure 1. Identification of SERCA at the Intersection of Two High-Throughput Screens

(A) Notch1 inhibitory modulators were identified using GE-HTS in DND41 cells, and these results were integrated with results from a cDNA library screen for factors enhancing the signaling activity of the leukemogenic *NOTCH1* allele, L1601PΔP. ORF, open reading frame; LMA, ligation-mediated amplification.

(legend continued on next page)

Thus, calcium modulators emerged at the nexus of two complementary screens.

Thapsigargin Targets the Notch Pathway

One of the small molecules that scored in our GE-HTS screen across four scoring metrics was thapsigargicin, an analog of thapsigargin, a highly potent natural product inhibitor of SERCA. Low nanomolar concentrations of thapsigargin induced the Notch1 *off* signature in a dose-dependent fashion in *NOTCH1* mutant T-ALL cells (Figure 2A) and reduced the expression of the direct Notch1 target genes *MYC*, *HES1*, and *DTX1* (Figure 2B). Subnanomolar concentrations of thapsigargin also inhibited the expression of a Notch reporter by L1601PΔP in U2OS cells (Figure 2C).

Notch1 inhibition results in G_0/G_1 arrest in human T-ALL cells (Weng et al., 2004) and decreased T-ALL cell size (Palomero et al., 2006b; Weng et al., 2006). As expected, thapsigargin also induced a G_0/G_1 arrest (Figure 3A) and a decrease in cell size (Figure 3B) in *NOTCH1*-mutated T-ALL cell lines. We next studied the effect of thapsigargin in a panel of T-ALL cell lines that contain activating mutations in the heterodimerization domain (HD) of Notch1 and/or deletions in the degradation domain (PEST). Three T-ALL cell lines reported to be highly sensitive to GSI (ALL/SIL, DND41, and KOPTK1) were more sensitive to thapsigargin as measured by inhibition of cell growth and induction of apoptosis compared to two cell lines with intermediate sensitivity to GSI (MOLT4 and PF382) (Figure 3C). Furthermore, 24 hr of thapsigargin treatment decreased ICN1 levels in T-ALL cells (Figure 4A). As a further test of the idea that thapsigargin acts by preventing Notch1 activation, the Notch1-dependent T-ALL cell lines MOLT4 and DND41 were transduced with an empty MigR1 vector or with MigR1-ICN1 (Figure 4B). Transduction of ICN1, which lies downstream of the γ-secretase cleavage step in Notch activation, prevented induction of the Notch1 *off* signature (Figure 4C), growth inhibition (Figure 4D), G_0/G_1 cell cycle arrest (Figure 4E), and induction of apoptosis (Figure 4F) by thapsigargin. In contrast, empty MigR1 had no effect on these readouts of Notch inhibition. These results are consistent with a Notch pathway inhibitory effect of thapsigargin at low nanomolar concentrations.

Thapsigargin Interferes with Notch1 Maturation

Multiple compounds scoring in our screen, including thapsigargin, are predicted to alter intracellular calcium. For example, thapsigargin and cyclopiazonic acid are known Ca^{2+}ATPase inhibitors, impairing calcium entry into the ER. Of note, multiple EGF repeats and all three Lin12/Notch repeats in the extracellular domains of Notch receptors require calcium ions for proper folding (Aster et al., 1999; Gordon et al., 2007; Hambleton et al., 2004; Rand et al., 1997). We thus hypothesized that thapsigargin, by altering ER Ca^{2+} concentrations, would inhibit Notch1 maturation in T-ALL cells.

To test this hypothesis, we first determined if thapsigargin affected furin processing of Notch1, an event that occurs in the late Golgi compartment. Lysates from T-ALL cell lines treated with thapsigargin were immunoblotted with an antibody specific for the cytoplasmic portion of Notch1 that recognizes both unprocessed Notch1 (~270 kDa) and the furin-processed transmembrane subunit (~110 kDa). Thapsigargin reduced the levels of the furin-processed transmembrane Notch1 subunit, but not the unprocessed full-length Notch1 precursor, in multiple T-ALL cell lines (Figure 5A). Similar results were observed with the less potent SERCA inhibitor cyclopiazonic acid (Figure S2). Misfolded Notch1 receptors are expected to be retained in the ER/Golgi compartment. Immunostaining revealed that thapsigargin treatment reduced the levels of Notch1 on the cell surface (Figures 5B and 5C) and resulted in the colocalization of Notch1 and giantin, a Golgi membrane protein (Figure 5D). Thus, thapsigargin leads to defective Notch1 maturation in cultured T-ALL cells.

SERCA Antagonism Inhibits Notch Function and T-ALL Growth In Vivo

To confirm that chemical and genetic inhibition of SERCA lead to Notch inactivation in vivo, we evaluated a *Drosophila* intestinal stem cell model in which Notch inhibition perturbs differentiation. The adult midgut is maintained by pluripotent stem cells that give rise to two populations of terminally differentiated daughter cells: a large class of polyploid enterocyes (EC) and a smaller class of diploid enteroendocrine (ee) cells (Micchelli and Perrimon, 2006; Ohlstein and Spradling, 2007). The stem cells express escargot (esg), a transcription factor, and Delta, a membrane-bound ligand of the Notch receptor. High levels of Notch activation are required for daughter cells to adopt the EC cell fate, whereas lower levels of Notch activation specify daughters to adopt the ee fate. Thus, when Notch is completely inhibited, daughter cells fail to differentiate and remain as stem cells. By contrast, when Notch signaling is partially inhibited, daughter cells fail to differentiate into ECs and remain as stem cells or differentiate into ee cells.

To enhance the sensitivity of fly-based drug assays, we used transgenic flies that express a human *RAF* gain-of-function cDNA, *RAF*(gof), in their intestinal stem cells. Expression of the *RAF*(gof) cDNA results in rapid expansion of the esg+ population,

(B) Notch1 *off* signature genes derived from the expression profiling of T-ALL cell lines treated with Cpd E. The columns represent individual cell lines treated in duplicate with Cpd E (0.5 μM) or vehicle for 24 hr. The rows represent the 28 genes selected for the Notch *off* signature. Dark red indicates high gene expression, and dark blue indicates low gene expression by Affymetrix microarray profiling.

(C) The x axis indicates the number of methods (summed score, weighted summed score, naive Bayes, K-nearest neighbor, and support vector machine), and the y axis the fraction of chemicals that scored for the number of methods. SERCA inhibitors are indicated. The number of compounds scoring by the indicated number of methods is noted above each column.

(D) Notch1 gain-of-function primary screen data for the negative (empty vector) and positive (MAML) controls versus SERCA-encoding cDNAs hits. Depicted is the fold induction of luciferase signal for each replicate normalized to the population median of reporter readout values of pcDNA3-L1601PΔP (n = 184).

(E) Retesting of cDNAs scoring in the Notch-sensitive luciferase reporter. Luciferase activity is expressed as relative activity compared to the pcDNA3 control. Errors bars denote the mean ± SD of 10 replicates. Statistical significance relative to pcDNA3 ($^{*}p < 0.05$) and to pcDNA3-L1601PΔP ($^{\#}p < 0.05$; $^{\#\#}p < 0.01$) was determined by Student's t test.

See also Figure S1 and Table S1.

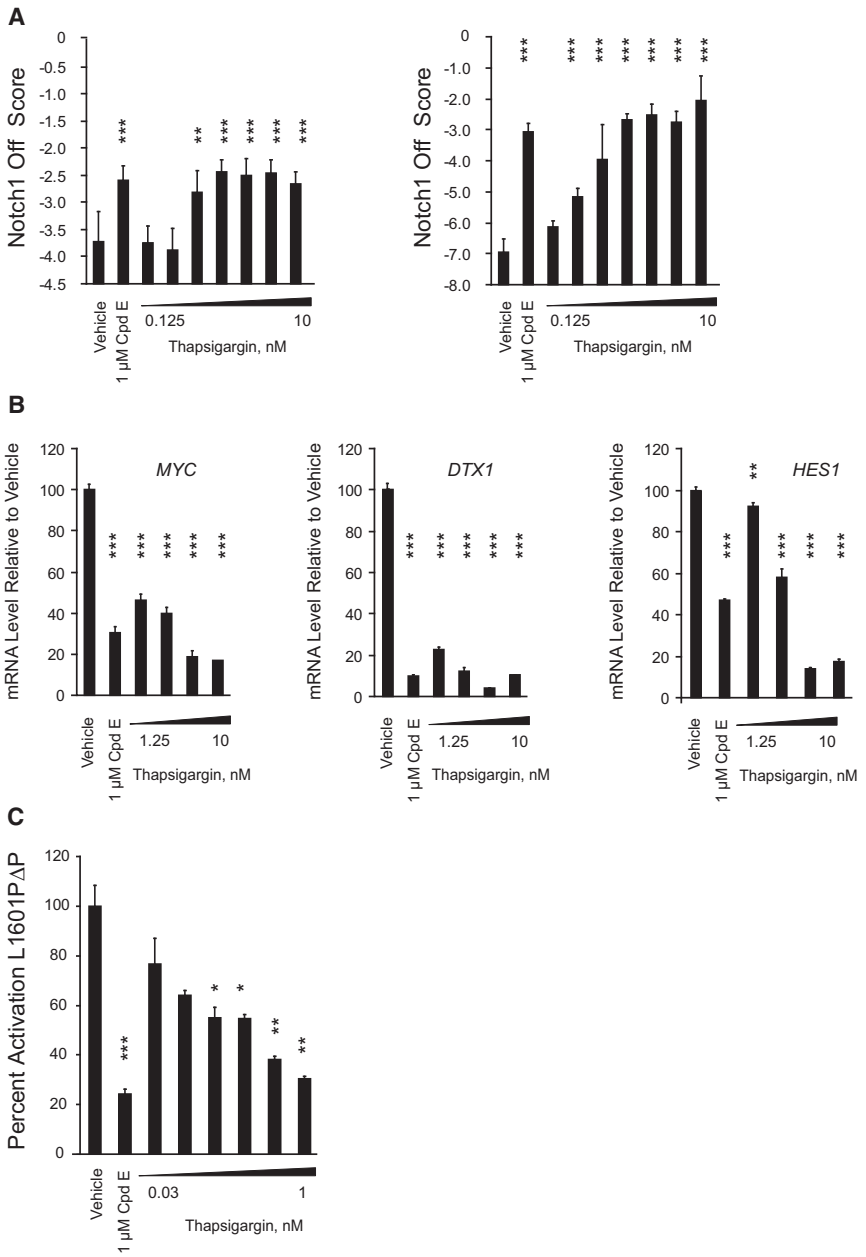

Figure 2. Validation of SERCA as a Notch1 Modulator

(A) Induction of the Notch1 *off* score (weighted summed score) measured by GE-HTS in DND41 (left) and MOLT4 (right) cells treated with thapsigargin in 2-fold dilution for 72 hr. Error bars denote the mean ± SD of 12 replicates for vehicle-treated (DMSO 0.06%) cells and six replicates for thapsigargin-treated cells.

(B) Expression of indicated Notch1 target genes in DND41 treated in 2-fold dliution for 24 hr was determined by quantitative RT-PCR. Error bars indicate the mean ± SD of three replicates. Data were analyzed using the ΔΔCT method and plotted as a percentage relative to the control gene *RPL13A*.

(C) Effects of thapsigargin on the activation of a Notch1 luciferase reporter by L1601PΔP in U2OS cells. Normalized luciferase activity relative to a Renilla control was expressed as a percentage of vehicle treatment. Error bars denote mean ± SD of four replicates. Statistical significance (*$p < 0.05$; **$p < 0.01$; ***$p < 0.001$) in all panels was determined by one-way analysis of variance (ANOVA) using Bonferroni's correction for multiple comparison testing.

which is composed of not only diploid stem cells but also polyploid EC daughter cells. When Notch is inhibited by feeding flies either DAPT or Cpd E, both GSIs, stem cell daughters fail to differentiate into EC cells and instead give rise mostly to additional stem cells, as well as some ee daughters (Figure 6A). Cyclopiazonic acid and thapsigargin treatment also expanded the stem cell and ee cell populations, thus phenocopying the effects of GSI (Figure 6B).

If thapsigargin inhibits Notch signaling through effects on calcium channels, then genetic modulation of SERCA should produce similar phenotypes. Indeed, knockdown of Ca-P60A, the only SERCA expressed in *Drosophila*, produced effects on stem cell and ee cell pools similar to those induced by GSI, thapsigargin, or cyclopiazonic acid treatment (Figure 6C). Thus, the results of chemical and genetic studies are consistent with a model in which SERCA inhibition by thapsigargin impairs Notch signaling in vivo.

We next tested thapsigargin in a human T-ALL xenograft model. Systemic administration of thapsigargin to SCID-beige mice bearing MOLT-4 tumors inhibited tumor growth compared to vehicle-treated controls (Figure 6D). In addition, ICN1 protein levels were diminished in the thapsigargin-treated tumors compared to vehicle-treated tumors (Figures 6E and S3A), linking growth inhibition to Notch inhibition.

To demonstrate further that thapsigargin impairs leukemic progression via Notch signaling inhibition, we established a second T-ALL xenograft model in which DND41 cells were transduced with MigR1 or MigR1-ICN1 and subsequently propagated in NSG mice. Thapsigargin treatment markedly decreased the growth of control tumors but had little effect on tumors expressing ICN1 (Figures 6F and 6G), indicating that tumor growth suppression by thapsigargin is mediated by inhibition of Notch1 signaling in the leukemic cells.

Prior studies demonstrated that gastrointestinal toxicity and lack of sustained response were the major limitations of first-generation GSIs (DeAngelo et al., 2006). It was hypothesized that gastrointestinal toxicity was due to blockade of wild-type Notch1 and Notch2 in the gut leading to intestinal secretory metaplasia, increased number of goblet cells, and arrested proliferation in the crypts of the small intestine (Milano et al., 2004;

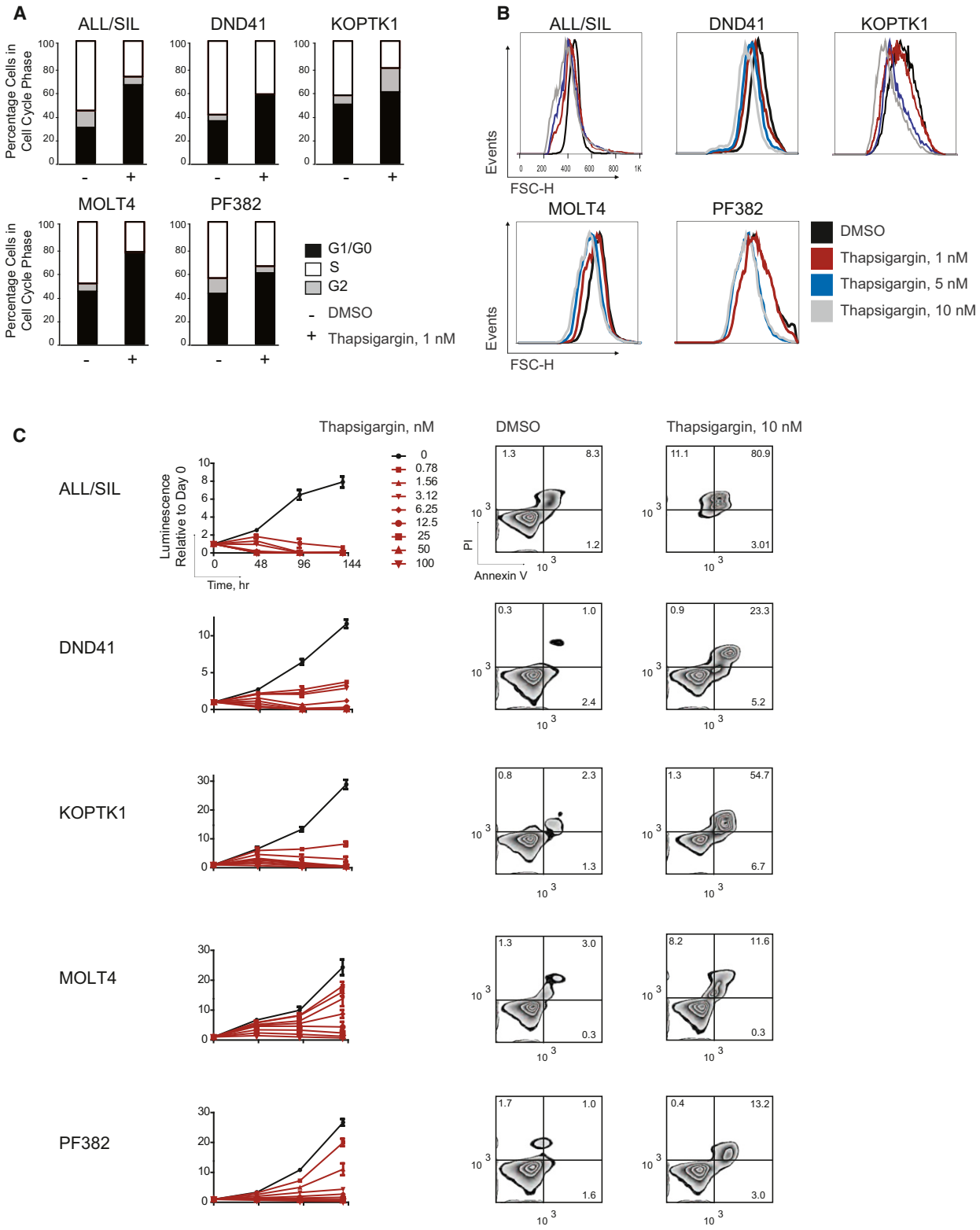

Figure 3. Thapsigargin Demonstrates Anti-Notch1 and Antileukemia Properties in T-ALL In Vitro

(A) Effect of thapsigargin treatment (6 days) on cell cycle of T-ALL cell lines, as assessed by measurement of DNA content on the viable fraction of cells.

(B) Effect of thapsigargin treatment for 24 hr on cell size as measured by forward-scatter flow cytometry.

(C) Effect of thapsigargin treatment on cell growth (left) and induction of apoptosis (right). Error bars denote mean ± SD of four replicates. Annexin V/PI staining of T-ALL cells following 72 hr of treatment with 10 nM thapsigargin.

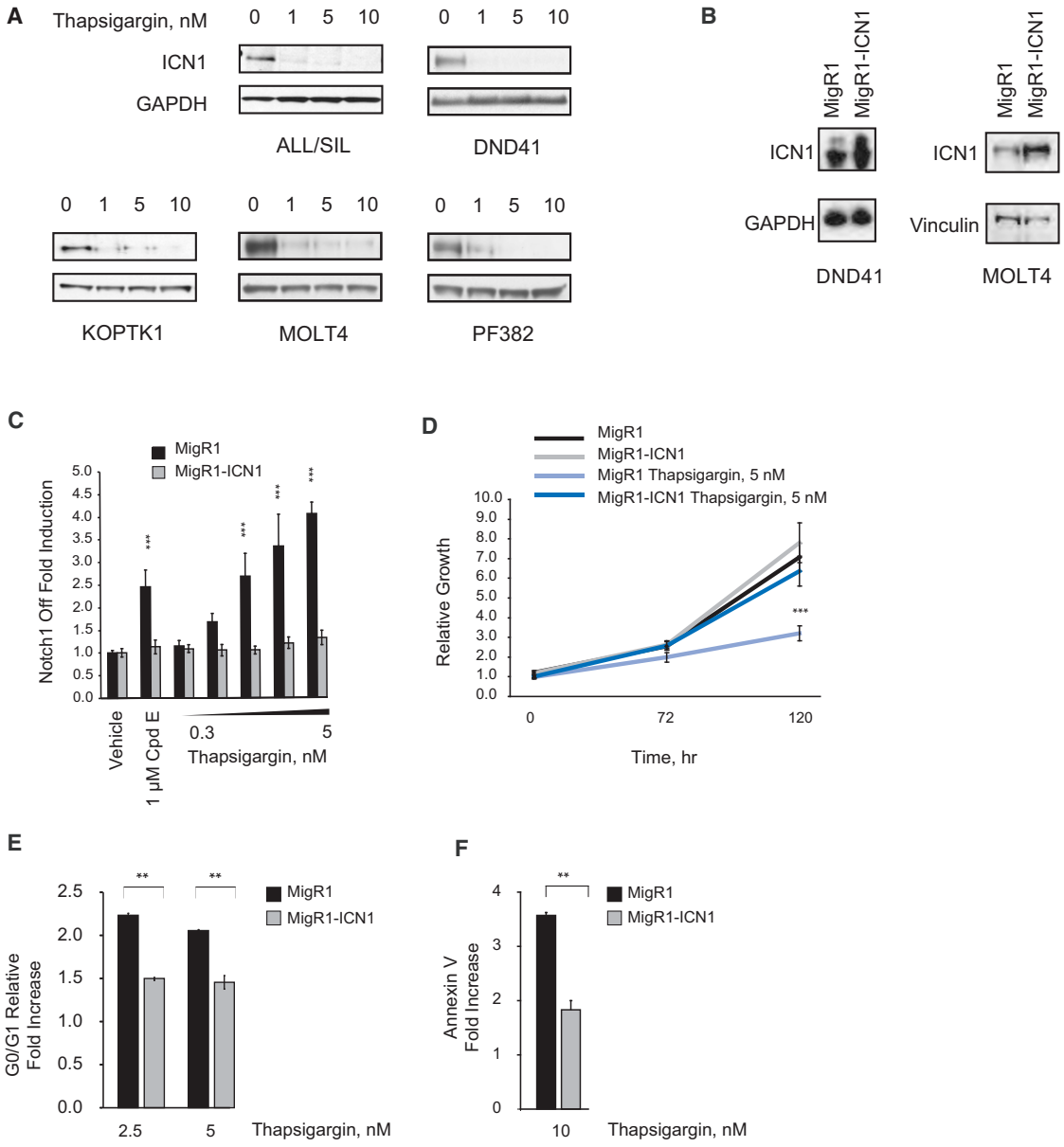

Figure 4. Thapsigargin Demonstrates Notch1 On-Target Activity In Vitro

(A) Effect of 24 hr of thapsigargin treatment on the ICN1 level in T-ALL cells. The immunoblot was stained with anti-ICN1 antibody.

(B) ICN1 level in MigR1- or MigR1-ICN1-transduced cells. ICN1 is detected using an anti-ICN1 antibody.

(C) The weighted summed score fold induction is shown for the Notch1 *off* signature after treatment of cells with thapsigargin or Cpd E for 48 hr. Error bars indicate the mean ± SD of 12 replicates for vehicle-treated and six replicates for GSI- or thapsigargin-treated cells. Statistical significance (***$p < 0.001$) was determined by one-way ANOVA using Bonferroni's correction for multiple comparison testing.

(D) Effect of thapsigargin on the growth of MigR1- or MigR1-ICN1-transduced DND41 cells. Normalized data are plotted relative to time 0. Error bars indicate mean ± SD of four replicates. Statistical significance (***$p < 0.001$) was determined by two-way ANOVA with Bonferroni's correction for multiple comparison testing.

(E) Effect of 3 days of thapsigargin treatment on DNA content of MigR1- or MigR1-ICN1-transduced MOLT4 cells. Error bars indicate mean ± SD of two replicates with results expressed relative to vehicle treatment. Statistical significance was determined by Student's t test (**$p < 0.01$).

(F) Effect of 3 days of thapsigargin treatment on apoptosis of MigR1- or MigR1-ICN1-transduced DND41 cells. Error bars indicate mean ± SD of two replicates with results expressed relative to vehicle. Statistical significance was determined by Student's t test (**$p < 0.01$).

Real et al., 2009). Mice treated with thapsigargin did not develop gastrointestinal toxicity (Figures S3B and S3C), suggesting that HD-mutated Notch1 receptors were more sensitive to the effects of thapsigargin than wild-type Notch1/Notch2 receptors expressed in normal cells. These preclinical studies support SERCA as a possible therapeutic target in T-ALL.

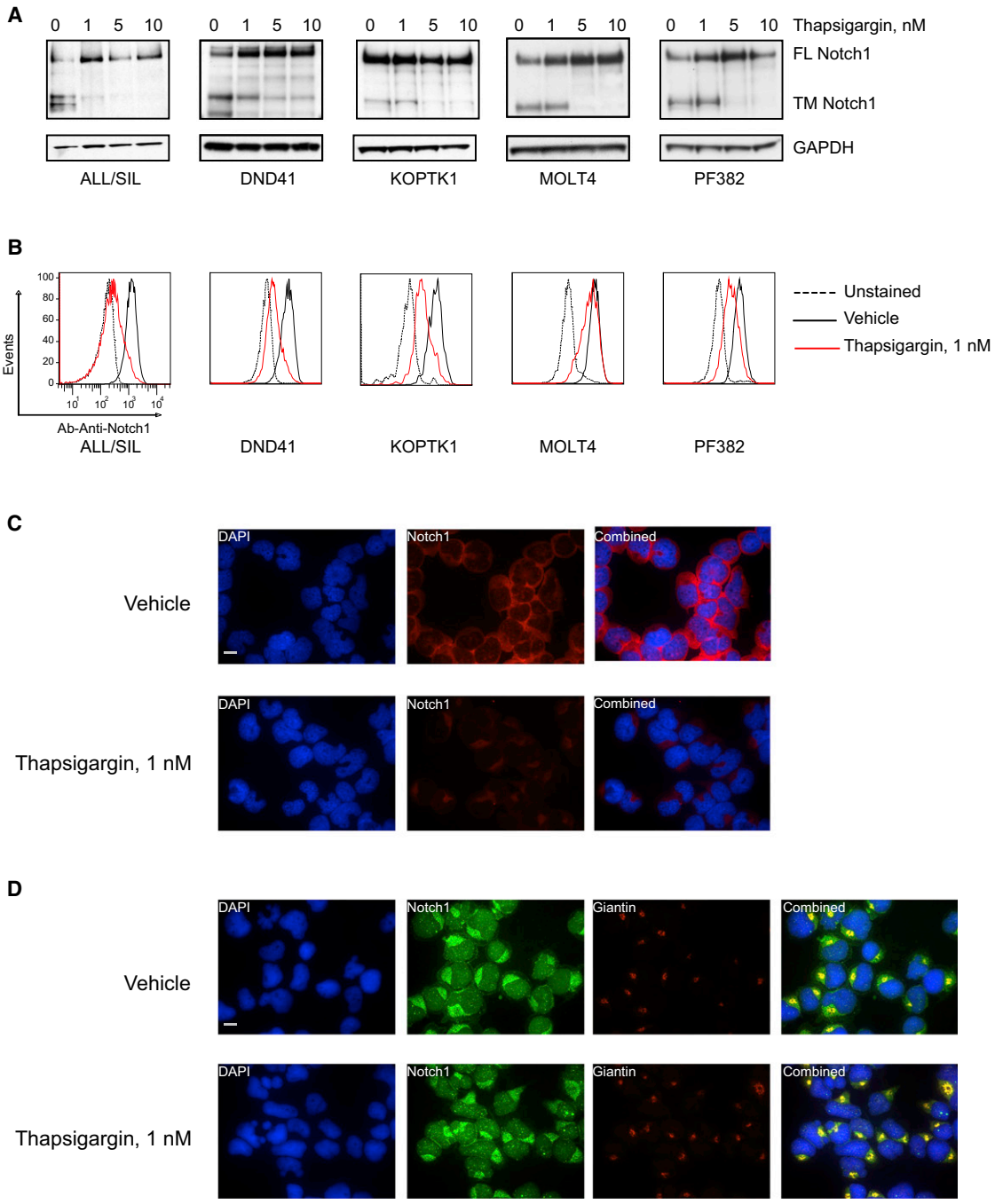

Figure 5. Thapsigargin Impairs Notch1 Maturation in T-ALL Cell Lines

(A) Effect of thapsigargin treatment (24 hr) on Notch1 processing in T-ALL cell lines all with HD mutations, DND41 and ALL/SIL (L1594PΔPEST), KOPTK1 and MOLT4 (L1601PΔPEST), and PF382 (L1575PΔPEST). The blot was stained with an antibody against the C terminus of Notch1 that recognizes both the furin-processed Notch1 transmembrane subunit (TM) and the unprocessed Notch1 precursor (FL).

(B and C) Effect of thapsigargin treatment (24 hr) on Notch1 cell surface staining, as assessed by flow cytometry (B) and staining of nonpermeabilized cells (C). Scale bar, 10 μm.

(D) Effect of thapsigargin treatment (24 hr) on the subcellular localization of Notch1. Double-immunofluorescence staining of permeabilized DND41 cells stained with anti-Notch1 (green) and Giantin (red) is shown. Colocalization is indicated by yellow signal. Scale bar, 10 μm.

See also Figure S2.

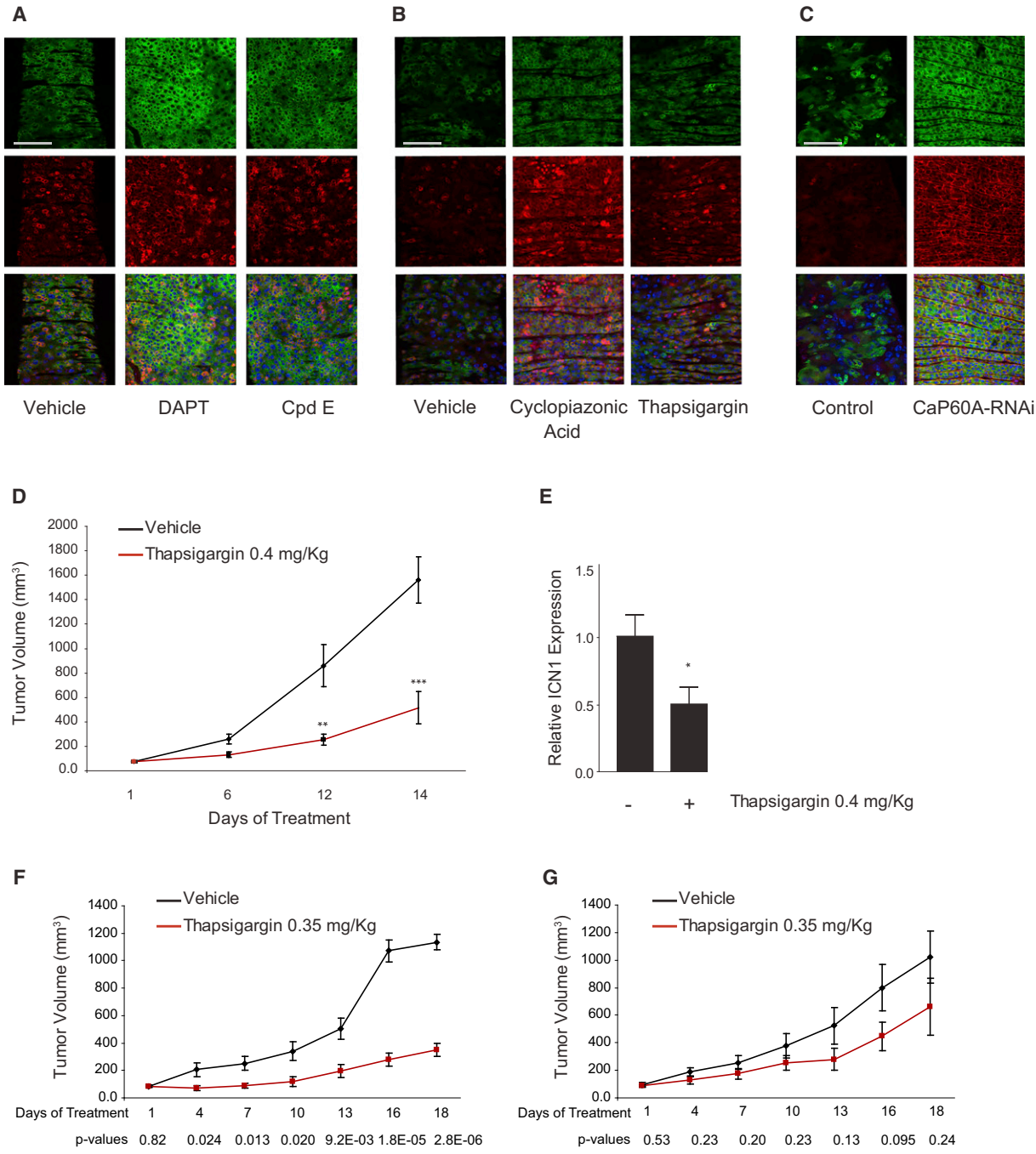

Figure 6. SERCA Inhibition Causes Notch Loss-of-Function In Vivo

(A–C) Immunofluorescence staining of *Drosophila* midguts expressing GFP (green) and stained with anti-Delta (membrane red), antiprospero (nuclear red), and DAPI (blue) is depicted. Treatment was with DAPT (400 μM) or Cpd E (100 μM) for 7 days in (A) and with cyclopiazonic acid (1 mM) or thapsigargin (100 μM) for 7 days in (B). In (C), effects of knockdown of Ca-P60A are shown. Scale bars, 75 μm.

(D) Effect of thapsigargin on the growth of xenografted MOLT4 tumors. Error bars indicate mean ± SD of six replicates for the thapsigargin-treated and nine replicates for the vehicle-treated mice. Statistical significance (**$p < 0.01$; ***$p < 0.001$) was determined by two-way ANOVA using Bonferroni's correction for multiple comparison testing.

(E) Effect of thapsigargin treatment on ICN1 levels in xenografted MOLT4 tumors was measured by western blotting, and statistical significance was determined by Student's t test (*$p < 0.05$). Error bars represent the mean ± SD of six replicates for each group.

(F and G) Effect of thapsigargin on the growth of DND41 cells transduced with MigR1 (F) or MigR1-ICN1 (G) xenografted in NSG mice. Error bars indicate mean ± SD of replicates for each cohort. Statistical significance was determined by Student's t test as indicated.

See also Figure S3.

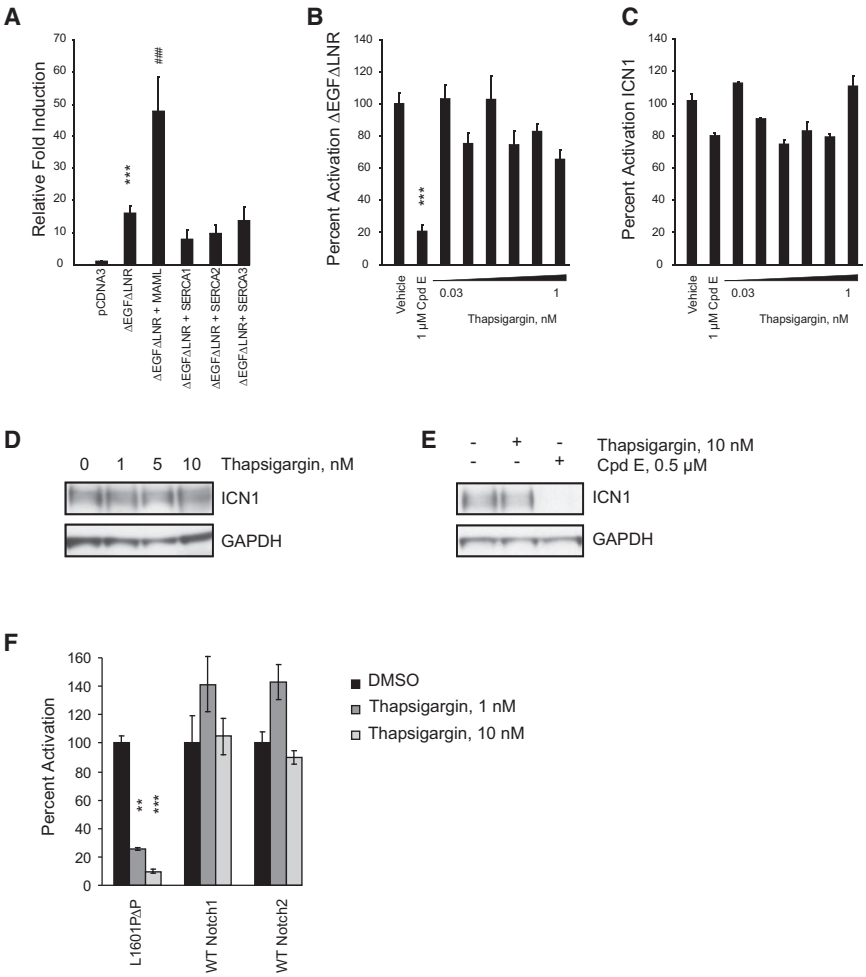

Figure 7. Notch1 Ca^{2+} Binding Modules Are Required for the Anti-Notch1 Activity of Thapsigargin

(A) Effect of SERCA coexpression on the activity of ΔEGFΔLNR in a Notch reporter assay. Normalized firefly luciferase activity was expressed as fold induction relative to the empty plasmid. Error bars denote the mean ± SD of 10 replicates. Statistical significance relative to pcDNA3 (***$p < 0.001$) and to pcDNA3-ΔEGFΔLNR ($^{###}p < 0.001$) was determined by one-way ANOVA using Bonferroni's correction for multiple comparison testing.

(B and C) Effects of thapsigargin or Cpd E on the activity of ΔEGFΔLNR (B) and ICN1 (C) in a Notch reporter assay. Assay conditions and interpretations were as in (A). Errors bars denote mean ± SD of four replicates. Statistical significance (***$p < 0.001$) was determined by one-way ANOVA using Bonferroni's correction for multiple comparison testing.

(D and E) The ICN1 protein level in SUPT1 cells treated for 24 hr as indicated was determined using immunoblots stained with anti-ICN1 antibody.

(F) Ligand-mediated activation of Notch activity was determined using U2OS cells stably (Notch1 and Notch2) or transiently (L1601PΔP) expressing Notch-Gal4 fusion receptors and treated as indicated. Normalized Gal4 firefly luciferase activity was expressed relative to vehicle treated control. Error bars denote mean ± SD of four replicates. Statistical significance (**$p < 0.01$; ***$p < 0.001$) was determined by Student's t test.

NOTCH1 Mutational Status Influences Thapsigargin Sensitivity

The aforementioned results suggest that thapsigargin inhibits signaling through wild-type and mutated Notch receptors but may have stronger effect for mutated Notch1. Prior work has shown that many activating HD mutations found in T-ALL result in destabilization of the Notch negative regulatory region and have deleterious effects on Notch1 folding and maturation (Malecki et al., 2006). Because the Lin12/Notch repeats (LNRs) of the Notch negative regulatory region rely on calcium for folding and function (Aster et al., 1999), mutated Notch1 might be more sensitive to reduced calcium availability than wild-type Notch1, providing a therapeutic window for SERCA inhibitors.

One simple prediction of the aforementioned model is that constitutively active forms of Notch1 lacking Ca^{2+} binding modules should be insensitive to SERCA inhibitors. To test this prediction, we performed Notch1 reporter assays in U2OS cells transfected with a plasmid encoding ΔEGFΔLNR, a membrane-tethered form of Notch1 lacking the extracellular epidermal growth factor (EGF) repeats and LNRs, or ICN1. As anticipated, coexpression of SERCA did not enhance reporter gene activation by ΔEGFΔLNR (Figure 7A), nor was reporter gene activation by ΔEGFΔLNR (Figure 7B) or ICN1 (Figure 7C) affected by thapsigargin. In contrast, ΔEGFΔLNR was highly sensitive to GSI (Figure 7B). Taken together, these results indicate that, at low nanomolar concentrations, thapsigargin inhibits Notch1 through a mechanism that requires the Ca^{2+}-binding modules of the Notch1 extracellular domain.

To determine if the Notch1 extracellular domain is important for the ability of thapsigargin to inhibit leukemia cell growth, we studied the human T-ALL cell line SUPT1, which has two copies of a t(7;9)(q34,q34) fusing the 3′ end of *NOTCH1* with enhancer/promoter elements of the T cell receptor β locus (*TCRB*) and has no normal *NOTCH1* allele (Ellisen et al., 1991). The rearranged *NOTCH1* alleles in SUPT1 cells drive the expression of a series of truncated mRNAs encoding N-terminally deleted polypeptides lacking the Notch1 extracellular domain, some of which are inserted into membranes and require γ-secretase cleavage for activation (Das et al., 2004). As anticipated, thapsigargin had no effect on ICN1 levels in SUPT1 cells (Figure 7D), whereas Cpd E eliminates the generation of ICN1 (Figure 7E). In line with this idea that protein structure affects drug response, thapsigargin failed to inhibit wild-type Notch1 or Notch2 at concentrations that impaired signaling of Notch1-bearing leukemogenic HD mutations (Figure 7F).

To further test the effect of thapsigargin on wild-type Notch1 maturation, we tested two Notch1 wild-type T-ALL and one chronic myelogenous leukemia (CML) cell lines in which high expression of Notch1 was previously reported (Palomero et al.,

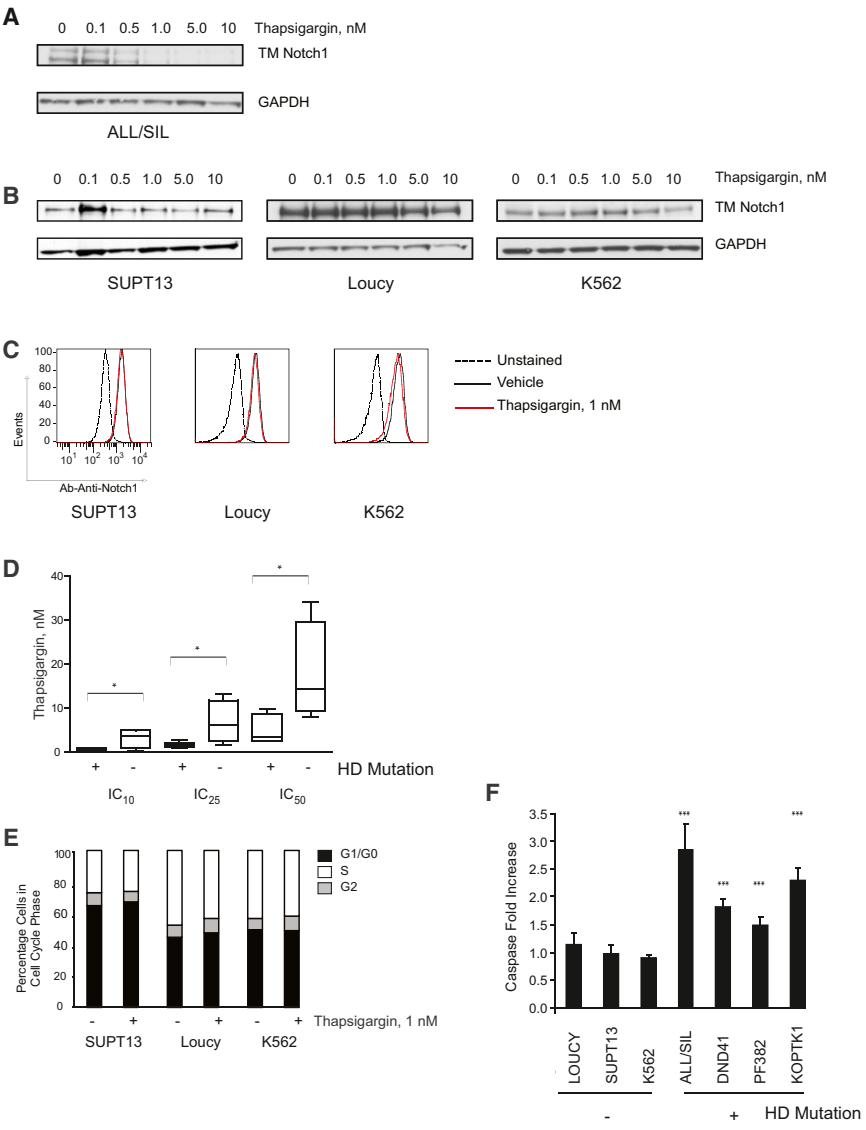

Figure 8. *NOTCH1* Mutational Status Influences the Sensitivity to Thapsigargin

(A and B) Effect of thapsigargin treatment (6 hr) on processing of HD mutant (A) or wild-type (B) Notch1. Notch1 was detected with an antibody against the C terminus of Notch1 that recognizes the furin-processed Notch1 transmembrane subunit (TM).

(C) Effect of thapsigargin treatment (24 hr) on Notch1 cell surface staining, as assessed by flow cytometry.

(D) The relative growth of thapsigargin-treated T-ALL cell lines with wild-type (LOUCY, MOLT16, and SUPT13) or rearranged alleles (SUPT1) of *NOTCH1* versus those with HD mutations (ALL/SIL, DND41, KOPTK1, MOLT4, and PF382). The line in the box plots represents the median. The upper edge (hinge) of the box indicates the 75th percentile of the data set, and the lower hinge indicates the 25th percentile. The ends of the vertical line indicate the minimum and the maximum data values. Statistical significance was determined by Student's t test (*$p < 0.05$).

(E) Effect of thapsigargin treatment on cell cycle progression in Notch1 wild-type cell lines, as assessed by measurement of DNA content on the viable fraction of cells.

(F) Effect of thapsigargin treatment (1 nM) on apoptosis induction as assessed by the luminescence Caspase 3/7 assay. Errors bars denote mean ± SD of four replicates. Statistical significance (***$p < 0.001$) was determined by one-way ANOVA using Bonferroni's correction for multiple comparison testing.

2006a). Compared to HD mutant, wild-type proteins appear to be less affected by thapsigargin treatment (Figures 8A–8C). The effects of thapsigargin on cell viability were then determined in a larger panel of human T-ALL cell lines of known *NOTCH1* mutational status (Weng et al., 2004). Cell lines carrying *NOTCH1* alleles with HD domain mutations were more sensitive to thapsigargin than cells with wild-type *NOTCH1* alleles or lacking the Notch1 extracellular domain (Figures 8D–8F).

In summary, these data suggest that Notch1 receptors bearing leukemogenic HD domain mutations are more sensitive to SERCA inhibitors, such as thapsigargin, than normal receptors.

DISCUSSION

Integrating Cell-Based Screens for Small Molecule and Protein Target Discovery

While there is a strong rationale for target-based therapies for cancer, with the exception of the nuclear hormone receptors, transcription factors have largely been refractory to conventional small-molecule screening approaches due to the challenges in developing high-throughput, robust screening assays. By definition, any therapeutic agent that modulates a transcription factor must alter the expression of its target genes. While there have been significant advances in our ability to assess global gene expression changes, almost all existing approaches cannot yet be applied to large-scale screening efforts due to cost and throughput limitations. Recognizing these shortcomings, we developed an approach that allows measurement of the expression of hundreds of endogenous genes in 384-well format and applied it to identify antagonists of leukemogenic increases in Notch signaling in T-ALL.

A limitation of both phenotypic and expression-based screening, however, is that identification of the relevant target of lead compounds can be difficult. The development of alternative genomic and chemical proteomic approaches for identifying protein targets holds the promise of accelerating the elucidation of underlying mechanism. Integrating results of a cDNA screen with GE-HTS data allowed us to identify SERCAs as Notch1 modulators and potential therapeutic targets in Notch1-associated leukemias.

Altering Maturation of Mutant Notch1 by SERCA Inhibition

We show here that SERCA inhibitors such as thapsigargin cause a Notch1 maturation defect marked by the accumulation of unprocessed Notch1 in the ER/Golgi compartment. The resulting effects on Notch1 signaling and leukemia cell growth depend on the nature of the *NOTCH1* mutations. The most common activating *NOTCH1* mutations in human T-ALL, the so-called class I *NOTCH1* mutations, consist of point substitutions or small in-frame deletions or insertions in the extracellular heterodimerization domain, which disrupt heterodimerization domain structure and permit ligand-independent ADAM-type metalloprotease cleavages (Gordon et al., 2009; Malecki et al., 2006). Folding and maturation of Notch1 are partially impaired by these mutations (Malecki et al., 2006), and it appears that Notch1 receptors bearing such mutations are more sensitive to the inhibitory effects of thapsigargin than wild-type Notch1 receptors. Another possible contributing factor to the greater sensitivity to thapsigargin in cells with mutated Notch1 receptors is that the presence of these mutated polypeptides may itself engender ER stress and thus render these cells more susceptible to the ER stress induced by thapsigargin. Indeed, this may account for the inability to rescue fully the effects of thapsigargin with ICN1 in some of our experiments. Taken together, these data suggest the potential for a therapeutic window for thapsigargin in T-ALLs bearing this type of mutation.

Other types of activating *NOTCH1* mutations also exist. Rarely, juxtamembrane in-frame tandem duplications create new "deprotected" ADAM-metalloprotease cleavage sites (class II mutations) (Malecki et al., 2006), or translocations create *NOTCH1* alleles encoding polypeptides that lack the Notch1 extracellular domain (Ellisen et al., 1991; Palomero et al., 2006a). As anticipated, we observed that a T-ALL cell line with two translocated *NOTCH1* alleles is relatively resistant to thapsigargin. Our proposed mechanism of action also predicts that murine T-ALLs, which often have Notch1 deletions that remove the Notch1 ectodomain coding sequence (Ashworth et al., 2010), as well as uncommon human breast cancers with *NOTCH1* rearrangements (Robinson et al., 2011), will be more resistant to thapsigargin and other SERCA inhibitors. It will be of importance to determine if CLLs, which have recently been reported to have frequent Notch1 PEST domain deletions (Di Ianni et al., 2009; Puente et al., 2011) but lack heterodimerization domain mutations, are sensitive to SERCA inhibitors.

Connecting *NOTCH1* and *SERCA* Mutations in Human Disease

Germline mutations in *ATP2A1* are reported in the congenital disorder Brody syndrome, characterized by impaired muscle relaxation and myopathy (Odermatt et al., 1996). *ATP2A2* mutations are reported in Darier's disease (Sakuntabhai et al., 1999), an autosomal dominant skin disorder characterized by loss of adhesion between keratinocytes, scaling due to hyperkeratosis, and thickening of the epidermis due to keratinocyte hyperproliferation. Skin cancers have been reported in patients with Darier's disease (Robertson and Sauder, 2012). Moreover, in aged $Atp2a2^{+/-}$ mice, tumors develop from the keratinized squamous epithelia (Liu et al., 2001) while the wild-type *Atp2a2* allele is retained and expressed, supporting a role for SERCA2 haploinsufficiency in tumor development (Prasad et al., 2005). In addition, thapsigargin acts as a tumor promoter in a skin carcinogenesis mouse model (Hakii et al., 1986).

There is also mounting evidence that Notch signaling suppresses the transformation of squamous epithelial cells. Genetically engineered mice with decrements in Notch signaling in the skin have a high incidence of skin cancers (Nicolas et al., 2003; Proweller et al., 2006). Recent human clinical trial data revealed that semagacestat, a GSI, is associated with an increased risk of skin cancer (discussed in Crump et al., 2011), possibly due to inhibition of Notch in the skin by chronic GSI administration. Furthermore, Notch pathway loss-of-function mutations have been reported in squamous cell carcinomas of the head and neck (Agrawal et al., 2011; Stransky et al., 2011) and of the skin and lung (Wang et al., 2011). Of note, at least one *NOTCH1* point substitution in human cutaneous squamous cell carcinoma impairs Ca^{2+} binding and folding of EGF repeat 12 (Hambleton et al., 2004; Wang et al., 2011) and a second (R1549Q) impacts folding of the LNRs (Wang et al., 2011), thus recapitulating the proposed pharmacologic effect of thapsigargin. Additional murine studies indicate that Notch signaling may have a tumor suppressive function in other cell lineages as well, including myeloid progenitors (Klinakis et al., 2011) and endothelial cells (Liu et al., 2011; Yan et al., 2010). It is intriguing that several recent studies report SERCA mutations in head and neck squamous cell carcinoma (Korosec et al., 2008; Stransky et al., 2011), in acute myeloid leukemia (Yan et al., 2011), and in other malignancies (Korosec et al., 2009), implicating loss-of-function mutations of SERCA as an additional possible mechanism for Notch inactivation in these diseases. Indeed, while *NOTCH1* mutations enhance sensitivity to SERCA inhibitors, providing a potential therapeutic window for application of this compound class, wild-type Notch1 is also sensitive to SERCA inhibition but at higher concentrations of the compound. One hypothesis to explain a Notch1 and SERCA functional dependency is by a physical interaction. It has been previously shown that presenilin and SERCA2b colocalize in the ER (Green et al., 2008). Since presenilin immunoprecipitation is also reported to preferentially recover the full-length Notch1 precursor prior to Notch1 cleavage in the Golgi (Ray et al., 1999), it is possible that Notch1, SERCA, and presenilin are part of a macromolecular complex.

Toward Translating SERCA Inhibitors to the Clinic

Our studies and other recent work bring to light a challenge in targeting Notch1 in cancer: its pleiotropic roles. *NOTCH1* is an oncogene in some human cancers, such as T-ALL and CLL, whereas it is a tumor suppressor in others, most notably, squamous cell carcinomas. Several strategies have been explored to inhibit Notch1 including the use of GSIs, Notch1-directed antibodies, and direct inhibition of the Notch complex with a hydrocarbon stapling approach (reviewed in Roti and Stegmaier, 2011). Each of these, however, is anticipated to also inhibit wild-type Notch1. One strategy to mitigate potential cancer-promoting effects in nondiseased cells is intermittent dosing of Notch inhibitors. A second approach is the selective targeting of the oncogenic protein. Our results suggest that common heterodimerization domain mutations in Notch1 render the protein more susceptible to the thapsigargin-induced maturation defect,

allowing for a therapeutic window in targeting mutant versus wild-type Notch1 (we observed an antileukemia effect with no measureable gut toxicity). The selective targeting of BRAF kinase bearing an activating V600E mutation by vemurafenib in melanoma is an example of successful application of this strategy (Bollag et al., 2010), although acquired resistance with RAS pathway lesions is common (Nazarian et al., 2010; Su et al., 2012). Similarly, reactivation of Notch1 signaling, for example, by altered EGF/LNR repeats, may pose a resistance mechanism in SERCA-targeted therapy in T-ALL.

Given the pervasive role of calcium signaling in normal physiology, it is unlikely that pan-SERCA inhibitors such as thapsigargin will have an immediate clinical application unless additional development is pursued. One strategy might be the development of isoform-specific small-molecule inhibitors of SERCA. A second is to derivatize thapsigargin for specific delivery to T-ALL cells. This tactic has already been used for a derivative of thapsigargin that is designed to treat prostate cancer, which is currently in clinical trials (NCT01056029 and NCT01734681) (Denmeade et al., 2003). Successful "targeted" delivery of SERCA inhibitors to T-ALL cells would further improve the therapeutic window with this class of drugs and enhance the likelihood of clinical translation.

In summary, this study demonstrates the power of an integrative screening strategy to identify alternative ways to target aberrant transcription factors, identify the modulation of SERCA as a tractable approach for inhibiting Notch1 in Notch-driven cancers, and implicate SERCA mutation as another potential pathogenic mechanism for Notch downregulation in human cancers in which the Notch pathway has a tumor suppressive role.

EXPERIMENTAL PROCEDURES

Full experimental details are in the Supplemental Experimental Procedures.

Cell Culture, Compounds, and Antibodies

Cells were cultured in RPMI 1640 (Cellgro) with 10% fetal bovine serum (Sigma-Aldrich) and 1% penicillin-streptomycin. Cpd E, thapsigargin, and cyclopiazonic acid were obtained from ENZO Life Sciences; and bepridil hydrochloride, ionomycin, salinomycin, methotrexate, dexamethasone, vincristine and DAPT were obtained from Sigma-Aldrich. We obtained western blot antibodies against Notch1 from Cell Signaling and Santa Cruz Biotechnology, Actin from Thermo Scientific, Vinculin from AbCAM, and GAPDH from Santa Cruz Biotechnology. Antibodies for immunofluorescence include Notch1 [A6] and Giantin (AbCAM). Cell surface Notch1 was evaluated by staining nonpermeabilized cells with monoclonal antihuman Notch1 antibody (R&D).

Notch1 *Off* Signature Detection

Marker and control genes for the Notch1 *on* versus *off* signature were chosen using publicly available Affymetrix microarray expression profiling data sets (GEO ID GSE5716) (Palomero et al., 2006b). Probes are shown in Supplemental Experimental Procedures. The signature was adapted to GE-HTS as described elsewhere (Peck et al., 2006). Signature performance was evaluated by calculating the summed score and weighted summed score (Hahn et al., 2008).

Small-Molecule Library Screening

DND41 cells were incubated with compounds at approximately 20 μM in dimethyl sulfoxide (DMSO) for 72 hr. We screened 3,801 compounds in triplicate, including the BSPBio collection (Prestwick, Biomol, and Spectrum libraries) and the HSCI1 collection (Broad Institute). The GE-HTS assay was performed as described elsewhere (Peck et al., 2006; Stegmaier et al., 2004). Compounds that induce the Notch1 *off* signature were identified using five discrete analytic metrics: summed score, weighted summed score, K-nearest neighbor analysis, naive Bayes classification, and support vector machine as described (Hahn et al., 2009).

cDNA Library Screen and Validation

The cDNA screening strategy involved the use of three key components: (1) a pcDNA3 plasmid encoding a modestly strong *NOTCH1* gain-of-function mutant, L1601PΔP, driven from a CMV promoter; (2) a Notch firefly luciferase reporter; and (3) a preplated cDNA library cloned into the Sport6 plasmid. Luminescence was measured 48 hr postplating.

Viral Transduction

Sequences targeted by each shRNA are listed in Supplemental Experimental Procedures. Viral supernatant production and MigR1 retroviral infections were performed as described (Aster et al., 2000).

Cell Growth, Apoptosis, and DNA Content Assays

Cell growth was assessed using the Promega Cell-Titer Glo ATP-based assay (Promega), apoptosis using a Caspase-Glo 3/7 assay (Promega) or Annexin V and propidium iodide (PI) staining by flow cytometry (eBioscience), and cellular DNA content by staining with PI. Values for IC_{10}, IC_{25}, and IC_{50} (the concentration of an inhibitor where the response is reduced by 10%, 25%, and 50%, respectively) were calculated using Prism 5 Software (Version 5.03).

Reporter Gene Assays

Expression plasmids for L1601PΔP (Weng et al., 2004), L1601PΔP-GAL4 (Malecki et al., 2006), ΔEGFΔLNR (Chiang et al., 2008), and ICN1 (Aster et al., 2000) have been described. Cotransfection of U2OS cells with expression plasmids, a Notch firefly luciferase reporter gene, and an internal Renilla luciferase control gene, was performed as described elsewhere (Aster et al., 2000). A second approach used a Notch1-Gal4 receptor ligand stimulation assay (Malecki et al., 2006).

RT-PCR

Primers and probes for real-time (RT)-PCR were obtained from Applied Biosystems. The data were analyzed using the ΔΔCT method and plotted as percentage of transcript compared to vehicle.

Drosophila Experiments

To generate RAF(gof) tumors in the adult *Drosophila* midgut, we created a stock containing the UAS-RAF(gof) transgene on the X chromosome (Brand and Perrimon, 1994) and the esg-Gal4, UAS-GFP, Tubulin, Gal80(ts) transgenes on the second chromosome (Micchelli and Perrimon, 2006). Drugs were prepared in DMSO, mixed with fly food 1:100, and fed to flies for 7 days. Flies were given freshly prepared drug every 2–3 days. Drug effects were evaluated by immunofluorescence microscopy.

T-ALL Xenograft Studies

MOLT4 xenografts were established by injecting 1.7×10^6 cells subcutaneously into 6-week-old female severe combined immunodeficiency (SCID)-beige mice (Charles River Laboratories). Tumor volume was determined by caliper measurements using this formula: volume = 0.5 × length × weight squared. When tumors reached a mean volume of 75 mm^3, mice were divided into two groups: 0.4 mg/kg thapsigargin or vehicle by intraperitoneal injection daily. Three mice that died prematurely due to drug toxicity were excluded from the study, leaving six evaluable mice in the thapsigargin-treated arm and nine in the vehicle arm. DND41 MigR1 and DND41 MigR1-ICN1 xenografts were established by injecting 10×10^6 cells subcutaneously into NSG mice (n = 20 per line). When tumor volume reached over 50 mm^3, mice were divided into two groups: 0.35 mg/kg thapsigargin or 10 ml/kg vehicle by intraperitoneal injection daily. Mice that were not ready at start of treatment were subsequently added to treatment groups when their tumors reached appropriate sizes. Mice were treated daily through the course of the study, and tumors were measured every 3 days. Five thapsigargin-treated mice were found dead during the course of the study with no prior weight loss or clinical signs of illness. All animal studies were performed under a protocol

approved by the Dana-Farber Cancer Institute Institutional Care and Use Committee.

SUPPLEMENTAL INFORMATION

Supplemental Information includes three figures, one table, and Supplemental Experimental Procedures and can be found with this article online at http://dx.doi.org/10.1016/j.ccr.2013.01.015.

ACKNOWLEDGMENTS

This work was supported by the Leukemia and Lymphoma Society (LLS) and the William Lawrence and Blanche Hughes Foundation (to K.S., J.C.A., and S.C.B.); the SynCure Cancer Research Foundation and the National Cancer Institute grant P01 CA 068484-11A1 (to K.S.); the European Hematology Association-American Society of Hematology International Fellowship Award, the American-Italian Cancer Foundation Post-Doctoral Research Fellowship, the Lady Tata International Award for Research in Leukaemia, and the LLS Special Fellow award and Fondazione Umberto Veronesi (to G.R.); the LLS Fellow (to K.P.); National Institutes of Health (NIH)/National Center for Research Resources grant 5 UL1 RR025758 (to N.P. and M.M.); and NIH grant R01 CA 092433 (to S.C.B.). We thank Zi Peng Fan and Amanda L. Christie for their technical support, Nicola Tolliday for stewardship of the chemical screen, the TRiP at Harvard Medical School for providing transgenic RNAi fly stocks used in this study, and Maria Pia Briziarelli, AULL (Associazione Umbra per lo studio e la terapia delle Leucemie e Linfomi), for grant management (G.R.).

Received: March 15, 2012
Revised: November 30, 2012
Accepted: January 22, 2013
Published: February 21, 2013

REFERENCES

Agrawal, N., Frederick, M.J., Pickering, C.R., Bettegowda, C., Chang, K., Li, R.J., Fakhry, C., Xie, T.X., Zhang, J., Wang, J., et al. (2011). Exome sequencing of head and neck squamous cell carcinoma reveals inactivating mutations in NOTCH1. Science *333*, 1154–1157.

Ashworth, T.D., Pear, W.S., Chiang, M.Y., Blacklow, S.C., Mastio, J., Xu, L., Kelliher, M., Kastner, P., Chan, S., and Aster, J.C. (2010). Deletion-based mechanisms of Notch1 activation in T-ALL: key roles for RAG recombinase and a conserved internal translational start site in Notch1. Blood *116*, 5455–5464.

Aste-Amézaga, M., Zhang, N., Lineberger, J.E., Arnold, B.A., Toner, T.J., Gu, M., Huang, L., Vitelli, S., Vo, K.T., Haytko, P., et al. (2010). Characterization of Notch1 antibodies that inhibit signaling of both normal and mutated Notch1 receptors. PLoS ONE *5*, e9094.

Aster, J.C., Simms, W.B., Zavala-Ruiz, Z., Patriub, V., North, C.L., and Blacklow, S.C. (1999). The folding and structural integrity of the first LIN-12 module of human Notch1 are calcium-dependent. Biochemistry *38*, 4736–4742.

Aster, J.C., Xu, L., Karnell, F.G., Patriub, V., Pui, J.C., and Pear, W.S. (2000). Essential roles for ankyrin repeat and transactivation domains in induction of T-cell leukemia by notch1. Mol. Cell. Biol. *20*, 7505–7515.

Banerji, V., Frumm, S.M., Ross, K.N., Li, L.S., Schinzel, A.C., Hahn, C.K., Kakoza, R.M., Chow, K.T., Ross, L., Alexe, G., et al. (2012). The intersection of genetic and chemical genomic screens identifies GSK-3α as a target in human acute myeloid leukemia. J. Clin. Invest. *122*, 935–947.

Bollag, G., Hirth, P., Tsai, J., Zhang, J., Ibrahim, P.N., Cho, H., Spevak, W., Zhang, C., Zhang, Y., Habets, G., et al. (2010). Clinical efficacy of a RAF inhibitor needs broad target blockade in BRAF-mutant melanoma. Nature *467*, 596–599.

Brand, A.H., and Perrimon, N. (1994). Raf acts downstream of the EGF receptor to determine dorsoventral polarity during Drosophila oogenesis. Genes Dev. *8*, 629–639.

Brou, C., Logeat, F., Gupta, N., Bessia, C., LeBail, O., Doedens, J.R., Cumano, A., Roux, P., Black, R.A., and Israël, A. (2000). A novel proteolytic cleavage involved in Notch signaling: the role of the disintegrin-metalloprotease TACE. Mol. Cell *5*, 207–216.

Carpenter, A.E. (2007). Image-based chemical screening. Nat. Chem. Biol. *3*, 461–465.

Chiang, M.Y., Xu, L., Shestova, O., Histen, G., L'heureux, S., Romany, C., Childs, M.E., Gimotty, P.A., Aster, J.C., and Pear, W.S. (2008). Leukemia-associated NOTCH1 alleles are weak tumor initiators but accelerate K-ras-initiated leukemia. J. Clin. Invest. *118*, 3181–3194.

Corsello, S.M., Roti, G., Ross, K.N., Chow, K.T., Galinsky, I., DeAngelo, D.J., Stone, R.M., Kung, A.L., Golub, T.R., and Stegmaier, K. (2009). Identification of AML1-ETO modulators by chemical genomics. Blood *113*, 6193–6205.

Crump, C.J., Johnson, D.S., and Li, Y.M. (2011). Target of γ-secretase modulators, presenilin marks the spot. EMBO J. *30*, 4696–4698.

Cullion, K., Draheim, K.M., Hermance, N., Tammam, J., Sharma, V.M., Ware, C., Nikov, G., Krishnamoorthy, V., Majumder, P.K., and Kelliher, M.A. (2009). Targeting the Notch1 and mTOR pathways in a mouse T-ALL model. Blood *113*, 6172–6181.

Darnell, J.E., Jr. (2002). Transcription factors as targets for cancer therapy. Nat. Rev. Cancer *2*, 740–749.

Das, I., Craig, C., Funahashi, Y., Jung, K.M., Kim, T.W., Byers, R., Weng, A.P., Kutok, J.L., Aster, J.C., and Kitajewski, J. (2004). Notch oncoproteins depend on gamma-secretase/presenilin activity for processing and function. J. Biol. Chem. *279*, 30771–30780.

DeAngelo, D.J., Stone, R.M., Silverman, L.B., Stock, E.C., Attar, I., Fearen, A., Dallob, A., Matthews, C., Stone, J., Freedman, S.J., and Aster, J.C. (2006). A phase I clinical trial of the Notch inhibitor MK-0752 in patients with T-cell acute lymphoblastic leukemia/lymphoma (T-ALL) and other leukemias. J. Clin. Oncol. *24*, 6585.

Denmeade, S.R., Jakobsen, C.M., Janssen, S., Khan, S.R., Garrett, E.S., Lilja, H., Christensen, S.B., and Isaacs, J.T. (2003). Prostate-specific antigen-activated thapsigargin prodrug as targeted therapy for prostate cancer. J. Natl. Cancer Inst. *95*, 990–1000.

Di Ianni, M., Baldoni, S., Rosati, E., Ciurnelli, R., Cavalli, L., Martelli, M.F., Marconi, P., Screpanti, I., and Falzetti, F. (2009). A new genetic lesion in B-CLL: a NOTCH1 PEST domain mutation. Br. J. Haematol. *146*, 689–691.

Ellisen, L.W., Bird, J., West, D.C., Soreng, A.L., Reynolds, T.C., Smith, S.D., and Sklar, J. (1991). TAN-1, the human homolog of the Drosophila notch gene, is broken by chromosomal translocations in T lymphoblastic neoplasms. Cell *66*, 649–661.

Gordon, W.R., Vardar-Ulu, D., Histen, G., Sanchez-Irizarry, C., Aster, J.C., and Blacklow, S.C. (2007). Structural basis for autoinhibition of Notch. Nat. Struct. Mol. Biol. *14*, 295–300.

Gordon, W.R., Roy, M., Vardar-Ulu, D., Garfinkel, M., Mansour, M.R., Aster, J.C., and Blacklow, S.C. (2009). Structure of the Notch1-negative regulatory region: implications for normal activation and pathogenic signaling in T-ALL. Blood *113*, 4381–4390.

Green, K.N., Demuro, A., Akbari, Y., Hitt, B.D., Smith, I.F., Parker, I., and LaFerla, F.M. (2008). SERCA pump activity is physiologically regulated by presenilin and regulates amyloid beta production. J. Cell Biol. *181*, 1107–1116.

Hahn, C.K., Ross, K.N., Warrington, I.M., Mazitschek, R., Kanegai, C.M., Wright, R.D., Kung, A.L., Golub, T.R., and Stegmaier, K. (2008). Expression-based screening identifies the combination of histone deacetylase inhibitors and retinoids for neuroblastoma differentiation. Proc. Natl. Acad. Sci. USA *105*, 9751–9756.

Hahn, C.K., Berchuck, J.E., Ross, K.N., Kakoza, R.M., Clauser, K., Schinzel, A.C., Ross, L., Galinsky, I., Davis, T.N., Silver, S.J., et al. (2009). Proteomic and genetic approaches identify Syk as an AML target. Cancer Cell *16*, 281–294.

Hakii, H., Fujiki, H., Suganuma, M., Nakayasu, M., Tahira, T., Sugimura, T., Scheuer, P.J., and Christensen, S.B. (1986). Thapsigargin, a histamine secretagogue, is a non-12-O-tetradecanoylphorbol-13-acetate (TPA) type tumor

promoter in two-stage mouse skin carcinogenesis. J. Cancer Res. Clin. Oncol. *111*, 177–181.

Hambleton, S., Valeyev, N.V., Muranyi, A., Knott, V., Werner, J.M., McMichael, A.J., Handford, P.A., and Downing, A.K. (2004). Structural and functional properties of the human notch-1 ligand binding region. Structure *12*, 2173–2183.

Inglese, J., Johnson, R.L., Simeonov, A., Xia, M., Zheng, W., Austin, C.P., and Auld, D.S. (2007). High-throughput screening assays for the identification of chemical probes. Nat. Chem. Biol. *3*, 466–479.

Klinakis, A., Lobry, C., Abdel-Wahab, O., Oh, P., Haeno, H., Buonamici, S., van De Walle, I., Cathelin, S., Trimarchi, T., Araldi, E., et al. (2011). A novel tumour-suppressor function for the Notch pathway in myeloid leukaemia. Nature *473*, 230–233.

Kopan, R., and Ilagan, M.X. (2009). The canonical Notch signaling pathway: unfolding the activation mechanism. Cell *137*, 216–233.

Korosec, B., Glavac, D., Volavsek, M., and Ravnik-Glavac, M. (2008). Alterations in genes encoding sarcoplasmic-endoplasmic reticulum Ca(2+) pumps in association with head and neck squamous cell carcinoma. Cancer Genet. Cytogenet. *181*, 112–118.

Korosec, B., Glavac, D., Volavsek, M., and Ravnik-Glavac, M. (2009). ATP2A3 gene is involved in cancer susceptibility. Cancer Genet. Cytogenet. *188*, 88–94.

Kridel, R., Meissner, B., Rogic, S., Boyle, M., Telenius, A., Woolcock, B., Gunawardana, J., Jenkins, C., Cochrane, C., Ben-Neriah, S., et al. (2012). Whole transcriptome sequencing reveals recurrent NOTCH1 mutations in mantle cell lymphoma. Blood *119*, 1963–1971.

Lee, S.Y., Kumano, K., Masuda, S., Hangaishi, A., Takita, J., Nakazaki, K., Kurokawa, M., Hayashi, Y., Ogawa, S., and Chiba, S. (2005). Mutations of the Notch1 gene in T-cell acute lymphoblastic leukemia: analysis in adults and children. Leukemia *19*, 1841–1843.

Liu, L.H., Boivin, G.P., Prasad, V., Periasamy, M., and Shull, G.E. (2001). Squamous cell tumors in mice heterozygous for a null allele of Atp2a2, encoding the sarco(endo)plasmic reticulum Ca2+-ATPase isoform 2 Ca2+ pump. J. Biol. Chem. *276*, 26737–26740.

Liu, Z., Turkoz, A., Jackson, E.N., Corbo, J.C., Engelbach, J.A., Garbow, J.R., Piwnica-Worms, D.R., and Kopan, R. (2011). Notch1 loss of heterozygosity causes vascular tumors and lethal hemorrhage in mice. J. Clin. Invest. *121*, 800–808.

Malecki, M.J., Sanchez-Irizarry, C., Mitchell, J.L., Histen, G., Xu, M.L., Aster, J.C., and Blacklow, S.C. (2006). Leukemia-associated mutations within the NOTCH1 heterodimerization domain fall into at least two distinct mechanistic classes. Mol. Cell. Biol. *26*, 4642–4651.

Mansour, M.R., Linch, D.C., Foroni, L., Goldstone, A.H., and Gale, R.E. (2006). High incidence of Notch-1 mutations in adult patients with T-cell acute lymphoblastic leukemia. Leukemia *20*, 537–539.

Micchelli, C.A., and Perrimon, N. (2006). Evidence that stem cells reside in the adult Drosophila midgut epithelium. Nature *439*, 475–479.

Milano, J., McKay, J., Dagenais, C., Foster-Brown, L., Pognan, F., Gadient, R., Jacobs, R.T., Zacco, A., Greenberg, B., and Ciaccio, P.J. (2004). Modulation of notch processing by gamma-secretase inhibitors causes intestinal goblet cell metaplasia and induction of genes known to specify gut secretory lineage differentiation. Toxicol. Sci. *82*, 341–358.

Nazarian, R., Shi, H., Wang, Q., Kong, X., Koya, R.C., Lee, H., Chen, Z., Lee, M.K., Attar, N., Sazegar, H., et al. (2010). Melanomas acquire resistance to B-RAF(V600E) inhibition by RTK or N-RAS upregulation. Nature *468*, 973–977.

Nicolas, M., Wolfer, A., Raj, K., Kummer, J.A., Mill, P., van Noort, M., Hui, C.C., Clevers, H., Dotto, G.P., and Radtke, F. (2003). Notch1 functions as a tumor suppressor in mouse skin. Nat. Genet. *33*, 416–421.

Odermatt, A., Taschner, P.E., Khanna, V.K., Busch, H.F., Karpati, G., Jablecki, C.K., Breuning, M.H., and MacLennan, D.H. (1996). Mutations in the gene-encoding SERCA1, the fast-twitch skeletal muscle sarcoplasmic reticulum Ca2+ ATPase, are associated with Brody disease. Nat. Genet. *14*, 191–194.

Ohlstein, B., and Spradling, A. (2007). Multipotent Drosophila intestinal stem cells specify daughter cell fates by differential notch signaling. Science *315*, 988–992.

Palomero, T., Barnes, K.C., Real, P.J., Glade Bender, J.L., Sulis, M.L., Murty, V.V., Colovai, A.I., Balbin, M., and Ferrando, A.A. (2006a). CUTLL1, a novel human T-cell lymphoma cell line with t(7;9) rearrangement, aberrant NOTCH1 activation and high sensitivity to gamma-secretase inhibitors. Leukemia *20*, 1279–1287.

Palomero, T., Lim, W.K., Odom, D.T., Sulis, M.L., Real, P.J., Margolin, A., Barnes, K.C., O'Neil, J., Neuberg, D., Weng, A.P., et al. (2006b). NOTCH1 directly regulates c-MYC and activates a feed-forward-loop transcriptional network promoting leukemic cell growth. Proc. Natl. Acad. Sci. USA *103*, 18261–18266.

Peck, D., Crawford, E.D., Ross, K.N., Stegmaier, K., Golub, T.R., and Lamb, J. (2006). A method for high-throughput gene expression signature analysis. Genome Biol. *7*, R61.

Periz, G., and Fortini, M.E. (1999). Ca(2+)-ATPase function is required for intracellular trafficking of the Notch receptor in Drosophila. EMBO J. *18*, 5983–5993.

Prasad, V., Boivin, G.P., Miller, M.L., Liu, L.H., Erwin, C.R., Warner, B.W., and Shull, G.E. (2005). Haploinsufficiency of Atp2a2, encoding the sarco(endo) plasmic reticulum Ca2+-ATPase isoform 2 Ca2+ pump, predisposes mice to squamous cell tumors via a novel mode of cancer susceptibility. Cancer Res. *65*, 8655–8661.

Proweller, A., Tu, L., Lepore, J.J., Cheng, L., Lu, M.M., Seykora, J., Millar, S.E., Pear, W.S., and Parmacek, M.S. (2006). Impaired notch signaling promotes de novo squamous cell carcinoma formation. Cancer Res. *66*, 7438–7444.

Puente, X.S., Pinyol, M., Quesada, V., Conde, L., Ordóñez, G.R., Villamor, N., Escaramis, G., Jares, P., Beà, S., González-Díaz, M., et al. (2011). Whole-genome sequencing identifies recurrent mutations in chronic lymphocytic leukaemia. Nature *475*, 101–105.

Rand, M.D., Lindblom, A., Carlson, J., Villoutreix, B.O., and Stenflo, J. (1997). Calcium binding to tandem repeats of EGF-like modules. Expression and characterization of the EGF-like modules of human Notch-1 implicated in receptor-ligand interactions. Protein Sci. *6*, 2059–2071.

Ray, W.J., Yao, M., Nowotny, P., Mumm, J., Zhang, W., Wu, J.Y., Kopan, R., and Goate, A.M. (1999). Evidence for a physical interaction between presenilin and Notch. Proc. Natl. Acad. Sci. USA *96*, 3263–3268.

Real, P.J., Tosello, V., Palomero, T., Castillo, M., Hernando, E., de Stanchina, E., Sulis, M.L., Barnes, K., Sawai, C., Homminga, I., et al. (2009). Gamma-secretase inhibitors reverse glucocorticoid resistance in T cell acute lymphoblastic leukemia. Nat. Med. *15*, 50–58.

Robertson, L., and Sauder, M.B. (2012). Basal cell carcinoma in Type 2 segmental Darier's disease. J. Skin Cancer *2012*, 839561.

Robinson, D.R., Kalyana-Sundaram, S., Wu, Y.M., Shankar, S., Cao, X., Ateeq, B., Asangani, I.A., Iyer, M., Maher, C.A., Grasso, C.S., et al. (2011). Functionally recurrent rearrangements of the MAST kinase and Notch gene families in breast cancer. Nat. Med. *17*, 1646–1651.

Roti, G., and Stegmaier, K. (2011). Targeting NOTCH1 in hematopoietic malignancy. Crit. Rev. Oncog. *16*, 103–115.

Sakuntabhai, A., Ruiz-Perez, V., Carter, S., Jacobsen, N., Burge, S., Monk, S., Smith, M., Munro, C.S., O'Donovan, M., Craddock, N., et al. (1999). Mutations in ATP2A2, encoding a Ca2+ pump, cause Darier disease. Nat. Genet. *21*, 271–277.

Stegmaier, K., Ross, K.N., Colavito, S.A., O'Malley, S., Stockwell, B.R., and Golub, T.R. (2004). Gene expression-based high-throughput screening(GE-HTS) and application to leukemia differentiation. Nat. Genet. *36*, 257–263.

Stransky, N., Egloff, A.M., Tward, A.D., Kostic, A.D., Cibulskis, K., Sivachenko, A., Kryukov, G.V., Lawrence, M.S., Sougnez, C., McKenna, A., et al. (2011). The mutational landscape of head and neck squamous cell carcinoma. Science *333*, 1157–1160.

Su, F., Viros, A., Milagre, C., Trunzer, K., Bollag, G., Spleiss, O., Reis-Filho, J.S., Kong, X., Koya, R.C., Flaherty, K.T., et al. (2012). RAS mutations in cutaneous squamous-cell carcinomas in patients treated with BRAF inhibitors. N. Engl. J. Med. *366*, 207–215.

Wang, N.J., Sanborn, Z., Arnett, K.L., Bayston, L.J., Liao, W., Proby, C.M., Leigh, I.M., Collisson, E.A., Gordon, P.B., Jakkula, L., et al. (2011). Loss-of-function mutations in Notch receptors in cutaneous and lung squamous cell carcinoma. Proc. Natl. Acad. Sci. USA *108*, 17761–17766.

Weng, A.P., Ferrando, A.A., Lee, W., Morris, J.P., 4th, Silverman, L.B., Sanchez-Irizarry, C., Blacklow, S.C., Look, A.T., and Aster, J.C. (2004). Activating mutations of NOTCH1 in human T cell acute lymphoblastic leukemia. Science *306*, 269–271.

Weng, A.P., Millholland, J.M., Yashiro-Ohtani, Y., Arcangeli, M.L., Lau, A., Wai, C., Del Bianco, C., Rodriguez, C.G., Sai, H., Tobias, J., et al. (2006). c-Myc is an important direct target of Notch1 in T-cell acute lymphoblastic leukemia/lymphoma. Genes Dev. *20*, 2096–2109.

Wong, G.T., Manfra, D., Poulet, F.M., Zhang, Q., Josien, H., Bara, T., Engstrom, L., Pinzon-Ortiz, M., Fine, J.S., Lee, H.J., et al. (2004). Chronic treatment with the gamma-secretase inhibitor LY-411,575 inhibits beta-amyloid peptide production and alters lymphopoiesis and intestinal cell differentiation. J. Biol. Chem. *279*, 12876–12882.

Yan, M., Callahan, C.A., Beyer, J.C., Allamneni, K.P., Zhang, G., Ridgway, J.B., Niessen, K., and Plowman, G.D. (2010). Chronic DLL4 blockade induces vascular neoplasms. Nature *463*, E6–E7.

Yan, X.J., Xu, J., Gu, Z.H., Pan, C.M., Lu, G., Shen, Y., Shi, J.Y., Zhu, Y.M., Tang, L., Zhang, X.W., et al. (2011). Exome sequencing identifies somatic mutations of DNA methyltransferase gene DNMT3A in acute monocytic leukemia. Nat. Genet. *43*, 309–315.

Cancer Cell
Article

Selective Requirement of PI3K/PDK1 Signaling for Kras Oncogene-Driven Pancreatic Cell Plasticity and Cancer

Stefan Eser,[1,9] Nina Reiff,[1,9] Marlena Messer,[1,9] Barbara Seidler,[1] Kathleen Gottschalk,[1] Melanie Dobler,[1] Maren Hieber,[1] Andreas Arbeiter,[1] Sabine Klein,[1] Bo Kong,[2] Christoph W. Michalski,[2] Anna Melissa Schlitter,[3] Irene Esposito,[3,8] Alexander J. Kind,[4] Lena Rad,[5] Angelika E. Schnieke,[4] Manuela Baccarini,[6] Dario R. Alessi,[7] Roland Rad,[1,5,8] Roland M. Schmid,[1,8] Günter Schneider,[1] and Dieter Saur[1,8,*]
[1]Department of Internal Medicine 2
[2]Department of Surgery
[3]Institute of Pathology
[4]Livestock Biotechnology
Technische Universität München, Ismaningerstr. 22, 81675 München, Germany
[5]Wellcome Trust Sanger Institute, Genome Campus, Hinxton-Cambridge CB10 1SA, UK
[6]Department of Microbiology and Immunobiology, University of Vienna, Max F. Perutz Laboratories, Doktor-Bohr-Gasse 9, 1030 Vienna, Austria
[7]MRC Protein Phosphorylation Unit, University of Dundee, Dow Street, Dundee DD1 5EH, Scotland, UK
[8]German Cancer Consortium (DKTK) and German Cancer Research Center (DKFZ), Im Neuenheimer Feld 280, 69120 Heidelberg, Germany
[9]These authors contributed equally to this work
*Correspondence: dieter.saur@lrz.tum.de
http://dx.doi.org/10.1016/j.ccr.2013.01.023

SUMMARY

Oncogenic Kras activates a plethora of signaling pathways, but our understanding of critical Ras effectors is still very limited. We show that cell-autonomous phosphoinositide 3-kinase (PI3K) and 3-phosphoinositide-dependent protein kinase 1 (PDK1), but not Craf, are key effectors of oncogenic Kras in the pancreas, mediating cell plasticity, acinar-to-ductal metaplasia (ADM), and pancreatic ductal adenocarcinoma (PDAC) formation. This contrasts with Kras-driven non-small cell lung cancer, where signaling via Craf, but not PDK1, is an essential tumor-initiating event. These in vivo genetic studies together with pharmacologic treatment studies in models of human ADM and PDAC demonstrate tissue-specific differences of oncogenic Kras signaling and define PI3K/PDK1 as a suitable target for therapeutic intervention specifically in PDAC.

INTRODUCTION

Pancreatic ductal adenocarcinoma (PDAC) is nearly uniformly fatal despite maximal treatment, with fewer than 1% of patients surviving 5 years (Carpelan-Holmström et al., 2005). A wealth of molecular studies have identified mutant Kras as the initiating event (Hidalgo, 2010; Hingorani et al., 2003; Morris et al., 2010; Pylayeva-Gupta et al., 2011). Expression of $Kras^{G12D}$ or $Kras^{G12V}$ in the murine pancreas induces acinar cell dedifferentiation, acinar-to-ductal metaplasia (ADM), and premalignant precursor lesions, called pancreatic intraepithelial neoplasia (PanIN) that progress to metastatic PDAC (Guerra et al., 2007; Hingorani et al., 2003; Morris et al., 2010; Pinho et al., 2011; Seidler et al., 2008). Oncogenic Kras activates a plethora of signaling pathways, including canonical Raf/MEK/ERK, PI3K/AKT, RalGDS/p38 MAPK, Rac and Rho, Rassf1, NF1, p120GAP, and PLC-ε (Castellano and Downward, 2011; Pylayeva-Gupta et al., 2011). However, which of these effector pathways of oncogenic Kras control cell fate decisions and PDAC formation remains an outstanding question (Morris et al., 2010; Pylayeva-Gupta et al., 2011).

The PI3K/AKT pathway is uniformly activated in human PDAC and mouse models of Kras-driven pancreatic cancer

Significance

Kras-driven tumors such as PDAC, NSCLC, or colon cancer differ in prognosis and response to targeted therapies. However, the underlying molecular mechanisms are largely unknown. Oncogenic Kras activates diverse signaling pathways but the functional relevance of specific Kras effectors is unclear for most cancer types. Because Kras is considered undruggable, this has hampered progress toward targeted therapeutic interventions. We provide in vivo genetic evidence for context-specific effector pathways of oncogenic Kras in PDAC and NSCLC and define cell autonomous Kras → PI3K → PDK1 signaling as a critical and therapeutically tractable axis in pancreatic cancer initiation and maintenance.

(Jimeno et al., 2008; Kennedy et al., 2011; Ying et al., 2011). PI3Ks are a family of heterodimeric lipid kinases composed of catalytic and regulatory subunits that, on stimulation, catalyze production of the second messenger phosphatidylinositol-3,4,5-triphosphate (PIP3), which activates downstream kinases, such as PDK1 and AKT (Castellano and Downward, 2011; Bader et al., 2005). p110α, which is encoded by *PIK3CA*, is the catalytic subunit of the ubiquitously expressed class IA PI3Kα. Hotspot mutations of p110α that activate PI3K signaling have been identified in the helical domain (E542K and E545K) and the catalytic domain (H1047R) in a variety of human cancers, including breast and lung (Bader et al., 2005; Liu et al., 2009). Transgenic expression of $p110\alpha^{H1047R}$ in mice induces breast and lung cancer (Adams et al., 2011; Engelman et al., 2008; Liu et al., 2011).

Taking advantage of genetically engineered murine and patient-derived humanized cancer models, we set out to analyze the contribution of Kras effector pathways to PDAC and NSCLC development.

RESULTS

Pancreas-Specific PI3K Pathway Activation by Expression of Oncogenic $p110\alpha^{H1047R}$ Induces ADM and Premalignant PanIN

To explore the role of the PI3K/AKT signaling pathway in Kras-induced cell plasticity, ADM, and PDAC formation, we generated a latent oncogenic $PIK3CA^{H1047R}$ (encoding $p110\alpha^{H1047R}$) allele silenced by a lox-stop-lox (LSL) cassette as a knock-in at the mouse *Rosa26* locus (*LSL-PIK3CA*^{H1047R} mouse line; Figures S1A–S1C available online). To activate the expression of $p110\alpha^{H1047R}$ and thus PI3K signaling, specifically in the pancreas, we used the well-established $Ptf1a^{Cre}$ driver line to direct recombination in pancreatic acini, ducts, and islets (Figures S1D and S1E) (Nakhai et al., 2007; Seidler et al., 2008; von Werder et al., 2012).

Transgenic expression of $p110\alpha^{H1047R}$ from the *Rosa26* locus resulted in moderately increased PIP3 levels in the pancreas, similar to expression of $Kras^{G12D}$ from the endogenous *Kras* locus in the established $Kras^{G12D}$ knock-in mouse model (Figures 1A and 1B). Importantly, we observed no obvious difference in the p110α protein levels in pancreatic tissue lysates between $Ptf1a^{Cre/+}$;*LSL-PIK3CA*$^{H1047R/+}$ animals and $Ptf1a^{Cre/+}$;*LSL-Kras*^{G12D} knock-in mice (Figure 1B), even though $Ptf1a^{Cre/+}$;*LSL-PIK3CA*$^{H1047R/+}$ animals carried $PIK3CA^{H1047R}$ in the *Rosa26* locus in addition to their endogenous *Pik3ca*. $Ptf1a^{Cre/+}$;*LSL-PIK3CA*$^{H1047R/+}$ mice were viable and revealed no overt phenotype after birth. However, pancreatic size and weight were increased, as previously shown in the $Kras^{G12D}$ model (Figure 1C).

Histopathologic analyses revealed that all $Ptf1a^{Cre/+}$;*LSL-PIK3CA*$^{H1047R/+}$ mice developed massive induction of ADM, a condition where terminally differentiated acinar cells dedifferentiate into a progenitor-like state and acquire features of ductal cells (Figure 1D) (Pinho et al., 2011). Furthermore, all animals developed PanIN, a precursor lesion of PDAC (Figure 1D) (Hruban et al., 2006). The amount and grade of these lesions increased over time from PanIN-1A, already present in 1-month-old mice, to PanIN-3, found in some 9-month-old animals, which represents carcinoma in situ (Figures 1D and 1E). The $PIK3CA^{H1047R/+}$ and $Kras^{G12D/+}$ models showed very similar patterns of ADM induction and PanIN progression (Figures 1D and 1E) and markers of PI3K pathway activation were almost identical, as shown by immunohistochemistry and western blot analysis of tissue lysates (Figures 1F and 1G). Indicators of PI3K signaling, such as proliferation of PanIN lesions, were consistently similar in both models (Figures S1F and S1G). These observations support the view that pancreas-specific activation of PI3K signaling phenocopies $Kras^{G12D}$-induced cellular plasticity and PanIN formation.

To confirm that acinar cell plasticity via ADM is indeed involved in PanIN and PDAC development, we used an *elastase-1 Cre* driver line (Stanger et al., 2005) to specifically activate $p110\alpha^{H1047R}$ in acinar cells. This induced ADM and PanIN lesions with the same frequency as expression of oncogenic $Kras^{G12D}$ (Figures S1H–S1J). In contrast, pancreas-specific constitutive activation of Rac1 signaling by expressing a dominant active $Rac1^{G12V}$ allele from the *Rosa26* locus ($Ptf1a^{Cre/+}$;*LSL-Rac1*$^{G12V/+}$ mice) (Srinivasan et al., 2009) failed to induce ADM and PanINs (Figure S1K). Since Rac1 is a downstream effector of PI3K and is activated in the $Kras^{G12D}$ model of pancreatic cancer (Heid et al., 2011), failure of $Rac1^{G12V}$ to induce ADM and PanINs argues for the specific involvement of canonical PI3K/AKT signaling in pancreatic tumor formation.

Expression of Oncogenic $p110\alpha^{H1047R}$ in the Pancreas Phenocopies $Kras^{G12D}$-Induced Metastatic PDAC

To test whether $p110\alpha^{H1047R}$ is also capable of inducing pancreatic cancer, we aged $Ptf1a^{Cre/+}$;*LSL-PIK3CA*$^{H1047R/+}$ mice. All animals in the tumor watch cohort developed PDAC within 800 days (Figures 2A, 2B, and S2A). Comparison of tumor formation and survival of $PIK3CA^{H1047R}$ and $Kras^{G12D}$ mutant animals revealed striking similarities, with nearly identical survival times and similar rates of metastasis (Figures 2A and S2B). $p110\alpha^{H1047R}$-induced tumors were histopathologically indistinguishable from human and murine $Kras^{G12D}$-induced PDAC and showed the full spectrum of the human disease, ranging from well-differentiated ductal PDAC to undifferentiated tumors and typical metastasis to lymph nodes, liver, and lung (Figures 2B, S2A, and S2B) (Hruban et al., 2006).

To explore activation of PI3K signaling in $p110\alpha^{H1047R}$- and $Kras^{G12D}$-driven pancreatic cancer, we analyzed tissues from these animals using phospho-specific antibodies. Similar activation of the key downstream effectors of PI3K signaling, pAKT-T308, pAKT-S473, and pGSK3β-S9 was observed in both models (Figures 2C and 2D). Importantly, we found that mutant $p110\alpha^{H1047R}$ did not activate Ras in primary tissue specimens and PDAC cell lines from $Ptf1a^{Cre/+}$;*PIK3CA*$^{H1047R/+}$ animals, indicating that the effects observed in the *PIK3CA*^{H1047R} model were not due to Ras cross activation (Figures S2C and S2D). Consistent with data from pancreatic tissues of the $Ptf1a^{Cre/+}$;*LSL-PIK3CA*$^{H1047R/+}$ model (Figure 1B), we found no obvious increase of p110α expression levels in *PIK3CA*^{H1047R} mutant PDAC cell lines (Figure S2D). This accords with previous findings that p110α not bound to the p85 regulatory subunit is unstable and rapidly degraded (Engelman et al., 2008).

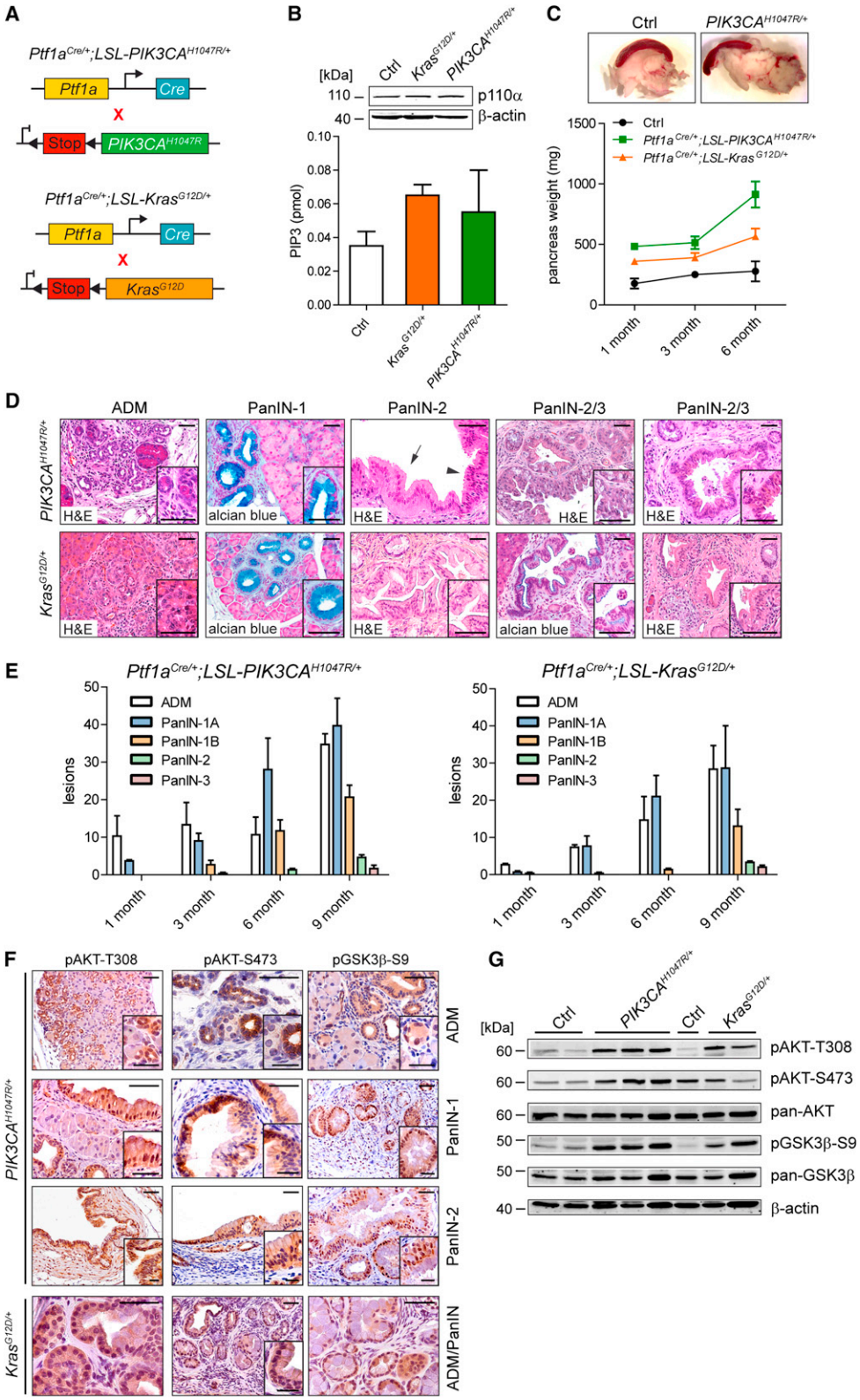

Figure 1. Constitutive Activation of PI3K Signaling Causes ADM and Neoplastic Changes in the Pancreas

(A) Genetic strategy used to activate p110α^{H1047R} or Kras^{G12D} expression in the pancreas.

(B) Immunoblot analysis of p110α expression levels (upper panel) and PIP3 activity (lower panel) in pancreata of 6-week-old control (Ctrl), *Ptf1a*$^{Cre/+}$;*LSL-Kras*$^{G12D/+}$ (*Kras*$^{G12D/+}$) and *Ptf1a*$^{Cre/+}$;*LSL-PIK3CA*$^{H1047R/+}$ (*PIK3CA*$^{H1047R/+}$) compound mutant mice (n = 3 per genotype).

(legend continued on next page)

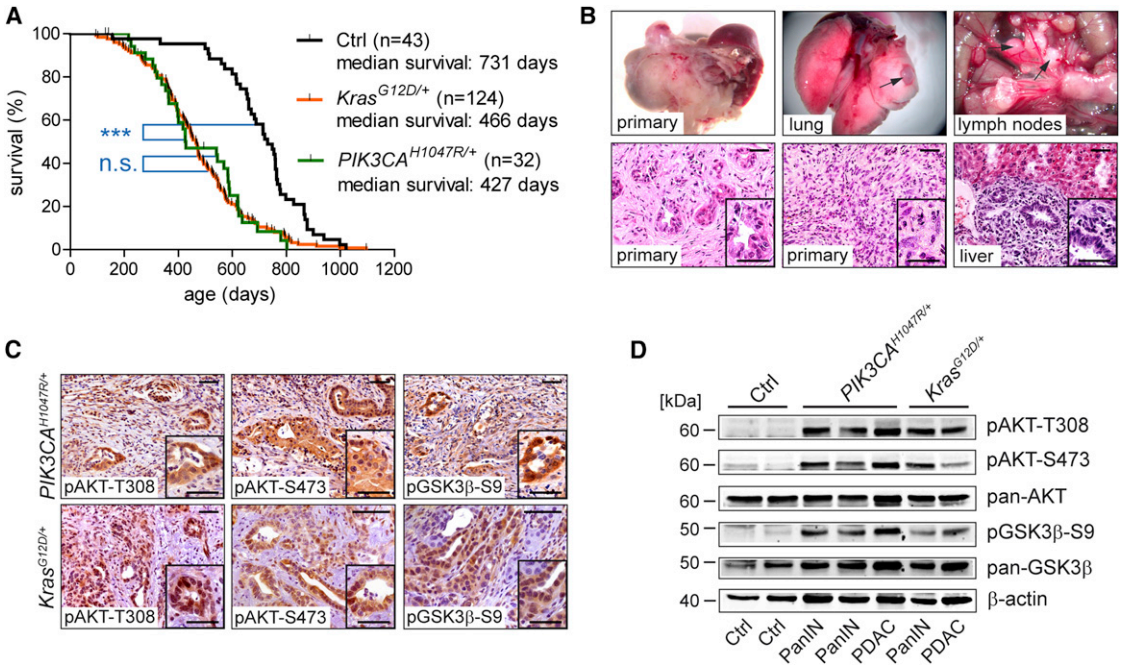

Figure 2. Expression of Oncogenic p110α^{H1047R} Induces Metastatic PDAC

(A) Kaplan-Meier survival curves of the indicated genotypes (n.s., not significant; ***p < 0.001, log-rank test).

(B) Macroscopic and microscopic images of PDAC and associated metastasis indicated by arrows in *PIK3CA*$^{H1047R/+}$ mutant mice.

(C) Immunohistochemical analysis of PI3K/AKT pathway activation in p110α^{H1047R} (upper panel) and Kras^{G12D} (lower panel) induced PDAC.

(D) Immunoblot analysis of PI3K/AKT pathway activation in the pancreas of 9-month-old Ctrl and age-matched PanIN-bearing pancreata and PDAC from *PIK3CA*$^{H1047R/+}$ and *Kras*$^{G12D/+}$ mutant mice. β-actin was used as loading control. Insets show representative lesions in high magnification. Scale bars, 50 μm for micrographs, 20 μm for insets.

See also Figure S2.

Oncogenic PI3K Signaling Activates a Senescence Program in the Pancreas that Is Bypassed by Loss of *Cdkn2a*

We next analyzed tumor-suppressive mechanisms in the *PIK3CA*^{H1047R} model. Expression of p110α^{H1047R}-induced a senescence program in the pancreas. All low-grade PanIN lesions examined stained positive for senescence-associated β-galactosidase (SA-β-Gal), which has been recently shown to be the only reliable oncogene-induced senescence biomarker in the pancreas (Figure S2E) (Caldwell et al., 2012). Importantly, these lesions showed concomitant upregulation of both *Cdkn2a* gene products, p16/Ink4a and p19/Arf, and activation of the p53/p21^{Cip1} pathway (Figures S2E and S2F).

In PDAC however, p16/Ink4a and p19/Arf expression is lost as demonstrated previously in the Kras^{G12D} model (Figure S2F and data not shown) (Bardeesy et al., 2006). Consistent with this, genomic analyses revealed frequent deletion of the *Cdkn2a* locus in p110α^{H1047R}-induced cancers (data not shown). Again, these observations demonstrate that the *PIK3CA*^{H1047R} model phenocopies Kras^{G12D}-induced PDAC with respect to tumor suppressor usage (Bardeesy et al., 2006). Accordingly, mimicking loss of heterozygosity of *Cdkn2a* by inactivation of one allele using floxed *Cdkn2a* mice (Bardeesy et al., 2006) accelerated PDAC formation in the *PIK3CA*^{H1047R} and *Kras*^{G12D} model (Figures S2G and S2H). To investigate the effect of *Cdkn2a* inactivation on oncogene-induced senescence of PanIN lesions, we inactivated both *Cdkn2a* alleles. As expected, this completely

(C) Representative images and weight of *Kras*$^{G12D/+}$ and *PIK3CA*$^{H1047R/+}$ mutant pancreata.

(D) Representative alcian blue and hematoxylin and eosin (H&E) stained sections of ADM and different grades of pancreatic intraepithelial neoplasia (PanIN) in *Ptf1a*$^{Cre/+}$;*PIK3CA*$^{H1047R/+}$ (upper panel) and *Ptf1a*$^{Cre/+}$;*LSL-Kras*$^{G12D/+}$ (lower panel) mutant animals (age from left to right, respectively: 1 month, 3 months, 6 months, 9 months, 9 months). The arrow indicates a PanIN-1 and the arrowhead a PanIN-2 lesion. Insets show representative lesions in high magnification. Scale bars, 50 μm.

(E) Quantification of ADM and PanIN progression in the *Kras*$^{G12D/+}$ and *PIK3CA*$^{H1047R/+}$ models (n = 3 per time point; 3 representative slides per mouse).

(F) Immunohistochemical analysis of PI3K/AKT pathway activation in ADMs and PanINs of 6-month-old *Ptf1a*$^{Cre/+}$;*PIK3CA*$^{H1047R/+}$ and *Ptf1a*$^{Cre/+}$;*LSL-Kras*$^{G12D/+}$ mutant mice. Insets show representative lesions in high magnification. Scale bars, 50 μm for micrographs, 20 μm for insets.

(G) Immunoblot analysis of PI3K/AKT pathway activation in control (Ctrl), *PIK3CA*$^{H1047R/+}$ and *Kras*$^{G12D/+}$ mutant pancreata of 6-month-old mice. β-actin was used as loading control. Error bars, ± SEM.

See also Figure S1.

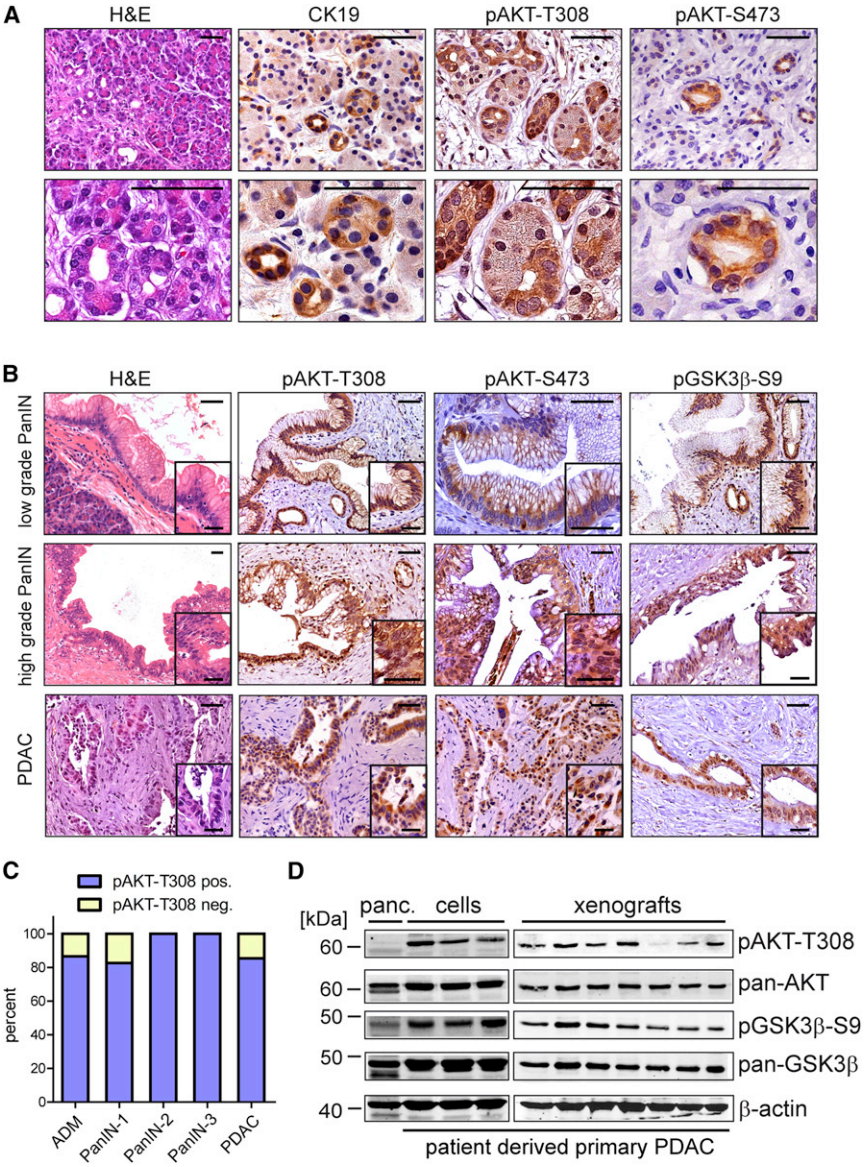

Figure 3. PI3K/AKT Pathway Activation in Human Pancreatic ADM and Neoplasia

(A) H&E stains and immunohistochemical analysis of CK19 and PI3K/AKT pathway activation in human ADM.

(B) H&E staining and immunohistochemical PI3K/AKT pathway analysis of human low- and high-grade PanINs and PDAC.

(C) Frequency of PI3K pathway activation in ADM, PanINs and PDAC. Bar graphs show the percentage of lesions that stained positive or negative on human tissue microarrays for pAKT-T308. ADM (n = 21 patients), PanINs (n = 32 patients), and PDAC (n = 205 patients).

(D) Immunoblot analysis of PI3K/AKT pathway activation in protein lysates of normal human pancreatic cells (panc.), patient-derived low passaged primary PDAC cells (n = 3 patients), and primary patient-derived PDAC xenografts (n = 7 patients). β-actin was used as loading control. Insets show representative lesions in high magnification. Scale bars, 50 μm for micrographs, 20 μm for insets.

blocked senescence of early PanIN lesions (Figures S2I and S2J). These findings demonstrate the importance of the *Cdkn2a* tumor suppressor locus for PDAC progression. Interestingly, median survival times were indistinguishable between both heterozygous deletion models, arguing that identical pathways and tumor suppressors operate in $p110\alpha^{H1047R}$- and $Kras^{G12D}$-driven PDAC formation.

Taken together, these murine in vivo modeling studies clearly demonstrate that PI3K signaling induces acinar cell plasticity, ADM, PanIN formation, senescence via upregulation of p16/Ink4a and p19/Arf, bypass of senescence by inactivation of *Cdkn2a*, and ultimately PDAC formation.

PI3K Pathway Activation in Human ADM, PanIN, and PDAC

PI3K/AKT activation is a classical and uniform feature of human PDAC (Jimeno et al., 2008; Kennedy et al., 2011; Reichert et al., 2007; Ying et al., 2011). However, the role of PI3K/AKT signaling during the early stages of human pancreatic carcinogenesis, namely ADM and PanIN formation, remains unclear. To test our hypothesis that the PI3K/AKT pathway is activated in human ADM, PanIN and PDAC, we analyzed key surrogates of PI3K signaling: AKT-T308/S473 and GSK3β-S9 phosphorylation (Figures 3A and 3B). In accordance with the murine in vivo studies, we observed strong activation of PI3K signaling in tissue microarrays of nearly all human ADM (n = 21), PanIN (n = 32), and PDAC (n = 205) specimens (Figure 3C).

In addition, we validated PI3K pathway activation in human PDAC using patient-derived primary xenografted tumors, early-passage cell lines, and normal pancreatic tissue (Figure 3D). These data suggest that PI3K/AKT signaling is activated at the earliest stages of tumor evolution in humans and controls pancreatic cell plasticity and carcinogenesis.

Elimination of PDK1 Invariably Blocks Kras-Driven ADM, PanIN, and PDAC In Vivo

PI3K activates various downstream effectors by converting phosphatidylinositol (4,5)-bisphosphate (PIP2) into the second messenger PIP3. PIP3 transmits PI3K signals by directly binding to proteins with pleckstrin homology (PH) domains, such as PDK1 and AKT (Cantley, 2002), targeting them to the cell membrane. In turn, PDK1 activates AKT by threonine 308 phosphorylation (Alessi et al., 1997; Currie et al., 1999).

To test whether cell autonomous signaling of the direct PI3K downstream target PDK1 is essential for Kras-driven pancreatic plasticity and PDAC formation, we inactivated *Pdk1* specifically in the epithelial compartment of the pancreas using floxed *Pdk1*

mice (Lawlor et al., 2002). *Ptf1a*$^{Cre/+}$-induced deletion of *Pdk1* in the pancreas was verified by PCR, quantitative RT-PCR, Western blot analysis and immunohistochemistry (Figures S3A–S3C and S3E–S3G). Consistent with our hypothesis, PDK1 inactivation completely blocked PanIN and PDAC formation in the *Kras*^{G12D} model (Figures 4A–4D). Pancreata showed normal weight and morphology with some areas of fatty degeneration in older animals, a common sign of cellular stress due to *Kras* oncogene expression (Figures 4B and 4C). Inactivation of PDK1 resulted in normal life expectancy in the *Kras*^{G12D} model (*Ptf1a*$^{Cre/+}$;*LSL-Kras*$^{G12D/+}$;*Pdk1*$^{f/f}$), whereas deletion of one *Pdk1* allele (*Ptf1a*$^{Cre/+}$;*LSL-Kras*$^{G12D/+}$;*Pdk1*$^{f/+}$) did not alter PanIN and PDAC formation (Figures 4B, 4D, 4F, and S3G). Loss of epithelial PDK1 expression in the *Kras*^{G12D} model correlated well with PI3K/AKT pathway inactivation (Figures 4E, 4F, and S3I) without affecting Ras activity (Figure 4G) or PIP3 levels (Figure S3F). Importantly, we did not observe hypoplasia or developmental defects of the pancreas, pancreatic islets, and beta cells, or overt hyperglycemia and lethality due to PDK1 inactivation in pancreas epithelia as reported by other groups using different Cre-driver lines and genetic backgrounds (Figures 4B, 4D, S3D, S3G, and S3H) (Hashimoto et al., 2006; Westmoreland et al., 2009). We did however observe impaired glucose tolerance, but this did not progress to diabetes mellitus (Figures S3D and S3H).

Besides AKT, PDK1 also transmits PI3K-dependent signals to SGK and S6K. The PDK1 effectors RSK and isoforms of PKC are probably not directly controlled by PI3K (Pearce et al., 2010). To determine whether PDK1 substrates other than AKT play a role in Kras^{G12D}-induced pancreatic carcinogenesis, we investigated whether their phosphorylation states were affected by the *Pdk1* knockout in vivo. Deletion of *Pdk1* in the *Kras*^{G12D} model blocked PKC, RSK (p90RSK-T359/S363), AKT-T308, and GSK3β-S9 phosphorylation (Figure S3I). Notably, we observed considerable variation in the phosphorylation levels of PKC and RSK in *Ptf1a*$^{Cre/+}$;*LSL-Kras*$^{G12D/+}$ pancreata, whereas AKT and GSK3β phosphorylation was always uniformly present (Figure S3I). These results provide biochemical evidence that canonical AKT-dependent signaling downstream of PI3K/PDK1 contributes significantly to the observed effects, although the importance of additional PDK1 substrates and alternate effectors cannot be completely excluded (Pearce et al., 2010).

PDK1 Is Essential for Kras-Induced Upregulation of p16/Ink4 and p19/Arf

To test our hypothesis that PI3K/PDK1 signaling transmits oncogenic Kras^{G12D}-induced failsafe mechanisms, we investigated regulation of p16/Ink4 and p19/Arf in pancreata in which the PI3K signaling pathway had been disrupted (*Ptf1a*$^{Cre/+}$;*LSL-Kras*$^{G12D/+}$;*Pdk1*$^{f/f}$ model, Figure 4F). PDK1 deficiency significantly reduced p16/Ink4a and p19/Arf induction compared to *Ptf1a*$^{Cre/+}$;*LSL-Kras*$^{G12D/+}$ animals (Figure 4H). These in vivo genetic studies therefore support the view that Kras^{G12D}-dependent oncogenic stress fluxes through PDK1 to induce upregulation of the p16/Ink4a and p19/Arf tumor suppressors.

Elimination of PDK1 Blocks PDAC, but not NSCLC Formation

We next evaluated the role of cell autonomous PDK1 signaling in pancreatic carcinogenesis in *PIK3CA*$^{H1047R/+}$ single and *PIK3CA*$^{H1047R/+}$;*Kras*$^{G12D/+}$ double mutant mice (Figures S4A and S4B). Deletion of *Pdk1* in both models led to complete inhibition of ADM, PanIN formation, and PDAC development, indicating that PDK1 is indeed a central node and essential for pancreatic carcinogenesis in diverse in vivo models (Figures S4A and S4B).

In contrast, deletion of *Pdk1* in Kras^{G12D}-driven NSCLC models had no effect on lung tumor formation (Figures S4C–S4F). Although both the Kras^{G12D}-driven lung and pancreatic cancer models are on a similar genetic background, it remains possible that subtle differences in the genetic background may affect Kras^{G12D} signaling and engagement of PDK1. We therefore used the *elastase-1 Cre* driver line that recombines loxP sites in the pancreas and the lung of the same animal (Figures 5A–5C). Simultaneous Kras^{G12D} expression in both organs of the same animal induced invasive grade 4 NSCLC and pancreatic tumorigenesis (Figure 5D). *Pdk1* deletion blocked pancreatic neoplasia completely, whereas NSCLC formation in the same animal was unaffected (Figures 5E and 5F). Importantly, *Pdk1* deletion did not affect overall survival in this model. All animals in the tumor watch cohort developed grade 3-4 NSCLC within 600 days (Figure 5F) and the number of lung lesions was comparable (Figure 5G). These in vivo findings support the view that each tissue has its own unique signaling requirement during Kras oncogene-induced transformation.

Craf Is Dispensable for Kras-Driven PDAC Formation

It has recently been shown that Craf is essential for Kras^{G12D}-induced NSCLC (Blasco et al., 2011; Karreth et al., 2011). To investigate the contribution of Craf in pancreatic carcinogenesis, we inactivated *Craf* in pancreas epithelium using floxed *Craf* mice (Jesenberger et al., 2001). *Ptf1a*$^{Cre/+}$-induced deletion of *Craf* in the Kras^{G12D}-driven PDAC model had no inhibitory effect on tumor development or progression and did not improve mouse survival (Figures 6A–6C). Efficient deletion of both *Craf* alleles and loss of Craf protein expression was verified by genotyping PCR, immunohistochemistry and western blot analysis of PDAC cells isolated from tumor specimens from *Ptf1a*$^{Cre/+}$;*LSL-Kras*$^{G12D/+}$;*Craf1*$^{f/f}$ mice (Figures 6D–6F). The possibility that tumors developed due to incomplete *Craf* deletion can thus be excluded. Signaling via Craf is therefore dispensable for initiation of Kras-driven PDAC, supporting the view that Kras exerts its oncogenic effects in a tissue-specific manner.

Disruption of PDK1 or Inhibition of PI3K Signaling Blocks Murine and Human ADM In Vitro

To gain insight into the cellular mechanisms of Kras^{G12D}-PI3K-PDK1-induced transformation, we analyzed early events of pancreatic carcinogenesis. As shown in Figure 4, deletion of *Pdk1* blocks not only PanIN development, but also ADM in the *Kras*^{G12D} model. ADM has recently been suggested to be an initiating event in human and murine PDAC formation (Aichler et al., 2012; Caldwell et al., 2012; Morris et al., 2010; Reichert and Rustgi, 2011). Previous studies demonstrated that transforming growth factor α (TGF-α)/epidermal growth factor receptor and Ras activation induces ADM in vitro (Means et al., 2005; Morris et al., 2010; Reichert and Rustgi, 2011).

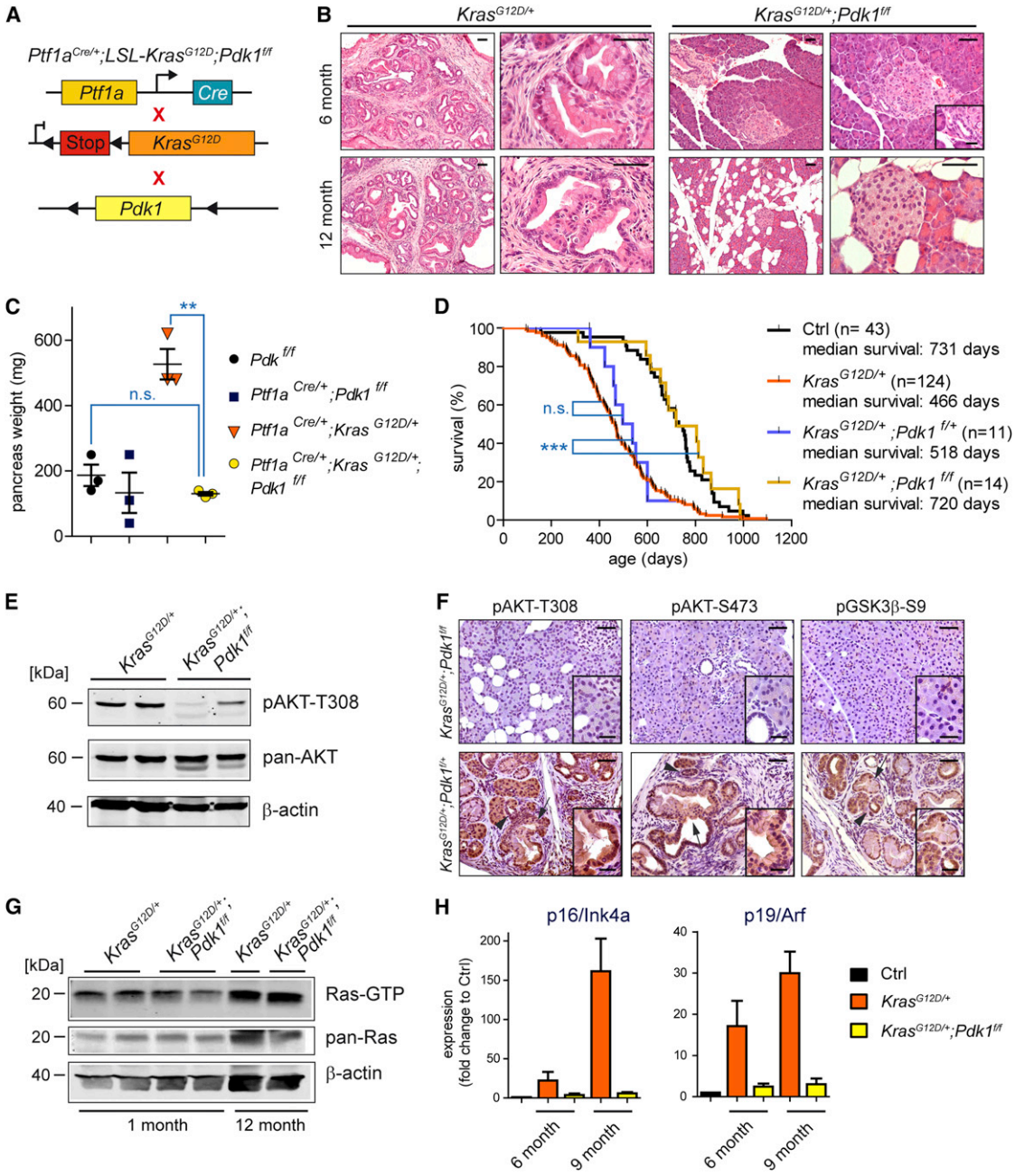

Figure 4. Epithelial PDK1 Is Essential for Kras^{G12D}-Driven Pancreatic Carcinogenesis

(A) Genetic strategy used to study the cell-autonomous role of the PI3K substrate PDK1 in Kras^{G12D}-driven pancreatic cancer formation.

(B) Representative H&E stains of control (*Ptf1a*$^{Cre/+}$;*LSL-Kras*$^{G12D/+}$) and conditional *Pdk1* knockout (*Ptf1a*$^{Cre/+}$;*LSL-Kras*$^{G12D/+}$;*Pdk1*$^{f/f}$) mice.

(C) Pancreatic weight of 6-month-old mice with the indicated genotypes (n.s., not significant; **p < 0.01, Student's t test).

(D) Kaplan-Meier survival analysis of the indicated conditional genotypes. + denotes the wild-type allele, f the conditional allele (n.s., not significant; ***p < 0.001, log-rank test).

(E) Immunoblot analysis of PI3K/AKT pathway activation in pancreata of 12-month-old *Ptf1a*$^{Cre/+}$;*LSL-Kras*$^{G12D/+}$ and *Ptf1a*$^{Cre/+}$;*LSL-Kras*$^{G12D/+}$;*Pdk1*$^{f/f}$ compound mutant mice.

(F) Immunohistochemical analysis of PI3K/AKT pathway activation in the pancreas of 12-month-old mice with the indicated genotypes. Arrowheads indicate ADM and arrows PanIN-1 lesions.

(G) Analysis of activated Ras (Ras-GTP) in the pancreas of 1- and 12-month-old *Ptf1a*$^{Cre/+}$;*LSL-Kras*$^{G12D/+}$ and *Ptf1a*$^{Cre/+}$;*LSL-Kras*$^{G12D/+}$;*Pdk1*$^{f/f}$ mice.

(H) qRT-PCR analysis of p16/Ink4a and p19/Arf mRNA expression in the pancreas of mice with the indicated genotypes. Data are shown as fold change versus Ctrl. Insets show representative histology in high magnification. Scale bars, 50 μm for micrographs, 20 μm for insets. Error bars, ± SEM.

See also Figure S3.

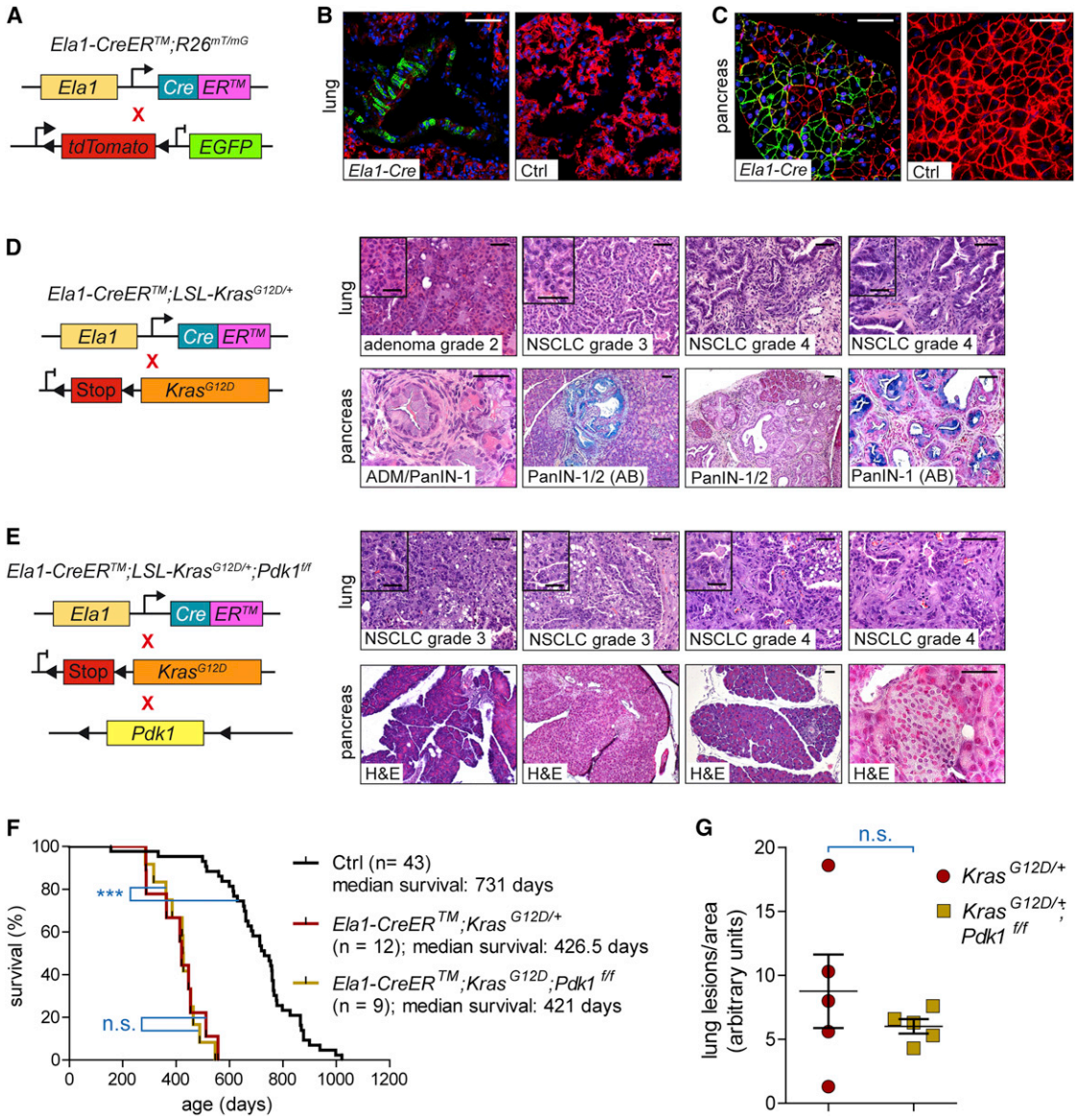

Figure 5. PDK1 Is Essential for Kras^{G12D}-Driven PDAC but not NSCLC Formation

(A) Genetic strategy used to analyze *Ela1-CreER^{TM}* mediated recombination in the lung and the pancreas of the same animal in the absence of tamoxifen with a double fluorescent floxed tdTomato-EGFP reporter line (*R26$^{mT/mG}$*).

(B and C) Confocal microscopic images of tdTomato (red) and Cre-induced EGFP (green) expression in the lung (B) and pancreas (C) of *Ela1-CreER^{TM};R26$^{mT/mG}$* (left panel) and Ctrl *R26$^{mT/mG}$* (right panel) animals. Nuclei were counterstained with TO-PRO-3 (blue). Note the constitutive Cre activity in the pancreas and lung in the absence of tamoxifen in *Ela1-CreER^{TM}* animals.

(D) Genetic strategy used to activate Kras^{G12D} in the lung and the pancreas of the same animal (left panel). H&E stained representative microscopic lung sections graded according to the established 4-stage NSCLC grading system from *Ela1-CreER^{TM};LSL-Kras$^{G12D/+}$* mouse (upper right panel). Lower right panel: Representative H&E or alcian blue (AB) stained microscopic pancreas sections from the same animal. Activation of oncogenic Kras^{G12D} in lung and pancreas using the *Ela1-CreER^{TM}* driver line induces grade 4 NSCLC and pancreatic neoplasia.

(E) Genetic strategy used to study the role of PDK1 in Kras^{G12D}-driven lung and pancreatic cancer formation in the same animal (left panel). Representative H&E stained microscopic lung sections graded according to the established 4-stage NSCLC grading system from *Ela1-CreER^{TM};LSL-Kras$^{G12D/+}$;Pdk1$^{f/f}$* mouse (upper right panel). Lower right panel: Representative H&E stained microscopic pancreas sections from the same animal. Deletion of *Pdk1* blocks ADM and PanIN formation in the pancreas completely but has no effect on NSCLC development and progression.

(F) Kaplan-Meier survival curves of the indicated genotypes (n.s., not significant; ***p < 0.001, log-rank test). Note: All *Ela1-CreER^{TM};LSL-Kras$^{G12D/+}$* and *Ela1-CreER^{TM};LSL-Kras^{G12D};Pdk1$^{f/f}$* animals developed NSCLC.

(G) Quantification of microscopic lung lesions of *Ela1-CreER^{TM};LSL-Kras$^{G12D/+}$* and *Ela1-CreER^{TM};LSL-Kras^{G12D};Pdk1$^{f/f}$* mice (n.s., not significant, Student's t test). Insets show representative lesions in high magnification. Scale bars, 50 μm for micrographs, 20 μm for insets. Note: All *Ela1-CreER^{TM}* animals were analyzed without Cre activation due to constitutive Cre activity (no tamoxifen treatment). Error bars, ± SEM.

See also Figure S4.

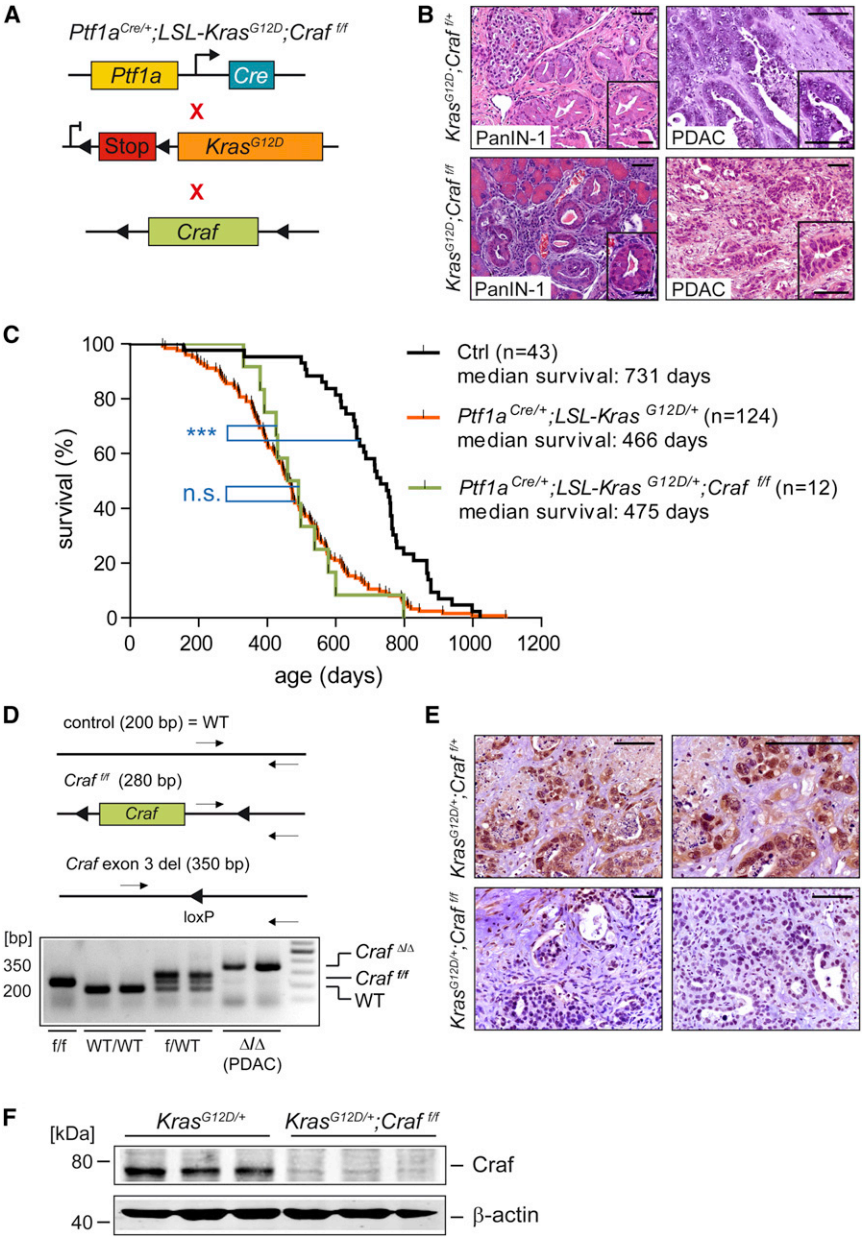

Figure 6. Craf Is Dispensable for Kras^{G12D}-Driven Pancreatic Carcinogenesis

(A) Genetic strategy used to study the cell-autonomous role of Craf in Kras^{G12D}-driven pancreatic cancer formation.

(B) Representative H&E stains of control (*Ptf1a*$^{Cre/+}$;*LSL-Kras*$^{G12D/+}$;*Craf* $^{f/+}$) and conditional *Craf* knockout (*Ptf1a*$^{Cre/+}$; *LSL-Kras*$^{G12D/+}$;*Craf* $^{f/f}$) mice.

(C) Kaplan-Meier survival analysis of the indicated conditional genotypes. + denotes the wild-type allele, f the conditional allele (n.s., not significant; ***p < 0.001, log-rank test).

(D) Genotyping strategy of the floxed Craf allele (upper panel). PCR analysis of DNA from wild-type (WT), heterozygous (f/WT) and homozygous (f/f) conditional floxed Craf mice and *Ptf1a*^{Cre} mediated deletion of exon 3 of *Craf* (*Craf*$^{\Delta/\Delta}$) in pancreatic cancer cells (PDAC) (lower panel). Sizes of WT and mutant PCR products are indicated. Note: Efficient recombination of both floxed *Craf* alleles in PDAC cells from *Ptf1a*$^{Cre/+}$;*Kras*$^{G12D/+}$;*Craf*$^{f/f}$ mice.

(E) Immunohistochemical analysis of Craf expression in PDAC of *Ptf1a*$^{Cre/+}$;*Kras*$^{G12D/+}$;*Craf*$^{f/f}$ and *Ptf1a*$^{Cre/+}$;*Kras*$^{G12D/+}$;*Craf* $^{f/+}$ mice. + denotes the WT allele, f the conditional allele.

(F) Immunoblot analysis of Craf expression in primary PDAC cells from mice with the indicated genotypes. β-actin was used as loading control. Insets show representative lesions in high magnification. Scale bars, 50 μm for micrographs, 20 μm for insets.

To test whether TGF-α/Kras-induced ADM formation depends on intact PDK1 signaling, we isolated acini from *Ptf1a*$^{Cre/+}$;*Kras*$^{G12D/+}$ and *Ptf1a*$^{Cre/+}$;*Kras*$^{G12D/+}$;*Pdk1*$^{f/f}$ pancreata and performed an in vitro ADM assay (Means et al., 2005). Consistent with the in vivo data (Figures 7A and 7B), we observed that deletion of *Pdk1* completely blocked ADM in the presence and absence of TGF-α (Figures 7C and 7D). Acini isolated from *Ptf1a*$^{Cre/+}$;*Kras*$^{G12D/+}$ and *Ptf1a*$^{Cre/+}$;*Kras*$^{G12D/+}$;*Pdk1*$^{f/f}$ pancreata were equally viable (data not shown), thus excluding differences in cellular vulnerability as a possible cause. ADM was also blocked by the pan class I PI3K inhibitor GDC 0941, the PDK1 inhibitor BX912, the dual pan class I PI3K-mTOR inhibitor NPV-Bez235, and the AKT inhibitor MK-2206 (Figure 7E). Interestingly, the RSK inhibitor BI-D1870 had no effect on ADM formation even at concentrations as high as 10 μM (Figure 7E). These data confirm our in vivo genetic studies in mice and indicate that disruption of the canonical PI3K-PDK1-AKT, but not the PDK1-RSK axis, blocks ADM and therefore, tumor initiation in the pancreas.

To test if our murine model system is relevant to humans, we established primary acinar cell culture from human pancreas and performed functional ADM assays with various PI3K-PDK1-AKT pathway inhibitors (Figures 7F, 7G, S5A, and S5B). As shown in Figure 7F, TGF-α treatment of human acinar cells induced ADM, as indicated by CK19 staining, with concomitant PI3K pathway activation, as evidenced by AKT-T308 phosphorylation. Treatment with GDC 0941 blocked ADM significantly in a dose-dependent manner (Figures 7G and S5A–S5C) and inhibited AKT-T308 phosphorylation and CK19 expression (Figure S5C).

Overall, these data support the notion that PI3K/PDK1 signaling is essential for pancreatic cell plasticity and tumor initiation and important to transmit the oncogenic Kras-induced program in the pancreas. However, we cannot completely exclude a role for indirect mechanisms of PI3K activation via alternate effectors such as receptor tyrosine kinases, rather than a direct Kras/PI3K interaction (Ardito et al., 2012; Ebi et al., 2011; Navas et al., 2012).

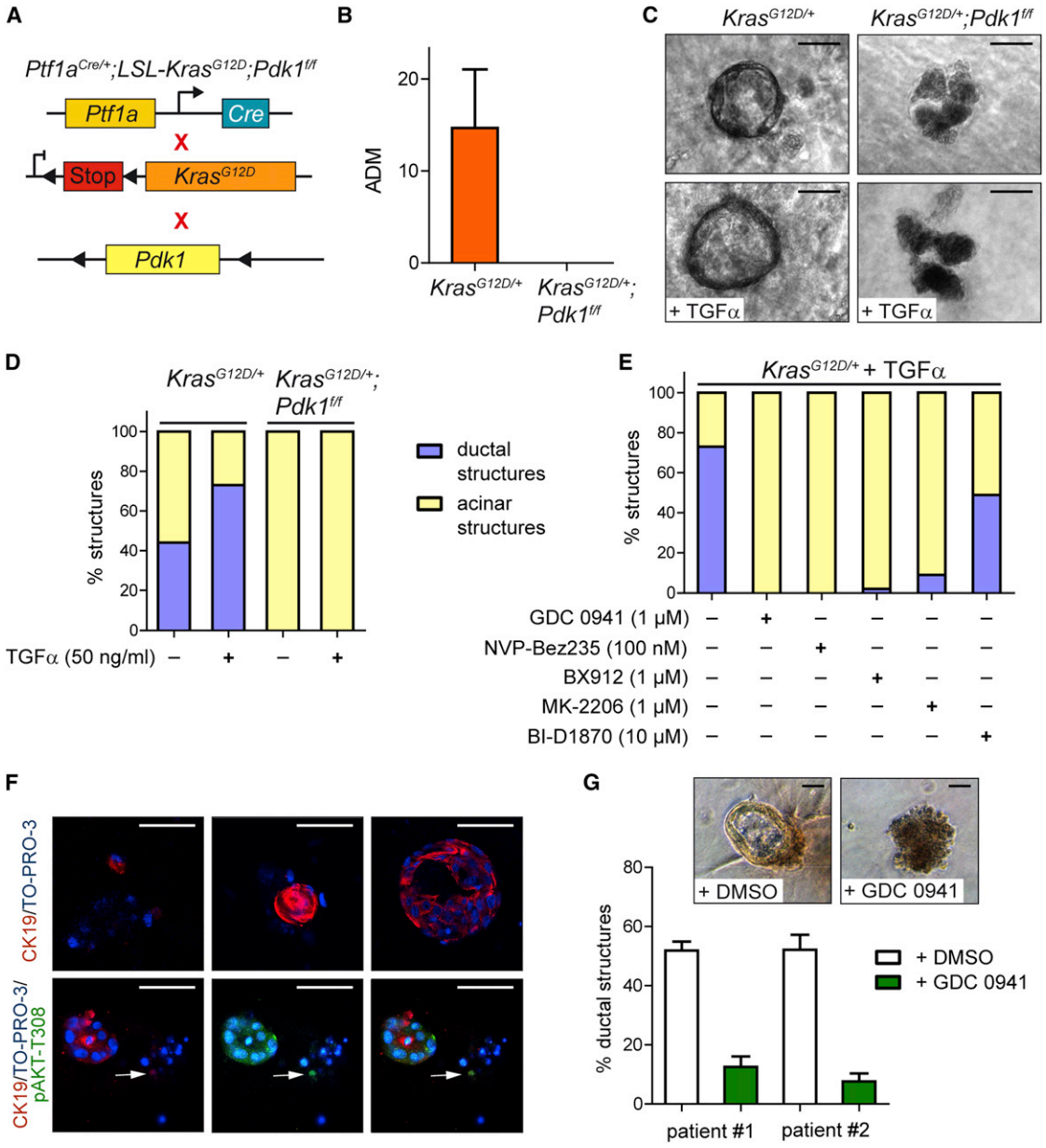

Figure 7. PI3K Signaling Regulates Human and Murine ADM

(A) Genetic strategy used to study the role of PDK1 in Kras^{G12D}-driven ADM.

(B) Quantification of ADM in 6-month-old *Ptf1a*$^{Cre/+}$;*LSL-Kras*$^{G12D/+}$ and *Ptf1a*$^{Cre/+}$;*LSL-Kras*$^{G12D/+}$;*Pdk1*$^{f/f}$ mice (n = 3; 3 representative slides per mouse).

(C) Phase contrast images of pancreatic acinar cells with the indicated genotypes 5 days after isolation and treatment with or without TGF-α (50 ng/ml).

(D) Quantification of ductal and acinar structures after 5 days in culture. Bar graph shows percentage of structures of the indicated genotypes with and without TGF-α treatment.

(E) Quantification of ductal and acinar structures after 5 days in culture with and without treatment with the indicated chemicals. Bar graph shows percentage of structures of indicated genotype treated with TGF-α and the indicated chemicals.

(F) Confocal microscopic images of TGF-α-induced human ADM. Upper panel: CK19 expression (red) in ADM after 5 days of TGF-α (50 ng/ml) treatment. Lower panel: CK19 expression (red) and AKT-T308 phosphorylation (green) after 5 days TGF-α treatment. Arrow indicates a cell with acinar morphology but positive staining for CK19 and pAKT-T308. Nuclei were counterstained with TO-PRO-3 (blue).

(G) Upper panel: Phase contrast images of human pancreatic acinar cells 5 days after isolation and treatment with TGF-α (50 ng/ml) with or without GDC 0941 (1 μM). Lower panel: Quantification of human ductal and acinar structures from two independent patients after 5 days in culture with and without GDC 0941 treatment. Scale bars, 50 μm. Error bars, ± SEM.

See also Figure S5.

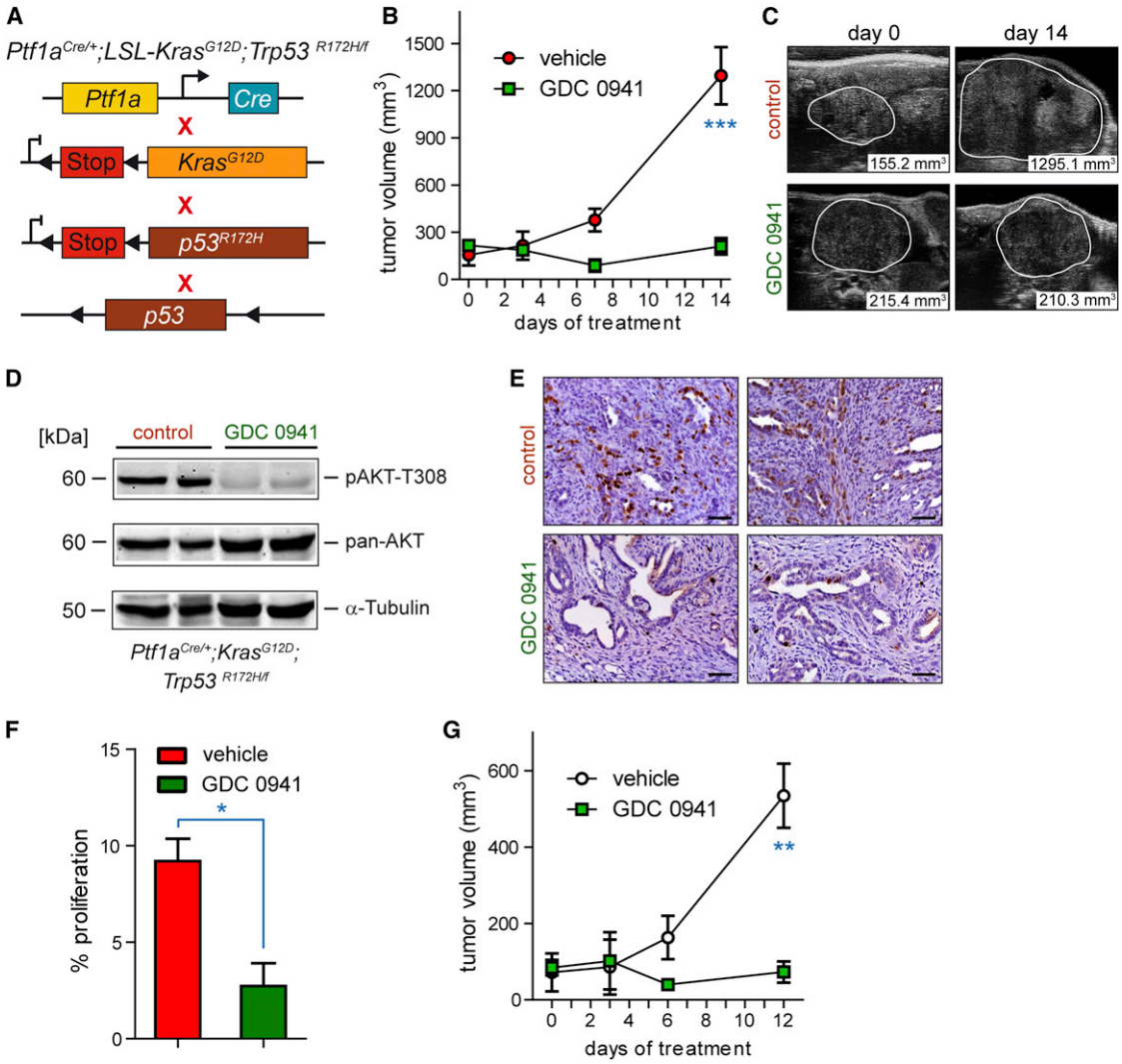

Figure 8. PI3K Signaling Is needed for Human and Murine Kras^{G12D}-Driven Pancreatic Tumor Maintenance

(A) Genetic strategy used to induce *Trp53*^{R172H} mutant PDAC (KPC mouse model).

(B) KPC mice with mean tumor diameters > 5 mm were enrolled and randomized into the GDC 0941 treatment or control (vehicle) group (n = 3 per group). Tumor growth was monitored by high-resolution ultrasound (Vevo 770 System, Visual Sonics). Data represent the mean tumor volumes ± SD (***p < 0.001, Student's t test).

(C) Representative high-resolution ultrasound images from KPC mice pre-treatment (left, day 0) and after 14 days on study (right). Visible lesions are outlined in white and mean tumor burden for each cohort is shown in mm^3 in the lower right corner.

(D) Immunoblot analysis of AKT-T308 phosphorylation in primary PDAC specimens from control and GDC 0941 treated KPC mice. α-Tubulin was used as loading control.

(E) Immunohistochemical BrdU staining of representative PDACs from control and GDC 0941-treated KPC mice indicates blockade of proliferation in the treatment group. Scale bars, 50 μm.

(F) Quantification of BrdU-positive proliferating cells (three representative slides per mouse; *p < 0.05, Student's t test). Error bars, ± SEM.

(G) Patient-derived primary PDAC cells (TUM-PaCa1; see Figure S6C) were orthotopically transplanted into the pancreas of *NOD-SCID-IL2Rγ* mice. After establishment of sizeable tumors, mice were randomized and treated with GDC 0941 or vehicle for 12 days (n = 3 per group). Data represent the mean tumor volumes ± SD (**p < 0.01, Student's t test).

See also Figure S6.

The PI3K/PDK1 Pathway Is a Target for Treatment of Murine and Human Pancreatic Cancer

To test whether PI3K-PDK1-AKT signaling could be a target for pancreatic cancer therapy, we used the well-established *Ptf1a*$^{Cre/+}$;*LSL-Kras*$^{G12D/+}$;*LSL-Trp53*$^{R172H/f}$ (KPC) model (Figure 8A) (Olive et al., 2009). KPC mice develop primary PDAC that faithfully recapitulates the molecular, histopathologic, and clinical features of the human disease (Olive et al., 2009).

To inhibit PI3K signaling in vivo, we used GDC 0941, a potent and selective oral pan class I PI3K inhibitor currently under clinical development (LoRusso et al., 2011; Yuan et al., 2013). GDC 0941 efficiently inhibited the growth of primary murine *Kras*^{G12D} and primary human patient-derived PDAC cells in vitro (Figures

S6A–S6C). To evaluate the in vivo efficacy of GDC 0941 against $Kras^{G12D}$-induced PDAC, KPC mice with established tumors of comparable size were treated for 14 days with vehicle or GDC 0941 at 150 mg/kg/day. GDC 0941 efficiently blocked tumor growth as measured by high-resolution ultrasound and reduced phosphorylation of AKT-T308, a surrogate marker of PI3K signaling via PDK1 (Figures 8B–8D). All GDC 0941-treated animals displayed stable disease, whereas vehicle-treated animals showed rapid disease progression (Figures 8B and 8C). Consistent with this, histopathologic analysis showed significantly decreased proliferation of GDC 0941-treated tumors (Figures 8E and 8F).

To demonstrate the relevance of the pathway for human pancreatic cancer therapy, we used primary patient-derived PDAC cells transplanted orthotopically into the pancreas of NOD-SCID-IL2Rγ (NSG) mice. We observed very similar antitumor effects of GDC 0941 in this humanized PDAC model (Figures 8G and S6D). These data strongly suggest that PI3K signaling is also necessary for proliferation and maintenance of established murine and human PDAC and that the PI3K-PDK1-AKT pathway is a promising target for therapeutic interventions.

DISCUSSION

There has been no major breakthrough in the treatment of PDAC in the past 30 years and no effective targeted therapies are available (Hidalgo, 2010). Nearly all PDAC harbor *KRAS* mutations, but efforts to develop effective Kras inhibitors have generally failed. It is therefore essential to understand and define the importance of effectors of mutant Kras and to identify nonredundant essential nodes of nononcogene addiction (Pylayeva-Gupta et al., 2011). Here, we show that PI3K-PDK1 signaling is such a node in Kras-driven pancreatic cancer initiation and maintenance.

It has recently become evident that Craf is essential for the onset of Kras-driven non-small cell lung cancer (Blasco et al., 2011; Karreth et al., 2011). However, ablation of *Craf* in our $Kras^{G12D}$-driven PDAC model had no significant inhibitory effect on tumor development, progression, or survival. This demonstrates that there are substantial tissue- and context-specific differences in Kras effector usage. Such differences may have important clinical implications because they could explain the diverse response to targeted therapies of different tumor types harboring oncogenic *KRAS* mutations. Indeed, a recent study showed no substantial response of $Kras^{G12D}$-driven NSCLC toward PI3K-mTOR inhibition in vivo (Engelman et al., 2008). In contrast, we demonstrate that targeting the PI3K pathway in $Kras^{G12D}$-driven PDAC efficiently blocks carcinogenesis and tumor progression. Our data thus provide in vivo evidence for the rationale to investigate Kras-driven oncogenic pathways in a tissue- and context-specific manner to characterize the relevant nodes engaged in different tumor entities.

Collisson and colleagues found that oncogenic $Braf^{V600E}$ is capable of inducing PanIN lesions in mice (Collisson et al., 2012). Using a tamoxifen-inducible transgenic *Pdx1-CreER*^{T2}-driver line, they activated a latent $Braf^{V600E}$ allele in the pancreas of adult mice and observed a greater number of PanIN lesions than in the classical $Kras^{G12D}$ model. These data and our findings clearly show that activation or deletion of different Kras-dependent signaling pathways can induce or block PanIN formation in vivo. This argues either for the existence of several distinct routes toward PanIN formation, or an essential crosstalk between the Raf-MEK-ERK and PI3K-PDK1-AKT pathway, which might depend on alternate effectors like receptor tyrosine kinases (Ardito et al., 2012; Ebi et al., 2011; Navas et al., 2012). Collisson and colleagues showed that PanIN formation can be caused by activation of the canonical Raf-MEK-ERK pathway at the level of Braf. Whether Braf is essential for PanIN formation in the $Kras^{G12D}$ model, as we show for the direct PI3K downstream target PDK1, needs to be investigated at the genetic level in the future.

In contrast to our study, Collisson and colleagues found no PanIN development after tamoxifen induced p110α^{H1047R} expression in the pancreas using the *Pdx1-CreER*^{T2} mouse line. This might be due to distinct target cells, or differences in *Pik3ca* copy number, Cre-induced recombination efficacy, or different expression and signaling levels of p110α in the $Ptf1a^{Cre}$ and *Ela1-CreER*^{TM} versus *Pdx1-CreER*^{T2} models (Collisson et al., 2012). Based on the similar phenotypes of our $Kras^{G12D}$ and $PIK3CA^{H1047R}$ models, the lack of Ras activation in $PIK3CA^{H1047R}$ mice, comparable levels of PI3K activation and expression as well as PIP3 levels in the $Kras^{G12D}$ and $PIK3CA^{H1047R}$ models, and by showing that deletion of the PI3K effector *Pdk1* blocks tumor formation, ADM, and PI3K activation in the $Kras^{G12D}$ model, we provide evidence at multiple levels that Kras acts through PI3K-PDK1 to induce pancreatic cancer. This conclusion is further supported using primary human material showing that PI3K signaling is active in human acinar-to-ductal metaplasia, premalignant pancreatic lesions and cancers, and is mechanistically involved in early processes of pancreatic cell plasticity and cancer formation as well as in tumor maintenance.

Downward and colleagues showed previously that the Ras-PI3K interaction plays an important role in Ras-induced skin and lung carcinogenesis (Gupta et al., 2007). They found that disruption of the direct Ras/p110α interaction—by constitutive expression of $Pik3ca^{T208D/K227A}$ in the mouse germline—dramatically reduced the number of Ras-induced papillomas and lung adenomas (Gupta et al., 2007). It is however unclear to what extent this was mediated by cell autonomous or non-cell autonomous effects in the host. Since p110α is required for angiogenesis (Graupera et al., 2008), disruption of the Ras-PI3K interaction in the vasculature, immune system, or stroma is likely to contribute significantly to the observed effects in this model.

Because PDK1 is a central node of PI3K signaling (Castellano and Downward, 2011), we evaluated its cell-autonomous role in Kras-induced NSCLC in vivo. Intriguingly, ablation of *Pdk1* specifically in the epithelial compartment of the lung using two different recombination strategies had no significant inhibitory effect on $Kras^{G12D}$-induced NSCLC development and progression. This suggests that PI3K signaling plays an important role in the tumor microenvironment rather than a cell autonomous function during NSCLC formation (Graupera et al., 2008). This is supported by the observation that Ras-induced NSCLC development is impaired but not completely blocked by constitutive expression of the $Pik3ca^{T208D/K227A}$ in the mouse germline (Gupta et al., 2007). In contrast to the lung, genetic inactivation of PDK1 in pancreas epithelium using two different Cre-driver lines completely blocked $Kras^{G12D}$-induced neoplastic transformation. These

data clearly demonstrate that each tissue has its own and unique cell autonomous signaling requirements during oncogenic transformation. This advance in our understanding of tissue-specific effects of oncogenic Kras may change clinical practice in the future because it clearly shows that results cannot simply be extrapolated from one Kras-driven tumor entity to another.

We have defined the tumor cell autonomous Kras-PI3K-PDK1 axis as an essential pathway of pancreatic cancer with the capacity to induce cell plasticity, ADM, PanIN, and cancer formation as well as tumor maintenance. A large variety of pharmacologic inhibitors directed against the PI3K pathway and the promising targetable node PDK1 are now available for clinical investigation (Engelman, 2009; Liu et al., 2009; Pearce et al., 2010). Recognition of the importance of the PI3K-PDK1 pathway in PDAC, as demonstrated in this study, will provide a more effective approach for targeted therapeutic interventions for this grave disease.

EXPERIMENTAL PROCEDURES

Mouse Strains and Tumor Models

LSL-Kras$^{G12D/+}$ (Hingorani et al., 2003), *Ptf1a*$^{Cre/+}$ (Eser et al., 2011; Nakhai et al., 2007; Seidler et al., 2008), *LSL-Rac1*$^{G12V/+}$ (Srinivasan et al., 2009), *LSL-Trp53*$^{R172H/+}$ (Hingorani et al., 2005), *Trp53*$^{f/+}$ (Jonkers et al., 2001), *LSL-R26*$^{lacZ/+}$ (Seidler et al., 2008), *R26*$^{mT/mG}$ (Muzumdar et al., 2007), *Ela1-CreER*^{TM} (Stanger et al., 2005), *Cdkn2a*$^{f/+}$ (Aguirre et al., 2003), *Craf*$^{f/+}$ (Jesenberger et al., 2001), and *Pdk1*$^{f/+}$ (Lawlor et al., 2002) mice have been described previously. The strains were interbred to obtain mice with activation of distinct pathways in the pancreas as previously described (Eser et al., 2011). All animal studies were conducted in compliance with European guidelines for the care and use of laboratory animals and were approved by the Institutional Animal Care and Use Committees (IACUC) of Technische Universität München, Regierung von Oberbayern and UK Home Office.

Human Pancreatic Tissue Samples

This study conformed to the Declaration of Helsinki and was approved by the ethics committee of the Technische Universität München. Informed consent was obtained from all patients included in the study.

Generation of Primary Human and Murine Ductal Pancreatic Cancer Cell Lines

Primary dispersed murine pancreatic cancer cells were established from *Ptf1a*$^{Cre/+}$;*LSL-Kras*$^{G12D/+}$ and *Ptf1a*$^{Cre/+}$;*LSL-PIK3CA*$^{H1047R/+}$ mice and cultivated as previously described (von Burstin et al., 2009). Primary dispersed human PDAC cells were isolated from surgically resected human PDAC as recently described (Conradt et al., 2011). Only early-passage (passage 3 to 4) dispersed cells were used for assays.

Establishment of Patient-Derived Xenograft Tumors from Primary Human PDAC

Tissues were placed into chilled sterile RPMI 1640 (Thermo Scientific/Hyclone, Waltham, MA) supplemented with 1% (v/v) penicillin/streptomycin/amphotericin B. The tumor was washed twice, dissected into 3 mm cubes and pieces were implanted subcutaneously into NOD SCIG IL2Rγ (NSG) mice (#005557; Jackson Laboratory, Bar Harbor, Maine) within 1 hour of resection.

Patient-Derived Orthotopic Human Pancreatic Cancer Xenotransplantation Model

One million patient-derived primary human pancreatic cancer cells in 20 μl Dulbecco's modified Eagle medium were implanted orthotopically into the pancreas of NSG mice as described (von Burstin et al., 2009; von Burstin et al., 2008).

Statistical Analyses

Comparisons between data sets were made with analysis of variance, followed by Students t test. A Bonferroni correction of the p values was performed for multiple testing. Kaplan-Meier survival curves were compared by log-rank test. Values of $p < 0.05$ or less were considered to be statistically significant.

SUPPLEMENTAL INFORMATION

Supplemental Information includes six figures and Supplemental Experimental Procedures and can be found with this article online at http://dx.doi.org/10.1016/j.ccr.2013.01.023.

ACKNOWLEDGMENTS

We would like to thank Dr. D. Melton, Dr. K. Rajewsky, Dr. N. Bardeesy, Dr. A. Berns, Dr. L. Luo, Dr. D. Tuveson, and Dr. T. Jacks for providing transgenic animals; Dr. P. Vogt for p110α^{H1047R} expression plasmid; and J. Götzfried, V. Klein, T. Schmid, and M. Zukowska for excellent technical assistance. This work was supported by funding from Deutsche Krebshilfe (# 108985 to D.S.), Helmholtz Preclinical Comprehensive Cancer Center (to D.S.), Novartis-Stiftung für therapeutische Forschung (to G.S. and D.S.), and DFG SFB824, TP C9 (to G.S. and D.S.). B.S., G.S., and D.S. designed research; S.E., N.R., M.M., B.S., K.G., M.D., M.H., A.A., S.K., B.K., L.R., R.R., and D.S. performed research; B.K., C.W.M., A.M.S., L.R., I.E., A.J.K., A.E.S., M.B., D.A., R.R., and R.M.S. contributed new reagents/analytic tools; S.E., N.R., M.M., B.S., K.G., M.D., M.H., A.A., A.M.S., I.E., L.R., R.R., and D.S. analyzed data; and B.S., G.S., and D.S. wrote the paper. All authors discussed the results and commented on the manuscript.

Received: October 4, 2012
Revised: December 27, 2012
Accepted: January 30, 2013
Published: February 28, 2013

REFERENCES

Adams, J.R., Xu, K., Liu, J.C., Agamez, N.M., Loch, A.J., Wong, R.G., Wang, W., Wright, K.L., Lane, T.F., Zacksenhaus, E., and Egan, S.E. (2011). Cooperation between Pik3ca and p53 mutations in mouse mammary tumor formation. Cancer Res. *71*, 2706–2717.

Aguirre, A.J., Bardeesy, N., Sinha, M., Lopez, L., Tuveson, D.A., Horner, J., Redston, M.S., and DePinho, R.A. (2003). Activated Kras and Ink4a/Arf deficiency cooperate to produce metastatic pancreatic ductal adenocarcinoma. Genes Dev. *17*, 3112–3126.

Aichler, M., Seiler, C., Tost, M., Siveke, J., Mazur, P.K., Da Silva-Buttkus, P., Bartsch, D.K., Langer, P., Chiblak, S., Dürr, A., et al. (2012). Origin of pancreatic ductal adenocarcinoma from atypical flat lesions: a comparative study in transgenic mice and human tissues. J. Pathol. *226*, 723–734.

Alessi, D.R., James, S.R., Downes, C.P., Holmes, A.B., Gaffney, P.R., Reese, C.B., and Cohen, P. (1997). Characterization of a 3-phosphoinositide-dependent protein kinase which phosphorylates and activates protein kinase Balpha. Curr. Biol. *7*, 261–269.

Ardito, C.M., Grüner, B.M., Takeuchi, K.K., Lubeseder-Martellato, C., Teichmann, N., Mazur, P.K., Delgiorno, K.E., Carpenter, E.S., Halbrook, C.J., Hall, J.C., et al. (2012). EGF receptor is required for KRAS-induced pancreatic tumorigenesis. Cancer Cell *22*, 304–317.

Bader, A.G., Kang, S., Zhao, L., and Vogt, P.K. (2005). Oncogenic PI3K deregulates transcription and translation. Nat. Rev. Cancer *5*, 921–929.

Bardeesy, N., Aguirre, A.J., Chu, G.C., Cheng, K.H., Lopez, L.V., Hezel, A.F., Feng, B., Brennan, C., Weissleder, R., Mahmood, U., et al. (2006). Both p16(Ink4a) and the p19(Arf)-p53 pathway constrain progression of pancreatic adenocarcinoma in the mouse. Proc. Natl. Acad. Sci. USA *103*, 5947–5952.

Blasco, R.B., Francoz, S., Santamaría, D., Cañamero, M., Dubus, P., Charron, J., Baccarini, M., and Barbacid, M. (2011). c-Raf, but not B-Raf, is essential for development of K-Ras oncogene-driven non-small cell lung carcinoma. Cancer Cell *19*, 652–663.

Caldwell, M.E., DeNicola, G.M., Martins, C.P., Jacobetz, M.A., Maitra, A., Hruban, R.H., and Tuveson, D.A. (2012). Cellular features of senescence

during the evolution of human and murine ductal pancreatic cancer. Oncogene *31*, 1599–1608.

Cantley, L.C. (2002). The phosphoinositide 3-kinase pathway. Science *296*, 1655–1657.

Carpelan-Holmström, M., Nordling, S., Pukkala, E., Sankila, R., Lüttges, J., Klöppel, G., and Haglund, C. (2005). Does anyone survive pancreatic ductal adenocarcinoma? A nationwide study re-evaluating the data of the Finnish Cancer Registry. Gut *54*, 385–387.

Castellano, E., and Downward, J. (2011). RAS Interaction with PI3K: More Than Just Another Effector Pathway. Genes Cancer *2*, 261–274.

Collisson, E.A., Trejo, C.L., Silva, J.M., Gu, S., Korkola, J.E., Heiser, L.M., Charles, R.P., Rabinovich, B.A., Hann, B., Dankort, D., et al. (2012). A central role for RAF→MEK→ERK signaling in the genesis of pancreatic ductal adenocarcinoma. Cancer Discov. *2*, 685–693.

Conradt, L., Godl, K., Schaab, C., Tebbe, A., Eser, S., Diersch, S., Michalski, C.W., Kleeff, J., Schnieke, A., Schmid, R.M., et al. (2011). Disclosure of erlotinib as a multikinase inhibitor in pancreatic ductal adenocarcinoma. Neoplasia *13*, 1026–1034.

Currie, R.A., Walker, K.S., Gray, A., Deak, M., Casamayor, A., Downes, C.P., Cohen, P., Alessi, D.R., and Lucocq, J. (1999). Role of phosphatidylinositol 3,4,5-trisphosphate in regulating the activity and localization of 3-phosphoinositide-dependent protein kinase-1. Biochem. J. *337*, 575–583.

Ebi, H., Corcoran, R.B., Singh, A., Chen, Z., Song, Y., Lifshits, E., Ryan, D.P., Meyerhardt, J.A., Benes, C., Settleman, J., et al. (2011). Receptor tyrosine kinases exert dominant control over PI3K signaling in human KRAS mutant colorectal cancers. J. Clin. Invest. *121*, 4311–4321.

Engelman, J.A. (2009). Targeting PI3K signalling in cancer: opportunities, challenges and limitations. Nat. Rev. Cancer *9*, 550–562.

Engelman, J.A., Chen, L., Tan, X., Crosby, K., Guimaraes, A.R., Upadhyay, R., Maira, M., McNamara, K., Perera, S.A., Song, Y., et al. (2008). Effective use of PI3K and MEK inhibitors to treat mutant Kras G12D and PIK3CA H1047R murine lung cancers. Nat. Med. *14*, 1351–1356.

Eser, S., Messer, M., Eser, P., von Werder, A., Seidler, B., Bajbouj, M., Vogelmann, R., Meining, A., von Burstin, J., Algül, H., et al. (2011). In vivo diagnosis of murine pancreatic intraepithelial neoplasia and early-stage pancreatic cancer by molecular imaging. Proc. Natl. Acad. Sci. USA *108*, 9945–9950.

Graupera, M., Guillermet-Guibert, J., Foukas, L.C., Phng, L.K., Cain, R.J., Salpekar, A., Pearce, W., Meek, S., Millan, J., Cutillas, P.R., et al. (2008). Angiogenesis selectively requires the p110alpha isoform of PI3K to control endothelial cell migration. Nature *453*, 662–666.

Guerra, C., Schuhmacher, A.J., Cañamero, M., Grippo, P.J., Verdaguer, L., Pérez-Gallego, L., Dubus, P., Sandgren, E.P., and Barbacid, M. (2007). Chronic pancreatitis is essential for induction of pancreatic ductal adenocarcinoma by K-Ras oncogenes in adult mice. Cancer Cell *11*, 291–302.

Gupta, S., Ramjaun, A.R., Haiko, P., Wang, Y., Warne, P.H., Nicke, B., Nye, E., Stamp, G., Alitalo, K., and Downward, J. (2007). Binding of ras to phosphoinositide 3-kinase p110alpha is required for ras-driven tumorigenesis in mice. Cell *129*, 957–968.

Hashimoto, N., Kido, Y., Uchida, T., Asahara, S., Shigeyama, Y., Matsuda, T., Takeda, A., Tsuchihashi, D., Nishizawa, A., Ogawa, W., et al. (2006). Ablation of PDK1 in pancreatic beta cells induces diabetes as a result of loss of beta cell mass. Nat. Genet. *38*, 589–593.

Heid, I., Lubeseder-Martellato, C., Sipos, B., Mazur, P.K., Lesina, M., Schmid, R.M., and Siveke, J.T. (2011). Early requirement of Rac1 in a mouse model of pancreatic cancer. Gastroenterology *141*, 719–730.

Hidalgo, M. (2010). Pancreatic cancer. N. Engl. J. Med. *362*, 1605–1617.

Hingorani, S.R., Petricoin, E.F., Maitra, A., Rajapakse, V., King, C., Jacobetz, M.A., Ross, S., Conrads, T.P., Veenstra, T.D., Hitt, B.A., et al. (2003). Preinvasive and invasive ductal pancreatic cancer and its early detection in the mouse. Cancer Cell *4*, 437–450.

Hingorani, S.R., Wang, L., Multani, A.S., Combs, C., Deramaudt, T.B., Hruban, R.H., Rustgi, A.K., Chang, S., and Tuveson, D.A. (2005). Trp53R172H and KrasG12D cooperate to promote chromosomal instability and widely metastatic pancreatic ductal adenocarcinoma in mice. Cancer Cell *7*, 469–483.

Hruban, R.H., Rustgi, A.K., Brentnall, T.A., Tempero, M.A., Wright, C.V., and Tuveson, D.A. (2006). Pancreatic cancer in mice and man: the Penn Workshop 2004. Cancer Res. *66*, 14–17.

Jesenberger, V., Procyk, K.J., Rüth, J., Schreiber, M., Theussl, H.C., Wagner, E.F., and Baccarini, M. (2001). Protective role of Raf-1 in Salmonella-induced macrophage apoptosis. J. Exp. Med. *193*, 353–364.

Jimeno, A., Tan, A.C., Coffa, J., Rajeshkumar, N.V., Kulesza, P., Rubio-Viqueira, B., Wheelhouse, J., Diosdado, B., Messersmith, W.A., Iacobuzio-Donahue, C., et al. (2008). Coordinated epidermal growth factor receptor pathway gene overexpression predicts epidermal growth factor receptor inhibitor sensitivity in pancreatic cancer. Cancer Res. *68*, 2841–2849.

Jonkers, J., Meuwissen, R., van der Gulden, H., Peterse, H., van der Valk, M., and Berns, A. (2001). Synergistic tumor suppressor activity of BRCA2 and p53 in a conditional mouse model for breast cancer. Nat. Genet. *29*, 418–425.

Karreth, F.A., Frese, K.K., DeNicola, G.M., Baccarini, M., and Tuveson, D.A. (2011). C-Raf is required for the initiation of lung cancer by K-Ras(G12D). Cancer Discov *1*, 128–136.

Kennedy, A.L., Morton, J.P., Manoharan, I., Nelson, D.M., Jamieson, N.B., Pawlikowski, J.S., McBryan, T., Doyle, B., McKay, C., Oien, K.A., et al. (2011). Activation of the PIK3CA/AKT pathway suppresses senescence induced by an activated RAS oncogene to promote tumorigenesis. Mol. Cell *42*, 36–49.

Lawlor, M.A., Mora, A., Ashby, P.R., Williams, M.R., Murray-Tait, V., Malone, L., Prescott, A.R., Lucocq, J.M., and Alessi, D.R. (2002). Essential role of PDK1 in regulating cell size and development in mice. EMBO J. *21*, 3728–3738.

Liu, P., Cheng, H., Roberts, T.M., and Zhao, J.J. (2009). Targeting the phosphoinositide 3-kinase pathway in cancer. Nat. Rev. Drug Discov. *8*, 627–644.

Liu, P., Cheng, H., Santiago, S., Raeder, M., Zhang, F., Isabella, A., Yang, J., Semaan, D.J., Chen, C., Fox, E.A., et al. (2011). Oncogenic PIK3CA-driven mammary tumors frequently recur via PI3K pathway-dependent and PI3K pathway-independent mechanisms. Nat. Med. *17*, 1116–1120.

LoRusso, P.M., Weiss, D., Guardino, E., Girish, S., and Sliwkowski, M.X. (2011). Trastuzumab emtansine: a unique antibody-drug conjugate in development for human epidermal growth factor receptor 2-positive cancer. Clin. Cancer Res. *17*, 6437–6447.

Means, A.L., Meszoely, I.M., Suzuki, K., Miyamoto, Y., Rustgi, A.K., Coffey, R.J., Jr., Wright, C.V., Stoffers, D.A., and Leach, S.D. (2005). Pancreatic epithelial plasticity mediated by acinar cell transdifferentiation and generation of nestin-positive intermediates. Development *132*, 3767–3776.

Morris, J.P., 4th, Wang, S.C., and Hebrok, M. (2010). KRAS, Hedgehog, Wnt and the twisted developmental biology of pancreatic ductal adenocarcinoma. Nat. Rev. Cancer *10*, 683–695.

Muzumdar, M.D., Tasic, B., Miyamichi, K., Li, L., and Luo, L. (2007). A global double-fluorescent Cre reporter mouse. Genesis *45*, 593–605.

Nakhai, H., Sel, S., Favor, J., Mendoza-Torres, L., Paulsen, F., Duncker, G.I., and Schmid, R.M. (2007). Ptf1a is essential for the differentiation of GABAergic and glycinergic amacrine cells and horizontal cells in the mouse retina. Development *134*, 1151–1160.

Navas, C., Hernández-Porras, I., Schuhmacher, A.J., Sibilia, M., Guerra, C., and Barbacid, M. (2012). EGF receptor signaling is essential for k-ras oncogene-driven pancreatic ductal adenocarcinoma. Cancer Cell *22*, 318–330.

Olive, K.P., Jacobetz, M.A., Davidson, C.J., Gopinathan, A., McIntyre, D., Honess, D., Madhu, B., Goldgraben, M.A., Caldwell, M.E., Allard, D., et al. (2009). Inhibition of Hedgehog signaling enhances delivery of chemotherapy in a mouse model of pancreatic cancer. Science *324*, 1457–1461.

Pearce, L.R., Komander, D., and Alessi, D.R. (2010). The nuts and bolts of AGC protein kinases. Nat. Rev. Mol. Cell Biol. *11*, 9–22.

Pinho, A.V., Rooman, I., Reichert, M., De Medts, N., Bouwens, L., Rustgi, A.K., and Real, F.X. (2011). Adult pancreatic acinar cells dedifferentiate to an embryonic progenitor phenotype with concomitant activation of a senescence programme that is present in chronic pancreatitis. Gut *60*, 958–966.

Pylayeva-Gupta, Y., Grabocka, E., and Bar-Sagi, D. (2011). RAS oncogenes: weaving a tumorigenic web. Nat. Rev. Cancer *11*, 761–774.

Reichert, M., and Rustgi, A.K. (2011). Pancreatic ductal cells in development, regeneration, and neoplasia. J. Clin. Invest. *121*, 4572–4578.

Reichert, M., Saur, D., Hamacher, R., Schmid, R.M., and Schneider, G. (2007). Phosphoinositide-3-kinase signaling controls S-phase kinase-associated protein 2 transcription via E2F1 in pancreatic ductal adenocarcinoma cells. Cancer Res. *67*, 4149–4156.

Seidler, B., Schmidt, A., Mayr, U., Nakhai, H., Schmid, R.M., Schneider, G., and Saur, D. (2008). A Cre-loxP-based mouse model for conditional somatic gene expression and knockdown in vivo by using avian retroviral vectors. Proc. Natl. Acad. Sci. USA *105*, 10137–10142.

Srinivasan, L., Sasaki, Y., Calado, D.P., Zhang, B., Paik, J.H., DePinho, R.A., Kutok, J.L., Kearney, J.F., Otipoby, K.L., and Rajewsky, K. (2009). PI3 kinase signals BCR-dependent mature B cell survival. Cell *139*, 573–586.

Stanger, B.Z., Stiles, B., Lauwers, G.Y., Bardeesy, N., Mendoza, M., Wang, Y., Greenwood, A., Cheng, K.H., McLaughlin, M., Brown, D., et al. (2005). Pten constrains centroacinar cell expansion and malignant transformation in the pancreas. Cancer Cell *8*, 185–195.

von Burstin, J., Eser, S., Seidler, B., Meining, A., Bajbouj, M., Mages, J., Lang, R., Kind, A.J., Schnieke, A.E., Schmid, R.M., et al. (2008). Highly sensitive detection of early-stage pancreatic cancer by multimodal near-infrared molecular imaging in living mice. Int. J. Cancer *123*, 2138–2147.

von Burstin, J., Eser, S., Paul, M.C., Seidler, B., Brandl, M., Messer, M., von Werder, A., Schmidt, A., Mages, J., Pagel, P., et al. (2009). E-cadherin regulates metastasis of pancreatic cancer in vivo and is suppressed by a SNAIL/HDAC1/HDAC2 repressor complex. Gastroenterology *137*, 361–371.

von Werder, A., Seidler, B., Schmid, R.M., Schneider, G., and Saur, D. (2012). Production of avian retroviruses and tissue-specific somatic retroviral gene transfer in vivo using the RCAS/TVA system. Nat. Protoc. *7*, 1167–1183.

Westmoreland, J.J., Wang, Q., Bouzaffour, M., Baker, S.J., and Sosa-Pineda, B. (2009). Pdk1 activity controls proliferation, survival, and growth of developing pancreatic cells. Dev. Biol. *334*, 285–298.

Ying, H., Elpek, K.G., Vinjamoori, A., Zimmerman, S.M., Chu, G.C., Yan, H., Fletcher-Sananikone, E., Zhang, H., Liu, Y., Wang, W., et al. (2011). PTEN is a major tumor suppressor in pancreatic ductal adenocarcinoma and regulates an NF-κB-cytokine network. Cancer Discov *1*, 158–169.

Yuan, W., Stawiski, E., Janakiraman, V., Chan, E., Durinck, S., Edgar, K.A., Kljavin, N.M., Rivers, C.S., Gnad, F., Roose-Girma, M., et al. (2013). Conditional activation of Pik3ca(H1047R) in a knock-in mouse model promotes mammary tumorigenesis and emergence of mutations. Oncogene *32*, 318–326.

Cancer Cell
Erratum

Dynein Light Chain 1, a p21-Activated Kinase 1-Interacting Substrate, Promotes Cancerous Phenotypes

Ratna K. Vadlamudi, Rozita Bagheri-Yarmand, Zhibo Yang, Seetharaman Balasenthil, Diep Nguyen, Aysegul Sahin, Petra den Hollander, and Rakesh Kumar*
*Correspondence: bcmrxk@gwu.edu
http://dx.doi.org/10.1016/j.ccr.2013.03.006

(Cancer Cell *5*, 575–585; June 1, 2004)
We became aware that the above paper contains some perceived errors wherein dotted lines were not used when lanes were brought together. We have now modified Figures 3D, 6D, 6I, and 8A to reflect this; the corrected figures are printed below. There is no change in the legend or text.

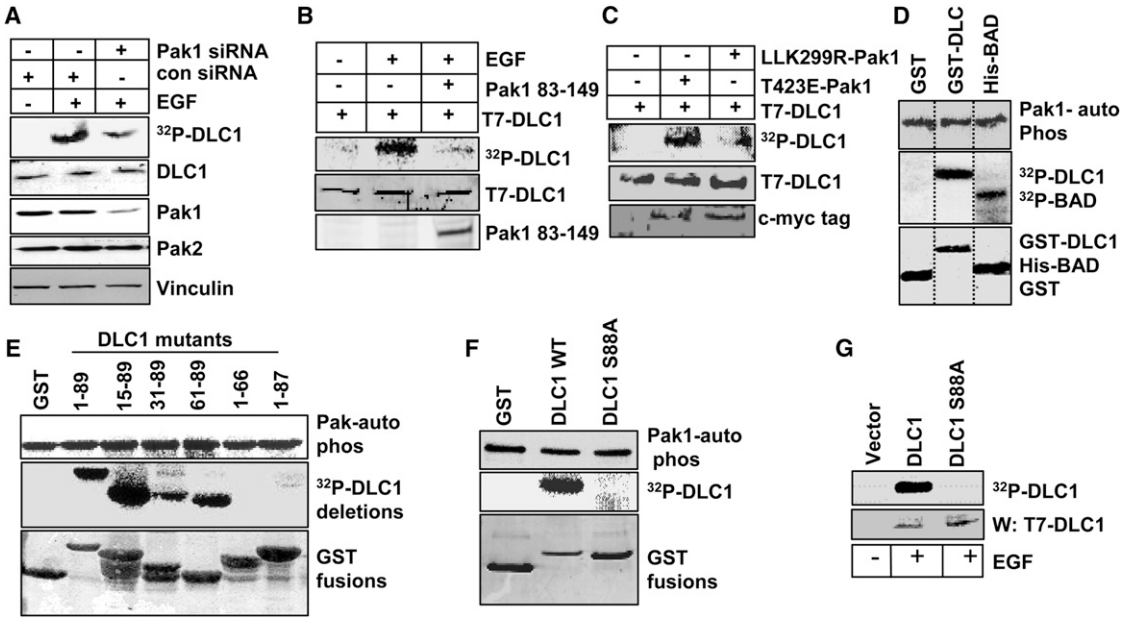

Figure 3. Pak1 Phosphorylation of DLC1

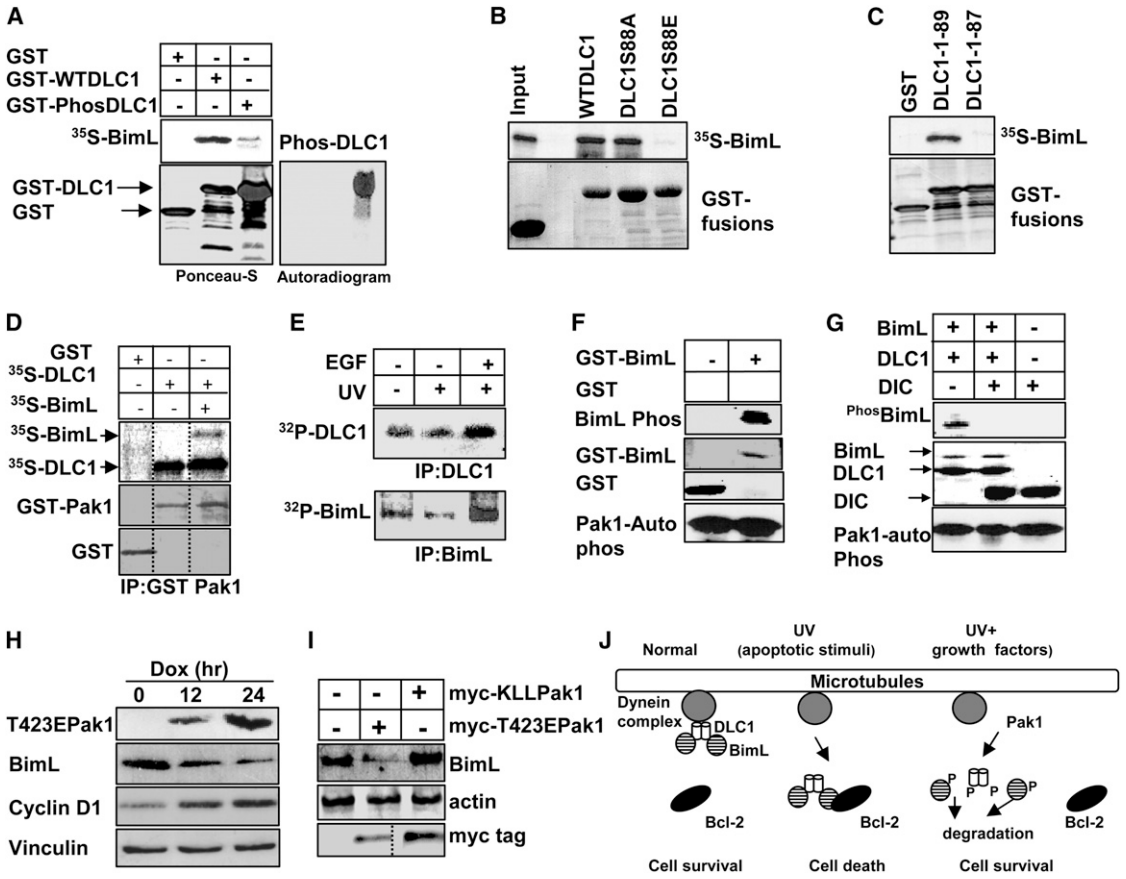

Figure 6. Pak1 Phosphorylation Regulates BimL and DLC1 Interactions

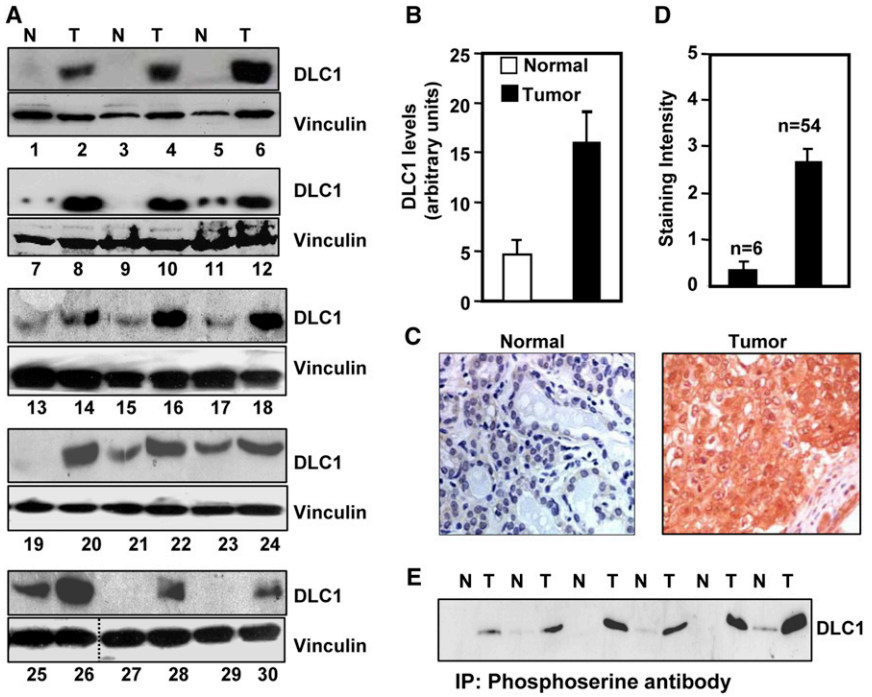

Figure 8. DLC1 Deregulation in Human Breast Tumors

SnapShot: Pancreatic Cancer

Haiyong Han and Daniel D. Von Hoff
Translational Genomics Research Institute, Phoenix, AZ 85004, USA

Cancer Cell

PATHOLOGY

Exocrine Pancreatic Cancer (95%)
- Ductal adenocarcinoma (90%)
  Premalignant: Carcinoma in situ (*PanIN-3)
- Mucinous cystadenocarcinoma (5%)
  (Acinar cell, pancreatoblastoma)
  Premalignant: **IPMN or mucinous cystadenoma

Endocrine Pancreatic Cancer (5%)
- Islet cell
- Carcinoid

*PanIN (Pancreatic intraepithelial neoplasia)

**IPMN (Intraductal papillary mucinous neoplasm)

HISTOPATHOLOGY

Photos by Christine Iacobuzio-Donahue

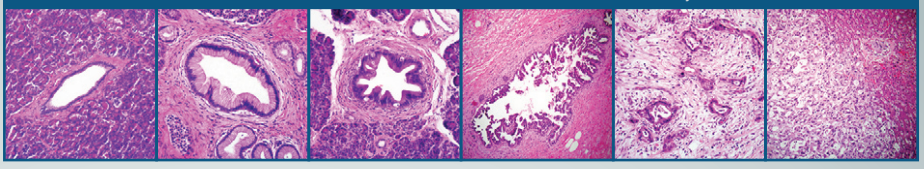

Normal | PanIN-1 | PanIN-2 | PanIN-3 | Cancer | Metastasis

ASSOCIATION WITH INHERITED CANCER SYNDROMES

- Mutation of *BRCA2* – Chromosome 13q12
- Peutz-Jeghers syndrome – autosomal dominant mutations in *LKB1/STK11* on chromosome 19p13
- Familial atypical multiple mole melanoma (FAMMM) syndrome – autosomal dominant mutation in *CDKN2A* tumor suppressor gene on 9p21
- Hereditary nonpolyposis colorectal cancer (HNPCC) – autosomal dominant mutations in DNA mismatch repair genes
- Familial kindreds - 2 or more first degree relatives
- *PALB2* mutation

GENOMIC VULNERABILITIES

Mutations
KRAS, BRCA2, PALB2, TP53,
other DNA repair genes

Amplifications
ERBB2 (HER2/neu)

Deletions (synthetic lethal possibility)
SMAD4 (DPC4)
CDKN2A (p16)

Hypermethylation
Inhibitors of DNMTs

CLINICAL AND MOLECULAR PROGNOSTIC FACTORS

Poor clinical prognostic factors
- Later stage
- R1 resection (tumor at margin, lymph node positive)
- Perineural invasion or vascular invasion
- Poor performance status
- Low serum albumin
- Liver metastasis
- Marker CA19-9 ≥ 59x ULN

Poor molecular prognostic factors
- Mutated *SMAD4*
- Mutated *TP53*

ORIGIN/EVOLUTION

Exact cell of origin not clear
(candidates include epithelium, acinar cell, islet cell)

Possible total time to evolve: 21-28 years
- 11.7 years: original gene mutation -> primary cancer
- 6.8 years primary -> metastasis
- 2.7 years appearance of metastases -> death.
  (Yachida et al., 2010)

Stem cell hypothesis
CD44, CD24, and epithelial-specific antigen (ESA) positive (Li et al., 2007)

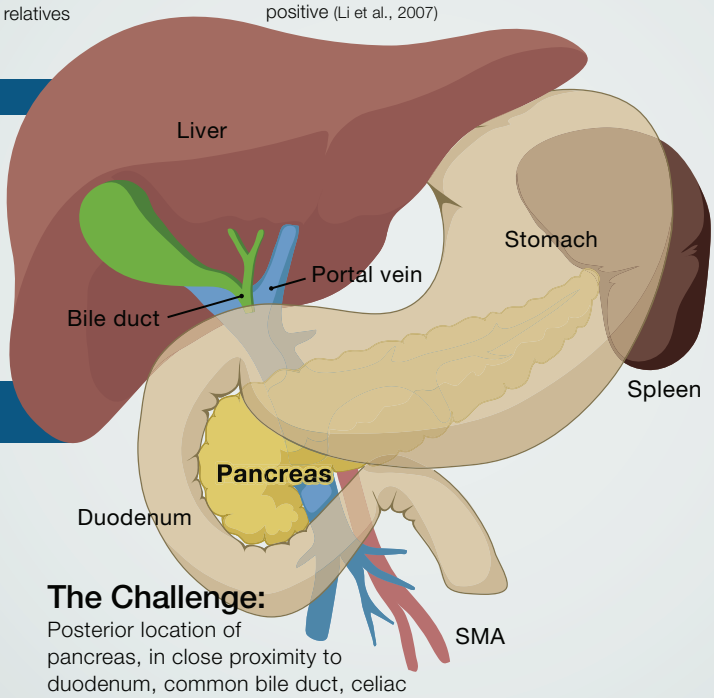

The Challenge:

Posterior location of pancreas, in close proximity to duodenum, common bile duct, celiac plexus, superior mesenteric artery (SMA), and portal vein, leads to late diagnosis as well as very bothersome symptoms of obstruction of biliary drainage, with infection, pain, and unresectability.

IN VIVO MODELS

- Genetically engineered mouse models (e.g., the KPC model by Hingorani et al., 2005)
- Primary patient-derived tumor xenografts (e.g., the PancXenoBank by Jimeno et al., 2009)

BREAKING TOLERANCE

- Anti-CTLA-4
- Anti-PD1
- Anti-PD-L1
- Anti-macrophage approaches

STROMA TARGETS

- Hypoxia
- Extracellular matrix
- Stellate cells - Vitamin D signaling
- SPARC
  (Secreted Protein Acidic, Rich in Cysteine)
- Collagen
- Hyaluronan
- Hedgehog signaling
- TGF-β signaling
- Inflammation:
  NF-κB, IL-6, JAK1/2, COX2
- High interstitial fluid pressure, growth induced solid stress

FUEL UTILIZATION

- Glucose (Aerobic glycolysis)
  PI3K, AKT, LDHA, PKM2
- Glutamine (Glutaminolysis)
  MYC, ASCT2, GLS, POL I
- Cellular constituents (Autophagy)
  AMPK
- Extracellular constituents (Macropinocytosis)
  RAS, SRC

CLINICAL STAGING AND USEFUL TREATMENTS

Resectable (localized): Surgical resection with possible follow-up XRT plus 5-FU or gemcitabine or with 6 cycles of gemcitabine, median survival = 12-19 months
- No encasement of celiac axis or superior mesenteric artery (SMA)
- Patent superior mesenteric – portal veins
- No extra pancreatic disease

Locally advanced: XRT plus 5-FU or gemcitabine, or chemotherapy alone, median survival = 6-10 months
- Encasement of arteries
- Venous occlusion (SMV or portal)
- No extra-pancreatic disease

Metastatic disease: Chemotherapy – See treatment regimens in the table to the right, median survival with treatment = 6-11 months

CLINICAL REGIMENS PROVEN TO INCREASE SURVIVAL FOR PATIENTS WITH ADVANCED METASTATIC PANCREATIC CANCER

Regimen	Control	Median Survival (Months)		p Value	Reference
		Regimen	Control		
gemcitabine	5-FU	5.6	4.4	0.0025	Burris, et al., 1997
gemcitabine + erlotinib	*GEM	6.24	5.91	0.038	Moore, et al., 2007
FOLFIRINOX**	*GEM	11.1	6.8	<0.001	Conroy, et al., 2011
nab-paclitaxel + gemcitabine	*GEM	8.5	6.7	0.000015	Von Hoff, et al., 2012

*GEM: gemcitabine **FOLFIRINOX: Folinic acid + 5-FU + Irinotecan + Oxaliplatin

SnapShot: Pancreatic Cancer

Haiyong Han and Daniel D. Von Hoff
Translational Genomics Research Institute, Phoenix, AZ 85004, USA

Cancer Cell

Pancreatic cancer can basically be divided into two major subtypes: adenocarcinoma, which is thought to arise in the exocrine portion of the pancreas (95% of cases), and rare endocrine tumors, which arise from islet cells (often designated as neuroendocrine tumors). This Snapshot concentrates on the most common and lethal type of adenocarcinoma of the pancreas: infiltrating ductal adenocarcinoma (designated here as pancreatic ductal adenocarcinoma or PDA).

Pancreatic cancer kills more than 37,000 people each year in the United States and more than 213,000 people worldwide. It has the worst 1 and 5 year survival rates of all cancers and, unfortunately, it is increasing in incidence. The highest rates of pancreatic cancer incidence are seen in industrialized and Western countries. In Europe, Nordic countries have the highest incidence rates (perhaps suggesting a role for Vitamin D). In the United States, the incidence is particularly high in Native Hawaiians, African Americans, and Korean Americans. The incidence of pancreatic cancer also increases sharply after age 50. Pancreatic cancer in young patients is frequently familial; there is a 40% increase in risk for pancreatic cancer if there is familial pancreatitis. Other risk factors include diabetes, metabolic syndrome, pancreatitis, cigarette smoking, heavy alcohol consumption, infectious agents (*H. pylori*, hepatitis B), and gastric resection. Diets low in fruits and vegetables and involving high intake of meat (particularly barbequed) are also associated with increased risk.

This Snapshot is designed to outline the pathology of PDA, its association with inherited cancer syndromes, information regarding the origin and evolution of the disease, clinical and molecular prognostic factors, and clinical staging along with common treatment regimens that have been proven to increase survival. Clearly, new ways to attack pancreatic cancer are needed. Also outlined in the SnapShot are four possible ways to attack the disease via genomic vulnerabilities, PDA's fuel utilization pathways, stroma targets, and breaking immune tolerance. These include some already discovered targets as well as some additional therapeutic possibilities. We hope that this cataloging of possibilities alongside the clinical aspects of the disease will help drive new approaches and ideas for development of new therapies and new methods for early detection of this awful disease.

ACKNOWLEDGMENTS

We would like to thank Drs. Richard Posner, Michael Barrett, Ramesh Ramanathan, and Derek Cridebring for insightful discussions during the preparation of this work. Studies in the authors' laboratories are supported by the National Foundation for Cancer Research, Stand Up to Cancer, and the NIH/NCI (U01 CA128454).

REFERENCES

Burris, H.A., 3rd, Moore, M.J., Andersen, J., Green, M.R., Rothenberg, M.L., Modiano, M.R., Cripps, M.C., Portenoy, R.K., Storniolo, A.M., Tarassoff, P., et al. (1997). Improvements in survival and clinical benefit with gemcitabine as first-line therapy for patients with advanced pancreas cancer: a randomized trial. J. Clin. Oncol. *15*, 2403–2413.

Conroy, T., Desseigne, F., Ychou, M., Bouché, O., Guimbaud, R., Bécouarn, Y., Adenis, A., Raoul, J.L., Gourgou-Bourgade, S., de la Fouchardière, C., et al.; Groupe Tumeurs Digestives of Unicancer; PRODIGE Intergroup (2011). FOLFIRINOX versus gemcitabine for metastatic pancreatic cancer. N. Engl. J. Med. *364*, 1817–1825.

Feig, C., Gopinathan, A., Neesse, A., Chan, D.S., Cook, N., and Tuveson, D.A. (2012). The pancreas cancer microenvironment. Clin. Cancer Res. *18*, 4266–4276.

Hingorani, S.R., Wang, L., Multani, A.S., Combs, C., Deramaudt, T.B., Hruban, R.H., Rustgi, A.K., Chang, S., and Tuveson, D.A. (2005). Trp53R172H and KrasG12D cooperate to promote chromosomal instability and widely metastatic pancreatic ductal adenocarcinoma in mice. Cancer Cell *7*, 469–483.

Iacobuzio-Donahue, C.A., Velculescu, V.E., Wolfgang, C.L., and Hruban, R.H. (2012). Genetic basis of pancreas cancer development and progression: insights from whole-exome and whole-genome sequencing. Clin. Cancer Res. *18*, 4257–4265.

Jimeno, A., Feldmann, G., Suárez-Gauthier, A., Rasheed, Z., Solomon, A., Zou, G.M., Rubio-Viqueira, B., García-García, E., López-Ríos, F., Matsui, W., et al. (2009). A direct pancreatic cancer xenograft model as a platform for cancer stem cell therapeutic development. Mol. Cancer Ther. *8*, 310–314.

Li, C., Heidt, D.G., Dalerba, P., Burant, C.F., Zhang, L., Adsay, V., Wicha, M., Clarke, M.F., and Simeone, D.M. (2007). Identification of pancreatic cancer stem cells. Cancer Res. *67*, 1030–1037.

Moore, M.J., Goldstein, D., Hamm, J., Figer, A., Hecht, J.R., Gallinger, S., Au, H.J., Murawa, P., Walde, D., Wolff, R.A., et al.; National Cancer Institute of Canada Clinical Trials Group (2007). Erlotinib plus gemcitabine compared with gemcitabine alone in patients with advanced pancreatic cancer: a phase III trial of the National Cancer Institute of Canada Clinical Trials Group. J. Clin. Oncol. *25*, 1960–1966.

Siegel, R., Naishadham, D., and Jemal, A. (2012). Cancer statistics, 2012. CA Cancer J. Clin. *62*, 10–29.

Stylianopoulos, T., Martin, J.D., Chauhan, V.P., Jain, S.R., Diop-Frimpong, B., Bardeesy, N., Smith, B.L., Ferrone, C.R., Hornicek, F.J., Boucher, Y., et al. (2012). Causes, consequences, and remedies for growth-induced solid stress in murine and human tumors. Proc. Natl. Acad. Sci. USA *109*, 15101–15108.

Von Hoff, D.D., Ervin, T.J., Arena, F.P., Chiorean, E.G., Infante, J.R., Moore, M.J., Seay, T.E., Tjulandin, S., Ma, W.W., Saleh, M.N., et al. (2012). Randomized phase III study of weekly nab-paclitaxel plus gemcitabine versus gemcitabine alone in patients with metastatic adenocarcinoma of the pancreas (MPACT). J. Clin. Oncol. *30* (*Suppl 34*), LBA148.

  DOI http://dx.doi.org/10.1016/j.ccr.2013.03.008